Editor's preface

Victor Gold wrote in the Preface to Volume 1 of Advances in Physical Organic Chemistry that "*The divisions of science, as we know them today, are man-made according to the dictates of practical expediency and the inherent limitations of the human intellect. As a direct result of this organization more effort has gone into the exploration of those natural phenomena that are clearly classifiable according to these divisions, with a comparative neglect of fields which, largely through historical accident do not rank as recognized 'branches' of science.*" Thus, Advances in Physical Organic Chemistry was born in an effort to establish a recognized branch of science that applies "*quantitative and mathematical methods to organic chemistry.*"

Nothing has occurred since Volume 1 of this series to diminish the value of a branch of Organic Chemistry which emphasizes the Physical over the Synthetic. A strong and vibrant community of Physical Organic Chemists continues to be desirable both to those whose work might fall within its boundaries and to members of the community of Synthetic Organic Chemists who sometimes find themselves faced with problems they are not entirely qualified to tackle.

The six chapters in Volume 40 of Advances in Physical Organic Chemistry describe work, which applies *quantitative and mathematical methods to organic chemistry.* These chapters are grouped into two general themes that reflect the merging of organic chemistry with biological and materials science.

Despite the efforts of synthetic chemists, biology remains the mother of most organic reactions. The simplicity and clarity of these reactions is apparent when examining catabolic and metabolic pathways. This examination shows that the individual steps in these pathways are variations of themes found in many other pathways, and that these themes seem innumerable. For example, a large number of compounds are metabolized by pathways that involve epoxidation of a double bond, followed by reaction with glutathione or water to give products that are readily excreted. Much of our knowledge of the mechanisms of hydrolysis and rearrangements of epoxides is due to the work of Dale Whalen. Professor Whelan's contribution to this volume is a comprehensive review of the subject that emphasizes the mechanism of reactions of high-energy carbocations that sometimes form as intermediates of nucleophile addition to the strained three-member epoxide ring.

Biological reactions are catalyzed by enzymes or ribozymes with efficiencies much greater than obtained from man-made small molecule catalysts. Many different interactions have been characterized that cause the modest rate accelerations for small molecule catalysts. By comparison, enzymes are mammoth catalysts and their size is clearly needed for the construction of an active site that enhances these individual stabilizing interactions and that favors additivity of several interactions. The chemical intuition that produces such generalizations has not led to a commonly accepted explanation for the rate acceleration achieved by any enzyme. Computational chemistry is an important tool which provides insight into important

questions in chemistry that cannot be easily addressed by experiments. Arieh Warshel is a leading practitioner of computer modeling of enzyme catalysis. He and co-workers, Sonja Braun-Sand and Mats Olson, present an overview of the computational methods that they have developed to obtain activation barriers for organic reactions at enzyme-active sites, and the insight their calculations have provided into the mechanism of action of several enzymes.

Organic molecules are often joined together in Biology through phosphate esters, and pyrophosphate esters serve as an energy reservoir that can be drawn upon to meet a variety of the needs of the cell. These phosphate and pyrophosphate esters are synthesized and degraded in enzyme-catalyzed phosphoryl transfer reactions. The present status of our understanding of the mechanism for enzymatic catalysis of these reactions is cogently reviewed by Alvan Hengge.

This editor views studies on organic chemistry in the solid state as one of the last frontiers in our field. The frontier may appear forbidding and mysterious to those of us who have spent our careers studying organic reactions within the comfortable confines of the condensed phase. However, an ever-increasing number of chemists are taming this frontier, driven by the understanding that an ignorance of the chemistry of the solid state is a major impediment to the rational design of solid organic materials. We are fortunate to have contributions from three authors whose work stands at the forefront of the areas they review.

The design and synthesis of organic compounds in which the electronic ground state possesses a very large total quantum spin number S are essential toward progress in the design of organic polymer magnets. Andrzej Rajca's chapter addresses the multiple challenges involved in the design, synthesis and characterization of very high-spin polyradicals. The substantial progress toward meeting these challenges is reviewed.

The high degree of order of crystalline organic compounds is easily characterized by X-ray crystallographic analysis. It is more difficult to define how crystal structure might be engineered to produce useful organic materials. Assemblies of organic molecules that form finite structures that exhibit properties that are independent of crystal packing represent important synthetic targets for crystal engineers. Progress toward the synthesis and structural analysis of such molecular assemblies is reviewed in a chapter by Tamara Hamilton and Leonard MacGillivray.

In recent years there have been many studies of organic reactions in cavities that exist in crystalline materials such as zeolites or in large macrocycles such as cyclodextrins. The relationship between the structure of these cavities, their microscopic environments, and the rates and products of organic reactions may be characterized in much the same way as solvent effects on organic reactivity. Murray Rosenberg and Udo Brinker summarize here what has been learned about the mechanism for formation and reaction of carbenes within cyclodextrins and zeolites.

Subject Index

Contributors to Volume 40

Sonja Braun-Sand   Department of Chemistry, University of Southern California, Los Angeles, CA 90089-1062, USA

Udo H. Brinker   Institut für Organische Chemie, Universität Wien, Währinger Str. 38, A-1090 Wien, Austria.

Tamara D. Hamilton   Department of Chemistry, University of Iowa, 423B Chemistry Building, Iowa City, IA 52212-1294, USA

Alvan Hengge   Department of Chemistry & Biochemistry, Utah State University, 0300 Old Main Hill, Logan, UT 84322-0300, USA

Leonard R. MacGillivray   Department of Chemistry, University of Iowa, 423B Chemistry Building, Iowa City, IA 52242-1294, USA

Mats H. M. Olsson   Department of Chemistry, University of Southern California, Los Angeles, CA 90089-1062, USA

Andrzej Rajca   Department of Chemistry, University of Nebraska, Lincoln, NE 68588-0304, USA

Murray G. Rosenberg   Institut für Organische Chemie, Universität Wien, Währinger Str. 38, A-1090 Wien, Austria

Ariel Warshel   Department of Chemistry, University of Southern California, Los Angeles, CA 90089-1062, USA

Dale Whalen   Department of Chemistry and Biochemistry, University of Maryland, Baltimore Country, 1000 Hilltop Circle, Baltimore, MD 21250, USA

Finite molecular assemblies in the organic solid state: toward engineering properties of solids

Tamara D. Hamilton and Leonard R. MacGillivray

Department of Chemistry, University of Iowa, Iowa City, IA 52242 1294, USA

Abstract

Assemblies of organic molecules that form finite structures represent targets for crystal engineers that can exhibit properties largely independent of crystal packing. Such finite molecular assemblies can display function, such as host–guest behavior and chemical reactivity. Here, we provide a review of finite molecular assemblies characterized in the organic solid state. The assemblies are classified as being either purely synthetic or functional. Examples from both the areas are presented and discussed.
© 2005 Elsevier B.V.
All rights reserved

1 Introduction

Crystal engineering involves the understanding of intermolecular interactions in the context of crystal packing and the utilization of such understanding in the design of new solids with desired physical and chemical properties.[1] A major aim of crystal engineering is to establish reliable connections between molecular and supramolecular structure on the basis of intermolecular forces.[2]

In this context, a central challenge in the engineering of organic solids has been to control crystal packing in one (1D) (e.g. chains), two (2D) (e.g. sheets), and three

dimensions (3D) (e.g. nets). In such a design, a crystal is regarded as an infinite network with molecules being the nodes and interactions between molecules being the node connections.[2] Through judicious selection of molecular components predisposed to self-assemble via directional noncovalent forces (e.g. hydrogen bonds), networks are engineered to give solids with desired bulk physical properties (e.g. electrical, optical, magnetic). It is for these reasons that reliable control over long-range packing is important for engineering organic solids.

Whereas infinite organic networks have been a major focus of engineering organic solids,[2] the design and construction of finite structures, or finite molecular assemblies, have received less attention. In contrast to a solid with a structure based on a network, properties of an organic solid with a structure based on a finite assembly of molecules may largely stem from the arrangement of molecules within the assembly rather than packing. In other words, properties of an organic solid based on a finite molecular assembly may be engineered largely independent of long-range packing. Indeed, although it can be difficult to identify interactions responsible for the formation of finite and infinite supramolecular structures in the solid state, recent advances in the fields of solution-phase molecular recognition and self-assembly,[3] coupled with an increasing understanding of structural consequences of intermolecular forces in the solid state,[2] provide a fertile ground to explore how finite assemblies of molecules can be used to influence bulk physical properties of organic solids.

It is with these ideas in mind that we focus here on the design and construction of finite molecular assemblies in the organic solid state. Our intention is to provide an overview of finite assemblies with emphasis on properties that such assemblies may provide solids. We will begin by outlining general criteria for constructing finite molecular assemblies in both the solid state and solution, and then describe assemblies isolated and characterized in the solid state to date. We will then use recent advances in our laboratory to illustrate how finite assemblies can be used to control solid-state reactivity and direct the synthesis of molecules.

2   Finite molecular assemblies

There are excellent reviews that address the structures of finite molecular assemblies.[3] The literature principally involves molecular assemblies designed, constructed, and characterized in the liquid phase. This is unsurprising since interests in finite molecular assemblies largely originate from studies of molecular recognition and self-assembly phenomena in solution.

In the minimalist case, a finite molecular assembly consists of either two identical (i.e. homodimer) or different (i.e. heterodimer) molecules that interact via a repeat of noncovalent forces (Scheme 1). The interactions propagate in a convergent fashion to give a discrete aggregate of molecules. Thus, the forces do not propagate ad infinitum. The vast majority of finite assemblies characterized both in solution and the solid state have components held together by hydrogen bonds.[3] Hydrogen bonds
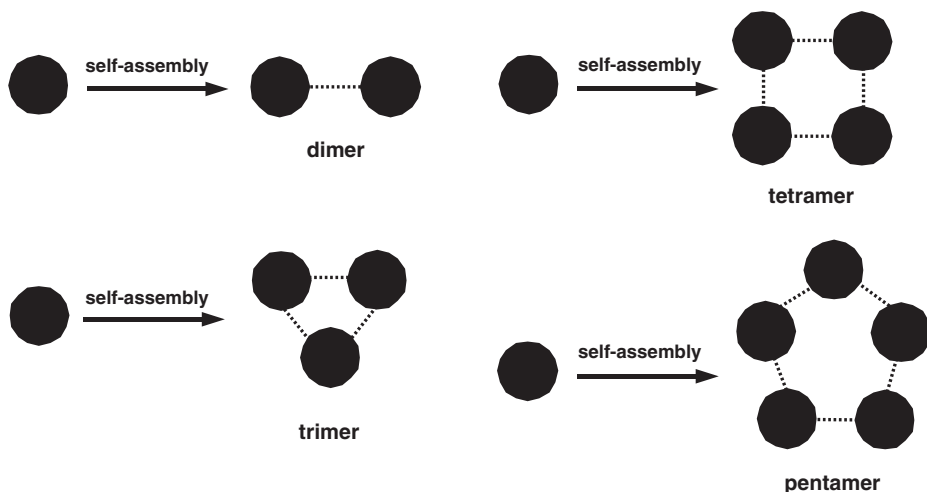
Scheme 1.

have dominated owing to the directionality, specificity, and biologic relevance of such forces.[4]

As the number of components that make up a finite molecular assembly increases so does the size and, generally, the complexity of the assembly. Thus, molecular assemblies with three, four, and five molecules as components may form 2D cyclic structures of increasing size in the form of trimers, tetramers, and pentamers, respectively (Scheme 1).[3a] The components may also be arranged in three dimensions to form a cage. Notably, useful classifications of the structures of finite assemblies based on principles of plane (i.e. polygons) and solid geometry (i.e. polyhedra) have been recently discussed.[4]

A major impetus for the design and construction of a finite molecular assembly is to create function not realized by the individual components.[3] The size, shape, and functionality of each component, which are achieved via methods of organic syntheses, are thus amplified within a final functional structure. The components may be synthesized, e.g., to give an assembly with cavities that host ions and/or molecules as guests.[3] The components may also react to form covalent bonds.[1] That a molecular assembly is, de facto, larger than a component molecule means that the components may be designed to assemble to form functional assemblies that reach nanometer-scale dimensions, and beyond.[4]

Although a finite molecular assembly may form in either the liquid phase or the solid state, such an assembly will exhibit markedly different structural behavior in each medium. In the liquid phase, a molecular assembly will be in equilibrium with its parts, as well as possible undesired complexes.[3a] Such equilibria will reduce the structural integrity of an assembly and may require stronger forces to hold the parts together. It has been suggested that the sensitivity of multiple equilibria to subtle environmental factors in solution (e.g. solvent effects) has hindered the development of finite assemblies that exhibit function.[3a] In the solid state, the structural integrity

of a molecular assembly is essentially maintained since the assembly cannot disso-
ciate back to the component parts. The crystalline environment may thus be used, in
effect, to sequester an assembly from the liquid phase,[3a] which can be used to
confirm the structure of an assembly via single-crystal X-ray diffraction. If a finite
assembly that exhibits function is sequestered to the solid state, then the function
(e.g. host–guest) may be transferred to the solid (e.g. inclusion). Inasmuch, however,
that structure effects of multiple equilibria can hinder the development of molecular
assemblies in the liquid phase, structure effects of crystal packing may hinder the
development of molecular assemblies in organic solids.

3 Supramolecular synthons, finite assemblies, and functional solids

To confront structural effects of packing in the organic solid state, Desiraju has
introduced the concept of a supramolecular synthon.[2] A supramolecular synthon is
a robust structural unit of molecules that can be transposed from solid to solid to
build solid-state structures and, ultimately, functional solids (Scheme 2). The con-
cept stems from the fields of supramolecular chemistry (i.e. intermolecular forces)
and organic synthesis (i.e. molecular synthons), and focuses upon an ability to
construct organic solids by design. The structural units can involve virtually any
organic molecule, as well as combinations of molecules and metal ions. The units
can be connected via relatively strong (e.g. O–H···O hydrogen bonds) and/or weak
(e.g. C–H···O hydrogen bonds) intermolecular forces, and may involve the same or
different molecules (i.e. co-crystal). A supramolecular synthon is important for de-
signing a solid-state structure since the synthon should successfully compete with
effects of crystal packing and, in doing so, aid the construction of a functional solid.[2]
The targeted structures of supramolecular synthons have largely been networks of
one, two, or three dimensions connectivity.

Although supramolecular synthons have been used to construct networks, it is
important to note that such structural units may also be used to construct functional
solids based on finite assemblies of molecules. That supramolecular synthons may be
used to construct such solids stems from the fact that the synthetic strategy to
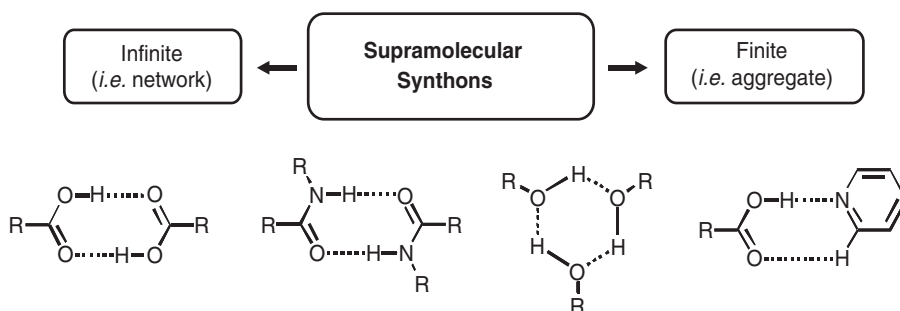
Scheme 2.

construct a finite assembly is virtually the same as that to construct a network, the primary difference being the spatial arrangements of the connecting intermolecular forces rather than the nature of the forces themselves.[2] This means that the forces that connect finite assemblies and networks in molecular solids must contend with the same effects of crystal packing. This also means that once a synthon[2] has been identified and used to form a finite assembly,[3] the same synthon may be used again and again, similar to networks, to construct analogous assemblies with desired changes to the components. If such assemblies exhibit function, then the changes may be used to affect properties of the resulting solids. Indeed, in aiding the construction of functional solids based on finite assemblies of molecules, supramolecular synthons can serve a more general role of contributing to the development of finite molecular assemblies in both the solid state and solution.[3]

4 Finite assemblies in the solid state

Having described the criteria for constructing finite molecular assemblies, we will now outline assemblies characterized in the solid state to date. In particular, our survey of the literature has led us to classify solid-state molecular assemblies into two categories: (1) synthetic and (2) functional (Scheme 3). In the former, we describe assemblies designed primarily for synthetic value and are generally not intended to contribute to properties of solids. Such assemblies either push assembly processes to new levels or confirm the structure of an assembly in solution. In the latter, we describe assemblies that contribute to properties of solids. In addition to being products of design, such assemblies may not have been originally constructed to contribute to solid-state properties but can, ex post facto, be regarded in such a light. As we shall see, many finite assemblies have not been designed a priori to affect bulk physical properties of solids. This observation is likely due to many studies in crystal engineering being focused on networks.[2] We also further classify finite assemblies as having intermolecular forces propagated in one, two, or three dimensions. Before describing the assemblies, we will first address the nature of the synthons used to form the finite structures.
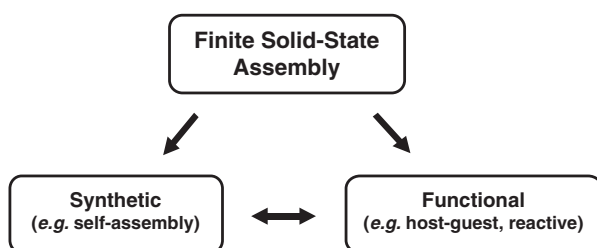
Scheme 3.

SYNTHONS

As stated, hydrogen bonds have been used to construct the majority of finite molecular assemblies. Thus, most synthons used to form finite assemblies in the solid state have been based on hydrogen bonds. Many such synthons have also been used to form networks.[2] Examples include single-point hydrogen bonds based on phenols and imidazoles, as well as multi-point hydrogen bonds based on carboxylic acid dimers, pyridone dimers, urea dimers, cyanuric acid–melamine complexes, and pyridine–carboxylic acid complexes.[2]

SYNTHETIC ASSEMBLIES

Finite assemblies constructed owing to synthetic reasons have been used to either sequester[3] assemblies from solution or develop new solid-state designs. Such assemblies have involved two components, as well as higher-order structures of 1D, 2D, and 3D connectivity.

Two-component assemblies

The smallest number of molecules that may form a finite assembly is two.[3,4] Thus, two molecules may assemble to form a finite structure in the form of either a homodimer or a heterodimer. Whereas single crystals of a homodimer are prepared via crystallization of the pure molecule, single crystals of a heterodimer are prepared via co-crystallization of the different individual components.

Molecules that form homodimers in the solid state are well documented.[2] In the minimalist case, such a molecule is monofunctional, possessing a functional group that acts as both a hydrogen-bond donor and acceptor. Thus, carboxylic acids[5] and amides,[2] e.g., self-assemble to form homodimers in the solid state held together by two hydrogen bonds.[6] Heterodimers based on different carboxylic acids, such as (α-cyclooctyl-4-carboxypropio-phenone)·(acetic acid), have also been reported (Fig. 1).[7]

A bifunctional molecule may also form a homodimer in the solid state. Such a molecule will typically possess a U-shaped structure with two identical hydrogen-bonding functionalities oriented in a parallel or convergent geometry.

Symmetrical U-shaped molecules shown to form homodimers in the solid state include 1,8-naphthalenedicarboxylic acid (1,8-nap)[8] and 2,7-di-tert-butyl-9,9-dimethyl-4,5-xanthenedicarboxylic acid.[9] The structures of the dimers are sustained by two carboxylic acid synthons that converge at the center of each assembly (Fig. 2).

Ducharme and Wuest have demonstrated that an unsymmetrical bis(2-pyridone) self-assembles as a homodimer in the solid state (Fig. 3).[10] The 2-pyridone units were separated by an acetylenic spacer that allowed the molecule to adopt a *syn* conformation, wherein the two pyridone groups are oriented along the same side of the molecule. The molecule self-assembled via four N–H···O hydrogen bonds. A symmetrical analog was also shown to form a hydrogen-bonded polymer.
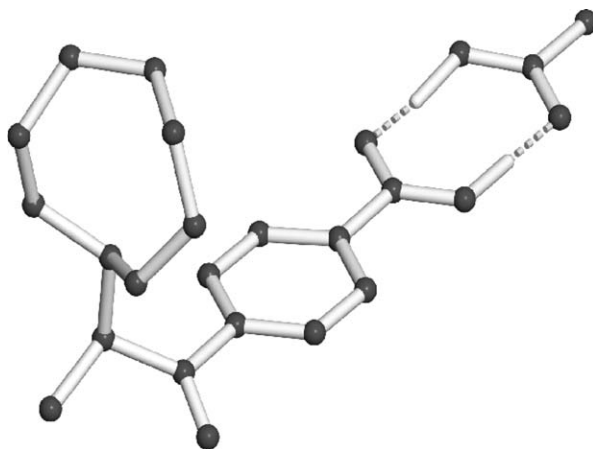
Fig. 1 X-ray crystal structure of the mixed carboxylic acid dimer (α-cyclooctyl-4-car-boxypropiophenone)·(acetic acid).
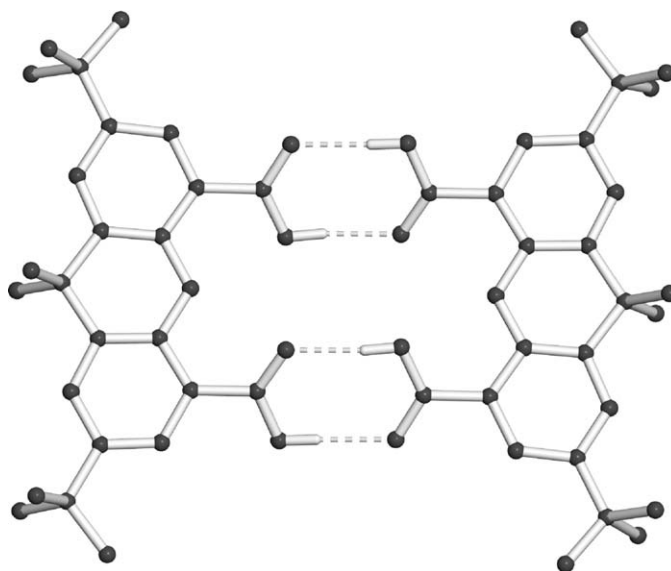
Fig. 2 Self-assembly in the X-ray crystal structure of the homodimer of 2,7-di-tert-butyl-9,9-dimethyl-4,5-xanthenedicarboxylic acid.

Unsymmetrical U-shaped molecules with two different hydrogen-bonding groups that give homodimers have also been reported. Specifically, a molecular cleft known as Rebek's imide has been shown to self-assemble in the solid state via two N–H···O and two O–H···O hydrogen bonds of two imide-carboxylic acid synthons (Fig. 4).[11]
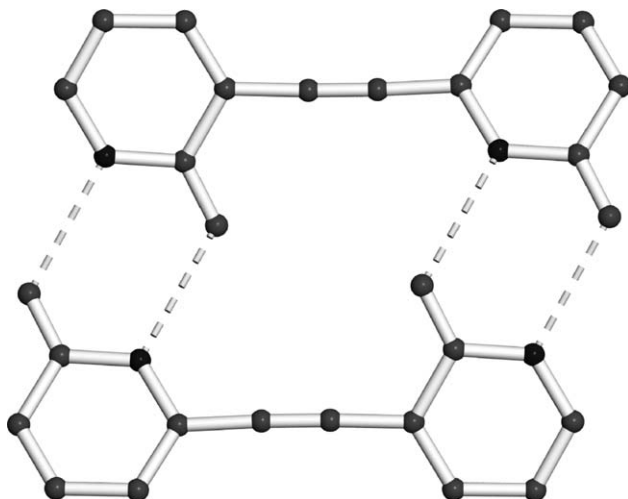
Fig. 3   Solid-state homodimer of an unsymmetrical bis(2-pyridone).
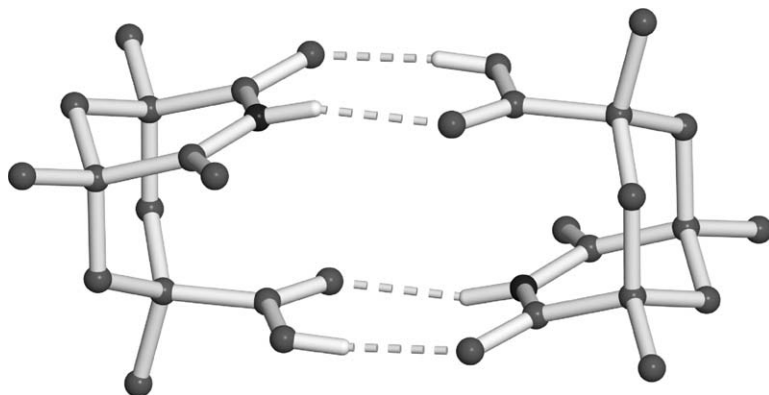
Fig. 4   Self-assembly of Rebek's imide in the crystalline state.

The ability of an unsymmetrical 2,2-dimethylbutynoic acid with a 2-pyridone terminus to form a homodimer has also been reported.[12]

   In addition to a bifunctional molecule, a trifunctional molecule has been illustrated to self-assemble to give a homodimer. Specifically, Alajarin and Steed have demonstrated the ability of a tris(o-ureido-benzyl)amine to form a homodimer in the solid state (Fig. 5).[13] Urea residues formed a belt of 12 hydrogen bonds along the equator to hold the two components together.

   There has been much interest, particularly in recent years, in the design and construction of molecules that self-assemble via quadruple hydrogen bonding.[14–19] Such bonding may be used to construct molecular assemblies of high stability. In
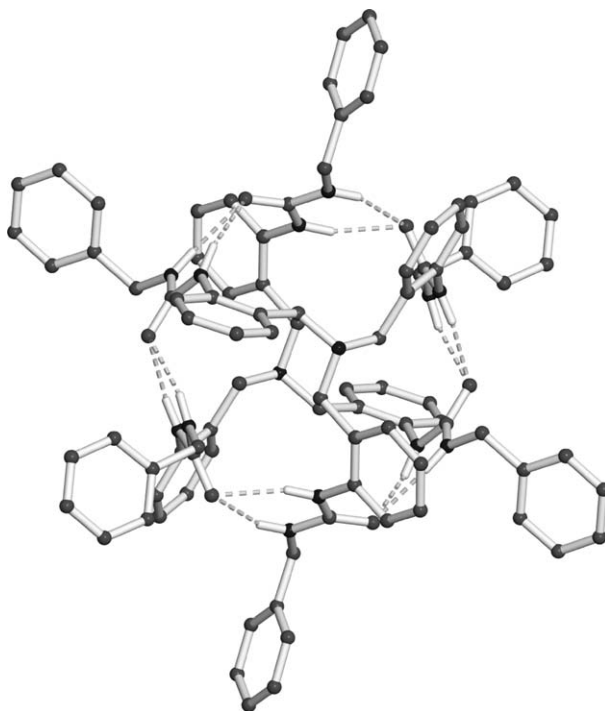
Fig. 5 X-ray crystal structure of the homodimer of tris(o-ureido-benzyl)amine.

particular, Meijer has described a series of acetylated diaminotriazenes and di-aminopyrimidines that self-assemble via quadruple hydrogen bonding.[14] The peripheries of the molecules exhibited differing patterns of hydrogen-bond donor (D) and acceptor (A) groups. In the case of two pyrimidines involving a DADA sequence, the molecules self-assembled as homodimers in the solid state (Fig. 6).[14] Notably, an intramolecular hydrogen bond contributed to the structure of one of the dimers. The same group has also demonstrated that an ureido-pyrimidone with a DDAA sequence forms a solid-state homodimer.[15] The dimer was more stable than the dimer based on the DADA sequence. This observation was rationalized on the basis of interplay between attractive and repulsive secondary electrostatic forces.[16] A related bifunctional 2-ureido-4-pyrimidinone involving an *m*-xylylene spacer was also shown to form a homodimer held together by eight N–H$\cdots$X (where X$=$N or O) forces in the crystalline state.[17] The molecule gave three isomeric dimers in solution.

Gong has recently described a class of oligoamides that employ quadruple hydrogen bonding to form solid-state homodimers (Fig. 7).[18] The monomers were derived from 3-aminobenzoic acid, 1,3-benzenedicarboxylic acid, and 1,3-diamino-benzene and, similar to Meijer's group , formed via DADA and DDAA sequences. In contrast to Meijer and colleagues, however, the donor and acceptor units were separated within the monomers such that secondary interactions were less prevalent
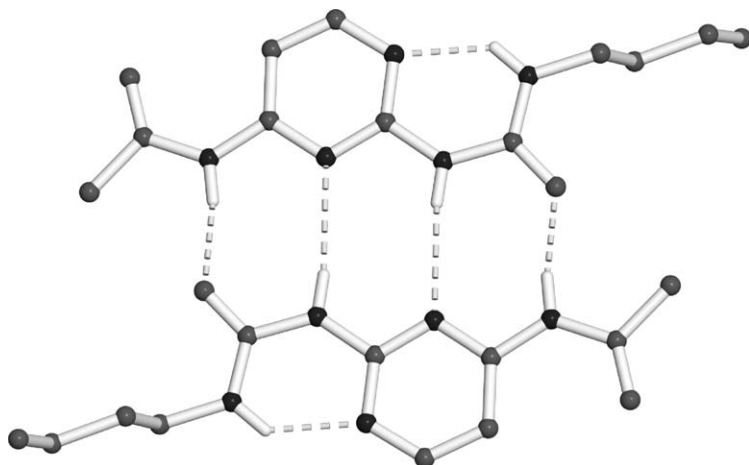
Fig. 6 Self-assembly of a pyrimidine with a DADA sequence in the solid state.
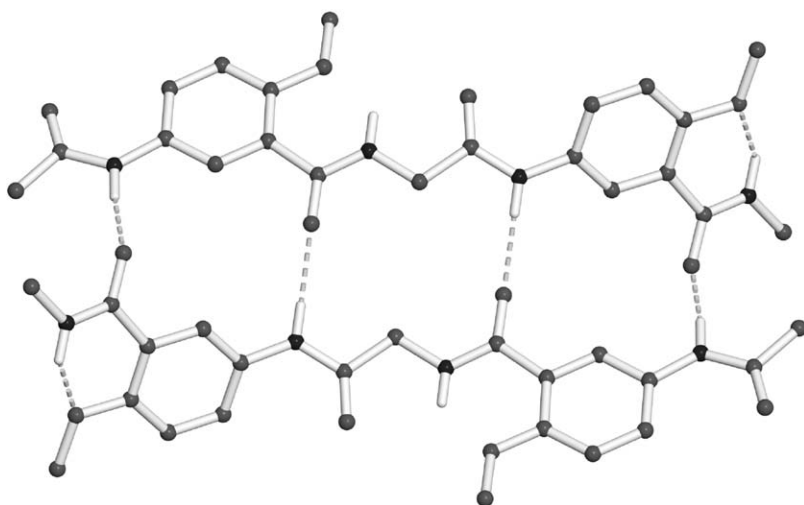
Fig. 7 Structure of the homodimer of an oligoamide with a DADA sequence.

and, as a result, the two sequences exhibited comparable stabilities. Davis has also shown that a related *N*-carbamoyl squaramide self-assembles to form a crystalline homodimer via quadruple hydrogen bonding.[19] The dimer was held together by two three-centered N–H⋯O forces.

1D assemblies

Three or more molecules may assemble to form a finite assembly based on a 1D geometry. Such an assembly will involve a central core "capped" by two mono-functional components.
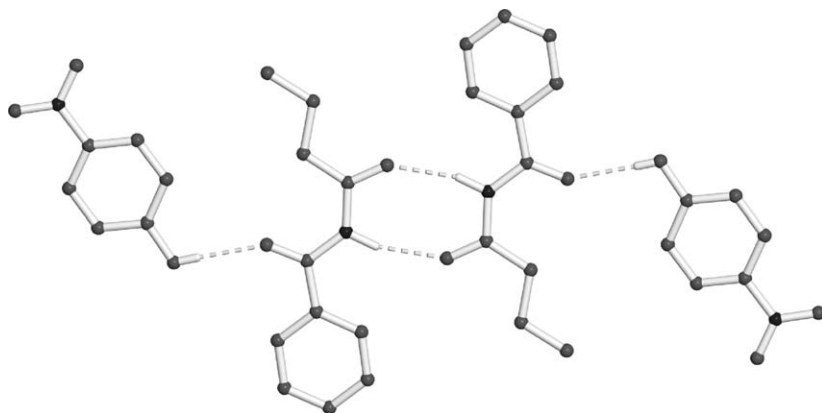
Fig. 8 X-ray crystal structure of 2(p-nitrophenol) · (N-butyrylbenzamide).

Etter and Reutzel have demonstrated that the components of co-crystals of p-nitrophenol with either diacetamide or N-butyrylbenzamide form finite 1D assemblies of composition 2(p-nitrophenol) · 2(amide) (Fig. 8).[20] In each case, the amide produced a dimer within the center of the structure. The remaining carbonyl groups pointed away from the core and served as hydrogen-bond acceptors, participating in $C=O\cdots H-O$ hydrogen bonds with the phenols. The structures of the 1D assemblies were rationalized according to relative hydrogen-bond donor and acceptor strengths of the components.

Finite 1D assemblies, of composition 2(carboxylic acid) · 2(amide), have been described by Aakeröy et al.[21] Specifically, co-crystallization of isonicotinamide with benzoic acid produced a four-component molecular assembly wherein, similar to the 1D assembly of Etter, an amide dimer defined the core. Each pyridyl group served as a hydrogen-bond acceptor by participating in an $O-H\cdots N$ hydrogen bond with a hydroxyl group of each acid (Fig. 9). Thus, according to Etter's rules,[22] the best hydrogen-bond donors (i.e. –OH groups) interacted with the best hydrogen-bond acceptors (i.e. pyridyl groups) while the second-best hydrogen-bond donors and acceptors (i.e. imide groups) interacted with each other. The scope of the assembly process was expanded to eight different carboxylic acids of various chemical functionalities (e.g. alkyl).[23]

2D assemblies

Three or more molecules may form a finite assembly with a 2D geometry. The connecting forces of such assemblies will be propagated within a plane. The components may assemble to adopt a cyclic geometry or branch from a central point.

Early work of Whitesides demonstrated the formation of heteromeric cyclic assemblies of barbital and N,N′-bis(4-tert-butylphenyl)-melamine that formed a 2D hydrogen-bonded "rosette", of composition 3(barbital) · 3(melamine), in the solid state.[24] The components assembled via 18 hydrogen bonds based on alternating ADA and DAD sequences of a cyanuric acid–melamine lattice. Covalent
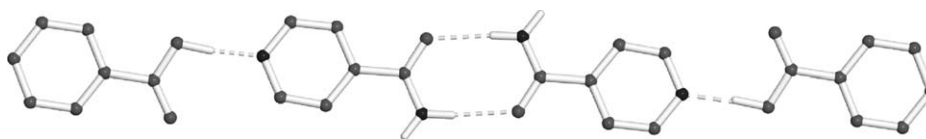
Fig. 9 The crystalline 1D assembly of 2(benzoic acid)·2(isonicotinamide).
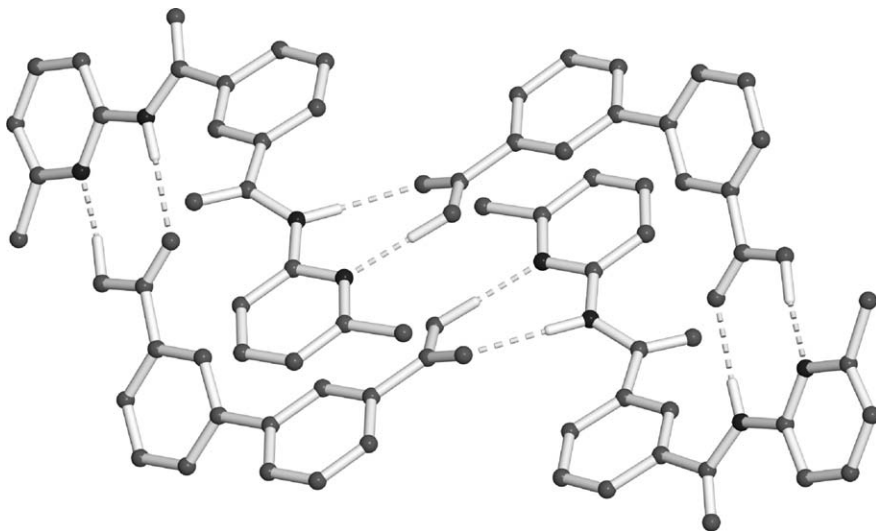
Fig. 10 X-ray crystal structure of 2(biphenyl-3,3′-dicarboxylic acid)·2(isophthalyl bis(aminopyridine).

preorganization was utilized along the periphery of the melamine component to favor the formation of the rosette over an alternative polymeric structure.

Following the work of Whitesides, Hamilton reported a cyclic assembly based on a biphenyl-3,3′-dicarboxylic acid and an isophthalpyl bis(aminopyridine) (Fig. 10).[25] The four-component assembly, of composition 2(acid) 2(bipyridine), was held together by eight hydrogen bonds. The components adopted a "figure-of-eight" structure in the solid state, wherein the diacids and bipyridines participated in face-to-face π–π forces.

Yang has also described the self-assembly of a 5-substituted isophthalic acid that produced a cyclic hexamer.[26] Each component occupied a corner of a hexagon. Similar to Whitesides the synthesis of the assembly was achieved by design. Specifically, Hamilton recognized the ability of trimesic acid to form an infinite hexagonal sheet in the solid state.[27] Moreover, it was hypothesized that replacing one of the carboxylic acid groups of trimesic acid with a substituent unable to participate in hydrogen bonds could terminate the assembly process to give a finite structure. Isophthalic acid had also been demonstrated to crystallize to give an infinite hydrogen-bonded ribbon.[28] Thus, a bulky group in the 5-position could disrupt the
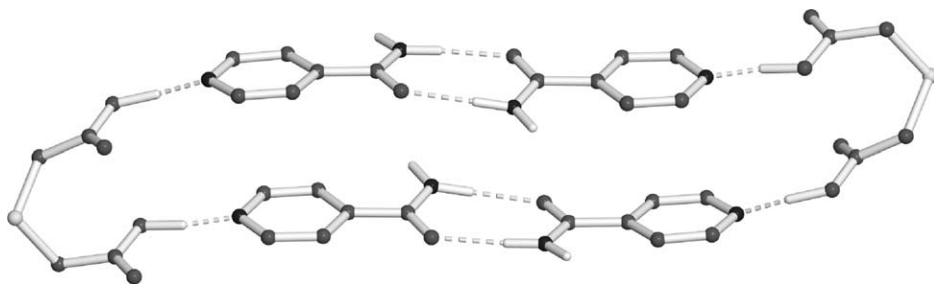
Fig. 11   The crystalline six-component assembly of 2(thiodiglycolic acid) · 4(isonicotinamide).
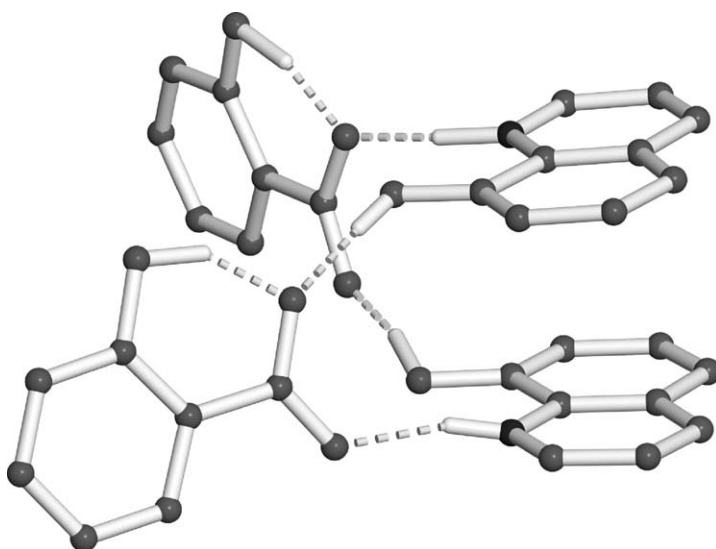
Fig. 12   Self-assembly of the four-component cyclic assembly of 2(oxine) · 2(salicyclic acid) in the solid state.

linear packing and form the six-component structure. The resulting hexamer possessed a cavity approximately 14 Å in diameter.[26]

A heteromeric, as opposed to a homomeric, six-component solid-state assembly, of composition 2(thiodiglycolic acid) · 4(isonicotinamde), has been described by Aakeröy et al. (Fig. 11).[23] As in the case of 2(carboxylic acid) · 2(amide), the central core was based on an amide dimer. The two diacids served as U-shaped units that forced two amide dimers to stack via hydrogen bonding to give the monocyclic structure.

Smith et al. have recently described a heteromeric four-component assembly, of composition 2(oxine) 2(salicyclic acid) (Fig. 12).[29] The components formed a cyclic tetramer in the solid state, wherein proton transfer occurred from the carboxylic acid to the quinoline. O–H···O and N^+–H···O hydrogen bonds, as well as face-to-face

(a)

(b)
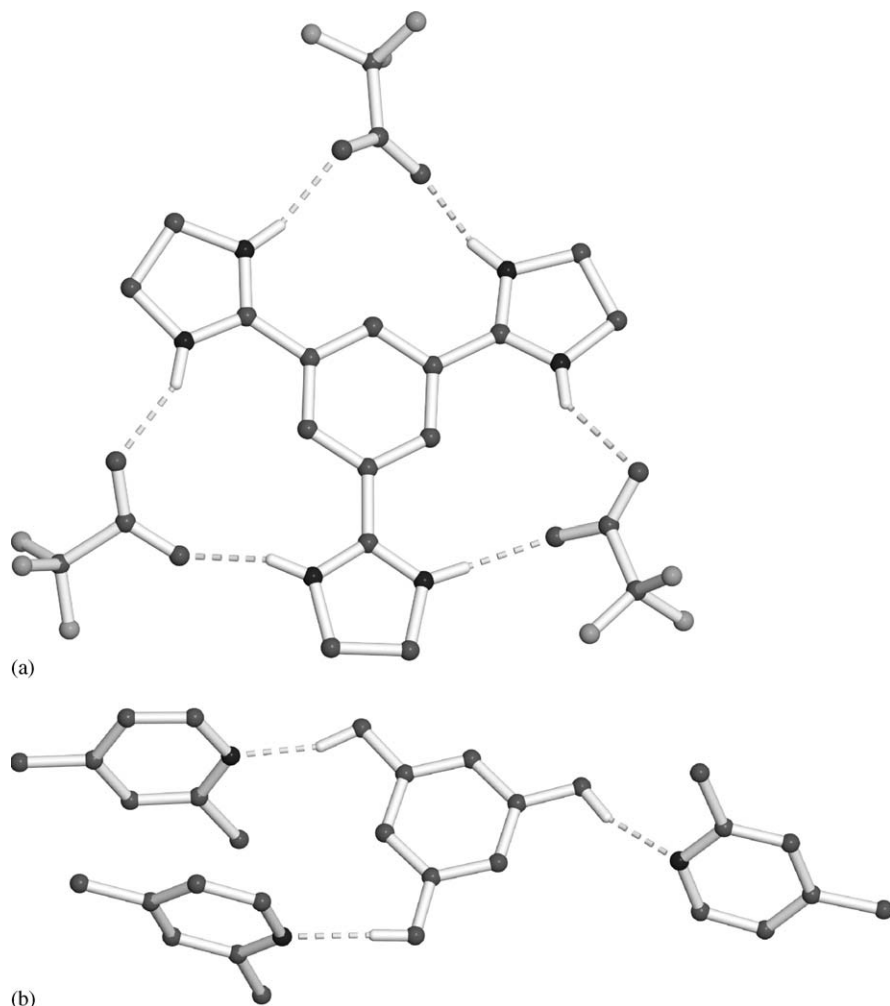
Fig. 13 X-ray crystal structures of two 2D assemblies with components that radiate from a central core: (a) tris(imidazolium) triflate salt and (b) phloroglucinol and 2,4-dimethyl-pyridine solid.

π–π forces involving the quinolinium cations, held the components together. The salicylate anions provided two U-shaped units, in the form of two carboxylato-O,O' bridges, which terminated the assembly process. The structure of the heteromeric assembly was based on a "bent" monocycle.

Whereas most 2D finite crystalline assemblies exhibit a cyclic structure, 2D assemblies with components that radiate, or branch, from a central core have also been reported (Fig. 13).[30,31] In particular, Kraft and Fröhlich have reported a tris(imidazolium) triflate salt with anions that assemble along the exterior of a 1,3,5-trisubstituted benzene (Fig. 13a).[30] Three imidazoline groups directed the assembly

of the anions via N–H$\cdots$O and N$^+$–H$\cdots$O$^-$ hydrogen bonds. The synthesis replaced a tedious covalent synthesis of a dendritic structure. Biradha and Zaworotko have also described a 2D assembly with components that branch from a 1,3,5-trisubstituted benzene core.[31] Specifically, co-crystallization of phloroglucinol with either 4-methyl or 2,4-dimethyl-pyridine produced a four-component heteromeric assembly sustained by three O–H$\cdots$N hydrogen bonds (Fig. 13b). In the case of 4-methyl-pyridine, the assemblies clustered, via C–H$\cdots\pi$ forces, to give a supramolecular cyclohexane analog.

3D assemblies

Three or more molecules may assemble in the solid state to form a finite assembly with connecting forces propagated in 3D. The components of such an assembly will typically form a polyhedral shell. The shell may accommodate chemical species as guests. The polyhedron may be based on a prism or antiprism, as well as one of the five Platonic (e.g. cube, tetrahedron) or 13 Archimedean (e.g. truncated tetrahedron) solids.[4]

   An example of a molecule that self-assembles to give a finite 3D assembly is triphenylmethanol.[32] The alcohol has been shown to self-assemble in the solid state, via O–H$\cdots$O hydrogen bonds, to form a tetramer, with the point group C_3 and a structure that conforms to a molecular tetrahedron (Fig. 14). The hydrogen bonds exhibited substantial dynamic disorder in the solid. Each molecule sits at the corner of the tetrahedron with the phenyl rings in propeller-like conformations.

FUNCTIONAL ASSEMBLIES

Whereas the finite assemblies described above have been isolated owing largely to synthetic reasons, the assemblies that follow exhibit a particular function. Examples of such function include host–guest behavior, chemical reactivity, and chirality. In doing so, the assembly affects or contributes to a property of a solid (e.g. inclusion, reactivity). Importantly, the functions arise owing to the geometric arrangement of the constituent components within the assemblies.

Two-component assemblies

Desiraju has reported a crystalline supramolecular "wheel-and-axle" compound with a structure based on a carboxylic acid dimer.[33] Specifically, the group predicted that 4-(triphenylmethyl)benzoic acid would self-assemble to give a homodimer. The dimer was expected, owing to an inability to efficiently pack, to form inclusion compounds that host solvent molecules as guests. Such inclusion would be reminiscent of structurally similar organic molecules that serve as wheel-and-axle compounds in the solid state. The homodimer would, thus, circumvent a covalent synthesis. As predicted, the carboxylic acid formed a homodimer that produced solids that exhibited solvent inclusion (Fig. 15). The packing was dominated by
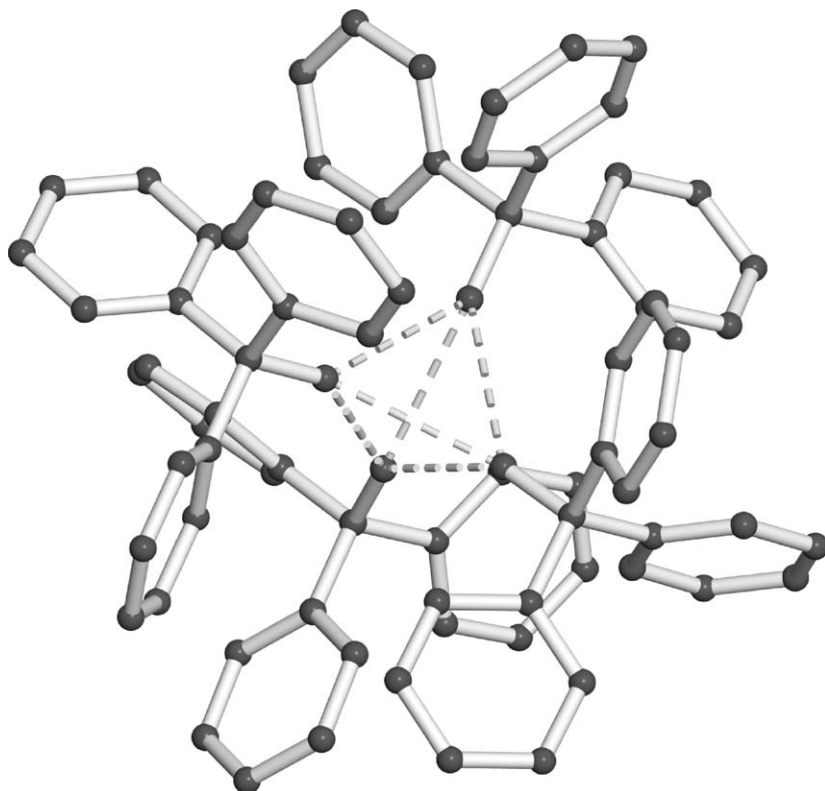
Fig. 14 Solid-state structure of the molecular tetrahedron based on triphenylmethanol.
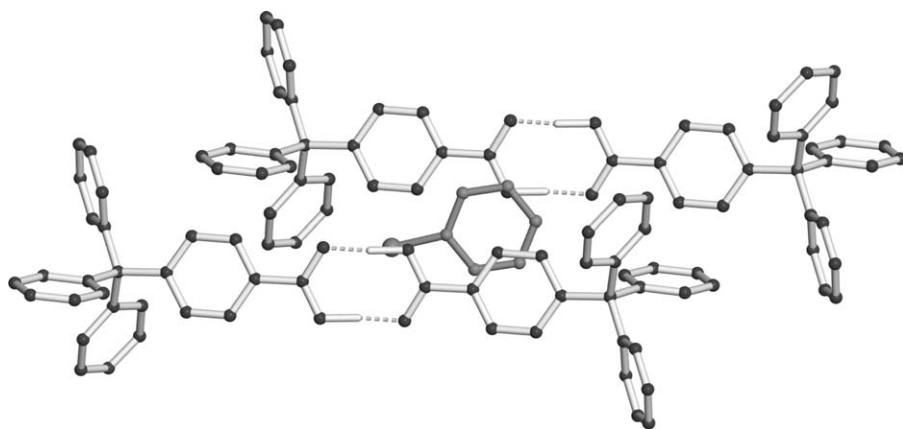
Fig. 15 The solid-state supramolecular ''wheel-and-axle'' compound involving 4-(triphenyl-methyl)benzoic acid. Included 4-chlorobenzene is shown between the dimers.
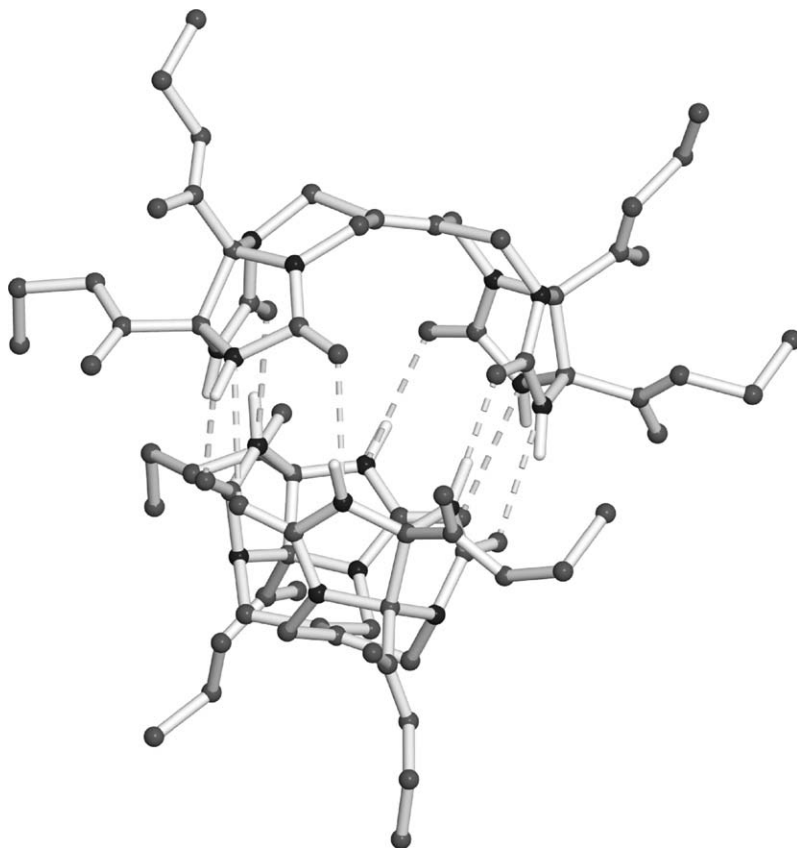
Fig. 16 X-ray crystal structure of Rebek's molecular tennis ball.

phenyl···phenyl interactions that produced voids with aromatic solvent molecules as guests.

Rebek has conducted extensive studies on curve-shaped molecules that self-assemble to form homodimers, in the form of molecular capsules, in both solution and the solid state.[34] In particular, Valdés et al. have demonstrated the ability of two glycoluril units separated by a benzene spacer to self-assemble in the solid state via eight N–H···O hydrogen bonds to form a capsule with a structure that conforms to a "tennis ball" (Fig. 16).[34a] A disordered guest, identified as probably being methanol, occupied the interior. A related dimer based on an ethylene spacer was also prepared and shown to accommodate a guest, also identified as probably being methanol, in the crystalline state.[34b]

Böhmer has reported the ability of a bowl-shaped molecule known as a calixarene to self-assemble in the solid state to form a homodimer.[35] A calix[4]arene with four urea groups attached to the upper rim self-assembled via 16 hydrogen bonds to give a cavity with an approximate volume of 200 Å^3 (Fig. 17). The cavity hosted a highly
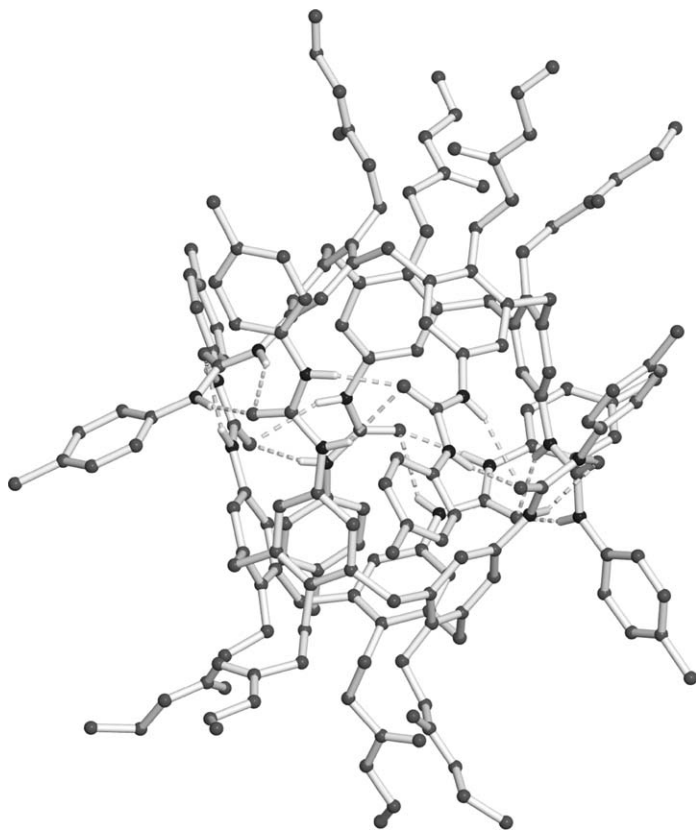
Fig. 17 Crystallographic structure of the urea-derivatized calix[4]arene homodimer.

disordered benzene molecule as a guest. The molecular capsules packed to form exterior cavities that also hosted benzene molecules.

Calix[5]arenes have also been demonstrated to form crystalline capsule-like dimers. Specifically, a tetra-substituted calix[5]arene with four methyl and iodo groups attached at opposite rings along the upper rim formed a dimer that encapsulated buckminsterfullerene, or C_{60} (Fig. 18).[36] Raston has also described dimers based on tetrabenzyl-derivatized calix[3]- and calix[5]arenes that encapsulate C_{60} in the solid state.[37,38] The components assembled via van der Waals forces.

In addition to calixarenes, Sherman has reported the ability of a resorcin[4]arene, a bowl-shaped molecule with eight hydroxyl groups at the upper rim, to form a homodimer in the solid state.[39] Deprotonation of two hydroxyl groups of a resorcin[4]arene using 1,8-diazabicyclo[5.4.0]undec-7-ene (DBU) as a base produced a dianion that self-assembled to form an anionic capsule. The dimer hosted a molecule of pyrazine. Four H^{+}–DBU ions also interacted with the periphery of the dimer via four N^{+}–H$\cdots$O^{-} hydrogen bonds (Fig. 19).
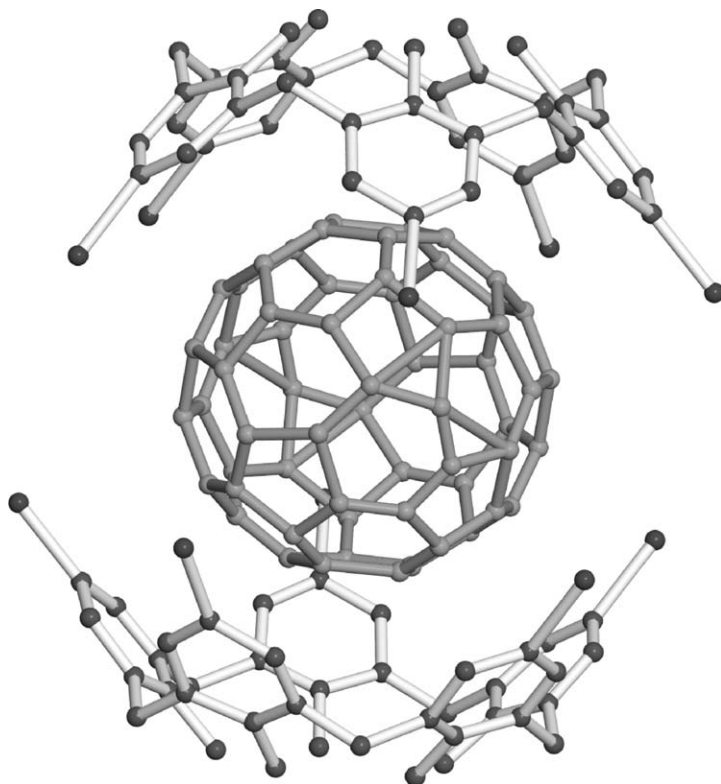
Fig. 18 X-ray crystal structure of the encapsulation complex between two molecules of an iodo-derivatized calix[5]arene and C_{60}.

Following the work of Sherman, work of Shivanyuk et al. described a hydrogen-bonded capsule based on a tetraester-substituted resorcin[4]arene.[40] The components were held together by eight O–H$\cdots$O hydrogen bonds and hosted a single tropylium cation as a guest (Fig. 20). A BF_4^- counter ion was located along the exterior of the dimer in a pocket created by pendant pentyl chains at the lower rim of the bowl-shaped molecule.

Whereas Alajarin and Steed demonstrated the ability of *ortho*-substituted tris (*o*-ureido-benzyl)amine to form a homodimer in the solid state,[13] the same group later revealed the ability of the *meta*-derivative, tris(*m*-ureido-benzyl)amine, to give a dimeric capsule (Fig. 21).[41] In particular, the amines self-assembled via hydrogen bonds involving the urea groups to form a dimer larger than the *ortho*-structure. The dimer possessed a central cavity that hosted an ordered dichloromethane molecule as a guest.

A synthetic cyclic peptide has been demonstrated by Ghadiri to form a cylindrical dimer in the crystalline state (Fig. 22).[42] The homodimer formed owing to selective *N*-methylation along the backbone of the peptide which mitigated the formation of an infinite structure. A total of eight hydrogen bonds held the two components
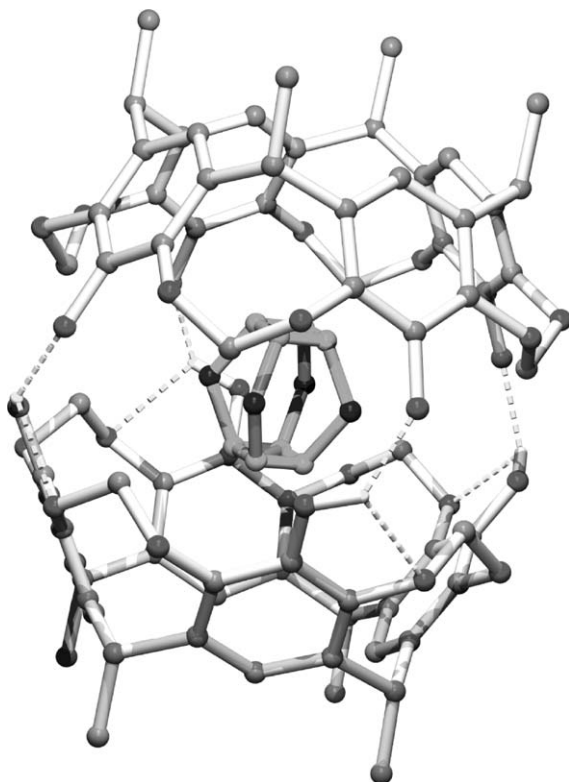
Fig. 19 A resorcin[4]arene homodimer in the solid state. Disordered pyrazine guest shown in dark gray.

together. An internal cavity was created by the peptide dimer that accommodated loosely held water molecules. The dimer packed to form a continuously channeled superlattice structure.

Zaworotko has recently demonstrated the ability of the drug carbamazepine to form a crystalline homodimer.[43] The structure was sustained by an amide dimer synthon (Fig. 23). The dimer possessed two pendant –NH groups that participated in hydrogen bonds with solvent molecules (e.g. acetone). The solids were generated to develop new solid compositions of the drug. Such compositions are anticipated to lead to pharmaceutical materials that exhibit properties (e.g. bioavailability) not realized by previous crystalline forms of the drug molecule.

Whereas most homodimers have been shown to exhibit host–guest behavior, Feldman and Campbell have described a crystalline homodimer that exhibits chemical reactivity (Fig. 24).[44] In particular, two J-shaped dicarboxylic acids based on 1,8-disubstituted naphthalene units directed the assembly of two olefinic groups via two carboxylic acid synthons in an arrangement suitable for a [2+2] photo-dimerization.[45] The two double bonds of the homodimer were organized parallel and separated by 3.65 Å. Ultraviolet (UV) irradiation of the solid induced the
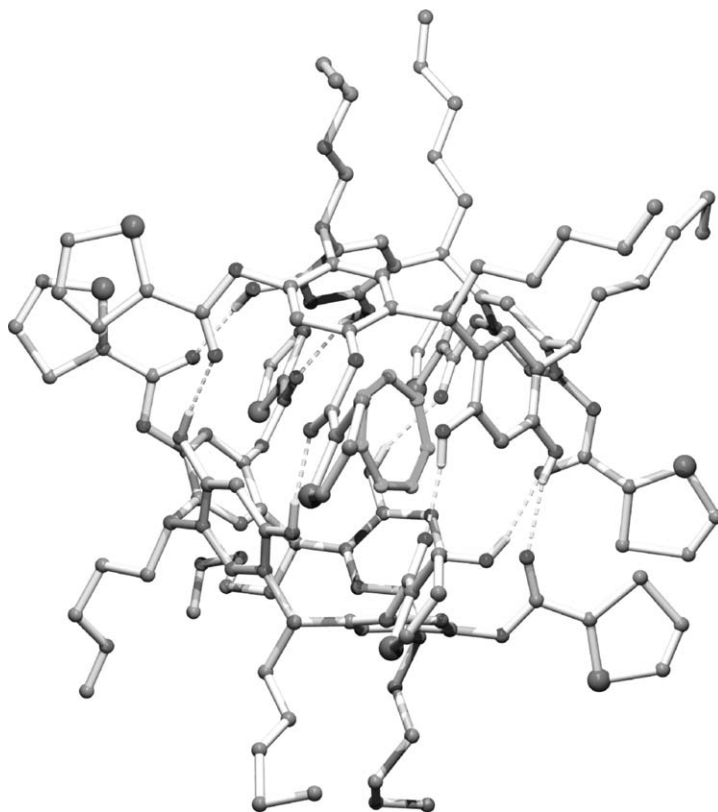
Fig. 20 Solid-state structure of the tetraester-substitued resorcin[4]arene capsule. Tropylium guest shown in dark gray.

molecules of the hydrogen-bonded dimer to cross-link regiospecifically and in quantitative yield to give the corresponding cyclobutane photoproduct.

In addition to host–guest properties and reactivity, the ability of the components of a dimer to form a finite chiral assembly has been described by Lightner. Specifically, a chiral dipyrrinone diester was shown to self-assemble in the solid state to give a doubly hydrogen-bonded dimer.[46] Hydrogen bonds formed from the pyrrole N–H group to the ester carbonyl oxygen to give the resulting chiral structure.

1D assemblies

A spectacular series of 1D assemblies based on *three different* components has been recently described by Aakeröy[21] Specifically, 1:1:1 assemblies involving 3,5-dinitrobenzoic acid and isonicotinamide co-crystallized with either 3-methylbenzoic acid, 4-(dimethylamino)benzoic acid, or 4-hydroxy-3-methoxycinnamic acid have been described (Fig. 25).[21] In each case, the components produced a linear three-component assembly with isonicotinamide at the center. The pyridyl group formed a
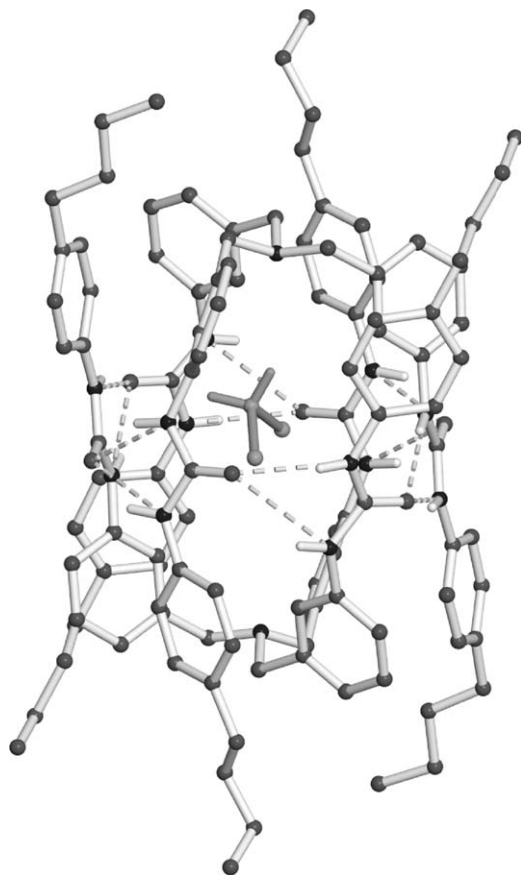
Fig. 21 X-ray crystal structure of the tris(*o*-ureido-benzyl)amine homodimer. Dichloromethane guest is shown in dark gray.

hydrogen bond with the strongest acid (i.e. best hydrogen-bond donor) and the amide formed a hydrogen bond with the weakest acid (i.e. second-best hydrogen-bond donor). The 1D assemblies stacked in an antiparallel fashion that displayed considerable donor–acceptor overlap between the strong acids and weak bases. The resulting solids were orange to deep red in color owing to the charge-transfer properties.

2D assemblies

Etter has described a crystalline hexamer composed of six molecules of cyclohexanedione. The molecules, each of which adopted a *syn–anti* configuration, self-assembled via six O–H⋯O hydrogen bonds (Fig. 26).[47] Each ketone, similar to the hexamer of Hamilton, was located at the corner of a hexagon. In contrast to Hamilton, however, the cavity of the assembly accommodated a solvent molecule as
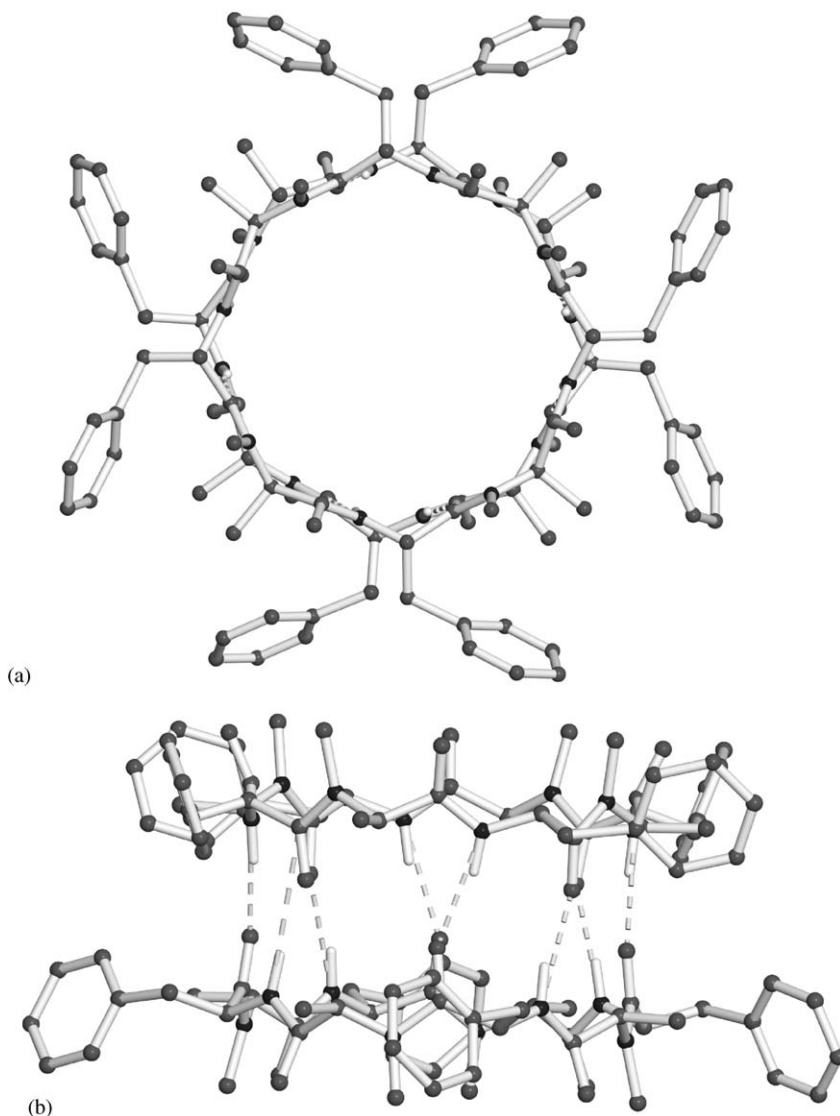
Fig. 22 The cylindrical dimer of a synthetic cyclic peptide in the solid state: (a) plane of the peptide and (b) perpendicular to the plane of the peptide.

a guest. In particular, the cavity accommodated a molecule of benzene. Importantly, the assembly process was shown to be specific. Thus, the hexamer formed with benzene and deuteriobenzene as guests, but not thiophene, pyridine, alcohols, or chloroform.

Mascal has demonstrated the ability of a bent molecule with AAD and DDA sequences of hydrogen bonds to self-assemble in the solid state to form a cyclic
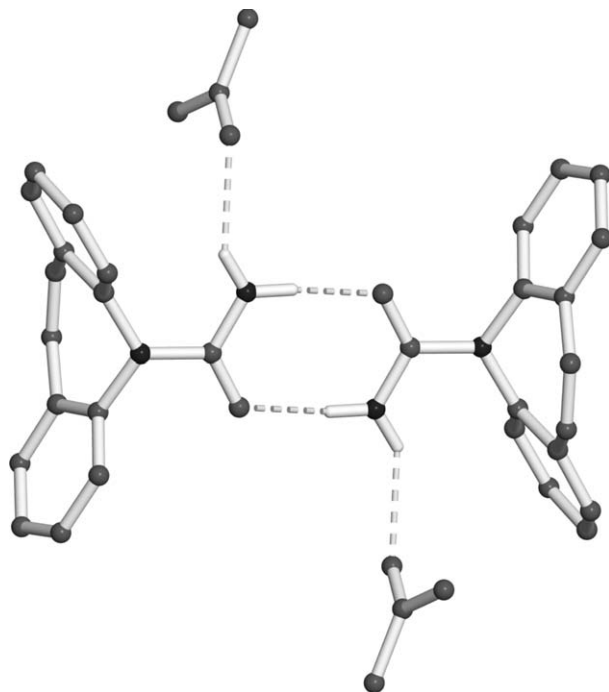
Fig. 23 X-ray crystal structure of the carbamazapine homodimer with hydrogen-bonded acetone molecules.
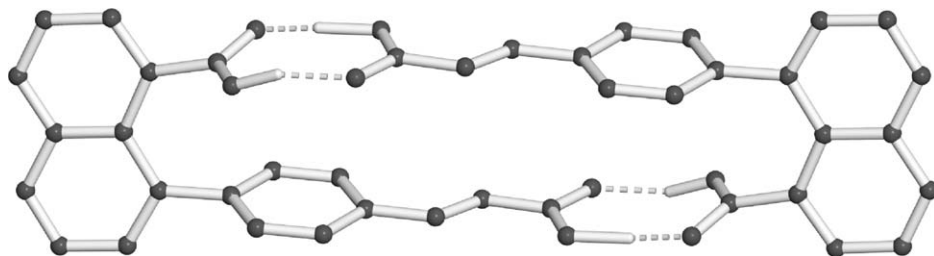
Fig. 24 Solid-state structure of the homodimer of a J-shaped napthalenedicarboxylic acid.

hexamer (Fig. 27). The AAD and DDA sequences were derived from cytosine and guanine, respectively, and were subtended by an angle of 120°.[48] The components self-assembled via 18 hydrogen bonds to give a macrocycle with an internal cavity approximately 11 Å in diameter. The hexamers packed to produce large, solvent-filled channels in the solid state. Interestingly, the 2D assembly crystallized in the rare cubic space group Ia–3d, which exhibits the highest symmetry of all space groups.

Whereas Hamilton, Etter, and Mascal have demonstrated the self-assembly of six identical molecules to form a hexamer with a planar structure, Grossman has
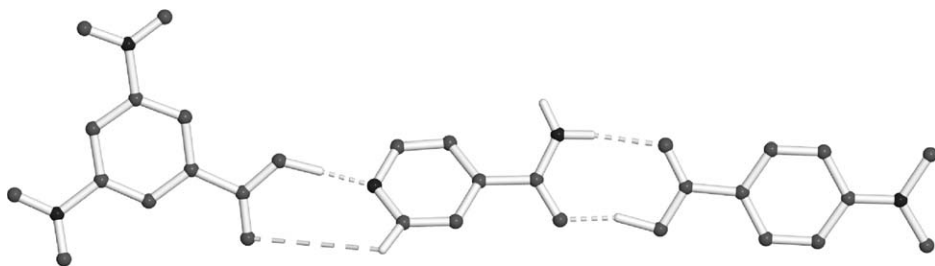
Fig. 25 The 1D assembly of (3,5-dinitrobenzoic acid) · (isonicotinamide) · (4-(dimethylami-no)benzoic acid) in the solid state.
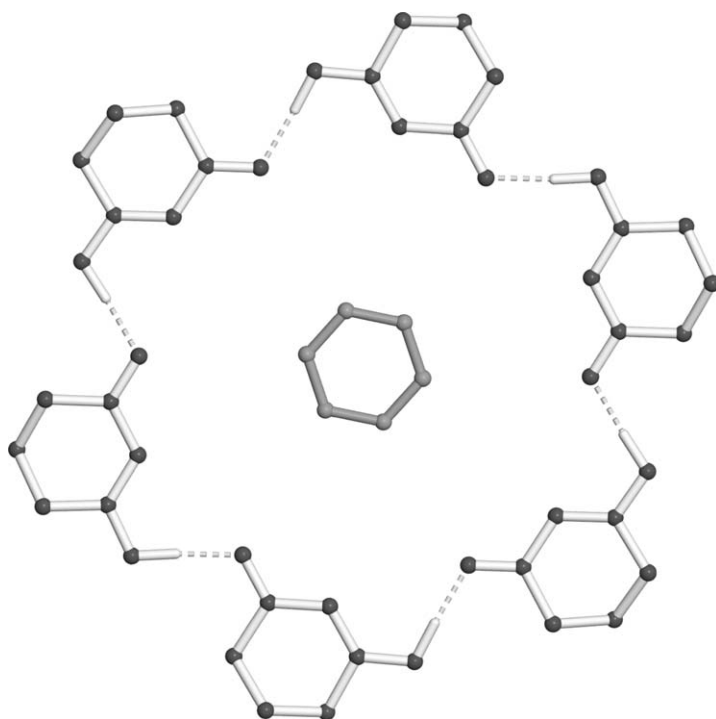
Fig. 26 Solid-state cyclic hexamer based on 1,3-cyclohexanedione. Benzene guest is shown in dark gray.

demonstrated the self-assembly of six identical tricyclic amidals, via amide dimers, to form a solid-state hexamer with a non-planar structure (Fig. 28).[49] In particular, the hexameric assembly exhibited a topology, held together by 12 N–H···O hydro-gen bonds, that conformed to the chair conformation of cyclohexane. The cyclic structure also possessed a central cavity occupied by multiple solvent molecules (e.g. nitrobenzene). In the absence of a suitable guest, a 1D tape was shown to form.
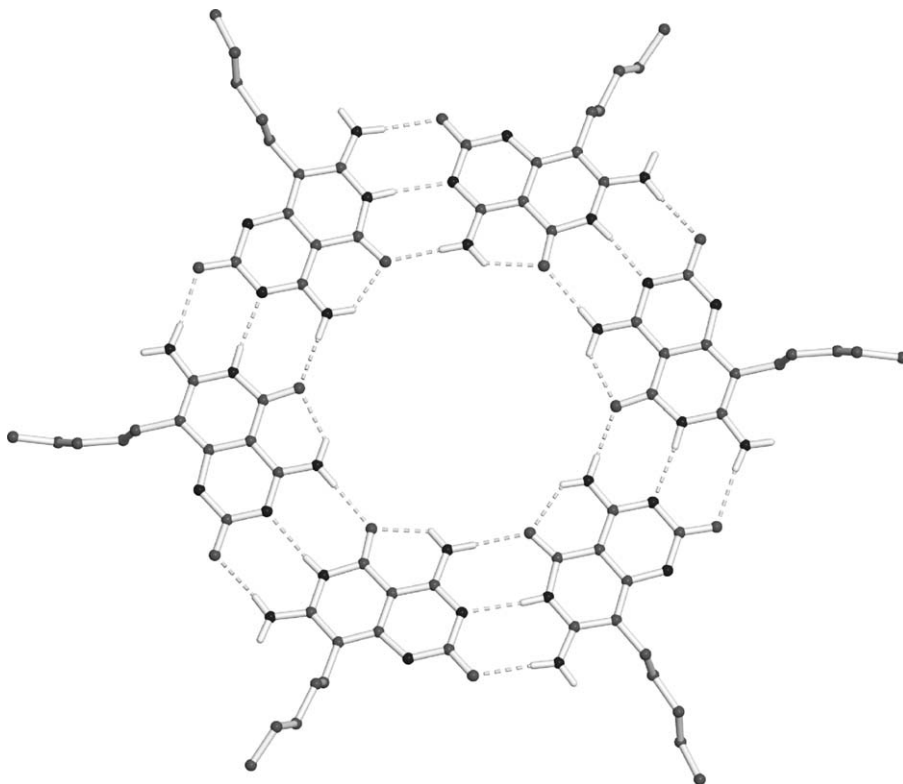
Fig. 27 The cyclic hexamer based on AAD and DDA sequences of hydrogen bonds.

In addition to dimers, Zaworotko has demonstrated the ability of cabamazepine to form four-component assemblies in the solid state with carboxylic acids (Fig. 29).[43] Each hydroxyl group and carbonyl unit of each acid (e.g. formic acid) formed an O–H···O=C and C=O···H–N hydrogen bond with each carbonyl and amine unit of the amide, respectively, to produce the heteromeric structures. Earlier work by Weber et al. involving a triarylmethanol based on fluorene also revealed the formation of similar cyclic assemblies with alcohols[50] while very recent work of Biradha and Mahata have described the formation of four-component heteromeric assemblies involving racemic-bis-β-naphthol and 4,4′-bipyridine.[51] Specifically, co-crystallization of the diol with the bipyridine gave a finite assembly, of composition 2(diol)·2(bipyridine), held together by four O–H···N hydrogen bonds. The packing of the assembly produced voids that accommodated solvent molecules as guests.

Whereas most functional 2D assemblies have been constructed using hydrogen bonds, Atwood et al. have recently described a functional 2D assembly sustained via van der Waals forces.[52]

In particular, the simplest calix[4]arene has been shown to self-assemble in the solid state to give a cyclic trimer with a shape that approximates a sphere (Fig. 30).
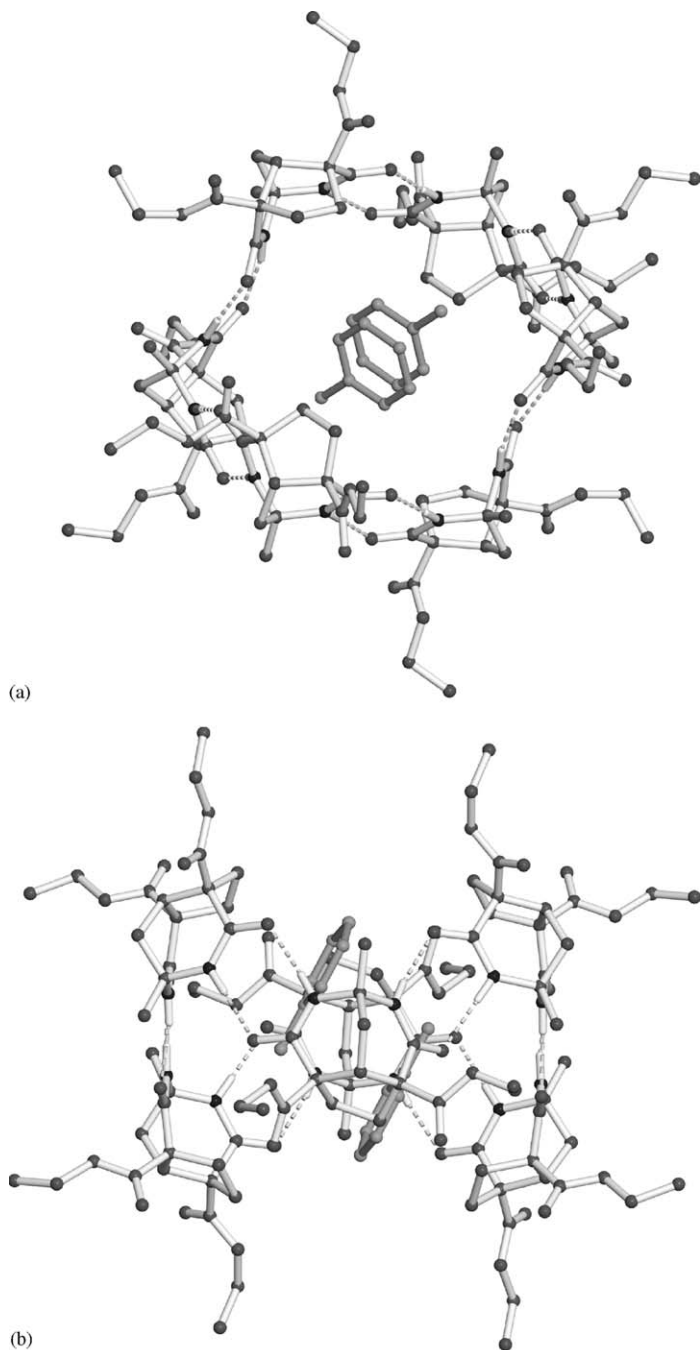
Fig. 28 Crystallographic structure of the hexamer of based on a tricyclic amidal: (a) central axis and (b) perpendicular to central axis. Two nitrobenzene guests are shown in dark gray.
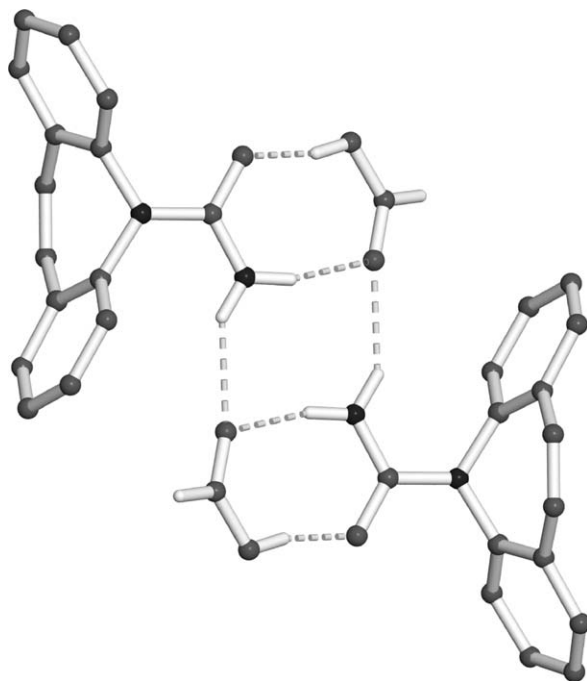
Fig. 29 Solid-state structure of the cyclic four-component assembly of 2(carbamazapine)-2(formic acid).

Owing to the spherical shape of the trimer, the assembly formed an extended structure based on hexagonal close packing. The packing produced a 3D network of parallel and oblique channels and voids that stabilized highly volatile guests, such as gases (e.g. freons), in the solid.

3D assemblies

As stated, a finite assembly with components arranged in 3D will possess a structure that conforms to a polyhedron. The simplest polyhedra are the prisms while polyhedra of increasing complexity include Platonic and Archimedean solids.

   Of those functional crystalline assemblies with structures that conform to polyhedra, it is the prisms that have, thus far, been most studied. In particular, Reinhoudt has described a 3D assembly with a structure that conforms to the simplest prism; namely, a trigonal prism.[53] Specifically, three calix[4]arenes functionalized at the upper rim with two melamine units have been shown to assemble with six barbituric acid molecules via 36 hydrogen bonds to form a nine-component assembly with a structure that approximated a trigonal prism (Fig. 31). Although the cavity of the assembly was too small to accommodate a guest, the assembly packed to produce voids that included toluene molecules as guests.
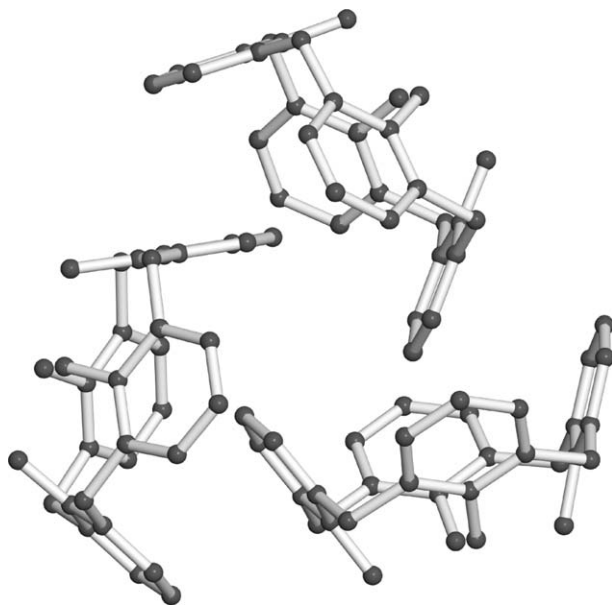
Fig. 30   Crystalline cyclic trimer of calix[4]arene.

In addition to calix[4]arenes, resorcin[4]arenes have been shown to give heteromeric assemblies in the solid state with structures that conform to prisms. In particular, two tetraphenethylresorcin[4]arenes have been shown by Atwood to assemble with eight 2-propanol molecules to form a 10-component assembly held together by 16 hydrogen bonds (Fig. 32).[54] The alcohols served as hydrogen-bond bridges between the resorcin[4]arenes, which were organized rim-to-rim, to give a framework that conforms to a tetragonal prism. The assembly possessed an interior volume of $230\,\text{Å}^3$ that encapsulated disordered solvent molecules.

Murayama and Aoki have also revealed the ability of a resorcin[4]arene to assemble with hydroxylated solvent molecules to form an assembly with a structure that conforms to a tetragonal prism. Specifically, two tetraethylresorcin[4]arenes assembled with eight water molecules to give an anionic capsule in the solid state.[55] The capsule accommodated a tetraethylammonium cation, which interacted with the inner walls of the host via cation–π forces. Similar assemblies involving derivatized resorcin[4]arenes have also been described.[56] In particular, the resorcin[4]arene of Aoki et al.[56] was also shown to assemble with 10 water molecules to give a capsule that hosted both a triethylammonium cation and a water molecule.[57] The encapsulated guests assembled via a N^+–H O··· hydrogen bond. Shivanyuk et al. have also described the ability of two hydroxylated resorcin[4]arenes to assemble with 16 water molecules to form a capsule that accommodated either four acetonitrile molecules or a quinuclidinium ion.[58]

Resorcin[4]arenes that adopt a boat conformation have also been demonstrated to form finite assemblies in the solid state. In particular, members of a series of

(a)

(b)
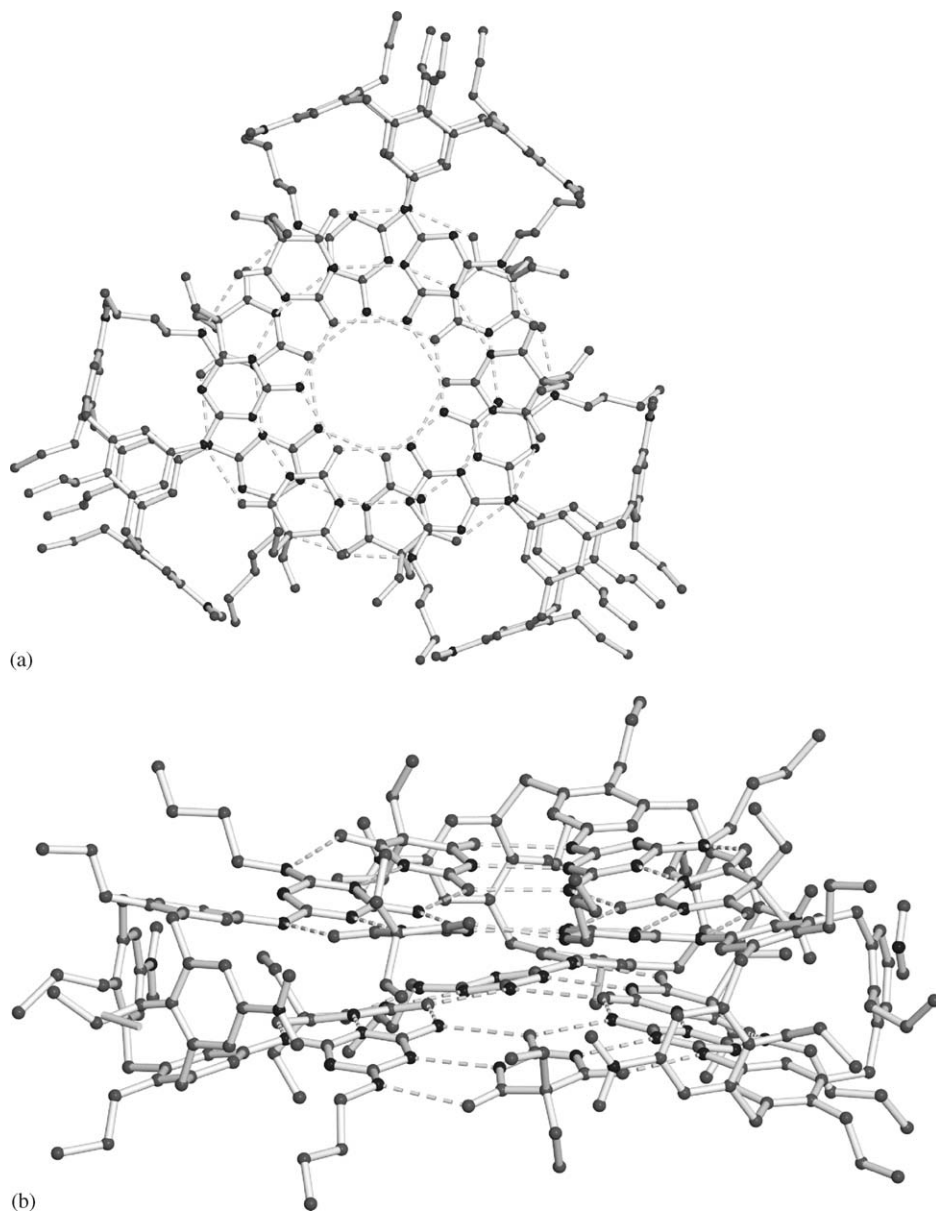
Fig. 31 The nine-component trigonal-prismatic solid-state assembly of 3(calix[4]arene de-
rivative) · 6(babituric acid): (a) plane of hydrogen-bonding and (b) perpendicular to hydrogen-
bonding.
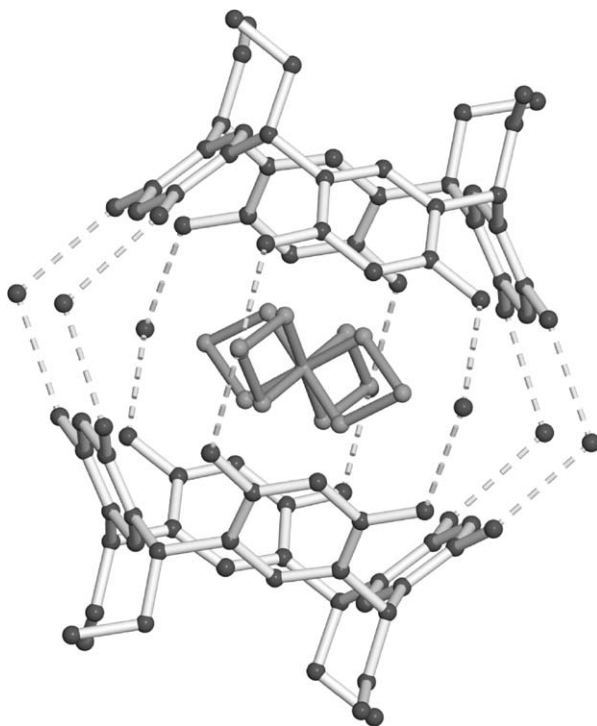
Fig. 32 X-ray crystal structure of the capsule involving tetraethylresorcin[4]arene and water molecules. Disordered tetraethylammonium guest is shown in dark gray.

C_2-symmetric tetraester resorcin[4]arenes have been shown by Shivanyuk et al. to form capsules that host two triethylammonium cations.[59] The capsules were held together by hydrogen bonds that involve chloride anions located along the peripheries of the assemblies.

   Whereas the synthesis of functional heteromeric assemblies based on resorcin[4]arenes have been achieved using solvent molecules as bridges, reports by Kobayashi et al. and MacGillivray et al. have demonstrated the construction of similar heteromeric assemblies that involve synthetic building units (Fig. 33)[60,61]. In particular, Kobayashi et al. have revealed the ability of a cavitand tetracarboxylic acid to assemble with four molecules of 2-aminopyrimidine to give a six-component crystalline capsule held together by 16 hydrogen bonds.[60] The cavitands defined the upper and lower hemispheres of the assembly while the pyrimidines formed the bridges (Fig. 33a). MacGillivray et al. have also demonstrated the ability of two molecules of a tetramethylresorcin[4]arene to assemble with four molecules of 4,4′-bipyridine to form a six-component capsule (Fig. 33b).[61] The capsule was held together by eight intermolecular, as well as eight intramolecular, hydrogen bonds. The structures of both capsules conformed to a tetragonal prism and accommodated two nitrobenzene molecules as guests. Similar prismatic assemblies of Coppens[62]

(a)

(b)
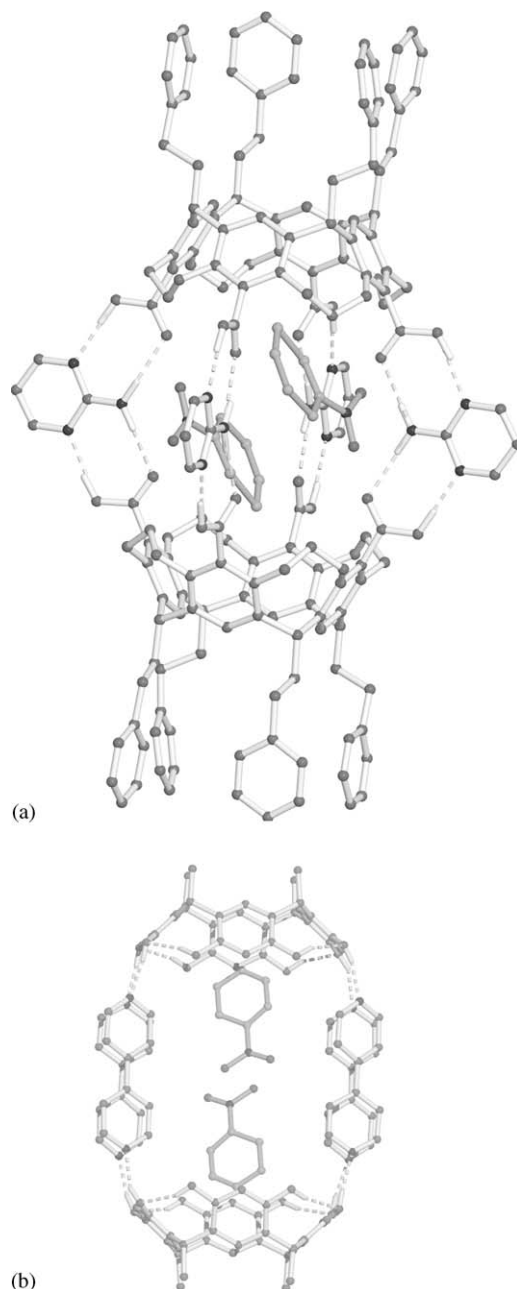
Fig. 33 Two heteromeric resorcin[4]arene-based assemblies: (a) capsule involving two ca-
vitand tetracarboxylic acids and four 2-aminopyrimidines and (b) capsule involving two
molecules of tetramethylresorcin[4]arene and four 4,4-bipyridine molecules. Guest nitroben-
zenes are shown in dark gray.
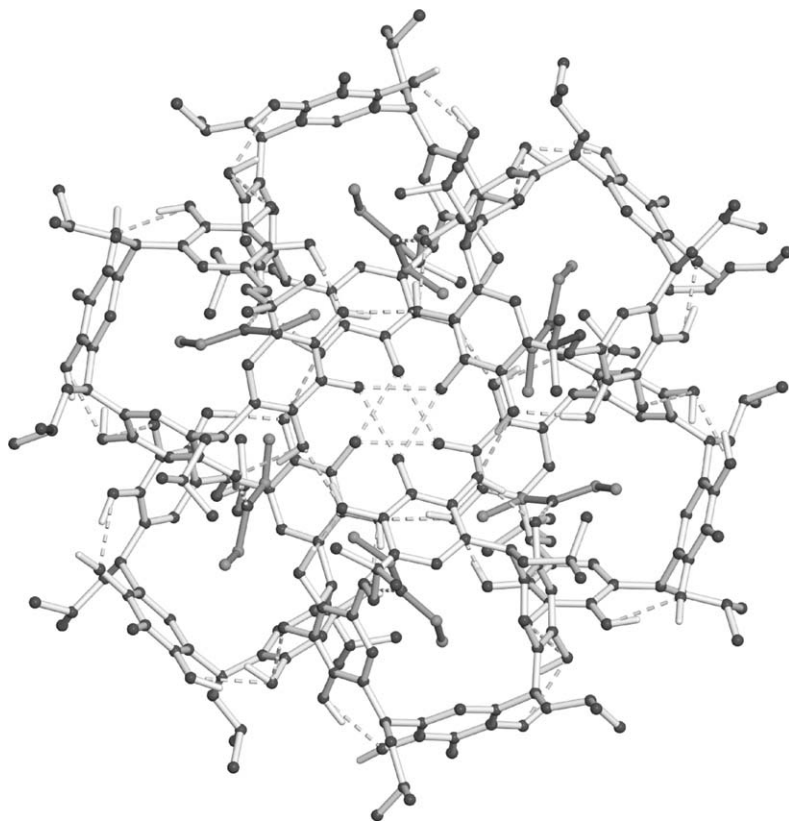
Fig. 34 Solid-state structure of the mixed-macrocycle hexameric capsule. Diethyl ether guests are shown in dark gray.

and Raston[63] have been shown to accommodate benzophenone and multiple toluene molecules, respectively.

A crystalline molecular capsule with a structure that conforms to a trigonal antiprism has been reported by Atwood et al.[64] In particular, a mixed macrocycle based on one resorcinol (res) and three pyrogallol units formed a hexamer sustained by 24 intermolecular and 18 intramolecular hydrogen bonds (Fig. 34). An additional 18 hydrogen-bond donor groups interacted with guests located inside and outside the capsule. The assembly possessed an interior volume of approximately $860\,\text{Å}^3$. The assembly crystallized reproducibly from a mixture of six macrocycles and three non-cyclized pyrogallol, and/or res molecules illustrating remarkable recognition properties of the mixed macrocycle.

A tetrameric capsule of ideal D_2 symmetry has been reported by Rebek.[65] In particular, a molecule with glycoluril and sulfamide functionality self-assembled in the solid state via 24 hydrogen bonds to form a finite assembly that accommodated 2,6-adamantanedione as a guest. The volume of the cavity of the capsule was determined to be approximately $184\,\text{Å}^3$ (Fig. 35). Each carbonyl oxygen atom of the
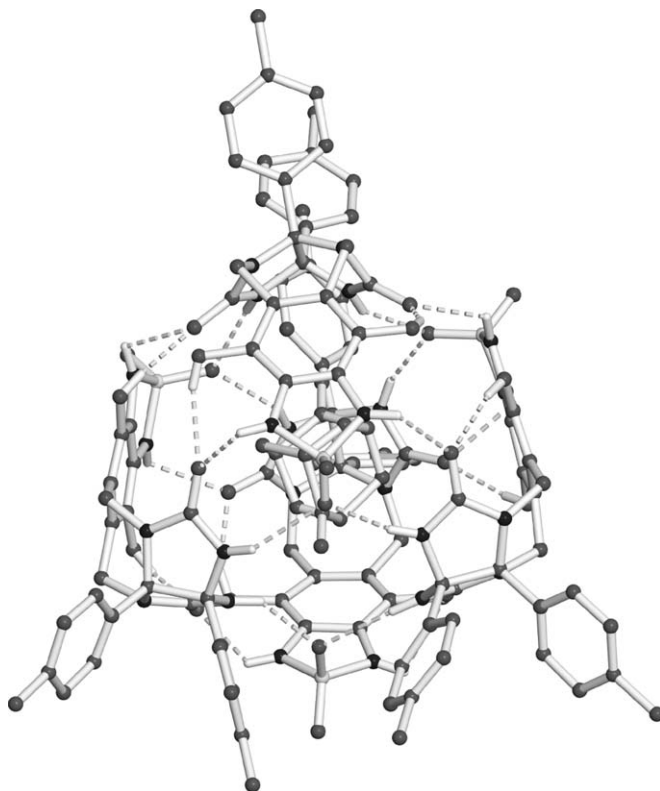
Fig. 35 Rebek tetrameric crystalline capsule of D2 symmetry.

guest participated in two hydrogen bonds with two donor N–H groups of the host.
The capsule did not form in the absence of a suitable guest.

A four-component capsule with a structure that conforms to a tetrahedron has
been recently described by Venkataraman[66] Specifically, triphenylamine *ortho*-
tricarboxylic acid self-assembled via 12 O–H···O hydrogen bonds to form a mo-
lecular tetrahedron (Fig. 36). The hydroxyl groups of the polyhedron participated in
hydrogen bonds with single ethanol molecules embedded within each triangular face
of each tetrahedron. The assembly crystallized in the rare cubic crystal system. The
ability of the acid to form a tetrahedron was reminiscent of the ability of triphenyl-
methanol to form a tetrahedron, which also forms inclusion compounds with solvent
guests that occupy voids between the polyhedra.[32]

MacGillivray and Atwood have demonstrated the ability of six resocin[4]arenes to
self-assemble to give a very large molecular capsule of octahedral symmetry.[67] Spe-
cifically, six molecules of tetramethylresorcin[4]arene assembled with eight water
molecules via 60 hydrogen bonds to form a capsule, approximately 2.5 nm in dia-
meter, that accommodated multiple solvent molecules as guests. The assembly was
chiral, possessing a structure that conformed to an Archimedean solid known as a
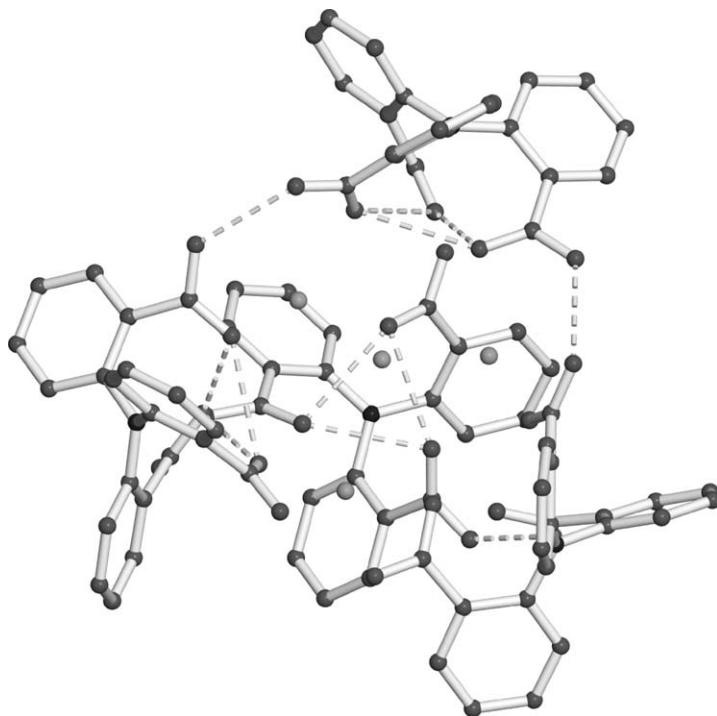
Fig. 36 Structure of the tetrahedral capsule based on triphenylamine *ortho*-tricarboxylic acid. Oxygen atoms of ethanol molecules embedded in each face of the tetrahedron are shown in medium gray.

snub cube. The internal volume of the assembly was determined to be approximately 1375 Å^3 (Fig. 37). A similar spherical assembly was also isolated and characterized by Mattay[68] In particular, tetraisobutylpyrogallo[4]arene was revealed to form a hexameric assembly held together by 48 hydrogen bonds. Ten acetonitrile molecules occupied the interior of the capsule.

5 Our approach: template-controlled solid-state reactivity

The molecular assemblies described above have inspired us, in recent years, to develop finite assemblies in the solid state that exhibit chemical reactivity. Specifically, we,[69] and others,[70] have been utilizing principles of molecular recognition and self-assembly to develop a method to direct the formation of covalent bonds in organic solids. The method builds on the work of Schmidt on the reactivity of cinnamic acids in the organic solid state.[45] Specifically, Schmidt has described topochemical postulates that dictate geometry criteria for a [2+2] photodimerization to occur in a solid. The postulates state that two carbon–carbon double (C═C) bonds should be aligned in parallel and separated by a distance <4.2 Å to react.
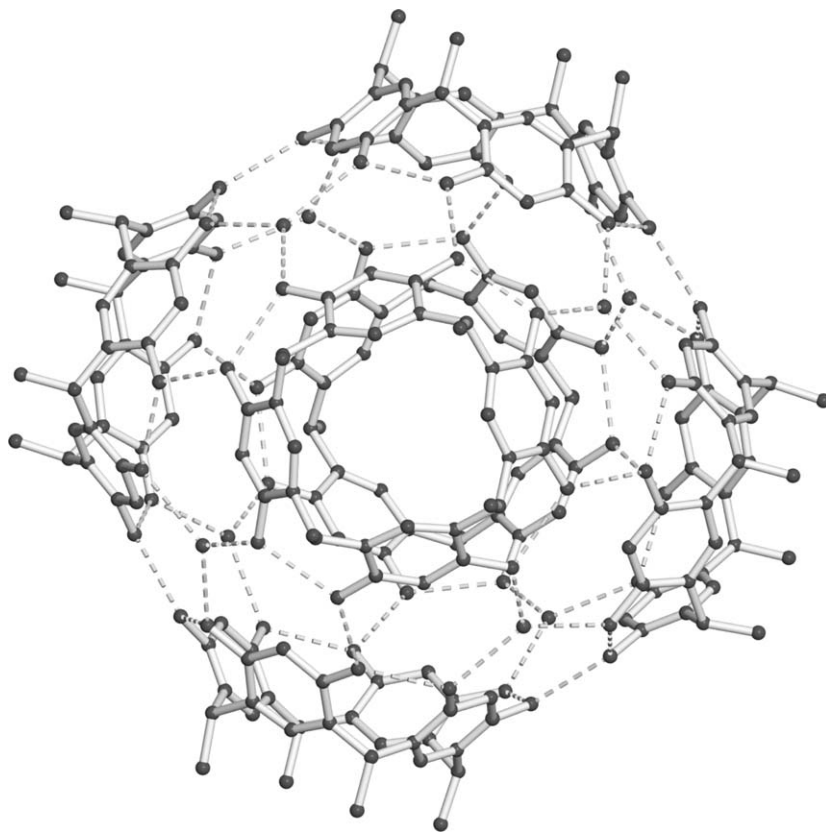
Fig. 37 Structure of the resorcin[4]arene sphere formed from six molecules of tetra-methylresorcin[4]arene and eight water molecules.

LINEAR TEMPLATES

In particular, we have been using rigid U-shaped molecules, in the form of linear templates, to assemble suitably functionalized olefins, via hydrogen bonds, within finite molecular assemblies for reaction (Scheme 4).[69] We reasoned that by directing reactivity within a finite assembly, we could establish control of reactivity that is largely independent of crystal packing. Moreover, we anticipated that such a template method could make directing reactivity in the solid state reliable such that the method could be used to construct molecules of varying size, shape, and functionality.

By following such reasoning, we have shown that molecules based on res[69g] and 1,8-nap[69f] can be used as linear templates to direct the [2 + 2] photodimerization in the solid state. Thus, co-crystallization of either res or 1,8-nap with *trans*-1,2-bis(4-pyridyl)ethylene (4,4′-bpe) produced solids, of composition 2(res) · 2(4,4′-bpe)[70] and
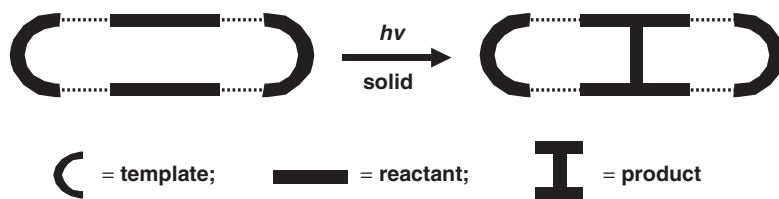
Scheme 4.
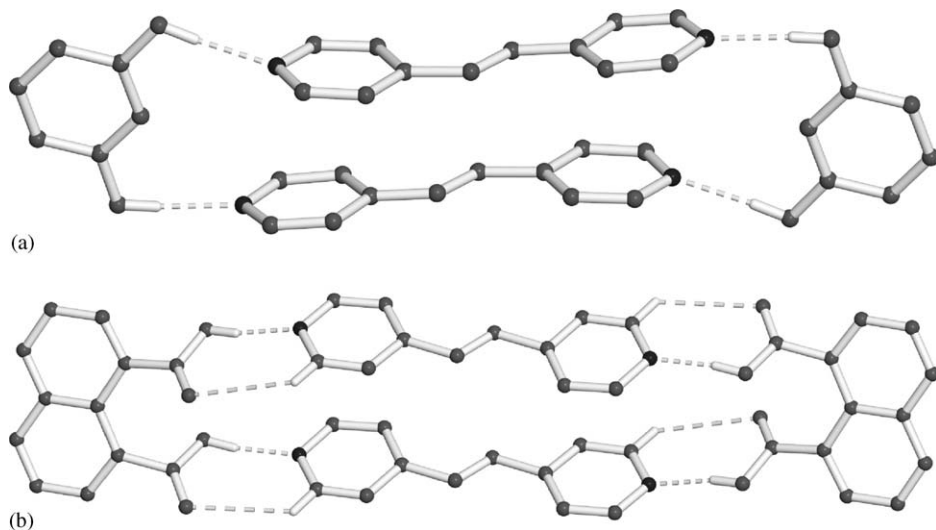
Fig. 38 Solid-state structures of four-component assemblies of 2(template)·2(4,4′-bpe): (a) res as template and (b) 1,8-nap as template.

2(1,8-nap)·2(4,4′-bpe), respectively, that consisted of finite four-component assemblies held together via four O–H···N hydrogen bonds (Fig. 38). Each molecule organized the C=C bonds of 4,4′-bpe in a parallel arrangement and at a distance <4.2 Å, geometries that satisfied the requirements of Schmidt for reaction.[45] Moreover, UV-irradiation of each solid produced the corresponding cyclobutane, *rctt*-tetrakis(4-pyridyl)cyclobutane (4,4′-tpcb), with a stereochemistry consistent with the stereochemistry of the reactants within each assembly. The photoproduct, in each case, formed in 100% yield and gram quantities.

By exploiting the modularity of the template method, we have shown that linear templates can be used to organize unsymmetrical reactants to achieve regiospecific control of reactivity. Specifically, co-crystallization of 4-chlororesorcinol (4-Cl-res) with 2,4′-bpe produced an unsymmetrical assembly, 2(4-Cl-res) 2(2,4′-bpe), with two molecules of 2,4′-bpe oriented in a head-to-head geometry.[71] UV-irradiation of the solid produced the head-to-head photoproduct 2,4′-tpcb in 100% yield. Similarly, co-crystallization of 1,8-nap with 3,4′-bpe produced the unsymmetrical assembly, 2(1,8-nap) 2(3,4′-bpe), with two molecules of 3,4′-bpe oriented in a head-to-head

geometry. The olefins also reacted to form the corresponding head-to-head pho-
toproduct in 100% yield.[69d]

TARGET-ORIENTED SYNTHESES

That the linear templates assembled along the periphery of each finite assembly
involving 4,4′-, 2,4′-, and 3,4′-bpe also suggested to us that the template molecules
may adapt to additional changes to the reactants (e.g. size). Moreover, an ability of
the templates to adapt to a variety of structural changes could, in principle, be
exploited as a means to construct targeted molecules.[72] Thus, to construct various
molecules using linear templates in the solid state, our efforts have focused on
molecular targets with structural elements that code for the [2 + 2] photodimerizat-
ion. In particular, we have identified a [2.2]-paracyclophane and [n]-ladderanes as
targets.

To construct a paracyclophane and ladderanes, we identified precursors to a
[2.2]paracyclophane[69b] and a [3]- and [5]-ladderane[69a] from retrosynthetic analyses
of the corresponding cyclobutanes. Specifically, the diolefin 1,4-bis[2-(4-pyridyl)et-
henyl]benzene (1,4-bpeb) was selected as the precursor to an assembly that
reacts to give the [2.2]-paracyclophane tetrakis(4-pyridyl)-1,2,9,10-diethano[2.2]-
paracyclophane (4,4′-tppcp) while the polyenes *trans,trans*-1,4-bis(4-pyridyl)-1,3-
butadiene (1,4-bpbd) and *trans,trans,trans*-1,6-bis(4-pyridyl)-1,3,5-hexatriene
(1,6-bpht) were selected as precursors that react to give the [3]- and [5]-ladderanes
all-*trans*-tetrakis(4-pyridyl)-[3]-ladderane (4-tp-3-lad) and all-*trans*-tetrakis(4-pyri-
dyl)-[5]-ladderane (4-tp-5-lad), respectively (Scheme 5). Notably, each target
molecule would be longer than 4,4′-, 2,4′-, and 3,4′-, which could allow us to test
the tolerance of the assembly process to lengthening of the reactants.

That a res derivative could be used to organize 1,4-bpeb for [2 + 2] photo-
dimerization to give 4,4′-tppcp was realized by a single-crystal X-ray structure
analysis of a co-crystal involving 4-benzylresorcinol (4-bn-res) as the template in 2(4-
bn-res)·2(1,4-bpeb) (Fig. 39). In this assembly, both C=C bonds of the diolefin
were organized parallel and separated by 3.77 and 3.91 Å (Fig. 39a). Moreover, UV-
irradiation of the solid produced the targeted photoproduct 4,4′-tppcp, regio-
specifically in gram quantities and 100% yield. The structure of the cyclophane was
identified via single-crystal X-ray structure analysis and ^{1}H NMR spectroscopy
(Fig. 39b). Similarly, single-crystal X-ray structure analyses of two solids involving
5-methoxy-resorcinol (5-OMe-res) as the template in 2(5-OMe-res)·2(1,4-bpbd) and
2(5-OMe-res)·2(1,6-bpht) revealed the ability of the res to organize the two polyenes
for reaction (Fig. 39c). The C=C bonds of each solid were parallel with C=C
separations ranging from 3.78 to 3.82 Å [2(5-OMe-res)·2(1,4-bpbd)] and 3.69 to
3.97 Å [2(5-OMe-res)·2(1,6-bpht)], respectively. UV-irradiation of each solid pro-
duced the targeted [3]- and [5]-ladderanes in gram quantities and 100% yield. The
structures of the targets were also confirmed via single-crystal X-ray diffraction and
^{1}H NMR spectroscopy (Fig. 39d).[69a,b] Whereas the synthesis of 4-tp-3-lad was the

4,4'-tppcp

4-tp-4-lad

4-tp-5-lad

1,4-bpeb

1,4-bpbd
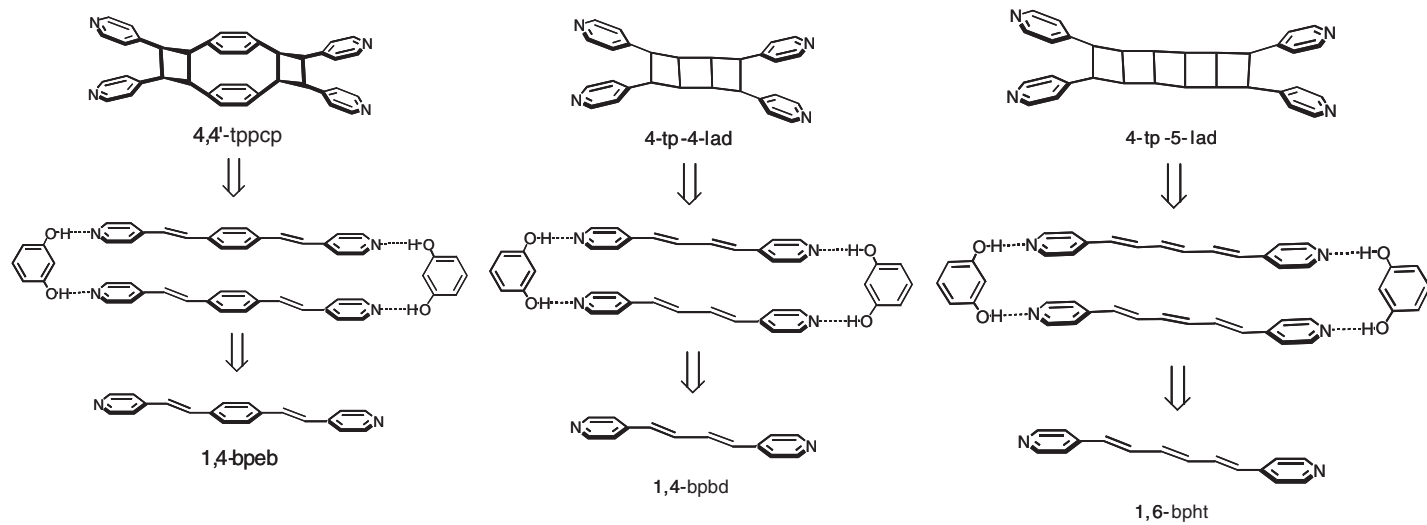
1,6-bpht

Scheme 5.
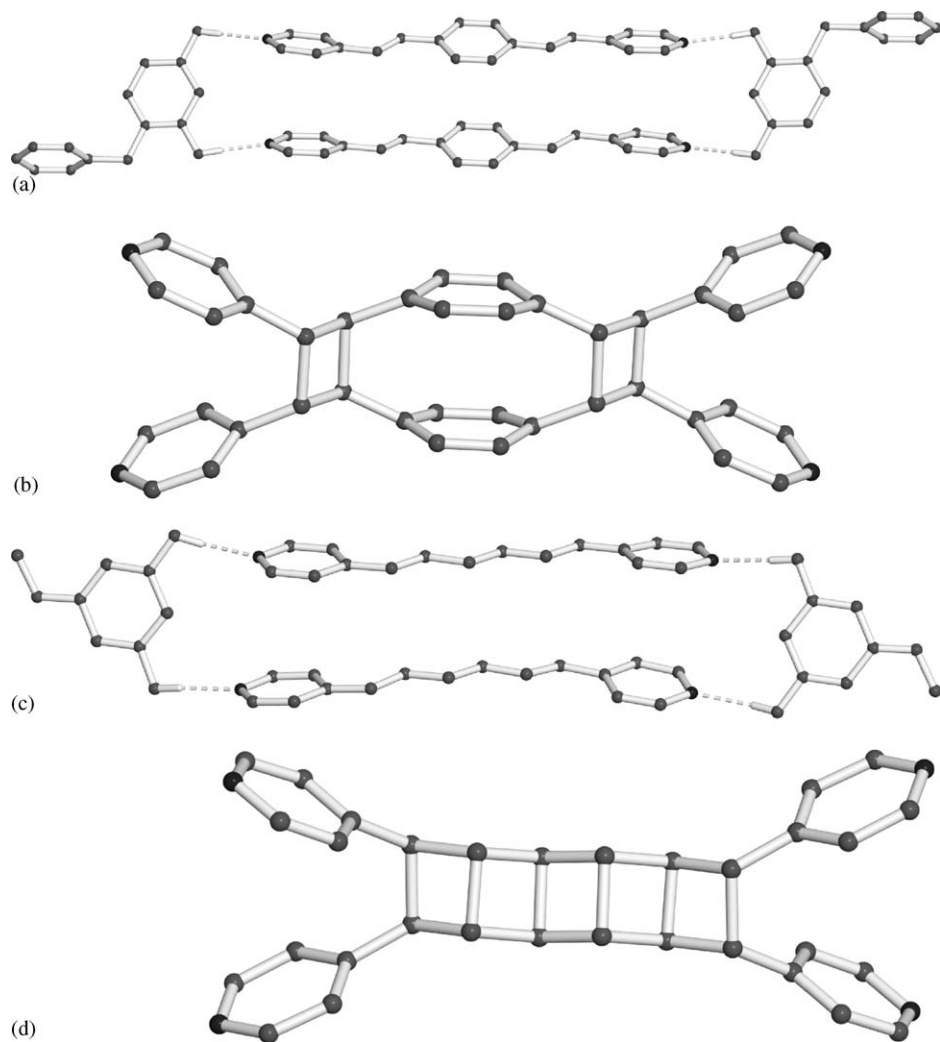
Fig. 39 Template-controlled solid-state reactivity, X-ray crystal structures of: (a) four-component assembly 2(4-bn-res)·2(1,4-bpeb); (b) targeted cyclophane; (c) four-component assembly 2(5-OMe-res)·2(1,6-bpht); and (d) targeted [5]-ladderane.

first example of a quantitative construction of a [3]-ladderane in the solid state, the synthesis of 4-tp-5-lad was the sole quantitative synthesis of a [5]-ladderane.

6 Summary and outlook

In this chapter, we have described the design and construction of finite molecular assemblies in the organic solid state. Whereas principles of crystal engineering have

largely focused on networks to control properties of organic solids,[1] we have revealed how finite assemblies can play a similar role. In particular, we have shown that, in contrast to a network,[2] a finite assembly of molecules provides a means to control properties of organic solids largely independent of long-range packing. We have demonstrated that those finite assemblies described to date can be classified as being constructed for either purely synthetic reasons or to develop functionality within solids. The assemblies have been based on structures of 1D, 2D, and 3D connectivity and have been shown to be held together, primarily, by hydrogen bonds.[3]

Although a variety of finite solid-state molecular assemblies have been reported, it is clear that much remains to be accomplished. Moreover, although methods of supramolecular synthesis have developed such that it is possible to construct a finite structure with a reasonable degree of accuracy,[2] it still remains unclear how changes to the structures of finite assemblies in the solid state may influence and fine-tune properties of organic solids. Indeed, it seems that an increasing ability of chemists to achieve control of self-assembly processes in the solid state may enable chemists to construct assemblies of technological importance (e.g. switches, devices, machines), particularly where effects of dynamics encountered in less-organized media, such as the liquid phase, can be avoided.[73]

Acknowledgment

References

1. Desiraju, G.R. (1989). *Crystal Engineering: The Design of Organic Solids*. Elsevier, Amsterdam
2. Desiraju, G.R. (1995). *Angew. Chem., Int. Ed. Engl.* **34**, 2311–2327
3. (a) Lawrence, D.S., Jiang, T. and Levett, M. (1995). *Chem. Rev.* **95**, 2229–2260; (b) Whitesides, G.M., Simanek, E.E., Mathias, J.P., Seto, C.T., Chin, D., Mammen, M. and Gordon, D.M. (1995). *Acc. Chem. Res.* **28**, 37–44; (c) Krische, M.J. and Lehn, J.-M. (2000). *Struct. Bond.* **96**, 1–30; (d) Zimmerman, S.C. and Corbin, P.S. (2000). *Struct. Bond.* **96**, 63–94
4. MacGillivray, L.R. and Atwood, J.L. (1999). *Angew. Chem., Int. Ed.* **38**, 1018–1033
5. Leiserowitz, L. (1976). *Acta Crystallogr. Sect. B* **32**, 775–802
6. Allen, F.H., Motherwell, W.D.S., Raithby, P.R., Shields, G.P. and Taylor, R. (1999). *New J. Chem.*, 25–34
7. Evans, S.V. and Trotter, J. (1988). *Acta Crystallogr. Sect. B* **44**, 533–538
8. Fitzgerald, L.J., Gallucci, J.C. and Gerkin, R.E. (1991). *Acta Crystallogr. Sect. B* **47**, 776–782
9. MacGillivray, L.R. and Siebke, M.M. (2001). *J. Chem. Crystallogr.* **31**, 373–376
10. Ducharme, Y. and Wuest, J.D. (1988). *J. Org. Chem.* **53**, 5787–5789
11. Gao, X., Friščić, T., Papaefstathiou, G.S. and MacGillivray, L.R. (2004). *J. Chem. Crystallogr.* **34**, 371–374

12. Walsh, P.W., Maverick, E., Chiefari, J. and Lightner, D.A. (1997). *J. Am. Chem. Soc.* **119**, 3802–3806

13. Alajarin, M., López-Lázaro, A., Pastor, A., Prince, P.D., Steed, J.W. and Arakawa, R. (2001). *Chem. Commun.*, 169–170

14. Beijer, F.H., Kooijman, H., Spek, A.L., Sijbesma, R.P. and Meijer, E.W. (1998). *Angew. Chem., Int. Ed. Engl.* **37**, 75–78

15. Beijer, F.H., Sijbesma, R.P., Kooijman, H., Spek, A.L. and Meijer, E.W. (1998). *J. Am. Chem. Soc.* **120**, 6761–6769

16. (a) Jorgensen, W.L. and Pranata, J. (1990). *J. Am. Chem. Soc.* **112**, 2008; (b) Pranata, J., Wierschke, S.G. and Jorgensen, W.L. (1991). *J. Am. Chem. Soc.* **113**, 2810

17. Folmer, B.J.B., Sijbesma, R.P., Kooijman, H., Spek, A.L. and Meijer, E.W. (1999). *J. Am. Chem. Soc.* **121**, 9001–9007

18. Gong, B., Yan, Y., Zeng, H., Skrzypczak-Jankunn, E., Kim, Y.W., Zhu, J. and Ickes, H. (1999). *J. Am. Chem. Soc.* **121**, 5607–5608

19. Davis, A.P., Draper, S.M., Dunne, G. and Ashton, P. (1999). *Chem. Commun.*, 2265–2266

20. Etter, M.C. and Reutzel, S.M. (1991). *J. Am. Chem. Soc.* **113**, 2586–2598

21. Aakeröy, C.B., Beatty, A.M. and Helfrich, B.A. (2001). *Angew. Chem., Int. Ed. Engl.* **40**, 3240–3242

22. Etter, M.C. (1990). *Acc. Chem. Res.* **23**, 120–126

23. Aakeröy, C.B., Beatty, A.M. and Helfrich, B.A. (2002). *J. Am. Chem. Soc.* **124**, 14425–14432

24. Mathias, J.P., Simanek, E.E., Zerkowski, J.A., Seto, C.T. and Whitesides, G.M. (1994). *J. Am. Chem. Soc.* **116**, 4316–4325

25. Yang, J., Fan, E., Geib, S.J. and Hamilton, A.D. (1993). *J. Am. Chem. Soc.* **115**, 5314–5315

26. Yang, J., Marendaz, J.-L., Geib, S.J. and Hamilton, A.D. (1994). *Tetrahedron Lett.* **35**, 3665–3668

27. Duchamp, D.J. and Marsh, R.E. (1969). *Acta Crystallogr.* **B25**, 5–19

28. Alcala, R. and Martinez-Carrera, S. (1972). *Acta Crystallogr.* **B28**, 1671–1677

29. Smith, G., Wermuth, U.D. and White, J.M. (2003). *Cryst. Eng. Comm.* **5**, 58–61

30 Kraft, A. and Fröhlich, R. (1998). *Chem. Commun.*, 1085–1086

31. Biradha, K. and Zaworotko, M.J. (1998). *J. Am. Chem. Soc.* **120**, 6431–6432

32. Ferguson, G., Gallagher, J.F., Glidewell, C., Low, J.N. and Scrimgeour, S.N. (1992). *Acta Crystallogr. Sect. C* **48**, 1272–1275

33. Jetti, R.K.R., Kuduva, S.S., Reddy, D.S., Xue, F., Mak, T.C.W., Nangia, A. and Desiraju, G.R. (1998). *Tetrahedron Lett.* **39**, 913–916

34. (a) Valdés, C., Spitz, U.P., Toledo, L.M., Kubik, S.W. and Rebek Jr., J. (1995). *J. Am. Chem. Soc.* **117**, 12733–12745; (b) Valdés, C., Toledo, L.M., Spitz, U. and Rebek Jr., J. (1996). *Chem. Eur. J.* **2**, 989–991.

35 Mogck, O., Paulus, E.F., Böhmer, V., Thondorf, I. and Vogt, W. (1996). *Chem. Commun.*, 2533–2534

36. (a) Haino, T., Yanase, M. and Fukuzawa, Y. (1997). *Angew. Chem., Int. Ed. Engl.* **36**, 259–260; (b) Haino, T., Yanase, M. and Fukuzawa, Y. (1997). *Tetrahedron Lett.* **38**, 3739–3742

37 Makha, M., Hardie, M.J. and Raston, C.L. (2002). *Chem. Commun.*, 1446–1447

38. Atwood, J.L., Barbour, L.J., Nichols, P.J., Raston, C.L. and Sandoval, C.A. (1999). *Chem. Eur. J.* **5**, 990–996

39. Chapman, R.G., Olovsson, G., Trotter, J. and Sherman, J.C. (1998). *J. Am. Chem. Soc.* **120**, 6252–6260

40. Shivanyuk, A., Paulus, E.F. and Böhmer, V. (1999). *Angew. Chem., Int. Ed. Engl.* **38**, 2906–2909

41. Alajarin, M., Pastor, A., Orenes, R.-Á. and Steed, J.W. (2002). *J. Org. Chem.* **67**, 7091–7095

42. Ghadiri, M.R., Kobayashi, K., Granja, J.R., Chadha, R.K. and McRee, D.E. (1995). *Angew. Chem., Int. Ed. Engl.* **34**, 93–95

43. Fleischman, S.G., Kuduva, S.S., McMahon, J.A., Moulton, B., Bailey Walsh, R.D., Rodriguez-Hornedo, N. and Zaworotko, M.J. (2003). *Cryst. Growth Des.* **3**, 909–919

44. Feldman, K.S. and Campbell, R.F. (1995). *J. Org. Chem.* **60**, 1924–1925

45. Schmidt, G.M.J. (1971). *Pure Appl. Chem.* **27**, 647–678

46. Boiadjiev, S.E., Anstine, D.T., Maverick, E. and Lightner, D.A. (1995). *Tetrahedron: Asymmetr.* **6**, 2253–2270

47. Etter, M.C., Urbańczyk-Lipkowska, Z., Jahn, D.A. and Frye, J.S. (1986). *J. Am. Chem. Soc.* **108**, 5871–5876

48. Mascal, M., Hext, N.M., Warmuth, R., Moore, M.H. and Turkenburg, J.P. (1996). *Angew. Chem., Int. Ed. Engl.* **35**, 2203–2206

49. Grossman, R.B., Hattori, K., Parkin, S., Partick, B.O. and Varner, M.A. (2002). *J. Am. Chem. Soc.* **124**, 13686–13687

50. Weber, E., Dörpinghaus, N. and Csöregh, I. (1990). *J. Chem. Soc. Perkin Trans.* **2**, 2167–2177

51. Biradha, K. and Mahata, G. (2005). *Cryst. Growth Des.* **5**, 61–63

52. Atwood, J.L., Barbour, L.J. and Jerga, A. (2002). *Science* **296**, 2367–2369

53. Timmerman, P.T., Vreekamp, R.H., Hulst, R., Verboom, W., Reinhoudt, D.N., Rissanen, K., Udachin, K.A. and Ripmeester, J. (1997). *Chem. Eur. J.* **3**, 1823–1832

54 Rose, K.N., Barbour, L.J., Orr, G.W. and Atwood, J.L. (1998). *Chem. Commun.*, 407–408

55 Murayama, K. and Aoki, K. (1998). *Chem. Commun.*, 607–608

56. Aoki, K., Nagae, T., Matsubara, R. and Fujisawa, I. (2004). *Chem. Lett.* **33**, 1264–1265

57 Shivanyuk, A., Rissanen, K. and Kolehmainen, E. (2000). *Chem. Commun.*, 1107–1108

58 Shivanyuk, A., Friese, J.C., Döring, S. and Rebek, J.Jr. (2003). *J. Org. Chem.* **68**, 6489–6496

59. Shivanyuk, A., Paulus, E.F., Rissanen, K., Kolehmainen, E. and Böhmer, V. (2001). *Chem. Eur. J.* **7**, 1944–1951

60. Kobayashi, K., Shirasaka, T., Yamaguchi, K., Sakamoto, S., Horn, E. and Furukawa, N. (2000). *Chem. Commun.*, 41–42

61. MacGillivray, L.R., Diamante, P.R., Reid, J.L. and Ripmeester, J.A. (2000). *Chem. Commun.*, 359–360

62. Ma, B.-Q., Zhang, Y. and Coppens, P. (2001). *Cryst. Growth Des.* **1**, 271–275

63. Cave, G.W.V., Hardie, M.J., Roberts, B.A. and Raston, C.L. (2001). *Eur. J. Org. Chem.*, 3227–3231

64. Atwood, J.L., Barbour, L.J. and Jerga, A. (2002). *Proc. Nat. Acad. Sci. USA* **99**, 4837–4841

[65] Johnson, D.W., Hof, F., Iovine, P.M., Nuckolls, C. and Rebek, J.Jr. (2002). *Angew. Chem., Int. Ed. Engl.* **41**, 3793–3796

66. Field, J.E., Combariza, M.Y., Vachet, R.W. and Venkataraman, D. (2002). *Chem. Commun.*, 2260–2261

67. MacGillivray, L.R. and Atwood, J.L. (1997). *Nature* **389**, 469–472

68. Gerkensmeier, T., Iwanek, W., Agena, C., Frölich, R., Kotila, S., Näther, C. and Mattay, J. (1999). *Eur. J. Org. Chem.* 2257–2262

69. (a) Gao, X., Friščić, T. and MacGillivray, L.R. (2004). *Angew. Chem., Int. Ed.* **43**, 232–235; (b) Friščić, T. and MacGillivray, L.R. (2003). *Chem. Commun.* 1306–1307; (c) MacGillivray, L.R. (2002). *Cryst. Eng. Commun.* **4**, 37–42; (d) Varshney, D.B., Papaefstathiou, G.S. and MacGillivray, L.R. *Chem. Commun.* 1964–1965; (e) MacGillivray, L.R., Reid, J.L., Ripmeester, J.A. and Papaefstathiou, G.S. (2002). *Indust. Eng. Chem. Res.* **41**, 4494–4497; (f) Papaefstathiou, G.S., Kipp, A.J. and MacGillivray, L.R. (2001). *Chem. Commun.* 2432–2433; (g) MacGillivray, L.R., Reid, J.L. and Ripmeester, J.A. (2000). *J. Am. Chem. Soc.* **122**, 7817–7818

70. (a) Ito, Y., Borecka, B., Trotter, J. and Scheffer, J.R. (1995). *Tetrahedron Lett.* **36**, 6083–6086; (b) Amirakis, D.G., Garcia-Garibay, M.A., Rowan, S.J., Stoddart, J.F., White, A.J.P. and Williams, D.J. (2001). *Angew. Chem., Int. Ed.* **40**, 4256–4261; (c) Phba, S., Hosomi, H. and Ito, Y. (2001). *J. Am. Chem. Soc.* **123**, 6349–6352; (d) Shan, N. and Jones, W. (2003). *Tetrahedron Lett.* **44**, 3687–3689; (e) Caronna, T., Liantonio, R., Logothetis, T.A., Metrangolo, P., Pilati, T. and Resnati, G. (2004). *J. Am. Chem. Soc.* **126**, 4500–4501
71. Hamilton, T.D., Papaefstathiou, G.S. and MacGillivray, L.R. (2002). *J. Am. Chem. Soc.* **124**, 11606–11607
72. Nicolaou, K.C., Vourloumis, D., Winssinger, N. and Baran, P.S. (2000). *Angew. Chem., Int. Ed. Engl.* **39**, 44
73. Balzani, V., Gómez-López, M. and Stoddart, J.F. (1998). *Acc. Chem. Res.* **31**, 405–414
74. *POV-ray*. Computer program for creating 3D graphics. POV-team[TM], 2002

Mechanisms of hydrolysis and rearrangements of epoxides

DALE L. WHALEN

Department of Chemistry and Biochemistry, University of Maryland, Baltimore County (UMBC), Baltimore, MD, USA

1   Introduction

The epoxide functional group has played very important and versatile roles in organic synthesis, and a number of early review articles on their reactions have been published.[1,2] Numerous natural products contain the epoxide group,[3–7] and the biological activities of certain compounds are linked to the facile reactivity and unique reactions of this group.

A large number of nonpolar, unsaturated compounds are metabolized by pathways that involve epoxidation of the unsaturated substance by the cytochrome P-450 enzymes, followed by epoxide hydrolase-catalyzed hydrolysis or glutathione transferase-catalyzed addition of glutathione to the epoxide.[8,9] The resulting metabolites are then secreted as glucuronide or glutathione derivatives. Although these metabolic pathways serve as a detoxification mechanism for some compounds, the intermediate epoxide metabolites of many unsaturated materials undergo covalent binding with DNA, proteins and other biological macromolecules. The reactions of compounds containing the epoxide functional group with biological molecules having acidic and nucleophilic groups are critical steps in the initiation of biosynthetic pathways that on the one hand may lead to the elimination of exogenous chemicals, but on the other hand may cause mutations that lead to disease and other detrimental physiological effects.[10–18]

An understanding of the mechanisms by which epoxides react with acidic and nucleophilic species is therefore of special importance. The purpose of this chapter is not to provide an extensive survey of the literature of epoxide reactions, but rather to summarize how pH, concentrations of added acidic and nucleophilic reagents, and epoxide structure determine the mechanisms by which epoxides undergo reactions in aqueous solutions. A review of the hydrolysis reactions of simple epoxides is presented, followed by discussions of the effects of charge-stabilizing groups such as vinyl and aryl on the mechanisms of epoxide reactions. Special attention is given to the lifetimes of carbocation intermediates formed from the reactions of epoxides with acidic reagents, and to the roles that carbocation conformation and transition-state effects play in determining the stereochemistry of the products formed from reaction of solvent with these carbocations.

2   Limiting mechanisms of epoxide reactions

The epoxide (oxirane) functional group has special features that allow it to play very important roles in synthesis and as an electrophilic species in biologically reactive intermediates. The epoxide group has an estimated strain energy of $27\,\mathrm{kcal\,mol^{-1}}$,[19] and its reactions with both acidic and nucleophilic reagents result in epoxide ring

opening and the release of strain energy. The strain energy of an epoxide group, however, is very similar to that of an oxetane. Yet epoxides are much more reactive than oxetanes toward acidic and nucleophilic reagents. The greater reactivity of a three-membered ring compared to a four-membered ring has been rationalized in several ways. Houk and co-workers proposed that the transition state for opening of a three-membered ring has aromatic stabilization.[20] Hoz and co-workers attributed the greater reactivity of three-membered rings, including the epoxide group, to "earlier" transition-state structures in which the strain energy is lost faster than in ring-opening reactions of four-membered rings.[21]

In an acidic environment, the epoxide oxygen acts as a base, and several reaction pathways are available that result in cleavage of a C–O bond and release of the strain energy of the epoxide ring. One possible pathway involves protonation of the epoxide oxygen by an acid HA, followed by C–O bond cleavage to yield a reactive carbocation that undergoes subsequent reaction with nucleophilic reagents (Scheme 1). For this to occur, the carbocation must be stabilized sufficiently by adjacent groups to exist as an intermediate. If the adjacent groups do not stabilize a carbocation sufficiently, then alternate pathways in which either a nucleophile
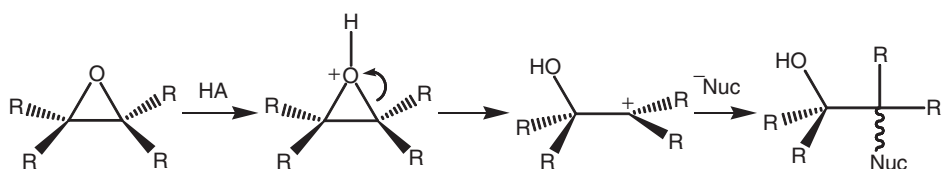
Scheme 1.
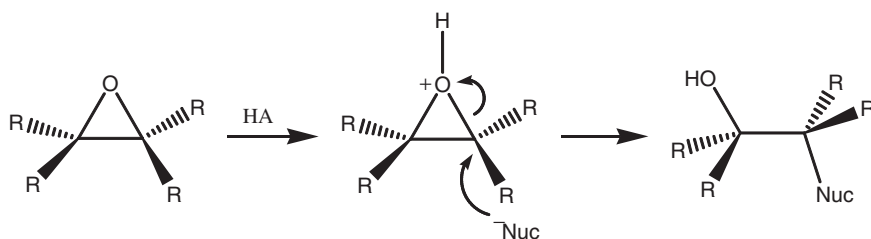
Scheme 2.
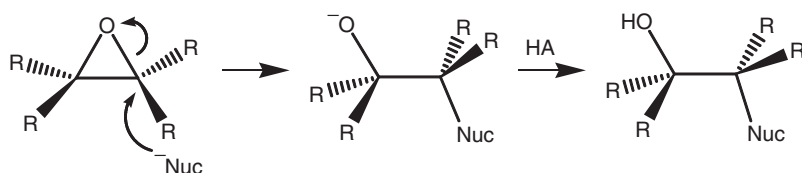
Scheme 3.

attacks a protonated epoxide (Scheme 2) or proton transfer concerted with
nucleophile addition are followed. In basic solution, either nucleophile addition to
the epoxide group precedes addition of a proton by a weakly acidic solvent or other
molecule **HA** (Scheme 3), or nucleophile addition concerted with proton donation
by a weakly acidic group occurs. In an aqueous solution, the actual mechanism of
reaction of a given epoxide will depend on the pH of the solution, the structure of
the epoxide, and the concentrations of any added acidic and nucleophilic reagents.

3   Mechanisms of hydrolysis of epoxides derived from simple alkenes and cycloalkenes

KINETIC STUDIES

Early mechanistic studies by Brønsted et al. of the reactions of ethylene oxide,
glycidol and glycidyl chloride in aqueous $HClO_4$ solutions established that there are
two kinetically distinct hydrolysis reactions.[22] These two reactions for ethylene oxide
are given by Equations (a) and (b) in Scheme 4, and correspond to hydronium
ion-catalyzed hydrolysis and "pH-independent" hydrolysis, respectively. Upon sub-
stitution of HCl for $HClO_4$, two additional kinetically distinct mechanisms are ob-
served and are given by Equations (c) and (d) in Scheme 4.

Kinetic and isotopic labeling studies by Long and Pritchard on the hydrolyses of
ethylene oxide, propylene oxide and isobutylene oxide to their corresponding glycols
provide additional insight on the hydrolysis mechanisms of simple aliphatic epox-
ides.[23] In each case, three kinetically distinct mechanisms for their reactions in water
solutions were observed: acid-catalyzed hydrolysis, pH-independent hydrolysis and
hydroxide-catalyzed hydrolysis. Thus, the rate law for hydrolyses of these simple
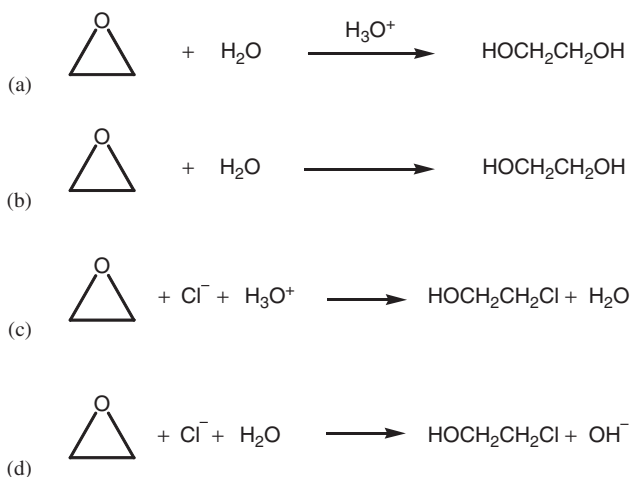
Scheme 4.
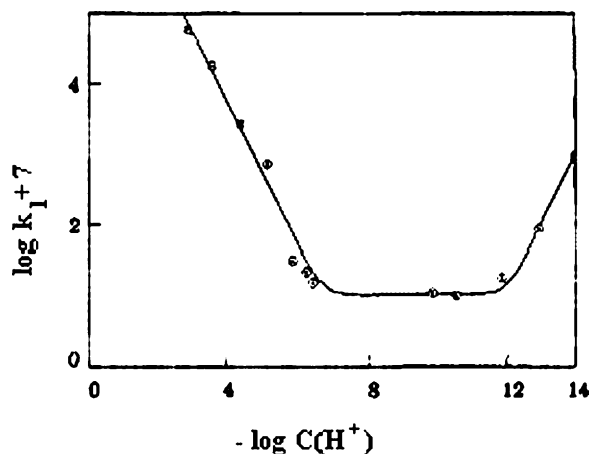
Fig. 1 Observed first-order rate coefficient, k_1 (s^{-1}), for hydrolysis of isobutylene oxide at 25 °C plotted against $-\log C(\text{H}^+)$. Reproduced with permission from Refs 23 and 24. Copyright 1956 American Chemical Society.

aliphatic epoxides is given by Equation (1), where k_{H} is the bimolecular rate constant for the acid-catalyzed hydrolysis, k_{o} is the first-order rate constant for the pH-independent reaction and k_{OH} is the bimolecular rate constant for the hydroxide-catalyzed hydrolysis:

$$k_{\text{obsd}} = k_{\text{H}}[\text{H}^+] + k_{\text{o}} + k_{\text{OH}}[\text{HO}^-] \tag{1}$$

The rate expression given in Equation (1) also applies to the hydrolyses of many other epoxides, and the shape of the pH-rate profile for a given epoxide will reflect the relative magnitudes of k_{H}, k_{o} and k_{OH}. In the hydrolyses of some epoxides, k_{o} is small relative to $k_{\text{H}}[\text{H}^+]$ and $k_{\text{OH}}[\text{HO}^-]$, and cannot be easily detected. In other cases, k_{o} is very large relative to $k_{\text{OH}}[\text{HO}^-]$, and consequently hydroxide ion-catalyzed epoxide hydrolysis may not be detected. The pH-rate profile for hydrolysis of isobutylene oxide is given in Fig. 1. For this compound, acid-catalyzed hydrolysis predominates at pH < ~ 6, the pH-independent reaction predominates at pH~8–11, and hydroxide ion-catalyzed hydrolysis predominates at pH > ~ 12.

ACID-CATALYZED HYDROLYSIS OF ALIPHATIC EPOXIDES

Simple primary and secondary epoxides

Several conclusions are drawn from the product studies of the reactions of propylene oxide and isobutylene oxide in H_2^{18}O.[23] In the acid-catalyzed hydrolysis of propylene oxide, cleavage of the secondary C–O bond is favored by a factor of 2–3 over cleavage of the primary C–O bond. In the acid-catalyzed hydrolysis of isobutylene oxide, cleavage of the tertiary C–O bond is highly favored (>99%). These results show that in acid-catalyzed epoxide hydrolysis, cleavage of the C–O bond leading to

A-1 Mechanism

A-2 Mechanism
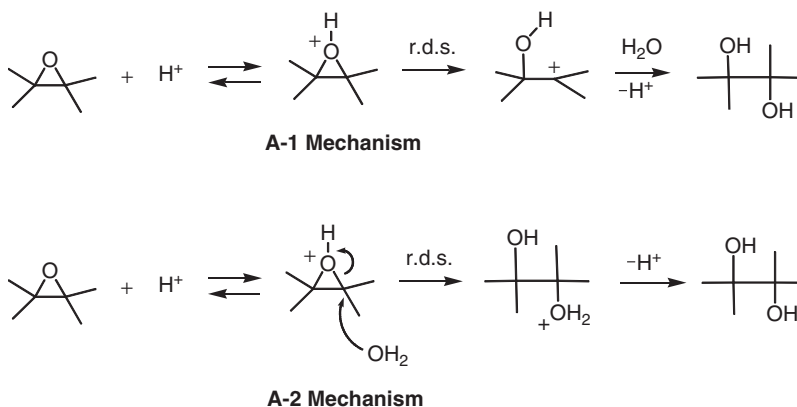
Scheme 5.

the carbon that can better stabilize positive charge is favored. For a number of simple alkyl-substituted epoxides, $\log k_{obsd}$ for acid-catalyzed hydrolysis correlates more closely with H_0, the Zucker–Hammett acidity function, than with $\log[H^+]$.[24] On the basis of the Zucker–Hammett postulate, it was proposed that the activated complex does not contain a water molecule, thus supporting the A-1 mechanism involving a carbocation intermediate for acid-catalyzed hydrolysis of these epoxides, including ethylene oxide (Scheme 5). However, the validity of the Zucker–Hammett hypothesis was later brought into question,[25,26] and an A-2 mechanism in which there is concerted addition of a water molecule to the protonated epoxide was suggested for the acid-catalyzed hydrolysis of epoxides containing only primary and secondary carbons.[27]

Simple tertiary carbocations react with water/trifluoroethanol (H_2O/TFE) solvent with an estimated rate constant of $\sim 10^{12}\,s^{-1}$, which is somewhat faster than bulk solvent reorganizes.[28] Simple primary and simple secondary carbocations are predicted to be even more reactive with nucleophilic solvent than tertiary carbocations. In water solutions, therefore, the rates at which simple primary and secondary carbocations are predicted to react with solvent would exceed the rate of a bond vibration ($\sim 10^{13}\,s^{-1}$), and consequently they would not be sufficiently stable to exist as an intermediate. An A-2 mechanism would therefore be enforced on the acid-catalyzed hydrolysis of those epoxides that potentially undergo ring opening to form primary or secondary carbocations.

Simple tertiary epoxides

The estimated rate at which a simple tertiary carbocation reacts with water solvent ($\sim 10^{12}\,s^{-1}$)[28] is very close to the rate at which solvent reorganizes (10^{11}–$10^{12}\,s^{-1}$).[29] It has been suggested that simple tertiary carbocations that are formed as part of ion pairs or ion-molecule pairs react with a solvent molecule that is already present within the solvent shell that is present at the time of formation of the carbocation.[30]

In the solvolysis of tertiary substrates in which there is a negative or neutral leaving group other than solvent, the leaving group will shield one side of the reaction center, and therefore attack of a solvent molecule leading to inversion of configuration at the reaction center is more likely to occur. In the ionization of RX to form a carbocation R^+ and X^-, the first step is the heterolytic cleavage of the RX bond to form an ion pair (R^+X^-) or ion-molecule pair. For retention of configuration at carbon to be observed, the lifetime of the ion pair or ion-molecule pair would have to be long enough for X^- to be replaced by a water molecule. However, C–O bond cleavage of a protonated epoxide yields a hydroxycarbocation that is completely solvated, without a counter ion or molecule, and if the carbocation has a significant lifetime, then some retention of configuration might be expected.

Several pieces of information suggesting an A-1 mechanism for the acid-catalyzed hydrolysis of isobutylene oxide are (1) isobutylene oxide is several orders of magnitude more reactive than propylene oxide and (2) the entropy of activation for hydrolysis of isobutylene oxide is ~13 units more positive that the entropies of activation for acid-catalyzed hydrolysis of propylene oxide and epichlorihydrin.[31] However, the acid-catalyzed hydrolyses of tertiary epoxide **1**[32] and di-tertiary epoxides **2** and **3**[33] are reported to proceed with complete inversion of configuration at carbon to yield only *trans* diols, which suggest an A-2 mechanism. Since the lifetime of a simple tertiary carbocation is very similar to the time required for solvent reorganization, epoxide ring opening may be nearly complete at the transition state, with little bond formation from the solvent to the carbocation. A mechanism in which proton transfer from hydronium ion to the epoxide oxygen and epoxide O–C bond breaking are more complete than bond formation between solvent and carbon has been referred to as "borderline S_N2."[34] Although complete inversion at carbon in the acid-catalyzed hydrolyses of **1–3** is predicted if there is some bond formation between solvent and carbon at the transition state, complete inversion might also be observed if carbocation formation is complete, and solvent collapses from within a solvent shell before solvent reorganization or conformational change occurs.
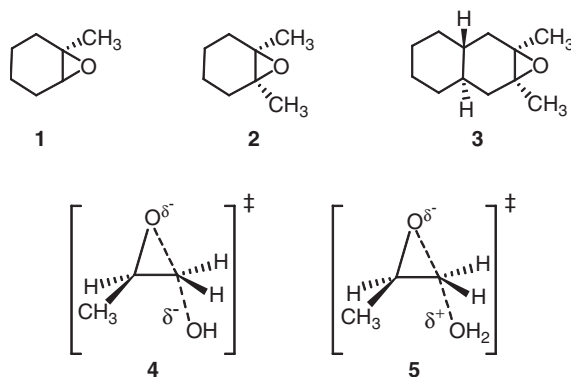
PH-INDEPENDENT AND HYDROXIDE ION-CATALYZED HYDROLYSES OF ALIPHATIC
PRIMARY AND SECONDARY EPOXIDES
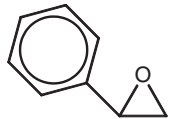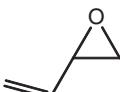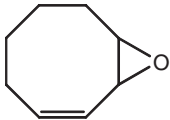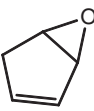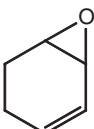
In the second-order reaction of propylene oxide with sodium hydroxide in water
solution, hydroxide ion attack at the primary carbon ($\sim$80%) is favored over attack
at the secondary carbon ($\sim$20%).[23] The ratio of attack by hydroxide ion at the
primary versus secondary carbons in hydroxide-catalyzed epoxide hydrolysis ($\sim$4) is
therefore lower than the ratio of second-order rate constants for displacement
of bromide by labeled bromide ion in the reactions of propyl and isopropyl brom-
ides in aqueous acetone ($\sim$15).[35] In the pH-independent reaction of propylene oxide,
solvent also adds preferentially to the primary carbon, but to a slightly lesser extent
of $\sim$60–70%.[23] The pH-independent reactions and the second-order reactions of
simple primary and secondary epoxides with hydroxide ion, which yield diol prod-
ucts, can be regarded as following very similar mechanistic pathways in which
epoxide C–O bond breaking is concerted with nucleophile O–C bond making.
Transition states for attack of hydroxide ion and for attack of water at the primary
carbon of propylene oxide are given by structures **4** and **5**. The newly developing
oxyanion is presumably stabilized by strong hydrogen bonding with the solvent, or
perhaps proton addition to the oxyanion is concerted with epoxide C–O bond
breaking and nucleophile O–C bond making. Reactions involving nucleophilic at-
tacks of hydroxide ion or water on simple tertiary epoxide carbons have not been
characterized.

4   Acid-catalyzed hydrolyses of alkyl- and vinyl-substituted epoxides

RELATIVE REACTIVITIES

A summary of bimolecular rate constants for the acid-catalyzed hydrolysis of a
series of alkyl-, vinyl- and phenyl-substituted epoxides is given in Table 1. Propylene
oxide (**7**) is 6.6 times more reactive than ethylene oxide, and from a study of its
reaction in H_2O^{18}, it was shown that $\sim$70% of the glycol product results from
addition of solvent to the secondary carbon and $\sim$30% from addition of solvent to
the primary carbon. The reactivity per primary carbon of ethylene oxide is one-
half of the observed reactivity of ethylene oxide, and thus the introduction of a
methyl group on ethylene oxide results in an increase in reactivity at the primary
carbon by a factor of $\sim$4 and an increase in reactivity at the secondary carbon by a
factor of $\sim$9. These results are consistent with A-2 mechanisms for the acid-
catalyzed hydrolyses of ethylene oxide and propylene oxide, in which some amount
of positive charge generated on carbon at the transition state is stabilized by a
methyl group.

Table 1   Bimolecular rate constants for hydronium ion-catalyzed hydrolysis of a series of epoxides in water, $25\,^{\circ}$C

Compound	k_H $(M^{-1}\,s^{-1})$	Compound	k_H $(M^{-1}\,s^{-1})$
6	9×10^{-3a}	**7**	6×10^{-2a}
8	6.8^{a}	**9**	2.7^{b}
10	1.7^{b}	**11**	3.6^{b}
12	3.7×10^{3b}	**13**	1.1×10^{4b}

[a]Taken from Ref. 23.
[b]Taken from Ref. 36.

SIMPLE VINYL EPOXIDES

Acid-catalyzed hydrolysis of isobutylene oxide (**8**) is > 750 times faster than that of ethylene oxide (**6**), and $> 99\%$ of the glycol product is from addition of solvent at the tertiary carbon.[23] These results are consistent with a mechanism in which there is significant positive charge on the tertiary carbon at the transition state, as discussed in the previous section. Butadiene monoepoxide (**10**) is slightly less reactive than isobutylene oxide,[36] and its acid-catalyzed hydrolysis can potentially proceed via a resonance-stabilized allyl cation (Scheme 6). However, the acid-catalyzed hydrolysis of **10** yields 96% of 3-buten-1,2-diol (**15**) and only 4% of 2-butene-1,4-diol (**16**),[36] and the acid-catalyzed methanolysis of **10** is reported to yield only 2-methoxy-3-buten-1-ol.[37] An A-2 mechanism proceeding via transition state **17** may account for the observation that 1,2-diol **15** is the predominant product from acid-catalyzed hydrolysis of **10**. The minor yield of the 1,4-diol **16** may be formed from reaction of
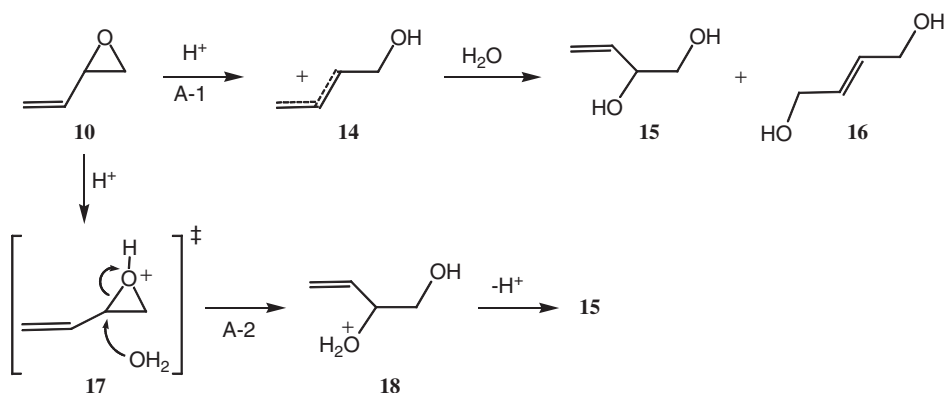
Scheme 6.
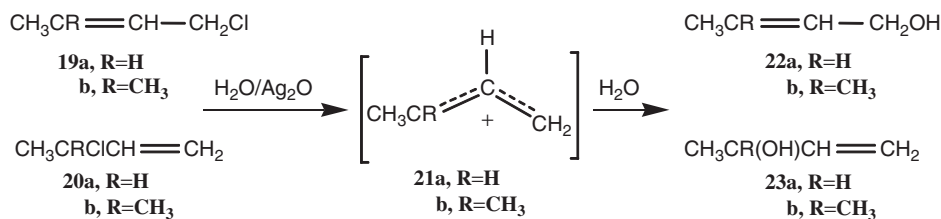
Scheme 7.

allylic carbocation **14** with solvent, although a concerted reaction for formation of this diol from attack of water on **17** is also possible.

It is interesting to compare the hydrolysis of butadiene oxide (**10**) with those of 1-chloro-2-butene and 3-chloro-1-butene.[38] 1-Chloro-2-butene (**19a**) solvolyzes in water to yield 45% of 2-butene-1-ol (**22a**) and 55% of 3-butene-2-ol (**23a**) (Scheme 7). 3-Chloro-1-butene (**20a**) also solvolyzes to yield alcohols **22a** and **23a**, but in a different ratio (34%:66%, respectively). The lifetime of the allylic carbocation intermediate **21a** is therefore not sufficient to allow dissociation of chloride ion and equilibration of solvent about the carbocation. However, hydrolyses of **19b** and **20b** (R = CH$_3$ instead of H) yield identical ratios of allylic alcohol products **22b** and **23b** (15%:85%, respectively).[38] Allylic cation **21b**, with a second methyl group to stabilize positive charge, must have a longer lifetime, which allows departure of the leaving group and equilibration of solvent about the carbocation.

Whereas the hydrolysis of 1-chloro-2-butene gives comparable yields of products from attack of solvent at both primary and secondary carbons, very little product from the acid-catalyzed hydrolysis of butadiene oxide **10** is formed from the attack of solvent at the primary carbon. The transition state for acid-catalyzed epoxide ring opening has a relatively reactant-like geometry, and therefore positive charge delocalization into the adjacent double bond at the transition state is expected to be less than that for allyl chloride hydrolysis.

CYCLIC VINYL EPOXIDES

The mechanisms and rates of acid-catalyzed vinyl epoxide hydrolysis depend markedly on whether the vinyl group is part of a ring system. When the epoxide group and vinyl group are both part of a five- or six-membered ring, the rate of acid-catalyzed hydrolysis (Table 1) is increased dramatically, and both 1,2- and 1,4-diols are formed as products.[36] The bimolecular rate constant k_H for acid-catalyzed hydrolysis of cyclopentadiene oxide (12) and cyclohexadiene oxide (13) are 2.2×10^3 times larger and 6.5×10^3 times larger, respectively, than that for acid-catalyzed hydrolysis of butadiene monoxide (10). Acid-catalyzed hydrolysis of cyclopentadiene oxide (12) yields major amounts of both *cis* and *trans* 1,2- and 1,4-diols (Scheme 8).[36b] The presence of all four diols in the product mixture provides strong evidence that a discrete cyclopentadienyl carbocation 24 is an intermediate, and that the reaction proceeds via an A-1 mechanism.

Cyclohexadiene oxide (13) is even more reactive toward acid-catalyzed hydrolysis than cyclopentadiene oxide (12), and comparable yields of both 3-cyclohexene-*trans*-1,2-diol (30) (60%) and 2-cyclohexene-*trans*-1,4-diol (31) (36%) are formed (Scheme 9), along with minor amounts of *cis* 1,2- and *cis* 1,4-diols (total 4%).[36a,c] As a significant yield of *trans* 1,4-diol 31 is formed, it was suggested that 13 also hydrolyzes via the A-1 mechanism (Scheme 9).[36] The cyclohexenyl carbocation 29 should have a lifetime in water comparable to that of the cyclopentenyl carbocation 24. The greater stabilities of the cyclic allylic carbocations 24 and 29 compared to that of acyclic allylic carbocation 14 are partly due to the stabilizing effect of substitution: both of the terminal carbons in cyclic allylic carbocations 24 and 29 are secondary, whereas one terminal carbon atom in allylic carbocation 14 is primary and one is secondary. The observation that cyclohexadiene oxide yields mostly *trans* 1,2- and *trans* 1,4-diols and very low yields of *cis* 1,2- and *cis* 1,4-diols is attributed to conformational factors[36] that will be discussed separately. Cycloheptadiene oxide
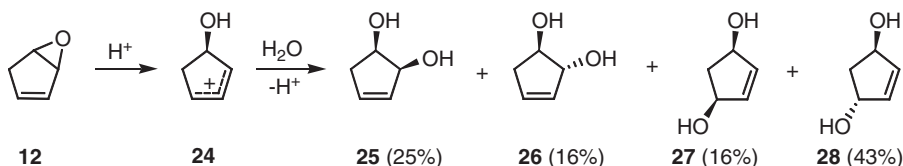
Scheme 8.
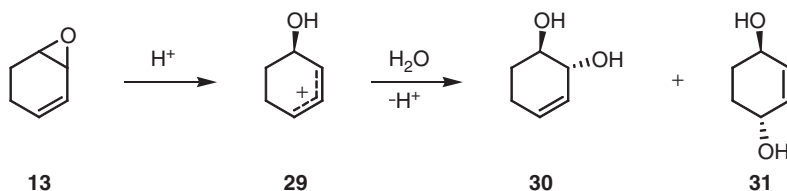
Scheme 9.

and cyclooctadiene oxide (**11**) also undergo acid-catalyzed hydrolysis to give substantial yields of *cis* and *trans* 1,2- and 1,4-diols, suggesting that they, too, react via A-1 mechanisms. The low reactivity of **11** is rationalized by the fact that the allylic C–O bond in each of its two principal conformations is twisted substantially with respect to the p-orbitals of the C–C double bond,[39] and substantial strain is developed in the transition state for the formation of the allylic carbocation in which there is maximum overlap of the newly developing p-orbital with the C–C π-bond.

5   Mechanisms of hydrolysis of styrene oxides

ACID-CATALYZED HYDROLYSIS OF STYRENE OXIDES

Acid-catalyzed hydrolysis of styrene oxide and of its *cis* and *trans* β-methyl derivatives in $H_2^{18}O$ are reported to yield glycol products in which all of the ^{18}O label is located in the benzyl positions.[40a] Also, the acid-catalyzed methanolysis of *p*-nitrostyrene oxide yields a mixture of hydroxy ethers in which the major isomer (95%) is the result of benzyl C–O bond cleavage.[40b,c] Thus, an aryl group, even the electron-withdrawing *p*-nitrophenyl group, stabilizes the transition state in which positive charge is developed at the benzyl carbon. The rates of acid-catalyzed hydrolysis and methanolysis of substituted styrene oxides give good Hammett correlations, yielding a ρ^+ value for hydrolysis of -4.2[41] and a ρ value for methanolysis of -4.1.[42] Thus, significant positive charge is developed on the benzylic carbon at the transition state for both hydrolysis and methanolysis. For comparison, ρ^+ values for the solvolysis of 1-phenylethyl halides and esters in aqueous organic solvents range from -5 to -6,[43,44] indicating a greater extent of carbocation formation at the transition state for solvolysis reactions.

In a study by Berti et al., acid-catalyzed hydrolysis of styrene oxide was reported to occur with 67% inversion and 33% retention at the benzyl carbon.[45] In a later study, it was reported that the styrene glycol product formed in the acid-catalyzed hydrolysis of chiral styrene oxide is completely racemic, which would indicate an A-1 mechanism.[46] As these two results indicate quite different mechanisms for this reaction, the glycol product from acid-catalyzed hydrolysis of chiral styrene oxide was converted to its bis-(+)-α-(methoxy-α-trifluoromethyl)phenylacetate diester derivative, and the composition of the diastereomeric diester mixture was determined by ^1H NMR.[47] This study agreed with those of Berti et al. and showed that acid-catalyzed hydrolysis of styrene oxide occurs with 67% inversion and 33% retention at the benzyl carbon. Acid-catalyzed methanolysis of styrene oxide is reported to occur with 89% inversion at the benzyl carbon.[48] The fact that the diol product from acid-catalyzed hydrolysis of chiral styrene oxide is not completely racemic demonstrates that the lifetime of the carbocation is not sufficiently long for it to become symmetrically solvated.

A mechanistic scheme for the acid-catalyzed hydrolysis of styrene oxide (**32**) is given in Scheme 10. If reaction of H^+ with **32** occurs with benzyl C–O bond
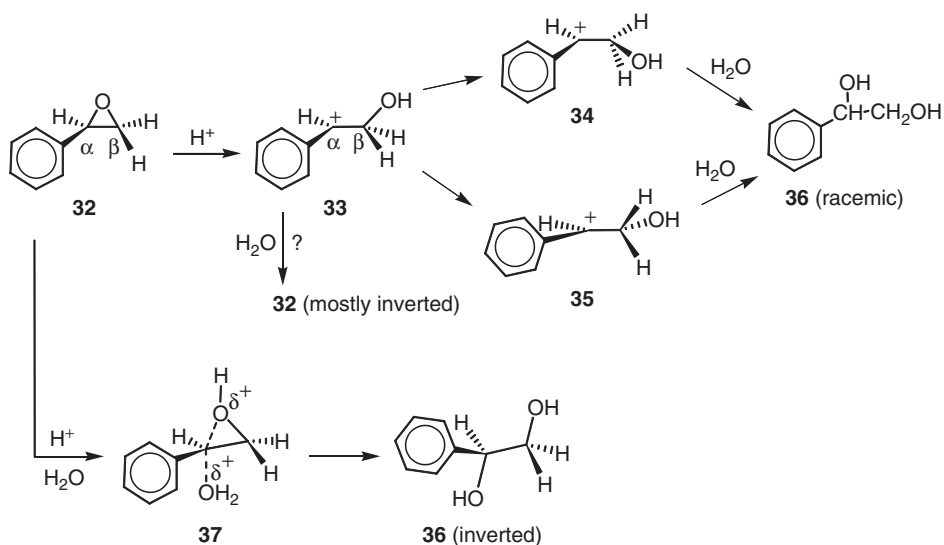
Scheme 10.

breaking, but without rotation about the C_α–C_β bond, then a carbocation with structure **33** will be formed. Quantum chemical calculations of the 2-hydroxy-1-phenylethyl carbocation in the gas phase at the MP2/6-31G* level of theory indicate that structure **33** collapses without activation to either structure **34** or **35**.[49] Structure **34** is calculated to be 3.9 kcal mol^{-1} more stable than structure **35** in the gas phase. After inclusion of a solvation energy term, structure **34** is still calculated to be 2.3 kcal mol^{-1} more stable than structure **35**. Structure **33**, in which the C–O bond is constrained to be co-linear with the empty p-orbital on the benzylic carbon, is calculated to be 6.2 kcal mol^{-1} higher in energy than structure **34**. Rotation of the C_α–C_β bond of the initially formed carbocation structure **33** in one direction will yield structure **34**, and rotation of this bond in the opposite direction will yield structure **35**. Conformers **34** and **35** possess planes of symmetry, however, and will react with solvent to yield completely racemic diol.

When the stability of the benzylic carbocation **33** is such that the rate of solvent attack on the carbocation is similar to the rate of rotation about the C_α–C_β bond of **33**, then reaction pathways other than fully concerted attack of solvent at the benzylic carbon accompanied with epoxide C–O bond breaking (A-2 mechanism) and attack of solvent on a symmetrically solvated carbocation intermediate (A-1 mechanism) become possible. The rate constant for reaction in 50:50 TFE/H$_2$O solvent of the 1-phenylethyl carbocation, which is similar in structure to the 2-hydroxy-1-phenylethyl carbocation, is estimated to be approximately 10^{11} s^{-1}.[43] Reorganization of water solvent is on the order of 10^{11}–10^{12} s^{-1},[29] and therefore an unstable species such as **33** might react with water to give either retained or inverted diol product at a rate that is comparable to the rate at which it undergoes C_α–C_β bond rotation to form **34** or **35**. In one mechanism, a water molecule that is hydrogen

bonded to the newly formed hydroxyl group may be in position to collapse with the carbocationic center in an encounter mechanism to yield diol with retention of configuration at the benzyl carbon. However, attack of water from the side of the carbocationic center opposite to the newly formed hydroxyl group would involve fewer nonbonding interactions at the transition state, and this reaction would lead to inversion of configuration.

In a comparison of the rates of acid-catalyzed racemization of and ^{18}O exchange in chiral 1-phenylethanol, it was concluded that the departing $–OH_2$ group shields that side of the benzyl carbocation from attack by other solvent molecules.[26] The lifetime of the β-phenylethyl carbocation, which should be similar to that of the β-hydroxy benzylic carbocation formed in the acid-catalyzed hydrolysis of styrene oxide **32**, is therefore too short to allow complete solvent equilibration about the carbocation.

The benzylic carbocation formed from the reaction of styrene oxide with H^+, like the 1-phenylethyl carbocation and simple tertiary carbocations, most likely reacts with water molecules from within the inner solvent shell that are present when the carbocation is formed.[30] The lifetime of the carbocation formed in the acid-catalyzed hydrolysis of styrene oxide must be similar to the time required for solvent relaxation and rotation about the C_α–C_β bond.

The lifetimes of 2-hydroxy-1-phenylethyl carbocations in which there are substituents in the phenyl ring are expected to vary with the ability of the substituent to stabilize positive charge at the benzyl carbon, and therefore the mechanism of acid-catalyzed hydrolysis will depend on the substituent. For example, a methoxy group substituted at the para position of the phenyl ring in **33** is expected to stabilize the carbocation and increase its lifetime, whereas a nitro group substituted at the para position of the phenyl ring is expected to destabilize the carbocation and decrease its lifetime. If the *p*-nitro group destabilizes charge at the benzyl carbon sufficiently, then addition of water at the benzyl carbon will be concerted with benzyl C–O bond cleavage (A-2 mechanism). Such a range in mechanism has been observed in the solvolysis of ring-substituted 1-phenylethyl derivatives in 50:50 H_2O/TFE solution, where strongly electron-donating substituents stabilize benzyl carbocations sufficiently so that the reaction occurs via a carbocation intermediate (S_N1 mechanism), and strongly electron-withdrawing substituents destabilize benzyl carbocations sufficiently so that concerted addition of solvent is enforced (S_N2 mechanism).[50]

The acid-catalyzed hydrolysis of *p*-methylstyrene oxide (**38a**) and *p*-methoxystyrene oxide (**38b**) in solutions of varying azide ion concentrations have been interpreted by the mechanism shown in Scheme 11. Azide ion reacts with **38** by direct nucleophilic opening of the epoxide ring at pH 9.5 to yield azido alcohols and also by trapping of an intermediate carbocation **39**, subsequent to its rate-limiting formation, at lower pH.[41] At pH 5.75, the rate of reaction of **38b** in dilute sodium azide solutions is independent of the concentration of azide ion. However, the yield of an azide product increases with increasing azide ion concentration, suggesting that an intermediate carbocation is trapped, subsequent to its rate-limiting formation. By using the azide "clock" technique[43] to estimate carbocation lifetimes, the rate constant for reaction of **39b** with water (k_s) is estimated to be $1.5 \times 10^8 \, s^{-1}$. This

38 a, X = CH$_3$
        b, X = OCH$_3$

H$^+$

39

k_s
H$_2$O

40

k_N[N$_3^-$]

Azido Alcohols

k_{az}[N$_3^-$]

41

Scheme 11.

42a, X = CH$_3$
b, X = OCH$_3$

H$^+$

43a, X = CH$_3$
b, X = OCH$_3$

H$^+$

44a, X = CH$_3$
b, X = OCH$_3$
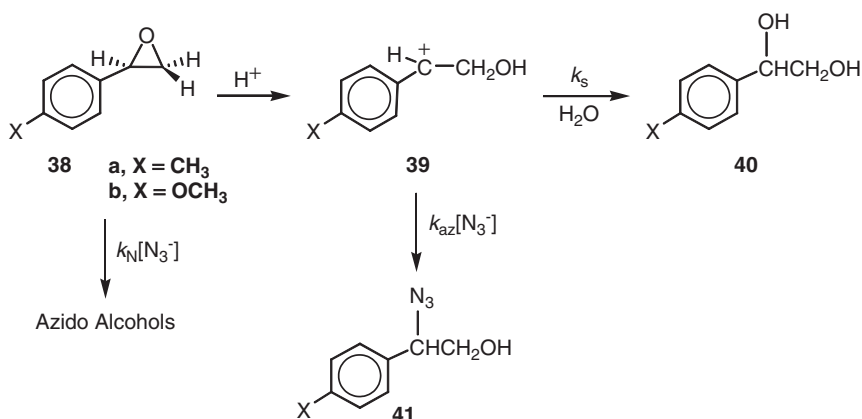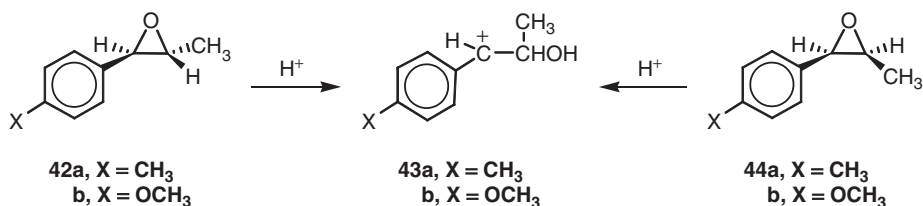
Scheme 12.

value of k_s for reaction of **39b** with water solvent is slightly larger than that estimated for reaction of 1-(p-methoxyphenyl)ethyl cation with 50:50 TFE/H$_2$O solvent ($5 \times 10^7 \, \text{s}^{-1}$),[43] and indicates that the lifetime of **39b** is longer than the time required for solvent reorganization and most likely the time required for conformational equilibration.

The acid-catalyzed hydrolysis of p-methylstyrene oxide (**38a**) in azide solutions has also been studied, but the yields of azido alcohols are only very slightly greater than the yields predicted if all of the azido alcohol is formed from the bimolecular (k_N) pathway.[41] For example, in water containing 0.025 M azide ion, pH 5.75, the observed yield of azido alcohol from **38a** is 22%. The calculated yield from the bimolecular reaction is 19%. This yield is very close, perhaps within experimental error, to that expected from only the bimolecular pathway (k_N). If it is assumed that ~3% of azido alcohol is actually from trapping of the intermediate carbocation **39a** with azide ion, then a *lower limit* of $\sim 3 \times 10^9 \, \text{s}^{-1}$ can be estimated for k_s. This value is fortuitously close the value of k_s estimated for reaction of 1-(p-methylphenyl)ethyl carbocation with 50:50 TFE/H$_2$O ($4 \times 10^9 \, \text{s}^{-1}$), and is most likely an underestimate.

In closely related studies, the acid-catalyzed hydrolyses of *cis*- and *trans*-β-methylstyrene oxides (**42a** and **44a**)[51–52] and of *cis*- and *trans*-anethole oxides (**42b** and **44b**)[53] have been reported (Scheme 12). Reactions of the *cis* and *trans* epoxides in

each series with H^+ yield the same carbocation **43**, and if the lifetime of this carbocation is sufficiently long to allow solvent reorganization and conformational equilibration to occur, then the same mixture of erythro and threo diols should be formed from both *cis* and *trans* epoxides. However, the isomeric *cis* and *trans* epoxides **42a** and **44a** undergo acid-catalyzed hydrolysis to yield different erythro/threo diol product mixtures resulting from syn and anti addition of solvent, and therefore the lifetime of carbocation **43a** must be shorter than the time required for conformational equilibration of the intermediate carbocation. The lifetime of **43a** is expected to be comparable to that of the hydroxybenzylic carbocation that is formed in the acid-catalyzed hydrolysis of styrene oxide **32**. In contrast, **42b** and **44b** undergo acid-catalyzed hydrolysis to yield identical mixtures of erythro and threo diols resulting from retention and inversion of configuration at the benzyl carbon. Thus, carbocation **43b** has a lifetime sufficient for both solvent relaxation and conformational equilibration of the carbocation to occur. By using the azide "clock" technique[43] to estimate carbocation lifetimes, the rate constant for reaction of **43b** with water (k_s) is calculated to be $2 \times 10^8 \, s^{-1}$. This rate constant is very similar to that calculated for reaction of the 2-hydroxy-1-(p-methoxyphenyl)ethyl carbocation **39b** with water ($1.5 \times 10^8 \, s^{-1}$).

SUBSTITUENT EFFECTS ON ADDITION OF AMINES AND HYDROXIDE ION TO STYRENE OXIDES

Laird and Parker studied[54] the reactions of benzylamine with m- and p-substituted styrene oxides in ethanol and showed that the Hammett ρ value for attack of amine at the primary β-carbon is positive and opposite in sign to that for attack of amine at the α-benzylic carbon. Thus, the regiochemistry of addition of amines to substituted styrene oxides (cf. Scheme 13) is dependent on the nature of the phenyl substituent. In the reaction of styrene oxide with benzylamine, 83% of product arises from attack at the primary carbon and only 17% arises from attack at the benzyl carbon. In the reaction of 3,4-dimethylstyrene oxide with benzylamine, only 19% of product arises from attack of amine on the primary carbon and 81% arises from attack of amine at the benzylic carbon.

It was originally reported that attack of hydroxide ion on styrene oxide occurs only at the primary carbon.[55] Later studies on the hydroxide ion-catalyzed hydrolysis of styrene oxide in $H_2^{18}O$ and of chiral styrene oxide, however, showed that
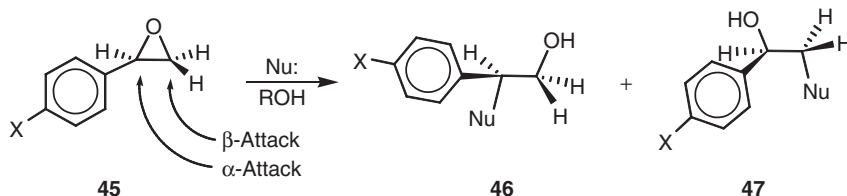
Scheme 13.

attack of hydroxide ion occurs equally at the benzylic α-carbon and primary β-carbon.[41,47] The effects of *p*-substituents on the rate of addition of hydroxide ion to the α-carbon is opposite to that for addition of hydroxide ion to the β-carbon, as found earlier for the addition of benzylamine to substituted styrene oxides. Addition of hydroxide ion and methoxide ion[41] to the α-carbon is favored by electron-donating groups, and addition of these nucleophiles to the β-carbon is favored by electron-withdrawing groups.

SUBSTITUENT EFFECTS ON THE PH-INDEPENDENT REACTIONS OF STYRENE OXIDES

The only products from the pH-independent reactions of styrene oxide and its *p*-chloro and *p*-methyl derivatives are the corresponding styrene glycols.[41] From analysis of the mass spectra of glycol products from the pH-independent reactions of styrene oxide and *p*-methylstyrene oxide in H_2O^{18}, it was determined that >95% of glycol was derived from attack of water at the benzylic α-carbon. Attack of water at the benzylic carbon of chiral styrene oxide also occurs with inversion of stereochemistry.[47] The pH-independent reactions of styrene oxide, *p*-methylstyrene oxide and most likely *p*-chlorostyrene oxide, therefore, appear to involve attack of water at the benzyl carbon concerted with epoxide C–O bond breaking as shown in **48**. Hydrogen bonding of solvent to the epoxide oxygen at the transition state is also expected, or proton transfer from solvent to the epoxide oxygen might be coupled with C–O bond breaking.

48
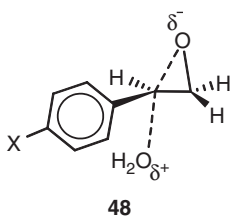
The observation that water attacks only the benzylic α-carbon of styrene oxide, whereas hydroxide ion attacks equally at both the α-carbon and β-carbon indicates that the aromatic ring stabilizes the transition state for α-attack of water (relative to β-attack) more than it does the transition state for α-attack of hydroxide ion. The transition state for attack of water must be a "looser" structure in which the nucleophile is less bonded to the benzylic carbon.

The pH-independent reactions of *p*-methoxystyrene oxide and of *p*-nitrostyrene oxide have different mechanisms than those for reactions of styrene oxides without strongly electron-donating or strongly electron-withdrawing groups. Both of these compounds are much more reactive than predicted from a Hammett sigma–rho plot of $\log k_{obsd}$ versus σ for the pH-independent reactions of styrene oxide and its *p*-methyl and *p*-chloro derivatives.[41] The most likely explanation for the enhanced reactivity of *p*-nitrostyrene oxide is that attack of water at the β-carbon, which is

expected to be favored by strongly electron-withdrawing groups in the phenyl ring, becomes the major reaction instead of attack of water at the benzylic carbon. The pH-independent reaction of *p*-methoxystyrene oxide is clearly different because the major product is *p*-methoxyphenylacetaldehyde, and *p*-methoxystyrene glycol is only a minor product. The mechanisms of pH-independent reactions of epoxides will be discussed in more detail in a later section.

6   Mechanisms of acid-catalyzed hydrolysis of 1-phenylcyclohexene oxides, indene oxides and 1,2,3,4-tetrahydronaphthalene-1,2-epoxides

ACID-CATALYZED HYDROLYSIS OF 1-PHENYLCYCLOHEXENE OXIDES

The acid-catalyzed hydrolysis of *p*-phenyl-substituted cyclohexene oxides **49a–d** yields diols resulting from "*cis*" and "*trans*" addition of water to the epoxide group (Scheme 14). It was initially reported that the *cis/trans* diol ratio correlates well with the electronic effect of the *p*-substituent, and varied from 7.5:93.5 for *p*-nitro-substituted oxide **49d** to 95.3:4.7 for *p*-methoxy-substituted epoxide **49a**.[56–58] Later work established that methoxy-substituted diols **50a** and **51a** underwent isomerization under the conditions of acid-catalyzed epoxide hydrolysis, and that the *cis/trans* diol ratios for hydrolysis of **49a–c** are quite similar.[59]

A mechanism that explains some of the more important observations in the acid-catalyzed hydrolysis of epoxides **49a–d** is outlined in Scheme 15. The *cis/trans* diol product ratios from the acid-catalyzed hydrolysis of **49a–c**, which have either hydrogen- or electron-donating groups in the para position of the phenyl ring, are 74:26, 83:17 and 65:35, respectively. An intermediate carbocation **52a** is trapped by azide ion in the acid-catalyzed hydrolysis of **49a** and the rate constant for reaction of **52a** with water in 10:90 dioxane–water solvent is estimated, by the azide "clock" technique, to be $1.7 \times 10^8 \, \text{s}^{-1}$. Azide ion also traps an intermediate **52b** in the acid-catalyzed hydrolysis of **49b**, but somewhat less efficiently. The rate constant k_s for reaction of **52b** with solvent is estimated to be $\sim 2 \times 10^9 \, \text{s}^{-1}$. The somewhat greater reactivity of **52b** compared to that of **52a** is consistent with the observation that
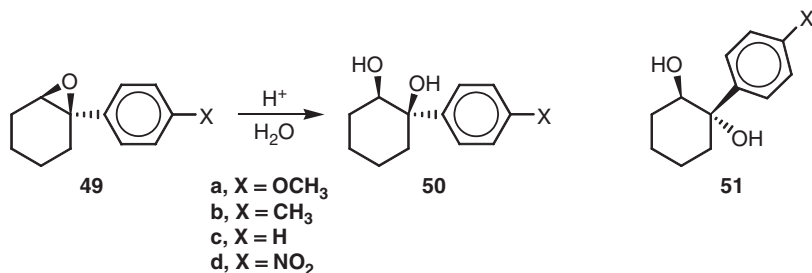
Scheme 14.
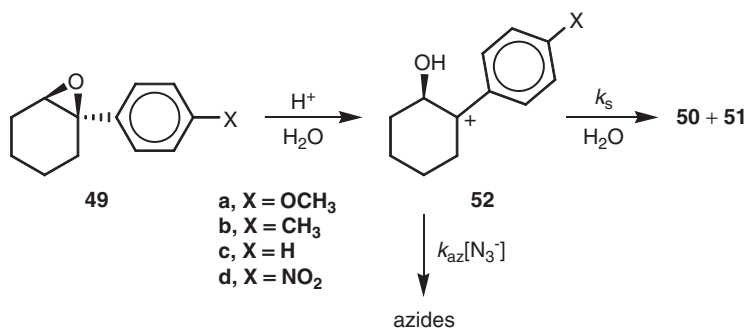
Scheme 15.
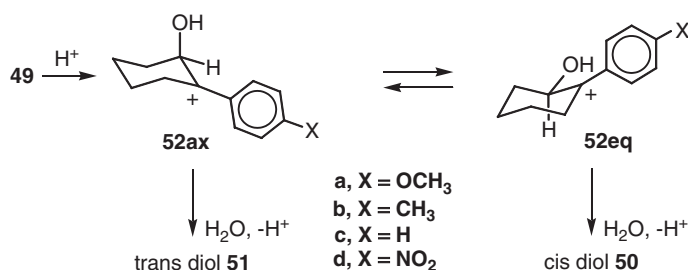
Scheme 16.

tertiary α-substituted *p*-methylbenzyl carbocations are more reactive with solvent than the corresponding α-substituted *p*-methoxybenzyl carbocations.[60] The acid-catalyzed hydrolysis of **49a–c** can therefore be regarded as proceeding via discrete carbocation intermediates **52a–c**.

In a study of the acid-catalyzed equilibration of *cis* and *trans* diols **50a, b** and **51a, b**, it was determined that the *cis* diol in each system is more stable than the *trans* diol.[59] A mechanism for hydrolysis of **49** that takes into account the relative stabilities of the diol products and also conformational factors was proposed, and is given in Scheme 16. In this mechanism, the reaction of **49** with H$^+$ occurs with axial C–O bond breaking to yield a carbocation with an axial hydroxyl group (**52ax**). Inversion of the ring yields a second carbocation conformation **52eq**, in which the hydroxyl group occupies an equatorial position. It was suggested that axial attack of solvent on each conformation would be favored, and that those factors contributing to the greater stability of the *cis* diol product would also contribute to lowering of the transition-state energy leading to it. *However, this assumption is not always valid, and factors other than the stabilities of the hydrolysis products may play very important roles.*[61]

The mechanism of acid-catalyzed hydrolysis of **49d**, which yields >92% of *trans* diol,[57] is clearly different than that for hydrolysis of **49a–c**. The lifetime of the carbocation **52d** is expected to be considerably shorter than the lifetimes of **52a** and

b. If **52d** were sufficiently unstable, then addition of solvent, concerted with proton transfer and benzylic C–O bond breaking, would occur and would yield only *trans* diol. Another possibility is that carbocation conformation **52d(ax)** is formed from the reaction of **49d** with H^+, and undergoes axial attack by solvent faster than it undergoes ring inversion to form **52d(eq)**, i.e. the lifetime of **52(ax)** is short relative to the time required for conformational change.

ACID-CATALYZED HYDROLYSIS OF INDENE OXIDES: TRANSITION-STATE EFFECTS ON STEREOCHEMISTRY OF DIOL FORMATION

The *cis/trans* hydrolysis ratio from the acid-catalyzed hydrolysis of indene oxide (**53a**, Scheme 17) is 75:25,[62,63] and that from acid-catalyzed hydrolysis of 5-methoxyindene oxide (**53b**) is 80:20.[61] Thus, the introduction of a methoxy group into position 5 does not result in any significant change in the *cis/trans* hydrolysis ratio. There is evidence that **54b**, which is stabilized by the 5-methoxy group, is sufficiently stable to be trapped by external nucleophiles. The very similar *cis/trans* diol product ratio from acid-catalyzed hydrolyses of both **53a** and **b** suggest that **54a** is also a discrete intermediate.

The *cis* and *trans* diols **55b** and **56b** are sufficiently reactive in dilute acid solution to undergo equilibration, and the *trans* diol was determined to be more stable than the *cis* diol by a factor of ~3. *In this system, therefore, the major diol from acid-catalyzed hydrolysis is the less stable isomer.* This result contrasts with the results from acid-catalyzed hydrolysis of phenyl-substituted cyclohexene oxides, where the major *cis* diol product is also more stable than the corresponding *trans* diol. In the hydrolysis of indene oxides **53a, b**, therefore, effects that are present in the transition state but absent in the products must play major roles in controlling the *cis/trans* product ratio.

Quantum chemical calculation of carbocation **54** suggests that it occupies only one ground-state conformation in which the five-membered carbon ring is near planar.[61] If there is no hydroxyl substitution at the β-carbon of **54**, the resulting carbocation would have a plane of symmetry, and solvent would attack equally from both sides of the electron-deficient benzylic carbon. The presence of the β-hydroxyl group is therefore responsible in some way for lowering the transition-state energy for *cis* attack of water leading to the less stable *cis* diol (or perhaps increasing the transition-state energy for *trans* attack of water). As pointed out in a review article
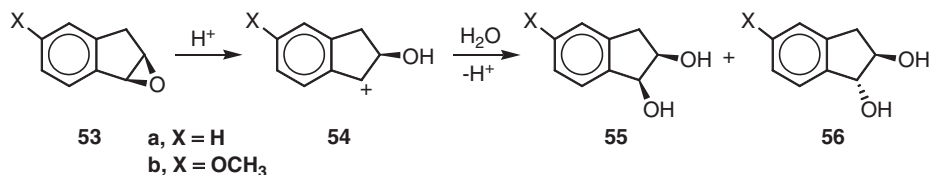
Scheme 17.

by Richard et al., the Marcus intrinsic barrier leading to the less stable *cis* diol must be lower than the intrinsic barrier leading to the *trans* diol.[64] Intramolecular hydrogen bonding between the attacking water molecule and the *β*-hydroxyl group is possible in the transition state **57** leading to the *cis* diol, but not in the transition state **58** leading to the *trans* diol. This intramolecular hydrogen bonding may contribute to lowering the intrinsic barrier in a number of ways. One possibility is that this internal hydrogen bond in **57** is stronger than the hydrogen bonding between the attacking water molecule and solvent in the transition state for *trans* attack of water (**58**). Nearby solvent molecules other than the one attacking the benzylic carbocation must also play a role in the selective stabilization of **57**. A second factor that may contribute to the greater stabilization of the transition state for *cis* attack of water is that intramolecular hydrogen bonding may result in an "earlier" transition state with less hybridization change of the benzylic carbon than that occurring in the formation of the transition state for *trans* attack of water.[61] A greater change in hybridization of the benzylic carbon for *trans* attack of water would result in a greater imbalance between loss of resonance stabilization and lowering of energy due to bond formation at the transition state, resulting in a raising of the intrinsic barrier for *trans* attack of water.

Transition-state effects in which a *β*-hydroxy group stabilizes the transition state for *cis* attack of water on a *β*-hydroxycarbocation may also be responsible for the observation that *cis* diols are the major diols formed in the acid-catalyzed hydrolysis of acenaphthylene oxide and cyclopenta[*cd*]pyrene oxide.[65] Due to this rate-enhancing effect, *β*-hydroxycarbocations may be more reactive with solvent than their parent carbocations that do not contain the *β*-hydroxy group.

57   **58**
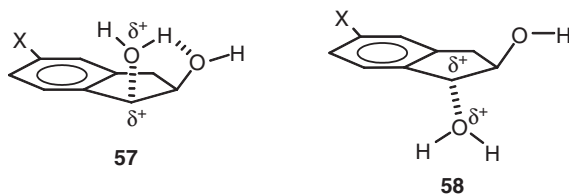
TETRAHYDRONAPHTHALENE EPOXIDE HYDROLYSIS: CONFORMATIONAL EFFECTS ON STEREOCHEMISTRY OF DIOL FORMATION

The stereochemical outcomes of the acid-catalyzed hydrolyses of 1,2,3,4-tetrahydronaphthalene 1,2-oxide **59a** and its 6-methoxy derivative **59b** (Scheme 18) are quite different from those of the corresponding indene oxide systems. For example, acid-catalyzed hydrolysis of **59a** yields only 5% of *cis* diol **61a** and 95% of *trans* diol **62a**.[66] However, acid-catalyzed hydrolysis of its 6-methoxy derivative **59b** yields 80% of *cis* diol **61b** and 20% of *trans* diol **62b**.[67] One might argue that carbocation **60a** does not have a sufficiently long lifetime compared to solvent relaxation, whereas **60b** does, and that this difference in lifetime leads to different mechanisms
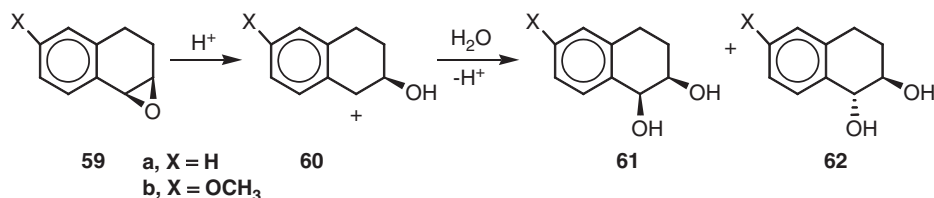
Scheme 18.

and different stereochemical outcomes. However, the *cis/trans* diol ratio from hydrolysis of **59a** at acidic pH in KCl solution is different from hydrolysis of **59a** in NaClO$_4$ solution, although the rate of hydrolysis does not change.[66] This observation indicates that there is an intermediate in the reaction, formed in a rate-limiting step. This intermediate is presumed to be a carbocation. Further, carbocation **60a** should have about the same reactivity with solvent as **54a**, which appears to have a lifetime longer than the time required for solvent relaxation. To reconcile the different stereochemical outcomes of the hydrolyses of indene oxides and tetrahydronaphthalene oxides, it was proposed that conformational factors play important roles in the stereochemistry of diol formation from **60a** and **b**.[67]

Whereas indene oxide and its 2-hydroxy-1-indanyl carbocation are each calculated to occupy one stable conformation, tetrahydronaphthylene oxide **59a** and carbocation **60a** are each calculated at the B3LYP/6-31G* level of theory to have two minimum-energy conformations, shown in Scheme 19. The mechanism for hydrolysis of this system should therefore take into consideration these additional conformations.

Tetrahydronaphthalene oxide 59**a** has two conformations, **63a** and **63b**. From analysis of vicinal H–C–C–H coupling constants in the ^{1}H NMR spectrum of **59a**, it was concluded that conformation **63a**, in which the bonds of the angular ring have fewer eclipsing interactions than those of **63b**, is the more stable.[67] This conclusion is supported by quantum chemical calculations in which conformation **63a** is calculated at the B3LYP/6-31G* level of theory to be $> 4\,\text{kcal}\,\text{mol}^{-1}$ more stable than **63b** in the gas phase.[49]

Addition of H$^+$ to the more stable conformation **63a** yields carbocation **64ax**, in which the newly formed hydroxyl group occupies an axial position. Conformational inversion of the cyclohexenyl ring in **64ax** leads to a second conformation of the carbocation in which the hydroxyl group occupies an equatorial position. This carbocation can also be formed directly by the reaction of the less stable epoxide conformation **63b** with H$^+$. These two carbocation conformations are related in structure to the cyclohexenyl carbocation. From the work of Goering and Josephson, it was shown that the cyclohexenyl carbocation undergoes energetically favorable axial attack of solvent, which converts the intermediate carbocation to the product possessing an energetically favorable half-chair conformation.[68] Equatorial attack of water on the cyclohexenyl carbocation, on the other hand, leads to product with an energetically unfavorable half-boat conformation.
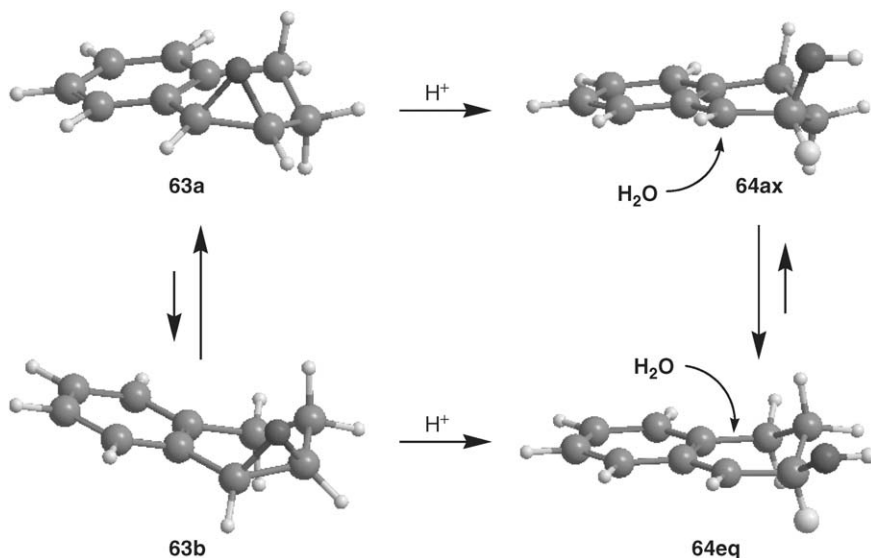
Scheme 19.

Application of these principles to Scheme 19 leads to the prediction that conformation **64ax** should react with solvent to preferentially form *trans* diol, whereas reaction of conformation **64eq** with water should lead preferentially to *cis* diol. Conformation **64eq**, in which the hydroxyl group occupies an equatorial position, is calculated to be more stable than conformation **64ax** in the gas phase by 1.25 kcal mol^{-1}.[49] A possible explanation for the observed results is that tetra-hydronaphthalene oxide reacts with H$^+$ only from the more stable ground conformation **63a** to yield the less stable carbocation conformation **64ax**. Carbocation **64ax** then reacts with water to form *trans* diol faster than it undergoes conformation inversion to form carbocation **64eq**. When a methoxy group occupies position 6, it stabilizes the carbocation, resulting in a smaller rate constant for reaction of **64ax**(6-OCH$_3$) with solvent. However, substitution of the 6-methoxy group should not significantly change the energy barrier for inversion of the carbocation ring. Therefore, ring inversion that transforms **64ax**(6-OCH$_3$) to **64eq**(6-OCH$_3$) may occur faster than the attack of water on **64ax**(6-OCH$_3$), and axial attack of water on this carbocation conformation would yield *cis* diol as the major product.

The mechanism in Scheme 19 is somewhat speculative, and relies heavily on the assumption that axial attack of solvent is more energetically favorable than equatorial attack of solvent on carbocations similar in structure to **64.** However, the stereochemistry of acid-catalyzed hydrolysis of two diastereomeric hexa-hydrophenanthrene 9,10-epoxides (**65** and **67**) provides support for this proposal. These two epoxides contain transfused cyclohexane moieties that restrict the geometry of each epoxide to a single conformation. Reaction of **65** with H$^+$ yields a single carbocation conformation **66**, in which the hydroxyl group is forced to occupy an axial position (Scheme 20).

65a, X = H
b, X = OCH₃

66a, X = H
b, X = OCH₃

Scheme 20.

67a, X = H
b, X = OCH

68a, X = H
b, X = OCH₃
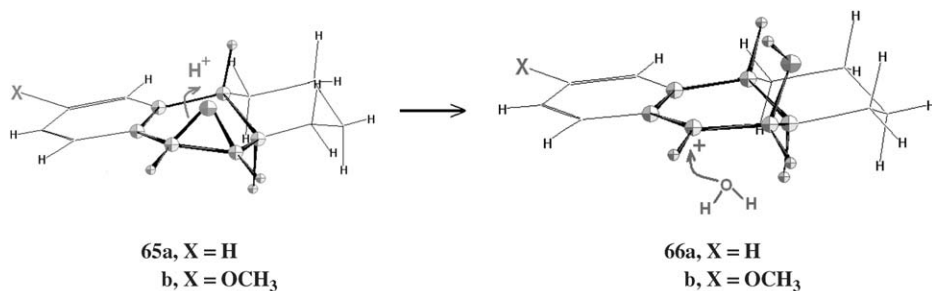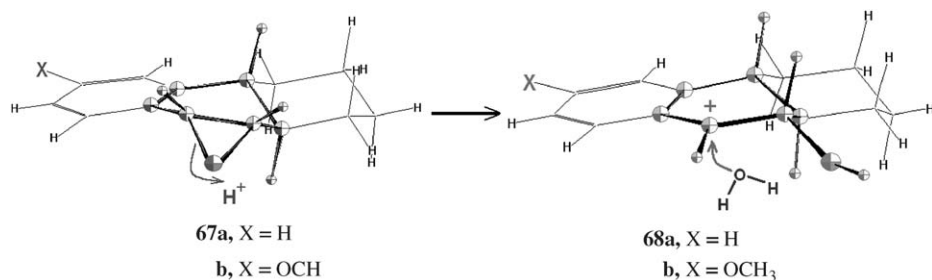
Scheme 21.

Acid-catalyzed hydrolysis of **65a** yields *trans* diol as the only detectable product,[69] and this diol product is rationalized by axial attack of water on carbocation **66a**. Since the lifetime of a simple benzyl carbocation is very short, an argument might be made that the *trans* diol is instead formed by an A-2 mechanism. However, we have also synthesized the methoxy derivative **65b**, and its acid-catalyzed hydrolysis also yields >98% *trans* diol.[70] The lifetime of carbocation **65b** is sufficiently long that it can be captured, subsequent to its rate-limiting formation, by azide ion. This result clearly shows that the *trans* diol product from acid-catalyzed hydrolysis **65b** is formed by axial attack of water on a discrete carbocation (**66b**).

Whereas acid-catalyzed hydrolyses of **65a** and **b** yield almost exclusively *trans* diol products, the acid-catalyzed hydrolysis of **67a** yields 85% of *cis* diol and 15% of *trans* diol.[69] The reaction of **67** with H⁺ also yields a single carbocation conformation **68**, in which the hydroxyl group is forced to occupy an equatorial position (Scheme 21). The major *cis* diol product can be rationalized by energetically favored axial attack of water on carbocation **68**. In unpublished work, we have also determined that the acid-catalyzed hydrolysis of **67b**, which is much more reactive than **67a** and yields a stabilized carbocation **68b**, also yields *cis* and *trans* diols in a ratio of ~85:15. Axial attack of water on **68** to yield *cis* diol is therefore favored over equatorial attack to yield *trans* diol, but not to the same extent that axial attack of water on carbocation **66** is favored.

7   General acid catalysis in epoxide reactions

ETHYLENE OXIDE AND SIMPLE PRIMARY AND SECONDARY EPOXIDES

In the early studies by Brønsted et al. of the rates of hydrolysis of epichlorohydrin (**69**) in water solutions containing formic acid, acetic acid, benzoic acid and trimethylacetic acid buffers, it was observed that the rate of reaction depends on the concentration of the buffer base, but not the buffer acid.[22] Therefore, nucleophilic addition of carboxylate ions to epichlorohydrin was observed, but general acid catalysis was not observed. However, the maximum concentration of the buffer acids used in this study was only 0.02 M, and the observation of general acid catalysis might not be expected. In a later study by Swain, it was observed that the rate of reaction of epichlorohydrin (**69**) in 0.15 M NaI/4.0 M HOAc/1.0 M NaOAc solution is 2.2 times faster that its rate in 0.15 M NaI/0.4 M HOAc/0.1 M NaOAc/ 0.90 M NaClO$_4$ solution.[71] General acid-catalyzed addition of iodide ion to epichlorohydrin by a mechanism outlined in Scheme 22 was proposed. This mechanism involves concerted proton transfer from acetic acid to the epoxide oxygen, coupled with C–O bond breaking and C–I bond making at the transition state; a carbocation is not involved in this proposed mechanism. Control experiments in which it was shown that added sodium perchlorate actually resulted in a lowering of the rate of hydrolysis of epichlorohydrin and that addition of other organic solvents such as dioxane and acetamide had little effect on the rate provide evidence that the proposed mechanism is correct. The concentration of epichlorohydrin is quite high (0.13 M), and the reaction presumably involves attack of iodide ion on an association complex of epichlorohydrin and acetic acid. Although this study presents evidence for general acid-catalyzed addition of iodide ion to a simple epoxide, general acid-catalyzed addition of solvent to a primary or secondary epoxide has not been observed, and may not be a viable mechanism because solvents such as water are much less nucleophilic than iodide ion.

   The interpretation of the observed rate increase of the reaction of epichlorohydrin with iodide ion in the presence of acetic acid was questioned by Long and Paul, who suggested that specific effects of the medium brought about by 4.0 M acetic acid may be responsible for the rate increase rather than general acid catalysis.[72] However, the alternative mechanism for acid-catalyzed epoxide hydrolysis proposed by these workers, an A-1 mechanism involving a carbocation intermediate, has been ruled
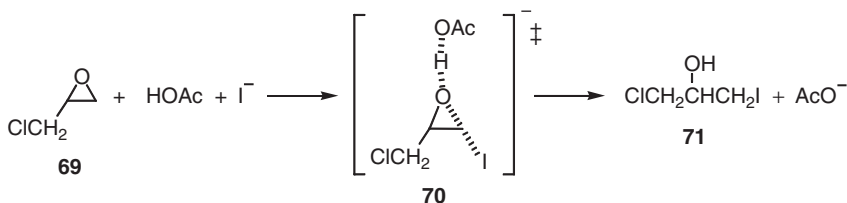
Scheme 22.

out for primary and secondary epoxides (Section 3). It is important to note that Swain's results provide evidence for general acid-catalyzed addition of iodide ion to a simple epoxide, epichlorohydrin, but not for general acid-catalyzed addition of solvent to simple epoxides.

TERTIARY EPOXIDES

Although general acid-catalyzed hydrolysis of a simple tertiary epoxide by formic acid is reported, the kinetic term in formic acid is difficult to detect over the background hydronium ion-catalyzed reaction. The rate of reaction of tetramethylethylene oxide in solutions with ionic strength held constant at 2.0 M and buffer ratio held constant increases by only $\sim$22% as the concentration of formic acid is varied up to 1.0 M.[73] It was estimated that two-thirds of the rate increase could be accounted for by a formate ester product, formed by nucleophilic attack of formate ion on protonated epoxide. The remaining one-third of the rate increase ($\sim$7%) was attributed to general acid catalysis. A specific-acid–general-base mechanism, in which there is a pre-equilibrium protonation of the epoxide group followed by rate-determining formate-assisted attack of water on protonated epoxide, was suggested for this reaction. Additional studies of the reactions of this and other simple tertiary epoxides with general acids, including but not limited to formic acid, would be helpful in confirming the interpretation of these results.

ACETALS AND EPOXY ETHERS

General acid catalysis in the hydrolysis of simple acetals is usually not observed.[74] However, general acid catalysis has been observed in the hydrolysis of acetals with phenolic leaving groups when the intermediate oxocarbocations possess moderate stability.[75] General acid catalysis has also been observed in the hydrolysis of acetals that yield an alkoxytropylium ion[76] or an oxocarbocation stabilized with a 4-methoxyphenyl group.[77] The mechanism proposed for the general acid-catalyzed hydrolysis of 2-(4-nitrophenoxy)tetrahydropyran (**72**) is concerted, with proton transfer from the general acid coupled with C–O bond breaking at the transition state **73** (Scheme 23).[78]

General acid catalysis by dihydrogen phosphate ion is also observed in the hydrolysis of an epoxy ether **74**.[79] Although the authors did not discuss the nature of the dihydrogen phosphate-catalyzed reaction, they proposed that in the hydronium ion-catalyzed reaction of **74**, proton transfer from hydronium ion to the epoxide oxygen is concerted with epoxide O–C bond breaking in a reactant-like transition state. Although the reaction of H^+ with **74** does not yield a highly stabilized oxocarbocation, the free energy change associated with the breaking of the C–O bond of the epoxide ring provides a driving force for the reaction. Thus, **74** is very reactive toward acid-catalyzed hydrolysis; the bimolecular rate constant for its hydronium ion-catalyzed hydrolysis in 10:90 dioxane/water at 25 $^\circ$C is $1.57 \times 10^5 \, M^{-1} \, s^{-1}$.

72 + RCO$_2$H $\longrightarrow$ **73**

Scheme 23.

74
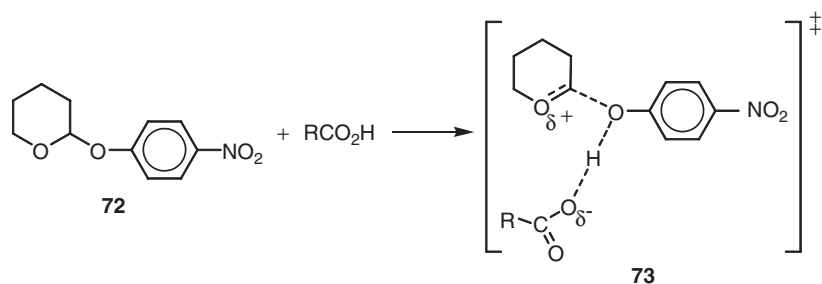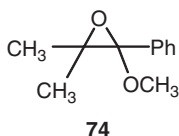
VINYL EPOXIDES

General acid catalysis has also been observed in the hydrolysis of epoxides that react with H$^+$ to yield stabilized carbocations. For example, the hydrolysis of 1,3-cyclohexadiene oxide **13** is catalyzed by dihydrogen phosphate and cacodylic acid.[36a] Other general acids such as cyanomethylamine hydrochloride are not catalytic. The bimolecular rate constant for general acid catalysis of **13** by dihydrogen phosphate ion (k_{HA}) is 0.074 M^{-1} s^{-1}, a rate constant sufficient to increase the rate of hydrolysis of **13** by ~60% at pH 5.78 in 0.1 M H$_2$PO$_4^-$. The allylic carbocation **29** is not highly stabilized, and the rate increase due to general acid catalysis is not large. The fact that dihydrogen phosphate ion catalyzes the hydrolysis whereas ammonium ions do not may be due to electrostatic stabilization of the partially formed allylic cation by the negatively charged dihydrogen phosphate ion at the transition state **75** (Scheme 24).[80–82]

Cyclohexadiene oxide **13** is very reactive toward hydronium ion-catalyzed hydrolysis; the bimolecular rate constant for acid-catalyzed hydrolysis $k_H = 1.6 \times 10^4$ M^{-1} s^{-1}. General acid catalysis by dihydrogen phosphate or other general acids was not observed in the hydrolysis of 1,3-cyclooctadiene oxide **11**, which is much less reactive toward hydronium ion-catalyzed hydrolysis ($k_H = 3.6$ M^{-1} s^{-1} at 25 °C) than **13**.[36a] The magnitude of general acid catalytic terms for hydrolysis of a particular epoxide is expected to correlate with its reactivity with hydronium ion. So it is not surprising that general acid catalysis in the hydrolysis of simple tertiary epoxides such as tetramethylethylene oxide ($k_H = 38$ M^{-1} s^{-1} at 36 °C)[73] and isobutylene oxide ($k_H = 6.8$ M^{-1} s^{-1} at 25 °C)[23]
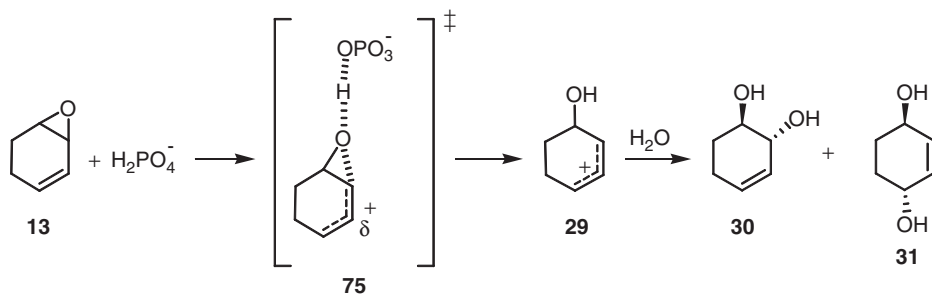
Scheme 24.

is difficult to detect. Values of k_{HA} for general acid-catalyzed hydrolysis of simple tertiary epoxides by general acids with pK_as > 4 are expected to be orders of magnitude smaller than k_H.

BENZYLIC EPOXIDES AND ARENE OXIDES

Relatively little is published on general acid-catalyzed hydrolysis of benzylic epoxides and arene oxides. The hydrolysis of phenanthrene 9,10-oxide is catalyzed by a number of general acids,[83] and general acid catalysis by dihydrogen phosphate in the hydrolysis of *cis*- and *trans*-anethole oxides (4-methoxy-β-methylstyrene oxides) is readily observed.[84] General acid catalysis in the hydrolysis of benzene oxide ($k_H = 32\,M^{-1}\,s^{-1}$), however, is not detectable.[85] The magnitude of general acid catalysis observed in epoxide hydrolysis is correlated with the ability of substituent groups to stabilize the carbocation resulting from epoxide ring opening.

Precocene I oxide (**76**) exhibits a particularly interesting pH-rate profile, and shows striking general acid catalysis.[86] Reaction of this epoxide with H^+ yields a highly stabilized benzylic carbocation **77** (Scheme 25). The hydronium ion-catalyzed hydrolysis of **76** is very facile ($k_H = 1.2 \times 10^5\,M^{-1}\,s^{-1}$), and yields only *cis* and *trans* diols **78** and **79**. A most interesting observation is that general acid catalysis by MES (2-[*N*-morpholino]ethanesulfonic acid, $pK_a = 6.17$), and BES (*N*,*N*-bis[2-hydroxy-ethyl]-2-aminoethanesulfonic acid, $pK_a = 7.08$) in the hydrolysis of **76** results a linear dependence of rate on the concentration of general acid, whereas plots of k_{obsd} versus general acid concentration for Tris (2-amino-2-[hydroxymethyl]-1,3-propane-diol, $pK_a = 8.06$), HEPES (*N*-[2-hydroxyethyl]piperazine-*N'*-2-ethanesulfonic acid, $pK_a = 7.49$) and CHES (2-[*N*-cyclohexylamino]ethanesulfonic acid, $pK_a = 9.28$), respectively, are nonlinear. Implications of this observation and the complicated pH-rate profile will be discussed in a later section. Catalytic constants for general acid catalysis in the hydrolysis of **76** are especially large and, of course, vary with the pK_a of the general acid. The bimolecular rate constant for general acid-catalyzed hydrolysis of **76** by MES, e.g., is $152\,M^{-1}\,s^{-1}$. Reaction of the acid form of MES or
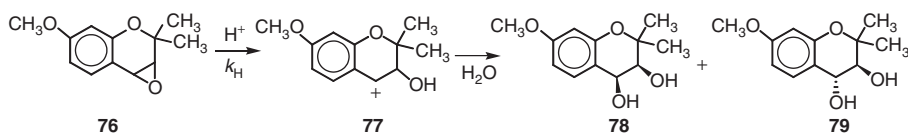
Scheme 25.

BES buffers ($pK_a < 7.5$) with **76** to form benzylic carbocation **77** is solely rate limiting, whereas increase in Tris, HEPES and CHES ($pK_a > 7.5$) buffer concentrations bring about a change in mechanism from rate-determining epoxide ring opening at low buffer concentration to attack of solvent on the carbocation at high buffer concentration.

Pronounced general acid catalysis by acetic acid ($pK_a = 4.8$), dihydrogen phosphate ion ($pK_a = 6.9$), Tris H$^+$ ($pK_a = 8.2$), hydroxyethylammonium ion ($pK_a = 9.5$) and phenol ($pK_a = 10.0$) has been observed in the hydrolysis of benzo[a]pyrene 7,8-diol 9,10-epoxides **80** and **81**.[87] Only the acid form of each buffer was found to be catalytic, and it was proposed that the mode of general acid catalysis involves rate-determining reactions of general acid with diol epoxides **80** and **81** to yield benzylic carbocations **82** and **83**, respectively. Plots of k_{obsd} for reactions of **80** and **81** versus [$H_2PO_4^-$] are provided in Fig. 2. A concentration of 0.05 M $H_2PO_4^-$ is sufficient to increase the rate of reaction of diol epoxide **81** by a factor of ~20–25. Brønsted plots of log k_{HA} versus pK_a for general acid-catalyzed hydrolysis of diol epoxide **81** by a series of ammonium ions[88] with pK_as varying between 5.4 and 10.6, and of both **80** and **81** by dihydrogen phosphate and a series of phosphonate anions[89] provide reasonable Brønsted α values of 0.45–0.50.
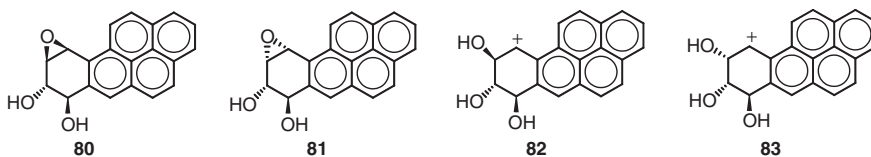
Kinetic solvent deuterium isotope effects for the hydronium ion-catalyzed hydrolyses ($k(H_3O^+)/k(D_3O^+)$) of diol epoxides **80** and **81** are 0.67 and 0.70, respectively, which are considerably larger than the solvent kinetic deuterium isotope effects observed for the hydronium ion-catalyzed hydrolyses of acetals that are thought to hydrolyze via specific acid catalysis ($k(H_3O^+)/k(D_3O^+) \sim 0.37$).[75] The observed solvent deuterium isotope effects for the acid-catalyzed hydrolyses of **80** and **81** are very close to the value of 0.75 observed for the acid-catalyzed hydrolysis of 2-(p-nitrophenoxy)-tetrahydropyran, an acetal that is thought to hydrolyze by a mechanism in which hydronium ion acts as a general acid.[75] The kinetic isotope effects and the fact that hydronium ion fits rather well on a Brønsted plot of log k_{HA} for reactions of **80** and **81** catalyzed by a series of phosphonate ions versus pK_a of the general acid suggest that hydronium ion is acting as a general acid in the
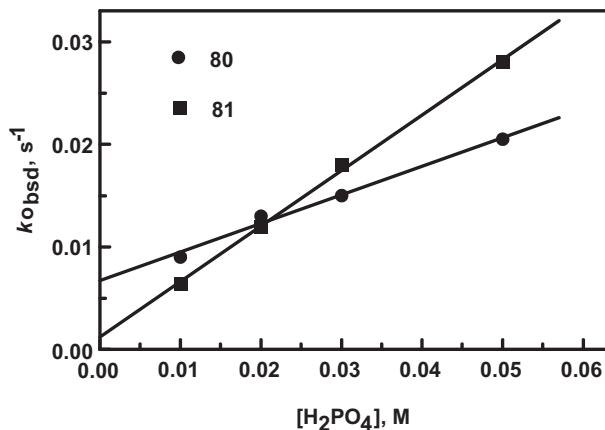
Fig. 2 Plot of k_{obsd} versus ph for reaction of **80** and **81** in 10:90 dioxane/water, pH 6.9. Reproduced with permission from Ref. 87. Copyright 1979 American Chemical Society.
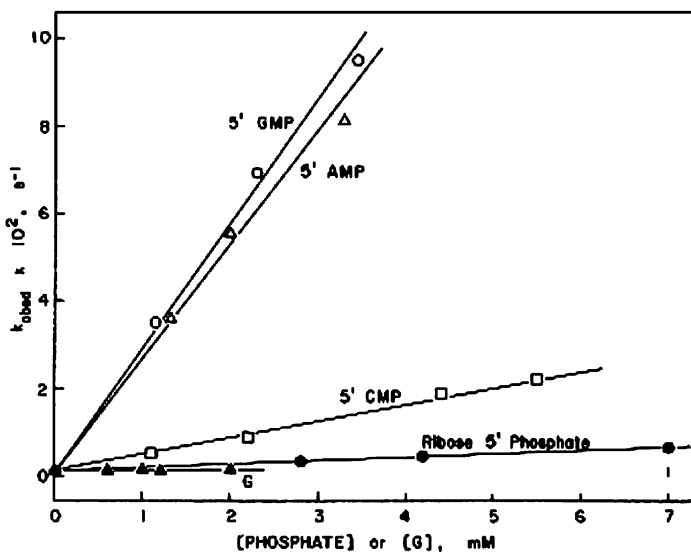
Fig. 3 Plots of k_{obsd} versus total concentration of monophosphate ester, 10:90 dioxane/water, 25 °C. Reproduced with permission from Ref. 90b. Copyright 1987 American Chemical Society.

hydrolyses of these diol epoxides and may act as a general acid in the hydrolysis of other epoxides that hydrolyze to form sufficiently stable carbocations.

Even more pronounced general acid catalysis by nucleoside monophosphates in the hydrolysis of diol epoxides **80** and **81** is observed.[90] In Fig. 3 are plots of k_{obsd} versus total concentrations of guanosine (G), ribose 5′-phosphate, 5′-cytosine mono-phosphate (5′-CMP), 5′-adenosine monophosphate (5′-AMP) and 5′-guanosine

monophosphate (5′-GMP). Whereas guanosine does not catalyze the hydrolysis of **81**, monophosphate esters of cytosine, adenosine and guanosine are catalytic. Ribose 5′-phosphate ($pK_a = 6.6$) is slightly more effective than dihydrogen phosphate ($pK_a = 6.9$), but 5′-AMP and 5′-GMP ($pK_a s \sim 6.3$–6.5) are 50–60 times more effective than dihydrogen phosphate as general acids. The greater catalytic efficiencies of 5′-AMP and 5′-GMP compared to dihydrogen phosphate ion (similar $pK_a s$) are attributed to a favorable stacking interaction or association of the nucleotide base with the polycyclic arene portion of the diol epoxide at the transition state.[90]

8   pH-independent reactions of epoxides

SIMPLE ALKYL EPOXIDES

Ethylene oxide, propylene oxide and isobutylene oxide each undergoes hydrolysis to form a 1,2-glycol by a reaction whose rate is independent of pH.[22,23] This reaction has been referred to as a "spontaneous" reaction,[22] a "water" reaction[23] and a "pH-independent" reaction. The pH-independent reaction of propylene oxide in H_2O^{18} yields glycol with ~65% of O^{18} located on the primary carbon and ~35% located on the secondary carbon.[23] These results suggest that the pH-independent reaction of simple epoxides with primary and secondary carbon centers occurs by nucleophilic addition of water, with attack at a less hindered primary carbon slightly favored over attack at a secondary carbon. An attempt to study the pH-independent reaction of isobutylene oxide in $H_2^{18}O$ was made, but the pH of the solution drifted from its initial value where the pH-independent reaction predominates to a value of ~4, where the acid-catalyzed reaction predominates, over the long 80-h reaction time.[23] Some ^{18}O (~10–20%) was incorporated at the primary carbon in these experiments, whereas >99% ^{18}O is located at the tertiary carbon of the glycol formed in the acid-catalyzed reaction. The only conclusion that can be made from this result is that attack of water at the primary carbon in the pH-independent reaction of isobutylene oxide is at least a minor reaction pathway (>20%).

ARENE OXIDES

A number of aromatic hydrocarbons are metabolized to phenols via intermediate arene oxides.[91] In a very important study of the rates of rearrangements of benzene oxide and 1,2-naphthalene oxide to their corresponding phenols, it was demonstrated that the rearrangement reaction occurs by two kinetically distinct pathways, an acid-catalyzed route and a pH-independent route.[92] From deuterium labeling studies, it was shown that each pathway involves a 1,2-hydrogen migration to yield an intermediate ketone, which then rearranges rapidly to phenol product.[93] This 1,2-hydrogen migration has been referred to as the "NIH" shift.[91] Proposed

mechanisms for the acid-catalyzed rearrangement of benzene oxide to phenol are outlined in Scheme 26. One mechanism involves reversible protonation of benzene oxide, followed by rate-limiting epoxide C–O bond breaking to yield a carbocation **86**, rearrangement with 1,2-hydrogen migration of **86** to oxocarbocation **87**, and loss of a proton from **87** to yield phenol (**88**). A second possible mechanism is concerted, with hydrogen migration and epoxide C–O bond breaking occurring concurrently. On the basis of a great sensitivity of the reaction to substituent effects and the lack of a primary kinetic deuterium isotope effect on hydrogen migration, the concerted mechanism was ruled out.[94]

The kinetic deuterium isotope effects on the pH-independent reactions of per-deuterobenzene oxide and 1-^{2}H-dihydronaphthalene-1,2-oxide to form phenols have been determined.[94] The lack of primary kinetic isotope effects on these reactions was taken as evidence that hydrogen migration does not occur in the rate-limiting step. If the reaction were concerted and 1,2-hydrogen migration were part of the rate-limiting step, then k_o^H/k_o^D should be ~2–3. Instead, values for $k_o^H/k_o^D = 1.05$ for each reaction were obtained. On the basis of a lack of a primary kinetic deuterium isotope effect and a very large negative Hammett ρ value (−7.3), a stepwise mechanism for the pH-independent reactions of these arene oxides was proposed as outlined in Scheme 27 for the rearrangement of dihydronaphthalene oxide **89** to 1-naphthol. In this mechanism there is rate-limiting epoxide C–O bond breaking in **89** to form a zwitterion intermediate **90**, with 1,2-hydrogen migration occurring after the rate-limiting step. The observation that ~80% of the original deuterium is located at C-2 of the 1-naphthol product **92** requires a 1,2-deuterium migration and the interme-diacy of ketone **91** in the reaction.[93] An isotope effect on the reaction of **91** to form phenol **92** is expected, which will result in a greater loss of hydrogen than deuterium from **91**.
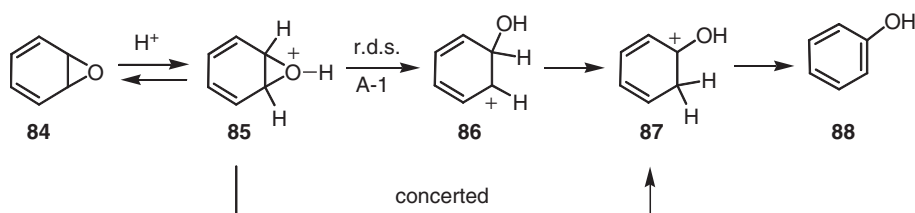
Scheme 26.
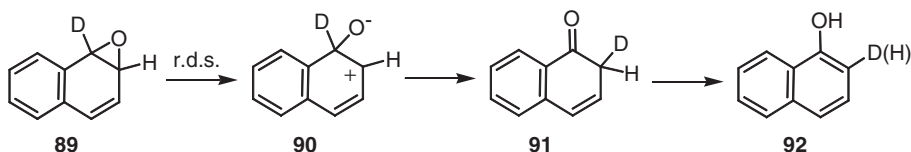
Scheme 27.

Arene oxides are also known to undergo an NIH shift in which there is 1,2-alkyl group migration. For example, 1,4-dimethylbenzene oxide undergoes acid-catalyzed and pH-independent reactions to yield both 2,4-dimethylphenol and 2,5-dimethyl-phenol.[95] 2,5-Dimethylphenol is formed from 1,2-hydrogen migration, and 2,4-di-methylphenol is formed from 1,2-methyl migration. A new mechanism for the NIH shift involving a diol intermediate was discovered in this study. The pH-independent reaction of 8,9-indane oxide to form 4-indanol occurs in part via a 1,2-alkyl migration to form an intermediate spiro ketone, which undergoes secondary isomerization to the observed phenol.[96]

CYCLIC VINYL EPOXIDES

Whereas the acid-catalyzed hydrolysis of cyclohexadiene oxide 13 gives comparable yields of 1,2- and 1,4-diols (Scheme 9), the pH-independent reaction of 13 yields only 3-cyclohexene-*trans*-1,2-diol.[36a,c] The hydroxide ion-catalyzed hydrolysis of 13 also yields only *trans* 1,2-diol. The observation that the pH-independent reaction of 13 yields only *trans* 1,2-diol suggests that epoxide C–O bond breaking and water O–C bond making are concerted. There is a negative salt effect on the pH-independent reaction of 13,[36c] so the transition state must not have significant charge separation. The newly developing oxyanion is expected to be either strongly hydrogen bonded with solvent, or proton transfer from solvent to the oxyanion may also be part of the transition state (i.e. structure 93).

93
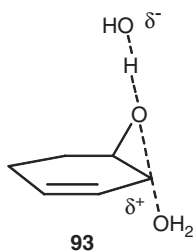
The pH-independent reaction of cyclopentadiene oxide 12 in water is clearly different from that of 13.[97] This reaction yields 33% of 3-cyclopentenone, 35% of *cis*-2,4-pentadienal and 35% of a mixture of *cis* and *trans* 1,2- and 1,4-diols (Scheme 28). When the reaction is carried out in D_2O instead of H_2O, no deuterium is incorporated into the ketone product. Thus, 1,2-hydrogen migration is required for this reaction just as it is in the rearrangement of arene oxides to phenols. The mechanisms of product formation in this reaction are not fully understood. The observation that the diol mixture is similar to that from the acid-catalyzed hydrolysis of 12 suggests that an allylic carbocation may be involved in the diol-forming reaction. Ketone (**96**) and dienal (**97**) products are potentially formed either by stepwise or concerted mechanisms, and there is insufficient evidence to rule out either one. There is a significant normal salt effect on this pH-independent
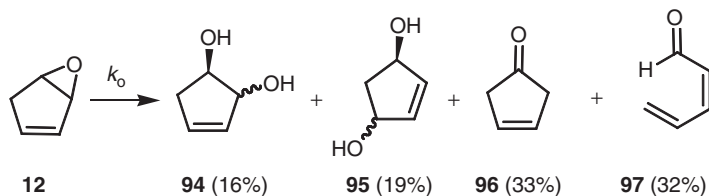
Scheme 28.

reaction,[36c] so there must be substantial charge separation in the transition states leading to products.

BENZYLIC EPOXIDES THAT UNDERGO RATE-LIMITING 1,2-HYDROGEN MIGRATION

Many benzylic epoxides undergo rearrangements to ketones in their pH-independent reactions. For example, the pH-independent reactions of indene oxide[63] and 5-methoxyindene oxide[61] yield 75–80% of 2-indanones, along with *cis* and *trans* diols. The pH-independent reaction of 6-methoxy-1,2,3,4-tetrahydronaphthalene-1,2-epoxide (**98**, Scheme 29) also gives ∼76% of ketone (**99**), along with *cis* and *trans* diols **100** (2.4:1.0 *cis/trans* ratio).[67] However, the pH-independent reaction of 1,2,3,4-tetrahydronaphthalene-1,2-epoxide yields only a *trans* 1,2-diol, presumably from nucleophilic attack of water at the benzylic carbon.[66] The transition state for the rearrangement pathway from benzylic epoxide to ketone must possess significant positive charge on the benzylic carbon, since an electron-donating *p*-substituted methoxy group promotes the rearrangement pathway over the diol-forming pathway.

The kinetic deuterium isotope effect k_o^H/k_o^D on the pH-independent reaction of **98** is reported to be 1.59.[98] This isotope effect is in the range expected for rate-determining 1,2-hydrogen migration. If it is assumed that the isotope effect on the minor diol-forming reaction of **98** is near unity, then the isotope effect on the ketone-forming reaction is calculated to be 2.0. This observation indicates that migration of hydrogen in the ketone-forming reaction of **98** is rate limiting. The observed kinetic deuterium isotope effect on the reaction of precocene I oxide **76** at pH 11, which yields 75% of rearranged ketone, is 2.15. The deuterium isotope effect on 1,2-hydrogen migration is estimated to be ∼4, which is somewhat larger than isotope effects on most 1,2-hydrogen migrations and indicates substantial hydrogen migration at the transition state.[86]

The observed kinetic isotope effect k_o^H/k_o^D on the pH-independent reaction of 5-methoxyindene oxide (**101**), which yields ketone **102** as the major product,[63] is 2.22 (Scheme 30).[99] This *observed* kinetic isotope effect is even larger than those for reaction of **98** and **76**. The large substituent effect of the methoxy group on this reaction suggests that epoxide C–O bond breaking is more advanced than 1,2-hydrogen migration, leaving substantial positive charge on the benzylic carbon at
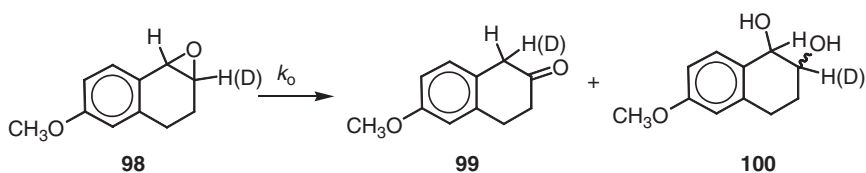
Scheme 29.
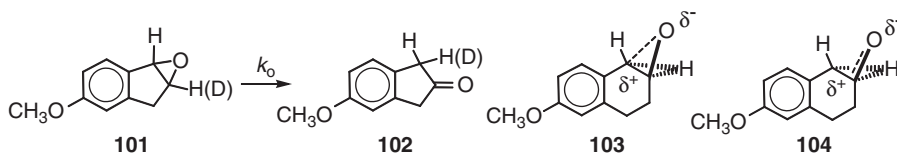
Scheme 30.

the transition state as shown in structure **103**. Another possibility is that epoxide C–O bond breaking is completed before 1,2-hydrogen migration occurs, as shown in **104**. Calculations at the MP2/6-31G*//MP2/6-31G* level of theory for the rearrangement of protonated propene oxide to protonated propanal in the gas phase show a concerted, asynchronous pathway in which the epoxide C–O bond is broken before hydrogen migration starts.[100]

The observations that the pH-independent reactions of deuterium-labeled 5-methoxyindene oxide and 6-methoxy-1,2,3,4-tetrahydronaphthalene-1,2-oxide show significant primary kinetic deuterium isotope effects for the ketone-forming reactions, whereas the pH-independent reactions of deuterium-labeled naphthalene oxide and benzene oxide do not, are quite puzzling. Clearly, more work needs to be done to fully understand why transition-state structures for rearrangement of arene oxides to phenols differ from those for rearrangement of benzylic epoxides to ketones.

BENZO[*a*]PYRENE 7,8-DIOL 9,10-EPOXIDES

Rate data for the reaction of benzo[*a*]pyrene diol epoxide **80** between pH 4 and 10 in water fit the equation $k_{obsd} = k_H[H^+] + k_o$.[101] The changeover in mechanism from acid-catalyzed hydrolysis to pH-independent hydrolysis occurs at pH $\sim$ 5. Products of the pH-independent reaction of **80** are tetrols resulting from *cis* and *trans* addition of water to the benzylic epoxide group and ketone resulting from 1,2-hydrogen migration (Scheme 31). The ketone product is quite unstable, especially in base solution, and the original yield of ketone product was underestimated.[102] The ratio of *cis* and *trans* tetrols (**105** and **106**) from this pH-independent reaction is identical with the *cis/trans* tetrol ratio from the acid-catalyzed hydrolysis of **80**. An
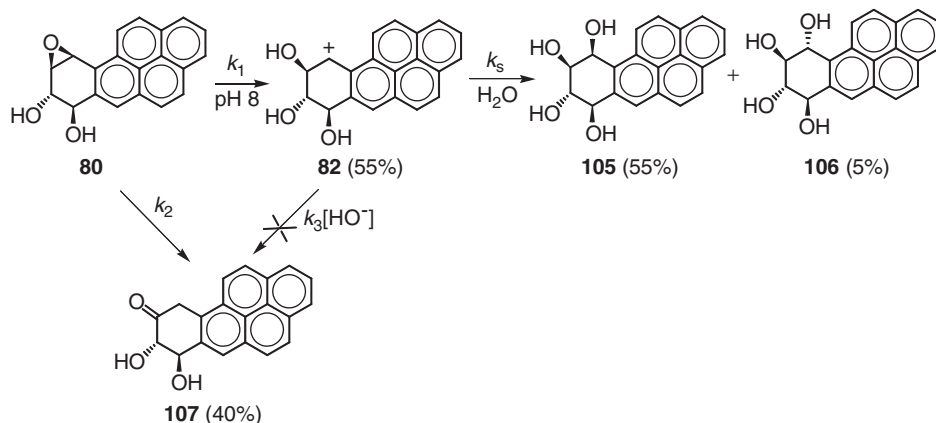
Scheme 31.

intermediate leading to tetrol products is trapped, subsequent to its rate-limiting formation, by azide ion.[89] This intermediate is presumed to be carbocation **82**, the same intermediate formed in the acid-catalyzed hydrolysis of **80**, since it leads to the same ratio of *cis* and *trans* tetrols. Ketone **107** is formed from either attack of hydroxide ion on carbocation **82**, coupled with 1,2-hydrogen migration ($k_3[HO^-]$), or from a separate reaction pathway (k_2) by either a concerted mechanism or a mechanism that involves a zwitterion intermediate. Attack of hydroxide ion on **82** as a pH-independent route leading to ketone can be ruled out on the following basis. The rate of this k_3 route would have to be comparable to or greater than the rate of the k_s route. The value of k_s is known to be $\sim 2 \times 10^8 \, s^{-1}$, so $k_3[HO^-]$ would have to be comparable in magnitude. However, at pH 6–11 the value of k_3 would have to exceed the diffusional limit of $\sim 10^{10} \, M^{-1} \, s^{-1}$. Yet in this pH range, the yield of ketone is $\sim 40\%$. Carbocation **82** is therefore not an intermediate in the formation of ketone **107**. The pH-independent reaction of diol epoxide **80** is therefore a combination of two nonintersecting reaction pathways, one stepwise pathway leading to tetrols via a carbocation intermediate and a second pathway (k_2) leading to ketone.

   The mechanism of carbocation formation in the pH-independent reaction of **80** is especially interesting. A neutral water molecule must serve at the proton source, i.e. a general acid, in the carbocation-forming reaction. Concerted general acid catalysis is to be expected if the pK_a of the catalyst is between the pK_a of the substrate site and the pK_a of the final substrate site (Jenck's rule for concerted catalysis).[103] General acid-catalyzed formation of carbocation **82** by acids with pK_a less than that of **82** (~ 13) is in accord with Jenck's rule and supports a concerted mechanism.[89] However, the pK_a of water is higher than the pK_a of carbocation **82**, and Jenck's rule is violated if water acts as a general acid in a concerted mechanism as outlined in Scheme 32. A concerted mechanism for this reaction is enforced, however, if the zwitterion **108** is too unstable to exist.[104] If the reaction is concerted, a physical process such as ion dissociation, not proton transfer, must occur in the rate-limiting
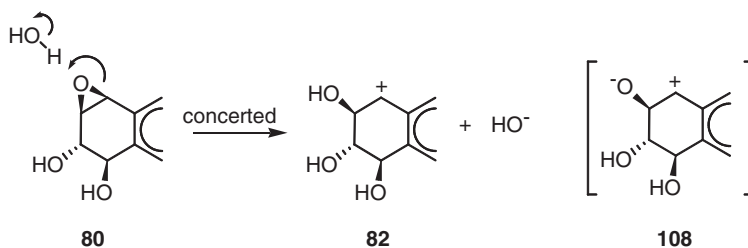
Scheme 32.

step. In this sense, water is not a "true general acid catalyst" in the pH-independent reaction of **80**.

The pH-independent reaction of diol epoxide **81** is quite different from that of diol epoxide **80**, although their chemical structures are similar. Subtle differences in conformation clearly are sufficient to cause different pH-independent mechanisms. Whereas one of the pH-independent reaction pathways of **80** involves a carbocation intermediate, carbocation **83** cannot be detected in the pH-independent reaction of **81**.[89] The mechanism of the diol-forming reactions in the pH-independent reactions of **81** are not clear, but may involve concerted reactions of **81** with solvent.

SUMMARY OF PH-INDEPENDENT MECHANISMS

The pH-independent reaction of a given epoxide may follow one or more of a number of possible mechanisms. For simple alkyl-substituted primary and secondary epoxides, nucleophilic addition of a water molecule, concerted with epoxide C–O bond breaking, occurs. The pH-independent reactions of simple vinyl- and phenyl-substituted epoxides also follow this mechanism. When epoxide C–O bond breaking yields a stabilized carbocation, a number of other reaction mechanisms are possible. Water may act as a proton donor in converting some epoxides to stabilized carbocations, which react with solvent in a second step to form *cis* and *trans* diols. Competing with diol-forming reactions of epoxides are reactions involving 1,2-hydrogen migrations that yield carbonyl compounds. Certain epoxides also undergo rearrangement to isomeric epoxides by mechanisms outlined in the following section.

9   Epoxide isomerization accompanying pH-independent reactions

8,9-Indane oxide (**109**) undergoes a pH-independent reaction to form 4-indanol (**115**), and part of this product is formed by a 1,2-alkyl migration.[96] However, most of the 4-indanol is formed as a result of the isomerization of 8,9-indane oxide to 4,9-indane oxide (**111**) via an "oxygen walk."[96a,b] A minor amount of 5-indanol (**116**) is
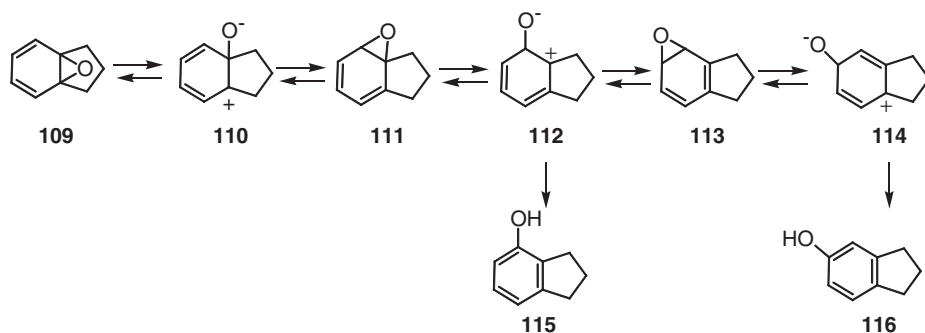
Scheme 33.
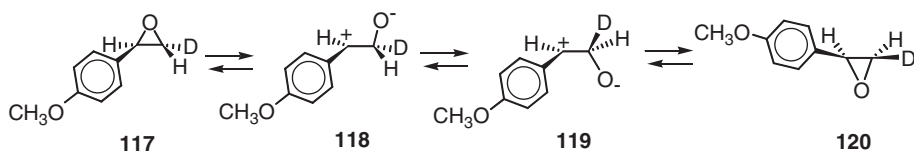
Scheme 34.

formed as a result of an additional "oxygen walk" in which 4,9-indane oxide (**111**) rearranges to 4,5-indane oxide (**113**). Scheme 33 outlines the mechanism, involving zwitterions **110**, **112** and **114**, proposed to explain the observed products. Zwitterions **110**, **112** and **114** must be very short-lived intermediates, or the interconversions of **109**, **111** and **116** might also take place by concerted suprafacial 1,5-sigmatropic rearrangements, which are thermally allowed.[105]

The pH-independent reaction of *p*-methoxystyrene oxide yields *p*-methoxyphenylacetaldehyde as a major product and *p*-methoxystyrene glycol as a minor product.[106] If deuterium is substituted for hydrogen at the *trans-β* position and the reaction is followed by ^{1}H NMR, scrambling of deuterium between the *trans-β* and *cis-β* positions during the course of the reaction is observed (Scheme 34). The mechanism must involve benzylic C–O bond breaking, rotation about the C_α–C_β bond via structures **118** and **119**, and epoxide ring closure to form **120** at a rate somewhat faster than the final products, *p*-methoxyphenylacetaldehyde and *p*-methoxystyrene glycol, are formed. The rearrangement of **117** to **120** is either stepwise via a very short-lived intermediate zwitterion, or it is concerted.

Another example of an epoxide isomerization occurring by a similar mechanism is the pH-independent reaction of *cis*-anethole oxide **121**, which yields (*p*-methoxyphenyl)acetone **125** along with threo and erythro 1-(*p*-methoxyphenyl)-1,2-propanediols **126**.[107] During the course of the reaction, *trans*-anethole oxide (**124**) builds up to a level that is detected by ^{1}H NMR (Scheme 35). The mechanism for this reaction involves benzylic C–O bond breaking, rotation about the C_α–C_β bond via zwitterionic structures **122** and **123**, and epoxide ring closure to form *trans*-anethole
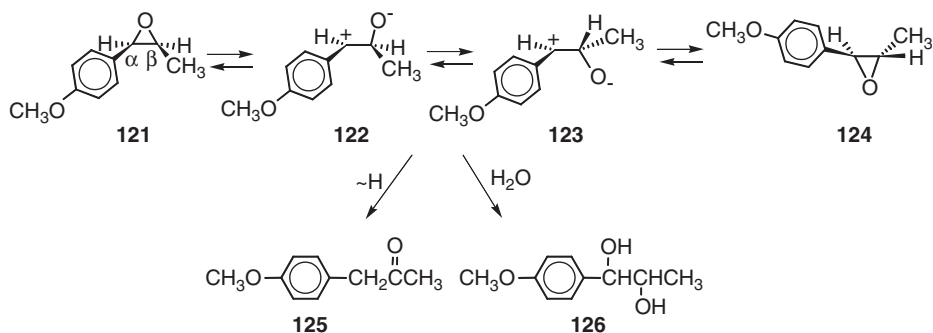
Scheme 35.

oxide **124** in a mechanism similar to that outlined in Scheme 34. Whereas zwitterion structures **118** and **119** in Scheme 34 are equivalent except for deuterium labeling, structures **122** and **123** in Scheme 35 have very different steric interactions.

The acid-catalyzed hydrolyses of both *cis*-anethole oxide (**121**) and *trans*-anethole oxide (**124**) yield identical product mixtures of 20% erythro and 80% threo 1-(*p*-methoxyphenyl)-1,2-propanediols, suggesting that there is a common benzylic car-bocation intermediate (**127**) and common product-forming steps.[108] These results indicate that rotation about the C_α–C_β bond of the carbocation intermediate **127** is faster than attack of water on the carbocation. However, the ratio of diol and ketone products from the pH-independent reaction of *cis*-anethole oxide is very different than that from *trans*-anethole oxide, so rotation about the C_α–C_β bond in the transformation of **121** to **124** is not rapid compared to the rates of ketone and diol product formation.

127
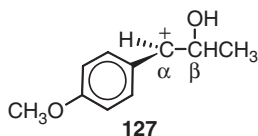
The rates and products of the reaction of **121** were compared with the rates and products of the reaction of *β*-deuterium-labeled *cis*-anethole oxide **121**-*d*.[107] The reaction pathway to ketone **125** involves a 1,2-hydrogen migration, and this step should exhibit a primary kinetic isotope effect of ~2–3. The diol-forming step, however, does not involve a 1,2-hydrogen migration, and the kinetic isotope effect on this step should be near unity. Since ketone **125** is the major product from the pH-independent reaction of **121**, then if the reaction of **121** to form **125** is either concerted or occurs via an intermediate **122/123** in a rate-limiting step, then the observed kinetic isotope effect k_o^H/k_o^D should be ~ 2. However, the value of k_o^H/k_o^D was measured to be 1.06, which is too much small for rate-limiting hydrogen mi-gration in which the hydrogen is substantially migrated at the transition state.

If there is a kinetic isotope effect on the *ketone-forming step* but not the *diol-forming step*, there will be a *partitioning isotope effect* that would result in a decrease in ketone yield relative to diol yield in the reaction of **121**-*βd*. However, the relative yields of ketone and diol products from the pH-independent reactions of both **121** and **121**-*βd* are the same. Therefore, ketone and diol products from the pH-independent reaction of **121** must be formed from nonintersecting reaction pathways. The absence of both kinetic and partitioning deuterium isotope effects was rationalized by a mechanism in which benzylic C–O bond breaking is followed by rotation about the C_α–C_β bond either in a clockwise or in a counterclockwise direction. Rotation of this bond in one direction must give one product mixture, and rotation in the other direction must give a different product mixture. In other words, epoxide ring opening and rotation of the C_α–C_β bond in a given direction commits to the formation of a given product mixture. Thus, the hydrogen migration step will not be rate limiting. The rearrangement pathways for the isomerization of **121** to **124** and ketone product may be examples of asynchronous concerted reactions.[100]

10 Benzylic epoxides that exhibit complicated pH-rate profiles

PRECOCENE I 3,4-OXIDE

Several highly reactive benzylic epoxides show more complicated pH-rate profiles that indicate a change in mechanism or rate-limiting step in the intermediate pH range. Instead of a simple biphasic profile indicating the presence of acid-catalyzed hydrolysis at low pH and pH-independent hydrolysis at intermediate pH for the reaction of precocene-I 3,4-oxide (**76**), a more complicated profile with a negative inflection point at pH ~ 10 is observed (Fig. 4).[86] There is also a nonlinear dependence of rate on buffer concentration for buffers with $pK_a > 7.5$. These observations were attributed to a change in rate-limiting step from epoxide ring opening at low pH (Regions A and B in Fig. 4) and low buffer concentrations to rate-limiting carbocation capture at higher pH and higher buffer concentrations of those buffers with $pK_a > 7.5$.

In Region A of Fig. 4, there is rate-limiting carbocation formation by the reaction of **76** with H^+ to yield **77** (Scheme 36). The carbocation is then captured by water to yield *cis* and *trans* diols **78** and **79**. In Region B, reaction of **76** yields 20% of ketone **128**, in addition to diols **78** and **79**. An intermediate in the diol-forming reaction is captured, subsequent to its rate-limiting formation, by acetylhydrazine. Rate-limiting reaction of **76** with water to form carbocation **77**, which is the intermediate captured by acetylhydrazine, was proposed (Scheme 37, $k_3 > k_{-2}[HO^-]$). This mechanism is similar to that proposed for the pH-independent reaction of benzo[*a*]pyrene diol epoxide **80** (Section "Benzylic epoxides and arene oxides"). At pH > 9, however, $k_3 < k_{-2}[HO^-]$, and carbocation formation becomes reversible. In Region D of Fig. 4, capture of carbocation **77** by hydroxide or its kinetic equivalent becomes rate limiting. In Region D of Fig. 4, ketone **128** is the major product (75%).
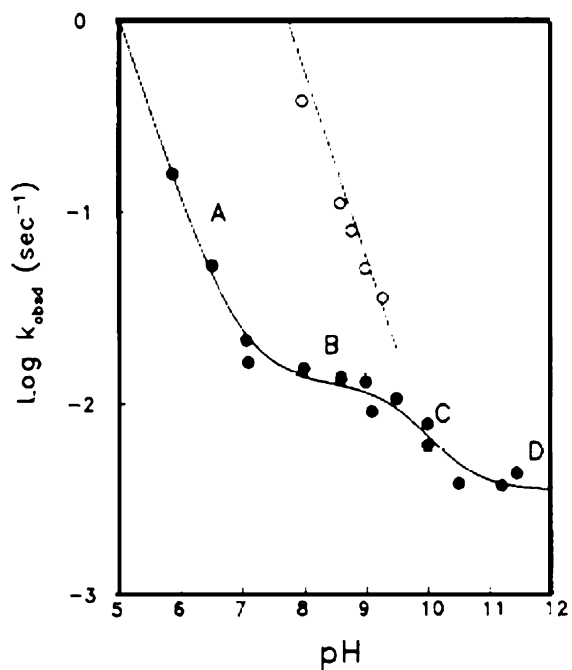
Fig. 4 Plot of log k_{obsd} (solid circles) versus pH for the hydrolysis of precocene I oxide. Reproduced with permission from Ref. 86. Copyright 1988 American Chemical Society.
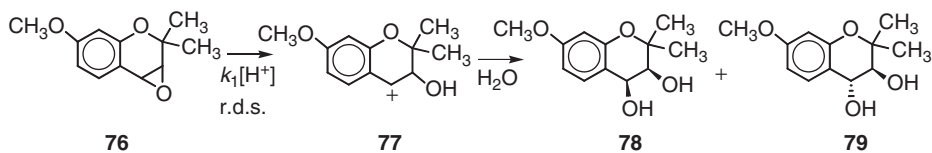
Scheme 36.
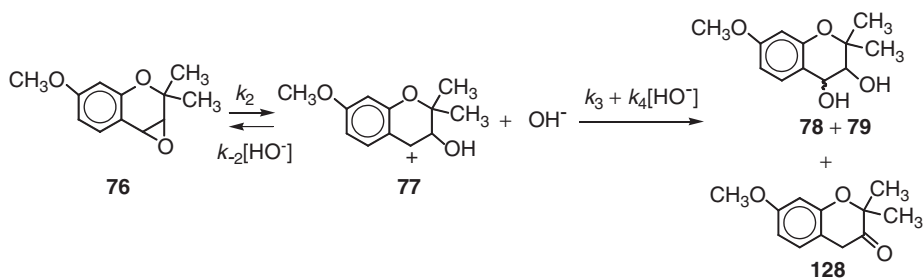
Scheme 37.

A number of very interesting conclusions are arrived at in this study.[86] (1) Re-action of hydroxide ion as a base on carbocation **77** to form epoxide ($k_{-2}[HO^-]$) is energetically more favorable than its reaction with **77** as a nucleophile to form diols. (2) The reaction pathway for formation of ketone **128** is completely separate from the stepwise mechanism for diol formation. (3) The *observed* kinetic deuterium isotope effect for reaction of **76**-β-d at pH 11 is 2.15; the kinetic deuterium isotope effect on the 1,2-hydrogen migration is estimated to be ∼4. Hydrogen migration must be occurring at the transition state for ketone formation.

BENZO[*a*]PYRENE 7,8-DIOL 9,10-EPOXIDE (**80**)

A more complicated pH-rate profile is also observed for the hydrolysis reactions of benzo[*a*]pyrene diol epoxide epoxide **80**, and is shown in Fig. 5.[102] This profile shows Regions A–D that are similar to those for reaction of precocene I oxide **76** (Fig. 4), except that Region B reaches a full plateau that extends from pH 5 to 9 in water. The interpretation of this pH-rate profile is essentially the same as the interpretation of the profile for hydrolysis of precocene I oxide (Fig. 4). The pH-independent reaction of **80** in Region B (discussed in detail in Section "Benzylic epoxides and arene oxides") yields 60% tetrols in a stepwise mechanism involving a carbocation inter-mediate and 40% ketone from a completely separate pathway (Scheme 31). The negative inflection of the profile at pH 10–11.5 indicates that hydroxide ion reacts as a base with the intermediate carbocation to reform diol epoxide **80** and thus slow the reaction rate. There is a corresponding increase in the yield of ketone **107** at pH > 11.
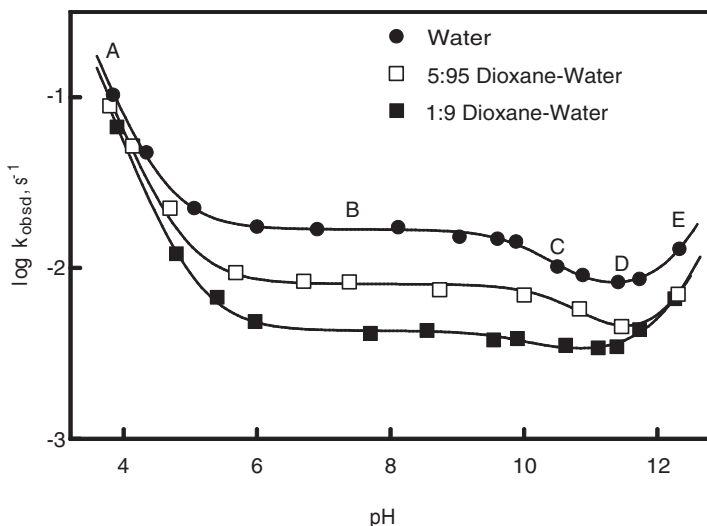
Fig. 5 Plots of log k_{obsd} versus pH for the reaction of diol epoxide **80** in water, 5:95 dioxane/water (v/v), 0.1 M NaClO$_4$, 25 °C. Reproduced with permission from Ref. 102. Copyright 2001 American Chemical Society.

The reaction of hydroxide ion with carbocation **82** is expected to occur at the diffusion-controlled limit because proton transfer from the β-OH is thermodynamically favorable, and the activation barrier for collapse of the resulting zwitterion (**108**, Scheme 32) to reform the epoxide ring should be absent or very small. A concerted mechanism for this reaction is "enforced" if zwitterion **108** is too unstable to exist as an intermediate.[104] The attack of hydroxide ion as a base on **82** as shown in Scheme 38 must be energetically more favorable than attack as a nucleophile to yield tetrol product. The exact yield of tetrol from direct combination of hydroxide ion with carbocation **82** could not be estimated, but is negligible or very small.

The reactions of stable carbocations with water are generally base catalyzed,[109,110] and their reactions with hydroxide ion are slower than their reactions with azide ion and sulfhydryl ions. The less favorable reaction of hydroxide ion with carbocations has been attributed to the fact that deprotonation of a water molecule by hydroxide ion is not a thermodynamically favorable reaction, and activation energy to generate a desolvated hydroxide ion is required.[110] These factors would also account for the less favorable reaction of hydroxide ion as a nucleophile with **82** to form tetrols instead of as a base to bring about epoxide ring closure.

At pH > 12 (Region E, Fig. 5), the rate of reaction of **80** increases due to the incursion of a second-order reaction of **80** with hydroxide ion. The ratio of *trans/cis* tetrols **106**/**105** (Scheme 31) increases somewhat, indicating that hydroxide ion attacks diol epoxide **80** to give some *trans* tetrol product.[102] However, the yield of *trans* tetrol does not increase substantially, indicating that the reaction of hydroxide ion with **80** may form some other product(s) such as unstable ketone **107**.

The pH-rate profile for diol epoxide **81** does not exhibit a negative inflection in the intermediate pH region similar to that for diol epoxide **80**, and its pH-independent reaction does not proceed via an intermediate carbocation, even though the carbocation formed from reaction of this epoxide with H$^+$ has a sufficient lifetime to be detected.[88] Tetrol products from the pH-independent reaction of **81** must occur by some other mechanism(s), possibly concerted.

General acid catalysis in the hydrolysis of **81** is quite facile. This reaction, as discussed in Section "Benzylic epoxides and arene oxides" and shown in Scheme 39, involves proton transfer to the epoxide oxygen concerted with epoxide C–O bond breaking to form a carbocation **83**. For primary ammonium ions with pK_a < ~ 8, only the acid form of the amine is reactive, and carbocation formation is irreversible,

82   **80**
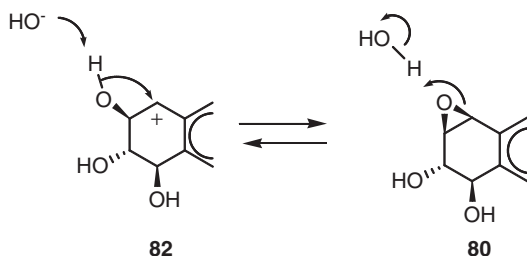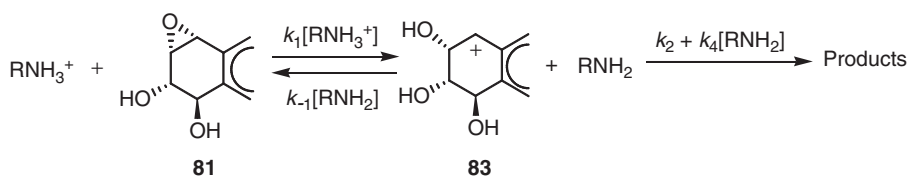
Scheme 38.

Scheme 39.

i.e. **83** reacts with water (k_2) faster than it reacts with RNH_2 to reform epoxide ($k_{-1}[RNH_2]$) or with RNH_2 to form product(s) ($k_4[RNH_2]$). However, for ammonium ions with $pK_a > \sim 8$, the base form of the buffer reacts with **81** as a nucleophile and with carbocation **83** as a base to reform epoxide **81** ($k_{-1}[RNH_2]$). For these amine buffers, the rate at which RNH_2 reacts with carbocation **83** to reform epoxide ($k_{-1}[RNH_2]$) exceeds the rate that it reacts with **83** as a nucleophile or general base to form other products ($k_4[RNH_2]$), and, under these conditions, carbocation formation is partially reversible. Thus, although there is a change in mechanism and rate-limiting step for the general acid-catalyzed hydrolysis of diol epoxide **80** by water as a function of pH and not for diol epoxide **81**, there is a change in mechanism and rate-limiting step in the general acid-catalyzed hydrolysis of diol epoxide **81** by amine buffers as a function of amine basicity.

SPECIFIC EFFECTS OF CHLORIDE ION IN EPOXIDE HYDROLYSIS

The pH-rate profiles for the reactions of a number of epoxides in solutions containing chloride salts show the same general shape as that in Fig. 4 for reaction of precocene I oxide. For example, indene oxide,[62] phenanthrene 9,10-oxide,[111] cyclohexadiene oxide,[36c] cyclopentadiene oxide,[36c] styrene oxide,[36c] 7-methyl-benzo[*a*]anthracene 5,6-oxide,[112] 7,12-dimethylbenzo[*a*]anthracene 5,6-oxide[112] and diol epoxide **81**[113] all show more complicated pH-rate profiles resembling Fig. 4 or 5 when their rates are determined in solutions containing chloride ion, but not when their rates are determined in solutions containing sodium perchlorate, a non-nucleophilic salt. The pH-rate profiles for reactions of these epoxides in solutions containing chloride ion are more complicated due to the nucleophilicity of chloride ion. Bromide ion and iodide ion, being more nucleophilic than chloride ion, have even greater effects on shapes of the pH-rate profiles of epoxides that are susceptible to reaction with nucleophiles.

Scheme 40 shows the mechanism of reaction of diol epoxide **81** in solutions containing chloride, bromide or iodide salts.[113] At sufficiently low pH, $k_H[H^+]$ is the dominant term of the rate equation, and **81** reacts with H^+ to form carbocation **83**. Carbocation **83** partitions between reaction with water (k_s) and capture by halide ion ($k_2[X^-]$). Iodide ion reacts with **83** at or near the diffusion-controlled limit, and is 3–4 times more reactive than bromide ion and $\sim$28 times more reactive than chloride
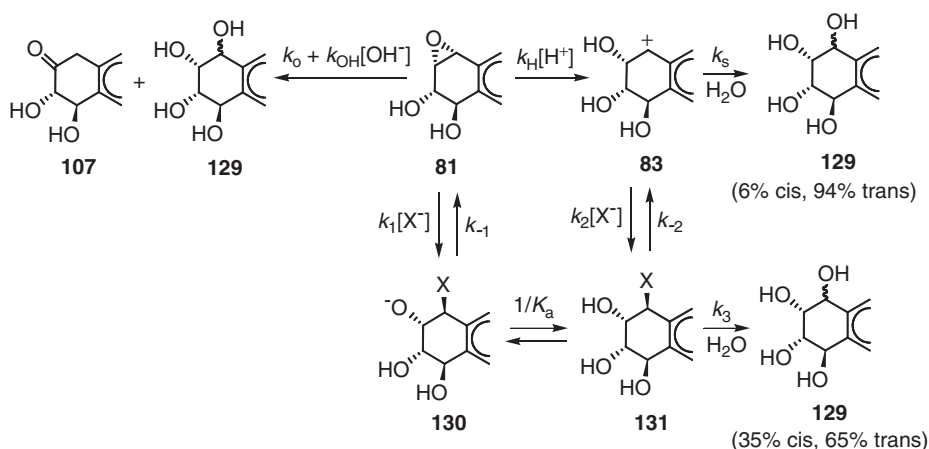
Scheme 40.
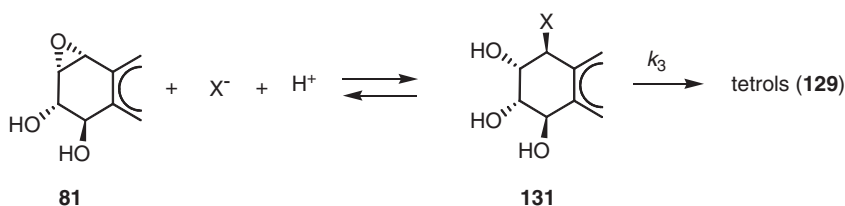
Scheme 41.

ion. Thus, chloride ion reacts with carbocation **83** within one or two orders of magnitude of the diffusional limit.

At somewhat higher pH, direct nucleophilic attack of halide ion on diol epoxide **81** ($k_1[X^-]$) becomes important, and a rate plateau is reached in which this term is the main one. If the pH is sufficiently low, the pH-dependent equilibrium between halohydrin **131** and diol epoxide **81** (shown in Scheme 41) favors halohydrin, which reacts via an S_N1 reaction (k_3) to form tetrols **129**. As the pH is increased, however, the pH-dependent equilibrium between halohydrin **131** and diol epoxide **81** shifts to favor diol epoxide, and there is a resulting rate decrease that gives an inflection point in the pH-rate profile at intermediate pH that resembles those in the profiles in Figs 4 and 5. Rate and product observations are rationalized by the mechanism of Scheme 40, and comparable mechanisms can be expected for reactions of other epoxides susceptible to reaction with nucleophiles.

11   Partitioning of hydroxycarbocations

The rates for reaction of highly stabilized carbocations such as triarylmethyl carbocations with water are sufficiently slow so that their reactions can be measured

directly.[109,110] The ratios of their rate constants with azide ion and with water are relatively constant, and are approximately 10^6–$10^7\,M^{-1}$. Other less stable carbocations have reduced k_{az}/k_s ratios, and these reduced ratios are interpreted to mean that these carbocations react with azide ion at the diffusional limit, whereas the reactions of more highly stabilized carbocations with solvent are activation limited.[43,114,115] For a series of ring-substituted 1-phenylethyl carbocations, values of k_{az}/k_s are between 1 and $130\,M^{-1}$.[43] It was concluded that their reactions with azide ion are diffusion limited. From direct measurements of these partitioning ratios, the assumption that $k_{az} = 5 \times 10^9\,M^{-1}\,s^{-1}$ and some extrapolation of structure–activity relationships, values of k_s for reactions of 1-phenylethyl carbocations with solvent were calculated and varied between $\sim 10^{13}\,s^{-1}$ for 1-(4-nitrophenyl)ethyl carbocation and $\sim 2 \times 10^3\,s^{-1}$ for 1-(4-dimethylaminophenyl)ethyl carbocation. The value of k_s for reaction of 1-(4-methoxyphenyl)ethyl carbocation was calculated to be $4 \times 10^7\,s^{-1}$.

For benzo[a]pyrene benzylic carbocations (**82** and **83**)[88,89] and 4-methoxyphenyl-stabilized carbocations (**52a**, **54b**, **66b**, **68b** and **127**),[59,63,70,108] values of k_{az}/k_s are in the range 25–600 M^{-1}. It is reasonable to assume that these carbocations also react with azide ion at the diffusional limit of $\sim 10^{10}\,M^{-1}\,s^{-1}$. The rate constants for reaction of these carbocations with water (k_s) are estimated to be $\sim (8 \times 10^6)$ to $(2 \times 10^8)\,s^{-1}$, which correspond to energies of activation of ~ 6.5–$8.0\,kcal\,mol^{-1}$. Benzo[a]pyrene 7,8-diol 9,10-epoxides (**80** and **81**) and tetrahydronaphthalene epoxide each has two optimized conformations similar to structures **132** and **134**, which are shown in Scheme 42. The carbocation formed from reaction of each of these
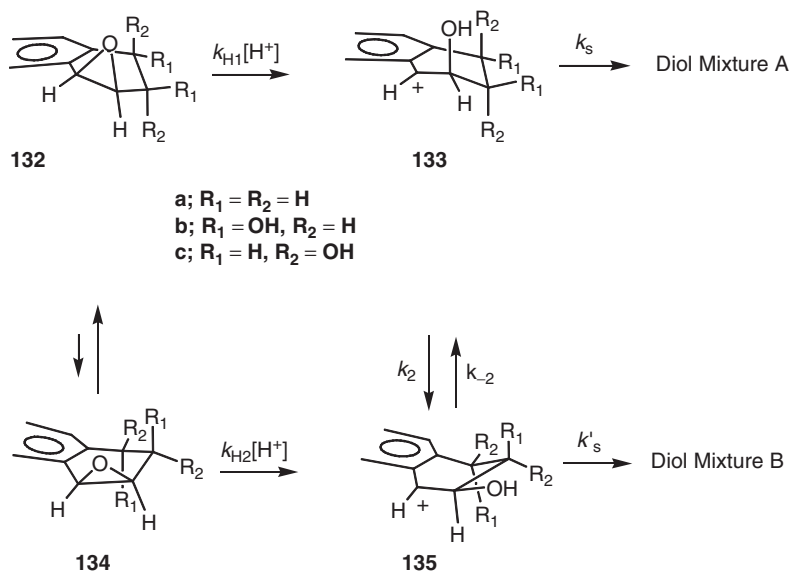
Scheme 42.

epoxides with H^+ also has two conformations, which are given by structures **133** and **135**. Since axial attacks of solvent on carbocation conformations **133** and **135** are energetically favored, each will yield a different ratio of *cis* and *trans* diols or tetrols from its reaction with water. When the k_{H1} pathway is faster than the k_{H2} pathway for reaction of epoxide with H^+, then the partitioning of carbocation conformation **133** and the relative stabilities of carbocation conformations **133** and **135** all play important roles in determining *cis/trans* product ratios. The value of k_s will depend on the ability of the aryl group to stabilize positive charge at the benzylic carbon, whereas the value of k_2 will depend on the size and nature of substituents R_1 and R_2. For systems in which the energy barrier for conformational interconversion of carbocations **133** and **135** is *small* relative to the energy barriers for attack of water on either carbocation, then the relative yields of diol or tetrol products are determined only by the difference in energy of the transition states leading to products (k_s versus k'_s steps). When the energy barrier for conformational interconversion of carbocations **133** and **135** is *large* relative to the energy barriers for attack of water on either carbocation, then the relative yields of diol or tetrol products are determined only by the difference in energy of the transition states leading to carbocation intermediates **133** and **135** (k_{H1} versus k_{H2} steps).

Conformation **132a** ($R_1 = R_2 = H$) is significantly more stable than **134a**, presumably due to fewer eclipsing interactions in the angular ring.[67] ^{1}H NMR evidence also indicates that diol epoxide conformation **132b** ($R_1 = OH$; $R_2 = H$) is substantially more stable than conformation **134b**.[116] In order to explain the observations that acid-catalyzed hydrolysis of diol epoxide **81** and solvolysis of its *trans* 9,10-chlorohydrin yields different *cis/trans* tetrol mixtures, even though each reaction proceeds via a carbocation intermediate with the same connectivity, it was proposed that (1) the *rate* at which diol epoxide conformation **132b** reacts with H^+ to form **133b** is greater than the *rate* at which diol epoxide conformation **134b** reacts with H^+ to form **135b**, and (2) the energy barrier for interconversion of carbocation **133b** to **135b** is large relative that for reaction of **133b** with water ($k_s > k_2$).[117] Therefore, products from the acid-catalyzed hydrolysis of **81** result mainly from reaction of **133b** with solvent, even though quantum chemical calculations suggest that carbocation conformations **133b** and **135b** have comparable stabilities.[117]

Product studies of the acid-catalyzed hydrolysis of diol epoxide **80** are somewhat more difficult to interpret. Epoxide conformation **132c** ($R_1 = H$; $R_2 = OH$) is estimated to be somewhat more stable than **134c**,[116] and carbocation conformation **135c** is calculated to be significantly more stable than **133c**.[118] The stereochemistry of diol products from reaction of **80** suggest that all or most of the tetrol products formed are from reaction of **135c** with solvent. One possible explanation of the results is that carbocation conformation **133c** is formed faster than **135c** and the barrier for interconversion of **133c** and **135c** is small relative to the energy barrier for attack of water on **133c**. However, the energy barrier for interconversion of **133c** and **135c** ($R_1 = H$; $R_2 = OH$) might be similar to that for interconversion of **133b** and **135b** ($R_1 = OH$; $R_2 = H$) because the substituent groups are the same, and this energy barrier may be larger than the barriers for attack of solvent on either carbocation conformation. A second possible explanation for the observed

results is that the transition-state energy of the k_{H2} pathway for reaction of **80** via conformation **134c** leading directly to the more stable carbocation conformation **135c** is lower than that for the k_{H1} pathway, and tetrol products are formed from reaction of this carbocation with solvent. Additional research is needed to clarify this mechanism.

In summary, the reactions of aryl epoxides with H^+ are generally irreversible. In some cases where the energy barrier for conformational interconversion of the intermediate carbocation is sufficiently high, then the relative rates of reaction of each epoxide conformation (k_{H1}[**132**] versus k_{H2}[**134**]) determine the diol product ratio, since each reaction pathway commits the products to be formed from a given intermediate carbocation. However, when interconversion of the carbocation conformations is rapid relative to the rate of carbocation capture by solvent, then the product distribution is determined only by the transition-state energy difference of the product-forming steps (k_s versus k'_s pathways, Curtin–Hammett principle).[119] The partitioning of a carbocation between reaction with solvent and ring inversion to form a second carbocation conformation is expected to vary significantly with both the ability of the aryl group to stabilize positive charge on the benzylic carbon and the magnitude of the energy barrier for conformational interconversion.

12   Overall summary

The mechanism of hydrolysis of a given epoxide is a function of many variables. The pH of the solution will determine whether a given epoxide will react via an acid-catalyzed reaction, a pH-independent reaction or a base-catalyzed reaction. The relative rate of each kinetically distinct reaction will vary with the epoxide structure. The relative rate of the acid-catalyzed reaction increases with the abilities of the substituent groups to stabilize positive charge in the transition state for epoxide ring opening. The pH-independent reaction has a number of completely different mechanisms as discussed in Section 8, and the mechanism followed will also depend on the abilities of substituent groups to stabilize positive charge in the transition state and, in many cases, an intermediate. The lifetimes of the intermediates in the acid-catalyzed and pH-independent reactions of epoxides play crucial roles in determining the reaction mechanisms, and both conformational effects and transition-state effects are important factors in affecting the stereochemistry of the hydrolysis products.

Acknowledgments

References

1. Rosowsky, A. (1964). In *Heterocyclic Compounds with Three- and Four-Membered Rings*. Weissberber, A. (ed.), Part 1, pp. 1–523, Wiley-Interscience, New York
2. Buchanan, J.G. and Sable, H.Z. (1972). In *Selective Organic Transformations*, Thyagarajan, B.S. (ed.), vol. 2, pp. 1–95, Wiley-Interscience, New York
3. Cross, A.D. (1960). *Quart. Rev.* **14**, 317–335
4. Nicolaou, D.C. and Smith, A.L. (1992). *Acc. Chem. Res.* **25**, 497–503
5. Bierl, B.A., Beroza, M. and Collier, C.W. (1970). *Science* **170**, 87–89
6. Persoons, C.J., Verwiel, P.E.J., Ritter, F.J., Talman, E., Nooijen, P.J.F. and Nooigen, W.J. (1976). *Tetrahedron Lett.* **24**, 2055–2058
7. Dahm, K.H., Trost, B.M. and Roller, H. (1967). *J. Am. Chem. Soc.* **89**, 5292–5294
8. El Masri, A.M., Smith, J.N. and Williams, R.T. (1958). *J. Biochem.* **68**, 199–204
9. Boyland, E., Ramsay, G.S. and Sims, P. (1961). *J. Biochem.* **78**, 376–384
10. Wogan, G.N. (1992). *Cancer Res.* **52**, 2114–2118
11. Olson, J.H., Dragsted, L. and Autrup, H. (1988). *Br. J. Cancer* **58**, 392–396
12. Hayes, R.B., Van Nieuwenhuize, J.P., Raatgever, J.W. and ten Kate, F.J.W. (1984). *Food Chem. Toxicol.* **22**, 39–43
13. Ivers, R.S., Coles, B.F., Raney, K.D., Thier, R., Guengerich, F.P. and Harris, T.M. (1994). *J. Am. Chem. Soc.* **116**, 1603–1609
14. Dipple, A., Moschel, R.C. and Bigger, C.A.H. (1984). In *Chemical Carcinogens*, Searle, C.E. (ed.) (2nd edn), vol. 1, ACS Monograph 182, pp. 41–163. American Chemical Society, Washington, DC
15. Harvey, R.G. (ed.) (1985) Polycyclic hydrocarbons and carcinogenesis, *ACS Symposium Series 283*. American Chemical Society, Washington, DC
16. Thakker, D.R., Yagi, H., Akagi, H., Koreeda, M., Lu, A.Y.H., Levin, W., Wood, A.W., Conney, A.H. and Jerina, D.M. (1977). *Chem. Biol. Interact.* **16**, 281–300
17. For historical reviews, see (a) Phillips, D.H. (1983). *Nature* **303**, 468–472; (b) Rubin, H. (2001). *Carcinogenesis* **22**, 1903–1930
18. Luch, A., Platt, K.L. and Seidel, A. (1998). *Carcinogenesis* **19**, 639–648
19. Greenberg, A. and Liebman, J.F. (1978). *Strained Organic Molecules*, p. 281. Academic Press, New York
20. Sawicka, D., Wilsey, S. and Houk, K.N. (1999). *J. Am. Chem. Soc.* **121**, 864–865
21. Wolk, J.L., Sprecher, M., Basch, H. and Hoz, S. (2004). *Org. Biomol. Chem.* **2**, 1065–1069
22. Brønsted, J.N., Kilpatrick, M. and Kilpatrick, M. (1929). *J. Am. Chem. Soc.* **51**, 428–461
23. Long, F.A. and Pritchard, J.G. (1956). *J. Am. Chem. Soc.* **78**, 2663–2667
24. Long, F.A. and Pritchard, J.G. (1956). *J. Am. Chem. Soc.* **78**, 2667–2670
25. (a) Bunnett, J.F. (1961). *J. Am. Chem. Soc.* **83**, 4956–4967; (b) Bunnett, J.F. (1961). *Ibid.* **83**, 4968–4973; (c) Bunnett, J.F. (1961). *Ibid.* **83**, 4973–4977; (d) Bunnett, J.F. (1961). *Ibid.* **83**, 4978–4983; (e) Bunnett, J.F. and Olsen, F.P. (1966). *Can. J. Chem.* **44**, 1899–1916
26. Grunwald, E., Heller, A. and Klein, F.S. (1957). *J. Chem. Soc.*, 2604–2613
27. Wohl, R.A. (1974). *Chimia* **28**, 1–5
28. Toteva, M.M. and Richard, J.P. (1996). *J. Am. Chem. Soc.* **118**, 11434–11445
29. (a) Billing, G.D. and Mikkelsen, K.V. (1996). *Molecular Dynamics and Chemical Kinetics*, p. 108, Wiley, New York; (b) Castner Jr., E.W., Maroncelli, M. and Fleming, R. (1987). *J. Chem. Phys.* **86**, 1090–1097
30. Richard, J.P. (1992). *J. Org. Chem.* **57**, 625–629
31. Pritchard, J.G. and Siddiqui, I.A. (1973). *J. Chem. Soc. Perk. II*, 452–457
32. Archer, I.V.J., Leak, D.J. and Widdowson, D.A. (1996). *Tetrahedron Lett.* **37**, 8819–8822
33. Henbest, H.B., Smith, M. and Thomas, A. (1958). *J. Chem. Soc.* 3293–3298

34. Parker, R.E. and Isaacs, N.S. (1959). *Chem. Rev.* **59**, 737–799
35. Data were taken from Streitwieser, A. (1962). *Solvolytic Displacement Reactions*, p. 12. McGraw-Hill, New York
36. (a) Whalen, D.L. (1973). *J. Am. Chem. Soc.* **95**, 3432–3434; (b) Whalen, D.L. and Ross, A.M. (1974). *J. Am. Chem. Soc.* **96**, 3678–3679; (c) Ross, A.M., Pohl, T.M., Piazza, K., Thomas, M., Fox, B. and Whalen, D.L. (1982). *J. Am. Chem. Soc.* **104**, 1658–1665
37. (a) Bartlett, P.D. and Ross, S.D. (1948). *J. Am. Chem. Soc.* **70**, 926–929; (b) Kadesch, R.G. (1946). *Ibid.* **68**, 41–45
38. DeWolfe, R.H. and Young, W.G. (1956). *Chem. Rev.* **56**, 753–901
39. Anet, F.A. and Yavari, I. (1978). *J. Am. Chem. Soc.* **100**, 7817–7819
40. (a) Audier, H.E., Dupin, J.F. and Jullien, J. (1968). *Bull. Soc. Chim. Fr.* **9**, 3850–3856; (b) Hanzlik, R.P. and Westkaemper, R.B. (1980). *J. Am. Chem. Soc.* **102**, 2464–2467; (c) Jacober, S.P. and Hanzlik, R.P. (1986). *Ibid.* **108**, 1594–1597
41. Blumenstein, J.J., Ukachukwu, V.C., Mohan, R.S. and Whalen, D.L. (1993). *J. Org. Chem.* **58**, 924–932
42. Biggs, J., Chapman, N.B., Finch, A.F. and Wray, V. (1971). *J. Chem. Soc. B,* 55–63
43. Richard, J.P., Rothenberg, M.E. and Jencks, W.P. (1984). *J. Am. Chem. Soc.* **106**, 1361–1372
44. (a) Tsuno, Y., Kusuyama, Y., Sawada, M., Fuji, T. and Jukawa, Y. (1975). *Bull. Soc. Chem. Jpn.* **48** (1), 3337–3346; (b) Richard, J.P. and Jencks, W.P. (1984). *J. Am. Chem. Soc.* **106**, 1383–1396
45. Berti, G., Bottari, F., Ferrarini, P.L. and Macchia, B. (1965). *J. Org. Chem.* **30**, 4091–4096
46. Dupin, C. and Dupin, J.-F. (1970). *Bull. Soc. Chim. Fr.* **11**, 249–251
47. Lin, B. and Whalen, D.L. (1994). *J. Org. Chem.* **59**, 1638–1641
48. Biggs, J., Chapman, N.B. and Wray, V. (1971). *J. Chem. Soc. B* 71–74
49. Whalen, D.L., unpublished results
50. Richard, J.P. and Jencks, W.P. (1982). *J. Am. Chem. Soc.* **104**, 4689–4691
51. Audier, H.E., Dupin, J.F. and Jullien, J. (1966). *Bull. Soc. Chim. Fr.* **7**, 2811–2816
52. Audier, H.E., Dupin, J.F. and Jullien, J. (1968). *Bull. Soc. Chim. Fr.* **9**, 3850–3855
53. Mohan, R.S. and Whalen, D.L. (1993). *J. Org. Chem.* **58**, 2663–2669
54. Laird, R.M. and Parker, R.E. (1961). *J. Am. Chem. Soc.* **83**, 4277–4281
55. Audier, H.E., Dupin, J.F. and Jullien, J. (1968). *Bull. Soc. Chim. Fr.* **9**, 3844–3850
56. Battistini, C., Balsamo, A., Berti, G., Crotti, P., Macchia, B. and Macchia, F. (1974). *J. Chem. Soc. Chem. Commun.*, 712–713
57. Battistini, C., Crotti, P., Donatella, D. and Macchia, F. (1979). *J. Org. Chem.* **44**, 1643–1647
58. Crotti, P., Dell'Omodarme, G., Ferretti, M. and Macchia, F. (1987). *J. Am. Chem. Soc.* **109**, 1463–1469
59. Doan, L., Bradley, K., Gerdes, S. and Whalen, D.L. (1999). *J. Org. Chem.* **64**, 6227–6234
60. Amyes, T.L., Stevens, L.W. and Richard, J.P. (1993). *J. Org. Chem.* **58**, 6057–6066
61. Sampson, K., Paik, A., Duvall, B. and Whalen, D.L. (2004). *J. Org. Chem.* **69**, 5204–5211
62. Balsamo, A., Berti, G., Crotti, P., Ferretti, M., Macchia, B. and Macchia, F. (1974). *J. Org. Chem.* **39**, 2596–2598
63. Whalen, D.L. and Ross, A.M. (1976). *J. Am. Chem. Soc.* **98**, 7859–7861
64. Richard, J.P., Amyes, T.L. and Toteva, M.M. (2001). *Acc. Chem. Res.* **34**, 981–988
65. Whalen, D., Doan, L., Poulose, B., Friedman, S., Gold, A., Sangaiah, R., Ramesha, A., Sayer, J. and Jerina, D.M. (2000). *Polycycl. Aromat. Hydrocarb.* **21**, 43–52
66. Becker, A.R., Janusy, J.M. and Bruice, T.C. (1979). *J. Am. Chem. Soc.* **102**, 5679–5687
67. Gillilan, R.E., Pohl, T.M. and Whalen, D.L. (1982). *J. Am. Chem. Soc.* **104**, 4481–4482
68. Goering, H.L. and Josephson, R.R. (1962). *J. Am. Chem. Soc.* **84**, 2779–2785

69. Sayer, J.M., Yagi, H., Silverton, J.V., Friedman, S.L., Whalen, D.L. and Jerina, D.M. (1982). *J. Am. Chem. Soc.* **104**, 1972–1978

70. (a) Doan, L. and Whalen, D.L., unpublished results; (b) Chini, M., Crotti, P., Ferretti, M. and Macchia, F. (1988). *Tetrahedron*, **44**, 2001–2004

71. Swain, C.G. (1951). *J. Am. Chem. Soc.* **74**, 4108–4110

72. Long, F.A. and Paul, M.A. (1957). *Chem. Rev.* **57**, 935–1010

73. Pocker, Y. and Ronald, B.P. (1978). *J. Am. Chem. Soc.* **100**, 3122–3127

74. Fife, T.H. (1972). *Acc. Chem. Res.* **5**, 254–272

75. (a) Fife, T.H. and Jao, L.K. (1968). *J. Am. Chem. Soc.* **90**, 4081–4085; (b) Fife, T.H. and Brod, L.H. (1970). *J. Am. Chem. Soc.* **92**, 1681–1684; (c) Anderson, E. and Capon, B. (1969). *J. Chem. Soc. B*, 1033–1037

76. Anderson, E. and Fife, T.H. (1969). *J. Am. Chem. Soc.* **91**, 7163–7166

77. Fife, T.H. (1967). *J. Am. Chem. Soc.* **89**, 3228–3231

78. Fife, T.H. and Hutchins, H.E.C. (1976). *J. Am. Chem. Soc.* **98**, 2536–2543

79. Mori, A.L. and Schaleger, L.L. (1972). *J. Am. Chem. Soc.* **94**, 5039–5043

80. (a) Dunn, B.M. and Bruice, T.C. (1971). *J. Am. Chem. Soc.* **93**, 5725–5731; (b) Vitullo, V.P. and Grossman, N.R. (1973). *J. Org. Chem.* **38**, 179–180

81. Kresge, A.J. and Chiang, Y. (1973). *J. Am. Chem. Soc.* **95**, 803–806

82. Whalen, D.L., Weimaster, J.F., Ross, A.M. and Radhe, R. (1976). *J. Am. Chem. Soc.* **98**, 7319–7324

83. Bruice, P.Y., Bruice, T.C., Dansette, P., Selander, H.G., Yagi, H. and Jerina, D.M. (1976). *J. Am. Chem. Soc.* **98**, 2965–2973

84. Mohan, R.S. and Whalen, D.L., unpublished results

85. Kasperek, G.J. and Bruice, T.C. (1972). *J. Am. Chem. Soc.* **94**, 198–202

86. Sayer, J.M., Grossman, S.J., Adusei-Poku, K.S. and Jerina, D.M. (1988). *J. Am. Chem. Soc.* **110**, 5068–5074

87. Whalen, D.L., Ross, A.M., Montemarano, J.A., Thakker, D.R., Yagi, H. and Jerina, D.M. (1979). *J. Am. Chem. Soc.* **101**, 5086–5088

88. Lin, B., Islam, N., Friedman, S., Yagi, H., Jerina, D.M. and Whalen, D.L. (1998). *J. Am. Chem. Soc.* **120**, 4327–4333

89. Islam, N.B., Gupta, S.C., Yagi, H., Jerina, D.M. and Whalen, D.L. (1990). *J. Am. Chem. Soc.* **112**, 6363–6369

90. (a) Gupta, S.C., Pohl, T.M., Friedman, S.L., Whalen, D.L., Yagi, H. and Jerina, D.M. (1982). *J. Am. Chem. Soc.* **104**, 3101–3104; (b) Gupta, S.C., Islam, N., Whalen, D.L., Yagi, H. and Jerina, D.M. (1987). *J. Org. Chem.* **52**, 3812–3815

91. (a) Jerina, D.M., Daly, J., Witkop, B., Zaltaman-Nirenberg, P. and Udenfriend, S. (1968). *Arch. Biochem. Biophys.* **128**, 176–183; (b) Jerina, D.M., Daly, J.W., Witkop, B., Zaltaman-Nirenberg, P. and Udenfriend, S. (1970). *Biochemistry* **9**, 147–156; (c) Jerina, D.M., Daly, J.W. and Witkop, B. (1968). *J. Am. Chem. Soc.* **90**, 6523–6525; (d) Jerina, D.M., Daly, J.W., Witkop, B., Zaltaman-Nirenberg, P. and Udenfriend, S. (1968). *J. Am. Chem. Soc.* **90**, 6525–6527; (e) Boyd, D.R., Jerina, D.M. and Daly, J.W. (1970). *J. Org. Chem.* **35**, 3170–3172

92. Kasperek, G.J. and Bruice, T.C. (1972). *J. Am. Chem. Soc.* **94**, 198–202

93. Boyd, D.R., Daly, J.W. and Jerina, D.M. (1972). *Biochemistry* **11**, 1961–1966

94. Kasperek, G.J. and Bruice, T.C. (1972). *J. Chem. Soc. Chem. Comm.*, 784–785

95. Kasperek, G.J., Bruice, T.C., Yagi, H., Kaubisch, N. and Jerina, D.M. (1972). *J. Am. Chem. Soc.* **94**, 7876–7882

96. (a) Bruice, P.Y., Kasperek, G.J. and Bruice, T.C. (1973). *J. Am. Chem. Soc.* **95**, 1673–1674; (b) Kasperek, G.J., Bruice, P.Y., Bruice, T.C., Yagi, H. and Jerina, D.M. (1973). *J. Am. Chem. Soc.* **95**, 6041–6046; (c) Vögel, E. and Günther, H. (1967). *Angew. Chem. Int. Ed. Engl.* **6**, 385–401

97. Whalen, D.L. and Ross, A.M. (1974). *J. Am. Chem. Soc.* **96**, 3678–3679

98. Gillilan, R.E., Pohl, T.M. and Whalen, D.L. (1982). *J. Am. Chem. Soc.* **104**, 4482–4484

99. Sridharan, S. and Whalen, D. L., unpublished results

100. Coxon, J.M., Maclagan, R.G.A.R., Rauk, A., Thorpe, A.J. and Whalen, D.L. (1997). *J. Am. Chem. Soc.* **119**, 4712–4718

101. Whalen, D.L., Montemarano, J.A., Thakker, D.R., Yagi, H. and Jerina, D.M. (1977). *J. Am. Chem. Soc.* **99**, 5522–5524

102. Doan, L., Lin, B., Yagi, H., Jerina, D.M. and Whalen, D.L. (2001). *J. Am. Chem. Soc.* **123**, 6785–6791

103. Jencks, W.P. (1972). *J. Am. Chem. Soc.* **94**, 4731–4732

104. Jencks, W.P. (1980). *Acc. Chem. Res.* **13**, 161–169

105. Woodward, R.B. and Hoffman, R. (1970). *The Conservation of Orbital Symmetry*. Verlag Chemie, GmbH, Academic Press

106. (a) Ukachukwu, V.C., Blumenstein, J.J. and Whalen, D.L. (1986). *J. Am. Chem. Soc.* **108**, 5039–5040; (b) Ukachukwu, V.C. and Whalen, D.L. (1988). *Tetrahedron Lett.* **29**, 293–296

107. Mohan, R.S., Gavardinas, K., Kyere, S. and Whalen, D.L. (2000). *J. Org. Chem.* **65**, 1407–1413

108. Mohan, R.S. and Whalen, D.L. (1993). *Org. Chem.* **58**, 2663–2669

109. Ritchie, C.D. and Virtanen, P.O.I. (1972). *J. Am. Chem. Soc.* **94**, 4966–4971

110. Ritchie, C.D. (1972). *Acc. Chem. Res.* **5**, 348–354

111. Whalen, D.L., Ross, A.M., Dansette, P.M. and Jerina, D.M. (1977). *J. Am. Chem. Soc.* **99**, 5672–5676

112. Nashed, N.R., Balani, S.K., Loncharich, R.J., Sayer, J.M., Shipley, D.Y., Mohan, R.S., Whalen, D.L. and Jerina, D.M. (1991). *J. Am. Chem. Soc.* **113**, 3910–3919

113. Lin, B., Doan, L., Yagi, H., Jerina, D.M. and Whalen, D.L. (1994). *Chem. Res. Toxicol.* **11**, 630–638

114. Richard, J.P. and Jencks, W.P. (1982). *J. Am. Chem. Soc.* **104**, 4689–4691

115. For a review and discussion of literature data for reactions of carbocations with azide ion, see: Ta-Shma, R. and Rappoport, Z. (1983). J. Am. Chem. Soc. **105**, 6082–6095

116. (a) Yagi, H., Hernandez, O. and Jerina, D.M. (1975). *J. Am. Chem. Soc.* **97**, 6881–6883; (b) Whalen, D.L., Ross, A.M., Yagi, H., Karle, J.M. and Jerina, D.M. (1978). *J. Am. Chem. Soc.* **100**, 5218–5221

117. Doan, L., Yagi, H., Jerina, D.M. and Whalen, D.L. (2002). *J. Am. Chem. Soc.* **124**, 14382–14387

118. Doan, L., Yagi, H., Jerina, D.M. and Whalen, D.L. (2004). *J. Org. Chem.* **69**, 8012–8017

119. (a) Curtin, D.Y. (1954). *Rec. Chem. Prog.* **15**, 111; (b) Eliel, E.L. (1962). *Stereochemistry of Carbon Compounds*, pp. 151–152, McGraw-Hill, New York

Mechanistic studies on enzyme-catalyzed phosphoryl transfer

Alvan C. Hengge

Department of Chemistry and Biochemistry, Utah State University, Logan, UT, USA

Abstract

Phosphoryl transfer reactions have essential roles throughout biochemistry. The enzymes that catalyze these reactions result in tremendous rate enhancements for their normally unreactive substrates. This fact has led to great interest in the enzymatic mechanisms, and debate as to whether the mechanisms for enzyme-catalyzed hydrolysis of phosphate esters differ from those of uncatalyzed reactions. This review summarizes the uncatalyzed reactions of monoesters, diesters and triesters. A selection of enzymatic phosphoryl transfer reactions that have been the most studied and are the best understood are discussed, with examples of phosphatases, diesterases, and triesterases.

1 Introduction

As stated in the opening words of a 1987 Science article by Frank Westheimer, "phosphate esters and anhydrides dominate the living world."[1] That article discusses the unique properties of these phosphoric acid derivatives that allow them to fill their many roles in biochemistry. Phosphate esters have well-known roles in genetic materials, in coenzymes, and in energy reservoirs, and as intermediates in biochemical transformations. In addition, research in recent years has revealed the tremendous role played by protein phosphorylation in the regulation of a host of processes including cell division, differentiation and development, metabolism, learning, and memory. It has been estimated that one-third of all proteins in organisms undergo reversible phosphorylation, often at multiple sites.[2]

Phosphoric acid may be esterified in one, two, or three positions, forming a monoester, diester, or triester, respectively (Fig. 1). The kinetic stability of monoesters and diesters is a major factor in their suitability for biological roles. The hydrolysis of phosphate esters is thermodynamically favorable, but the negative charge of ionized monoesters and diesters repel nucleophiles. As a result, they are very stable kinetically. The half-life for attack of water on alkyl phosphate dianions is $\sim 1.1 \times 10^{12}$ years ($k = 2 \times 10^{-20}\,\mathrm{s}^{-1}$) at $25\,^{\circ}\mathrm{C}$.[3] Such species (serine or threonine phosphate, along with the aryl counterpart tyrosine phosphate) are the substrates for phosphatases involved in signal transduction and regulation, which produce the largest enzymatic rate enhancements ($\sim 10^{21}$-fold) that have yet been identified relative to the uncatalyzed reactions of their substrates. Enzymatic phosphodiester hydrolysis is similarly impressive. The rate for the uncatalyzed hydrolysis of the diester dimethyl phosphate at $25\,^{\circ}\mathrm{C}$ is estimated at $10^{-15}\,\mathrm{s}^{-1}$.[4] Comparison with reported kinetic constants for the reaction catalyzed by staphylococcal nuclease indicate that this enzyme raises the rate of P–O bond fission in its diester substrate by 10^{16}-fold, as a lower estimate.[5]

These tremendous rate enhancements have led to speculations that enzymatic phosphoryl transfer might proceed by altered mechanisms, or different transition states, than the uncatalyzed reactions. This review will begin by describing what is known about the mechanisms of phosphoryl transfer in solution, followed by a

$$
\begin{array}{ccc}
\mathrm{O} & \mathrm{O} & \mathrm{O} \\
\parallel & \parallel & \parallel \\
\mathrm{HO-P-OR} & \mathrm{HO-P-OR} & \mathrm{RO-P-OR} \\
\mid & \mid & \mid \\
\mathrm{OH} & \mathrm{OR} & \mathrm{OR}
\end{array}
$$
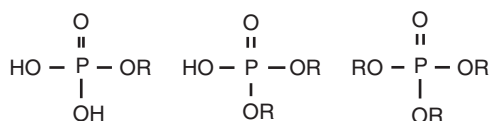
Fig. 1 From left to right, the structures of a phosphate monoester, diester, and triester. Depending upon pH, monoesters may be neutral, monoanionic, or dianionic; diesters may be neutral or anionic. The first pK_a of an alkyl phosphomonoester, and the pK_a of a dialkyl diester, is ~ 2. The second pK_a of an alkyl monoester is ~ 6.8. Oxygen atoms bonded to ester groups (OR) are called bridging oxygen atoms; the other oxygen atoms are nonbridging. Thus, a triester has one nonbridging oxygen atom, an ionized diester has two, and a fully ionized monoester has three.

Dissociative ($D_N + A_N$):

metaphosphate
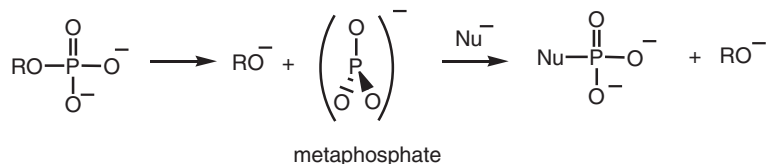
Associative ($A_N + D_N$):
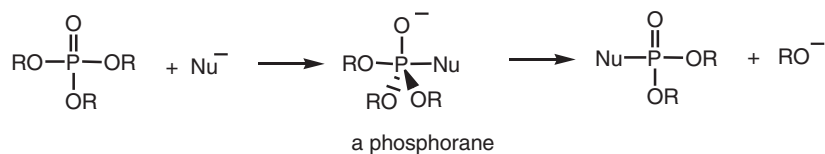
a phosphorane
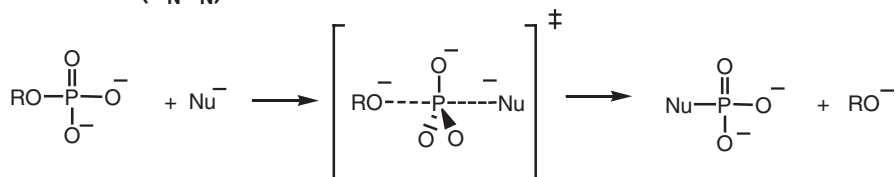
Concerted ($A_N D_N$):

Fig. 2 The dissociative, associative, and concerted mechanistic pathways of phosphoryl transfer. The dissociative and concerted mechanisms are shown for the dianion form of a phosphomonoester. The associative mechanism is shown for a phosphotriester.

summary of a portion of the enzymatic phosphoryl transfer literature. This field is too voluminous and ever-growing for a comprehensive coverage, so this review will focus on enzymatic reactions that have been the most studied and are the best understood, with examples of enzymatic reactions of phosphomono-, di-, and triesters.

MECHANISTIC POSSIBILITIES FOR PHOSPHORYL TRANSFER

Phosphoryl transfer reactions are substitution reactions at phosphorus, and can occur by three limiting mechanisms (Fig. 2). One is a dissociative, S_N1-type mechanism, designated $D_N + A_N$ in the IUPAC nomenclature.[6] In this mechanism, a stable metaphosphate ion (PO_3^{1-}) forms that is attacked by a nucleophile in a subsequent step. Metaphosphate is usually represented as structure (a) in Fig. 3, but computational studies indicate that the phosphorus and oxygen atoms bear significant partial charges.[7,8] This, and data from isotope effects,[9] suggest that metaphosphate is more properly represented as a resonance hybrid of the three structures shown in Fig. 3, the major contributors being (b) and (c). If so, the P–O bond order in metaphosphate is little changed from that between phosphorus and the nonbridge oxygen atoms in a phosphomonoester.
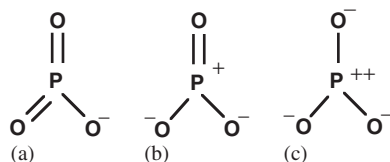
Fig. 3 Resonance contributors for metaphosphate ion.
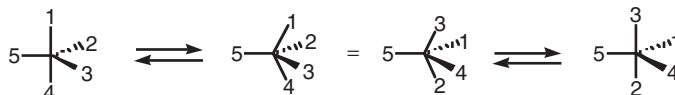
Scheme 1 During pseudorotation, a pair of equatorial ligands exchange with the apical ligands in a concerted fashion via the intermediacy of a tetragonal–pyramidal transition state. The pivot point is one of the equatorial ligands (in the example above). This process can be visualized as one in which the two apical ligands (1 and 4) undergo a motion in which their bond angles close down from 180° to 120°, and two equatorial ligands (2 and 3) open their bond angles from 120° to 180°.

Other phosphoryl transfer mechanisms are an associative, two-step mechanism $(A_N + D_N)$; and a concerted mechanism $(A_N D_N)$ with no intermediate. The $A_N + D_N$ mechanism is an addition–elimination pathway in which a stable pentacoordinate intermediate, called a phosphorane, is formed. This mechanism occurs in some reactions of phosphate triesters and diesters, and has been speculated to occur in enzymatic reactions of monoesters. In the concerted $A_N D_N$ mechanism, bond formation to the nucleophile and bond fission to the leaving group both occur in the transition state. This transition state could be loose or tight, depending upon the synchronicity between nucleophilic attack and leaving group departure. The concerted mechanism of Fig. 2 is drawn to indicate a loose transition state, typical of phosphate monoester reactions.

Phosphate esters, as well as other compounds of phosphorus in the same oxidation state and bearing a formal double bond to phosphorus, are tetrahedral. The addition of a nucleophile can result in a pentacoordinate phosphorane intermediate with a trigonal bipyramidal geometry. If nucleophilic addition and leaving group departure occur in the same step, then the transition state is similarly trigonal bipyramidal, but with extended distances to the apical groups. Although there are some exceptions when steric constraints demand, it is generally accepted that nucleophiles add, and leaving groups depart, from the apical positions. Thus, in a concerted process, these two groups and the phosphorus atom must assume an "in-line" orientation, and nucleophilic substitution will result in inversion of configuration if the phosphorus atom is chiral. The reorganization of apical and equatorial ligands of a phosphorane can occur by a process termed pseudorotation[10] illustrated in Scheme 1. In an $A_N + D_N$ mechanism, nucleophilic addition, if followed by pseudorotation to bring the leaving group from an equatorial into an apical

position, will result in retention of stereochemistry if the phosphorus is chiral. Thus, the observation of retention requires that a phosphorane intermediate forms and subsequently undergoes pseudorotation. Inversion of stereochemistry does not require that a reaction is concerted, but it does impose the condition that if a phosphorane intermediate forms, leaving group departure must occur before pseudorotation can take place. This carries the requirement that the leaving group must reside in an apical position in the phosphorane that forms as a result of nucleophilic addition. Further details pertinent to the pseudorotation phenomenon can be found in other reviews, and references therein.[11,12]

NOMENCLATURE ISSUES

Care must be taken in the description of mechanisms in any reaction, and particularly for phosphoryl transfer reactions, where there are a number of mechanistic possibilities. There has been confusion in the use of the terms associative and dissociative in the literature, particularly in enzyme-catalyzed phosphoryl transfer. An associative *mechanism* is an addition–elimination, $A_N + D_N$ process. Many authors have described transition states as associative based on the degree of bond formation to the nucleophile, regardless of whether or not a pentavalent intermediate forms. Similarly, a transition state characterized by extensive bond fission to the leaving group and little bond formation to the nucleophile is often called a dissociative transition state, even when a metaphosphate intermediate does not form. It seems a poor idea to use the terms associative or dissociative to describe *transition states*, since these terms can be taken to imply an associative or dissociative *mechanism*. In this review, transition states will be described as loose or tight, depending on the sum of the bond orders to incoming nucleophile and the departing leaving group. In a phosphoryl transfer reaction (or, for that matter, any substitution reaction) this sum is 1 in the reactant and product states. In an addition intermediate this bond order sum is 2. A tight transition state is one in which bond formation to the nucleophile is more advanced than leaving group bond fission, giving a sum of >1. In a loose transition state, this sum is <1. This is merely a way of describing in words what is conveyed in a More-O'Ferrall–Jencks diagram[13,14] (Fig. 4).

2 Uncatalyzed reactions of phosphomonoesters

Depending upon pH, a phosphate monoester exists as a neutral, monoanionic, or dianionic species. The neutral form is present only under very acidic conditions, and the reactions of neutral monoesters have not been subjected to much study. With the exception of monoesters with highly activated leaving groups like 2,4-dinitrophenol, the dianion is much less reactive than the monoanion.[15]
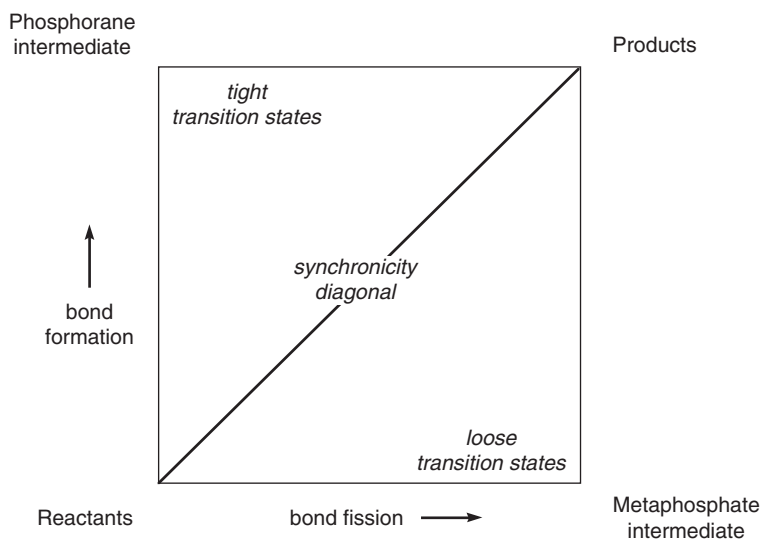
Fig. 4 A transition state for phosphoryl transfer in which bond fission is ahead of bond formation to the phosphoryl acceptor (nucleophile) is loose, and resides in the lower right region. In the reverse situation a tight transition state results in the upper left region. If the sum of bond order to nucleophile plus leaving group is unity, the transition state will lie on the synchronicity diagonal.

DIANIONS OF PHOSPHOMONOESTERS

When the phosphoryl group is fully deprotonated a monoester is in the dianion form, except for phosphorylated pyridines, which carry a formal net charge of −1. A large body of evidence indicates that esters with a dianionic phosphoryl group, including acyl phosphates and phosphorylated pyridines,[16] undergo phosphoryl transfer via a concerted process with a loose transition state. The supporting data include near zero entropies of activation, small dependencies of rates on nucleophile basicity (low Brønsted β_{nuc} values) and large dependencies of rates on leaving group pK_a (β_{lg}),[15] and large $^{18}k_{bridge}$ isotope effects[9,17] (Fig. 5 shows the isotope effect designations[18]). Despite very loose transition states, there is no evidence for the formation of free metaphosphate.[16] The collected evidence in favor of this mechanism has been reviewed.[19,20] When the phosphoryl group is made chiral using ^{16}O, ^{17}O, and ^{18}O, phosphoryl transfer occurs with inversion of configuration except in the very nonnucleophilic solvent and phosphoryl acceptor t-butanol, where racemic t-butyl phosphate forms from chiral p-nitrophenyl phosphate (pNPP).[21,22] The reaction in t-butanol also exhibits a significantly more positive entropy of activation, +24 eu,[23] compared to +0.3 eu[24] for the aqueous hydrolysis. These data suggest that the reaction in t-butanol has become a two-step $D_N + A_N$ mechanism with a metaphosphate intermediate. The β_{lg} value ($\beta_{lg} = -1.2$) is similar for the two reactions, and the kinetic isotope effects (KIEs) in the nonbridging phosphoryl oxygen atoms ($^{18}k_{nonbridge}$), the bridging oxygen ($^{18}k_{bridge}$), and in the nitrogen atom (^{15}k),

a) The nonbridge oxygen atoms ($^{18}k_{nonbridge}$)

b) The bridge oxygen atom, of the scissile bond ($^{18}k_{bridge}$)

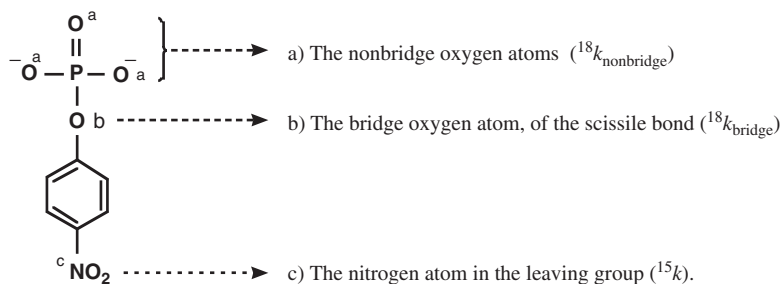c) The nitrogen atom in the leaving group (^{15}k).

Fig. 5 The designation and location of kinetic isotope effects measured on reactions of phosphate esters. Diesters have two, and triesters have one nonbridging oxygen atom, respectively. $^{18}k_{nonbridge}$ gives an indication of the state of the phosphoryl group; loss of a pi-bond to form a phosphorane results in a normal $^{18}k_{nonbridge}$, while a metaphosphate-like transition state exhibits a slight inverse effect. $^{18}k_{bridge}$ is sensitive to the extent of P–O(R) bond fission. Protonation of the leaving group in the transition state reduces the magnitude of this effect. When the leaving group is *p*-nitrophenol, ^{15}k measures negative charge delocalized into the aromatic moiety. The table below gives some expected KIEs for representative extremes of transition state structure. Normal isotope effects are >1, inverse isotope effects are <1.

Leaving group KIEs	*Loose TS*: Extensive leaving group bond fission, no protonation	For *p*-nitrophenol, $^{15}k \approx 1.003$, $^{18}k_{bridge} \approx 1.03$. Maximum $^{18}k_{bridge}$ is larger for alkyl-leaving groups; for *m*-nitrobenzyl alcohol, $^{15}k = 1$, maximum $^{18}k_{bridge} \approx 1.05$
	Tight TS: Phosphoryl group resembles pentacoordinate phosphorane, no bond fission to leaving group	$^{15}k \approx 1.000$, $^{18}k_{bridge} \approx 1.000$
Nonbridge KIEs	*Loose TS*: Metaphosphate-like phosphoryl group	Small, inverse $^{18}k_{nonbridge} \approx 0.995$
	Tight TS: Phosphoryl group resembles pentacoordinate phosphorane	Normal $^{18}k_{nonbridge}$ up to 1.04[25]

TS: transition state.

corrected for the difference in temperature at which the KIEs were measured, are also similar[9] (Table 1, Fig. 5).

This indicates a similar transition state in terms of leaving group bond fission for the reactions in water and in *t*-butanol. Fig. 6 shows a More-O'Ferrall–Jencks diagram with the loose transition state for the aqueous hydrolysis denoted in the lower right-hand region. The reaction in *t*-butanol proceeds along the bottom axis via the intermediate in the lower right corner.

Table 1   KIEs for phosphoryl transfer from pNPP to water and to t-butanol[9]

Reaction	^{15}k	$^{18}k_{\text{bridge}}$	$^{18}k_{\text{nonbridge}}$
pNPP dianion, H_2O, 95 °C	1.0028 ± 0.0002	1.0189 ± 0.0005	0.9994 ± 0.0005
pNPP dianion, t-butanol, 30 °C	1.0039 ± 0.0003	1.0202 ± 0.0008	0.9997 ± 0.0016

The reaction is several orders of magnitude faster in t-butanol, necessitating different temperatures for the two experiments.

The data and mechanistic conclusions summarized above come from work with aryl phosphomonoesters; as predicted by the steep β_{lg} value, alkyl ester dianions react at very slow rates. A recent study of methyl phosphate found the rate of the dianion hydrolysis to be below the threshold of detectability, with an estimated rate constant of $2 \times 10^{-20}\,\text{s}^{-1}$ at 25 °C.[3] Since this value is close to the rate predicted from an extrapolation of the Brønsted plot of aryl phosphomonoester dianions, a similar mechanism is likely to be followed for alkyl and aryl esters.

In a tight transition state, negative charge on the phosphoryl group increases. Thus, interactions with metal ions or positively charged amino acids, which are found at the active sites of enzymes that catalyze phosphoryl transfers, would intuitively favor an associative mechanism.

This simple approach neglects the influence of geometrical differences in the phosphoryl group in the ground state and transition state, which have been shown to have the potential to result in preferential enzymatic stabilization of a loose, metaphosphate-like transition state.[26,27] While there have been many reports of the accelerating effect of metal ions on phosphoester hydrolysis,[28–31] few of these reactions have been studied mechanistically to ascertain how the transition state for phosphoryl transfer might have been affected.

Do metal ions change the mechanism of phosphoryl transfer? The results are mixed. It has been shown that Mg^{2+} or Ca^{2+} ions do not alter the loose transition states for the hydrolysis of aryl phosphate monoesters[32] or of ATP.[33] Kinetic experiments with $Co(en)_2(OH)p$NPP, with $Co(NH_3)_5p$NPP, and with a Co(cyclen) complex, in all of which pNPP is complexed in a monodentate fashion to Co(III), are consistent with either concerted mechanisms, or stepwise mechanisms via phosphorane intermediates.[34,35] In these reactions the phosphoryl transfer is to an adjacent, coordinated nucleophile. KIE experiments with these complexes[36] are more consistent with a concerted mechanism, with a transition state not significantly different from the uncatalyzed hydrolysis. However, for $Co(NH_3)_5p$NPP complex, the leaving group KIEs are smaller and $^{18}k_{\text{nonbridge}}$ values are small and normal, indicating a tighter transition state for the reaction of this complex, in which the nucleophile is more basic than in the other two.

KIEs, including the ^{18}O nucleophile KIE, show that pNPP coordinated to a dinuclear Co(III) complex (Fig. 7) reacts by a single-step, concerted mechanism with significantly more nucleophilic participation in the transition state than the hydrolysis of the uncomplexed ester.[37] Labeling studies using ^{18}O show that the model complex uses one of the bridging oxygen atoms as a nucleophile.[38] This dicobalt
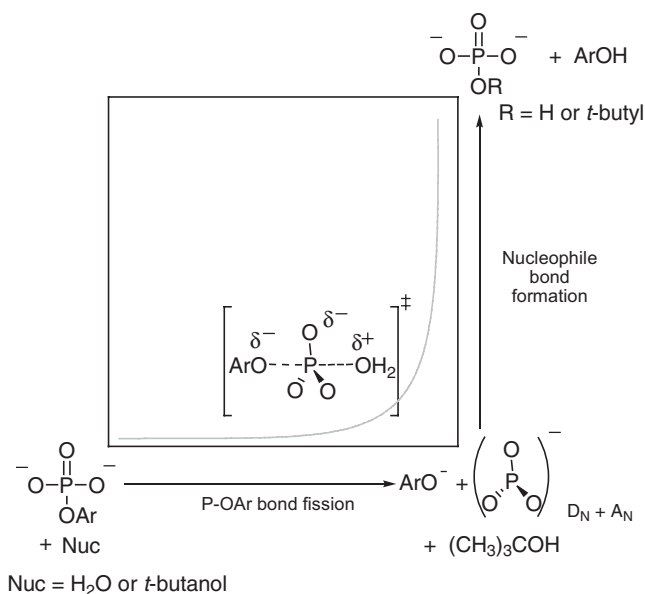
Fig. 6 More-O'Ferrall–Jencks diagram illustrating the mechanisms for the reactions of aryl phosphates with water (hydrolysis) and *t*-butanol. The hydrolysis reaction is concerted but not synchronous; in the transition state, bond fission to the leaving group is ahead of bond formation to the nucleophile. In *t*-butanol, *p*-nitrophenyl phosphate undergoes reaction by a two-step $D_N + A_N$ mechanism. The transition state for the rate-limiting first step is similarly late with regard to leaving group bond fission.
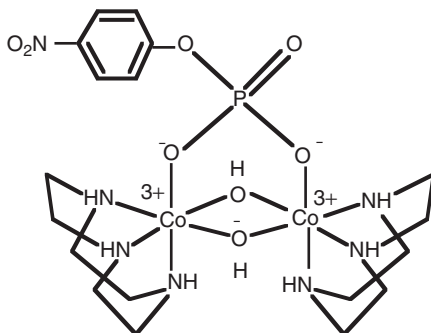
Fig. 7 *p*NPP coordinated to a complex that mimics the geometry of the binuclear metal centers of a number of phosphatases.

complex has been shown to greatly accelerate the reactions of both coordinated phosphodiesters and monoesters. For *p*NPP, coordination provides a rate enhancement of $\sim 10^{12}$.[38]

The KIE results show that coordination to a metal center can change the transition state for phosphoryl transfer, although it must be pointed out that Co(III) is a

stronger Lewis acid than the metal ions found in enzymes that catalyze phosphoryl transfer.

MONOANIONS OF PHOSPHOMONOESTERS

Linear free-energy relationships (LFER) with monoanionic phosphorylated pyridines indicate a loose transition state in which metaphosphate is not an intermediate.[16] The hydrolysis of the monoanion of 2,4-dinitrophenyl phosphate is thought to be concerted,[39] but the possibility of a metaphosphate intermediate has not been ruled out with esters having less activated leaving groups. A stereochemical study of the hydrolysis of phenyl phosphate monoanion indicates that the reaction proceeds with inversion.[21] This result implies either a concerted mechanism, or a discrete metaphosphate intermediate in a pre-associative mechanism.

A small β_{lg} (–0.27)[15] for the hydrolysis of monoanions suggests that the leaving group is protonated in the transition state. There has been some debate over the timing of proton transfer and P–O bond fission. Kirby[15] proposed that for less basic leaving groups, protonation occurs simultaneously with leaving group departure and is partially rate-limiting, while for more basic leaving groups, a bridge-protonated intermediate forms followed by rate-limiting P–O bond fission. Either timing of proton transfer and P–O(R) bond fission could occur in concert with nucleophilic attack, or with formation of metaphosphate (Fig. 8).

A solvent isotope effect (k_{H2O}/k_{D2O}) of 1.45 for the hydrolysis of 2,4-dinitrophenyl phosphate monoanion,[15] suggests that proton transfer occurs in the rate-limiting step of the hydrolysis of this ester, but not in the hydrolysis of the methyl phosphate monoanion, where $^D k$ is 0.87.[40] Similar small inverse solvent isotope effects are found for the hydrolyses of the monoanions of pNPP (0.96 ± 0.01) and m-nitrobenzyl phosphate (mNBP) (0.94 ± 0.01).[41] In general, a proton in flight in the transition state manifests itself in a normal k_{H2O}/k_{D2O}. This would suggest that the reactions exhibiting inverse values for k_{H2O}/k_{D2O} proceed by a mechanism in which proton transfer occurs in a pre-equilibrium step, prior to P–O bond fission. However, exceptions are known; there is precedent for a very early or late transition state resulting in a very small primary KIE which is then masked by fractionation factors to give an inverse observed effect. The acid-catalyzed hydrolysis of ortho esters [42,43] has an observed k_{H2O}/k_{D2O} of 0.7,[43] despite being general acid catalyzed.[44] This was ascribed to a KIE of near unity in a very late transition state for proton transfer from hydronium ion, and an inverse secondary isotope effect arising from fraction factors.[43] The primary $^{18}k_{bridge}$ isotope effect in the hydrolysis of mNBP monoanion (0.9981 ± 0.0002) gives additional information. The magnitude of $^{18}k_{bridge}$ is affected by protonation (which produces an inverse effect) and P–OR bond fission (a normal effect). The inverse value implies that protonation is ahead of P–OR bond fission, either in a pre-equilibrium step, or in the same step as P–OR fission. By contrast, for the hydrolysis of the monoanion of pNPP, the normal $^{18}k_{bridge} = 1.0094$ at 35 °C indicates a difference in the timing of proton transfer, or the synchronicity between proton transfer and P–O fission, in the two reactions.
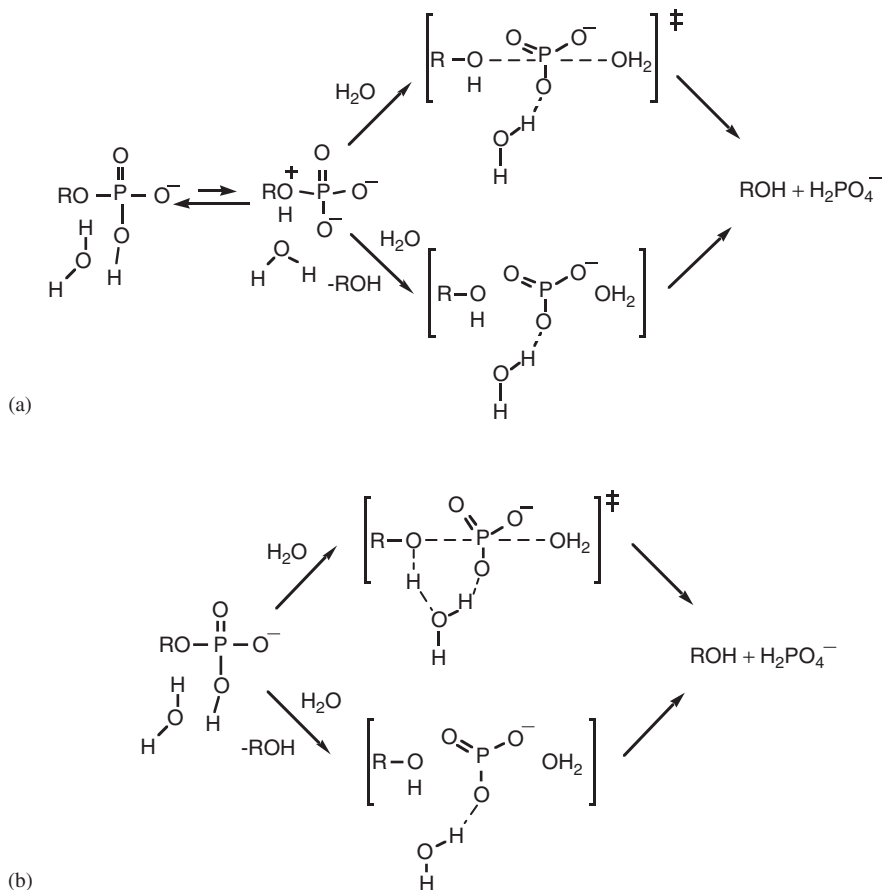
Fig. 8 Potential mechanisms for hydrolysis of phosphomonoester monoanions. In mechanism (a), proton transfer from the phosphoryl group to the ester oxygen (probably via the intermediacy of a water molecule) yields an anionic zwitterion intermediate. This may react in either concerted fashion (upper pathway) or via a discrete metaphosphate intermediate in a preassociative mechanism (bottom pathway). Mechanism (b) denotes proton transfer concerted with P–O(R) bond fission. As with (a), such a mechanism could either occur with concerted phosphoryl transfer to the nucleophile (upper pathway) or via a discrete metaphosphate intermediate in a preassociative mechanism (bottom pathway).

The hydrolysis reactions of monoanions share a key feature of the reaction of many enzymatic phosphoryl transfers, namely, protonation of the leaving group. For example, the protein–tyrosine phosphatases (PTPases) contain a conserved general acid, an aspartic acid residue, that swings into position to accomplish this task during catalysis. Ribonuclease (RNase) A utilizes a protonated histidine (His) to protonate the leaving group during phosphodiester cleavage. The catalytic benefit of leaving group protonation is a major reason why the uncatalyzed hydrolysis of

phosphomonoesters exhibits a pH optimum at pH $\sim$ 4, where concentration of the monoanion is highest.

3   Uncatalyzed reactions of phosphodiesters

As with monoesters, the majority of mechanistic studies have been carried out with diesters bearing an activated, i.e. aryl, leaving group. The reaction rates of various nucleophiles with a series of aryl methyl phosphate diesters is sensitive to both the nucleophile and the leaving group, which has been taken as evidence for a concerted mechanism.[45,46] The Brønsted β_{nuc} for attack by substituted pyridines and oxyanions on methyl 2,4-dinitrophenyl phosphate is 0.31, intermediate between the β_{nuc} for attack on the triester $ArOP(O)(OCH_3)_2$ and the monoester dianion $ArOPO_3^{2-}$. For attack by substituted pyridine nucleophiles on diesters of the form $ArOP(O)(OCH_3)O^-$, the leaving group dependence, β_{lg}, ranges from –0.98 to –1.06. The β_{lg} for the alkaline hydrolysis is somewhat smaller, –0.64, in keeping with Hammond Postulate predictions that the stronger nucleophile should result in an earlier transition state.

KIEs also support a concerted mechanism for diesters with an aryl leaving group. The $^{18}k_{bridge}$ for the alkaline hydrolysis of several diesters of the type p-nitrophenyl-$OP(O)(OR)O^-$, where the second ester group R is alkyl or aryl, range from 1.004 to 1.006,[18] indicative of some bond fission in the transition state, but much less than in the very loose transition states of reactions of monoesters. In this respect, the KIEs mirror the comparative Brønsted β_{lg} values for diesters compared with monoesters. An observed nucleophile ^{18}O KIE of 6.8% (1.068 ± 0.007) is found for the attack of hydroxide on the diester thymidine-5′-pNPP.[47] This observed KIE consists of an equilibrium isotope effect of 1.040 for the deprotonation of water, and a 1.027 KIE for nucleophilic attack. The large normal KIE is evidence for direct attack by hydroxide in the rate-limiting step, and together with the presence of a normal ^{18}O KIE in the scissile oxygen atom, points to a concerted mechanism.

Together the Brønsted LFER and the KIE data indicate that transition states for phosphodiesters lie more toward the central area of the More-O'Ferrall–Jencks diagram of Fig. 4 than the monoester transition state. The precise location is dependent upon nucleophile and leaving group, but the reactions of diester anions are concerted and exhibit more nucleophilic participation in the transition state, and less bond fission to the leaving group, than monoesters.

P–O bond fission is the usual mode of attack by nucleophiles on phosphodiesters, although there are exceptions. The labile diester methyl-2,4-dinitrophenyl phosphate shows significant amounts of attack at aromatic carbon (nucleophilic aromatic substitution, with loss of methyl phosphate) in competition with attack at phosphorus, most notably with hydroxide and with primary amines.[46] Due to the small size of the methyl group it is sterically susceptible to nucleophilic attack in phosphate esters; the hydrolysis of the dimethyl phosphate anion occurs almost exclusively by C–O bond fission.[4] With larger or less labile leaving groups, even

p-nitrophenyl, attack at phosphorus seems to be the only pathway. An isotope labeling study of the alkaline hydrolysis of ethyl 4-NPP indicated only P–O fission occurs even at 1N [OH$^-$].[48]

As with aryl monoesters, methyl aryl phosphodiesters react significantly faster when coordinated to a dinuclear Co(III) complex (Fig. 9); the methyl pNPP complex reacts about 10^{11} times faster than the hydrolysis rate of the uncomplexed diester.[49,50] Mechanistic investigations revealed that the acceleration in rate is accompanied by a change in mechanism. A specific base mechanism, in which the nucleophile is a deprotonated bridging oxide, is indicated by pH-rate studies.[49] The β_{lg} of –1.38 for reactions of coordinated phosphodiesters is larger than the $\beta_{lg} = -0.64$ for the alkaline hydrolysis of uncoordinated phosphodiesters.[49] Large KIEs in the leaving group (both $^{18}k_{bridge}$ and ^{15}k) of complexed methyl pNPP indicate much greater P–O bond fission and more negative charge on the leaving group in the transition state than in the hydrolysis of uncomplexed alkyl-p-nitrophenyl phosphodiesters, consistent with the larger β_{lg}.[51] The large inverse nucleophile ^{18}O KIE of 0.937 ± 0.002 is most consistent with a mechanism in which the bond to the nucleophile has been fully formed before the rate-determining transition state.[51] This is best accommodated by a stepwise mechanism, in which nucleophilic attack occurs to form a coordinated phosphorane intermediate, followed by rate-limiting expulsion of the leaving group. In this mechanism, the observed nucleophile isotope effect is, in effect, an equilibrium isotope effect between the reactant shown in Fig. 9, and the phosphorane intermediate. Since there is no nucleophile bond formation taking place in the transition state, there is no imaginary frequency factor contribution to the isotope effect to counter the inverse zero point energy factor. In the transition state of the rate-limiting step, the P–O bond is substantially broken and there is a substantial negative charge on the departing nitrophenolate. Thus, coordination to the complex results in a change from a concerted to a stepwise mechanism.

Considerable study has been devoted to the reactions of dinucleotides and related molecules, like those in Fig. 10, because of the biological significance of RNA and interest in the mechanism of RNase, which catalyzes its cleavage. The β_{lg} values were measured for the cyclization reaction of a series of aryl esters 10A (to yield a 2′,3′ cyclic phosphate) under alkaline conditions. For the imidazole general
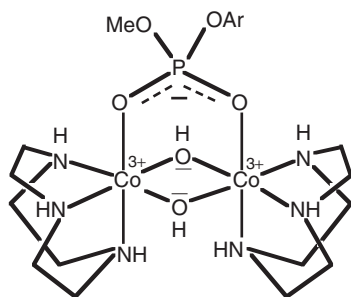

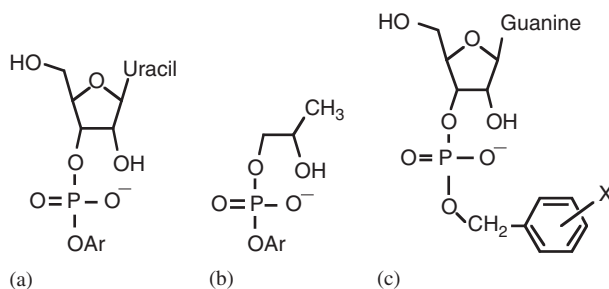Fig. 9   A dinuclear Co(III) complex that accelerates the reactions of coordinated methyl–aryl phosphodiesters.

Fig. 10 Chemical models for the cyclization of RNA.

base-catalyzed reaction, $\beta_{lg} = -0.59$, and for the hydroxide specific base reaction, $\beta_{lg} = -0.54$.[52] A very similar β_{lg} of –0.56 was found by Brown and Usher for the hydrolysis of 10B.[53] For the general base-catalyzed reaction of 10A, the dependency of rate on base strength yielded a Brønsted slope of $+0.67$. These data indicate that the general base acquires a charge of approximately $+0.67$ in the transition state, implying that the deprotonated nucleophile acquires a negative charge of similar magnitude.

Normalization of β_{lg} using the β_{eq} of 1.74 for the net reaction yields a Leffler α index of 0.34, indicating that only about a third of a negative charge is transmitted to the leaving group.[52] The rest of the negative charge resides either on the 2′-hydroxyl or the phosphoryl group. These data were taken as evidence for a concerted mechanism with a phosphorane-like transition state.

Rate constants extrapolated from the aryl compounds 10A agreed within an order of magnitude with those measured previously for less-activated compounds 10C.[54] This suggests a similar mechanism for this reaction whether the leaving group is alkyl or aryl. The β_{lg} value is –0.9, yielding a Leffler α for the cyclization of 10C of 0.5, compared to 0.34 for 10A. Under alkaline conditions, the fission of series of uridine-3′-alkylphosphates to form the 2′, 3′ cyclic phosphate yields a β_{lg} value of –1.28.[55] The fact that hydroxide-ion-catalyzed isomerization to yield a uridine-2′-alkylphosphate is not observed argues against the formation of a phosphorane intermediate, and the reaction is thought to proceed by a concerted mechanism with the attacking 2′ oxyanion nucleophile and the departing oxyanion occupying the apical positions in a trigonal bipyramidal phosphorane-like transition state. The more negative β_{lg} values observed in reactions of esters with alkyl leaving groups is consistent with expectations of a later transition state in a concerted reaction.

Under acidic conditions, the hydrolysis of phosphodiesters takes place via the neutral species, and a pentacoordinate intermediate is formed. The phosphoryl cleavage and migration reactions of dinucleotide-3′-phosphate diesters and related compounds have been examined by several groups, most recently by Lonnberg and co-workers.[56,57] Under acidic conditions, alkylphosphate migration (to form a 2′-phosphate diester) and cyclization (to the cyclic 2′,3′ phosphate) (Fig. 11) proceed at
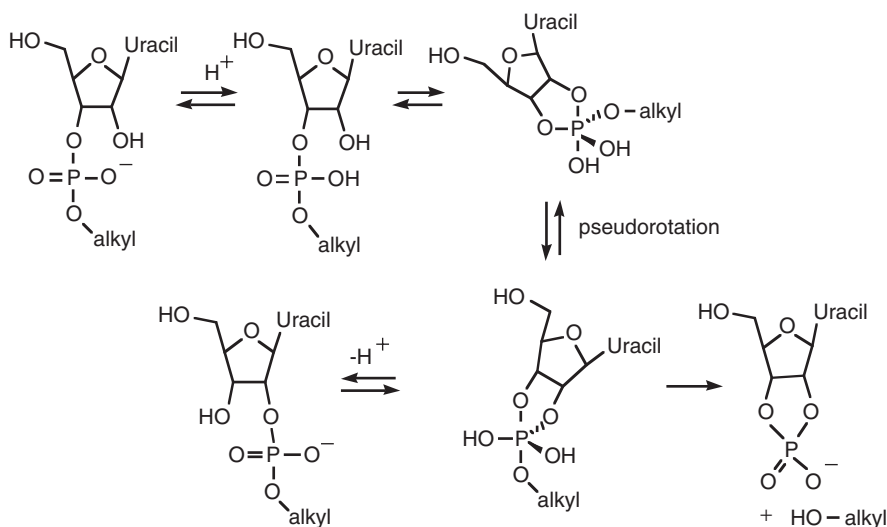
Fig. 11 The acid-catalyzed isomerization and cyclization reactions of uridine-3′-alkyl phosphates.

comparable rates via a common intermediate. The protonated (cationic) phosphate ester is the species attacked by the 2′-hydroxyl under strongly acidic conditions, and the neutral phosphodiester is the electrophile at lower acid concentrations. Near neutral pH, the diester is anionic, and a pH-independent isomerization of the diester is the major reaction. Under alkaline conditions, hydrolysis of the phosphodiester bond is the only reaction observed.[56,57] These reactions mirror the results obtained with the benzyl esters 10C.

The ^{18}O KIEs have been measured for the isomerization and cleavage reactions of uridine 3′-mNBP.[58] At pH 2.5, an inverse $^{18}k_{nonbridge}$ KIE of 0.9904 for the cleavage reaction is consistent with protonation of the phosphoryl group. The $^{18}k_{nonbridge}$ and $^{18}k_{bridge}$ KIEs are unity for the pH-independent isomerization at neutral pH. These indicate that no P–O(R) bond fission occurs in the rate-limiting step, and are consistent with protonation of a nonbridge oxygen atom (with an associated inverse nonbridge effect) and formation of a phosphorane (with a normal effect due to loss of a pi-bond). Thus, these KIEs support a stepwise mechanism with a monoanionic phosphorane intermediate. The isomerization reaction does not take place in anhydrous t-butanol, implying that solvent water is required for mediation of the proton transfer accompanying formation of the phosphorane intermediate. Finally, the $^{18}k_{bridge}$ of 1.0272 for the cleavage reaction at pH 10.5 is consistent with a concerted reaction in which the leaving group departs with a substantial negative charge.[58] This pH-dependent range of mechanisms is consistent with the notion that a dianionic phosphorane is viable as a transition state, but not an intermediate.[59]
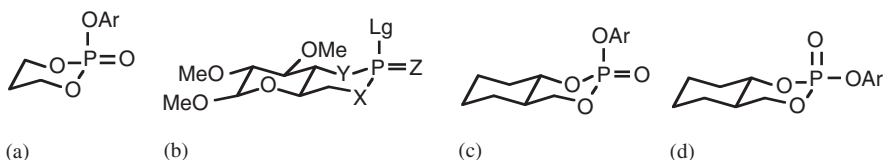
Fig. 12 Cyclic phosphotriesters used for mechanistic studies. In (b), the leaving group is denoted by Lg, Z is oxygen or sulfur. X and Y represent oxygen, sulfur, or N-methyl.

4 Uncatalyzed reactions of phosphotriesters

The kinetic stability of monoesters and diesters is due largely to their negative charge when ionized, which repels nucleophiles. Thus, it is not surprising that as neutral compounds, triesters are the most reactive of the three classes of phosphate esters. A significant portion of the mechanistic studies on triesters have been carried out using six-membered ring cyclic triesters (Fig. 12).[46] Such esters react at comparable rates to their acyclic counterparts, in contrast to five-membered cyclic phosphate esters, which react at much faster rates.

LFER for a series of esters (12a) showed that the dependency of the rate on the leaving group (β_{lg}) is smallest with the most basic oxyanion nucleophiles (such as hydroxide, for which $\beta_{lg} = -0.4$) and becomes more negative with less-basic nucleophiles (for acetate, $\beta_{lg} = -0.88$). This and other observations were interpreted to favor, although not require, a two-step mechanism involving a phosphorane intermediate.[46]

Stereochemical studies of related compounds (Fig. 12b), with various nucleophiles and leaving groups, show that whether the reaction occurs with retention or inversion of configuration depends not only on the nucleophile and leaving group, but also the solvent, counterions present, and other heteroatoms in the six-membered ring.[60] The latter effect is shown in the contrast between the displacement of p-nitrophenoxide by ethoxide, which proceeds predominantly (88%) by retention when X = O, but predominantly (68%) by inversion when X = N–CH$_3$ (Fig. 12b where Y and Z = O, Lg = p-nitrophenol).[60] Studies with analogs of Fig. 12b with both axial and equatorial orientations of Z and Lg revealed that the stereochemical outcome is independent of the initial axial or equatorial orientation of the leaving group.

In these reactions, retention can only be accommodated by formation of a phosphorane intermediate, followed by pseudorotation, before loss of the leaving group. Inversion could result either from a concerted reaction, or a stepwise process, if the phosphorane collapses before pseudorotation can occur. The stereochemical and LFER data indicate that both mechanisms occur. In a study of similar cyclic triesters (Fig. 12c and d) that combined LFER studies, stereochemical analysis, and solvent isotope effects, Rowell and Gorenstein found a trend in β_{lg} values as a function of attacking nucleophile.[61] These, and the stereochemical data, are strong evidence for a mechanistic continuum from concerted to stepwise reactions of six-membered cyclic phosphate triesters.[61]

LFER data support a concerted reaction with no intermediate in reactions of acyclic phosphotriesters with aryl leaving groups, as the second-order rate constants for reactions of a number of phenoxide nucleophiles with substituted phenyl diphenylphosphate esters are linear across the range spanning the pK_a of the leaving group.[62,63] When the leaving group is p-nitrophenol, $\beta_{nuc} = 0.53$, and is reduced to 0.12 when the leaving group is 2,4-dinitrophenol. The cumulative LFER data for aryl diphenyl and aryl diethyl phosphates indicate concerted mechanisms, but with transition states that vary depending on the leaving group, as well as the other ester moieties. It was concluded that a very loose transition state exists for the attack of phenolate ions on 2,4-dinitrophenyl diphenylphosphate, a more synchronous mechanism for triphenylphosphate, and a tighter transition state with an almost associative mechanism for phenyl diethylphosphate.[63]

[18]O isotope effects in the nonbridging oxygen atom and in the leaving group have been measured for a series of acyclic diethyl phosphate triesters with different leaving groups. A normal $^{18}k_{nonbridge}$ is observed in the reactions of all of the triesters, reflecting loss of double bond character to the P–O bond in the transition states for alkaline hydrolysis. The magnitude of this isotope effect increases from 1.0063 when the leaving group is p-nitrophenol ($pK_a = 7.41$), to 1.025 for p-carbamoylphenol ($pK_a = 8.6$), to 1.041 for the leaving group choline iodide ($pK_a = 13.9$).[25] The calculated isotope effect for reducing this bond from a double bond to a single bond is 1.04.[25] The experimental values point to an increasingly associative transition state as the leaving group basicity increases. Unexpectedly, the primary [18]O isotope effects in the scissile P–O bond also increase with leaving group basicity, from 1.006 with p-nitrophenol, to 1.052 with the leaving group m-nitrobenzyl alcohol ($pK_a = 14.9$).[25] The large magnitudes were attributed to the imaginary frequency factor contribution to the isotope effect.

The roles of solvation and buffer catalysis have been examined for the phosphoryl transfers to methanol from the triesters tris(p-nitrophenyl)phosphate (PNNN), methyl bis(p-nitrophenyl)phosphate (PMNN) and dimethyl p-nitrophenyl phosphate (PMMN).[64] In acetate buffer, the reaction with PNNN exhibits general base catalysis by acetate ion, but no significant catalysis by acetic acid. The reaction is accompanied by a solvent isotope effect, k_{CH3OH}/k_{CH3OD}, of from 1.68 to 1.77, depending on the ionic strength. A linear proton inventory suggests that the isotope effect arises from the proton abstraction from the nucleophile by the general base in the transition state, with the small normal magnitude of the KIE reflecting an asymmetric position of the proton between the donor and acceptor in the transition state. The reactions of all three triesters with methoxide anion produce small inverse solvent isotope effects, from 0.83 to 0.91. These are less inverse than the value of 0.4 expected to arise from full desolvation of the methoxide nucleophile. Thus, the methoxide reaction is accompanied by isotope-sensitive solvent interactions in the transition state that prefer hydrogen over deuterium.

Summary. In summary, the transition states for the uncatalyzed phosphoryl transfer reactions of the three classes of phosphate esters can be generally represented on the More-O'Ferrall–Jencks diagram in Fig. 13. It has been noted that phosphoryl transfer reactions follow a trend for the phosphoryl group to bear a
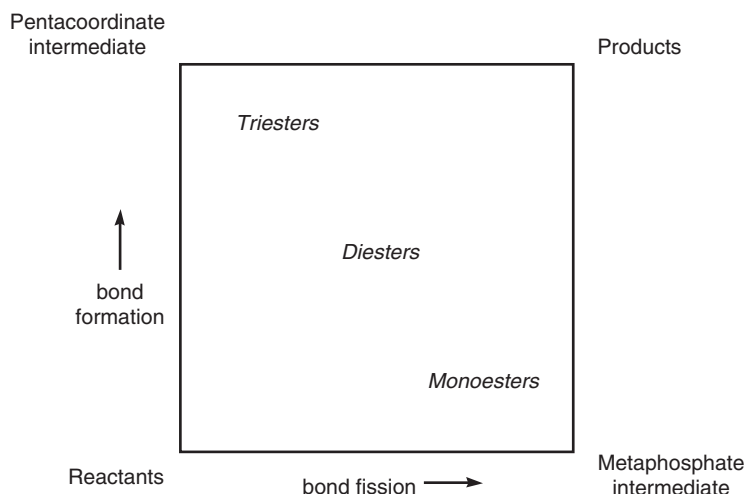
Fig. 13   More-O'Ferrall–Jencks' diagram depicting the general location of transition states of the uncatalyzed phosphoryl transfer reactions of phosphomono-, di-, and triesters. In general, the transition states become tighter as the alkylation state of the ester increases.

charge of about –1 in the transition state.[65] Thus, monoester dianions react by a loose transition state in which the dinegative phosphoryl group of the reactant sheds nearly a full negative charge to the leaving group in a late transition state. Diesters have roughly synchronous transition states in which they maintain a uninegative charge, and neutral triesters react by tighter transition states, in which the phosphoryl accepts the negative charge.

5   Implications for enzymatic catalysis

Comparisons of the structures of enzymes that catalyze phosphoryl transfer show that the only similarity at the active site is the presence of positive charge, in the form of either a binuclear metal center and/or positively charged amino acid side chains. For phosphatases, which catalyze the hydrolysis of phosphomonoesters, it has been suggested that metal ions or cationic side chains might change the normally loose transition state into a more associative process by promoting electron withdrawal from the phosphorus atom, thus promoting nucleophilic attack. One can postulate that strong interactions with metal ions by the nonbridging oxygen atoms could bring about a change to a more associative mechanism such as that resulting from alkyl substitution; as mentioned earlier, transition states become more associative in the continuum from monoesters to triesters (Fig. 13). While coordination to a di-Co(III) complex indeed results in a change to a mechanism involving more nucleophilic participation in the transition state for monoesters and diesters,[51] phosphatases utilize divalent metal ions, and mechanistic studies to date with such
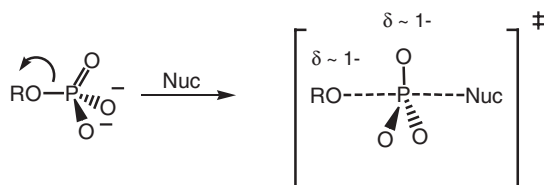
Fig. 14 The changes in charge distribution and in geometry in a loose, metaphosphate-like transition state for phosphoryl transfer involving the dianion form of a monoester. The reactant is tetrahedral at phosphorus, the nonbridging oxygen atoms have a total charge of 2- and an average P–O bond order of 4/3. In the transition state the PO_3 moiety is trigonal, the oxygen atoms share a charge of approximately 1-. The metaphosphate-like phosphoryl group is shown with single bonds for simplicity; see Fig. 3 for the resonance contributors to meta-phosphate.

ions show that they do not significantly alter the transition state for phosphoryl transfer.[32,33]

The notion that enzymatic phosphoryl transfer mechanisms differ from uncataly-zed processes arises in part because of a perceived difficulty in rationalizing how enzymes can stabilize a loose, metaphosphate-like transition state. In such a trans-ition state (Fig. 14), it is assumed that the net flow of electron density is away from the nonbridge oxygen atoms to the leaving group. To achieve stabilization of such a transition state in preference to the ground state, the enzyme would have to de-stabilize negative charge on the nonbridge oxygen atoms. However, this seemingly runs counter to the presence of cationic groups present in all known phosphatases. By contrast, in a transition state for an associative process, electron density on the nonbridge oxygen atoms increases, and it is obvious how such a species will be preferentially stabilized by positively charged amino acids or metal ions. However, this simple approach neglects the influence of the geometric change that occurs in the phosphoryl group during phosphoryl transfer, which has been shown in computational studies to have the potential to result in preferential enzymatic stabilization of a loose, metaphosphate-like transition state in PTPases.[26,27] Fur-thermore, as previously noted, computational studies suggest that the amount of negative charge on the nonbridging oxygen atoms does not significantly change in a metaphosphate-like transition state (see Fig. 3).

Whether the transition state is loose or tight, negative charge develops on the leaving group, and the stabilization of this charge, either through protonation or coordination to a metal ion, is a common feature of nearly all known enzymatic phosphoryl transfer reactions.

One might suppose that in a loose transition state a phosphate substrate expands relative to the ground state, but this need not be the case.[66,67] Fig. 15 shows the geometric changes involved in the reaction of a phosphate monoester (or phospho-anhydride) when the reactants begin at the van der Waals contact distance, and the nucleophile and leaving group do not move during the reaction. In this geometry, the initial phosphorus-nucleophile distance is $\approx 3.3\,\text{Å}$ and the single bond to the leaving group $\approx 1.6\,\text{Å}$. The nonbridge oxygen atoms move very little, and only the
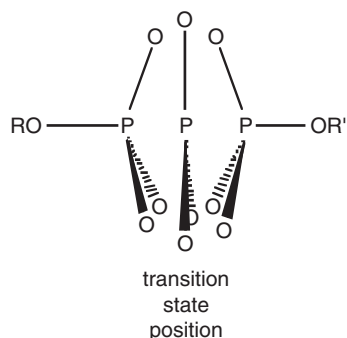
Fig. 15 Illustration of the relative movements of the phosphorus atom and the nonbridge oxygen atoms during phosphoryl transfer from OR to OR′ if the horizontal O–P–O distance remains constant at the van der Waals contact distance of 5.07 Å.

phosphorus atom undergoes significant translation. If the pK_as of the nucleophile and leaving group are similar, the transition state will be symmetric. If the axial O–P–O distance does not change, each P–O distance in the transition state will be ≈ 2.5 Å. Using Pauling's rule, the transition state bond orders to the nucleophile and leaving group, will each be approximately 0.08. For a tighter transition state with a bond order of 0.5 to entering and leaving groups, the O–P–O distance would be 3.6 Å. In enzymatic reactions the reaction coordinate may even be compressed somewhat, which has been suggested to be the case for alkaline phosphatase.[68] In this case the nonbridge oxygen atoms may not move at all, and the axial bond orders in the transition state will be approximately 0.15. This still describes a loose transition state. The volumes of activation for the hydrolysis reactions of acetyl phosphate and of 2,4-dinitrophenyl phosphate are near zero or negative,[69,70] consistent with this picture. This suggests that a phosphatase active site need not be significantly larger than the substrate in order to accommodate a loose transition state.

This puzzle of how a loose transition state can be stabilized has led to investigations of the manner in which metal ions accelerate phosphoryl transfer reactions in solution, and whether they result in alterations in the transition state for phosphoryl transfer. As mentioned earlier, while coordination to a dinuclear Co^{3+} complex results in significant mechanistic changes, coordination to divalent metal ions does not seem to result in significant alterations in the transition state for phosphoryl transfer. Studies in aqueous solution show that Mg^{2+} and Ca^{2+} catalyze the reaction of pNPP with substituted pyridines, but do not increase the associative character of the transition state, as indicated by the lack of a change in values of β_{nuc}.[32] A change to a more associative mechanism would show an increased β_{nuc}, reflecting greater nucleophilic participation. The solvolysis of ATP in alcohol/water mixtures with and without Mg^{2+} also yields values of β_{nuc} that are identical within experimental error, indicating that metal ions do not alter this aspect of the transition state.[33] It was found that Mg^{2+} and Ca^{2+} inhibit the reaction of phosphorylated pyridines, in contrast to their enhancement of the reaction of

pNPP.[32] These substrates differ in the charge developed on the leaving group in the transition state. The results suggest that interactions of the metal ions solely with the nonbridge oxygens of phosphomonoesters are anticatalytic, and that metal ion catalysis arises from interactions with the negatively charged leaving group in the transition state.[32]

Another mode for metal ion catalysis of phosphoryl transfer is by complexation with a nucleophile of the form R–OH, thereby facilitating its deprotonation to form the more nucleophilic alkoxide or hydroxide. An example is the catalysis of the aqueous hydrolysis of phosphorylated pyridines by $Mg(OH)^+$.[71] A rate enhancement of 10^4 was attributed to the greater nucleophilicity of the metal-bound hydroxide relative to water. A further rate enhancement of 10^2 was attributed to induced intramolecularity arising from interaction of the metal ion with both the hydroxide nucleophile and the nonbridge phosphoryl oxygens in the transition state.[71]

A metal-coordinated hydroxide ion can act not just as a nucleophile, but also as a base. A dinuclear Zn complex has been shown to catalyze the cleavage of the diester 2-hydroxypropyl-4-NPP[72,73] and of RNA[74] by such a mechanism (Fig. 16). The absence of a normal solvent deuterium KIE means that no proton is in flight in the transition state of the rate-limiting step.[75] This implicates a pre-equilibrium deprotonation of the nucleophilic 2′ hydroxyl group, as shown in Fig. 16. The significant catalytic power of the Zn complex, which equals about half that observed for enzymatic catalysts, is attributed primarily to electrostatic stabilization of the transition state. Dinuclear complexes can chelate both the ester and nucleophile, also providing a significant entropic advantage, a property shared by enzymes.

In summary, a number of potential interactions of enzymatic catalytic groups that can facilitate phosphoryl transfer can be identified. Metal ions can coordinate with a nucleophile to facilitate its deprotonation, to form the more nucleophilic anionic species, possibly by an enzymatic general base. Expulsion of the leaving group is facilitated by neutralization of its negative charge, either by protonation or by coordination to a metal ion. Lewis acid (electrophilic) activation of the phosphoryl group toward nucleophilic attack by interactions of the nonbridge oxygen atoms with hydrogen-bond donors or metal ions is only likely in an associative mechanism, and will be anticatalytic in a dissociative transition state. Electrostatic interactions
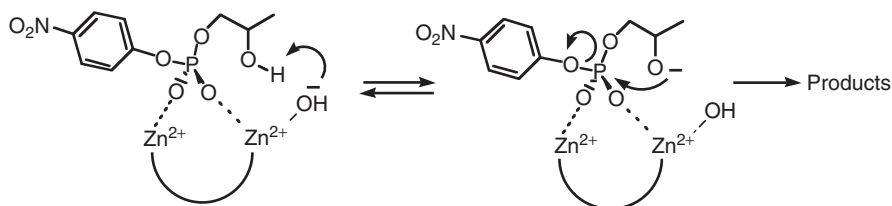
Fig. 16   The mechanism implicated by kinetic data by which a dinuclear zinc complex catalyzes the cyclization of RNA analogs. The pK_a of the Zn-coordinated water was found to be 8.0; once deprotonated, the resulting coordinated hydroxide acts as a base to deprotonate the secondary alcohol, which acts as the nucleophile in a subsequent step.

between the nonbridging oxygen atoms and cationic residues or metal ions can also stabilize a loose, metaphosphate-like transition state if a conformational change of the protein associated with the chemical step enhances these interactions in the transition state, or, if the geometric change from tetrahedral to trigonal bipyramidal serves to strengthen such interactions. The enzymatic reactions discussed in the subsequent sections are a representative sampling of those for which structural and/ or mechanistic data are sufficient to determine at least a partial understanding of the catalytic mechanism and the mode of catalysis.

6   Enzymes that catalyze transfer of the phosphoryl (PO$_3$) group

PHOSPHATASES: GENERAL

Phosphatases catalyze the transfer of a phosphoryl group from a phosphomonoester substrate to water, producing inorganic phosphate. Phosphatases fall into two categories with regard to their overall mechanism, with different stereochemical outcomes (Fig. 17). Some transfer the phosphoryl group directly to water; these enzymes characteristically possess a binuclear metal center and the nucleophile is a metal-coordinated hydroxide. Other phosphatases form a phosphoenzyme intermediate, via transfer of the phosphoryl group from the substrate to an enzymatic nucleophile. This intermediate is hydrolyzed by nucleophilic addition of water in a subsequent step. Some, but not all of this group of enzymes use binuclear metal catalysis as well. The binuclear metal ion containing phosphatases form a very heterogeneous group of enzymes, varying in the identities of the metal ions, ligands, and catalytic residues.

Table 2 lists phosphatases for which the stereochemical outcome has been determined by using chiral phosphomonoester substrates. In such experiments the phosphoryl group is made chiral using ^{16}O, ^{17}O, and ^{18}O, or, a phosphorothioate substrate is used that has a sulfur atom and two isotopes of oxygen in the nonbridging positions. Summaries of results for additional enzymes that catalyze phosphoryl transfer are available in other reviews.[20,76,77]

ALKALINE PHOSPHATASE

The *Escherichia coli* alkaline phosphatase (*E. coli* AP) is the most extensively studied phosphatase, and perhaps the most studied two-metal ion catalyst.[68,91–95] The AP-catalyzed reaction proceeds via an intermediate in which a serine residue (Ser-102 in *E. coli* AP) is phosphorylated. Thus, the stereochemical outcome of the overall reaction is retention. The hydrolysis of the intermediate by water to produce inorganic phosphate competes with phosphoryl transfer to other acceptors such as alcohols or nucleophilic buffers if such are present in solution. The rate-limiting step
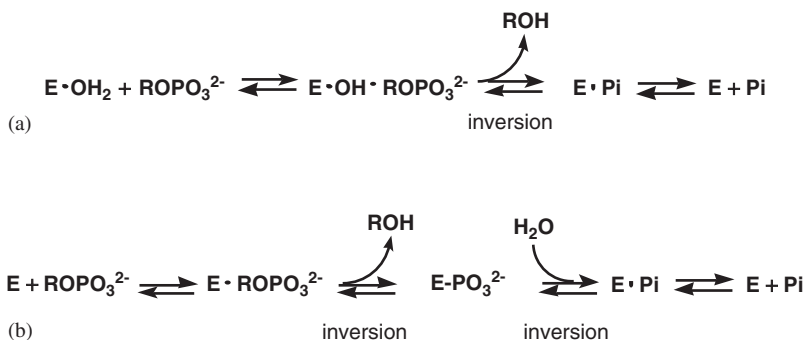
Fig. 17   The two typical reaction mechanisms employed by phosphatases. In (a), the phosphoryl group is transferred directly to a water molecule, which is typically bound to one or two metal ions; if the substrate is made chiral at phosphorus, the stereochemical outcome is inversion. In (b), the phosphoryl group is first transferred to an enzymatic residue. In a subsequent step the phosphoenzyme intermediate is hydrolyzed. Since each step occurs with inversion of configuration at phosphorus, the net outcome is retention. Pi: inorganic phosphate.

Table 2   Stereochemistry of some enzyme-catalyzed phosphoryl transfer reactions

Enzyme	Stereochemical result
Bovine liver acid phosphatase	Retention[78]
Human prostatic acid phosphatase	Retention[79]
Alkaline phosphatase	Retention[80]
ATPase (sarcoplasmic reticulum)	Retention[81]
ATPase (mitochondrial)	Inversion[82]
ATPase (thermophilic bacterium PS3)	Inversion[83]
Glucose-6-phosphatase	Retention[84]
GTPase (elongation factor G)	Inversion[85]
Myosin ATPase	Inversion[86]
Nucleoside phosphotransferase	Retention[87]
p21 Ras	Inversion[88]
Purple acid phosphatase	Inversion[89]
Pyrophosphatase	Inversion[90]

in the overall mechanism at pH > 7 is release of inorganic phosphate, and is hydrolysis of the phosphoserine intermediate at pH < 7.[96,97]

The AP from *E. coli* contains two Zn^{2+} ions and one Mg^{2+} ion in the active site.[68,91] The Zn ions play the most direct roles in catalysis; the Mg^{2+} has been suggested to function as the provider of the general base that deprotonates the Ser nucleophile, in the form of a Mg-coordinated hydroxide.[98] All known alkaline phosphatases have this conserved three metal ion center, as well as an arginine residue (Arg-166 in *E. coli* AP) that plays a role in binding and probably in transition state stabilization (Fig. 18).
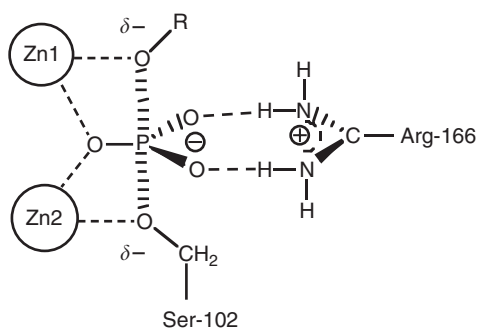
Fig. 18 A model of the transition state interactions in the reaction catalyzed by alkaline phosphatase, based on X-ray structures.

The substrate coordinates to both Zn ions and forms hydrogen bonds to the guanidinium group of Arg-166, with the leaving group oxygen atom coordinated to Zn1 and opposite from Ser-102. Coordination of the Ser-102 oxygen atom nucleophile to Zn2 facilitates its deprotonation to form the more nucleophilic serine alkoxide, while Zn1 facilitates P–O bond fission by stabilization of the negative charge that develops on the ester oxygen atom in the transition state. The replacement of the two Zn ions of native AP by Cd^{2+} enabled the crystallization and structural determination of the phosphoserine intermediate at 2.5 Å resolution.[68] Following formation of the intermediate and departure of the leaving group, Zn1 can coordinate to a water molecule. The Zn1 hydroxide is the nucleophile that displaces Ser from the phosphoryl group; its departure is stabilized by coordination with Zn2. Thus, the roles of the two Zn ions are exactly reversed in the two phosphoryl transfer steps.

Several attempts to probe the nature of the transition state of the first phosphoryl transfer step using Brønsted correlations on k_{cat}/K_m led to conflicting conclusions. The first such study found a small value for β_{lg} of –0.2 for a series of aryl and alkyl phosphates.[99] However, it was subsequently shown that for aryl phosphate ester substrates, a nonchemical step such as binding or an associated conformational change is rate-limiting for k_{cat}/K_m (the portion of the kinetic mechanism consisting of all steps from substrate binding up to the first irreversible step). Evidence for this comes from the viscosity dependence of k_{cat}/K_m[100] and from the absence of isotope effects for the AP-catalyzed hydrolysis of pNPP.[9] Thus, the LFER and KIE data did not provide information about the chemical step. In later work, a larger β_{lg} value of –0.6 was measured for a small group of alkyl monoester substrates with leaving group pK_a values from 14.1 to 16.2, where phosphorylation of Ser-102 is rate-limiting.[101] In a mutant AP where the nucleophilic Ser was replaced by cysteine (Cys), phosphorylation was rate-limiting for all substrates with leaving group pK_a's between 4 and 16, and the β_{lg} value was reduced to –0.3. This result and data on the hydrolysis of phosphorothioate monoesters[102,103] led to the conclusion that an

associative triester-like mechanism, or at least a tight transition state, is operative for both the native enzyme and the mutant.[101]

The phosphorothioate results were considered as evidence for such a mechanism on the basis of the direction of thio effects in uncatalyzed reactions of phosphate esters. In the hydrolysis reactions, which have loose transition states, phosphorothioate monoesters react faster than phosphates. In contrast, for triesters, which have tighter transition states, the thio analogs react more slowly. The fact that AP hydrolyzes phosphorothioates more slowly than it does, phosphates has been taken as an indication of a triester-like transition state in the AP reaction.[101,103] Subsequently, it was shown that while wild-type *E. coli* AP catalyzes the hydrolysis of *p*NPP ~70 times faster than *p*-nitrophenyl phosphorothioate, the R166A mutant AP hydrolyzes *p*NPP only about three times faster than *p*-nitrophenyl phosphorothioate. Despite this ~23-fold change in the magnitude of the thio effects, the magnitudes of Brønsted β_{lg} for a series of aryl phosphorothioate substrates for the native AP (–0.77 ± 0.09) and the R166A mutant (–0.78 ± 0.06) are the same. Unlike the case with phosphate ester substrates, the chemical step is rate-limiting in the enzymatic reaction of aryl phosphorothioate substrates. The identical β_{lg} values indicate that the transition states are similar for the reactions catalyzed by the wild-type and the R166A mutant enzymes. The fact that a significant change in the thio effect is not accompanied by a change in the β_{lg} indicates that the thio effect is not a reliable reporter for the transition state of the enzymatic phosphoryl transfer reaction.

AP is subject to product inhibition; the K_i for inorganic phosphate is ~1 μM. Reactions run under conditions conducive to traditional spectrophotometric assay methods quickly generate concentrations of inorganic phosphate in excess of this concentration, which affects the kinetic constants that are derived. Recently, a sensitive ^{32}P-based assay for measuring the hydrolysis of a series of alkyl phosphomonoester substrates was developed, and used to reexamine the AP mechanism.[94] The results confirmed that the chemical step of phosphoryl transfer is rate-limiting for k_{cat}/K_m for such substrates. The value of –0.85 ± 0.1[94] for β_{lg} is somewhat more negative than the earlier value of –0.6[101] that was obtained using a different kinetic method. The steep leaving group dependence indicates considerable P–O bond fission in the transition state. The pH dependence of the kinetic data also suggest that the nucleophilic Ser hydroxyl group has a $pK_a < 5.5$ in the free enzyme.[94]

The guanidinium group of Arg-166 plays a role in binding and in transition state stabilization, but is not essential for catalysis. The role of this residue in catalysis has been probed further using site-directed mutagenesis. Replacement of this residue results in an increased K_m and reduced k_{cat} but enzyme activity remains; R166A is reported to show 2.4% of native activity.[104,105] The k_{cat}/K_m for R166S is decreased ~10^4-fold relative to native AP.[106] The β_{lg} value of –0.66 ± 0.1 for the reaction of a series of alkyl phosphomonoester substrates with the R166S mutant is slightly less negative than the –0.85 ± 0.1 for native AP. If transition state interactions with the guanidinium group of the Arg favor a tighter transition state, then native AP should exhibit a less negative β_{lg} than the mutant, the opposite of what is observed.[106] As

previously mentioned, the β_{lg} values for native AP and R166A are identical for phosphorothioate substrates, for which chemistry is rate-limiting in both reactions. Thus, with both natural phosphomonoester substrates and phosphorothioate analogs, this residue does not seem to alter the transition state structure, which LFER data indicate is characterized by extensive bond fission to the leaving group. Data directly assessing the degree of nucleophile bond formation in the transition state have not been obtained, leaving the picture of the transition state incomplete. An indirect assessment of nucleophilic participation comes from the small inverse secondary $^{18}k_{nonbridge}$ KIE on the hydrolysis of glucose-6-phosphate (G6P) by AP, consistent with a loose transition state.[107]

ACID PHOSPHATASE

The *E. coli* acid phosphatase is a member of a class of nonspecific acid phosphatases that include human lysosomal, human prostatic, yeast, and plant phosphatases that contain a nucleophilic His, no metal cofactor, and which have molecular weights in the range of 50–60 kDa. The overall catalytic reaction proceeds via formation of a phosphohistidine intermediate, and these phosphatases exhibit acidic pH optima. This is a logical feature of these enzymes since nitrogen–phosphorus linkages are base stable, but acid labile. The nucleophilic His residue is part of the characteristic amino acid sequence RHGXRXP[108] (using the amino acid single-letter codes where X represents amino acid residues which are not conserved). Although acid phosphatases have not been subject to nearly as much mechanistic study as alkaline phosphatase, some mechanistic information has been obtained from X-ray structures,[109–111] mutagenesis studies, and LFER analyses.[112]

An X-ray structure of the rat enzyme with bound vanadate[111] (Fig. 19) is consistent with kinetic data from site-directed mutants that a conserved aspartate (Asp) residue found in members of this family of phosphatases is catalytically important. In the *E. coli* acid phosphatase, His-303 and Asp-304 correspond to His-257 and Asp-258 in the rat enzyme. LFER experiments show that the sensitivity of V_{max} to leaving group pK_a is small for the native enzyme (–0.08) and for the H303A mutant (–0.13). In contrast, the D304A mutant gives a slope of –0.51, indicating substantial negative charge resides on the leaving group in the reaction catalyzed by this mutant. It was also noted that the reduction in rate resulting from the D304A mutation is much smaller for the substrate *p*NPP, which has a good leaving group, than for an alkyl phosphomonoester substrate.[112]

The structural and kinetic data suggest a mechanism in which the first phosphoryl transfer step occurs by attack of the nitrogen atom of His accompanied by general acid protonation of the leaving group by the Asp carboxyl group. A logical assumption is that the carboxylate form of the Asp residue then acts as a general base to deprotonate a nucleophilic water molecule in the second step, hydrolysis of the phosphohistidine intermediate (Fig. 20).
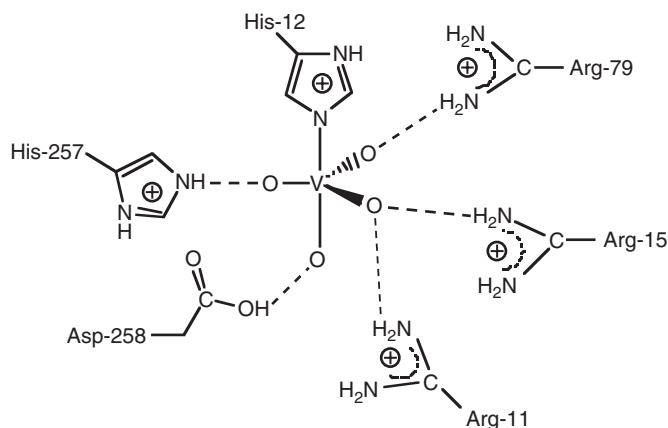
Fig. 19 Interactions with active site residues found in the X-ray structure of rat acid phosphatase with bound vanadate.
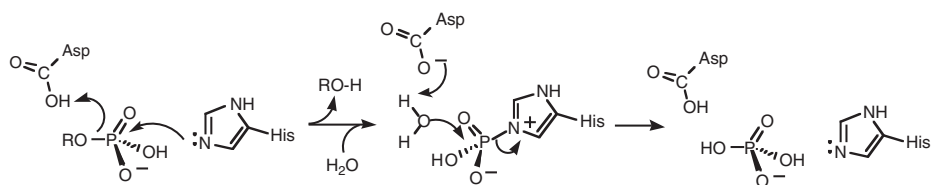
Fig. 20 The reaction mechanism of acid phosphatases implicated by structural, kinetic, and stereochemical data.

PURPLE ACID PHOSPHATASES

Purple acid phosphatases (PAPs) catalyze the hydrolysis of phosphate monoesters with mildly acidic pH optima (5–7) utilizing a binuclear metal center containing a ferric ion and a divalent metal ion. PAPs are also characterized by their purple color, the result of a tyrosine (Tyr) to Fe^{3+} charge transfer transition at about 560 nm.[113] All known mammalian PAPs are monomeric and have a binuclear Fe^{3+}–Fe^{2+} center, whereas the kidney bean and soybean enzymes are dimeric and have an Fe^{3+}–Zn^{2+} center in each subunit. The X-ray structures for kidney bean PAP[114] and the PAP[115] from rat bone reveal that despite a sequence similarity of only 18%, they share very similar catalytic sites. The structure of the kidney bean PAP shows the two metal ions at a distance of 3.1 Å, with a monodentate bridging Asp-164. These and other residues involved in metal coordination can be seen in Fig. 21.

Some evidence, including the observation of a burst of p-nitrophenol and the appearance of transphosphorylation products with the substrate pNPP, initially
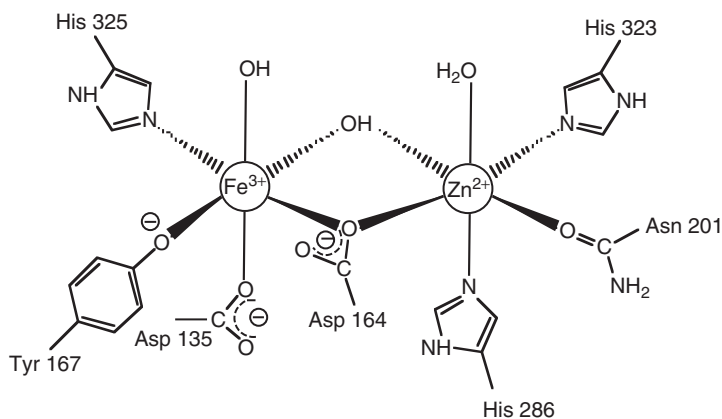
Fig. 21 The active site of kidney bean purple acid phosphatase.

suggested the formation of a phosphoenzyme intermediate.[116,117] However, it was subsequently found that the stereochemical course of the reaction occurs with inversion of configuration at phosphorus, which supports direct phosphoryl transfer to water.[89] A later study[118] found no transphosphorylation products with pNPP, and burst kinetics were observed only when the enzyme was added after the substrate, suggesting that the burst was an artifact of the order of addition of reagents.

Details of the catalytic mechanism, including the identity of the nucleophile, remain to be elucidated, not just for PAPs, but for the related Ser/Thr protein phosphatases, which share similar dinuclear metal active sites. Mechanistic proposals include nucleophilic attack by a bridging hydroxide (Scheme 2, pathway 2); a Fe^{3+}-bound hydroxide acting either as the nucleophile (pathway 1); or, alternatively, as a general base for nucleophilic attack by a free water molecule (pathway 3)[28,119,120]. Recently, spectroscopic evidence for the structure of the complex of inorganic phosphate with uteroferrin, a member of the PAP family, has been cited as evidence for a nucleophilic role for a bridging hydroxide ligand[121] (Fig. 22). This is an enzyme–product complex that would be expected from either pathway 1 or 2 in Scheme 2. Inorganic phosphate is both a product and a competitive inhibitor. It is therefore unclear whether structures of phosphatases with bound phosphate can be taken as models for an intermediate on the reaction pathway, or simply depict product-inhibited states.

The recombinant human PAP exhibits the bell-shaped pH-rate profile typical of the PAP family. The optimal pH is 5.5, $pK_{a1} = 4.6$, $pK_{a2} = 6.7$.[122] Nuclear magnetic resonance (NMR) spectra[123] revealed no differences in the hyperfine-shifted signals between pH 5.5 and 7.1, indicating that pK_{a2} does not involve a metal ligand, and may instead be due to ionization of one of two conserved His residues near the dinuclear site. It has been proposed that such a His residue may act as a general acid in protonation of the leaving group.[124] The structure of the kidney bean PAP has His-296, corresponding to His-216 in the rat PAP, in a location consistent with such a function, but experimental verification of the role of these His residues is lacking.
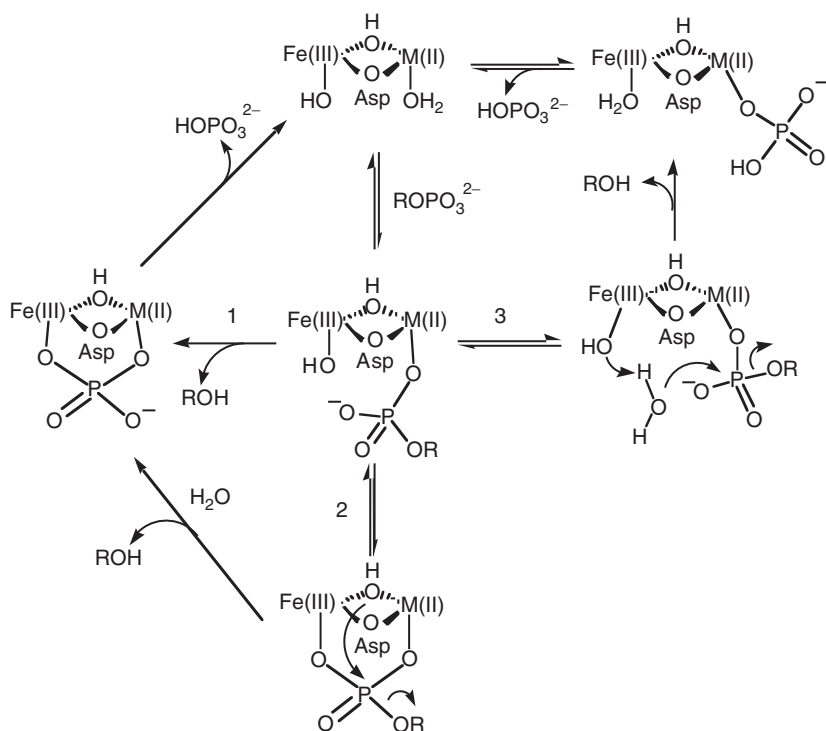
Scheme 2   Three possible roles for metal-assisted phosphoryl transfer to water by PAPs, and related Ser/Thr protein phosphatases, which contain similar binuclear metal centers. In 1, an Fe^{3+}-coordinated hydroxide is the nucleophile. In 2, a bridging hydroxide (or oxide) is the nucleophile, forming an intermediate that is subsequently opened by attack of water. In 3, an Fe^{3+}-coordinated hydroxide acts as a general base to facilitate attack by water.
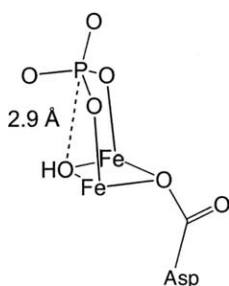
Fig. 22   The orientation of inorganic phosphate bound to the active site of uteroferrin, as implied from spectroscopic data.

Spectral changes found at pH < 5.5 indicate that pK_{a1} is due to a metal-bound moiety that is deprotonated in the active enzyme. A plausible candidate for such a group is a metal-bound water, which upon deprotonation could act as the nucleophile in phosphate ester hydrolysis.

The observation that pK_{a1} is also sensitive to changes in the identity of the metal at the divalent site is consistent with the proposal that the nucleophilic hydroxide is that bridging the divalent and trivalent metals,[125] as in pathway 2 of Scheme 2. By contrast, an electron paramagnetic resonance (EPR) study with the bovine spleen PAP showed that the EPR spectrum of the Fe^{3+}–Zn^{2+} form does not show significant changes upon addition of phosphate at pH 6.5, the optimal pH for k_{cat}, suggesting that phosphate binds only to the spectroscopically silent Zn^{2+}. Assuming that phosphate binds in a manner analogous to a phosphomonoester substrate, this observation is consistent with the notion that, at the pH where the enzyme is optimally active, hydroxide competes with phosphate and substrate for coordination to Fe^{3+} and that both phosphate and substrate coordinate only to the divalent metal ion in the catalytically active complex.[120] This is pathway 1 in Scheme 2.

Two PAPs have been isolated from sweet potato; one contains an Fe^{3+}–Zn^{2+} center with spectroscopic properties similar to the kidney bean PAP. The other contains an Fe^{3+}–Mn^{2+} center, the first of its kind seen in a biological system.[126] An LFER study of this novel sweet potato PAP revealed differences between it and the kidney bean and pig PAPs.[127] The β_{lg} values for k_{cat} and for k_{cat}/K_m, respectively, were found as 0.06 and 0.007 for sweet potato PAP; –0.47 and –0.62 for kidney bean PAP; and –0.27 and –0.39 for pig PAP. The lack of a significant β_{lg} for the sweet potato enzyme indicates that no significant charge develops on the leaving group in the transition state of the rate-determining step, in contrast to the other two PAPs. This could, in principle, result from a nonchemical step being rate-determining. However, another possibility comes to light from the X-ray structure of the Fe^{3+}–Mn^{2+} enzyme with bound phosphate.[127] This structure shows a hydrogen bond between a phosphate oxygen atom and glutamic acid (Glu)-365 in one subunit, while in the other subunit, phosphate is hydrogen bonded to His-295. A corresponding His residue is conserved in all PAPs as discussed above, but there is no carboxylic acid corresponding to Glu-365 in PAPs from animals, and in the kidney bean PAP the corresponding residue is a Tyr. Glu-365 may function as a more efficient proton donor to the leaving group at the low pH optimum of these enzymes, resulting in the smaller β_{lg} value. Another unique feature of this structure is the tripodal-binding mode of phosphate, in which two of the oxygen atoms bind to the Fe^{3+} and Mn^{2+} and a third oxygen atom bridges the two metal ions. Other structures of PAPs with bound phosphate lack the oxygen bridge interaction.

Mammalian purple acid phosphatases can be divided into two groups, which exhibit distinct spectroscopic and kinetics properties: PAPs that consist of a single 36 kDa polypeptide, and PAPs that have undergone limited proteolysis to give two fragments with masses of 16 and 20 kDa, respectively. Proteolysis results in an increase in enzymatic activity, an increase in the optimal pH for activity, and a change in the EPR spectrum.[122,125] Site-directed mutagenesis shows that a major contributor to these changes is the loss of interactions between active site residues

and Asp-146 in an exposed loop region that is proteolytically cleaved. Since both *p*NPP and osteopontin, a potential in vivo substrate, show the same level of activation upon proteolysis, the observed increase in catalytic activity upon proteolysis is not due to steric effects. EPR spectra of the Fe/Zn form before and after proteolysis suggest that loss of the loop region primarily affects the divalent metal site.

The role of the trivalent metal ion has been probed by examining the kinetic behavior of the bovine spleen PAP with several trivalent metal ions, including aluminum.[128] The kinetics and pH-rate dependency of the Al^{3+}–Zn^{2+} enzyme were similar to those of the Fe^{3+}–Zn^{2+} and the Ga^{3+}–Zn^{2+} forms. These results are unexpected, in light of the slow ligand exchange properties of trivalent metal ions. This would be disadvantageous in an enzymatic system where rapid product release is desirable. The results suggest that either the enzyme alters the properties of the trivalent metal ion to facilitate ligand exchange, or, that the catalytic mechanism does not involve phosphate dissociation from the trivalent metal ion, as in pathway 3 of Scheme 2. Clearly, further work is needed to clarify the mode of substrate binding and the identity of the nucleophilic water (or hydroxide).

SER/THR PROTEIN PHOSPHATASES

Phospho-protein phosphatases are generally grouped into the PTPases and the phosphoserine/phosphothreonine-specific phosphatases based on substrate specificity and genetic homology.[129] As their name implies, the Ser/Thr protein phosphatases dephosphorylate phosphoserine and phosphothreonine residues in proteins. These phosphatases have binuclear metal centers similar to those of the purple acid phosphatases, and are distinguished from the PTPases and the dual-specific protein phosphatases (discussed in the next section), which do not contain metal ions. On the basis of their catalytic domains, the Ser/Thr phosphatases fall into two structural families, designated PPP and PPM. The PPP family members share a conserved phosphoesterase motif, $DXH(X)_{25}GDXXDR(X)_{25}GNHE$. This family includes the protein phosphatases known as PP1, PP2A, PP2B (also called calcineurin), and lambda protein phosphatase (λPP). The PPM family is regarded as evolutionarily distinct from the PPP family, and is typified by PP2C, an Mn^{2+}- or Mg^{2+}-dependent Ser/Thr phosphatase. In PP2C, and others in its subfamily, the metal ligands consist almost entirely of carboxylates,[130] in contrast to the neutral His and amide carbonyls that comprise the ligands in the PPP phosphatases. PP2C homologs have been identified in bacteria, plants, yeast, and mammals, and have a conserved role in negatively regulating stress responses.

X-ray structures have been published of the catalytic subunit of rabbit muscle PP-1 complexed with the polypeptide microcystin[131] and of human PP-1 with tungstate.[132] The X-ray structures are also available of free human calcineurin (Fig. 23), as well as of human and bovine brain calcineurin complexed with the immunosuppressant complex FKBP12/FK506, which does not contact the active site, but binds adjacent in a manner that hinders access.[133,134] Calcineurin is involved in the
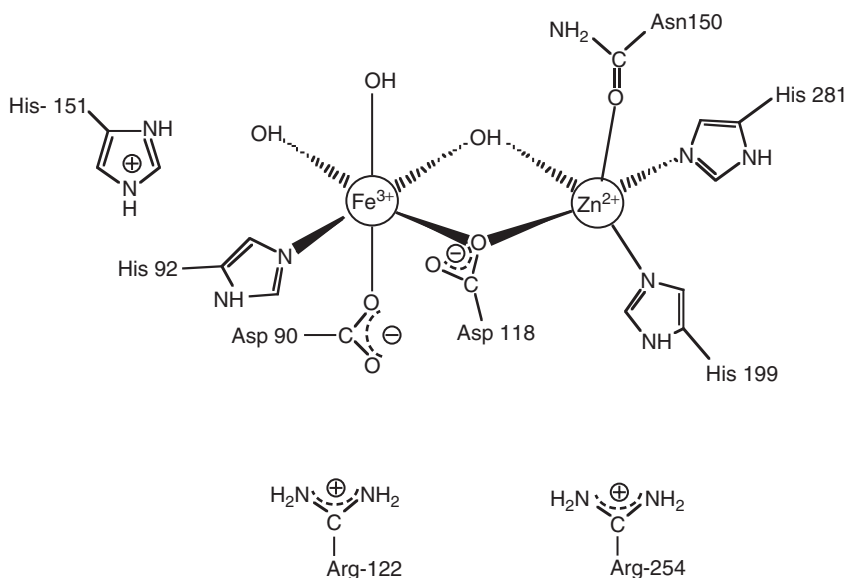
Fig. 23 The active site of human calcineurin (PP2B).

regulation of T-cell production, and is the target of a number of immunosuppressant drugs. The identities of the metal ions in PP1 and PP2A in vivo are not certain; some evidence indicates that calcineurin has a binuclear Fe^{+3}–Zn^{+2} center, although its best activators in vitro are Mn^{2+} and Ni^{2+}.[135]

The same mechanistic possibilities present themselves for the Ser/Thr phosphatases as for the PAPs (Scheme 2), and, like the PAPs, a His residue is found in the vicinity of all the known structures. A mechanism for PP1 catalysis has been proposed[132] based on the binding mode of tungstate, although these crystals were grown at low pH and may not reflect the active binding mode with substrate. The most solvent-exposed oxygen atom of the tungstate ion forms a hydrogen bond with His-125, and this oxygen atom is suggested to correspond to the scissile P–O(R) bond of a substrate. This proposed mechanism cites the bridging hydroxide as the most likely nucleophile, on the basis of its position approximately opposite the W–O bond that interacts with His-125. An essentially identical mechanism, with leaving group protonation by His-151, has been suggested for calcineurin.[134]

Kinetic studies with calcineurin yielded a modest solvent isotope effect of 1.35, and a proton inventory and fractionation factor data that were most consistent with a mechanism involving a single proton transfer from a water molecule coordinated to a metal ion.[136] No transphosphorylation products were found in the presence of alternate nucleophiles, consistent with direct phosphoryl transfer to a metal-coordinated water.[137] No calcineurin-catalyzed oxygen exchange of ^{18}O labeled water with phosphate could be detected.[138] In a study using pNPP as the substrate, product inhibition studies found that both phosphate and p-nitrophenol are

competitive inhibitors.[136] This pattern is consistent with a random uni–bi (one substrate, two products) mechanism. In contrast, an ordered uni–bi-mechanism should result if the mechanism involved a phosphoenzyme intermediate, since the product phenol would be released before the second product, phosphate, is produced by the hydrolysis of a phosphoenzyme intermediate.

Taken together, the data indicate direct phosphoryl transfer to a metal-bound water molecule without a phosphoenzyme intermediate. A Brønsted analysis found a value of β_{lg} of –0.3 for V/K,[137] similar to the value for the uncatalyzed hydrolysis of phosphate monoester monoanions, which could be indicative of charge neutralization on the leaving group in the transition state via protonation.

Like the PAPs, the Ser/Thr phosphatases share a conserved His residue that is not a metal ligand, but is within 5 Å of either metal ion. This residue (His-151 in calcineurin, His-76 in λ-PP) is hydrogen bonded to an Asp residue.[135] Kinetic studies have examined the consequences of mutating these His residues.[139,140] In both mutants, there were significant reductions in k_{cat} but only small effects on K_m.[139,140] Substrates with varying leaving groups were used in order to test the possible role of this His as a general acid. For calcineurin, pNPP (leaving group $pK_a = 7.14$) and a phosphoserine peptide (~14) were used; in the λ-PP study, pNPP and phenyl phosphate (leaving group $pK_a = 10.9$) were used. If the His residue functions as a general acid, its loss should result in a greater dependency of the rate on leaving group pK_a; in other words, the substrate with the more basic leaving group should show a greater reduction in rate. The calcineurin results showed less than a threefold difference in rate despite the ΔpK_a of >6 between the two substrates. With λ-PP, both substrates showed the same 500–600-fold decrease in k_{cat} in H76N relative to native enzyme. Using pNPP as a substrate, pH dependence studies were carried out with λ-PP.[141] Both the native and H76N proteins exhibit a bell-shaped profile, whereas the loss of a general acid should abolish the basic limb. However, kinetic data could not be obtained under the same conditions at all pH values; substrate inhibition at low pH necessitated higher metal ion concentrations. It was noted that the K_m with native λ-PP increases from 1–2 mM at low pH to >40 mM above pH 8, while H76N exhibits high K_m values across the pH range.[141] This suggests that substrate binding is facilitated when this residue is protonated.

KIEs have been measured for both the calcineurin and the λ-PP-catalyzed reactions.[141–143] With calcineurin, it was found that with pNPP as the substrate, phosphoryl transfer is only partially rate-limiting at the pH optimum and is more rate-limiting at pH 8. For λ-PP, phosphoryl transfer is fully rate-limiting, and the measured KIEs are the intrinsic ones for this step. With both enzymes the KIEs indicate that the dianion of pNPP is the substrate, which is also the major form present at the pH optima (pK_{a2} of pNPP = 5; for alkyl phosphomonoesters, pK_{a2}~6.8). The $^{18}V/K_{nonbridge}$ values (0.9942 ± 0.0007 and 0.9976 ± 0.0003) are most consistent with a loose transition state, similar to that seen for the uncatalyzed QJ;hydrolysis, and for PTPases (discussed in the next section). The $^{15}V/K$ on both reactions (1.0014 for calcineurin, 1.0006 for λ-PP) indicate partial charge neutralization on the leaving group in the transition state. The magnitude of $^{15}V/K$ increases in the reaction catalyzed by the H76N mutant of λ-PP to 1.0016, indicating the leaving

group bears more negative charge, consistent with a role of this residue as a general acid. However, this magnitude of $^{15}V/K$ is only about half as large as observed when a full negative charge resides on the leaving group, e.g., in reactions of PTPases when their general acids have been removed by mutagenesis. It is also possible that charge neutralization of the leaving group is assisted by a metal-coordinated water molecule. Thus, the role of the conserved His residue remains uncertain. It has also been suggested that this residue may serve as a general base to deprotonate the nucleophilic metal-coordinated water.[135]

Several groups have investigated the role of the conserved Arg residues in PPP catalysis. It has been demonstrated that a decrease in activity is observed in λ-PP, PP1, and PP2B when the conserved Arg residues are mutated.[139,144–146] In the crystal structures of PP1 and PP2B these conserved Arg residues form hydrogen bonds with the oxyanions of either bound phosphate or tungstate. It is possible that these residues may be important in not only binding of substrate, but also aligning the substrate over the bridging hydroxide ion for hydrolysis.

X-ray structural data for PP2C reveals the metal ligands to the binuclear metal center consist entirely of oxygen or oxyanions, in the form of carboxylates, water molecules, and the carbonyl oxygen of a glycine residue (Fig. 24).[130] This structure shows phosphate bound in a position not directly coordinated to the metal center.

Like most of the PPP family, the identity of the metal ions of PP2C in vivo is uncertain, but PP2C binds its catalytic metal ions loosely. Typically assayed with Mn^{2+} supplied in the buffer, saturation kinetics show that 10 mM $[Mn^{2+}]$ is needed to achieve full activation.[147] Values of K_{metal} for several divalent ions range from 1.42 mM for Mn^{2+} to 20.6 mM for Mg^{2+}.[147] The highest activity is observed with Fe^{2+}, which results in a 1000-fold higher k_{cat} and V/K than Mg^{2+}. A pH-rate profile of k_{cat}/K_m of the PP2C reaction using Mn^{2+} and Mg^{2+} with pNPP as
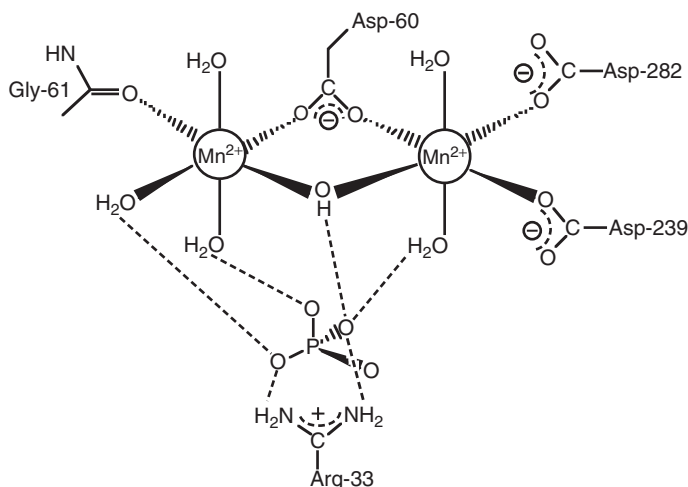
Fig. 24   The active site region of PP2C with phosphate ion.

substrate identified two critical ionizations required for activity.[147] A species with a pK_a ~7.5 must be unprotonated, while an ionization with a pK_a of 9 must be protonated for catalysis. It was proposed that the group having a pK_a value of approximately 7.5 might be the water molecule that bridges the two metal atoms in the active site. The identity of the other ionizable group is not yet clear. The only X-ray structure of PP2C[130] reported to date was obtained at pH 5, where the enzyme has very little activity.[147] In this structure, the conserved His-62 is located near the active site but the side chain is too far away to act as a general acid/base and, instead, hydrogen bonds with Asp-199. It is speculative to propose a role for the residues close to the active site based on this structure, because at this pH the environment surrounding the active site may not represent the active form of the enzyme. The structure has phosphate bound, but not directly coordinated to either of the metal ions, but connected to the metal center by shared hydrogen bonds to water molecules.

The possible roles of His-62 and Arg-33 were examined kinetically using site-directed mutants.[148] Analysis of H62Q and R33A yielded k_{cat} values that were 20- and 2-fold lower, respectively, than wild-type PP2C with the substrate pNPP. The mutant R33A showed a 8-fold higher K_m for substrate, while the K_m observed with H62Q was unaffected. The pH dependence of k_{cat} and k_{cat}/K_m with the H62Q mutant showed an order of magnitude decrease in k_{cat}, but no change in the bell-shaped behavior of k_{cat}. However, the k_{cat}/K_m profile showed loss of the basic limb resulting from the group whose pK_a is 9 in the wild-type enzyme. Brønsted analysis using several phosphomonoester substrates with different leaving group pK_a values were carried out. A Brønsted analysis with wild-type PP2C revealed that at pH 7.0 the phosphoryl transfer step is rate-limiting only for substrates with leaving group pK_a values >7.[147] Under such conditions, a β_{lg} of -0.32 was obtained, similar to that exhibited by calcineurin. The H62Q mutant gave a greater dependency ($\beta_{lg} = -0.84$) on leaving group pK_a, consistent with a role for His-62 as a general acid during the cleavage of the P–O bond.[148]

PROTEIN-TYROSINE PHOSPHATASES (PTPASES)

The PTPases share the signature motif $(H/V)C(X)_5R(S/T)$. This motif is also found in the low-molecular-weight PTPases, as well as in the VH1-like dual-specific phosphatases, so-called because they dephosphorylate phosphotyrosine as well as phospho-Ser/Thr residues.[129,149] These three groups of phosphatases have little sequence similarity other than the signature motif and the placement of the essential Cys and Arg residues in the active site.

The X-ray structures of a number of PTPases have been reported, including the catalytic domains of PTP1B complexed with tungstate[150] and of Yop51 from *Yersinia* (residues 163–468)[151] with and without complexed tungstate. The structure of the human dual-specific phosphatase VHR (Vaccina H1-related) has also been determined,[152] as well as those of several low-molecular-weight PTPases, including

the bovine enzyme complexed with sulfate[153] and with vanadate,[154] the human enzyme[155] and that from yeast.[156] The collective structural data show that these enzymes all share highly similar active-site clefts (see Fig. 25).

These enzymes have been the focus of intensive mechanistic study, and the functions of conserved Cys, Asp, and Arg residues are well understood. Mechanistic studies on the *Yersinia* PTP,[157,158] the mammalian PTP1,[159] the low-molecular-weight PTPase Stp1 from yeast,[160] and on the human VHR[161,162] show that these enzymes share a number of features. These include the requirement for the nucleophilic cysteine to be deprotonated for catalysis, the dianion of the phosphomonoester is the substrate, and a conserved Asp serves as a general acid to protonate the leaving group in the first step and as a general base to promote attack by water in the subsequent hydrolysis of the phosphocysteine intermediate.[163] The formation of a phosphocysteine intermediate has been demonstrated using ^{32}P-labeled substrates and ^{31}P NMR,[164–167] and using the Q262A mutant of PTP-1B, which permitted the accumulation of the intermediate and its observation by X-ray crystallography.[168]

The active-site cysteine in PTPases has a very depressed pK_a that ranges from ∼4.7 in the *Yersinia* enzyme[169] to 5.5 in VHR.[161] In the *Yersinia* PTPase (YopH), His-402 has been proposed to decrease the pK_a of Cys-403 by 2.7 pH units,[169] while Thr-410 additionally lowers this pK_a by 0.6 pH units.[170] Mutation of the His-402 residue in Yersinia PTP to Asp or Ala increases the pK_a of Cys-403 to 5.99 and 7.35, respectively.[169] This His residue does not directly hydrogen bond to the Cys residue, thus, the effect is most likely due to the disruption of the hydrogen-bond network
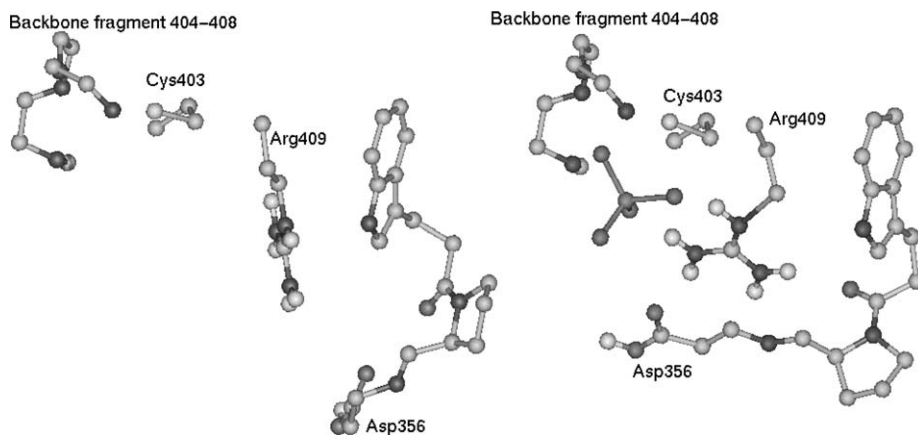
Fig. 25 The orientations of groups at the active site of free *Yersinia* PTPase (left) and when sulfate is bound (right). The binding of other oxyanions, such as tungstate, results in a similar conformational change. Hydrogen bonds form between the oxyanion and backbone amide groups and with Arg-409. The Arg side chain rotates to form two hydrogen bonds to the oxyanion, resulting in formation of a new hydrogen bond with the carbonyl oxygen atom of Trp-354. Associated movements of a protein loop bearing Asp-356 bring it into position to function as a general acid during catalysis. The structures shown are from published X-ray structures with computer-generated hydrogen atoms added to the Arg and Asp residues.

within the active site. The low pK_a of the conserved Cys ensures that it is in the thiolate form under physiological conditions.

The pH-rate profiles for V/K of the PTPases are invariably bell shaped, and pK_{a1} is assigned to the conserved Cys nucleophile. The second pK_a is ascribed to the conserved Asp residue that serves as a general acid in the first step of the catalytic reaction. This residue resides on a flexible loop that closes down on the active-site cleft upon oxyanion (phosphate, sulfate, or tungstate) binding. In the *Yersinia* PTP, the alpha carbon of the general acid Asp-356 moves by about 6 Å toward the active site upon binding of tungstate or sulfate, into a position ideally suited to protonate the leaving group in the catalytic reaction[151,171] (Fig. 25). This conformational change is triggered primarily by movement of the Arg-409 side chain. Oxyanion binding causes the guanidinium group to rotate 90° and shift by about 2 Å, allowing formation of two hydrogen bonds with the oxygen atoms. As Arg-409 moves toward the oxyanion, the side chain of Trp-354 slides into a hydrophobic crevice, optimizing van der Waals contacts.[172] The same loop movement, triggered by an invariant Arg residue, is observed in all of the X-ray structures of PTPases with bound oxyanions, as well as in the structure of a catalytically inactive mutant of the yeast low-molecular-weight PTPase complexed with the substrate *p*NPP.[156]

KIEs with the substrates *p*NPP and *m*NBP have been used to examine the transition state structure of the first phosphoryl transfer step, formation of the phosphocysteine intermediate. KIEs were measured for the reaction with the substrate *p*NPP with the *Yersinia* PTP and PTP1,[173] with VHR,[174] and with Stp1.[175] Kinetic studies, and the invariance of the isotope effects with pH, indicate that the chemical step is rate-limiting in each of these enzymes and thus the isotope effects reveal the transition state structure. For each of these PTPases, small, inverse magnitudes for $^{18}(V/K)_{nonbridge}$ suggest that the transition state is loose, resembling that in uncatalyzed phosphoryl transfer. Near-unity values for $^{15}(V/K)$ with all of the PTPases examined, except Stp1, mean that the leaving group is neutral in the transition state, implying that proton transfer to the leaving group is synchronous with P–O bond fission; in the Stp1 case, a partial negative charge remains on the leaving group, suggesting that proton transfer may slightly lag behind P–O bond fission. The magnitudes of the primary $^{18}(V/K)_{bridge}$ KIEs for all of the PTPases are those expected of a late transition state, in which both P–O bond fission and proton transfer are well advanced (Table 3).[176]

In all four of these enzymes, when the general acid Asp is mutated to Asn (Table 3), the values for $^{18}(V/K)_{nonbridge}$ become slightly normal, indicating that the transition state has somewhat more nucleophilic participation, although less than that in reactions of phosphodiesters or triesters. The magnitudes of $^{18}(V/K)_{bridge}$ and $^{15}(V/K)$ are significantly higher, indicating extensive bond cleavage to the leaving group, which now bears essentially a full negative charge.

KIEs and pH-rate dependencies for V/K were measured for the reactions of the dual-specificity phosphatase VHR[177] and the *Yersinia* PTP[178] with the alkyl phosphate *m*NBP, which, with a leaving group pK_a of 14.9, is a better mimic for physiological alkyl phosphate substrates like phosphoserine or phosphothreonine. In

Table 3 Kinetic isotope effects for reactions of pNPP with members of the PTPase family: the *Yersinia* PTPase (YopH), PTP1, the dual-specific VHR, and the low-molecular-weight PTPase Stp1

	$^{15}(V/K)$	$^{18}(V/K)_{\text{bridge}}$	$^{18}(V/K)_{\text{nonbridge}}$
YopH, PTP1, VHR (range)	0.9999–1.0001	1.0118–1.0152	0.9998–1.0003
Stp1	1.0007	1.0171	1.0007
D to N mutants of YopH, PTP1, VHR, Stp1 (range)	1.0024–1.0030	1.0275–1.0297	1.0019–1.0024

Standard errors are in the range of 0.0001–0.0008.

both enzymes, compared with pH-rate data for pNPP, the pH-rate profile showed a shift consistent with the change in pK_{a2} of the substrate, which is 6.2 for mNBP versus 5 for pNPP, consistent with the dianion form of the substrate as the catalytically active species. The small, slightly inverse $^{18}(V/K)_{\text{nonbridge}}$ KIEs (0.9999 for YopH, 0.9986 for VHR) are not measurably different from those with pNPP, and are consistent with a loose, metaphosphate-like transition state. The $^{18}(V/K)_{\text{bridge}}$ KIEs are much smaller with mNBP than with pNPP for both the YopH reaction (0.9995 ± 0.0008, versus 1.0152 ± 0.0006, respectively) as well as for VHR (1.0004 ± 0.0007 versus 1.0118 ± 0.0020). This isotope effect is affected both by the extent of protonation and P–O bond fission; protonation will result in an inverse contribution to $^{18}(V/K)_{\text{bridge}}$ while the contribution resulting from P–O bond fission is normal. The significantly smaller net $^{18}(V/K)_{\text{bridge}}$ KIEs with mNBP indicate that protonation is more advanced in the reactions with the alkyl phosphomonoester substrate than with the aryl substrate. This is a logical expectation from the relative basicities of the two substrates; some degree of P–O bond fission must occur to make the proton transfer from Asp thermodynamically favorable. For the more basic m-nitrobenzyl alcohol leaving group, this will occur sooner (with a smaller degree of bond fission) than when the leaving group is p-nitrophenol. A similar difference in timing of protonation of the leaving group with P–O bond fission was found in the uncatalyzed hydrolysis of the monoanions of mNBP and pNPP.[41] This leads to the conclusion that the transition states in the PTPase reactions are not significantly different from those in the uncatalyzed hydrolyses of their substrates.

To probe the role of the conserved Arg residue, the KIEs for the R409K and R409A mutants of the YopH were measured.[179] The data revealed an interesting interplay between the Arg and the functioning of the general acid. The values for k_{cat} are reduced by about four orders of magnitude by these mutations, but the rate for R409A is about 2.5 higher than that for R409K. For the reaction catalyzed by R409K, the isotope effects resemble those for the general acid mutant D356N. This means the general acid has been rendered nonfunctional, and the leaving group departs as an anion in the transition state. By contrast, in the reaction of R409A, the isotope effects are intermediate between those of the wild-type and general acid mutant.[179] This indicates that the general acid is still partially operative in R409A,

and the leaving group bears about half a charge. This is the opposite of what would be expected on the basis of the similarity of the side chains. Lysine (Lys), like Arg, is cationic, while Ala is much smaller, and neutral. Apparently, changing the position of the positive charge interferes more with the proper movement of the loop bearing the general acid than having no cationic residue at all in this position. This emphasizes the danger of attributing a change in rate to a particular effect without doing a mechanistic analysis. One might have reasonably attributed the lowered catalytic rate of the R409K mutant to a loss in transition state stabilization afforded by the positive charge of Arg-409, when, in fact, the majority of the effect is due to a disabling the general acid.

The transition state of the second chemical step of the PTPase reaction, dephosphorylation of the intermediate, was probed in Stp1 using LFER.[180] This method made use of the fact that the phosphocysteine intermediate can phosphorylate alcohols as well as water. The β_{nuc} value was found to be $+0.14$, a value indicative of little nucleophilic participation, and thus a loose transition state. The carboxylate of Asp-128 is thought to act as a general base in the dephosphorylation step, and deprotonation of the nucleophile could suppress the magnitude of β_{nuc} by neutralizing the positive charge that would otherwise accrue. A Glu residue in this position, a weaker general base, gives rise to a similar value ($+0.11$) for β_{nuc}, suggesting that the extent of deprotonation in the transition state is not significant.[180]

Interestingly, the β_{nuc} parameter for dephosphorylation of the intermediate increased to 0.26 in the S18A mutant of Stp1. The Ser-18 residue in Stp1 is representative of a conserved hydroxyl group that hydrogen bonds to the nucleophilic sulfur atom in the PTPase signature motif. Loss of this interaction presumably makes the sulfur a poorer leaving group, resulting in a somewhat later transition state, reflected in the increased β_{nuc}.[180] Fig. 26 shows the mechanisms of the first and second phosphoryl transfer steps, and a diagrammatic representation of the transition state, consistent with all of the experimental data for the PTPase family of phosphatases.

Several groups have used computational methods to address the PTPase mechanism. Computations have led some to propose an alternative mechanism, in which the reactive form of the substrate is the monoanion.[181–184] In one version of this mechanism, the dianion is proposed to bind to the form of the enzyme in which the Cys residue is protonated; the substrate then deprotonates the Cys nucleophile. A common feature of these proposals is the net charge of –2 in the Michaelis complex (ignoring the Arg) versus –3 as supported by the experimental data. The conflict with experimental data led proponents of the alternative mechanism to question the assignment of ionization constants in pH studies of PTPases, as well as the interpretation of KIEs.[183,184] Errors in these criticisms were subsequently presented,[185] and computational methods by others have yielded conclusions in complete agreement with the experimental data supporting a charge of –3 in the Michaelis complex.[26,27,186] One such study,[26] using the bovine low-molecular-weight PTPase, found through a structural analysis that the enzyme stabilizes the loose, metaphosphate-like transition state via enhanced hydrogen bonding during the inversion of the phosphoryl group.
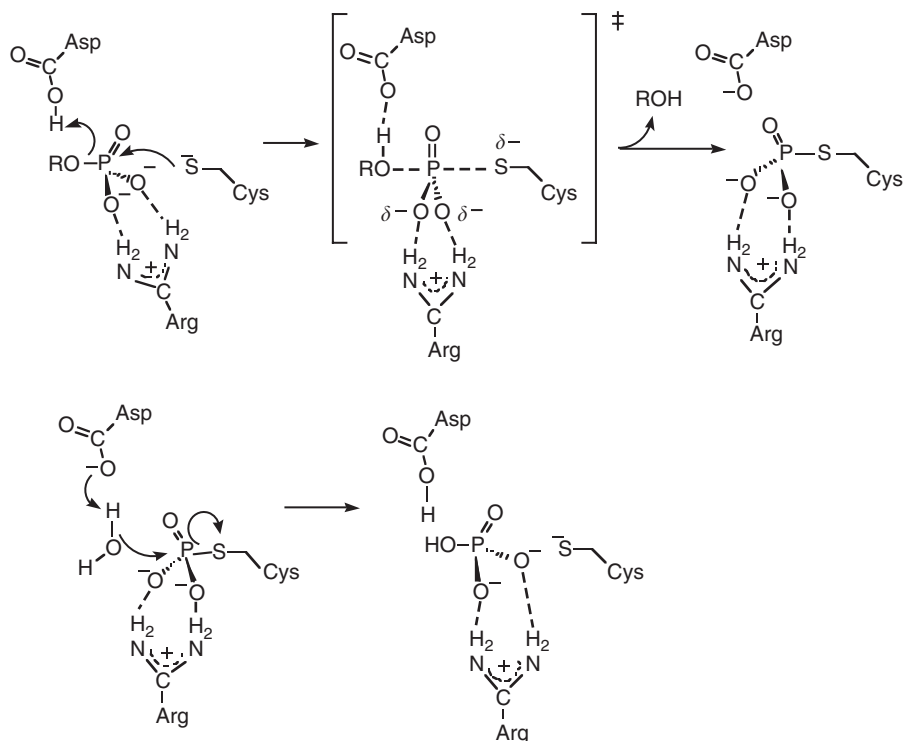
Fig. 26 In the first step of the reaction catalyzed by PTPases, the thiolate nucleophile of a conserved cysteine attacks the dianionic form of the substrate. The transition state is loose, and the leaving group is neutralized by proton transfer from the conserved Asp residue. In the second step the carboxylate of this residue deprotonates a nucleophilic water molecule. The transition state of the second step (not shown) is also loose, with a small degree of bond formation to the nucleophile.

RAS

The guanine triphosphate (GTP)-binding proteins, or G-proteins, regulate a host of cellular processes and act as molecular switches by catalyzing the conversion of GTP to guanine diphosphate (GDP). These proteins are "on" when bound to GTP, and are switched to their inactive or "off" state upon hydrolysis of GTP to produce GDP.[187,188] For the Ras family of G-proteins, stereochemical analysis has shown that the enzyme catalyzes phosphoryl transfer from GTP to water with inversion of configuration,[88] indicative of direct phosphoryl transfer to water. The GTPase reaction catalyzed by Ras alone is slow, with a half-life of 25 min at 37 °C; this rate is about 100-fold slower than typical G-proteins. The hydrolysis is substantially accelerated by GTPase-binding proteins, termed GTPase activating proteins (GAPs); those that are specific for Ras are called the RasGAPs. In the presence of GAP, the GTPase reaction of Ras is 10^5-fold faster. The mechanism of GTP hydrolysis catalyzed by these enzymes is the subject of interest, centering on the nature of the
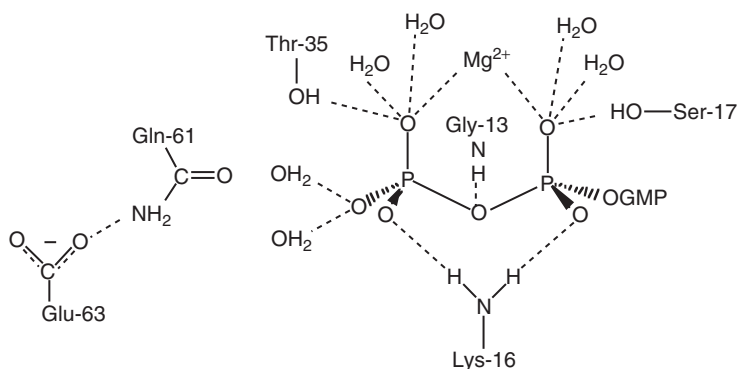
Fig. 27 A representation of the conformation of the substrate analog GppNp bound to Ras. Dashed lines indicate hydrogen-bonding interactions. In this drawing the NH moiety that joins the β- and γ phosphoryl groups in the X-ray structure is replaced by oxygen, as in the natural substrate.

transition state and the identity of the catalytic base that activates a water molecule for nucleophilic attack, or whether such a base is even necessary in the transition state.

The X-ray structure was obtained of the Ras protein complexed with a relatively unreactive GTP analog, GppNp (this molecule is a GTP analog in which the β–γ-bridging oxygen atom is replaced by NH) (Fig. 27).[189] A number of water molecules and side chains were found within hydrogen-bonding distance of all three phosphate groups. The structure led to the mechanistic proposal that glutamine (Gln-61) serves as a catalytic general base to deprotonate a nucleophilic water molecule.[189] It was further proposed that the carboxylate of Glu-63 could assist in properly orienting Glu-61, and/or increase its basicity. The finding that mutation of Glu-63 to Lys somewhat increases activity[190] was cited as evidence for involvement of this residue, at least indirectly, in catalysis. This Gln residue is conserved among small guanine nucleotide-binding proteins, except for those encoded by the *rap* genes. The *rap* p21 enzymes have Thr-61 in place of Gln-61 and have lower GTPase activity; mutation of Thr-61 to Gln increases the GTPase rate to the value found for p21 Ras. Replacement of Gln-61 by Glu increases the rate of GTP hydrolysis by 20-fold, which was also considered evidence that this residue acts as a general base.[191]

An amide is an unlikely candidate to serve as a base, and subsequent mechanistic proposals have centered on the possibility that the γ-phosphoryl group deprotonates the nucleophilic water molecule, or, whether a base is needed at all. To address the former possibility, an unusual type of LFER was obtained by altering the pK_a of the γ-phosphoryl group by means of mutating several residues in its vicinity.[192–194] The pK_a values were obtained either directly by titration using ^{31}P NMR, or, indirectly by analysis of the pH-rate profile of the GTP hydrolysis reaction. A correlation between k_{cat} and the pK_a of the γ-phosphoryl group was found, with a Brønsted slope of 2.1; in the presence of the activating protein GAP, the Brønsted slope increased to 4.9.[192,194] The significant Brønsted dependency of rate on pK_a is

consistent, although not exclusively so, with the notion that the γ-phosphoryl group deprotonates a nucleophilic water molecule. Alternatively, the correlation of hydrolysis rate with the basicity of the γ-phosphoryl group has been proposed to result from progressively stronger, cooperative hydrogen-bonding interactions of nearby cationic residues with the γ-phosphoryl group as its basicity increases, thus further stabilizing the transition state.[5] Gln-61 was proposed to stabilize or assist in positioning this water molecule (Fig. 28).[193] The finding of a small, inverse solvent isotope effect ($^{D}k = 0.7$)[192] implies that deprotonation occurs before the rate-limiting step, since proton transfer in this step usually results in a significant normal solvent isotope effect.

From model studies of the uncatalyzed reactions of GTP and related molecules in solution, the assumption that a base is necessary in the transition state of the Ras-catalyzed reaction has been questioned.[195] LFER experiments result in a Brønsted β_{nuc} of 0.07 for the phosphoryl transfer of the γ-phosphoryl group from ATP, GTP, and pyrophosphate to a series of alcohols, indicative of very little nucleophilic participation in the transition state.[33] The Brønsted $\beta_{lg} = -1.1$ for phosphoryl transfer to water from a series of phosphoanhydrides is suggestive of a large degree of bond fission to the leaving group.[33] The presence of Mg^{2+} has no measurable effect on the rates of the model reactions.

In a loose transition state for phosphoryl transfer, the greatest change in charge distribution relative to the ground state is the increased negative charge density on the bridge oxygen atom. In the GTP to GDP reaction charge also builds up on the nonbridging oxygen atoms of the scissile β-phosphoryl group; the bound Mg^{2+} and Lys-16 of native Ras are in position to stabilize such charge (Fig. 27). The structure of Ras with bound GppNp revealed that the $\beta\gamma$ bridge oxygen is exposed at the bottom of an exposed crevice. A prediction[195] that the GAPs might stimulate the GTPase activity of Ras by donation of a hydrogen bond to the $\beta\gamma$ bridge oxygen atom by an Arg residue, thereby further stabilizing the transition state, was confirmed by the X-ray structure of Ras-GDP-AlF$_3$ in a complex with GAP-334.[196] The so-called Arg finger residue (Arg-789 of GAP-334) was found inserted in the crevice in a location ideally suited to stabilize developing negative charge on the scissile oxygen atom in the transition state. Using a fluorescent GTP substrate analog, it was shown that mutation of this Arg residue to Lys reduces k_{cat} by three orders of magnitude.[197]
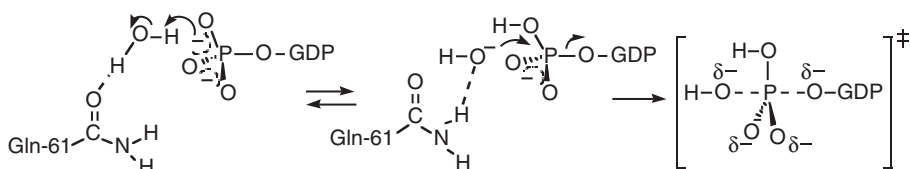
Fig. 28 A model of the proposed role of the conserved Glu and the γ-phosphoryl group in the Ras-catalyzed hydrolysis of GTP. The alternative of water attack upon a dianionic terminal phosphoryl group has also been proposed.

These findings suggest a late transition state with respect to bond fission to the β-phosphoryl group, which would result in substantial negative charge on the scissile bridge oxygen atom. This is in agreement with the uncatalyzed reactions of ATP and GTP. In a tight, triester-like transition state, little charge develops at this position, and catalysis would be better assisted by interactions with the nonbridging γ-phosphoryl oxygen atoms. The transition state of the Ras-catalyzed reaction cannot be fully described until information regarding the degree of nucleophile bond formation is obtained.

A recent time-resolved Fourier transform infrared (FTIR) study yielded interesting insights into the manner in which Ras promotes catalysis.[198] The reaction was initiated by the photolysis of caged GTP bound to Ras. The vibrations of the phosphoryl groups of GTP were assigned using ^{18}O-labeled caged GTP. The data indicate that, in contrast to the considerable coupling that exists between vibrations of the three phosphoryl groups of unbound GTP, in bound GTP the vibrations are uncoupled, and individual vibrations of the α-, β-, and γ-phosphate groups are observed. This observation indicates that binding to Ras forces the flexible GTP molecule into a restrained conformation. The binding also causes a downshift in the frequency of the GTP β-PO_2^- vibration, whereas the α-PO_2^- and γ-PO_3^{2-} vibrations shift to higher wave numbers. The downshift indicates a reduction in the bond order of the nonbridging P–O bonds of the β-phosphate group. The bond order changes can be explained by a shift of negative charge from the γ- to the β-oxygen atoms; in other words, a charge distribution that is more like that in the transition state. This charge shift may be a key factor contributing to catalysis by Ras, in addition to the correct positioning of the attacking water and stabilization of charge on the $\beta\gamma$ bridge oxygen atom of GTP. Ras appears to shift this negative charge by interactions with Mg^{2+}, backbone NH groups of several amino acids, and the Lys-16 side chain.[198]

Subsequently, this technique was applied to the Ras (GAP)-catalyzed reaction.[199] The complete GTPase reaction pathway was observed, with a time resolution of milliseconds. The shift of negative charge from the γ- to the β-phosphate found in the Ras study was shown to be enhanced by GAP binding. Thus, the charge distribution of the GAPRasGTP complex resembles that in a loose, metaphosphate-like transition state. Evidence for an intermediate species was observed on the reaction pathway, after the bond between β- and γ-phosphate is cleaved. The putative intermediate surprisingly shows bands expected of a phosphorylated enzyme intermediate. However, the existence of such an intermediate is at odds with the stereochemical outcome of the reaction, which is inversion. In addition, the FTIR analysis revealed that phosphate release is the overall rate-limiting step for the GAP-catalyzed reaction.[199]

PHOSPHOGLUCOMUTASES

The α- and β-phosphoglucomutases (α- and β-PGM) catalyze the interconversion of D-glucose-1-phosphate (G1P) and G6P (Scheme 3). These enzymes are named for the anomer of G1P on which they act; thus, α-PGM acts on the α-C(1) anomer of
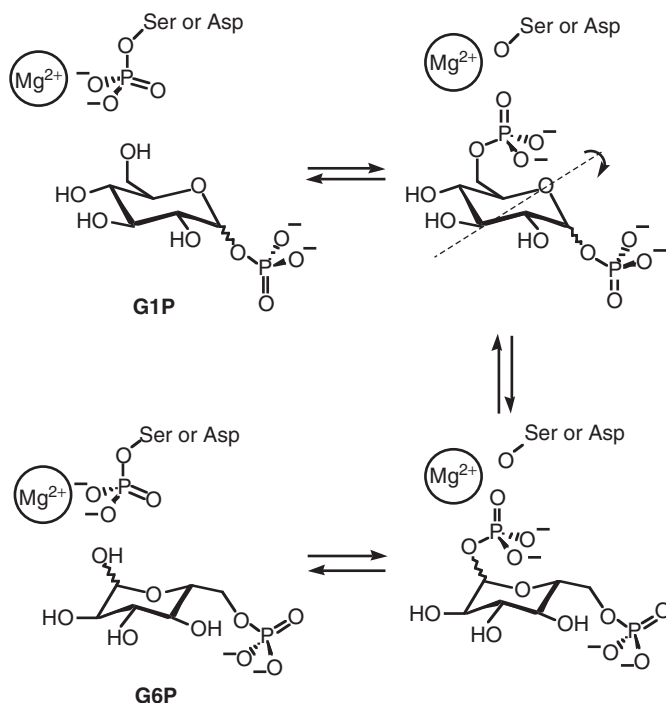
Scheme 3 Representations of the four enzyme–substrate complexes on the reaction pathway of PGMs. The α-PGMs utilize the α-anomers at C1, and a serine as the phosphoryl carrier. The β-PGMs utilize the β-anomers at C1 and an Asp as the phosphoryl carrier.

G1P, while α-PGM catalyzes the reaction of the β-C(1) anomer. Both mutases employ Mg^{2+} and α- or β-glucose 1,6-diphosphate (G1,6-diP) as cofactors.

Stereochemical analysis of the products using [^{16}O, ^{17}O, ^{18}O] phosphate ester methods show that the PGM reaction proceeds with overall retention of config-uration at phosphorus,[200] which indicates that an even number of phosphoryl transfers are involved. The catalytic reactions of both α- and β-PGM proceed via a phosphoenzyme intermediate, formed by the reaction of an active-site nucleophile with G1,6-diP. The α-PGM utilizes an active-site Ser nucleophile, while β-PGM uses an active-site Asp. The phosphorylated PGM binds either G1P or G6P and transfers the phosphoryl group to the C(6)OH or C(1)OH, respectively (Scheme 3).

The mechanism shown in Scheme 3 leaves open the question of whether the intermediate G1,6-diP dissociates from the enzyme during catalysis. Substrate re-orientation within the active site occurs at a faster rate than dissociation with PGM from rabbit muscle and from rat.[201] This means that the substrate reorients by flipping within the confines of the active site, rather than by dissociating and re-binding. In contrast, dissociation is more rapid with the PGM from *Bacillus cereus* and *Micrococcus lysodekticus*, and as a result, the latter enzymes have an absolute requirement for Gl,6-diP as a cofactor to rephosphorylate the enzyme.
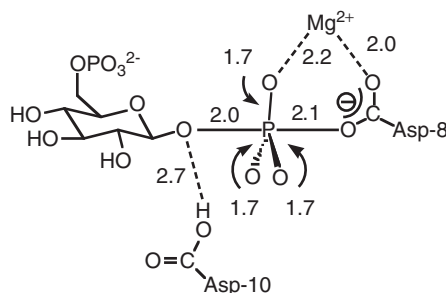
Fig. 29 The elongated pentacoordinate phosphorus species observed in the X-ray structure of β-PGM from *Lactococcus lactis*. Distances shown are in angstroms. In addition to the interactions shown, the PO_3 moiety also makes hydrogen-bonding contacts with two backbone amide N–H groups, and the hydroxyl of Ser-114.

The X-ray structure of the β-PGM from *Lactococcus lactis* reveals a small active-site cavity, seemingly too small to permit reorientation. Since the structure showed that the active site of this enzyme contains two neighboring Asp residues, Asp-8 and Asp-10, it was proposed that both Asp residues might function in phosphoryl transfer with one as the phosphoryl acceptor and the other as the donor, thus eliminating the need for dissociation and rebinding, or for reorientation of the G1,6-diP intermediate within the active site.[202]

On the basis of spectroscopic studies using the transition state analog glucose 1-phosphate 6-vanadate bound to the enzyme, the transition state for phosphoryl transfer was concluded to be S_N2-like in character, and tighter than the transition states of phosphomonoester dianions in uncatalyzed reactions.[203] Recently, a 1.2 Å resolution X-ray structure of β-PGM from *Lactococcus lactis* obtained at cryogenic temperature revealed a seeming intermediate in the reaction (Fig. 29).[204] There has been some question[205,206] and response[207] as to whether the pertinent four-atom moiety observed in the X-ray structure is PO_3 or MgF_3. Assuming it is a phosphorus species, it is certainly an unusual one. The authors refer to it as a pentacovalent phosphorane intermediate.[204] Pentacovalent phosphoranes exhibit typical P–O bond lengths of 1.7 Å. The apical P–O bond lengths in the X-ray structure correspond to bond orders of between 0.2 and 0.3, using Pauling's rule.[208] With such low bond orders to the apical oxygen atoms, there seems no reason why this structure could not be described as a stabilized metaphosphate, at least as accurately as a pentacovalent phosphorane. The metaphosphate anion has never been directly observed in solution, but it exists as a stable entity in the gas phase, where it is surprisingly nonreactive.[209] Metaphosphate has also been seen in the X-ray structure of crystals of fructose-1,6-bisphosphatase grown in an equilibrium mixture of substrate and product.[210] These results suggest that the stability of metaphosphate can be modulated by its environment.

In a computational study, the species from the X-ray structure did not converge to an energetic minimum, but instead to a transition state for phosphoryl transfer (with a moderate barrier of 14 kcal/mol) from substrate G6P to the product G1,6-diP. The

computationally modeled reaction is concerted with no phosphorane intermediate, and with proton transfer from the hydroxyl group of glucose to Asp-10 in the same step as phosphoryl transfer.[206] Further experimental data are needed to determine whether Asp-10 functions as an acid–base catalyst, as suggested by the calculations,[206] or as an alternate phosphoryl donor, as proposed on structural grounds.[202]

7 Phosphodiesterases

STAPHYLOCOCCAL NUCLEASE

Staphylococcal nuclease (SNase) is one of the most powerful enzymes known in terms of its rate acceleration, with a catalytic rate that exceeds that of the non-enzymatic reaction by as much as 10^{16}.[211] This enzyme is a phosphodiesterase, and utilizes a Ca^{2+} ion for catalysis to hydrolyze the linkages in DNA and RNA. In addition to the metal ion, the active site has two Arg residues in a position to interact with the phosphoryl group, and a glutamate. X-ray structures[212–215] of SNase have been solved for the wild-type enzyme and mutants, but the exact roles of active-site residues are still uncertain. SNase cleaves the 5'O–P nucleotide bond to yield a free 5'-hydroxyl group (Fig. 30).

Stereochemical experiments show that the reaction proceeds with inversion of configuration at phosphorus, consistent with a single in-line nucleophilic attack by a water molecule.[216] The Glu-43 residue was proposed to act as a general base on the basis of the first X-ray structure of the enzyme,[212] and the hydroxide could also be stabilized by electrostatic interactions with the Ca^{2+} ion. Mutation of Glu-43 to Asp results in a 200-fold reduction in k_{cat} at pH 9.5.[217] However, the E43D mutant was found to be significantly structurally altered compared to the native enzyme, by NMR[218] and by X-ray crystallography.[214] Similarly, an investigation of the roles of the Arg residues (Arg-35 and Arg-87) by mutation of these residues to Lys led to the
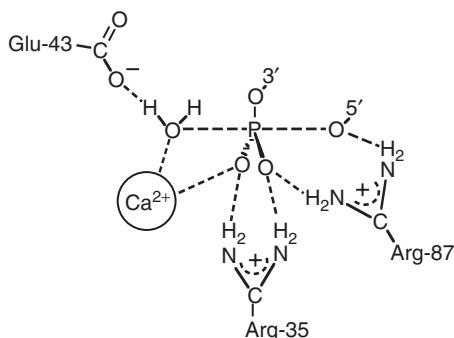
Fig. 30 A model of the proposed interactions involved in the hydrolysis of the phosphodiester bond of nucleotides by staphylococcal nuclease.

discovery that the mutations result in large reductions in catalytic activity, but also cause structural alterations.

The rate-limiting step for the hydrolysis of single-stranded DNA by SNase was subsequently shown to be product dissociation, and substrate binding is diffusion-controlled when the pH is >7.3.[219] The pH optimum is between 8.6 and 10.3, and the enzyme is routinely assayed at pH 9.5. Thus, under these conditions, kinetic studies cannot reveal the effect of mutations on the chemical step. On the basis of the dependence of rate on pH it was proposed that Glu-43 does not act as a general base.[219] It was also proposed that residues in a protein loop near the active site may be involved in the physical process that is the rate-determining step.[219]

It seems safe to say that the function of the two Arg residues includes stabilization of the transition state by forming hydrogen-bonding interactions with the phosphoryl group. The means by which the nucleophile is deprotonated is still to be clarified. The SNase story illustrates the need to insure that seemingly conservative mutations do not result in structural alterations, and exemplifies the difficulties that can accompany enzymatic mechanistic analysis, even when detailed structural data are available.

RIBONUCLEASE (RNASE)

RNase catalyzes the hydrolysis of the phosphodiester bonds of RNA, thus accomplishing its degradation. The initial reaction is attack of the 2′-hydroxyl group to form a 2′,3′ cyclic phosphate (Scheme 4). Hydrolysis of this intermediate results in a 3′-phosphomonoester. It has been shown by ^{31}P NMR[220] and chromatographic means[221–223] that the cyclic intermediate accumulates during the RNase-catalyzed reaction; the enzyme releases most of the cyclic intermediate. During the analogous buffer-catalyzed or alkaline reaction, hydrolysis of the cyclic phosphate is faster than its formation.[220]

RNase A is the paradigm of the RNase family and has been the subject of a number of reviews.[224–227] It was the first enzyme for which the amino acid sequence was determined, and the third enzyme for which an X-ray structure was obtained.[228] Stereochemical experiments show that both the transphosphorylation[229,230] and the hydrolysis of the cyclic intermediate[231] each proceed with inversion, suggesting a concerted, in-line phosphoryl transfer process. Scheme 4 shows the primary catalytic groups involved in catalysis, using the numbering for RNase A. The enzyme also has a Lys-41 in RNase A that is within hydrogen-bonding distance to the phosphoryl group. The catalytic reaction has a bell-shaped pH-rate dependency, indicative of general acid–base catalysis. His-12 and His-119 are the residues assigned to these roles. Among the data supporting this assignment are the recent semi-synthesis of a form of RNase A in which both His residues are replaced by 4-fluorohistidine, which has a pK_a of 3.5 compared to 6.8 for His. This RNase variant still exhibits a bell-shaped pH-rate profile, but with both pK_a values shifted to a lower pH.[232]

Elimination of the imidazole moiety of general base His-12 by mutation to Ala results in a 10^4-fold rate reduction for the cleavage of poly(C), UpA, or
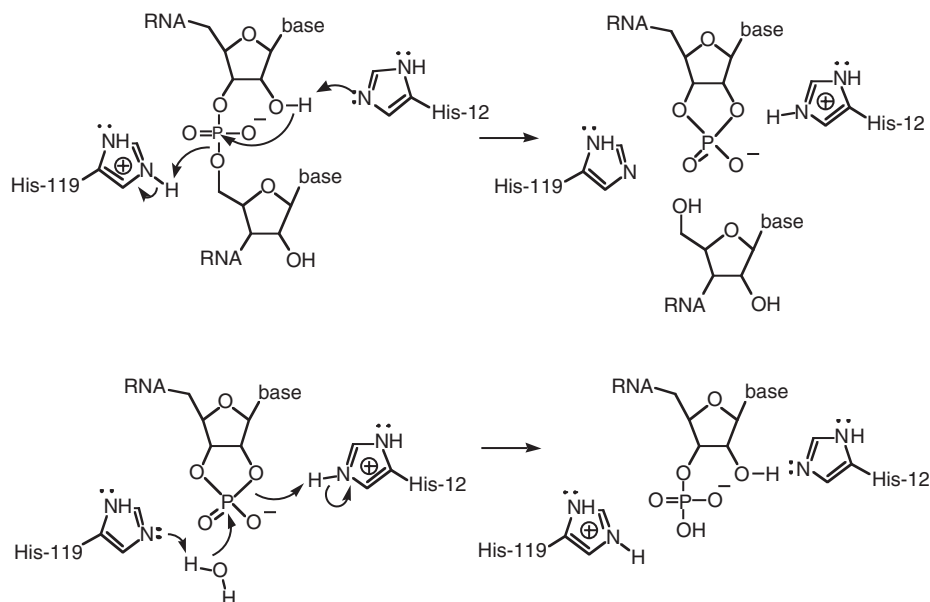
Scheme 4 The putative mechanisms for the two steps of the RNase A-catalyzed reaction. Despite the fact that after the initial transphosphorylation reaction to form the 2′,3′ cyclic phosphate, His-12 and His-119 are in the correct protonation states to immediately catalyze its hydrolysis by water, the cyclic phosphate is released by the enzyme faster than it is hydrolyzed.

uridine-3′-*p*-nitrophenyl phosphate.[233] The same mutation to the general acid His-119 causes a similar rate reduction for the reaction with the substrates poly(C) and UpA; however, the rate with uridine-3′-*p*NPP is little affected. The latter substrate has a leaving group with a much lower pK_a than the others. These results indicate that the importance of the general acid to catalysis diminishes for good leaving groups.

   The mechanism in Scheme 4 is consistent with all of the data collected for the enzymatic reaction. The reaction is concerted, with deprotonation of the nucleophilic 2′-hydroxide by His-12 accompanied by protonation of the leaving group by His-119. In the transition state the phosphorus becomes trigonal bipyramidal. KIEs with uridine-3′-*m*NBP, which has a leaving group pK_a very similar to that of the natural substrate, are consistent with a concerted mechanism with the moderately tight transition state expected of a diester ($^{18}(V/K)_{nonbridge} = 1.005$).[234] The magnitude of $^{18}(V/K)_{bridge}$ of 1.016 is that expected from a combination of P–O bond fission and protonation in the transition state, as seen in the reactions of PTPases (vide supra).

   Based on results obtained in imidazole buffers, an alternative mechanism has been proposed for RNase A.[235] This mechanistic proposal has been the subject of considerable debate, not always polite; the arguments in favor and against have been reviewed.[59,236] In this mechanism, His-119 is proposed to protonate the phosphoryl

group; the 2′-OH group then attacks to form a phosphorane intermediate. His-119 then deprotonates the phosphoryl group of the intermediate, and transfers this proton to the leaving group. No enzymatic data was obtained in these studies, and several lines of evidence obtained for the enzymatic reaction argue against this mechanism; yet, this mechanistic proposal has found its way into at least two textbooks as the mechanism of RNase A.[237,238] This mechanism is not consistent with the KIEs previously mentioned, which support a concerted mechanism.[234] Nor is it consistent with the observation of small thio effects on the ring-opening of both the (R_P) and the (S_P) thio-isomers of cUMP,[239] as thio effects in a triester mechanism are large. However, the thio effect for the reaction of the (S_P) thio isomer of UpA with RNase A is large (70–100) while that for the (R_P) isomer is small (2–4). This indicates that binding effects in the asymmetric active site are at work, complicating the interpretation of the thio effects. The revisionist mechanism is also not consistent with the fact that the H119A mutant cleaves uridine-3′-pNPP at about the same rate as wild-type RNase A.[233] This rules out a role for His-119 in formation of a phosphorane intermediate, at least for this substrate. While the results of each of these experiments may be rationalized in a manner that does not fully rule out the alternative mechanism, the fact remains that no evidence obtained on the enzymatic reaction favors it, and whether this mechanism is even followed in imidazole buffer has been the subject of debate. In the RNase active site, the substrate is ideally positioned for simultaneous acid–base catalysis to facilitate a concerted mechanism. Such a serendipitous arrangement in imidazole buffer would be highly disfavored on entropic grounds.

The role of Lys-41 is commonly attributed to stabilization of negative charge on the phosphoryl group in the transition state. It has generally been assumed that this is an electrostatic interaction, but it has also been proposed that stabilization occurs via formation of a short, strong (low-barrier) hydrogen bond in the transition state.[240] In a series of experiments to probe the nature of the interactions involving Lys-41, it was replaced by a Cys residue, which was then alkylated with several different haloalkylamines.[241] This served to introduce positive charge in several different forms (primary amine, tertiary amine, amidino group) and the resulting effect on catalysis was observed. The amidino group, which can donate a second hydrogen bond, did not enhance activity. An enzyme variant with a quaternary amino group had significantly less activity than the wild type. For variants with amine groups, it was found that superior activity correlated with low pK_a values for the protonated amine. Together these results suggested that the role of Lys-41 is not merely electrostatic, but that the donation of a single hydrogen bond in the transition state is important. This role seems to be the same for both the initial, transphosphorylation reaction, as well as for the subsequent RNase-catalyzed hydrolysis of the 2′,3′-cyclic phosphate.[227]

8 Phosphotriesterases

Phosphotriesters are not naturally occurring compounds, but have been introduced into the environment as pesticides and insecticides since the middle of the twentieth

century. Several phosphotriesterases have been identified, despite the limited time during which these compounds have been available in the environment for the evolution of enzymatic activity for their hydrolysis. These enzymes were discovered by means of the resistance of some insects to insecticides, and the ability of microbes to degrade pesticides.[242,243] Such compounds are close structural relatives to chemical warfare nerve agents; the essential core of these compounds is a neutral organophosphorus compound with a good leaving group. Fig. 31 shows the structures of several such compounds: parathion, used in mosquito control; its relative paraoxon; and sarin, a chemical warfare nerve agent.

The phosphotriesterase from the soil bacterium *Pseudomonas diminuta* is the only one that has been well characterized. The "natural" substrate for this enzyme is unknown; it hydrolyzes a large number of phosphotriester substrates, but the best substrate is paraoxon.[244] Phosphomonoesters are not substrates, and diesters are hydrolyzed only at greatly reduced rates.[245]

This phosphotriesterase catalyzes the hydrolysis of paraoxon and similar substrates with rate accelerations of $\sim 10^{12}$ above the uncatalyzed rates.[244] The active site has two Zn^{2+} ions, and an X-ray structure[246] with the competitive inhibitor diethyl-4-methylbenzyl phosphonate (Fig. 32) shows a binding mode that is strikingly absent of direct electrostatic interactions between the inhibitor and the active site; the phosphoryl oxygen atom is 3.5 Å distant from the more exposed of the two Zn ions. The methylbenzyl group resides in a hydrophobic pocket. The absence of specific interactions explains the ability of the enzyme to hydrolyze a wide range of substrates. The Zn ions are bridged by a hydroxide and by a carbamate moiety formed from the ε-amino group of Lys-169.[246]

The stereochemistry of the phosphotriesterase reaction proceeds with inversion of configuration at phosphorus.[247] Thus, the reaction was postulated to occur by a single phosphoryl transfer event to an activated water molecule. Modeling of a substrate, the S_P enantiomer of [O-ethyl-O-(4-nitrophenyl)benzenephosphonothioate], in place of the inhibitor in an orientation that preserves both the interaction between Zn and the phosphoryl oxygen, and the orientations of the non-leaving groups, led to the conclusion that the leaving group is positioned opposite the bridging hydroxide, suggesting it as the nucleophile.[246]

The native enzyme contains two Zn^{2+} ions, but the apoenzyme can be activated by a number of other divalent ion pairs including Co, Ni, Cd, and Mn, as well as mixed Zn/Cd. These metal substitutions yield enzyme forms that exhibit catalytic activities as high or higher than the native enzyme.[248,249]

Kinetic studies show that the enzymatic reaction depends on a group that must be deprotonated, with a pK_a of 6.1.[250] Kinetic studies with a range of metal ions in the active site show that this pK_a depends on the identities of the metals, consistent with the notion that this pK_a is that of a metal-coordinated water (or hydroxide) nucleophile. LFER obtained using substrates with a range of leaving groups reveal a break in the Brønsted β_{lg} plot, and for good leaving groups ($pK_a < 7$) the phosphoryl transfer step is only partially rate-limiting. For poorer leaving groups, the β_{lg} is very large and negative, –1.8, indicative of fully rate-limiting phosphoryl transfer.[251] This is significantly more negative than the uncatalyzed hydrolysis of the same
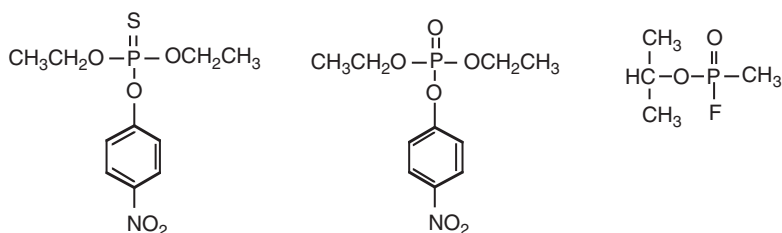
Fig. 31   The structures for parathion (left), paraoxon (middle), and sarin (right).
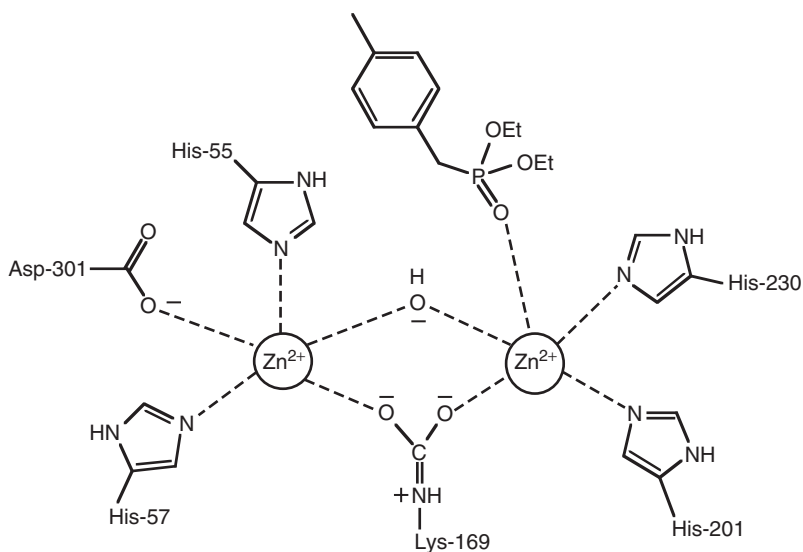
Fig. 32   The structure of the active site of the phosphotriesterase with the competitive inhibitor bound as determined by X-ray crystallography.

compounds, for which $\beta_{lg} = -0.44$. Primary and secondary KIEs on the enzymatic reaction with paraoxon and diethyl 4-carbamoylphenyl phosphate confirmed that chemistry is less rate-limiting with the more labile substrate. For paraoxon and diethyl 4-carbamoylphenyl phosphate, respectively, $^{18}(V/K)_{nonbridge} = 1.0021$ and 1.0181; $^{18}(V/K)_{bridge} = 1.0020$ and 1.036. The very small KIEs for paraoxon reflect the fact that the isotope effects for the chemical step are not expressed. The KIEs for diethyl 4-carbamoylphenyl phosphate also reflect the fact that the transition state for the enzymatic reaction has a transition state with greater bond fission than the alkaline hydrolysis, for which $^{18}k_{bridge} = 1.025$.[252]

The residue Asp-301, which is hydrogen bonded to His-254, has been proposed to deprotonate the bridging hydroxide nucleophile.[253] Mutation of His-245 to Ala or Asp reduces the rate of hydrolysis of paraoxon by 1–2 orders of magnitude. In contrast, the hydrolysis for the slower substrate diethyl *p*-chlorophenyl phosphate increases by from 2- to 33-fold.[253] This suggests that for the more activated
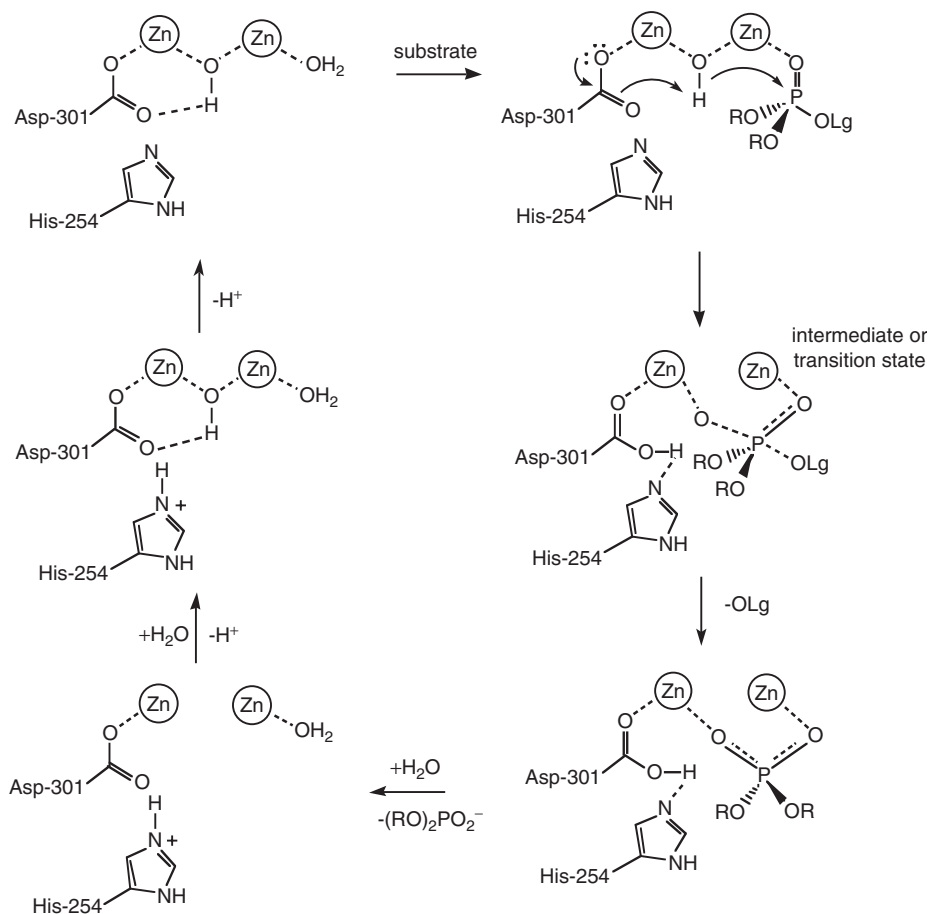
Scheme 5 A model for the mechanism of the phosphotriesterase reaction. The data do not clearly distinguish between a concerted mechanism of phosphoryl transfer, or a phosphorane intermediate; in the model above the reaction is shown as a concerted process. In either case, the P–OLg bond is largely broken in the transition state, requiring that breakdown of any putative intermediate is rate-limiting for less activated substrates. For more labile substrates, such as paraoxon, a step involving proton transfer that occurs after phosphoryl transfer is rate-limiting.

substrate, the rate-limiting step involves proton transfer that is assisted by the His-254/Asp-301 pair. The solvent isotope effects were measured for these two substrates to examine the kinetic significance of proton transfer steps in the mechanism. For the Zn/Zn form of the enzyme, the solvent isotope effects on k_{cat}/K_m are very small for both substrates. With the faster substrate paraoxon, $k_{catH2O}/k_{catD2O} = 2.0$ while with the slower substrate diethyl p-chlorophenyl phosphate, $k_{catH2O}/k_{catD2O} = 1.3$. Similar trends were seen with the Cd/Cd and the Zn/Cd forms of the triesterase. The

results support the proposal that in the hydrolysis of paraoxon, k_{cat} is limited by a step involving proton transfer that follows P–O bond fission.

In reactions of substrates exhibiting rate-limiting phosphoryl transfer, the very negative β_{lg} and the large $^{18}(V/K)_{bridge}$ indicate an absence of stabilization of the leaving group via protonation or electrophilic interactions with the metal center. The cumulative results support a mechanism involving attack by the bridging hydroxide, with a transition state in which bond fission to the leaving group is far advanced and the leaving group bears a substantial negative charge, without significant leaving group stabilization provided by the enzyme. The mutational studies and solvent isotope effects led to the mechanistic proposal shown in Scheme 5, which include a proposed mechanism for the proton shuttles involved in the regeneration of the active form of the enzyme.[253]

References

1. Westheimer, F.H. (1987). *Science* **235**, 1173–1178
2. Cohen, P. (2001). *Eur. J. Biochem.* **268**, 5001–5010
3. Lad, C., Williams, N.H. and Wolfenden, R. (2003). *Proc. Natl. Acad. Sci. USA* **100**, 5607–5610
4. Wolfenden, R., Ridgway, C. and Young, G. (1998). *J. Am. Chem. Soc.* **120**, 833–834
5. Mildvan, A.S. (1997). *Proteins* **24**, 401–416
6. Guthrie, R.D. and Jencks, W.P. (1989). *Acc. Chem. Res.* **22**, 343–349
7. Horn, H. and Ahlrichs, R. (1990). *J. Am. Chem. Soc.* **112**, 2121–2124
8. Rajca, A., Rice, J.E., Streitweiser Jr., A. and Schaefer, H.F. (1987). *J. Am. Chem. Soc.* **109**, 4189–4192
9. Hengge, A.C., Edens, W.A. and Elsing, H. (1994). *J. Am. Chem. Soc.* **116**, 5045–5049
10. Berry, R.S. (1960). *J. Chem. Phys.* **32**, 933–938
11. Holmes, R.R. (1978). *J. Am. Chem. Soc.* **100**, 433–446
12. Westheimer, F.H. (1968). *Acc. Chem. Res.* **1**, 70–78
13. Moore O'Ferrall, R.A. (1970). *J. Chem. Soc. B*, 274–277
14. Jencks, W.P. (1972). *Chem. Rev.* **72**, 705–718
15. Kirby, A.J. and Varvoglis, A.G. (1967). *J. Am. Chem. Soc.* **89**, 415–423
16. Herschlag, D. and Jencks, W.P. (1989). *J. Am. Chem. Soc.* **111**, 7579–7586
17. Gorenstein, D.G., Lee, Y.-G. and Kar, D.J. (1977). *Am. Chem. Soc.* **99**, 2264–2267
18. Hengge, A.C. (2002). *Acc. Chem. Res.* **35**, 105–112
19. Thatcher, G.R.J. and Kluger, R. (1989). *Adv. Phys. Org. Chem.* **25**, 99–265
20. Hengge, A.C. (1998). In *Comprehensive Biological Catalysis: A Mechanistic Reference*, Sinnott, M., (ed.), vol. 1, pp. 517–542, Academic Press, San Diego, CA
21. Buchwald, S.L., Friedman, J.M. and Knowles, J.R. (1984). *J. Am. Chem. Soc.* **106**, 4911–4916
22. Friedman, J.M., Freeman, S. and Knowles, J.R. (1988). *J. Am. Chem. Soc.* **110**, 1268–1275
23. Hoff, R.H. and Hengge, A.C. (1998). *J. Org. Chem.* **63**, 6680–6688
24. Kirby, A.J. and Jencks, W.P. (1965). *J. Am. Chem. Soc.* **87**, 3209–3216
25. Anderson, M.A., Shim, H., Raushel, F.M. and Cleland, W.W. (2001). *J. Am. Chem. Soc.* **123**, 9246–9253
26. Alhambra, C., Wu, L., Zhang, Z.-Y. and Gao, J. (1998). *J. Am. Chem. Soc.* **120**, 3858–3866
27. Asthagiri, D., Dillet, V., Liu, T., Noodleman, L., Van Etten, R.L. and Bashford, D. (2002). *J. Am. Chem. Soc.* **124**, 10225–10235

28. Strater, N., Lipscomb, W.N., Klabunde, T. and Krebs, B. (1996). *Angew. Chem. Int. Ed. Engl.* **35**, 2024–2055

29. Williams, N.H., Takasaki, B., Wall, M. and Chin, J. (1999). *Acc. Chem. Res.* **32** 485–493

30. Hendry, P. and Sargeson, A.M. (1990). *Prog. Inorg. Chem.* **38**, 201–258

31. Vichard, C. and Kaden, T.A. (2002). *Inorg. Chim. Acta.* **337**, 173–180

32. Herschlag, D. and Jencks, W.P. (1987). *J. Am. Chem. Soc.* **109**, 4665–4674

33. Admiraal, S.J. and Herschlag, D. (1995). *Chem. Biol.* **2**, 729–739

34. Harrowfield, J.M., Jones, D.R., Lindoy, L.F. and Sargeson, A.M. (1980). *J. Am. Chem. Soc.* **102**, 7733–7741

35. Jones, D.R., Lindoy, L.F. and Sargeson, A.M. (1983). *J. Am. Chem. Soc.* **105**, 7327–7336

36. Rawlings, J., Hengge, A.C. and Cleland, W.W. (1997). *J. Am. Chem. Soc.* **119**, 542–549

37. Humphry, T., Forconi, M., Williams, N.H. and Hengge, A.C. (2004). *J. Am. Chem. Soc.* **126**, 11864–11869

38. Williams, N.H., Lebuis, A.-M. and Chin, J. (1999). *J. Am. Chem. Soc.* **121**, 3341–3348

39. Admiraal, S.J. and Herschlag, D. (2000). *J. Am. Chem. Soc.* **122**, 2145–2148

40. Bunton, C.A., Llewellyn, D.R., Oldham, K.G. and Vernon, C.A. (1958). *J. Chem. Soc.* 3574–3587

41. Grzyska, P.K., Czyryca, P.G., Purcell, J. and Hengge, A.C. (2003). *J. Am. Chem. Soc.* **125**, 13106–13111

42. Jencks, W.P. (1987). *Catalysis in Chemsitry and Enzymology*. Dover, New York

43. Kresge, A.J. and Preto, R.J. (1965). *J. Am. Chem. Soc.* **87**, 4593–4596

44. Fife, T.H. (1972). *Acc. Chem. Res.* **5**, 264–272

45. Kirby, A.J. and Younas, M. (1970). *J. Chem. Soc. B*, 1165–1172

46. Khan, S.A. and Kirby, A.J. (1970). *J. Chem. Soc. B*, 1172–1182

47. Cassano, A.G., Anderson, V.E. and Harris, M.E. (2002). *J. Am. Chem. Soc.* **124**, 10964–10965

48. Hengge, A.C. and Cleland, W.W. (1991). *J. Am. Chem. Soc.* **113**, 5835–5841

49. Williams, N.H., Cheung, W. and Chin, J. (1998). *J. Am. Chem. Soc.* **120**, 8079–8087

50. Wahnon, D., Lebuis, A.-M. and Chin, J. (1995). *Angew. Chem. Int. Ed. Engl.* **34**, 2412–2414

51. Humphry, T., Forconi, M., Williams, N.H. and Hengge, A.C. (2002). *J. Am. Chem. Soc.* **124**, 14860–14861

52. Davis, A.M., Hall, A.D. and Williams, A. (1988). *J. Am. Chem. Soc.* **110**, 5105–5108

53. Brown, D.M. and Usher, D.A. (1965). *J. Chem. Soc.* **87**, 6558–6564

54. Satoh, K. and Inoue, Y. (1972). *Chem. Lett.*, 1097–1100

55. Kosonen, M., Youseti-Salakdeh, E., Stromberg, R. and Lonnberg, H. (1997). *J. Chem. Soc. Perkin Trans.* **2**, 2661–2666

56. Oivanen, M., Schnell, R., Pfleiderer, W. and Lonnberg, H. (1991). *J. Org. Chem.* **56**, 3623–3628

57. Jarvinen, P., Oivanen, M. and Lonnberg, H. (1991). *J. Org. Chem.* **56**, 5396–5401

58. Gerratana, B., Sowa, G.A. and Cleland, W.W. (2000). *J. Am. Chem. Soc.* **122**, 12615–12621

59. Perreault, D.M. and Anslyn, E.V. (1997). *Angew. Chem. Int. Ed. Engl.* **36**, 432–450

60. Hall, C.R. and Inch, T.D. (1980). *Tetrahedron* **36**, 2059–2095

61. Rowell, R. and Gorenstein, D.G. (1981). *J. Am. Chem. Soc.* **103**, 5894–5902

62. Ba-Saif, S.A., Waring, M.A. and Williams, A. (1990). *J. Am. Chem. Soc.* **112**, 8115–8120

63. Ba-Saif, S.A., Waring, M.A. and Williams, A. (1991). *J. Chem. Soc. Perkin Trans.* **2**, 1653–1659

64. Bryan, C.D., Schowen, K.B. and Schowen, R.L. (1996). *Can. J. Chem.* **74**, 931–938

65. Cleland, W.W. (1990). *FASEB J.* **4**, 2899–2905

66. Jones, J.P., Weiss, P.M. and Cleland, W.W. (1991). *Biochemistry* **30**, 3634–3639

67. Cleland, W.W. and Hengge, A.C. (1995). *FASEB J.* **9**, 1585–1594
68. Kim, E.E. and Wyckoff, H.W. (1991). *J. Mol. Biol.* **218**, 449–464
69. Di Sabato, G., Jencks, W.P. and Whalley, E. (1962). *Can. J. Chem.* **40**, 1220–1224
70. Ramirez, F., Marecek, J., Minore, J., Srivastava, S. and Le Noble, W. (1986). *J. Am. Chem. Soc.* **108**, 348–349
71. Herschlag, D. and Jencks, W.P. (1990). *Biochemistry* **29**, 5172–5179
72. Iranzo, O., Richard, J.P. and Morrow, J.R. (2004). *Inorg. Chem.* **43**, 1743–1750
73. Iranzo, O., Kovalevsky, A.Y., Morrow, J.R. and Richard, J.P. (2003). *J. Am. Chem. Soc.* **125**, 1988–1993
74. Iranzo, O., Elmer, T., Richard, J.P. and Morrow, J.R. (2003). *Inorg. Chem.* **42**, 7737–7746
75. Yang, M.Y., Iranzo, O., Richard, J.P. and Morrow, J.R. (2005). *J. Am. Chem. Soc.* **127**, 1064–1065
76. Frey, P.A., Richard, J.P., Ho, H.-T., Brody, R.S., Sammons, R.D. and Sheu, K.-F. (1982). In *Methods in Enzymology*, Purich, D.L. (ed.), vol. 87, pp. 213–235, Academic Press, New York
77. Eckstein, F., Romaniuk, P.J. and Connolly, B.A. (1982). In *Methods in Enzymology*, Purich, D.L. (ed.), vol. 87, pp. 197–212, Academic Press, New York
78. Saini, M.S., Buchwald, S.L., Van Etten, R.L. and Knowles, J.R. (1981). *J. Biol. Chem.* **256**, 10453–10455
79. Buchwald, S.L., Saini, M.S., Knowles, J.R. and Van Etten, R.L. (1984). *J. Biol. Chem.* **259**, 2208–2213
80. Jones, S.R., Kindman, L.A. and Knowles, J.R. (1978). *Nature* **275**, 564–565
81. Webb, M.R. and Trentham, D.R. (1981). *J. Biol. Chem.* **256**, 4884–4887
82. Webb, M.R., Grubmeyer, C., Penefsky, H.S. and Trentham, D.R. (1980). *J. Biol. Chem.* **255**, 11637–11639
83. Senter, P., Eckstein, F. and Kagawa, Y. (1983). *Biochemistry* **22**, 5514–5518
84. Lowe, G. and Potter, B.V. (1982). *Biochem. J.* **201**, 665–668
85. Webb, M.R. and Eccleston, J.F. (1981). *J. Biol. Chem.* **256**, 7734–7737
86. Webb, M.R. and Trentham, D.R. (1980). *J. Biol. Chem.* **255**, 8629–8632
87. Richard, J.P., Prasher, D.C., Ives, D.H. and Frey, P.A. (1979). *J. Biol. Chem.* **254**, 4339–4341
88. Feuerstein, J., Goody, R.S. and Webb, M.R. (1989). *J. Biol. Chem.* **264**, 6188–6190
89. Mueller, E.G., Crowder, M.W., Averill, B.A. and Knowles, J.R. (1993). *J. Am. Chem. Soc.* **115**, 2974–2975
90. Gonzalez, M.A., Webb, M.R., Welsh, K.M. and Cooperman, B.S. (1984). *Biochemistry* **23**, 797–801
91. Holtz, K.M. and Kantrowitz, E.R. (1999). *FEBS Lett.* **462**, 7–11
92. Coleman, J.E. (1992). *Annu. Rev. Biophys. Biomol. Struct.* **21**, 441–483
93. Reid, T.W. and Wilson, I.B. (1971). In *The Enzymes*, Boyer, P.D. (ed.), pp. 373–415, Academic Press, New York
94. O'Brien, P.J. and Herschlag, D. (2002). *Biochemistry* **41**, 3207–3225
95. Holtz, K.M., Stec, B. and Kantrowitz, E.R. (1999). *J. Biol. Chem.* **274**, 8351–8354
96. Bale, J., Huang, C. and Chock, P. (1980). *J. Biol. Chem.* **255**, 8431–8436
97. Bloch, W. and Schlesinger, M.J. (1973). *J. Biol. Chem.* **248**, 5794–5805
98. Stec, B., Holtz, K.M. and Kantrowitz, E.R. (2000). *J. Mol. Biol.* **299**, 1303–1311
99. Hall, A.D. and Williams, A. (1986). *Biochemistry* **25**, 4784–4790
100. Simopoulos, T.T. and Jencks, W.P. (1994). *Biochemistry* **33**, 10375–10380
101. Han, R. and Coleman, J.E. (1995). *Biochemistry* **34**, 4238–4245
102. Mushak, P. and Coleman, J.E. (1972). *Biochemistry* **112**, 201–205
103. Breslow, R. and Katz, I. (1968). *J. Am. Chem. Soc.* **90**, 7376–7377
104. Chaidaroglou, A., Brezinski, D.J., Middleton, S.A. and Kantrowitz, E.R. (1988). *Biochemistry* **27**, 8338–8343

105. Butler-Ransohoff, J.E., Rokita, S.E., Kendall, D.A., Banzon, J.A., Carano, K.S., Kaiser, E.T. and Matlin, A.R. (1992). *J. Org. Chem.* **57**, 142–145
106. O'Brien, P.J. and Herschlag, D. (1999). *J. Am. Chem. Soc.* **121**, 11022–11023
107. Weiss, P.M. and Cleland, W.W. (1989). *J. Am. Chem. Soc.* **111**, 1928–1929
108. Ostanin, K., Harms, E.H., Stevis, P.E., Kuciel, R., Zhou, M.M. and Van Etten, R.L. (1992). *J. Biol. Chem.* **267**, 22830–22836
109. Ishikawa, K., Mihara, Y., Gondoh, K., Suzuki, E. and Asano, Y. (2000). *EMBO J.* **19**, 2412–2423
110. Kostrewa, D., Wyss, M., D'Arcy, A. and van Loon, A.P. (1999). *J. Mol. Biol.* **288**, 965–974
111. Lindqvist, Y., Schneider, G. and Wihko, P. (1994). *Eur. J. Biochem.* **221**, 139–142
112. Ostanin, K. and Van Etten, R.L. (1993). *J. Biol. Chem.* **268**, 20778–20784
113. Vincent, J.B., Olivier-Lilley, G.L. and Averill, B.A. (1990). *Chem. Rev.* **90**, 1447–1467
114. Strater, N., Klabunde, T., Tucker, P., Witzel, H. and Krebs, B. (1995). *Science* **268**, 1489–1492
115. Lindqvist, Y., Johansson, E., Kaija, H., Vihko, P. and Schneider, G. (1999). *J. Mol. Biol.* **291**, 135–147
116. Vincent, J.B., Crowder, M.W. and Averill, B.A. (1992). *Biochemistry* **31**, 3033–3037
117. Vincent, J.B., Crowder, M.W. and Averill, B.A. (1991). *J. Biol. Chem.* **266**, 17737–17740
118. Wynne, C.J., Hamilton, S.E., Dionysius, D.A., Beck, J.L. and de Jersey, J. (1995). *Arch. Biochem. Biophys.* **319**, 133–141
119. Rusnak, F., Yu, L. and Mertz, P. (1996). *J. Biol. Inorg. Chem.* **1**, 388–396
120. Merkx, M., Pinkse, M.W. and Averill, B.A. (1999). *Biochemistry* **38**, 9914–9925
121. Smoukov, S.K., Quaroni, L., Wang, X., Doan, P.E., Hoffman, B.M. and Que Jr., L. (2002). *J. Am. Chem. Soc.* **124**, 2595–2603
122. Funhoff, E.G., Klaassen, C.H., Samyn, B., Van Beeumen, J. and Averill, B.A. (2001). *Chembiochem* **2**, 355–363
123. Dikiy, A., Funhoff, E.G., Averill, B.A. and Ciurli, S. (2002). *J. Am. Chem. Soc.* **124**, 13974–13975
124. Klabunde, T., Strater, N., Frohlich, R., Witzel, H. and Krebs, B. (1996). *J. Mol. Biol.* **259**, 737–748
125. Funhoff, E.G., Ljusberg, J., Wang, Y., Andersson, G. and Averill, B.A. (2001). *Biochemistry* **40**, 11614–11622
126. Schenk, G., Boutchard, C.L., Carrington, L.E., Noble, C.J., Moubaraki, B., Murray, K.S., de Jersey, J., Hanson, G.R. and Hamilton, S. (2001). *J. Biol. Chem.* **276**, 19084–19088
127. Schenk, G., Gahan, L.R., Carrington, L.E., Mitic, N., Valizadeh, M., Hamilton, S.E., de Jersey, J. and Guddat, L.W. (2005). *Proc. Natl. Acad. Sci. USA* **102**, 273–278
128. Merkx, M. and Averill, B.A. (1999). *J. Am. Chem. Soc.* **121**, 6683–6689
129. Jackson, M.D. and Denu, J.M. (2001). *Chem. Rev.* **101**, 2313–2340
130. Das, A.K., Helps, N.R., Cohen, P.T. and Barford, D. (1996). *EMBO J.* **15**, 6798–6809
131. Goldberg, J., Huang, H.B., Kwon, Y.G., Greengard, P., Nairn, A.C. and Kuriyan, J. (1995). *Nature* **376**, 745–753
132. Egloff, M., Cohen, P.T., Reinemer, P. and Barford, D. (1995). *J. Mol. Biol.* **254**, 942–959
133. Kissinger, C.R., Parge, H.E., Knighton, D.R., Lewis, C.T., Pelletier, L.A., Tempczyk, A., Kalish, V.J., Tucker, K.D., Showalter, R.E. and Moomaw, E.W. (1995). *Nature* **378**, 641–644
134. Griffith, J.P., Kim, J.L., Kim, E.E., Sintchak, M.D., Thomson, J.A., Fitzgibbon, M.J., Fleming, M.A., Caron, P.R., Hsiao, K. and Navia, M.A. (1995). *Cell* **82**, 507–522
135. Rusnak, F. and Mertz, P. (2000). *Physiol. Rev.* **80**, 1483–1521
136. Martin, B.L. and Graves, D.J. (1986). *J. Biol. Chem.* **261**, 14545–14550
137. Martin, B., Pallen, C., Wang, J. and Graves, D. (1985). *J. Biol. Chem.* **260**, 14932–14937
138. Martin, B.L. and Graves, D.J. (1994). *Biochim. Biophys. Acta* **1206**, 136–142

139. Mondragon, A., Griffith, E.C., Sun, L., Xiong, F., Armstrong, C. and Liu, J.O. (1997). *Biochemistry* **36**, 4934–4942

140. Mertz, P., Yu, L., Sikkink, R. and Rusnak, F. (1997). *J. Biol. Chem.* **272**, 21296–21302

141. Hoff, R.H., Mertz, P., Rusnak, F. and Hengge, A.C. (1999). *J. Am. Chem. Soc.* **121**, 6382–6390

142. Hengge, A.C. and Martin, B.L. (1997). *Biochemistry* **36**, 10185–10191

143. Martin, B.L., Jurado, L.A. and Hengge, A.C. (1999). *Biochemistry* **38**, 3386–3392

144. Zhang, J., Zhang, Z., Brew, K. and Lee, E.Y. (1996). *Biochemistry* **35**, 6276–6282

145. Huang, H.B., Horiuchi, A., Goldberg, J., Greengard, P. and Nairn, A.C. (1997). *Proc. Natl. Acad. Sci. USA* **94**, 3530–3535

146. Zhuo, S., Clemens, J.C., Stone, R.L. and Dixon, J.E. (1994). *J. Biol. Chem.* **269**, 26234–26238

147. Fjeld, C.C. and Denu, J.M. (1999). *J. Biol. Chem.* **274**, 20336–20343

148. Jackson, M.D., Fjeld, C.C. and Denu, J.M. (2003). *Biochemistry* **42**, 8513–8521

149. Zhang, Z.-Y. (1998). *CRC Crit. Rev. Biochem. Mol. Biol.* **33**, 1–52

150. Barford, D., Flint, A.J. and Tonks, N.K. (1994). *Science* **263**, 1397–1404

151. Stuckey, J.A., Schubert, H.L., Fauman, E.B., Zhang, Z.-Y., Dixon, J.E. and Saper, M.A. (1994). *Nature* **370**, 571–575

152. Yuvaniyama, J., Denu, J.M., Dixon, J.E. and Saper, M.A. (1996). *Science* **272**, 1328–1331

153. Su, X.D., Taddei, N., Stefani, M., Ramponi, G. and Nordlund, P. (1994). *Nature* **370**, 575–578

154. Zhang, M., Zhou, M., Van Etten, R.L. and Staufacher, C.V. (1997). *Biochemistry* **36**, 15–23

155. Zhang, M., Stauffacher, C.V., Lin, D. and Van Etten, R.L. (1998). *J. Biol. Chem.* **273**, 21714–21720

156. Wang, S., Tabernero, L., Zhang, M., Harms, E., Van Etten, R.L. and Stauffacher, C.V. (2000). *Biochemistry* **39**, 1903–1914

157. Zhang, Z.-Y., Wang, Y. and Dixon, J.E. (1994). *Proc. Natl. Acad. Sci. USA* **91**, 1624–1627

158. Zhang, Z.-Y., Malochowski, W.P., Van Etten, R.L. and Dixon, J.E. (1994). *J. Biol. Chem.* **269**, 8140–8145

159. Zhang, Z. (1995). *J. Biol. Chem.* **270**, 11199–11204

160. Wu, L. and Zhang, Z.-Y. (1996). *Biochemistry* **35**, 5426–5434

161. Denu, J.M., Zhou, G., Guo, Y. and Dixon, J.E. (1995). *Biochemistry* **34**, 3396–3403

162. Denu, J.M. and Dixon, J.E. (1995). *Proc. Natl. Acad. Sci. USA* **92**, 5910–5914

163. Zhang, Z.Y. (2003). *Prog. Nucl. Acid Res. Mol. Biol.* **73**, 171–220

164. Zhou, G., Denu, J., Wu, L. and Dixon, J. (1994). *J. Biol. Chem.* **269**, 28084–28090

165. Guan, K.L. and Dixon, J.E. (1991). *J. Biol. Chem.* **266**, 17026–17030

166. Denu, J.M., Lohse, D.L., Vijayalakshmi, Saper, M.A. and Dixon, J.E. (1996). *Proc. Natl. Acad. Sci. USA* **93**, 2493–2498

167. Cho, H., Krishnaraj, R., Kitas, E., Bannwarth, W., Walsh, C.T. and Anderson, K.S. (1992). *J. Am. Chem. Soc.* **114**, 7296–7298

168. Pannifer, A.D.B., Flint, A.J., Tonks, N.K. and Barford, D. (1998). *J. Biol. Chem.* **273**, 10454–10462

169. Zhang, Z.Y. and Dixon, J.E. (1993). *Biochemistry* **32**, 9340–9345

170. Zhang, Z.Y., Palfey, B.A., Wu, L. and Zhao, Y. (1995). *Biochemistry* **34**, 16389–16396

171. Fauman, E.B., Yuvaniyama, C., Schubert, H., Stuckey, J.A. and Saper, M.A. (1996). *J Biol. Chem.* **217**, 18780–18788

172. Schubert, H.L., Fauman, E.B., Stuckey, J.A., Dixon, J.E. and Saper, M.A. (1995). *Protein Sci.* **4**, 1904–1913

173. Hengge, A.C., Sowa, G.A., Wu, L. and Zhang, Z.-Y. (1995). *Biochemistry* **34**, 13982–13987

174. Hengge, A.C., Denu, J.M. and Dixon, J.E. (1996). *Biochemistry* **35**, 7084–7092
175. Hengge, A.C., Zhao, Y., Wu, L. and Zhang, Z.-Y. (1997). *Biochemistry* **36** 7928–7936
176. Hengge, A.C. (2001). *FEBS Lett.* **501**, 99–102
177. Grzyska, P.K., Kim, Y., Jackson, M.D., Hengge, A.C. and Denu, J.M. (2004). *Biochemistry* **43**, 8807–8814
178. McCain, D.F., Grzyska, P.K., Wu, L., Hengge, A.C. and Zhang, Z.Y. (2004). *Biochemistry* **43**, 8256–8264
179. Hoff, R.H., Wu, L., Zhou, B., Zhang, Z.-Y. and Hengge, A.C. (1999). *J. Am. Chem. Soc.* **121**, 9514–9521
180. Zhao, Y. and Zhang, Z.Y. (1996). *Biochemistry* **35**, 11797–11804
181. Hansson, T., Nordlund, P. and Aqvist, J. (1997). *J. Mol. Biol.* **265**, 118–127
182. Hart, J.C., Hillier, I.H., Burton, N.A. and Sheppard, D.W. (1998). *J. Am. Chem. Soc.* **120**, 13535–13536
183. Kolmodin, K. and Aqvist, J. (1999). *FEBS Lett.* **456**, 301–305
184. Kolmodin, K., Nordlund, P. and Aqvist, J. (1999). *Protein. Struct. Funct. Genet.* **36**, 370–379
185. Czyryca, P.G. and Hengge, A.C. (2001). *Biochim. Biophys. Acta* **1547**, 245–253
186. Dillet, V., Van Etten, R.L. and Bashford, D. (2000). *J. Phys. Chem. B* **104**, 11321–11333
187. Bourne, H.R., Sanders, D.A. and McCormick, F. (1990). *Nature* **348**, 125–132
188. Barbacid, M. (1987). *Annu. Rev. Biochem.* **56**, 779–827
189. Pai, E.F., Krengel, U., Petsko, G.A., Goody, R.S., Kabsch, W. and Wittinghofer, A. (1990). *EMBO J.* **9**, 2351–2359
190. Fasano, O., Aldrich, T., Tamanoi, F., Taparowsky, E., Furth, M. and Wigler, M. (1984). *Proc. Natl. Acad. Sci. USA* **81**, 4008–4012
191. Frech, M., Darden, T.A., Pedersen, L.G., Foley, C.K., Charifson, P.S., Anderson, M.W. and Wittinghofer, A. (1994). *Biochemistry* **33**, 3237–3244
192. Schweins, T., Geyer, M., Kalbitzer, H.R., Wittinghofer, A. and Warshel, A. (1996). *Biochemistry* **35**, 14225–14231
193. Schweins, T., Geyer, M., Scheffzek, K., Warshel, A., Kalbitzer, H.R. and Wittinghofer, A. (1995). *Nat. Struct. Biol.* **2**, 36–44
194. Schweins, T. and Warshel, A. (1996). *Biochemistry* **35**, 14232–14243
195. Maegley, K.A., Admiraal, S. and Herschlag, D. (1996). *Proc. Natl. Acad. Sci. USA* **93**, 8160–8166
196. Scheffzek, K., Ahmadian, M.R., Kabsch, W., Wiesmuller, L., Lautwein, A., Schmitz, F. and Wittinghofer, A. (1997). *Science* **277**, 333–338
197. Ahmadian, M.R., Stege, P., Scheffzek, K. and Wittinghofer, A. (1997). *Nat. Struct. Biol.* **4**, 686–689
198. Allin, C. and Gerwert, K. (2001). *Biochemistry* **40**, 3037–3046
199. Allin, C., Ahmadian, M.R., Wittinghofer, A. and Gerwert, K. (2001). *Proc. Natl. Acad. Sci. USA* **98**, 7754–7759
200. Lowe, G. and Potter, B.V.L. (1981). *Biochem. J.* **199**, 693–698
201. Ray Jr., W.J. Burgner II, J.W. and Post, C.B. (1990). *Biochemistry* **29**, 2770–2778
202. Lahiri, S.D., Zhang, G., Dunaway-Mariano, D. and Allen, K.N. (2002). *Biochemistry* **41**, 8351–8359
203. Deng, H., Ray Jr., W.J. Burgner II, J.W. and Callender, R. (1993). *Biochemistry* **32**, 12984–12992
204. Lahiri, S.D., Zhang, G., Dunaway-Mariano, D. and Allen, K.N. (2003). *Science* **99**, 2067–2071
205. Blackburn, G.M., Williams, N.H., Gamblin, S.J. and Smerdon, S.J. (2003). *Science* **301**, 5637
206. Webster, C.E. (2004). *J. Am. Chem. Soc.* **126**, 6840–6841
207. Allen, K.N. and Dunaway-Mariano, D. (2003). *Science* **301**, 5637

208. Pauling, L. (1960). *The Nature of the Chemical Bond*. 3rd edn pp. 255–260. Cornell University Press, Ithaca, NY
209. Henchman, M., Viggiano, A.A., Paulson, J.F., Freedman, A. and Wormhoudt, J. (1985). *J. Am. Chem. Soc.* **107**, 1453–1455
210. Choe, J.Y., Iancu, C.V., Fromm, H.J. and Honzatko, R.B. (2003). *J. Biol. Chem.* **278**, 16015–16020
211. Serpersu, E.H., Shortle, D. and Mildvan, A.S. (1987). *Biochemistry* **26**, 1289–1300
212. Cotton, F.A., Hazen Jr., E.E. and Legg, M.J. (1979). *Proc. Natl. Acad. Sci. USA*, **76**, 2551–2555.
213. Loll, P.J., Quirk, S., Lattman, E.E. and Garavito, R.M. (1995). *Biochemistry* **34**, 4316–4324
214. Loll, P.J. and Lattman, E.E. (1990). *Biochemistry* **29**, 6866–6873
215. Loll, P.J. and Lattman, E.E. (1989). *Proteins* **5**, 183–201
216. Mehdi, S. and Gerlt, J.A. (1982). *J. Am. Chem. Soc.* **104**, 3223–3225
217. Hibler, D.W., Stolowich, N.J., Reynolds, M.A., Gerlt, J.A., Wilde, J.A. and Bolton, P.H. (1987). *Biochemistry* **26**, 6278–6286
218. Wilde, J.A., Bolton, P.H., Dell'Acqua, M., Hibler, D.W., Pourmotabbed, T. and Gerlt, J.A. (1988). *Biochemistry* **27**, 4127–4132
219. Hale, S.P., Poole, L.B. and Gerlt, J.A. (1993). *Biochemistry* **32**, 7479–7487
220. Thompson, J.E., Venegas, F.D. and Raines, R.T. (1994). *Biochemistry* **33**, 7408–7414
221. Markham, R. and Smith, J.D. (1952). *Biochem. J.* **52**, 552–557
222. Brown, D.M. and Todd, A.R. (1953). *J. Chem. Soc.* (*London*), 44–52
223. Cuchillo, C.M., Pares, X., Guasch, A., Barman, T., Travers, F. and Nogues, M.V. (1993). *FEBS Lett.* **333**, 207–210
224. Barnard, E.A. (1969). *Annu. Rev. Biochem.* **38**, 677–732
225. Blackburn, P. and Moore, S. (1982). *Enzymes* **XV**, 317–433
226. Richards, F.M. and Wyckhoff, H.W. (1971). *Enzymes* **IV**, 647–806
227. Raines, R.T. (1998). *Chem. Rev.* **98**, 1045–1066
228. Kartha, G., Bello, J. and Harker, D. (1967). *Nature* **213**, 862–865
229. Eckstein, F., Saenger, W. and Suck, D. (1972). *Biochem. Biophys. Res. Commun.* **46**, 964–971
230. Usher, D.A., Erenrich, E.S. and Eckstein, F. (1972). *Proc. Natl. Acad. Sci. USA* **69**, 115–118
231. Usher, D.A., Richardson, D.I.J. and Eckstein, F. (1970). *Nature* **228**, 663–665
232. Jackson, D.Y., Burnier, J., Quan, C., Stanley, M., Tom, J. and Wells, J.A. (1994). *Science* **266**, 243–247
233. Thompson, J.E. and Raines, R.T. (1994). *J. Am. Chem. Soc.* **116**, 5467–5468
234. Sowa, G.A., Hengge, A.C. and Cleland, W.W. (1997). *J. Am. Chem. Soc.* **119**, 2319–2320
235. Anslyn, E. and Breslow, R. (1989). *J. Am. Chem. Soc.* **111**, 4473–4482
236. Lonnberg, H. (1998). *Chem. Rev.* **98**, 961–990
237. Zubay, G.L. (1998). *Biochemistry* (4th edn). Wm. C. Brown, Chicago, IL
238. Abeles, R.H., Frey, P.A. and Jencks, W.P. (1992). *Biochemistry*. Jones and Bartlett, Boston
239. Herschlag, D. (1994). *J. Am. Chem. Soc.* **116**, 11631–11635
240. Gerlt, J.A. and Gassman, P.G. (1993). *Biochemistry* **32**, 11943–11952
241. Messmore, J.M., Fuchs, D.N. and Raines, R.T. (1995). *J. Am. Chem. Soc.* **117**, 8057–8060
242. Scanlan, T.S. and Reid, R.C. (1995). *Chem. Biol.* **2**, 71–75
243. Dumas, D.P., Caldwell, S.R., Wild, J.R. and Raushel, F.M. (1989). *J. Biol. Chem.* **264**, 19659–19665
244. Donarski, W.J., Dumas, D.P., Heitmeyer, D.P., Lewis, V.E. and Raushel, F.M. (1989). *Biochemistry* **28**, 4650–4655
245. Shim, H., Hong, S.B. and Raushel, F.M. (1998). *J. Biol. Chem.* **273**, 17445–17450

246. Vanhooke, J.L., Benning, M.M., Raushel, F.M. and Holden, H.M. (1996). *Biochemistry* **35**, 6020–6025
247. Lewis, V.E., Donarski, W.J., Wild, J.R. and Raushel, F.M. (1988). *Biochemistry* **27**, 1591–1597
248. Omburo, G.A., Mullins, L.S. and Raushel, F.M. (1993). *Biochemistry* **32**, 9148–9155
249. Hong, S.B. and Raushel, F.M. (1996). *Biochemistry* **35**, 10904–10912
250. Dumas, D.P. and Raushel, F.M. (1990). *J. Biol. Chem.* **265**, 21498–21503
251. Caldwell, S.R., Newcomb, J.R., Schlecht, K.A. and Raushel, F.M. (1991). *Biochemistry* **30**, 7438–7444
252. Caldwell, S.R., Raushel, F.M., Weiss, P.M. and Cleland, W.W. (1991). *Biochemistry* **30**, 7444–7450
253. Aubert, S.D., Li, Y. and Raushel, F.M. (2004). *Biochemistry* **43**, 5707–5715

The physical organic chemistry of very high-spin polyradicals

Andrzej Rajca

Department of Chemistry, University of Nebraska, Lincoln, NE 68588 03044, USA

Abstract

This review outlines the design and characterization of very high-spin poly-radicals. The rational, ''bottom-up'' design and characterization of polyarylmethyl polyradicals with increasing number of exchange coupled unpaired electron spins are described.

1   Introduction

A very high-spin polyradical may be defined as a molecule or polymer in which the electronic ground state possesses very large value of total spin quantum number S (high-spin ground state). Since the values of S are related to the net number of ferromagnetically coupled unpaired electrons (parallel spins), such molecules and

polymers may be viewed as one of the key measures of progress toward organic polymer magnets.[1–6] For magnetic ordering at room temperature, the characteristic energy of the interaction between electron spins should be $\sim 1\,\mathrm{kcal\,mol^{-1}}$, significantly exceeding RT at room temperature. Thus, much stronger interactions associated with chemical bonding (antiparallel spins) will have to be overcome. To date, only through-bond interactions, especially mediated by π-systems, have been found to provide such strength and lead to high-spin ground states in organic molecules. Consequently, one of the key challenges in attaining very large values of S is the maintenance of through-bond interactions between very large number of sites with electron spins within the molecule or polymer.

The bottom-up approach to organic magnets relies on the design and synthesis of paramagnetic molecules and polymers with increasing values of S.[7,8] Such paramagnets, with controlled interactions between unpaired electrons, may be viewed as organic analogous of now much studied paramagnetic and superparamagnetic metal-ion clusters.[8–14] In particular, ambient stable polyradicals, in which the high-spin ground state is separated from the low-spin excited states by the energy gap significantly exceeding RT at room temperature, may provide well-defined and practical organic paramagnets, in principle exceeding the magnetic moments associated with any single metal-ion. In particular, organic paramagnetic contrast agents competing with metal-based complexes (e.g., Gd^{III}) can be envisioned.[15–17] In addition, paramagnets with multiple Lewis basic radical sites may be employed as ligands for metal-ions, to attain organometallic magnets with magnetic ordering at relatively high temperatures.[18–20]

In addition to magnetism, many other interesting phenomena in condensed matter are associated with weak interactions between electrons and/or nuclei. Thus, the lessons learned in very high-spin polyradicals may facilitate analogous single-macromolecule approaches to other collective phenomena. Extrapolating further, one can envision the advantages of single-macromolecule integration in molecular electronics or even in photonics.

This review will address multiple challenges that are involved in the design and characterization of very high-spin polyradicals. However, synthesis cannot be entirely omitted, as it is the most laborious and, perhaps, the most difficult aspect of this problem. Even with a good physical organic design and sophisticated methods for characterization in place, synthesis still does determine what can be done. Since each target is a macromolecule with multiple radical sites interacting through bonds, not only efficient and flexible synthetic approaches to varied molecular frameworks are needed but, most importantly, ultra-efficient methods for generation of radicals are absolutely necessary. In view of these multiple challenges, polyarylmethyls are the best systems by far. For example, among non-polyarylmethyls, the highest values of S are 9 and 5 for molecules and polymers, respectively (Fig. 1).[21–26]

These values of S are relatively low, compared to those attained in polyarylmethyl polyradicals, especially for the first organic polymer with magnetic ordering and its model compounds (Fig. 2).[7,8]

Polyarylmethyl polyradicals are derived from triphenylmethyl, the first organic free radical discovered by Moses Gomberg in 1900 (Fig. 2).[27,28] At that time, the
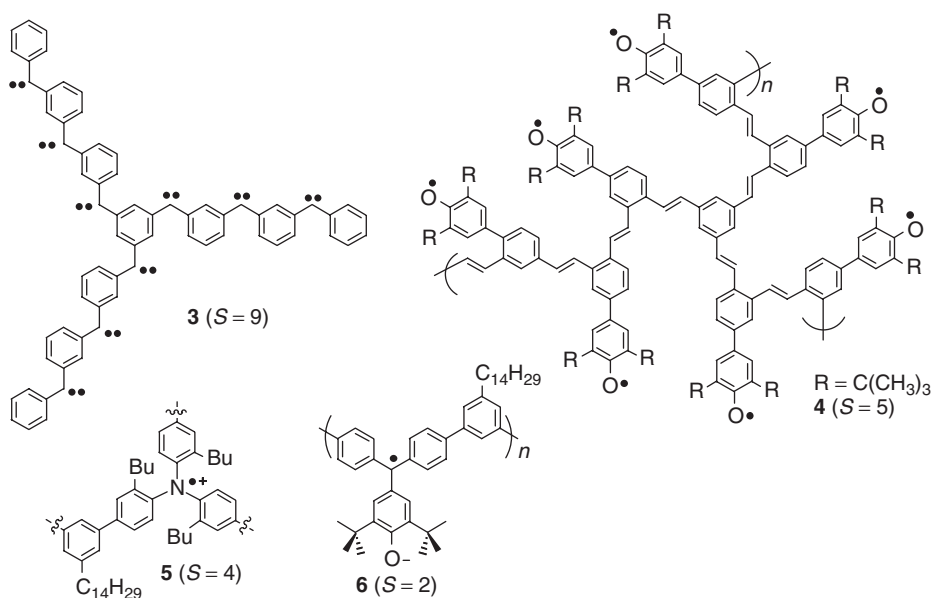
Fig. 1 Structures and values of S for selected high-spin organic molecules and polymers.

existence of organic free radicals stirred a considerable controversy, which was amplified by the difficulties in studies of the reaction of triphenylmethyl with oxygen and itself (dimerization).[29,30] Triphenylmethyl predominantly exists as a dimer,[31] with the CC bond between the α-C and *para*-C of the two triphenylmethyls (Fig. 3); however, the structure of the dimer was not established until 1968.[29,32] As expected, introduction of sterically bulky substituents at the *para* positions shifts monomer–dimer equilibrium toward the monomer;[33] e.g., tris-(4-*tert*-butylphenyl)methyl is practically monomeric in solution (Fig. 3).[33,34] Furthermore, alkyl substitution improves solubility in organic solvents. Nearly all carbon-centered radicals are air sensitive; their reaction with oxygen gives peroxides. Only most extreme sterically bulky substitution makes such radicals ambient stable or nearly so. Among notable examples of such stable radicals are perchlorinated triarylmethyls, selected perfluorinated alkyl radicals, and, in exceptional cases, hydrocarbon radicals.[35–37]

2   Exchange coupling and magnetism

Organic ferromagnets and ferrimagnets composed of crystals of small radicals (predominantly nitroxides) or charge transfer salts have been prepared.[38–43] Their Curie temperatures (T_C), the temperature above which ferromagnetism is destroyed and the material becomes paramagnetic, is generally below 2 K,[38] with the exception of the C_{60}-TDAE (tetrakis(dimethylamine)ethylene) charge transfer compound which
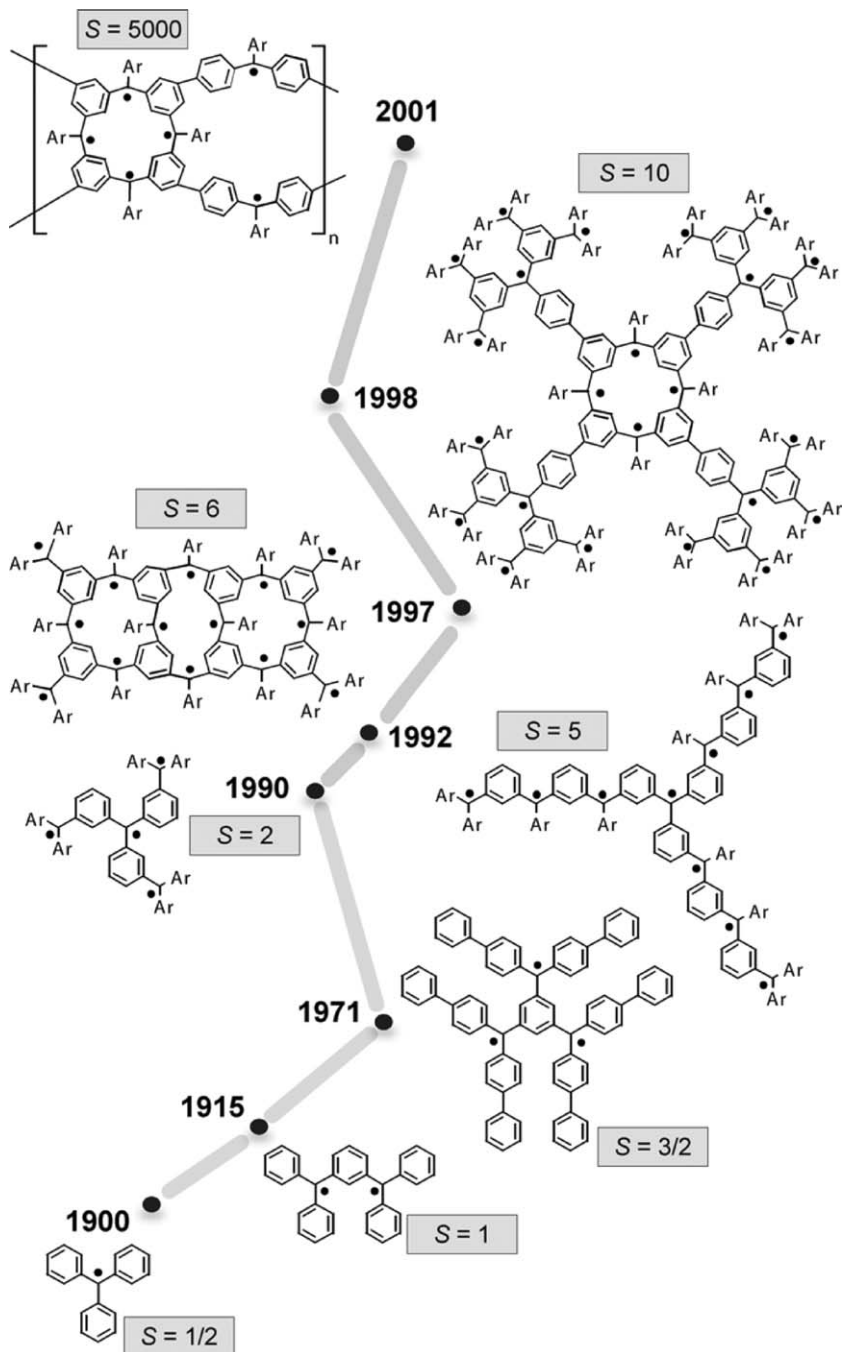
Fig. 2 Progress in high-spin polyarylmethyls: bottom-up approach to organic polymer magnets. Ar = 4-*tert*-butylphenyl.
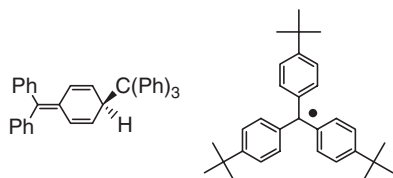
Fig. 3 Triphenylmethyl dimer and tris-(4-*tert*-butylphenyl)methyl.

has $T_C = 16\,K$.[39,40] The weakness of the through-space pairwise exchange couplings between the radicals in these molecular solids leads to low T_C.

An alternative approach to organic magnet may be based upon high-spin macromolecules and/or polymers with very large number of unpaired electrons, i.e., single macromolecule and/or polymer magnet. In this approach, through-bonds pairwise exchange couplings may be relatively very strong, promising relatively high T_C.

In 1968, Mataga, in an article entitled "Possible 'Ferromagnetic States' of Some Hypothetical Hydrocarbons," proposed three extended polycarbenes and polyradicals (**I–III**) as possible candidates for polymers and networks, in which topological degeneracies scale with the degree of polymerization (Fig. 4).[44] However, topological degeneracies, illustrated by Mataga, are just one of the prerequisites for either ferromagnets or paramagnetic molecules (or polymers) with high-spin ground states. In particular, all of Mataga's structures lack sufficient dimensionality for magnetic ordering of any type, including ferromagnetism. For polycarbene **II** (Fig. 4), $S = 0$ ground state is expected.

Organic macromolecules or polymers with magnetic ordering constitute a challenging goal as illustrated by the following three main questions:

(1) How to attain very large values of S?
(2) How to attain relatively strong exchange coupling in a three-dimensional (or greater than two-dimensional) structure?
(3) How to attain significant magnetic anisotropy barrier?

These three questions will be addressed in the reverse order, leaving the most important, first question for more detailed discussion.

Two primary sources of magnetic anisotropy barrier in magnetic materials are spin–orbit coupling and magnetic dipole–dipole interactions.[45] For metal-free, light element-based radicals, especially the carbon-based π-conjugated radicals with spin density primarily at tri-coordinated carbon atoms, spin–orbit coupling will be rather small.[46] In this case, the magnetic dipole–dipole interactions within the macromolecule will lead to the shape anisotropy barrier, E_A/k, in units of temperature, as shown in Equation (1):[45]

$$E_A/k = 0.5NVM_{sat}^2/k \tag{1}$$

In Equation (1), k is a Boltzman constant, N a shape factor (e.g., $0 \leqslant N \leqslant 2\pi$ with limiting values of 0 and 2π for a sphere and infinite rod, respectively), V the volume
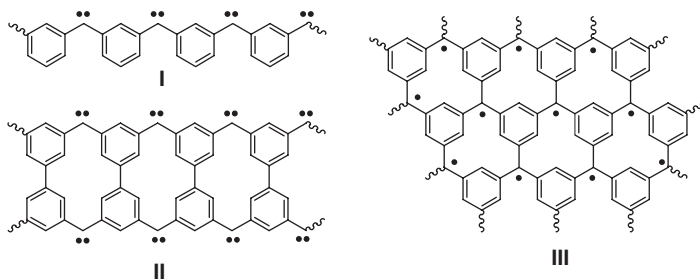
Fig. 4 Mataga's polymers and networks.

of macromolecule, and M_{sat} the magnetization at saturation (i.e., effectively, density of ferromagnetically coupled electron spin in a macromolecule). As an example, an early estimate for magnetic anisotropy barrier suggested that for $E_A/k \approx 2\,\mathrm{K}$, a moderately elongated shape polyarylmethyl polyradical with $N \approx 3$ (e.g., prolate ellipsoid with $a/b \approx 2$) and about 200 ferromagnetically coupled electron spins (i.e., $S \approx 100$) were needed.[47] This could provide organic-macromolecule-based blocked superparamagnets, analogous to nanometer-sized conventional magnetic particles or high-spin molecular metal-ion clusters.

However, for true magnetic ordering based upon isotropic exchange coupling, strong exchange coupling in a three-dimensional (or more than two-dimensional) structure must be maintained (magnetic dipole–dipole interactions may also lead to magnetic ordering, thus relaxing requirement for high dimensionality, however, only very low T_C are possible[19]). It should be emphasized that the pairwise connectivity between the radicals (electron spins), not to be confused with macromolecular shape, must have the above dimensionality. Due to the strong exchange couplings in high-spin organic molecules and polymers are mediated through π-conjugated systems, such three-dimensional π-conjugated macromolecule with thousands of exchange-coupled unpaired electrons poses the challenge for the physical organic design and synthesis.

For the most important question, concerning very large values of S for the ground state of a molecule or polymer, the most fundamental case of an effective pairwise interaction between electron spins in diradicals will be first considered. As the energy scale of the quantum mechanical exchange coupling is by far greater than that of classical magnetic dipole–dipole interaction,[45] only the former will be considered in discussion of electronic ground states.[48]

For two electron spins, their total spin, S, can be either $S = 1$ or $S = 0$, i.e., the corresponding spin multiplicities, $2S + 1$, can be either triplet or singlet (singlet–triplet mixing is neglected). For a diradical with the $S = 1$ ground state, the exchange coupling between unpaired electrons may be referred to as ferromagnetic coupling. This should not be confused with "ferromagnetic" or "ferromagnetism" when referring to magnetically ordered materials. Analogously, the $S = 0$ ground state corresponds to antiferromagnetic coupling. The energy difference between the

singlet and triplet states (ΔE_{ST}) may be viewed as a measure of strength for the pairwise exchange coupling (ferromagnetic or antiferromagnetic coupling).[3]

Pairwise exchange coupling between spins $\mathbf{S_1}$ and $\mathbf{S_2}$ with coupling constant J may be formulated in term of the well-known Heisenberg Hamiltonian, $-2J\mathbf{S_1} \bullet \mathbf{S_2}$.[49] This Hamiltonian will be especially useful for analyses of magnetic data for organic spin clusters, which are described in the following sections. In the case of two $S = 1/2$ electron spins (i.e., diradical), $\Delta E_{ST} = 2J$. The value of J/k (k = Boltzman constant), expressed in kelvin, will be a more general and convenient measure of pairwise exchange coupling, applicable both to diradicals and polyradicals. Positive and negative values of J/k correspond to ferromagnetic and antiferromagnetic coupling, respectively.

Ferromagnetic coupling is attained when the orbitals containing unpaired electron spins are orthogonal and coinciding in space.[2] The preference for the ferromagnetic versus antiferromagnetic coupling in non-Kekule π-conjugated diradicals may be illustrated by trimethylenemethane (TMM) and tetramethyleneethylene (TME). Both diradicals possess two degenerate (or nearly degenerate) half-occupied non-bonding moieties (MOs). In TMM, the degenerate half-occupied non-bonding MOs must have their lobes coincide significantly (non-disjoint MOs).[50] In TME, it is possible to write a linear combination of analogous near-degenerate half-occupied non-bonding MOs, lacking coinciding lobes (disjoint MOs). Thus, the $S = 1$ state in TMM would greatly relieve the electrostatic repulsion associated with non-disjoint MOs because the $S = 1$ state possesses an additional node in its spatial part of the wave function.[50] As this large effect is absent in TME, electron correlation might lead to the $S = 0$ ground state.

Dowd was the first to observe TMM and to study extensively TME by electron paramagnetic resonance (EPR) spectroscopy.[51] However, the ground states and ΔE_{ST} were best established by photoelectron spectroscopy studies of the corresponding radical anions in the gas phase.[52,53] These studies showed unequivocally very strong ferromagnetic coupling in TMM and relatively weaker antiferromagnetic coupling in TME (Fig. 5).

An alternative approach to determining the spin of the ground state is a qualitative method by Ovchinnikov,[54] which is illustrated in Fig. 6. One may consider, that the spin densities at the adjacent atomic centers of the π-system prefer opposite signs, leading to $\alpha\beta\alpha\beta$ pattern in alternate systems. The count of "arrows up" versus "arrows down" in TMM or m-xylylene (Fig. 6) indicates preference for the $S = 1$ ground state (in the gas phase, m-xylylene is the $S = 1$ ground state with $\Delta E_{ST} \approx 10\,\mathrm{kcal\,mol^{-1}}$ [55]). Analogously, the number of "arrows up" and "arrows down" are identical for TME or 3,3'-dimethylenebiphenyl (Fig. 6), consistent with the $S = 0$ ground state.

Conceptually pairwise ferromagnetic and antiferromagnetic couplings may be visualized as transmitted through ferromagnetic coupling units (fCUs) and anti-ferromagnetic coupling units (aCUs), respectively.[2] As illustrated in Fig. 6, 1,3-phenylene and 3,3'-biphenylene are fCU and aCU, respectively.

The concept of coupling units may be traced to McConnell's perturbation theory for ΔE_{ST} in diradicals, in which two weakly exchange-coupled radical moieties are separated by the bridging group.[56] In particular, 1,3-phenylene was predicted to be
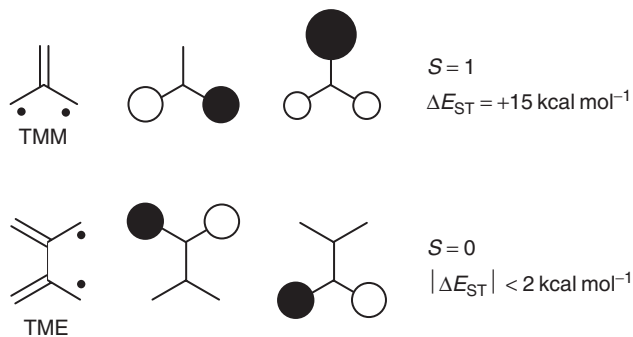
Fig. 5 Non-bonding MOs, ground states, and ΔE_{ST} for TMM and TME.
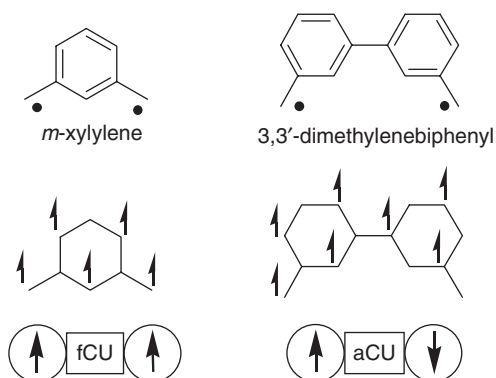
Fig. 6 *m*-Xylylene and 3,3′-dimethylenebiphenyl: Ovchinnikov's method and coupling units (fCU and aCU).
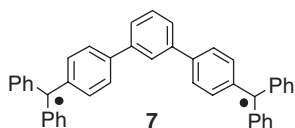
Fig. 7 Diradical 7.

an effective fCU, e.g., the $S = 1$ ground state with $\Delta E_{ST}/k = 34\,K$ was estimated for diradical **7** in 1960 (Fig. 7).[56]

However, when π-conjugated system comprising the radical site and fCU is twisted out-of-plane by nearly 90°, the singlet ground states with relatively small ΔE_{ST} were reported.[57] In general, the ground state and ΔE_{ST} may be affected by conformational equilibria, presence of heteroatoms, and substituent effects.[58,59]

How to attain large values of *S*? Three limiting coupling schemes for the spins of radicals are shown in Fig. 8.
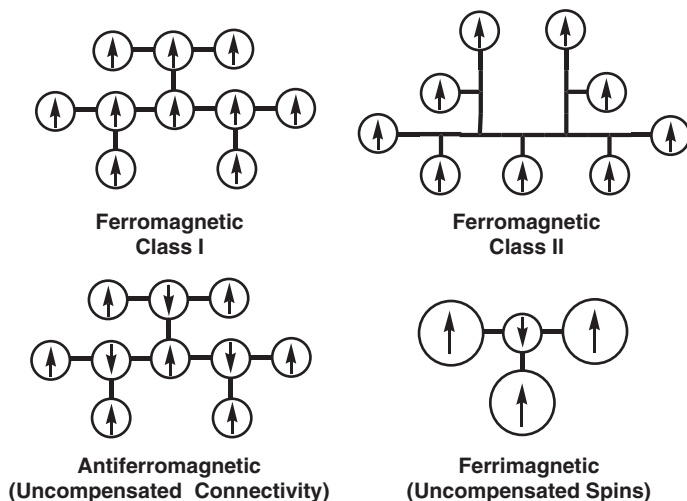
Fig. 8   Coupling schemes leading to high-spin ground states.

In the ferromagnetic coupling scheme, polyradical possesses the fCUs and the spin sites connected in an alternating mode. The resultant high-spin polyradical has ground state with $S = n/2$, where n is the number of spin sites. In this coupling scheme, there are two limiting ways of connecting the spin sites: the spin sites are within the π-system mediating exchange-coupling interaction (Class I polyradicals) and the spin sites are pendants attached to the π-system (Class II polyradicals), as illustrated in Fig. 8.

In the antiferromagnetic coupling scheme, polyradical possesses aCUs and the spin sites connected in an alternating mode. Equal values of S are associated with each spin site. The key to attaining high-spin ground state is the "uncompensated connectivity" between the spin sites that leads to uncompensated spin canceling, such as in hyper-branched structure shown in Fig. 8.

In the ferrimagnetic coupling scheme, polyradical possesses aCUs and the spin sites connected in an alternating mode. Furthermore, the spin sites with unequal values of S associated with each spin site alternate, i.e., large, small, large, small, etc. This leads to uncompensated spin canceling for most connectivities between the spin sites, e.g., linear, branched, macrocyclic, etc.

Overwhelming majority of organic polyradicals reported to date are based upon ferromagnetic coupling scheme, and in particular, Class I type of connectivity. However, the highest values of S are obtained using the coupling schemes which may be viewed as intermediate between ferrimagnetic and ferromagnetic.

3   Preparation and characterization of polyarylmethyl polyradicals

Polyarylmethyl polyradicals were prepared using the carbanion method (Fig. 9), as described in the original communications in 1990 and the other references cited
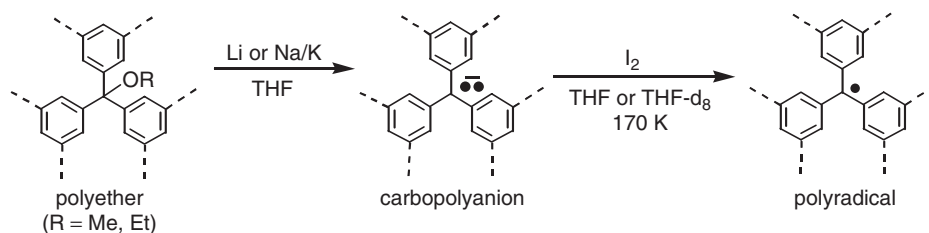
Fig. 9 Carbanion method for preparation of polyarylmethyl polyradicals.

throughout this review.[60,61] This method provides exceptional yields of radicals and it is applicable to very large polyradicals. The use of triarylmethylethers, instead of the corresponding halides, enabled the convergent syntheses and purification of the precursors to polyradicals.

Strict vacuum techniques had to be followed, especially for the generation of large polyradicals. For example, 0.5–1 mg polyether with $M_w \approx 10$ kDa, as in a typical procedure for quantitative measurement of magnetic data, implies handling of < 100 nmol of highly basic (moisture- and air-sensitive) polycarbanion in about 0.05 ml of ethereal solvent. This may be a far more demanding task than anionic polymerizations, which are typically carried out on a much larger scale, although requiring the near-perfect handling of highly sensitive intermediates. In more recent preparations of large polyradicals, THF-d_8 was used to minimize protonation (deuteration) of the polycarbanions.

Typical oxidations of carbopolyanions were carried out with iodine at temperatures near the freezing point of THF (or THF-d_8). Ultra-dry iodine was transferred over the vaccum line in small portions into the reaction mixture. Typically, a sharp color change occurred at the point of complete conversion of the carbopolyanion to the polyradical.

Typical reaction vessels are shown in Figs 10 and 11. Detailed description of the procedures of the carbanion method and their development since late 1980s until 2004 is available on our research group web site.[62]

Thermal instability and sensitivity to oxygen of polyarylmethyl polyradicals imposes experimental challenges in the preparation of samples for magnetic and other characterization techniques. However, these difficulties are worth overcoming. In particular, the ability to convert polyradical to diamagnetic species under mild conditions without opening the flame-sealed sample vessel has an inherent advantage in a field of study, in which many spurious reports of "room temperature organic magnets" appeared in the literature, including the most prestigious journals, allowed for unambiguous exclusion of metal-based impurities as source of the observed magnetic behavior. Furthermore, for more recent magnetic measurements, this enabled nearly exact point-by-point background subtraction, including an accurate correction for diamagnetism.
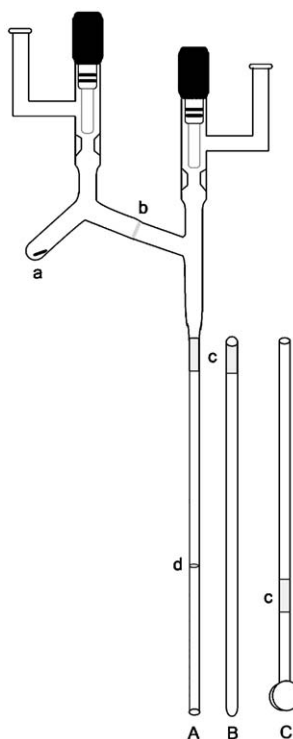
Fig. 10 Vessel for preparation of soluble polyanions and polyradicals for SQUID magneto-metry (tube A), EPR spectroscopy (tube B), SANS (cylindrical cell C), and NMR spectroscopy (sample tube not shown): (a) sample compartment with Teflon-coated magnetic stir-bar, (b) glass frit (course), (c) pyrex-to-quartz seal, (d) thin bottom ($\sim$6 cm from the end of the tube). Solv-seal joints and Kontes (or Chemglass) vacuum stopcocks are used. Reproduced with permission from Ref. 94. Copyright 2004 *Am. Chem. Soc.*

4   High-spin versus low-spin polyradicals

DIRADICALS

Schlenk hydrocarbons I (**8**) and II (**9**) are prototypical diradicals (Fig. 12), which are expected to possess ferromagnetic and antiferromagnetic coupling through their 1,3-phenylene and 3,3′-biphenylene coupling units, respectively. In two pioneering 1915 Berichte articles, Schlenk and Brauns reported the preparation of **8** and **9** via the reaction of the corresponding triarylchloromethanes with powdered zinc at room temperature.[63,64] Schlenk and Brauns' work on **8** followed the apparently unsuc-cessful attempts by Stark and coworkers, who reported "their **8**" as almost com-pletely unreactive with oxygen.[65–67] The Schlenk's contributions to the advancement
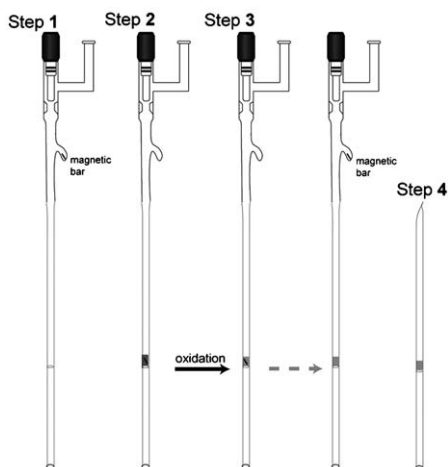
Fig. 11 Implementation of the carbanion method for insoluble (gel forming) polyethers. Steps 1–4 correspond to swelling of polyether with THF-d$_8$, generation of carbopolyanion, oxidation with removal of a Teflon-coated magnetic stirbar, and flame sealing of the quartz sample vessel for SQUID magnetic studies, respectively. Reproduced with permission from Ref. 62. Copyright 2004 Dr. Suchada Rajca.
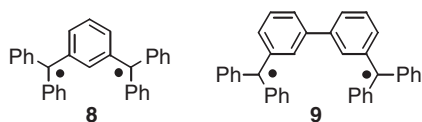
Fig. 12 Schlenk hydrocarbons: diradicals **8** and **9**.

of vacuum and inert atmosphere techniques were important to synthesis of **8** and **9**.[68]

In view of the subsequent work, the content of the actual monomeric diradicals in Schlenk hydrocarbons was rather miniscule. For Gomberg radical, the percentage of the monomeric radical in dilute solutions is relatively small ($K_{assoc} \approx 10^{-4}\,M^{-1}$ at 293 K);[31] thus, the content of the monomer for the corresponding diradicals is likely to be much smaller that less than few percent for triphenylmethyl in dilute solutions. Also, the reported violet color of **8** is unlikely to correspond to monomeric diradical.[63]

EPR spectra for **8** and **9** in glassy toluene matrices were consistent with the dominant content of $S = 1/2$ species, assigned to very intense center peak, and the minor content of $S = 1$ state species, assigned to very weak side peaks. No signal was detected in the $\Delta m_s = 2$ region. The most reliable EPR spectrum for **8** was obtained by Luckhurst and Pedulli, using freshly prepared solutions of **8**, according to the original procedure by Schlenk and Braun; values of $|D/hc| = 6.4 \times 10^{-3}\,cm^{-1}$ and $|E/hc| = 5.7 \times 10^{-4}\,cm^{-1}$ were reported for zero field splitting (zfs) parameters of the $S = 1$ state.[69] For **9**, value of $|D/hc| = 4.9 \times 10^{-3}\,cm^{-1}$ was reported.[70,71]

Based upon the I versus $1/T$ plots of the EPR intensity (I), the triplet ground states were assigned to both diradicals.[70,72] However, such results, even if obtained with utmost care, do not preclude the singlet ground state. The ambiguity of these results was further compounded by the technical difficulties in accurate double integration of minor resonances in partially overlapped spectrum of different species, especially in the absence of adequate numerical approaches to data handling in early 1970s. Furthermore, the studied temperature ranges were relatively narrow, which led to unreliable results. In particular, the assignment of the $S = 1$ ground state for **9**, and especially the singlet–triplet energy gap of $0.3\,\mathrm{kcal\,mol^{-1}}$,[70] was very likely an artifact of softening of glassy toluene matrix in the 153–183 K range.

More stable, alkyl-substituted analogous of Schlenk diradicals **8** and **9** were prepared in order to carry out rigorous studies of the ground states and the singlet–triplet energy gaps in Schlenk-like diradicals **10–20** (Fig. 13).[61,73–82]

1,3-Phenylene-based diradicals **10**, **13–15**, in which all p-positions (with respect to the α-carbon) are alkyl substituted, were sufficiently persistent to allow their isolation as solids. The solids could be stored at room temperature under argon for an
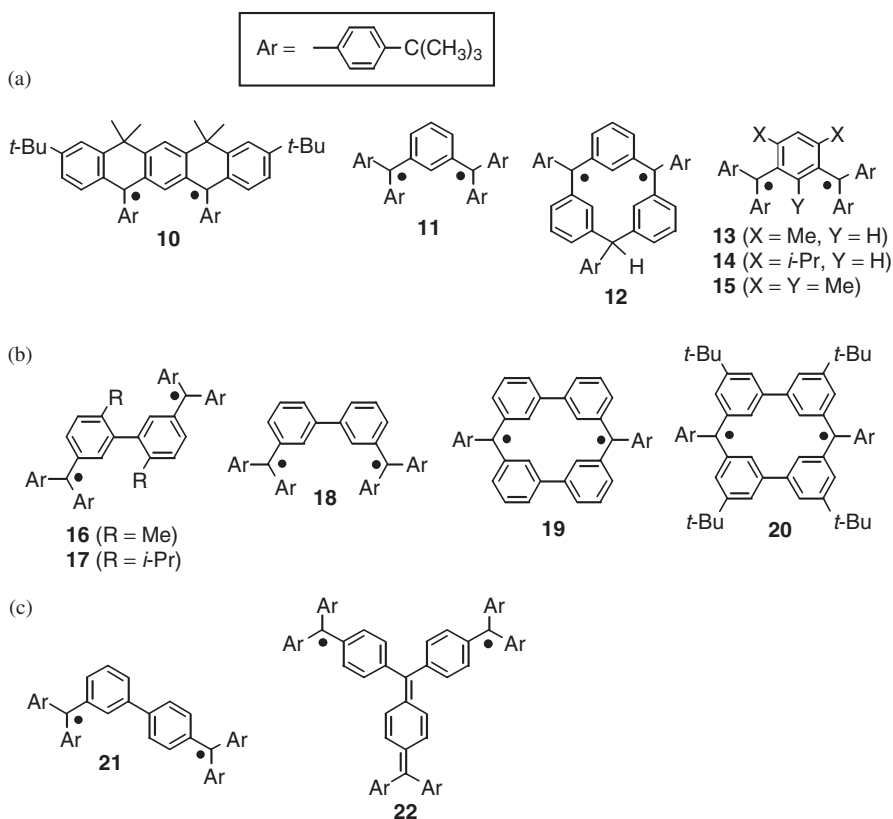
Fig. 13 Diradicals: (a) 1,3-phenylene-based, (b) 3,3′-biphenylene-based, and (c) 3,4′-biphenylene-based and diradical with antiferromagnetic coupling scheme.
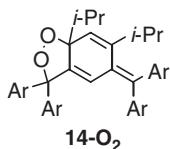
Fig. 14 Cyclic peroxide **14-O₂** obtained from diradical **14**.

extended period of time.[73,74] For each diradical, two reversible cyclic voltammetric waves of equal intensity and separated by about 0.2 V, and corresponding to radical anion and carbodianion were observed; these cyclic voltammograms were analogous to those that were obtained from solutions of the corresponding carbodianions[73] (for **10**, the strong basicity of the corresponding dianion, led to only partially reversible wave for dianion in THF/tetrabutylammonium perchlorate at room temperature and using scanning rates of $< 5\,\mathrm{V\,s^{-1}}$).[74] The reaction of diradicals **13–15** with oxygen gave peroxides; for **14**, cyclic peroxides with three different structures were isolated, e.g., cyclic peroxide **14-O₂**, with its structure confirmed by single crystal X-ray crystallography (Fig. 14).[83]

For 1,3-phenylene-based diradicals **10–15**, values of $|D/hc|/\mathrm{cm}^{-1}$ are 6.6 (dibr), 6.6, 7.2, 8.7, 9.9 and 10.7×10^{-3}, respectively.[73,74,76,77,79] In addition, values of $|E/hc|/\mathrm{cm}^{-1}$ are 22×10^{-4}, 8×10^{-4}, and 7×10^{-4} for **10**, **11**, and **12**, respectively, and they are negligible for diradicals **13–15**.[73,74,76,77,79] Assuming a simple localized magnetic dipole–dipole model in these hydrocarbon diradicals, the experimental values of $|D/hc|$ and $|E/hc|$ may provide qualitative insight into "average" molecular conformations. Value of $|E/hc| = 0$ is associated with effectively threefold (or higher) symmetry of the spin density distribution, while values of $|E/hc| \neq 0$ imply lower symmetry. The increasing values of $|D/hc|$ suggest the increasing "proximity" of the spin densities of the two triarylmethyls along the above series. Overall, the values $|D/hc|$ and $|E/hc|$ strongly suggest the increasing out-of-plane twisting for the $S = 1$ states in the series of diradicals **10–15**.

Superconducting QUantum Interference Device (SQUID) magnetic studies for solid **10** established its $S = 1$ ground state.[74] The plot of the product of magnetic susceptibility (χ) and temperature (T) versus temperature (T) was flat in the 20–110 K temperature range. The effective magnetic moment, $\mu_{\mathrm{eff}} = 2.7\ \mu_{\mathrm{B}}$, was in an agreement with the theoretical value of $\mu_{\mathrm{eff}} = 2.8\ \mu_{\mathrm{B}}$ for a diradical with exclusively populated $S = 1$ ground state. These results indicate that diradical **10** is relatively pure and monomeric in the solid state. Most importantly, strong ferromagnetic coupling was found in **10**, with no detectable thermal population of singlet excited state up to 110 K (the highest temperature studied).

SQUID magnetic studies of **11**, **12**, **13**, and **14** in THF or 2-MeTHF matrices established the $S = 1$ ground states. The strength of ferromagnetic coupling for **13** and **14** in 2-MeTHF was estimated using EPR spectroscopy. The IT versus T plot of the EPR $\Delta m_{\mathrm{s}} = 2$ signal in the 10–80 K range was flat for **13**, but a small drop off at the higher temperature was observed for **14**. However, the χT versus T plot, based upon SQUID magnetic studies, for **14** in THF was flat up to 80 K (the highest

temperature studied). These results suggested that the ferromagnetic coupling for **14** might be matrix dependent and, most likely, somewhat weaker than that for **13**.[77,79]

Mesitylene-based diradical **15** in THF or 2-MeTHF matrices was found as a mixture of two component diradicals, both possessing singlet ground states: the major and minor diradicals had $J/k \approx -40$ K and $J/k \approx -5$ K, respectively. These values of J/k were determined using the IT versus T plot of the EPR $\Delta m_s = 2$ signal and SQUID magnetometry for thermally populated triplet states. Values of $|D/hc|$ for the thermally populated triplet states of these two diradicals are too similar to allow for resolution of their spectra. However, upon lowering of the temperature from ~ 80 to ~ 4 K, the EPR spectral width ($2|D/hc|$) decreases by $\sim 5\%$. Although these changes are rather small, they are consistent with the "more planar" conformation for the thermally populated triplet state of the component diradical, for which the thermally populated triplet state is relatively less depopulated at upon lowering of the temperature, i.e., diradical with smaller $|J/k| \approx 5$ K is relatively less twisted out-of-plane. Probably, the two component diradicals are conformational isomers of **15**.[79]

For 3,3′-biphenylene-based diradicals **16–19**, values of $|D/hc|/\text{cm}^{-1}$ are 0.0041, 0.0041, 0.005, and 0.0081, respectively[75,78,80,81] (values of $|E/hc| \approx 0$ were found, except $|E/hc| = 8 \times 10^{-4}\,\text{cm}^{-1}$ for cyclophane-based diradical **19**). Assuming a simple localized magnetic dipole–dipole model in these hydrocarbon diradicals, the experimental values of $|D/hc|$ suggest the increasing "proximity" for centroids of the spin densities of the two triarylmethyls along the above series. This suggests that conformationally unrestricted diradical **18** was found predominantly in a "syn" rather than "anti" conformation in glassy 2-MeTHF/THF and toluene matrices (Fig. 15).

Detailed EPR and SQUID magnetic studies of **18** in 2-MeTHF/THF and THF matrices were interpreted in terms of the major ($>90\%$) and minor ($<10\%$) component "diradicals", with $J/k = -22 \pm 3$ K and $J/k = -5 \pm 2$ K, respectively. Thus, diradical **18** possessed singlet ($S = 0$) ground state, with rather weak antiferromagnetic coupling. Assuming that the two component "diradicals" correspond to the somewhat out-of-plane twisted "syn" and "anti" conformations, this suggests much greater antiferromagnetic coupling in the "syn" conformation.[78]

Analogouss studies of conformationally restricted cyclophane-based diradical **19** gave singlet ($S = 0$) ground state, with much greater antiferromagnetic coupling,
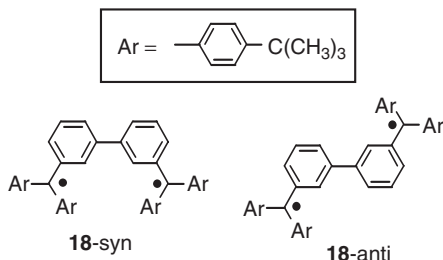
Fig. 15 "Syn" and "anti" isomers (conformers) for diradical **18**.

compared with that for acyclic diradical **18**. In particular, the EPR data in glassy 2-MeTHF/THF and the SQUID data in frozen THF gave $J/k = -53 \pm 3\,\mathrm{K}$ and $J/k = -60 \pm 2\,\mathrm{K}$, respectively.[80] Similar results were obtained for diradical **20**, with 5,5′-di-*tert*-butyl-3,3′-biphenylene moieties; this diradical could be isolated as an air-sensitive solid.[81] Cyclophane-based diradicals **19** and **20** may also be viewed as arylmethyl models for phenylcarbene-based Mataga polymer II (Fig. 4), suggesting $S = 0$ ground state for the polymer II.

In conjunction with Monte Carlo conformational searches (MM3* force field, with parametrization for arylmethyl radicals) for diradicals **18** and **19** in the gas phase, a concept of parallel exchange pathways was introduced. It was concluded that the relative strengths of antiferromagnetic coupling (singlet–triplet energy gaps) in **18** compared with **19** may be related to the number of parallel exchange-coupling pathways, i.e., one pathway in **18** and two parallel pathways in **19**.[80]

For Me- and *i*-Pr-substituted diradicals **16** and **17**, SQUID magnetic studies indicate very weak exchange couplings, as expected for severely out-of-plane twisted conformations. Although numerical fitting of magnetization data suggested $S = 1$ ground states, such assignments were complicated by the difficulty in the measurement of small ferromagnetic couplings and the presence of relatively strong, presumably intermolecular, antiferromagnetic couplings.[75]

The 3,4′-biphenylene-based diradical **21** emerged as an important building block for very high-spin polyradicals, described in the following sections. The EPR and SQUID magnetic studies establish the $S = 1$ ground state for **21** in 2-MeTHF/THF and THF matrices. As no thermal population of $S = 0$ excited states was detected at $T < 75\,\mathrm{K}$ (EPR), the strength of the ferromagnetic coupling is still significant, in spite elongation of the exchange-coupling pathway by 1,4-phenylene spacer, compared with simple 1,3-phenylene-based diradicals. Diradical **21** could be isolated as solid, which may be handled at room temperature under oxygen-free atmosphere. However, solutions of diradical, prepared from the solid, were somewhat less pure than those obtained directly as solutions via the standard low-temperature methods.[78]

Diradical **22** (Fig. 13) provided an example for implementation of the antiferromagnetic coupling scheme (Fig. 8). This diradical may also be viewed as an analog of TMM or phenoxy-based Young's biradical.[84] SQUID magnetic studies and EPR spectroscopy for **22** in THF-d_8 matrices established the $S = 1$ ground state with strong ferromagnetic coupling. Diradical **22** was persistent in THF-d_8 solution at room temperature.[81]

Thus, studies of alkyl-substituted and/or conformationally restrained diradicals **10–20**, derivatives of Schlenk hydrocarbons, indicate a delicate interplay between conformation and exchange coupling that is affected by both the molecular structures, conformations, and the medium. Although in most cases 1,3-phenylene is a ferromagnetic coupler, even a robust coupler, severe out-of-plane twisting (as measured via zfs parameters) may weaken the ferromagnetic exchange coupling and, in selected cases, lead to a weak antiferromagnetic coupling. Analogously, 3,3′-biphenylene-based diradicals possess singlet ground state, with modest strength of antiferromagnetic coupling; in this case, severe out-of-plane twisting diminishes the exchange coupling, with probable sign reversal from antiferromagnetic to ferromagnetic. At

least, in dilute frozen solutions (matrices), there is a qualitative correlation between the value of $|D/hc|$ (as a measure of out-of-plane twisting or conformation) and the value of J/k for diradicals of the analogous molecular structure.

TRIRADICALS

Three limiting topologies (Fig. 16), based upon 1,3-phenylene coupling unit, can be considered for Class I polyarylmethyl triradicals: quasi-linear, quasi-cyclic, and macrocyclic (calyx[3]arene-based).[3,85–89]

   In 1937, Leo reported the preparation of 1,3,5-tris-(diphenylmethyl)benzene, i.e., triradical **23** (Fig. 17), with quasi-cyclic connectivity. Synthetic methodology analogous to that for Schlenk hydrocarbon was used. Based upon cryoscopy (melting point depression of benzene), Leo claimed that brown, 2% solution of **23** is largely monomeric.[85a] Triradical **23** was reinvestigated in 1975 by Zimmermann and co-workers, who claimed that **23** in solution exists as a "diamagnetic tetramer". A cage-like structure, with the CC bond between the α-C and *para*-C of each of six pairs of triarylmethyl moieties, was proposed, however, the spectroscopic evidence for such unusual structure was nearly absent. ESR spectrum of freshly prepared **23** in toluene glass at 138 K showed a symmetrical pattern of six weak side lines and a very strong center line in the $\Delta m_s = 1$ region. This spectral pattern was interpreted as a mixture of $S = 3/2$, 1, and 1/2 states and/or species; in particular, the spectral width associated with the two most outer lines (210 G) was greater than that in Schlenk di-radical **8** (147 G).[85b] However, such spectral patterns does not prove even a presence
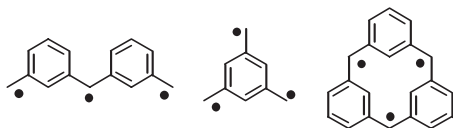
Fig. 16   Limiting topologies for triradicals.[3]
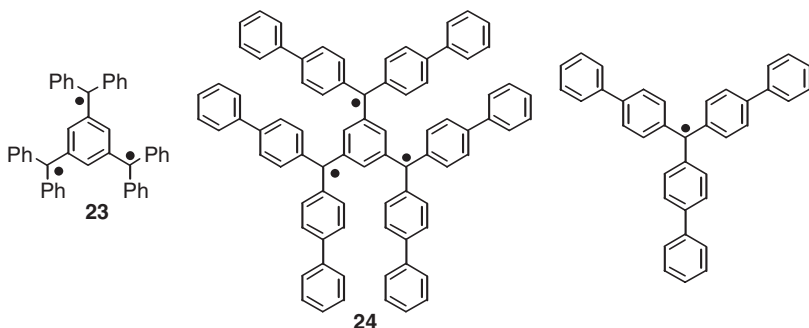
Fig. 17   Triradicals **23** and **24**, and tris-(4-biphenylyl)methyl.

of $S = 3/2$ state; instead, the spectrum may be associated with two $S = 1$ diradicals, with different zfs parameters (e.g., as in a σ-dimer of **29**), in addition to $S = 1/2$ monoradicals (from higher oligomers or other impurities). The $\Delta m_s = 2$ signal was detected and described only as "strong" but not shown; most likely a singlet was observed, which would be consistent with $S = 1$ state. Therefore, neither detection of $S = 3/2$ state nor, definitely, ground state for triradical **23** were established.

The evidence for $S = 3/2$ state for Zimmermann triradical **24**[86] (Fig. 17) is not definite either but it better withstands the scrutiny with the benefit of hindsight. The primary evidence for the $S = 3/2$ state is the agreement between the computed and the experimental ESR spectrum ($\Delta m_s = 1$) for **24** in glassy toluene at 93 K.[86] However, as outlined in the preceding paragraph such spectra may as well correspond to a mixture of $S = 1$ and $S = 1/2$ radicals. Zimmermann and coworkers reported three additional findings for **24** in toluene that cast additional doubt on the assignment of the $S = 3/2$ state: (1) for the zfs parameters assigned to the $S = 3/2$ state, the expected spectral pattern in the $\Delta m_s = 2$ region was absent, and instead, apparently a single line characteristic of $S = 1$ state was most likely observed (the $\Delta m_s = 2$ region was not shown),[86] (2) the average molecular weight for 3.5×10^{-3}–3.3×10^{-2} M **24** corresponds to a dimer,[86] (3) magnetic susceptibility at room temperature, as obtained by the very approximate EPR spin counting method, decreased with increased concentration of **24** and, for 10^{-2} M **24**, was only of the order of 10% of the expected value for pure $S = 3/2$ triradical.[86]

Tris-(4-biphenylyl)methyl, $S = 1/2$ monoradical, provides a valuable reference for triradicals **23** and **24** (Fig. 17). The first report of tris-(4-biphenylyl)methyl by Schlenk and coworkers in 1911 played an important role in validation of Gomberg's discovery of triphenylmethyl.[90] This was primarily because tris-(4-biphenylyl)methyl was more dissociated in solution, compared with triphenylmethyl. Nevertheless, subsequent authors, including Zimmermann, found by susceptibility studies that this monoradical is always significantly contaminated with diamagnetic impurities, especially in dilute solutions, i.e., formation of chemical defects cannot be avoided.[90] It is not clear whether this is an intrinsic problem, associated with the inefficient method preparation from the triarylchloromethane and metal, or inadequate exclusion of oxygen and light. This implies that chemical defects for triradicals **23** and **24** may have a significant impact. In 1976, Kurreck and coworkers reported for 10^{-2} M tris-(4-biphenylyl)methyl in glassy toluene at 160 K strong EPR resonances ($\Delta m_s = 1$ and $\Delta m_s = 2$) corresponding to $S = 1$ state. Based upon the observed value of $|D/hc|$, these resonances were assigned to a π-dimer of monoradicals, separated by 4.3–4.7 Å.[90] Although the ground state of the dimer was not established, the $S = 0$ ground state is likely; in such a case, the observed EPR spectrum might originate in a thermally populated $S = 1$ excited state of the dimer.

Zimmermann triradical **24** makes a reasonable case for the $S = 3/2$ state (Fig. 2), especially in view of the characterization tools and techniques available up to the mid-1970s. From the 2005 perspective, monomeric triradical **24** with $S = 3/2$ state was probably a very minor component in solution, i.e., **24** was largely oligomerized and it was likely to contain significant amounts of impurity diradicals and monoradicals
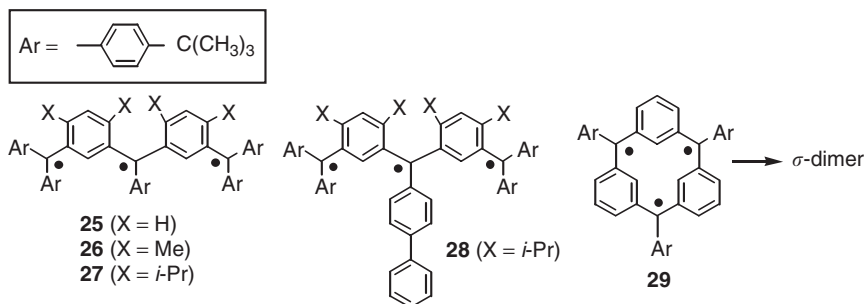
Fig. 18   Triradicals.

arising from chemical defects. There is no experimental evidence concerning the ground state of monomeric **24** or the strength of its exchange coupling.

Quasi-linear triradicals **25–28** (Fig. 18), which were prepared via carbanion method, possess $S = 3/2$ ground states.[87,88] The EPR spectra, recorded down to the temperature of 4 K in 2-MeTHF/THF glassy matrices, possessed the spectral patterns of the $S = 3/2$ state of five symmetrical peaks for **26–28** and more complicated pattern, assigned to two $S = 3/2$ states (e.g., diastereomers) for the least substituted triradical **25**. For Me-substituted **26** and biphenyl-*i*-Pr-substituted **28**, the well-defined, single resonance in the $\Delta m_s = 3$ region was observed at 4 K, unequivocally confirming the presence of $S = 3/2$ state. In addition, a symmetric spectral pattern of five resonances in the $\Delta m_s = 2$ region, indicated the $S = 3/2$ state (the four side lines) with a small admixture of an $S = 1$ state (the center line) impurity. Even for the high sterically hindered, *i*-Pr-substituted triradicals **27** and **28**, the SQUID magnetic data unequivocally support the $S = 3/2$ ground states. The strengths of the ferromagnetic coupling in **27** and **28** may require additional investigation, using improved preparation techniques for SQUID samples of air-sensitive solids, to allow for more reliable correction for diamagnetism.

Calix[3]arene-based triradical **29** (Fig. 18) may be viewed as the key fragment of Mataga network III.[77] Attempts to prepare monomeric triradical **29** via oxidation of the corresponding carbotrianion were not successful; oxidation with iodine at –95°C, followed by dilution with 2-methyltetrahydrofuran at temperatures below –95°C, gave ESR spectrum of which dipolar coupling patterns can be reasonably well fit to two $S = 1$ states with distinct zfs parameters.[77] Since the spectral width of $\Delta m_s = 1$ region was comparable with those for quasi-linear triradicals **25–28**, the failure to observe the $\Delta m_s = 3$ resonance, under analogous instrumental conditions, establishes the absence of any significant content of $S = 3/2$ state at 4 K. Furthermore, magnetic susceptibility studies using EPR spectroscopy and SQUID magnetometry showed the presence of weak antiferromagnetic interactions. Thus, calix[3]arene-based triradical **29** could not be obtained using our standard low-temperature solution techniques.[77] Possibly, relatively small out-of-plane twisting, associated with calix[3]arene moiety, led diminished persistence of **29**, analogously to that observed for simple triarylmethyl monoradicals.[91]

TETRARADICALS

Three limiting topologies, based upon 1,3-phenylene coupling unit, can be considered for Class I polyarylmethyl tetraradicals: quasi-linear, star branched, and macrocyclic (calix[4]arene based). Structures of polyarylmethyl tetraradicals are illustrated in Fig. 19.

No polyarylmethyl tetraradicals with quasi-linear connectivity were reported. However, polymer 30 was prepared and it was found to possess average $S \approx 2$, according to the magnetization studies at low temperatures (Fig. 20).[92] Synthesis of quasi-linear annelated tetraradical and hexaradical, homologs of diradical 10, was not successful, although states with $S > 1$ were found, as indicated by the EPR and magnetization data.[93] In particular, annelation of 30 and 31 under aromatic electrophilic substitution conditions leads to a complex mixture of diastereomers of corresponding hydrocarbons, which makes their adequate purification very difficult (Fig. 20). Another complicating factor is the possibility of formation of annelated regioisomers (constitutional isomers), which are precursors to low-spin oligoradicals.

Star-branched tetraradicals 33–35 possess $S = 2$ ground states, with relatively strong ferromagnetic couplings, as determined by EPR spectroscopy and magnetization studies (Fig. 21).[61,87] EPR spectra for sterically hindered tetraradicals were
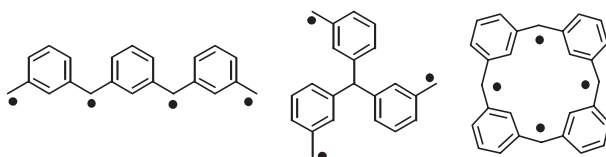
Fig. 19   Selected limiting topologies for tetraradicals.
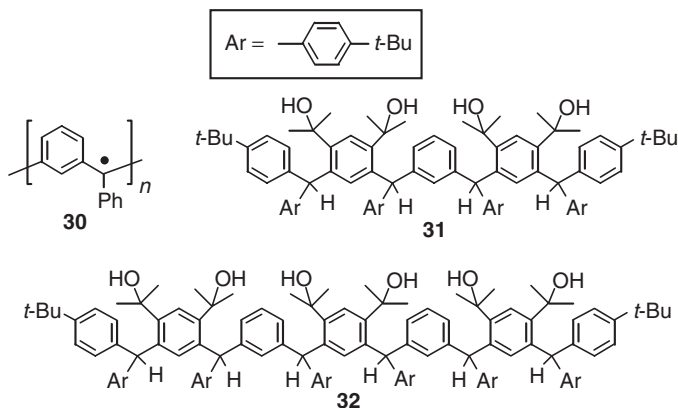
Fig. 20   Polymer 30. Precursors 31 and 32 to quasi-linear annelated tetraradicals and hexaradicals, homologs of diradical 10.
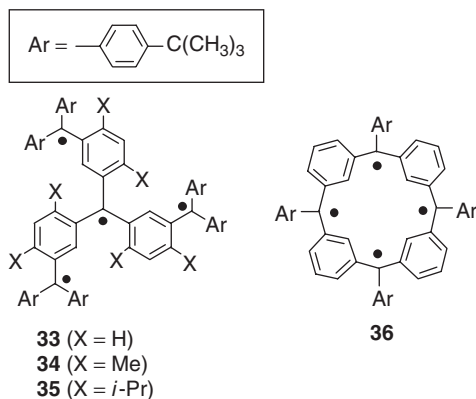
Fig. 21   Tetraradicals.

complicated by spectral broadening for Me-substituted **34** and additional resonances for *i*-Pr-substituted **35**, which may be associated with the effectively lowered symmetry ($|E/hc| \neq 0$) and/or the presence of propeller-like diastereomers. The best resolved EPR spectra were obtained for **33** in 2-MeTHF/THF glassy matrix: the $\Delta m_s = 1$ regions of the EPR spectra showed an excellent agreement with the $S = 2$ state and, in the $\Delta m_s = 2$ region, an unprecedented symmetrical five-line pattern was observed at 4 K, as expected for $S = 2$ state with $|E/hc| \approx 0$. At X-band, with $|D/hc| \approx 0.003 \, \text{cm}^{-1}$ and $|E/hc| \approx 0$, the theoretically predicted symmetrical four-line pattern in the $\Delta m_s = 3$ region, as well as a single resonance in the $\Delta m_s = 4$ region, would possess extremely low intensity and were not detected not only in **33–35** but in any $S = 2$ organic tetraradical. The I versus $1/T$ and IT versus T ($T = 10–100$ K) plots of the EPR $\Delta m_s = 2$ signals are straight lines, showing that **33–35** possessed either strong ferromagnetic coupling, leading to the $S = 2$ ground states with no significant thermal population of the low-spin excited states up to 100 K, or very weak coupling (ferromagnetic or antiferromagnetic), leading to the nearly degenerate $S = 2$ and low-spin excited states. This dilemma was resolved by SQUID magnetization studies, which clearly indicated $S = 2$ ground states.[87] Additional evidence for $S = 2$ with a significant strength of ferromagnetic coupling was obtained for **33** in dimethyl ether solution by Evan's NMR method, i.e., $\mu_{\text{eff}} \approx 4.3 \, \mu_{\text{B}}$ was obtained in the range 133–163 K, which is close to the theoretical value of $\mu_{\text{eff}} = 4.9 \, \mu_{\text{B}}$.[61]

Macrocyclic tetraradical **36** (Fig. 21) may be viewed as the key building for very high-spin polyradicals, including polymer with magnetic ordering described in later part of this chapter. The EPR and magnetic studies established the $S = 2$ ground state for **36** in THF and 2-MeTHF/THF.[77] In particular, SQUID magnetization studies at low temperatures unequivocally indicate the $S = 2$ ground state. The EPR spectra confirm the $S = 2$ state ($\Delta m_s = 1$ and $\Delta m_s = 2$ regions). The IT versus T ($T = 10–80$ K) plot of the EPR $\Delta m_s = 2$ signal is approximately flat. In conjunction with the magnetic data, this suggests strong ferromagnetic coupling in **36**, leading to negligible thermal population of low-spin excited states up to approximately 80 K.[77]

Monte Carlo conformational searches (MM3* force field, with parametrization for arylmethyl radicals) for tetraradical **36** in the gas phase gave 1,3-alternate-like conformations for of calix[4]arene moiety for the lowest energy structures.[94] The CCCC torsional angles along the inner macrocyclic carbon backbone are about $47°$,[94] which is consistent with the experimentally observed $S = 2$ ground state and a moderate strength of ferromagnetic coupling in 2-MeTHF/THF and THF matrices.

DIRADICAL ANIONS AND DIRADICAL DIANIONS

Trianions and tetraanions corresponding to triradicals **25–28** and tetraradicals **33–35** were studied by cyclic voltammetry at 200 K.[88] Especially useful data were obtained in the–1.0 to -2.2 V potential range (versus SCE) corresponding to the oxidation of polyanions to polyradicals and reduction of polyradicals to polyanions. Typically, three waves were resolved in this potential range with the relative peak currents 1:1:1 and 1:2:1 (or 1:1:2) for trianions and tetranions; for trianion, corresponding to triradical **28**, only two waves (relative peak currents, 2:1) were resolved.

Selected intermediate radical anion species could be prepared and studied, primarily in solution (Fig. 22).[88] Of particular interest were diradical anions **25$^{2.1-}$–28$^{2.1-}$** and diradical dianions **33$^{2.2-}$–35$^{2.2-}$**, i.e., "diradicals" related to the corresponding high-spin polyradicals by different occupancy of their non-bonding MOs (Fig. 22).

The EPR spectra in the $\Delta m_s = 1$ region for diradical anions **25$^{2.1-}$–27$^{2.1-}$** and diradical dianions **33$^{2.2-}$–35$^{2.2-}$** in 2-MeTHF/THF matrix showed typically four-line dipolar pattern assigned to $S = 1$ states with the values of $|D/hc|$ that were similar (but not identical) to those for the corresponding diradicals **11**, **13**, and **14**.[88] In conjunction with the EPR studies of selected diradical anions, this provided evidence for localization of spin density in diradical anions **25$^{2.1-}$–27$^{2.1-}$** and diradical dianions **33$^{2.2-}$–35$^{2.2-}$** at the two adjacent triarylmethyl sites (Fig. 22).[88] Also, the IT versus T plot of the EPR $\Delta m_s = 2$ signal drops off with decreasing temperature in the 10–80 K range.

For biphenyl-substituted diradical anion **28$^{2.1-}$**, the $S = 1$ state with $|D/hc| = 0.0027$ cm^{-1} was found in the 25–70 K range. This value was smaller by a factor of >2, compared to the values of $|D/hc|$ for **25$^{2.1-}$–27$^{2.1-}$** and **33$^{2.2-}$–35$^{2.2-}$**. In conjunction with the UV–vis absorption spectroscopy data, this suggested that the spin density in diradical anion **28$^{2.1-}$** was localized at the terminal triarylmethyl sites. Furthermore, the IT versus T plot of the EPR $\Delta m_s = 2$ signal drops off with decreasing temperature in the 10–80 K range indicating that the observed $S = 1$ was a thermally populated excited state; numerical fitting of the data gave the strength of the antiferromagnetic coupling, $J/k \approx -4$ K, in diradical anion **28$^{2.1-}$**.[88]

The relatively small perturbation of the triarylmethyl sites by biphenyl substitution allowed for both control of electron localization and exchange coupling. When the triarylmethyl spin sites were adjacent, the exchange coupling was ferromagnetic,
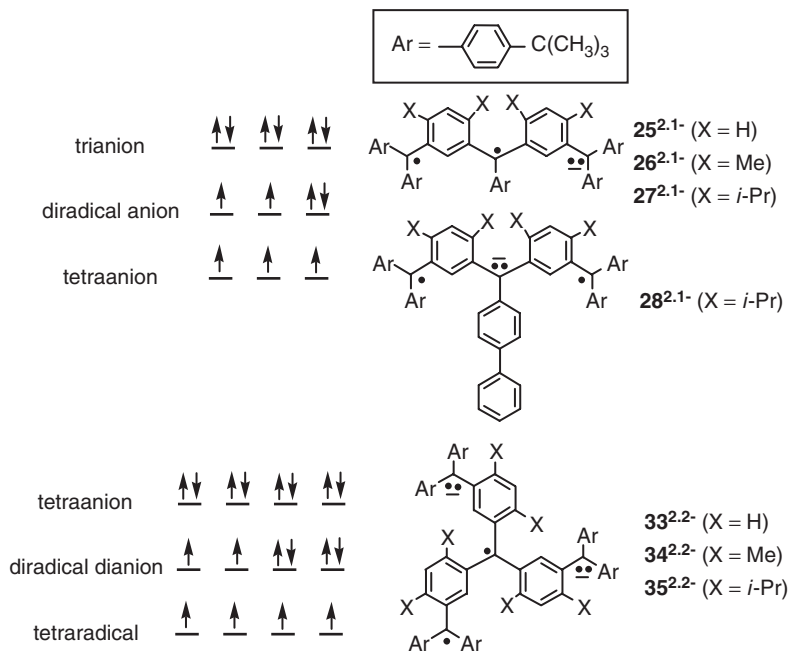
Fig. 22 Diradical anions and diradical dianions and their occupation of non-bonding MOs.[88]

and for non-adjacent sites, separated by a negatively charged site, the exchange coupling was antiferromagnetic.

5 Star-branched and dendritic polyarylmethyl polyradicals

Star-branched and dendritic polyradicals **37**–**42**, with 5–31 triarylmethyl sites for unpaired electrons were studied (Fig. 23).[47,77,95–98] With the increasing number of sites, the resolution of the EPR spectra in glassy matrices decreases dramatically, as expected for a series of high-spin homologs with approximately constant spin density (number of unpaired electrons per unit volume). In addition, the presence of diastereomers (conformers) may contribute to spectral broadening. In the dendritic series, the diminished resolution is further compounded by decreasing spectral width in the $\Delta m_s = 1$ region. The decreasing spectral width might be associated with more globular-like molecular shapes for larger dendrimers, e.g., spectral width, due to magnetic dipole–dipole interaction, tends to zero for a sphere. Alternatively, through-space exchange coupling between the proximate dendritic branches, especially in the presence of defects, may diminish the spectral width (exchange-narrowing mechanism). These intrinsic factors limit the identification of spin states by EPR spectroscopy to polyradicals with relatively few unpaired electrons.
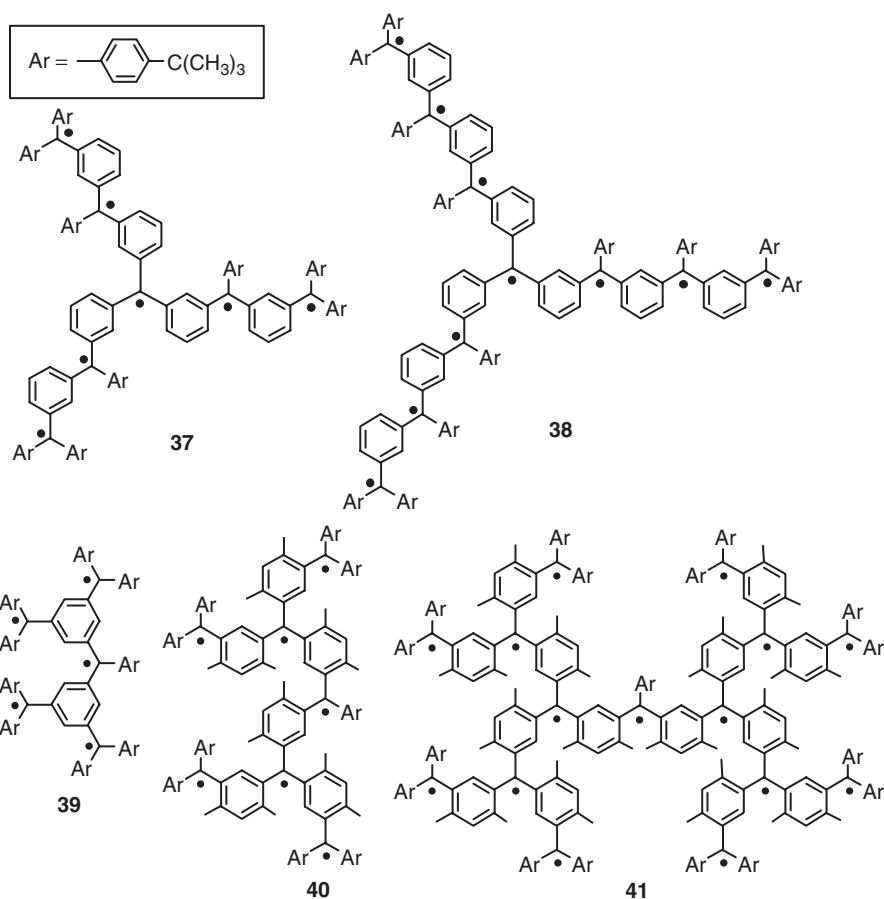
Fig. 23 Star-branched and dendritic polyradicals. (Dendritic 31-radical **42**, next higher homologs of **40** and **41**, is not shown.)

The EPR spectral changes, described in the preceding paragraph, are accompanied by the increased polydispersity of S, as obtained from magnetization studies at low temperatures. Most importantly, the average values of S did not scale with number of sites, especially in the dendritic series.

Star-branched heptaradical **37** and decaradical **38** possess the $S = 7/2$ and $S = 5$ ground states, respectively.[47,95] The relatively well-resolved EPR spectrum ($\Delta m_s = 1$) of 10^{-3} M **37** in 2-MeTHF/THF matrix at 100 K was numerically fitted to a threefold symmetric $S = 1/2$ state ($|E/hc| \approx 0$).[95] The much less-resolved spectrum for 10^{-3} M **38** consisted of a symmetrical progression of shoulders, of which positions agree reasonably well with calculated resonance positions for an $S = 5$ state.[95] At low temperatures, the EPR spectra for both polyradicals were highly susceptible to microwave saturation. Magnetic moment for 2×10^{-3} M decaradical

38 in dimethyl ether at 150 K, as measured by Evan's NMR method, was near the theoretical value of 11 μ_B. Owing to the technical reasons, the samples of **37** and **38** for magnetic studies had to be prepared in solvents such as THF or 2-MeTHF, the very low temperatures employed for preparation of **38** in dimethyl ether could not be used. Magnetization studies for **37** and **38** revealed somewhat polydisperse mixture of spin systems, with $7/2 > S > 5/2$ and $S \approx 4$, respectively.[47,95] The numerical fits of these magnetization data could be greatly improved using a simple percolation model, which takes into account chemical defects, i.e., the absence of radicals at some triarylmethyl sites (Section 6).[47]

For the relatively small dendritic pentaradical **39**, the EPR and magnetic studies were consistent with $S = 5/2$ ground state, as expected for five ferromagnetically coupled electron spins.[77,98] At 4 K, the observed EPR spectral pattern in the $\Delta m_s = 1$ region was consistent with the presence of two $S = 5/2$ states, assigned to two diastereomers (or frozen conformers); structured $\Delta m_s = 2$ and relatively simpler $\Delta m_s = 3$ signals were detected, as expected for $S > 1$ polyradical. Magnetization studies gave at least $S \approx 2.3$, which is close to the $S = 5/2$.[77,98]

For larger dendritic polyradicals **40–42**, magnetization studies gave similar values of $S \approx 3$ but with increased polydispersity of S for the higher homologs.[47,96] The value of $S \approx 3$ is perhaps not too far from the theoretically expected $S = 7/2$ for ferromagnetically coupled electron spins in heptaradical **40**, but nowhere near the expectation for the higher homologs. Analysis of the magnetization data, using a simple percolation model with chemical defects, suggested that **41** and **42** may consist of highly polydisperse spin systems.[47]

6   Design of very high-spin polyradicals

DEFECTS

1,3-Phenylene-based polyarylmethyl polyradicals with quasi-linear, star-branched, and dendritic connectivities gave only values of S that approach 5, i.e., only up to 10 sites with electron spins could be ferromagnetically coupled. Analogous results were obtained for 1,3-phenylene-based polycarbenes, with S approaching 9 or up 9 $S = 1$ ferromagnetically coupled carbene sites.[21,22] Evidence for interbranch C=C bond formation was reported for a dendritic polycarbene.[99] Such bond formation is an example of a failure to generate a radical or carbene; other examples of such "chemical defects", relevant to polyarylmethyls, are C–I bond, C–H bond, or carbanion at the triarylmethyl site. For linear, star-branched, and dendritic connectivities between the radical sites, the presence of chemical defect in the interior of polyradical may interrupt the exchange pathway and effectively divide polyradical into two (or more) parts with relatively low values of S, as illustrated for penta-decaradical **41** (Figs 23 and 24).[47]

Another type of defect may be associated with severe out-of-plane twisting within the exchange-coupling pathway connecting two sites with electron spin, which we

$S = 3/2, 3/2, 8/2$ $S = 8/2 − 7/2 = 1/2$
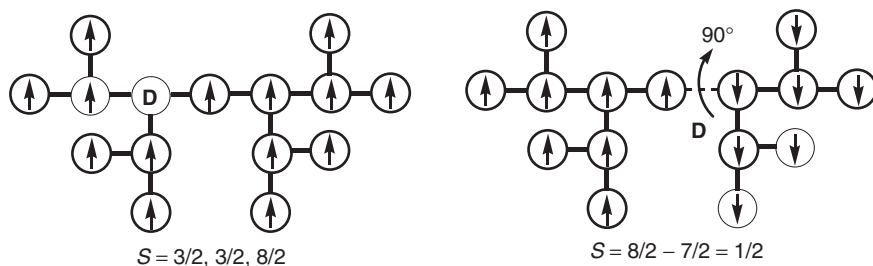
Fig. 24 Impact of chemical defects and exchange defects on values of *S*, as illustrated using pentadecaradical **41**.

● = radical site with unpaired electron

○ = chemical defect

$S = 7/2$ $S = 3/2$
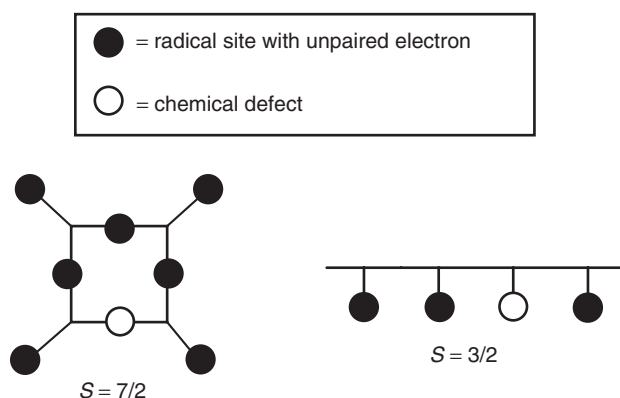
Fig. 25 Chemical defects in Class I and II high-spin polyradicals.

refer to as "coupling defect".[8] As demonstrated by studies of diradicals, such coupling defect may imply reversal of exchange coupling, e.g., a strong fCU may be replaced by a weak aCU, leading to a partial or complete cancellation of spins, as illustrated for pentadecaradical **41** (Fig. 24).

Two conceptual approaches to the problem of defects are illustrated by Class I and II polyradicals (Fig. 25).[3]

In Class I polyradicals,[3,8] macrocyclic connectivity between the spin sites provides an alternative exchange pathway to bypass chemical defects or coupling defects. Furthermore, with adequate choice of the macrocycle, macrocyclic conformational restriction may prevent significant out-of-plane twisting associated with coupling defects.

In Class II polyradicals,[3,8] the spin sites are attached to a shared π-system, analogously to pendants attached to a main chain in a polymer. Therefore, a defect in the pendant may be bypassed, however, the elongated exchange pathway causes significant decrease in exchange coupling. Coupling defects in the shared π-system (outside pendants), which remain an important problem, may possibly be addressed with macrocyclic connectivities.[100,101] Nishide group have developed the design of

Class II polyradicals and explored possible applications.[23,24,100–102] The effectiveness of exchange coupling in Class II polyradicals, as measured by the highest reported values of $S \approx 5$,[24] still remains the challenge.

The results of EPR studies for diradical dianions (Section 4) also suggest that for partially oxidized polyanions, corresponding to polyarylmethyls with large number of sites, the spin density may be localized at the terminal sites. Thus, a weak antiferromagnetic coupling through the negatively charged, "central" site would effectively provide another type of exchange defect.

MACROCYCLIC OCTARADICAL AND ANNELATED MACROCYCLIC TETRADECARADICAL

The concept of defects was initially tested using Class I macrocycle, such as calix[4]arene octaradical **43** (Fig. 26).[77,98] The EPR spectrum of 8×10^{-4} M **43** in 2-MeTHF/THF matrix consists a center peak with a symmetrical set of shoulder peaks.[77] The numerically computed and experimental values for the resonance fields of the shoulders agreed well with an $S = 4$ state, as expected for eight ferromagnetically coupled unpaired electrons. An odd-integral S state (e.g., $S = 7/2$ such as expected for **43** with one chemical defect) was tentatively assigned to the center peak. Most importantly, the SQUID magnetization data for $\sim 10^{-3}$ M **43** in THF at low temperature gave $S = 3.8$, indicating the $S = 4$ ground state for the defect-free octaradical. Most importantly, relatively low polydispersity was found for S in this case, suggesting that interruptions of exchange coupling by defects were not significant.

Octaradical **43** was an important proof of principle (Fig. 25) but its average value of $S \approx 4$ was still modest. Prerequisite for larger values of S is greater number of radical sites. For a constant yield for generation of each radical site, probability for polyradicals with two or more chemical defects, which may not be bypassed in a simple macrocycle, does increase. A parameter Q, which was defined as the percentage of those polyradicals with all unpaired electrons ferromagnetically coupled,
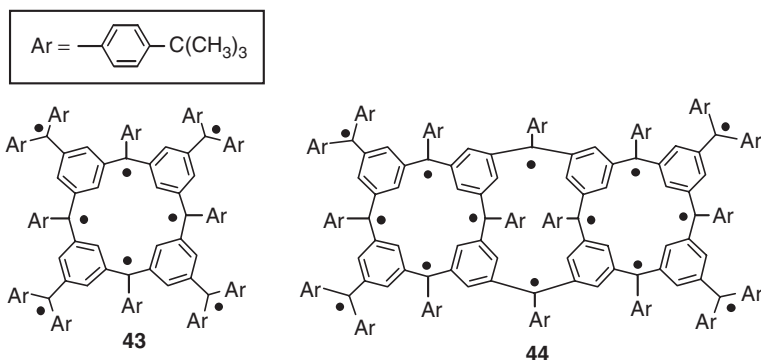
Fig. 26   Octaradical **43** and tetradecaradical **44**.

was introduced to evaluate the optimum connectivities for bypassing chemical defects.[103,104] One such connectivity, with relatively slowly decreasing value of Q in a homologous series, is represented by annelated, double stranded tetradecaradical **44** (Fig. 26).[105] For **44**, the lowest member of the double stranded series, $Q > 98\%$ was estimated, assuming the 95% yield for generation of each radical.[104]

SQUID magnetic studies of **44** in THF-d_8/2-MeTHF matrix revealed a relatively high average value of $S \approx 6$, although still below the expected $S = 7$ for 14 ferromagnetically coupled unpaired electrons.[105] Most importantly, quenching studies showed the presence of at least one chemical defect, i.e., for a polyradical originally prepared in THF-d_8 (and then diluted with 2-MeTHF) approximately one deuterium was incorporated from the deuterated solvent. Furthermore, low-spin excited states were populated at low temperatures. This suggested relatively weak exchange coupling for this 1,3-phenylene-based polyradical, in particular compared to the parent tetraradical **36**.[105]

A tentative structure for **44**, incorporating one chemical defect and possessing exchange coupling of a symmetric spin trimer, was proposed.[105] It was speculated that the annelation of calix[4]arene-based macrocycles leads to substantial strain, especially in the center macrocycle.[105] Such strain could have two consequences: (1) increased basicity of the arylmethyl carbanion sites, which would facilitate deuterium abstraction from the deuterated solvent, and (2) increased out-of-plane twisting of the π-system, which would weaken the exchange coupling.[105]

7 Organic spin clusters

The interpretation of the magnetic data for **44**, in terms of selective weakening of ferromagnetic coupling through out-of-plane twisting in the center part of the polyradical, led to the concept of organic spin clusters.[94,106–113] This borne-in-failure concept was among the most important advances that allowed for attaining very high-spin polyradicals, and ultimately magnetic ordering in a polymer-based polyradical.[7,8]

In this approach, a weak fCU was introduced by design. Thus, those spins 1/2, which were coupled through strong fCUs, could be effectively combined into larger component spins. Then, the component spins were coupled through weak fCUs (Fig. 27).

One of the key aspects of the design was to distribute weak fCUs in such way that a symmetrical spin cluster was obtained. Eigenvalues for Heisenberg Hamiltonian for such cluster could be readily solved, allowing for computation of both temperature and field dependence of magnetization for direct fitting of the experimental data.[94,107] Therefore, additional structure–property correlation could be obtained.

The practical implementation of organic spin clusters was through the synthesis of polyradicals, in which relatively weak and relatively strong fCUs were based upon 3,4′-biphenylene and 1,3-phenylene connectivities. Based upon the spin densities in conformationally unconstrained systems, factor of 6 was predicted for the relative strength of exchange coupling in 3,4′-biphenylene and 1,3-phenylene.[3,107,108]
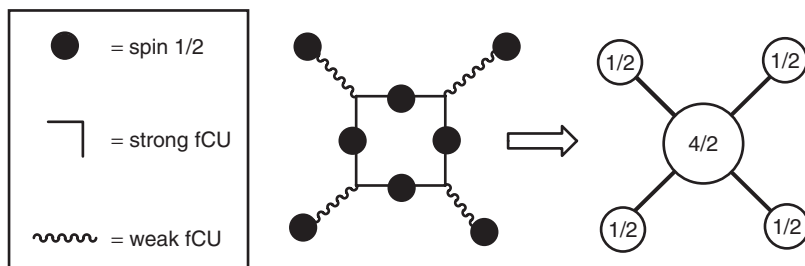
Fig. 27   Design of high-spin organic spin cluster.

Also, relative persistence of 3,4′-biphenylene diradical **21** suggested improved persistence for the corresponding organic spin clusters. The clusters were designed to possess the least possible number of the triarylmethyl sites where a single chemical defect could interrupt exchange coupling; in addition, all of those sites had at least one ''stabilizing'' biphenyl substitutent.

Three types of organic spin clusters were developed: dendritic–macrocyclic polyradicals, macrocyclic–macrocyclic polyradicals, and annelated macrocyclic polyradicals. These clusters may be viewed as model compounds for three essential aspects needed for an organic polymer with magnetic ordering: magnetic anisotropy, effective ferromagnetic correlation of $> 10^4$ electron spins, and dimensionality beyond two for pairwise exchange coupling between electron spins.

DENDRITIC–MACROCYCLIC POLYRADICALS

Dendritic–macrocyclic polyradicals were initially designed to test the concept of organic spin clusters.[94,107,108] One of the very important outcomes was the estimate of magnetic shape anisotropy and its scaling with the value of S, providing a stepping stone to an organic polymer with magnetic ordering.[94]

Dendritic–macrocyclic polyradicals consist of small dendritic branches which may be connected to calix[4]arene macrocyclic cores via 3,4′-biphenylene linkers. Polyradicals **45–50** correspond spin dimers, trimers, and pentamers, as illustrated in Fig. 28. Their connectivity is consistent with ferromagnetic coupling scheme.

The results of SQUID magnetic measurements for **45–50** were summarized in Fig. 28. The average values of S for **45–50** are slightly below the theoretical values for defect-free polyradicals with ferromagnetic coupling scheme.

All clusters showed ferromagnetic coupling ($J/k > 0$) through the 3,4′-biphenylene fCUs. The experimental values of $J/k \approx 90$ K for the simplest clusters, such as **45** and **46**, were direct measures of the pairwise coupling through 3,4′-biphenylene fCUs.[107,108] In the remaining clusters, such pairwise $J/k \approx 90$ K had to be scaled by a fraction of the spin density of the spin participating directly in the pairwise coupling, and then compared with the experimental values of J/k. Such scaling may be illustrated for pentamer **49**, in which each pairwise coupling involved the $S = 1/2$
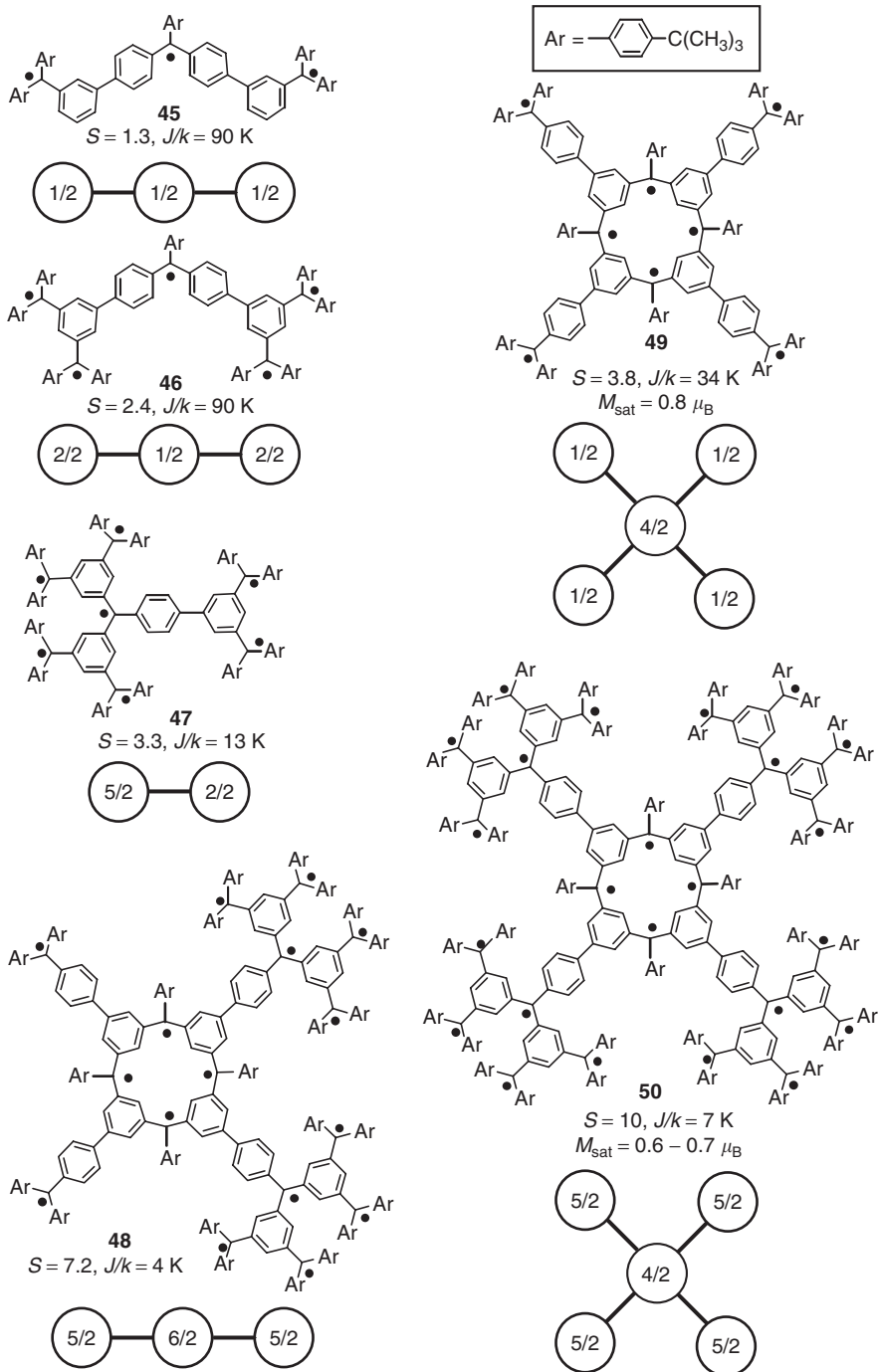
Fig. 28 Dendritic–macrocyclic organic spin clusters.

and $S = 2$; however, only two out of four sites in $S = 2$ participate in pairwise coupling through 3,4′-biphenylene fCU. Therefore, J/k should be scaled by a factor of $2/4 = 0.5$.[107,108] Analogous scaling was proposed previously by Dougherty.[114] Applicability of the spin density scaling is based on several interdependent factors, such as spin density distributions, molecular conformations, and the large ratio between the J/k through 1,3-phenylene versus 3,4′-biphenylene.[108] In particular, for the estimated factor of 6 for J/k through 1,3-phenylene versus 3,4′-biphenylene, the scaling factors were still accurate, based upon the analysis of Heisenberg Hamiltonians for selected clusters.[108]

For pentamers **49** and **50**, quantitative magnetic data, based upon the mass of the polyether precursor, were obtained (Fig. 28).[94] Magnetization at saturation (M_{sat}), expressed in Bohr magnetons (μ_B) per triarylmethyl site, gave the average fraction of unpaired electrons (spin concentration) in the limit of very low temperature and high-magnetic field. The value of M_{sat} was affected by the mass transfers during the preparation of polyradical. Also, intramolecular antiferromagnetic coupling, leading to spin cancellation may lower the value of M_{sat}.

It is important to point out that the values of S and M_{sat} in Fig. 28 correspond to (spin) weighed averages and number averages, respectively.[94] For example, this explained the result that average $S = 10$ was obtained for polyradical **50** with an average number of unpaired electrons in the 14–17 range. It was proposed that coupling defects had a major role in suppressing the values of S and M_{sat} (Fig. 29). The alternative explanation using chemical defects would require a rather unusual situation to occur, i.e., large density of defects and their very selective distribution at the periphery of the polyradical (Fig. 29).[94]

The feasibility of coupling defects was studied with Monte Carlo conformational searches (MM3* force field, with parametrization for arylmethyl radicals) for **50** in the gas phase. The representative low-energy conformation (Fig. 30) had
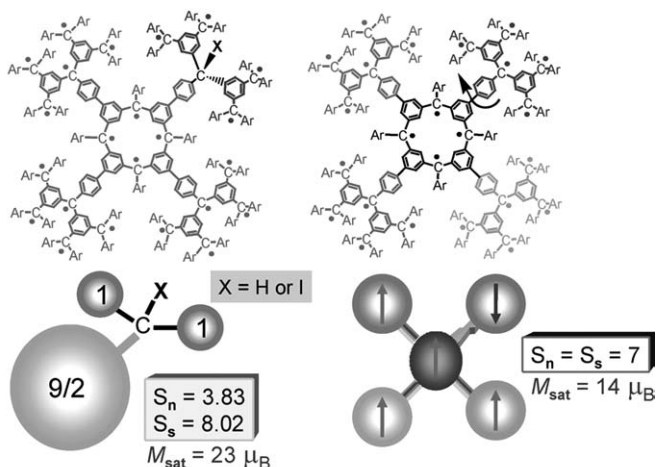
Fig. 29 Chemical (left structure) and exchange (right structure) defects in polyradical **50**.
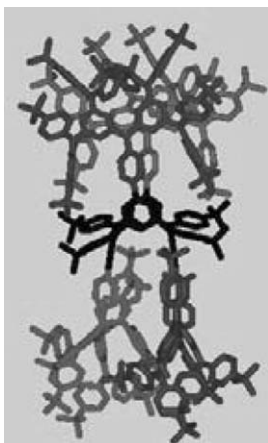
Fig. 30 Low-energy conformation for polyradical **50**.[94] Reproduced with permission from Ref. 94. Copyright 2004 *Am. Chem. Soc.*

approximately 1,3-alternate conformation of the macrocyclic core. Overall, the torsional angles were compatible with ferromagnetic coupling throughout the polyradical. However, the conformations, in which one of the biphenylene moieties possessed a near 90 out-of-plane twisting, were only a few kcal/mol higher in energy.[94]

Small-angle neutron scattering (SANS) studies of polyradical **50** in THF-d$_8$ at 170 K (slightly above melting point of the solvent) revealed the molecular structure (Fig. 31), which was analogous to that obtained from conformational searches.[94] Since SANS is a relatively low-resolution technique and the information content of the data is rather low, the structure of **50** might be best described as dumbbell-like with overall dimensions of $2 \times 3 \times 4$ nm. Also, this result confirms that polyradical **50** existed as a monomer in solution at low temperatures.

Magnetic shape anisotropy was estimated for polyradical **50** using the shape of a prolate ellipsoid. The barrier for inversion of magnetization, $E_A/k \approx 60$ mK, should be viewed as an upper for **50**.[94] This implies that polyradical **50** is still paramagnet at the readily accessible temperatures above 1.8 K, as found experimentally. However, for homologous prolate ellipsoids with $a/b = 2$ (and same spin density), $E_A/k \approx 5S$ mK. This implies that for S of the order of several thousands, E_A/k will be in tens of kelvins, leading to blocking of magnetization at the readily accessible temperatures near 10 K.

MACROCYCLIC–MACROCYCLIC POLYRADICALS

Macrocyclic–macrocyclic polyradicals were designed to attain the scaling of S with the number of radical sites, thus allowing for attaining very large values of S in
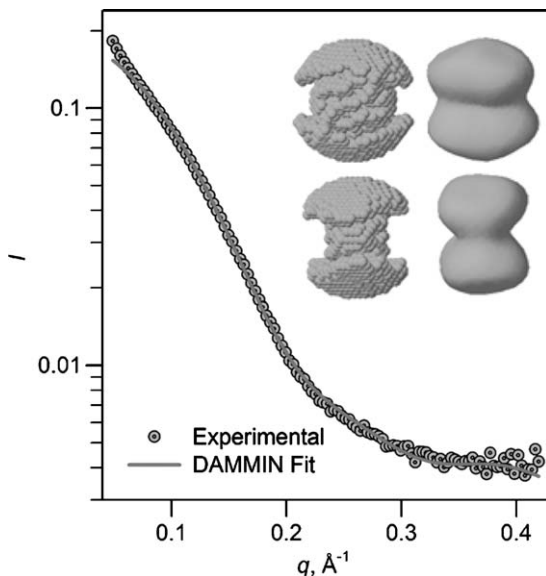
Fig. 31 Main plot: SANS intensity (I) versus momentum transfer ($q = 0.049–0.419 \,\text{Å}^{-1}$) for 9×10^{-4} M polyradical **50** in THF-d_8 at 170 K. The symbols and solid line correspond to the experimental data points and the numerical fit using GNOM/DAMMIN simulated annealing, respectively. Inset: low-resolution particle shape reconstruction for **50** obtained from the GNOM/DAMMIN fit. Two side views (rotated by 90°), using both the DAMMIN spheres and the spherical harmonics-based envelopes, are shown.[94] Reproduced with permission from Ref. 94. Copyright 2004 *Am. Chem. Soc.*

macromolecules.[112] Net ferromagnetic correlation of thousands of unpaired electrons is another stepping stone to an organic polymer with magnetic ordering.

Macrocyclic–macrocyclic polyradicals consist of macrocyclic branches connected to macrocyclic cores via bis(3,4′-biphenylene)methyl linkers (Figs 32 and 33). The connection of calix[4]arene-based macrocycles via bis(3,4′-biphenylene)methyl linkers provided special type of organic spin clusters, in which large component spins of the macrocycles were exchange coupled via much smaller spins 1/2 of the linkers, as illustrated in Figs 32 and 33 for polyradicals **51–53**.[8,112]

Organic spin clusters of unequal spin **51–53** were designed to alleviate the problem of coupling defects.[8] Since the macrocycles were conformationally constrained, the most likely coupling defects would involve out-of-plane twistings of the biphenylene fCUs. This was an analogous situation, as encountered in dendritic–macrocyclic polyradicals, with one important exception, i.e., the reversal of the exchange coupling from ferromagnetic to antiferromagnetic for unequal spins should lead to partial cancellation of the spins. This is illustrated for polyradical **51**, i.e., spin trimer 7/2–1/2–7/2, using the two-parameter percolation model (Fig. 34). The first parameter (q) allowed for the random distribution of ferromagnetic and antiferromagnetic couplings through biphenylene coupling units. The second parameter (p) allowed for the presence of chemical defects.[112]
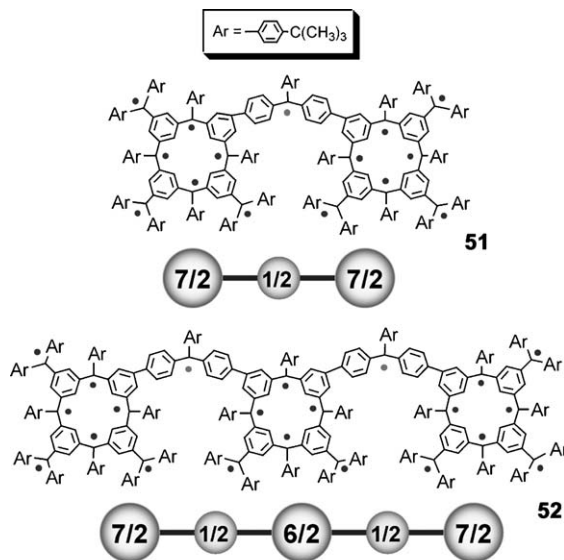
Fig. 32 Macrocyclic–macrocyclic organic spin clusters of unequal spins **51** and **52**.[112]

All spin systems were enumerated, as illustrated in Fig. 34 for polyradical **51**. Plots of the weighed average S and number average M_{sat} as functions of q and p for polyradicals **51** and **52** are shown in Fig. 35.[112] Most importantly, for any random distribution of coupling defects and limited density of chemical defects, the values of average S should scale with the molecular weight (or number of radical sites) of polyradical.[112]

The percolation model provided excellent quantitative fits to the magnetic data at low temperatures.[112] The weighed average values of S were 5–6, 7–9, and 11–13 for polyradicals **51**, **52**, and **53**, respectively. The value of $S \approx 13$ for **53** is the highest among organic molecules. Most importantly, the values of S scale with the number of radical sites (or molecular weights) in a polyradical.[112] This may allow for synthesis of polymers with very large values of S.

Although connectivities of polyradicals **51**, **52**, and **53** were consistent with ferromagnetic coupling scheme, the distribution of pairwise ferromagnetic and antiferromagnetic couplings between unequal spin modules may be viewed as ferromagnetic–ferrimagnetic coupling scheme (Fig. 8).[8]

ANNELATED MACROCYCLIC POLYRADICALS

Annelated macrocyclic polyradicals were designed to test the feasibility of highly cross-linked polymers, which possess significant content of structures with fractal dimensionality beyond one, and even beyond two.[113] Such fractal dimensionality beyond two for pairwise exchange coupling between the electron spins is a prerequisite for long-range magnetic ordering in an organic polymer.
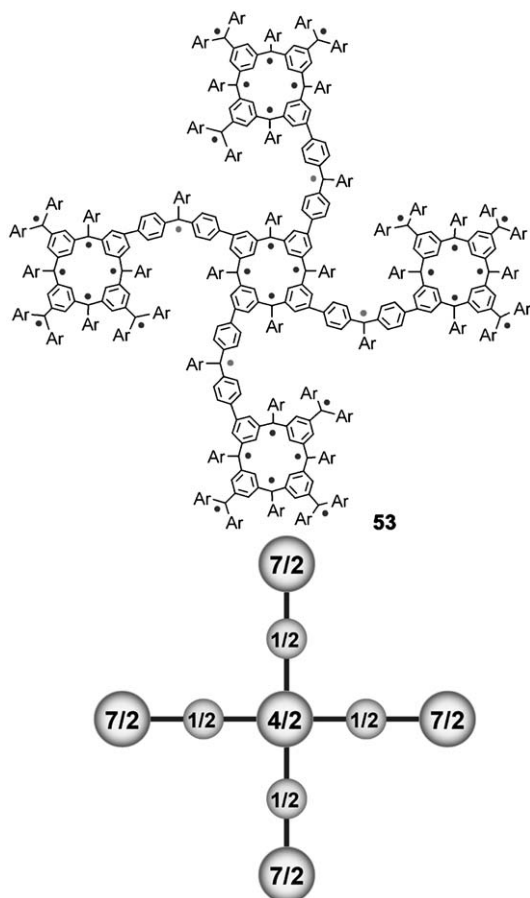
Fig. 33 Macrocyclic–macrocyclic organic spin cluster of unequal spin **53**.[112]

Annelated macrocyclic polyradicals consist of calix[4]arene-based macrocycles annelated via bis(3,4′-biphenylene)methyl linkers. This connectivity is consistent with the ferromagnetic–ferrimagnetic coupling scheme, for which scaling of S with the number of radical sites (or molecular weights) was attained.[8,112]

SQUID magnetic studies indicate average values of $S \approx 6$–7 and $S \approx 10$ for **54** and **55**, respectively (Fig. 36). Values of $M_{sat} \approx 0.6$ μ_B indicate that about 60% of unpaired electrons in the limit of very low temperature and high field for both polyradicals.[113]

The next higher homolog of 28-radical **55**, 42-radical **56**, in which six calix[4]arene rings were annelated to the center macrocycle, was prepared and studied. However, the SQUID magnetic studies gave relatively low average values of $S \approx 9$–12 and $M_{sat} \approx 0.3$ μ_B;[115] one of the possible reasons was insufficient purity of the 42-ether precursor of **56**.
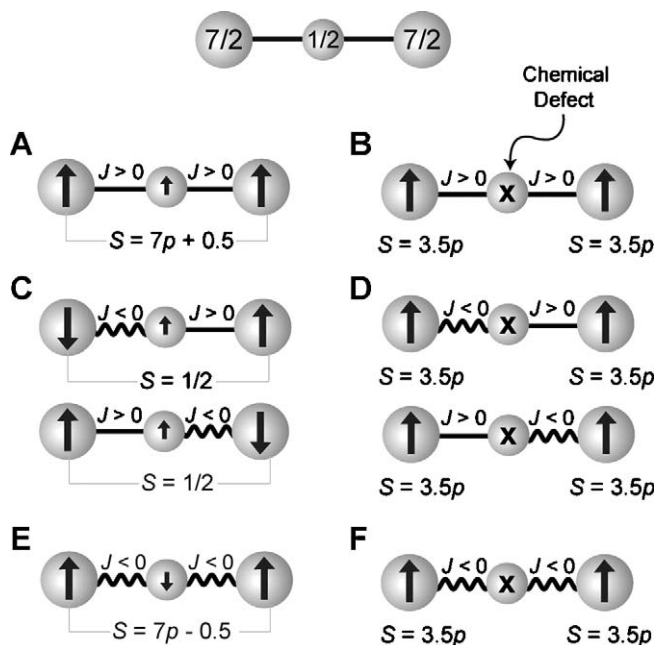
Fig. 34 Organic trimer of component spins, 7/2–1/2–7/2, corresponding to pentadecaradical **51**. (A)–(F) correspond to spin systems for the configurations with 0–2 antiferromagnetic couplings through the biphenylene coupling units and 0–1 chemical defects at the 4-biphenyl-substituted sites.

Notably, the Negishi cross-coupling of difunctionalized macrocyclic monomers produced the annelated polyether precursors to polyradicals **54**, **55**, and **56** in significant isolated yield for each polyether (Fig. 37). This suggested that analogous cross-couplings of multi-functionalized macrocyclic monomers could provide highly cross-linked polymers with fractal dimensionalities beyond one.

8 Very high-spin polyarylmethyl polymers

High-spin polymers **57** and **58** consist of calix[4]arene-based macrocycles either linked or annelated via bis(3,4′-biphenylene)methyl linkers. Their design, including ferromagnetic–ferrimagnetic coupling scheme with unequal spin modules, was derived from macrocyclic–macrocyclic polyradicals and annelated macrocyclic polyradicals (Fig. 38).

Polyether precursors to polymers **57** and **58** were prepared via Negishi cross-coupling between di- and tetra-functionalized macrocyclic monomers, respectively.[7,113,116] For **58**, one of the two limiting modes of cross-linking during the polymerization via Negishi cross-coupling involved formation of macrocycles
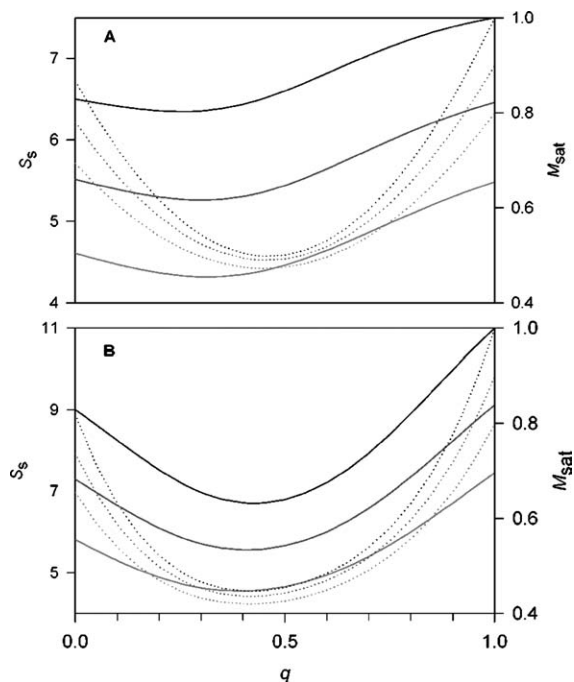
Fig. 35 Plots of weighed average spin (S_s, full lines) and magnetization at saturation (M_{sat}, dotted lines) for percolation model for pentadecaradical **51** (plot A) and 22-radical **52** (plot B). The black, red, and green lines correspond to parameter p set to 1.0, 0.9, and 0.8, respectively.[112] Reproduced with permission from Ref. 112. Copyright 2004 *Am. Chem. Soc.*

corresponding to polyethers, which were precursors to polyradicals **54**, **55**, **56**, and possibly their higher homologs. The important point is that the larger-sized macrocycles would correspond to higher dimensionality of the formed polymer network (Fig. 39).[113] As significant yields for the polyether precursors to polyradicals **54**, **55**, and **56** were obtained (Fig. 37), this suggested that polymer **58** was likely to possess significant content of annelated macrocyclic structures with dimensionality beyond one.[113]

In polymer **57**, the $S = 3$ component spins of the calix[4]arene macrocycles were exchange coupled with the $S = 1/2$ spins of the bis(3,4′-biphenylene)methyl linkers, forming "quasi-linear" chain of unequal spins of $S = 3$ and $S = 1/2$. Similarly, polymer **58** consists of exchange-coupled network of unequal spins, i.e., the $S = 2$ component spins of the calix[4]arene macrocycles and the $S = 1/2$ spins of the bis(3,4′-biphenylene)methyl linkers (Fig. 38).[8,113]

SQUID magnetic studies of **57** in THF-d$_8$ matrix revealed a relatively high average value of $S \approx 18$. Values of $M_{sat} \approx 0.4$–0.6 μ_B indicate 40–60% of unpaired electrons in the limit of very low temperature and high field for both polyradicals, which is consistent with the ferromagnetic–ferrimagnetic coupling scheme.[8,113] These results may be compared with the value of $S \approx 40$–50 expected for defect-free
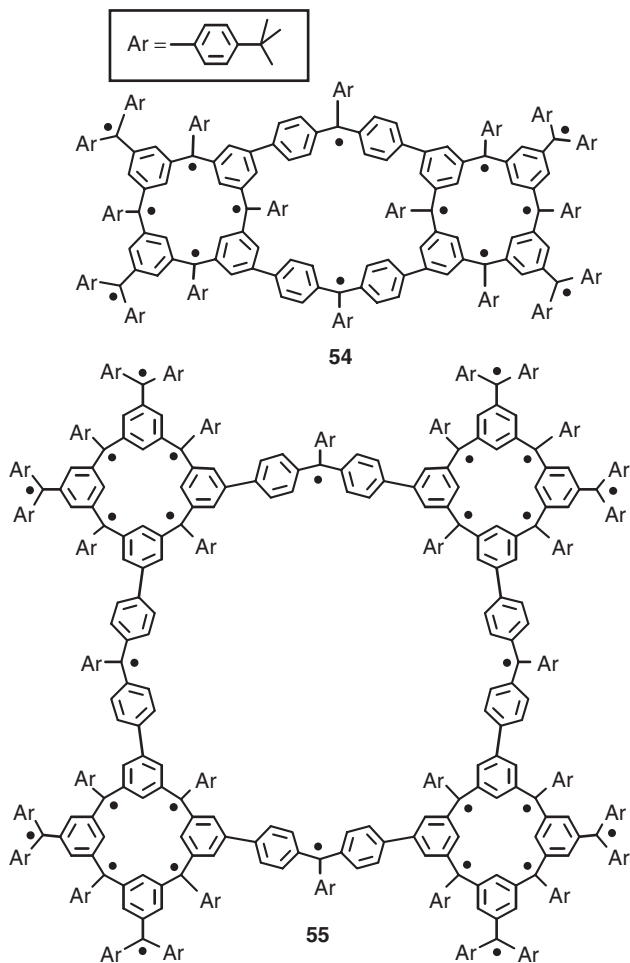
Fig. 36 Annelated macrocyclic polyradicals **54** and **55**.

polymer with the ferromagnetic coupling scheme and obtained from polyether precursor with weight average molecular weight, $M_w \approx 26$ kDa (Fig. 37). The value of $S \approx 18$ exceeds by far the highest values of $S \approx 5$, reported for other high-spin organic polymers.[23–26]

The results of SQUID magnetic measurements (and EPR spectroscopy) for polymer **58** were dependent upon the degree of polymerization and cross-linking for the polyether precursor.

For polymer **58**, prepared from THF-soluble polyether precursors with $M_w \approx 60$–70 kDa and $M_w \approx 300$–500 kDa, average values of $S \approx 8$–18 and $S > 40$ were obtained, respectively.[116] The THF-insoluble polyether precursor, of which polymerization was stopped near the gel point, gave average values of $S \approx 600$–1500; for longer polymerization time, average values of $S \approx 3000$–7000 were obtained.[7]
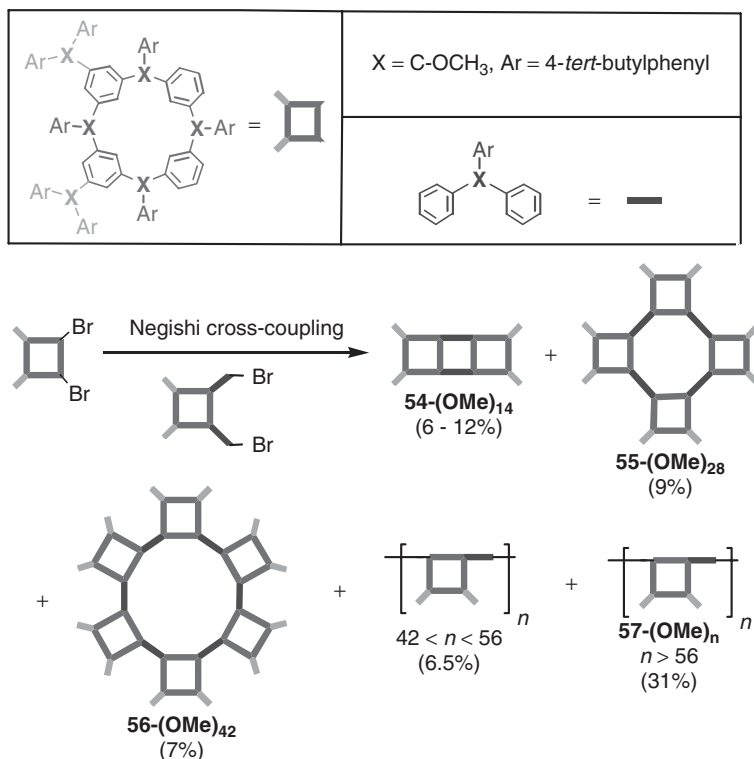
Fig. 37   Synthesis polyethers **54-(OMe)₁₄**, **55-(OMe)₂₈**, and **56-(OMe)₄₂**, precursors to po-
lyradicals **54**, **55**, and **56**, respectively. Polyether **57-(OMe)ₙ** ($n > 56$) is a precursor to high-spin
polymer **57**.

Values of $M_{sat} \approx 0.5 \ \mu_B$, indicating presence of approximately 50% of unpaired
electrons at low temperature, did not show any systematic dependence on degree of
polymerization of polyether. Overall, this results were consistent with the
ferromagnetic–ferrimagnetic coupling scheme and presence of chemical defects.[8]

   EPR spectra of **58** at 140–150 K were obtained on the identical samples, for which
SQUID magnetic studies were carried out. A single resonance at $g \approx 2$ in the $\Delta m_s = 1$ region was observed. For samples with the increasing values of S, the width of the
resonance decreased and its propensity to microwave saturation greatly increased.
These changes were mirrored by decreased intensity of the $\Delta m_s = 2$ signal.[117]

   Most interestingly, polymer **58** with very large values of S showed the onset of
magnetic ordering at temperature of approximately 10 K.[7] This is the first example
of a conjugated organic polymer with magnetic properties beyond simple paramag-
netism.[7] For a typical sample of **58** with an average value of $S \approx 5000$, a sharp
upturn in magnetic moment (an increase by two orders of magnitude) was ob-
served.[7,8] Below 10 K, magnetization increases very rapidly with applied fields,
reaching near saturation at relatively low fields. The observed values of $M_{sat} \approx 0.5$
μ_B correspond to about 10 emu g⁻¹. At zero or very low applied magnetic fields of the

$Ar = \langle\!\!\!\langle\!\!\!\rangle\!\!\!\rangle - C(CH_3)_3$

57

ferro
$S = 3.5n$

ferri
$S = 2.5n$

58
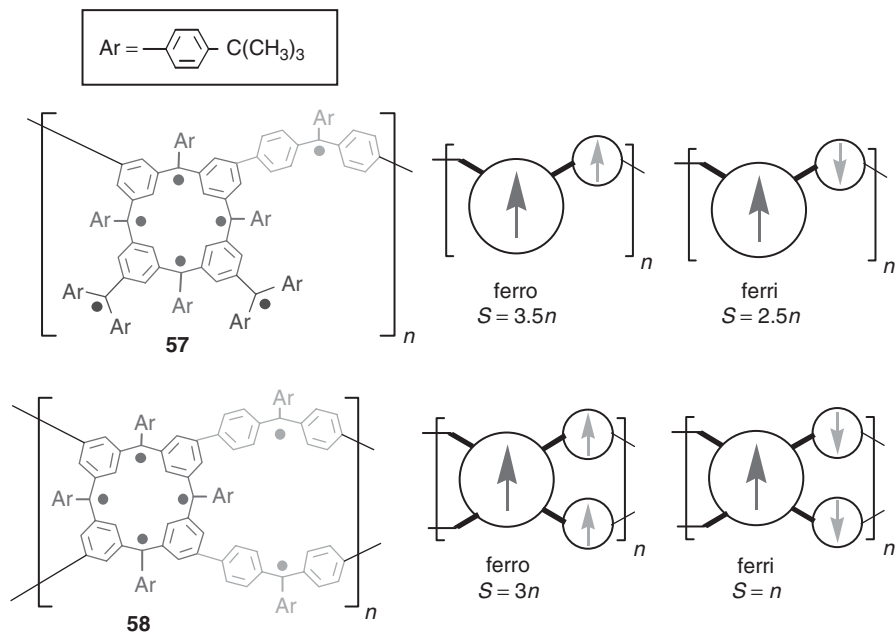
ferro
$S = 3n$

ferri
$S = n$

Fig. 38 Polymers **57** and **58** with the ferromagnetic–ferrimagnetic coupling scheme with the macrocyclic ($S = 3$ and $S = 2$) and cross-linking ($S = 1/2$) modules.

Dimensionality
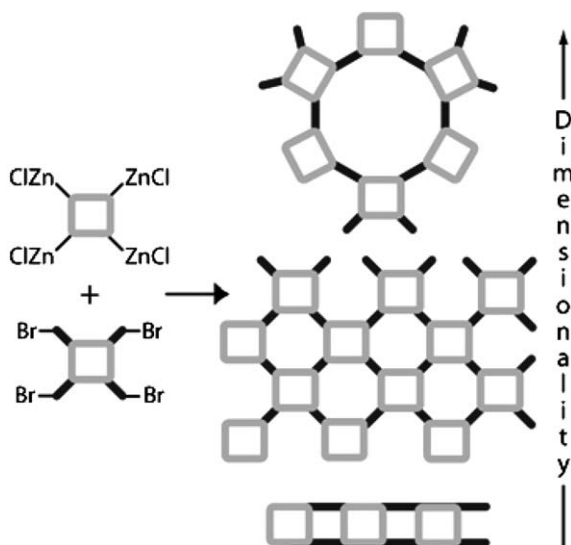
Fig. 39 One of the possible annelation modes in polymer **58**.[113]

order of earth's field (0.5–1.0 Oe), magnetization blocking was found. AC suscepti-bility studies suggested that the magnetic anisotropy barrier for inversion of magnetization was of the order of 15 K and the large magnetic moments (corres-ponding to a value of $S \approx 5000$) were frozen at low temperatures with some degree of cooperativity. When the upper bound for the shape anisotropy barrier $E_A/k \approx 60$ mK in polyradical **50** ($E_A/k \approx 60$ mK) is extrapolated to a polyradical with $S \approx 5000$, the upper bound of $E_A/k \approx 5S$ mK ≈ 25 K is obtained.[94] This suggests that one of the key contributors to the magnetic anisotropy barrier in polymer **58** might be shape anisotropy. The magnetic behavior of polymer **58** can be classified as being between insulating spin glasses and blocked superparamagnets, but closer to spin glasses.[7]

9   Conclusion and outlook

Implementation of a multi-step rational design for polyarylmethyl polyradicals res-ulted in the first conjugated polymer with magnetic ordering. This achievement should be viewed as a proof of principle, providing novel approach to magnetic materials with very low anisotropy. In order to attain practical materials, the further research should aim at attaining both stability of polyradicals at ambient conditions and magnetic ordering at room temperature.

Gomberg's statement, "This work will be continued and I wish to reserve the field for myself," with which he concluded one of his original articles on triphenyl-methyl,[27] may be paraphrased as follows. Indeed, this work was successfully con-tinued; polyarylmethyls reserved for themselves the field of high-spin polyradicals, but predictably, for not too long.

Acknowledgements

References

1. Iwamura, H. (1990). High-spin organic molecules and spin alignement in organic mo-lecular assemblies. *Adv. Phys. Org. Chem.* **26**, 179–253
2. Dougherty, D.A. (1991). Spin control in organic molecules. *Acc. Chem. Res.* **24**, 88–94
3. Rajca, A. (1994). Organic diradicals and polyradicals: from spin coupling to magnetism? *Chem. Rev.* **94**, 871–893
4. Lahti, P.M. (ed.) (1999). *Magnetic Properties of Organic Materials*, pp. 1–713. Marcel Dekker, New York

5. Crayston, J.A., Devine, J.N. and Walton, J.C. (2000). Conceptual and synthetic strategies for the preparation of organic magnets. *Tetrahedron* **56**, 7829–7857

6. Itoh, K. and Kinoshita, M. (eds) (2000). *Molecular Magnetism*, pp. 1–337. Gordon and Breach, Kodansha

7. Rajca, A., Wongsriratanakul, J. and Rajca, S. (2001). Magnetic ordering in an organic polymer. *Science* **294**, 1503–1505

8. Rajca, A. (2002). From high-spin organic molecules to polymers with magnetic ordering. *Chem. Eur. J.* **8**, 4834–4841

9. Rajca, A. (2004). Organic polyradical magnetic nanoclusters, In *Encyclopedia of Nanoscience and Nanotechnology*, Nalwa, H.S. (ed.), vol. 8, pp. 285–294. American Scientific Publishers, Stevenson Ranch, CA

10. Lis, T. (1980). *Acta Crystallogr. Sect. B* **B36**, 2042–2046

11. Sessoli, R., Gatteshi, D., Caneshi, A. and Novak, M.A. (1993). Magnetic bistability in a metal–ion cluster. *Nature* **365**, 141–143

12. Friedman, J.R., Sarachik, M.P., Tejada, J. and Ziolo, R. (1996). Macroscopic measurement of resonant magnetization tunneling in high-spin molecules. *Phys. Rev. Lett.* **76**, 3830–3833

13. Wernsdorfer, W., Allaga-Alcalde, N., Hendrickson, D.N. and Christou, G. (2002). *Nature* **416**, 406

14. Murugesu, M., Habrych, M., Wernsdorfer, W., Abboud, K.A. and Christou, G. (2004). Single-molecule magnets: a Mn_{25} complex with a record $S = 51/2$ spin for an isolated molecule. *J. Am. Chem. Soc.* **126**, 4766–4767

15. Caravan, P., Ellison, J.J., McMurry, T.J. and Lauffer, R.B. (1999). Gadolinium(III) chelates as MRI contrast agents: structure, dynamics, and applications. *Chem. Rev.* **99**, 2293–2352

16. Pierre, V.C., Botta, M. and Raymond, K.N. (2005). Dendrimeric gadolinium chelate with fast water exchange and high relaxivity at high magnetic field strength. *J. Am. Chem. Soc.* **127**, 504–505

17. Winalski, C.S., Shortkroff, S., Mulkern, R.V., Schneider, E. and Rosen, G.M. (2002). Magnetic resonance relaxivity of dendrimer-linked nitroxides. *Magn. Reson. Med.* **48**, 965–972

18. Iwamura, H., Inoue, K. and Kaga, N. (1998). Tacticity versus dimension of the extended structures in the crystals of heterospin magnets made of transition-metal complexes with the poly(aminoxyl) radical. *New J. Chem.* 201–210

19. Caneshi, A., Gatteschi, D. and Rey, P. (1991). The chemistry and magnetic properties of metal nitronyl nitroxide complexes. *Progr. Inorg. Chem.* **39**, 331–429

20. Manriquez, J.M., Yee, G.T., McLean, R.S., Epstein, A.J. and Miller, J.S. (1991). A room-temperature molecular/organic-based magnet. *Science* **252**, 1415–1417

21. Nakamura, N., Inoue, K. and Iwamura, H. (1993). A branched-chain nonacarbene with a nonadecet ground state: a step nearer to superparamagnetic polycarbenes. *Angew. Chem. Int. Ed.* **32**, 872–874

22. Iwamura, H. and Koga, N. (1993). Studies of organic di-, oligo-, and polyradicals by means of their bulk magnetic properties. *Acc. Chem. Res.* **26**, 346–351

23. Michinobu, T., Inui, J. and Nishide, H. (2003). *m*-phenylene-linked aromatic poly(aminium cationic radical)s: persistent high-spin organic polyradicals. *Org. Lett.* **5**, 2165–2168

24. Nishide, H., Ozawa, T., Miyasaka, M. and Tsuchida, E. (2001). Nanometer-sized high-spin polyradical: poly(4-phenoxyl-1,2-phenylenevinylene) planarily extended in a non-kekule fashion and its magnetic force microscopic images. *J. Am. Chem. Soc.* **123**, 5942–5946

25. Bushby, R.J. and Gooding, D. (1998). Higher-spin pi multiradical sites in doped polyarylamine polymers. *J. Chem. Soc. Perkin* **2**, 1069–1075

26. Anderson, K.K. and Dougherty, D.A. (1998). An improved model for one-dimensional polaronic ferromagnetism: electrochemically doped poly(*m*-phenylenefuchsone). *Adv. Mater.* **10**, 688–692

27. Gomberg, M. (1900). An instance of trivalent carbon: triphenylmethyl. *J. Am. Chem. Soc.* **22**, 757–771

28. Gomberg, M. (1900). *Ber. Dtsch. Chem. Ges.* **33**, 3150

29. McBride, J.M. (1974). The hexaphenylene riddle. *Tetrahedron* **30**, 2009–2022

30. Eberson, L. (2001). Gomberg and the nobel price. *Adv. Phys. Org. Chem.* **36**, 59–84

31. Extent of dissociation of triphenylmethyl, $K \approx 3 \times 10^{-4} \, M^{-1}$ at 293 K: Colle, K.S., Glaspie, P.S. and Lewis, E.S. (1975). Equilibrium dissociation of triphenylmethyl dimer. *Chem. Comm.* 266–267

32. Lankamp, H., Nauta, W.T. and MacLean, C. (1968). New interpretation of the monomer–dimer equilibrium of triphenylmethyl- and alkylsubstituted-diphenyl methyl-radicals in solution. *Tetrahedron Lett.* 249–254

33. Tris(4-*tert*-butylphenyl)methyl: Duennebacke, D., Neumann, W.P., Penenory, A. and Ulrich, S. (1989). Stabile 4,4',4''trisubstituierte triphenylmethyl-radicale. *Chem. Ber* **122**, 533–535

34. Utamapanya, S. and Rajca, A. (1991). Topological control of electron localization in π-conjugated polyarylmethyl carbopolyanions and radical anions. *J. Am. Chem. Soc.* **113**, 9242–9251

35. Ballester, M. (1985). *Acc. Chem. Res.* **18**, 380–387

36. $[(CF_3)_2CF]_3C$ radical: (a) Scherer Jr., K.V., Ono, T., Yamanouchi, K., Fernandez, R., Henderson, P. and Goldwhite, H. (1985). *J. Am. Chem. Soc.* **107**, 718–719; (b) Lemal, D.M. (2004). *J. Org. Chem.* **69**, 1–11

37. Koelsch radical: Koelsch, C.F. (1957). Syntheses with triarylvinylmagnesium bromides. α,γ-bisdiphenylene-β-phenylallyl, a stable free radical. *J. Am. Chem. Soc.* **79**, 4439–4441

38. Kinoshita, M. (1997). In *Handbook of Organic Conductive Molecules and Polymers*, Nalva, H.S. (ed.), vol. 1, Chapter 15, pp. 781–800. Wiley, New York

39. Allemand, P.-M., Khemani, K.C., Koch, A., Wudl, F., Holczer, K., Donovan, S., Gruner, G. and Thompson, J.D. (1991). *Science* **253**, 301–303

40. Narymbetov, B., Omerzu, A., Kabanov, V.V., Tokumoto, M., Kobayashi, H. and Mihailovic, D. (2000). *Nature* **407**, 883–885

41. Buchanenko, A.L. (1990). *Russ. Chem. Rev.* **59**, 307–319

42. Hosokoshi, Y., Katoh, K., Nakazawa, Y., Nakano, H. and Inoue, K. (2001). *J. Am. Chem. Soc.* **123**, 7921–7922

43. Shiomi, D., Kanaya, T., Sato, K., Mito, M., Takeda, K. and Takui, T. (2001). *J. Am. Chem. Soc.* **123**, 11823–11824

44. Mataga, N. (1968). Possible ferromagnetic states of some hypothetical hydrocarbons. *Theor. Chim. Acta.* **10**, 372–376

45. Aharoni, A. (2000). *Introduction to the Theory of Ferromagnetism* (2nd edn). Oxford University Press, Oxford

46. Havlas, Z. and Michl, J. (1999). *J. Chem. Soc. Perkin* **2**, 2299–2303

47. Rajca, A. and Utamapanya, S. (1993). Toward organic synthesis of a magnetic particle: dendrimeric polyradicals with 15 and 31 centers for unpaired electrons. *J. Am. Chem. Soc.* **115**, 10688–10694

48. Borden, W.T., Iwamura, H. and Berson, J.A. (1994). Violations of Hund's rule in non-kekule hydrocarbons: theoretical prediction and experimental verification. *Acc. Chem. Res.* **27**, 109–116

49. Belorizky, E. and Fries, P.H. (1993). Exact solutions for simple spin clusters with isotropic Heisenberg exchange interactions. *J. Chim. Phys.* (*Paris*) **90**, 1077–1100

50. Topological requirements for ferromagnetic coupling: Borden, W.T. and Davidson, E.R. (1977). Effects of electron repulsion in conjugated hydrocarbon diradicals. *J. Am. Chem. Soc.* **99**, 4587–4594

51. Dowd, P. (1966). *J. Am. Chem. Soc.* **88**, 2587–2589

52. TMM as triplet ground state with an estimated singlet–triplet energy gap of 13–16 kcal mol^{-1}: Wenthold, P.G., Hu, J., Squires, R.R. and Lineberger, W.C. (1996). Photoelectron spectroscopy of the trimethylenemethane negative ion. The singlet–triplet splitting of trimethylenemethane. *J. Am. Chem. Soc.* **118**, 475–476

53. TME as singlet ground state with a singlet–triplet energy gap of 2 kcal mol^{-1}: Clifford, E.P., Wenthold, P.G., Lineberger, W.C., Ellison, G.B., Wang, C.X., Grabowski, J.J., Vila, F. and Jordan, K.D. (1998). Properties of tetramethyleneethane (TME) as revealed by ion chemistry and ion photoelectron spectroscopy. *J. Chem. Soc. Perkin* **2**, 1015–1022

54. Ovchinnikov, A.A. (1978). Multiplicity of the ground state of large alternant organic molecules with conjugated bonds. *Theor. Chim. Acta.* **47**, 297–304

55. *m*-xylylene as triplet ground state with singlet–triplet energy gap of 9.6±0.2 kcal mol^{-1}: Wenthold, P.G., Kim, J.B. and Lineberger, W.C. (1997). Photoelectron spectroscopy of *m*-xylylene anion. *J. Am. Chem. Soc.* **119**, 1354–1359

56. McConnell, H.M. (1960). Theory of singlet–triplet splittings in large biradicals. *J. Chem. Phys.* **33**, 115–121

57. Dvolaitzky, M., Chiarelli, R. and Rassat, A. (1992). Stable N,N′-di-*tert*-butyl-*meta*-phenylene-bisnitroxides-unexpected ground state singlets. *Angew. Chem. Int. Ed.* **31**, 180–181

58. Effect of conformation on exchange coupling through 1,3-phenylene or TMM: (a) Berson, J.A. (1997). A new class of non-kekule molecules with tunable singlet–triplet energy spacings. *Acc. Chem. Res.* **30**, 238–244; (b) Shultz, D.A., Boal, A.K. and Farmer, G.T. (1997). The biradical, bis(3,5-di-*tert*-butyl-4-phenoxyl)methyleneadamantane, exhibits matrix-dependent EPR spectra suggesting rotamer bistability with differential exchange coupling. *J. Am. Chem. Soc.* **119**, 3846–3847; (c) Rajca, A., Lu, K., Rajca, S. and Ross, C.R. II (1999). Singlet–triplet bistability in a 1,3-phenylene-based bis(aminoxyl) diradical. *Chem. Commun.* 1249–1250; (d) "Karplus-Conroy-type" relationship for exchange coupling in trimethylene-based bis(semiquinone) diradicals was proposed: Shultz, D.A., Fico Jr., R.M., Bodnar, S.H., Kumar, K., Vostrikova, K.E., Kampf, J.W. and Boyle, P.D. (2003). *J. Am. Chem. Soc.* **125**, 11761–11771

59. Effect of hetereoatoms and substituents on exchange coupling through 1,3-phenylene: (a) West Jr., A.P., Silverman, S.K. and Dougherty, D.A. (1996). Do high-spin topology rules apply to charged polyradicals? Theoretical and experimental evaluation of pyridiniums as magnetic coupling units. *J. Am. Chem. Soc.* **118**, 1452–1463; (b) Shultz, D.A., Bodnar, S.H., Lee, H., Kampf, J.W., Incarvito, C.D. and Rheingold, A.L. (2003). Singlet–triplet gap in triplet ground-state biradicals is modulated by substituents effects. *J. Am. Chem. Soc.* **125**, 10054–10061

60. Rajca, A. (1990). A polyarylmethyl carbotetraanion. *J. Am. Chem. Soc.* **112**, 5889

61. Rajca, A. (1990). A polyarylmethyl quintet tetraradical. *J. Am. Chem. Soc.* **112**, 5890

62. Rajca, S. http://www.chem.unl.edu/rajca/Gomberg/rajcamagnet.html

63. Schlenk, W. and Brauns, M. (1915). Zur frage der metachinoide. *Chem. Ber.* **48**, 661–669

64. Schlenk, W. and Brauns, M. (1915). Uber einige bis-triarylmethyle. *Chem. Ber.* **48**, 716–728

65. (a) Stark, O. and Garben, O. (1913). Zur frage der metachinoide. *Chem. Ber.* **46**, 659–666; (b) Stark, O. and Garben, O. (1913). Zur Frage der metachinoide. II. *Chem. Ber.* **46**, 2252–2259

66. Stark, O., Garben, O. and Klebahn, L. (1913). Zur frage der metachinoide. III. *Chem. Ber.* **46**, 2542–2544

67. Stark, O. and Klebahn, L. (1914). Zur frage der metachinoide. IV. *Chem. Ber.* **47**, 125–130

68. Tidwell, T.T. (2001). Wilhelm Schlenk: the man behind the flask. *Angew. Chem. Int. Ed.* **40**, 331–337

69. Luckhurst, G.R. and Pedulli, G.F. (1971). Electron spin resonance of Schlenk's hydrocarbon. *J. Chem. Soc.* (*B*) 329–334

70. Schmidt, R. and Brauer, H.-D. (1971). The energetic positions of the lowest singlet and triplet state of the Schlenk and of the Müller hydrocarbon. *Angew. Chem. Int. Ed.* **10**, 506–507

71. Schmidt, R. and Brauer, H.-D. (1972). Uber das assoziationsverhalten des schlenkschen kohlenwasserstoffs. *Z. Naturforsch.* **B27**, 1363–1370

72. Kothe, G., Denkel, K.-H. and Sümmermann, W. (1970). Schlenk's biradical – a molecule in the triplet ground state. *Angew. Chem. Int. Ed.* **9**, 906–907

73. Rajca, A., Utamapanya, S. and Xu, J. (1991). Control of magnetic interactions in polyarylmethyl triplet diradicals using steric hindrance. *J. Am. Chem. Soc.* **113**, 9235–9241

74. Rajca, A. and Utamapanya, S. (1992). π-Conjugated systems with unique electronic structure: a case of "planarized" 1,3-connected polyarylmethyl carbodianion and stable triplet hydrocarbon diradical. *J. Org. Chem.* **57**, 1760–1767

75. Rajca, A., Utamapanya, S. and Smithhisler, D.J. (1993). Near-degeneracy between the low- and high-spin ground states in an alternant hydrocarbon diradical: topology and geometry. *J. Org. Chem.* **5**, 5650–5652

76. Rajca, A. (1994). High spin polyarylmethyl polyradicals. In *Advances in Dendritic Macromolecules*, Newkome, G.R. (ed.), vol. 1, pp. 133–168. JAI Press, Greenwich

77. Rajca, A., Rajca, S. and Desai, S.R. (1995). Macrocyclic π-conjugated carbopolyanions and polyradicals based upon calix[4]arene and calix[3]arene rings. *J. Am. Chem. Soc.* **117**, 806–816

78. Rajca, A. and Rajca, S. (1996). Intramolecular antiferromagnetic versus ferromagnetic spin coupling through biphenyl unit. *J. Am. Chem. Soc.* **118**, 8121–8126

79. Rajca, A. and Rajca, S. (1998). Alkyl-substituted Schlenk hydrocarbon diradicals with triplet and singlet ground states in frozen solutions. *J. Chem. Soc. Perkin* **2**, 1077–1082

80. Rajca, A., Rajca, S. and Wongsriratanakul, J. (2000). Singlet–triplet energy gap in a cyclophane-based diradical with parallel exchange coupling pathways. *Chem. Commun.* 1021–1022

81. (a) Diradical **20**: unpublished data from this laboratory. (b) Diradical **22**: Rajca, A., Shiraishi, K., Vale, M., Han, H. and Rajca, S. (2005). Stable Hydrocarbon Diradical, An Analogue of Trimethylenemethane. *J. Am. Chem. Soc.* **127**, 9014–9020

82. Perchlorinated Schlenk diradical: Veciana, J., Rovira, C., Crespo, M.I., Armet, O., Domingo, V.M. and Palacio, F. (1991). *J. Am. Chem. Soc.* **113**, 2552

83. Rajca, A., Rajca, S., Desai, S.R. and Day, V.W. (1997). Peroxides of sterically hindered derivatives of Schlenk hydrocarbon diradical. *J. Org. Chem.* **62**, 6524–6528

84. Yang, N.C. and Castro, A.J. (1960). *J. Am. Chem. Soc.* **82**, 6208

85. Leo triradical: (a) Leo, M. (1937). Uber radical emit mehreren dreiwertigen kohlenstofatomen. *Chem. Ber.* **70**, 1691–1694; (b) Wilker, W., Kothe, G. and Zimmermann, H. (1975). Uber da radical 1,3,5-benzoltris(diphenylmethyl). Tetramere und quartettzustand. *Chem. Ber.* **108**, 2124–2136

86. Zimmermann triradical: (a) Schmauss, G., Baumgartel, H. and Zimmermann, H. (1965). 1,3,5-tris(di-*p*-biphenylylmethyl)benzene, a new triradical. *Angew. Chem. Int. Ed.* **4**, 596; (b) Brickman, J. and Kothe, G. (1973). ESR of the quartet states of randomly oriented molecules: calculation of the line shape and detection of the zero-field splitting. *J. Chem. Phys.* **59**, 2807–2814; (c) Kothe, G., Ohmes, E., Brickmann, J. and Zimmermann, H. (1971). 1,3,5-benzenetriyltris[di-*p*-biphenyl)methyl)], a radical having quartet ground state that dimerizes by entropy bonding. *Angew. Chem. Int. Ed.* **12**, 938–940

87. Rajca, A. and Utamapanya, S. (1993). Polyarylmethyl quartet triradicals and quintet tetraradicals. *J. Am. Chem. Soc.* **115**, 2396–2401

88. Rajca, S. and Rajca, A. (1995). Novel high-spin molecules: π-conjugated polyradical polyanions. Ferromagnetic spin coupling and electron localization. *J. Am. Chem. Soc.* **117**, 9172–9179

89. Chlorinated triarylmethyl triradicals: Sedo, J., Ventosa, N., Ruiz-Molina, D., Mas, M., Molins, E., Rovira, C. and Veciana, J. (1998). Crystal structures of chiral diastereoisomers of a carbon-based high-spin molecule. *Angew. Chem. Int. Ed.* **37**, 330–333

90. Tris(4-biphenylyl)methyl: (a) Schlenk, W., Weickel, T. and Herzenstein, A. (1910). Ueber triphenylmethyl and analoga des triphenylmethyls in der biphenylreihe. *Justus Liebigs Ann. Chem.* **372**, 1–20; (b) Ohmes, E., Kothe, G., Naujok, A. and Zimmermann, H. (1971). Zur frage der association von tri-*p*-biphenyyl-methyl eine ESR-spectroskopische untersuchung zum selwood-effekt. *Ber. Bunsen-Gesselschaft* **75**, 895–901; (c) Broser, W, Kurreck, H. and Niemeier, W. (1976). Uber paramagnetische dimerenkomplexe des substituierten triphenylmethylradicals. *Tetrahedron* **32**, 1183–1187

91. Forrester, A.R., Hay, J.M. and Thomson, R.H. (1968). *Organic Chemistry of Stable Free Radicals*, Chapter 2, p. 64. Academic Press, New York

92. Utamapanya, S., Kakegawa, H., Bryant, L. and Rajca, A. (1993). High-spin polymers. Synthesis of 1,3-connected polyarylmethane and its carbopolyanion and polyradical. *Chem. Mater.* **5**, 1053–1055

93. Unpublished data from this laboratory

94. Rajca, S., Rajca, A., Wongsriratanakul, J., Butler, P. and Choi, S. (2004). Organic spin clusters. Dendritic–macrocyclic polyarylmethyl polyradical with very high-spin of $S = 10$ and its derivatives: synthesis, magnetic studies, and small angle neutron scattering. *J. Am. Chem. Soc.* **126**, 6972–6986

95. Rajca, A., Utamapanya, S. and Thayumanavan, S. (1992). Polyarylmethyl octet ($S = 7/2$) heptaradical and undecet ($S = 5$) decaradical. *J. Am. Chem. Soc.* **114**, 1884–1885

96. Rajca, A. and Utamapanya, S. (1993). Spin balls and spin barbells. Preparation and magnetic studies of $S = 7/2$ dendritic heptaradical and progress toward very high-spin dendrimers. *Liq. Cryst. Mol. Cryst.* **232**, 305–312

97. Rajca, A. (1994). Toward organic synthesis of a nanometer-size magnetic particle. *Adv. Mater.* **6**, 605–607

98. Rajca, A., Rajca, S. and Padmakumar, R. (1994). Calixarene-based macrocyclic nonet ($S = 4$) octaradical and its acyclic sextet ($S = 5/2$) pentaradical analogue. *Angew. Chem. Int. Ed.* **33**, 2091–2093

99. Matsuda, K., Nakamura, N., Inoue, K., Koga, N. and Iwamura, H. (1996). *Chem. Eur. J.* **2**, 259–264

100. Pu, Y.-J., Takahashi, M., Tsuchida, E. and Nishide, H. (1999). *Chem. Lett.* 161–162

101. Nishide, H., Takahashi, M., Takashima, J., Pu, Y.-J. and Tsuchida, E. (1999). *J. Org. Chem.* **64**, 7375–7380

102. Nishide, H., Kaneko, T., Nii, T., Katoh, K., Tsuchida, E. and Lahti, P.M. (1996). *J. Am. Chem. Soc.* **118**, 9695–9704

103. Rajca, A. (1997). Assembling triarylmethyls into mesoscopic-size polyradicals: How to maintain strong interactions between multiple sites in a single molecule? In *Modular Chemistry*, Michl, J. (ed.), pp. 193–200, Kluwer Academic Publishers, Dordrecht, The Netherlands

104. Rajca, A. (1996). Very-high-spin polyradicals. In *ACS Symposium Series 644, Molecule-Based Magnetic Materials*, Turnbull, M.M, Sugimoto, T. and Thompson, L.K. (eds), Chapter 17, pp. 258–265. American Chemical Society, Washington, DC

105. Rajca, A., Lu, K. and Rajca, S. (1997). High-spin polyarylmethyl polyradical: fragment of a macrocyclic 2-strand sased upon calix[4]arene rings. *J. Am. Chem. Soc.* **119**, 10335–10345

106. Rajca, A. (1997). High-spin organic polyradicals as simple spin clusters. *Mol. Cryst. Liq. Cryst.* **305**, 567–577

107. Rajca, A., Wongsriratanakul, J. and Rajca, S. (1997). Organic spin clusters: ferromagnetic spin coupling through biphenyl unit in polyarylmethyl tri-, penta-, hepta-, and hexadecaradicals. *J. Am. Chem. Soc.* **119**, 11674–11686

108. Rajca, A. (1999). High-Spin Organic Polyradicals. In *Magnetic Properties of Organic Materials*, Lahti, P.M. (ed.), Chapter 17, pp. 345–359. Marcel Dekker, New York

109. Rajca, A., Wongsriratanakul, J., Rajca, S. and Cerny, R. (1998). A dendritic macrocyclic organic polyradical with a very high-spin of $S = 10$. *Angew. Chem. Int. Ed.* **37**, 1229–1232

110. Rajca, S. and Rajca, A. (2001). Polyarylmethyl polyradicals as organic spin clusters. *J. Solid State Chem.* **159**, 460–465

111. Rajca, A. (2002). Organic spin clusters, fractals, and networks with very high-spin. In *Hyper-structured Molecules III*, Sasabe, H. (ed.), Chapter 3, pp. 46–60, Taylor & Francis, London

112. Rajca, A., Wongsriratanakul, J. and Rajca, S. (2004). Organic spin clusters: macrocyclic–macrocyclic polyarylmethyl polyradicals with very high-spin $S = 5$–13. *J. Am. Chem. Soc.* **126**, 6608–6626

113. Rajca, A., Wongsriratanakul, J., Rajca, S. and Cerny, R.L. (2004). Organic spin clusters: annelated macrocyclic polyarylmethyl polyradicals and polymer with very high-spin $S = 6$–18. *Chem. Eur. J.* **10**, 3144–3157

114. Jacobs, S.J., Shultz, D.A., Jain, R., Novak, J. and Dougherty, D.A. (1993). *J. Am. Chem. Soc.* **115**, 1744–1753

115. Annelated macrocyclic 42-radical **56**: unpublished data from this laboratory

116. Rajca, A., Rajca, S. and Wongsriratanakul, J. (1999). Very high-spin organic polymer: π-conjugated hydrocarbon network with average spin of $S \geqslant 40$. *J. Am. Chem. Soc.* **121**, 6308–6309

117. EPR spectroscopy of polymer **58**: unpublished data from this laboratory

Carbenes generated within cyclodextrins and zeolites

Murray G. Rosenberg and Udo H. Brinker

Institut für Organische Chemie, Universität Wien, Wien, Austria

1 Introduction

GUEST@HOST

Definition of guest@host

The symbol @ is used both in commerce and for e-mail addresses.[1] But recently, the symbol @ has been adopted by chemists to denote a guest "at" host inclusion complex (IC). A guest@host IC is defined as an addition compound between a guest molecule, which has divergent binding sites, and an inclusion compound (or clathrate), which has convergent binding sites. In a guest@host IC, the guest does not form ionic or covalent bonds with its host. Instead, other types of binding interactions exist.

Inclusion compounds are crystalline hosts that have channels in which a guest molecule may reside, e.g., templated urea. Non-stoichiometric ICs are typically formed. Clathrates, or cage compounds, are a special type of inclusion compound that possess fully enclosed voids. Integral stoichiometries for their ICs are expected. For example, hydroquinone (**1**) forms a hydrogen-bonded trimer that can confine a
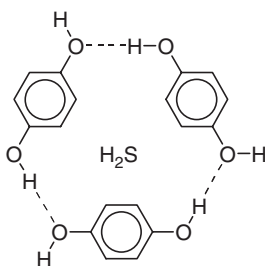
Fig. 1 $H_2S@(\mathbf{1})_3$ IC.

guest molecule, producing guest@$(\mathbf{1})_3$ (Fig. 1).[2] Carcerands and hemicarcerands (HCs) are two other examples of cage compounds (see p. 3).

Supramolecular chemistry

In 1967, Pedersen described the preparation and properties of crown ethers,[3] which are macrocyclic polyethers capable of sequestering metal cations. These catalysts can enhance the solubility and reactivity of salts in nonpolar solvents. For example, 18-crown-6, i.e., α,ω-*anhydro*-hexaethylene glycol, forms a host–guest complex with potassium cation (K^+) (Equation (1)). This association enables ionic potassium fluoride (KF) to dissociate in nonpolar benzene. And since the nucleophilic F^- counterions are not complexed,[4] the yield of the Finkelstein reaction,[5] i.e., halide–halide exchange, is increased:[6]

$$\text{(1)}$$
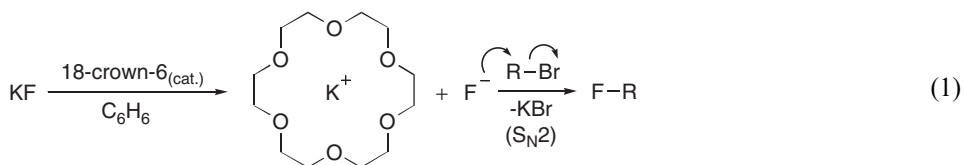
This innovation soon led Cram to extend the complexation concept to organic guests, by forming more rigid hosts made from benzene rings.[7] Calixarenes are one such example.[8] They can assemble into dimers that can entrap a guest molecule.

In 1987, supramolecular chemistry attained worldwide recognition when the Nobel Prize in Chemistry was awarded to Cram,[9] Pedersen,[10] and Lehn "for their development and use of molecules with structure-specific interactions of high selectivity."[11]

Not long after winning the 1987 Nobel Prize in Chemistry, Cram pioneered carceplex chemistry.[12,13] A carceplex is an IC formed when a guest molecule is imprisoned within the inner phase of a carcerand host, which consists of two hemispherical molecules linked together. Later, HCs were introduced (Fig. 2). These hinged, Pac-Man®-shaped hosts "gobble" guest molecules at high temperatures and retain them when the temperature is lowered. A milestone in organic chemistry was achieved when 1,3-cyclobutadiene was generated within a HC (see p. 3).
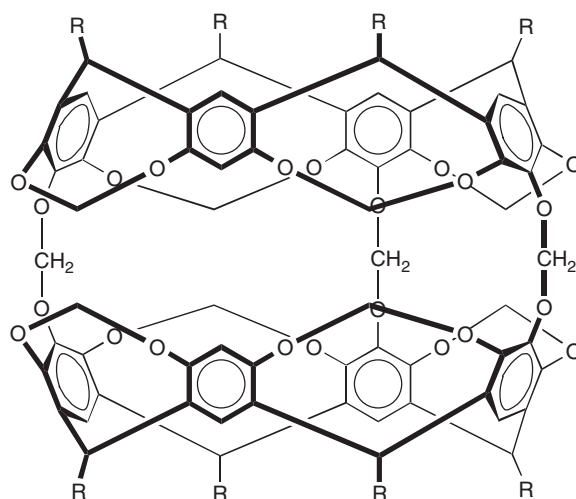
Fig. 2 A HC, e.g., R = CH$_2$CH$_2$Ph (phenethyl).

Characterizing the IC

Several physical methods have been employed to ascertain the existence and nature of ICs: infrared (IR) absorption spectroscopy; nuclear magnetic resonance (NMR) spectroscopy,[14] including ^{1}H nuclear Overhauser effect (NOE) difference spectroscopy, ^{1}H 2-D rotating-frame Overhauser effect spectroscopy (2-D ROESY),[15] and solid-state ^{13}C cross-polarization/magic angle spinning (CP/MAS) spectroscopy;[16] induced circular dichroism (ICD) absorption spectroscopy;[17] powder and single-crystal X-ray diffraction;[18] and fast atom bombardment mass spectrometry (FAB MS).

GUESTS

Neutral organic reaction intermediates

1,3-Cyclobutadiene. This was a much studied reactive intermediate during the twentieth century.[19] The shape (i.e., rectangle or square), ground-state electronic configuration (i.e., singlet or triplet), and Hückel anti-aromaticity of the ephemeral diene were all in question. When generated, e.g., from α-pyrone, 1,3-cyclobutadiene can rapidly undergo a Diels–Alder reaction with itself. It also photofragments into two equivalents of ethyne. One of the greatest achievements in supramolecular chemistry and a milestone in organic chemistry, was the trapping of 1,3-cyclobutadiene within a HC.[20]

Ortho-benzyne. The generation of *ortho*-benzyne within a HC was recently reported by Warmuth.[21] Like 1,3-cyclobutadiene, strained *ortho*-benzyne is a unstable,

reactive intermediate.[22] Its lifetime (τ) was limited, though, by unwelcomed *inner-molecular* Diels–Alder reaction with its HC host. It was also very sensitive to the presence of adventitious water molecules, forming 3-hydroxy-1(3*H*)-isobenzofuranone.

Carbenes. Although most organic compounds possess uncharged carbon atoms that have a Lewis octet of electrons in their valence shells, i.e., they form four bonds, neutral carbon fragments can nevertheless be generated as reaction intermediates. These include carbenes. The generation of transient carbene ICs is explored in detail in this chapter.

HOSTS

Cyclodextrins

Structure and stoichiometry. Cyclodextrins (CyDs) were discovered over 100 years ago by Villiers.[23] They are formed by *Bacillus macerans*, which is a type of bacteria that degrades starch,[24] using the enzyme cyclomaltodextrin gluconotransferase, or CyD glycosyl transferase.[25] CyDs were often called Schardinger dextrins because they were first popularized by Schardinger.[26]

A CyD is a nonreducing, cyclic oligosaccharide molecule composed of α-D-glucopyranose (α-D-Glc*p*) monomers linked at the 1 and 4 glycosidic positions. The general structure of CyDs is shown in Fig. 3. Their prefixes depend on the number of pyranose units present: six (α-CyD), seven (β-CyD), eight (γ-CyD), and nine (δ-CyD).[27]

These torus-shaped[28] hosts can accommodate many sorts of organic molecules that can reside within the nonpolar cavity. The strength of this noncovalent interaction is directly related to the position of the equilibrium for complex formation. This is evaluated by a binding constant (K)[29] that may be measured in a variety of different ways, e.g., spectrofluorometric methods based on competition experiments.[30] Recently, ICD has also been used to assess the binding constants of carbene-forming 3*H*-diazirine@CyD ICs.[17]

The driving forces responsible for CyD IC formation are (1) van der Waals (London dispersion) forces, (2) hydrophobic interactions, (3) dipole–dipole (electrostatic) interactions, (4) hydrogen (O–H···N, O–H···O, and/or O–H···F) bonding, (5) release of CyD distortional energy by the merging guest, and (6) expulsion of "high-energy water" from the CyD cavity upon IC formation.[31]

The host–guest stoichiometries of CyD ICs are difficult to predict because CyDs are versatile hosts that can act either as nonstoichiometric channel-forming inclusion compounds or as stoichiometric cage-forming clathrates. To complicate matters, CyDs can also form association complexes (ACs),[27b] in which the guests reside within the interstices between the hosts. Therefore, direct proof of a guest@host IC should be obtained so that structural information, such as host–guest stoichiometry and reactant orientation, can be ascertained. This can be obtained using well-developed methods, including single-crystal X-ray diffraction.[32]
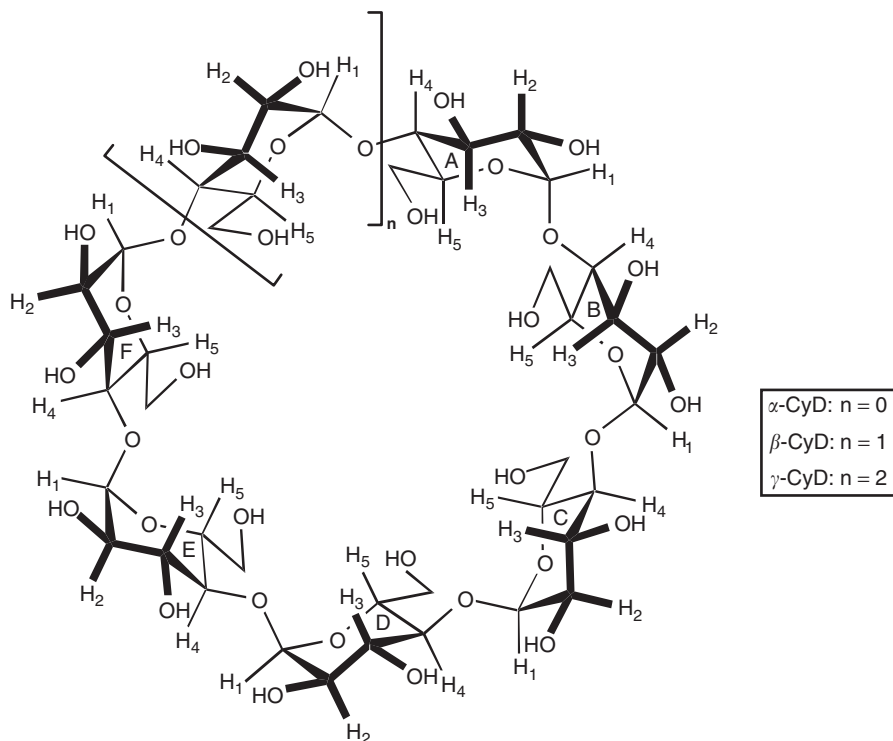
Fig. 3 Structure of CyD depicting the O1–C4 α-linkage of D-Gl*cp* monomers. Note the inward pointing H3 and H5 atoms.

Zeolites

Faujasite structure and stoichiometry. Zeolites were discovered in 1751 by the Swedish mining engineer, Cronstedt.[33] There are many naturally occurring forms,[34] like chabazite (CHA),[35] as well as synthetic ones, like MCM-41.[36]

Faujasite (FAU) zeolites are crystalline, highly polar, multicameral aluminosilicates wherein organic molecules may be entrapped. Both types (i.e., X and Y) are characterized by a tetrahedrally arranged network of interconnected sodalite cages (Fig. 4).[37] The voids that are created are called supercages. Inspection of the unit cell reveals that the number of sodalite cages and supercages are equivalent. Note that 10 sodalite cages are present in Fig. 4 but that three of them, i.e., at 12, 8, and 4 "o'clock," are eclipsed, or hidden. In a sense, the structure in Fig. 4 can be likened to that of adamantane (**2**), whereby sodalite cages are swapped for C atoms (Fig. 5).

Positively charged counterions, which balance $(AlO_2)^-$ moieties, are found within the FAU lattice. They can also be a source of acidity, e.g., H^+. These cations may be
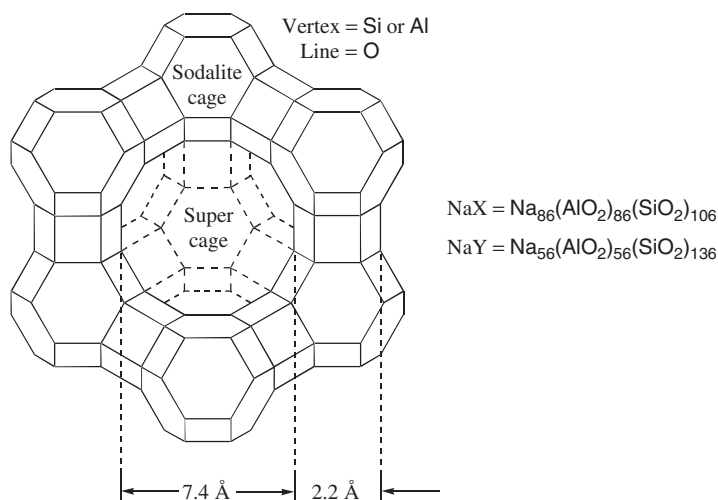
Fig. 4 Structure of FAU zeolites X and Y, depicting 13-Å diameter supercage and tetrahedral arrangement of 7.4-Å apertures.
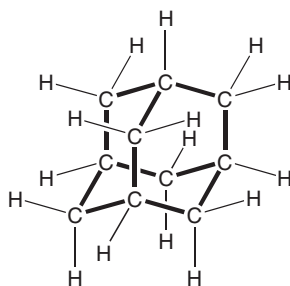
Fig. 5 Adamantane (**2**) structure.

exchanged,[38] thereby allowing chemists to alter the free volume (ΔV) of supercages by choosing ions of certain radii.[39]

The loading factor ($\langle s \rangle$) is a measure of the ratio of guest molecules to supercages. For instance, if $\langle s \rangle = 1.00$ then each filled supercage is adjoined to another filled supercage. In the limit of $\langle s \rangle = 0.25$, each filled supercage is surrounded by four empty ones.[40] The uptake of guest molecules can be determined experimentally.[41] Like CyDs, FAU zeolites allow a range of ultraviolet (UV) light to pass through and interact with photolabile guests, such as nitrogenous carbene precursors.

Choice of hosts

Recent advances in carbene chemistry demonstrate that constrictive hosts, like CyDs and FAUs zeolites are able to modify the selectivity of the high-energy reaction intermediate.[42]

α- and β-CyDs. CyDs has become readily available in recent years.[43] Indeed, their supply now exceeds demand, thus, making them affordable too. However, large volume uses for CyDs have yet to materialize,[44] though lucrative patents for their "real-world" applications are actively being sought. Therefore, CyDs are increasingly being applied as supramolecular hosts. Due to the size of typical carbene precursors, α-CyD and β-CyD have been deemed to be the most formfitting hosts, although γ-CyD has been used in some instances.

NaY FAU. Since carbenes, e.g., phenylcarbenes, can sometimes act as Brønsted–Lowry bases, acidic media should be avoided. In principle, protonation of carbenes will give *carben*ium ions, their conjugate acids. This will, of course, complicate product studies because carbenes and carbocations behave differently. Therefore, HX and HY zeolites, i.e., NH_4X and NH_4Y zeolites,[45] were not used.

The Lewis acidity of the zeolites can also be problematic since these may constitute catalytically active sites.[46] According to their empirical formulas, Y-type FAUs have a higher Si/Al ratio, i.e., Si/Al = 2.43, than do X-type FAUs, i.e., Si/Al = 1.23 (Fig. 4). Hence, Y-type FAUs should exhibit less (unwelcomed) Lewis acidity than the latter. Likewise, group 1 counterions would be preferred over group 2 counterions. This is because alkali metal cations exhibit less Lewis acidity than do alkaline earth metal cations. Since FAU zeolites exist in nature as hydrates, i.e., $NaX \cdot 264H_2O$ and $NaY \cdot 253H_2O$, and cannot be completely dehydrated upon heating, their inner water molecules can hydrolyze the charge-compensating cations, yielding $H^+_{(aq)}$. For example, $Na^+_{(aq)}$ behaves as a simple spectator ion when it is dissolved in water (Equation (2)). But $Mg^{2+}_{(aq)}$ is strong enough to bind the free $OH^-_{(aq)}$ that is formed during the autoionization of water (Equation (3)). Hence, *two* equivalents of $H^+_{(aq)}$ are formed per counterion and there exists less free $OH^-_{(aq)}$ to neutralize them:

$$Na^+_{(aq)} + H_2O_{(l)} \rightleftharpoons H^+_{(aq)} + Na^+_{(aq)} + OH^-_{(aq)} \tag{2}$$

$$Mg^{2+}_{(aq)} + 2H_2O_{(l)} \rightleftharpoons 2H^+_{(aq)} + Mg(OH)_{2(s)} \tag{3}$$
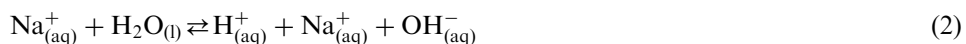
Finally, Na^+ cations are small enough so that guest inclusion should not be inhibited. And NaY zeolite is commercially available. Thus, NaY was the zeolite of choice for many studies.

2 Objectives

SHAPE SELECTIVITY

Molecular recognition is a term often used to describe the ability of a host molecule to bind a specific type of guest, typically from a mixture.[47] The 3-D hosts (i.e., cavitands) are more apt at this task than are flat, 2-D hosts (i.e., coronands). The concept of molecular recognition is reminiscent of Fischer's[48] "lock and key"

metaphor that is used to describe the specificity of enzymes.[49] Hence, host molecules, such as CyDs, have been used as simple enzyme mimics because they exhibit saturation kinetics and competitive inhibition.[25,50,51]

Enzymes not only catalyze reactions, but they do so with a high degree of specificity that originates from the shapes of their active sites. Shape selectivity can also be a property of other supramolecular hosts which, therefore, are said to be enzyme mimics.[52] If two products stem from a single reactant, i.e., $\mathbf{R} \rightarrow \mathbf{P_A} + \mathbf{P_B}$, then an enzyme mimic can bias the competition in favor of one product over the other.

It should be mentioned that modifying reaction outcomes is not a new concept. Manipulation of reactants through electronic effects, e.g., by adjoining either electron-donating groups or electron-withdrawing groups to $\mathbf{R}$, can alter the outcome. And appending bulky groups to $\mathbf{R}$ can introduce steric effects. However, both of these methods rely upon chemical modification of $\mathbf{R}$. Supramolecular inclusion of $\mathbf{R}$ within an appropriate host vessel is innovative because reaction selectivity is altered via physical modification.

Shape selectivity has also been demonstrated within FAU zeolites. For example, *meta* selectivity was observed for the NaY-mediated Friedel–Crafts alkylation of benzyl chloride (BnCl) with itself. In addition to polymer inhibition, the FAU zeolite favored the formation of the "banana-shaped" 1-(chloromethyl)-3-(phenyl-methyl)benzene (*m*-**3**) regioisomer (Equation (4)):[53]

$$2 \quad \xrightarrow{\text{-HCl}} \quad (4)$$

BnCl@NaY   *m*-**3**@NaY

STEERING REACTION OUTCOMES

The motive behind supramolecular carbene chemistry is to modify the inter- and intramolecular reactions of entrapped carbenes in order to manipulate product formation. Such would be achieved through *physical* modification as opposed to the more conventional *chemical* modification techniques, e.g., appending bulky substituents, which would necessarily alter the reactant's potential energy surface (PES). Selectively directing carbene reactions wherein more than one product may be formed would, therefore, confound conventional predictions.

The reactive behavior of a carbene within a molecular reaction vessel is expected to be very different from that of a carbene in any other reaction medium. Host vessels may have any variety of different channel or cavity sizes that can restrict the mobility of carbene guests and any other reaction partner that might also be included.[54] One should even be able to generate, within the host domain, a carbene that has no intramolecular reaction pathways available. Situated like a model ship

Fig. 6 A carbene may be constrained like a ship in a bottle.

within a bottle (Fig. 6),[55a] this highly reactive species will have been harnessed because no other molecules would be available with which to react. This might introduce the possibility to spectroscopically characterize carbenes in an unfettered state.[55b,c]

Supramolecular modification of carbene chemistry may be achieved, to some degree, by forming guest@host ICs of nitrogenous carbene precursors with CyDs and FAU zeolites. The results of these reactions should help physical organic chemists better understand the detailed mechanisms by which carbenes decay.

CONTROL CARBENE SPIN STATE

The spin multiplicity $(2S_z + 1)$ of a carbene is dependent upon whether or not its nonbonding electrons are magnetically paired. The spin states of carbenes are an important aspect since singlet and triplet carbenes do not react in the same manner. For instance, a singlet carbene adds to carbon–carbon double bonds with retention of the substrate's geometric configuration, whereas a triplet carbene reacts without stereospecificity under nonconcerted conditions.[56] In fact, triplet carbenes, which are geminate diradicals, behave much like other organic free radicals. They can abstract H atoms from organic solvents or can be photoreduced in protic solvents, like isopropyl alcohol (*i*-PrOH). Moreover, electron spin resonance (ESR) spectroscopy can be used to detect triplet carbenes since they are paramagnetic.[57]

Carbene bond angle distortion

The bond angle (θ) that a divalent carbon atom forms with the two atoms to which it is bonded is one factor that determines carbene ground and electronically excited spin states.[58] This geometric parameter might be susceptible to change when a carbene is generated in a supramolecular state. Moreover, carbenes may possess ground and excited states of unlike spin multiplicity that are significantly close in energy, e.g., $\Delta E_{ST} = 1$–$2 \, \text{kcal} \, \text{mol}^{-1}$. When compared with that of a mobile carbene, the reacting state of an entrapped carbene might display a change in its spin multiplicity. Thus, a constrictive molecular reaction vessel might foster exciting new chemistry from carbenes once dismissed as unimportant.

Facilitate intersystem-crossing

Intersystem crossing (ISC) of gaseous singlet methylidene ($^1CH_2$) to triplet methanediyl ($^3CH_2$) is facilitated by increased N_2 pressure.[59] This is due to collisional deactivation of electronically excited $^1CH_2$. A similar mechanism for ISC may be provided by cavitand hosts, due to their comparatively large molar masses.[60] Therefore, supramolecular inclusion of a carbene having a triplet ground state (GS) is expected to enhance radical-type reactions, such as H-abstraction/recombination.

CONTROL INTRAMOLECULAR REACTIONS

The high-energy content of carbene intermediates ensures that their decay processes are spontaneous, i.e., $\Delta G < 0$, with a low enthalpic barrier, i.e., $\Delta H^{\ddagger} \approx 0$ (but $\Delta G^{\ddagger} \neq 0$). Therefore, carbenes are highly indiscriminant, short-lived reagents. Yet their intramolecular reactions are still subject to certain limitations.

Constraint

Clathrates can exert a positive cage effect on entrapped reactive intermediates.[41,61] Likewise, they can shield certain reaction sites during radical recombination.[62,63] Therefore, it seems reasonable that cage compounds might also behave like molecular straitjackets.[64] For example, transannular C–H insertion reactions within large alicyclic carbenes should become more inhibited as the free volume (ΔV) of the host becomes smaller. Similarly, irreversible carbene fragmentation reactions might also experience a restriction since ample space is needed for the unraveling process to occur.

Topologic distortion

Since proper orbital alignment is a crucial requirement for an elementary reaction step to proceed, host-induced topologic distortion of a pliable carbene guest might cause its usual reactions to be foiled.[65] That is because misalignment of the guest's frontier orbitals could reduce overlap with those of the target moiety. Intramolecular hydride and alkyl shifts might be tunable, even in the absence of bystander effects.[66]

INHIBIT INTERMOLECULAR REACTIONS

For two molecules to react, they must first collide with each other. Intermolecular reactions within nanoscopic reaction vessels are limited because reactants are mostly isolated from one another. Both inclusion compounds and clathrates are expected to inhibit bimolecular reactions. Moreover, shape selectivity, cf. Equation (4), and reaction site shielding,[62,63] have been shown to preclude certain intermolecular

reactions. Indeed, with $\Delta H^{\ddagger} \approx 0$ for most carbene reactions, the entropic term $T\Delta S^{\ddagger}$ can become decisive in intermolecular reactions.

Limit guest mobility

The diffusion, or percolation,[41] of a molecule within the channels of CyD or FAU inclusion compounds is expected to be much less than that in conventional solvents. Often, the decay rate (k_0) of a carbene in a nonviscous organic solvent is diffusion limited, cf. $k_d(MeOH) = 1.20 \times 10^{10}\,M^{-1}\,s^{-1}$@ 25 °C.[67] Therefore, limited guest mobility not only will hamper intermolecular reactions but it should also prolong the lifetime (τ) of the carbene reaction intermediate, if intramolecular modes of decay are not accessible.

3 Supramolecular carbene chemistry

CARBENE REACTIONS

Carbene reactions are strictly those in which uncharged, divalent carbons are formed as reaction intermediates.[68] Besides intermolecular σ-bond insertions and π-bond additions, these unstable molecules can also undergo intramolecular electronic re-arrangements that either convert them to stable products or transform them into secondary carbenes of lesser energy content. The ephemeral carbene is electron deficient and, by various ways, gains an electron pair to completely fill its valence shell. Nevertheless, carbenes can also act as Brønsted–Lowry bases, e.g., protona-tion of a carbene to a *carben*ium ion.[67,69] Carbenes may be observed transiently under special reaction conditions. Sometimes, they are paramagnetic or possess chromophores that may be detected spectroscopically.[57,70] Other times, Lewis bases, such as pyridine, are used to reveal their fleeting presence.[71]

PHASE TRANSFER CATALYSIS

The history of supramolecular carbene chemistry is not long. Preliminary trials, during the 1970s, involved the generation of carbenes in the presence of micelles, e.g., quaternary ammonium salts, and crown ethers.[72] However, carbene@host ICs were not formed, nor were they sought. Instead, these hosts enable phase transfer catalysis (PTC) of Lewis acid–Lewis base reactions, e.g., the S_N2 reaction (Equation (1)).

CyD-mediated Reimer–Tiemann reaction

The formylation, i.e., formal carbon monoxide (CO) insertion, of phenols using chloroform and aqueous base is known as the Reimer–Tiemann reaction (Scheme 1).[73] It is generally accepted that base-induced α-elimination of chloroform (CHCl$_3$) yields the rate-determining, electrophilic dichlorocarbene (CCl$_2$) intermediate, which
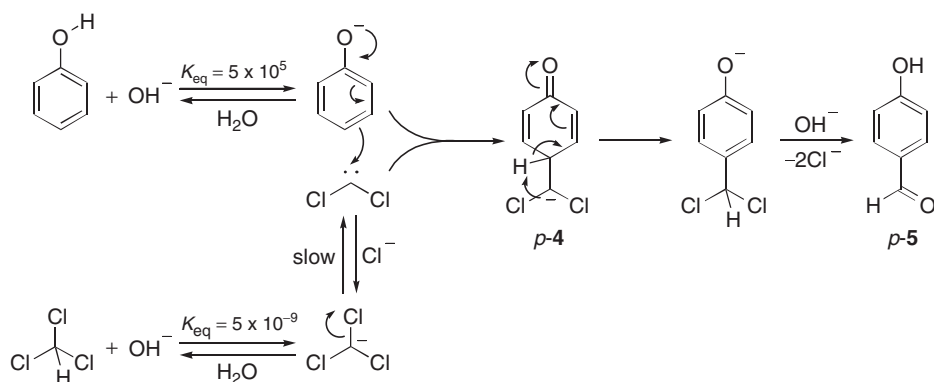
Scheme 1 Reimer–Tiemann reaction.

is then attacked by the very strongly activated *o-/p*-directing phenolate anion (PhO⁻).[74] Subsequent rearomatization of the initial intermediate **4** and base-mediated hydrolysis yields *o-* and *p*-hydroxybenzaldehydes (**5**). Remarkably, the *O*-formylated product is only formed during the photo-Reimer–Tiemann reaction, which proceeds not by dichlorocarbenes but rather by dichloromethyl radicals.[75]

The genesis of supramolecular carbene chemistry likely occurred when the Reimer–Tiemann reaction was conducted in the presence of CyDs.[76] Dehydrochlorination of $CHCl_3$ by OH⁻ was retarded due to the formation of armored $CHCl_3$@CyD ICs. Thus, the overall yield of **5** was even lower than usual. Indeed, at pH = 13, CyDs were likely deprotonated and behaved much like *anionic* micelles, which cannot transport the electrically repulsive OH⁻ base needed for $CHCl_3$-dehydrochlorination, thereby inhibiting CCl_2 formation.[77] However, α-elimination of $CHCl_3$ by the deprotonated CyD host itself was inexplicably deemed to be "less important."[76b] Encapsulation of CCl_2 within the CyD hydrophobic cavity is expected to impede hydrolysis of the carbene to CO. No *innermolecular* chlorination of the CyD hydroxyl groups of the CCl_2@CyD ICs occurred,[76b] which should have been possible.[78] Instead, the aryl end of the PhO⁻ dipped into the nonpolar cavity of the CyD and reacted with the ordinarily short-lived CCl_2 intermediates. Thus, increased *para* selectivity was observed, e.g., *p*-**5**/*o*-**5** = 4.65.[79]

CyD derivatization using nitrogenous carbene precursors

With the intent to selectively derivatize CyD oligosaccharides,[80] Abelt enlisted nitrogenous carbene precursors as labile guests.[81] The involvement of supramolecular carbenes could be inferred based on intramolecular products stemming from 1,2-H shifts. Of course, 3*H*-diazirines that possess α-C–H bonds, like 3-methyl-3-phenyl-3*H*-diazirine (**6**) (Scheme 2), are susceptible to rearrangements in the excited state (RIES) that mimic the results of carbene 1,2-H shifts,[82] e.g., **6*** → **10** (Scheme 2).

The styrene (**10**) that was formed also underwent a secondary reaction giving *cis*- and *trans*-1-methyl-1,2-diphenylcyclopropanes (**9**).[81a] These three-atom rings are not
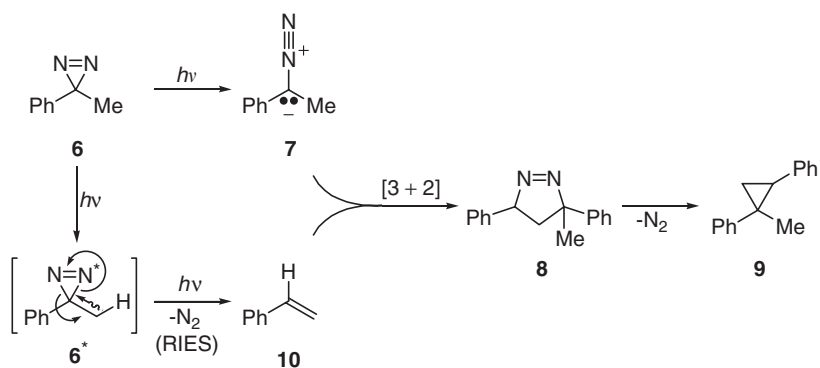
Scheme 2 Formation of styrene (**10**) and 1-methyl-1,2-diphenylcyclopropane (**9**) via non-carbenic pathways

necessarily formed via carbene [2 + 1] cheletropic addition, however, since they may be derived from homolytic scission of the pyrazoline 3-methyl-3,5-diphenyl-4,5-dihydro-3H-pyrazole (**8**),[83] which can be formed by the facile [3 + 2] dipolar addition of the diazo compound 1-(diazoethyl)benzene (**7**) to alkene **10** (Scheme 2).

The participation of carbenes was also surmised from the formation of the *innermolecular* O–H insertion products of CyDs that were originally sought. The innermolecular products, i.e., O-(1-phenylethyl)CyDs, can also be explained without invoking carbenes. Since most of the diazo compounds that were used decomposed during CyD IC formation,[81c] CyD derivatization may have occurred by a diazonium ion route.[84] And although 3H-diazirines survive CyD IC formation,[81b] excited-state diazirines, like **6***, might exhibit much greater Brønsted–Lowry basicities (pK_b^*) than GS diazirines (pK_b).[85] Thus, protonation of excited-state diazirines to the corresponding carbenes would give carbocations,[86] which could yield O-substituted CyDs.

Encapsulated methylene

In the early 1980s, the conversion of methyl alcohol (MeOH) to gasoline over synthetic zeolite catalysts was being studied. One set of experiments using MeOH@H-ZSM-5 led to the hypothesis that carbenes, like CH_2, were involved in this industrially important process.[87] However, a more explanatory mechanism was proposed[88] and, by decade's end, a rigorous study of this reaction using MAS ^{13}C NMR showed CO to be the key intermediate.[89] Recently, the precise role of H-ZSM-5 has even been questioned.[90]

The possible formation of the endohedral fullerene $CH_2@C_{70}$ was recently communicated by Dunsch.[91] The IC was isolated in > 90% purity by HPLC and, remarkably, was stable for months even though CH_2 is normally only short-lived.
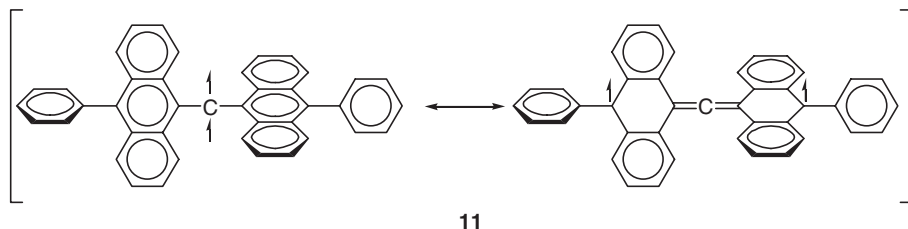
Fig. 7 Is triplet bis(10-phenylanthracen-9-yl)carbene (**11**) really a geminate diradical?

(a)   (b)

(c)   (d)
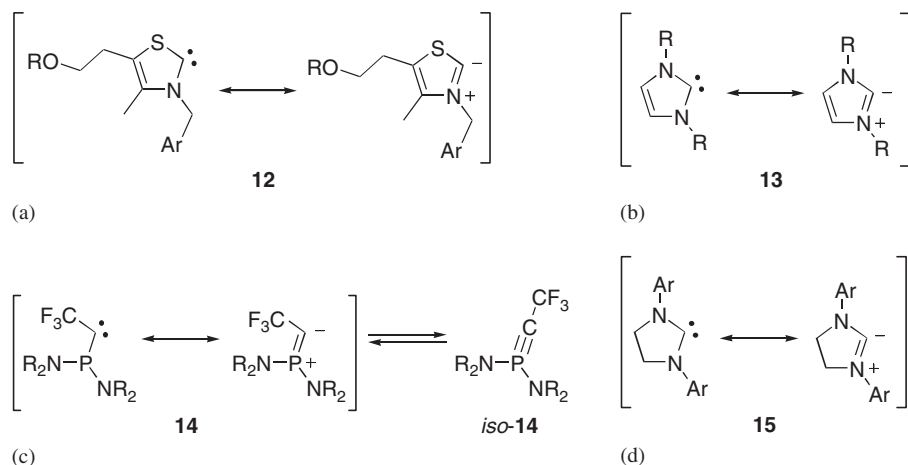
Fig. 8 Singlet carbene or pnictonium ylide? (a) Breslow, (b) Arduengo, (c) Bertrand, and (d) Wanzlick carbenes.

CHOICE OF CARBENES

Much time and effort has been spent in recent years seeking long-lived carbenes.[92] This flurry of activity has met limited success. Persistent triplet carbenes,[93] such as triplet bis(10-phenylanthracen-9-yl)carbene (**11**) ($t_{1/2} = 19$ min, $D/hc = 0.105$ cm^{-1}) (Fig. 7),[92a;93a,b;94] constitute one area of promising research. Ylide-like singlet carbenes, such as Breslow thiazol-2-ylidenes (**12**),[95] Arduengo imidazolin-2-ylidenes (**13**),[92f;96,97] Bertrand phosphinocarbenes (**14**),[92c,98] and Wanzlick imidazolidin-2-ylidenes (**15**),[97,99] comprise another (Fig. 8).[100] However, supramolecular inclusion of more *typical* carbenes within suitable hosts may offer distinct advantages.

CASE STUDIES

With so much uncertainty regarding true carbene intermediacy within molecular reaction vessels, a reaction demonstrating a unique process only attributable to carbenes needed to be performed.
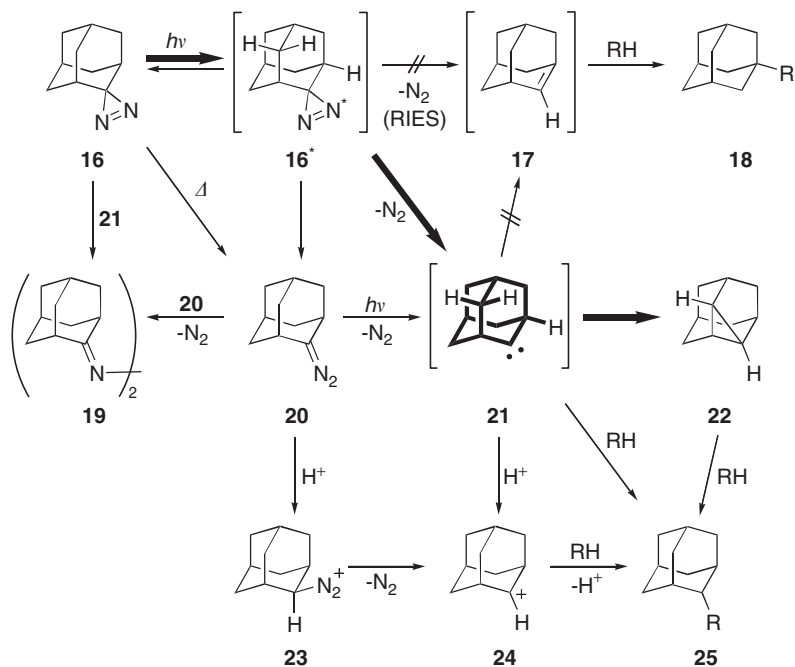
RH = (a) α-CyD, (b) β-CyD, (c) MeOH, (d) H$_2$O, (e) n-C$_7$H$_{16}$.

Scheme 3 Generation of 2-adamantanylidene (**21**) and its subsequent reactions.

2-Adamantanylidene

The reaction of aziadamantane (2-azitricyclo[3.3.1.1^{3,7}]decane, **16**) within the relatively inert confines of CyDs[101] and FAU zeolites[102] serves as a major achievement in carbene chemistry.[42] This 3*H*-diazirine, first prepared in the early 1970s,[103] has been studied to a considerable extent.[104,105] Diazirine **16** forms the azine di(2-adamantanylidene)hydrazine (**19**) and other bimolecularly derived products such as 2-alkyl(oxy)adamantane (**25**) when reacted in solution (Scheme 3), likely via the carbene intermediate 2-adamantanylidene (**21**). Believed to possess a singlet GS,[106] carbene **21** does not readily undergo 1,2-H shift to form singlet adamantene (**17**),[107] a strained *anti*-Bredt compound (Scheme 3). Thus, other nontrivial rearrangements of carbene **21** have the potential to flourish.

The dramatic increase in 2,4-didehydroadamantane (tetracyclo[3.3.1.1^{3,7}.0^{2,4}]decane, **22**) production when diazirine **16** is photolyzed in CyDs and FAU zeolites (Table 1) is demonstrative of the powerful influence these hosts can have on reaction outcomes. Since there are no solvent molecules with which supramolecular carbene **21** can react and because a 1,2-H shift by carbene **21** is prohibited, decay via 1,3-CH insertion is greatly enhanced. In contrast, cyclopropane **22** is only formed in trace amounts from diazirine **16** in organic solvents.[101,103] When a physical mixture

Table 1 Relative intra- and intermolecular product distribution for photolytic reactions of aziadamantane **(16)**

Medium	**22**	**19**	**25**
n-C$_7$H$_{16}$	0.2	54	10[a]
MeOH	6.5	0	93.5[b]
β-CyD	29	53[c]	5[d]
NaY	45[e]	0	50[f]

[a]**25e**.
[b]**25c**.
[c]Presumably due to a 2:2 IC, cf. Ref. 18.
[d]**25b**.
[e]Extrapolated value due to FAU-mediated **22**→**25d**.
[f]**25d**.

of β-CyD and diazirine **16** was photolyzed, less than 1% of cyclopropane **22** was formed.[101] Furthermore, photolysis of diazirine **16** in the solid state leads to no detectable **22**.

The formation of the three-membered ring of **22** can only be easily explained as an intramolecular 1,3-CH insertion of carbene **21**. This signature reaction of carbenes leaves little doubt that the **21**@β-CyD IC was the first verifiable supramolecular carbene. Indeed, more **22** may have been formed if the CyD host had been completely inert.

According to FAB and tandem mass spectrometry, carbene **21** also inserts into one of the 21 hydroxyl ($-$OH) moieties of β-CyD to make the covalently bound host–guest adduct O-(adamantan-2-yl)β-CyD (**25b**), which exhibits an [M–H]$^-$ ion with a mass to charge ratio (m/z) of 1267.4 Da.[101] Further proof was secured by treating a sample with D$_2$O to exchange the number of active H atoms left and also by collisionally activating the **25b** parent ion. No measurable loss of **22** could be detected. A low abundance ion of $m/z = 1401.5$ Da was also observed in the FAB mass spectrum, probably due to a β-CyD bearing *two* 2-adamantanyl substituents. Support for this was demonstrated by the fact that only 19 H atoms were exchanged upon D$_2$O treatment. Thus, two insertions by two different carbene intermediates **21** into two separate $-$OH sites of β-CyD had taken place. This finding, in addition to the observation that so much azine **19** was formed (Table 1), indicates that a 2:2 host–guest inclusion compound, i.e., (**21**@β-CyD)$_2$, was likely formed.

Recently, it was found that chemoselective O–H insertions of dimeric α-CyD hosts by their encapsulated carbene **21** guests produced 2-O-(2-adamantanyl)α-CyD (2-**25a**) and 3-O-(2-adamantanyl)α-CyD (3-**25a**).[108] Within the cavities of β-CyD at 30 °C, these innermolecular insertion products were isolated in 35% yield. Correspondingly, in the smaller confines of α-CyD, as much as 58% of 2- and 3-**25a** were formed.[109] In contrast, the yield of the intramolecular insertion product **22** remains unchanged at 10%. Innermolecular insertion products 2- and 3-**25a** were separated via reversed-phase high-pressure liquid chromatography (RP HPLC),[109]

and then identified by FAB MS and by 600 MHz pulsed field gradient enhanced [1]H-detected [1]H–[13]C heteronuclear correlation through binary quantum coherence (HMBC) NMR spectroscopy.[108,109]

2-Methylcyclohexanylidene

Since 2-adamantanylidene (**21**) is a fairly rigid molecule,[110] investigation of host–guest ICs of unscaffolded 2-methylcyclohexanylidene (**27**)[111] seemed appropriate (Scheme 4). If supramolecular constraint of the more flexible carbene **27** can promote its axial methyl conformation then that more compact conformer should be less prone to form 1-methylcyclohexene (**28**) and more apt to produce norcarane (bicyclo[4.1.0]heptane, **30**) and 3-methylcyclohexene (**29**) because it has been shown that orbital alignment plays a crucial role in carbene rearrangements,[112] such as 1,2-H shifts.[112,113] Therefore, 1-azi-2-methylcyclohexane (4-methyl-1,2-diazaspiro[2.5]oct-1-ene, **26**) was prepared,[114] and its supramolecular reactivity was examined.[42,115]

Products formed during the photolysis of diazirine **26** were initially assumed to arise from carbene **27** (Scheme 5). The CyD ICs of diazirine **26** were prepared in fair yields (Table 2).[115a] The amounts may reflect the increasing cavity sizes of the hosts.

Solid-state photolyses were conducted in argon-purged borosilicate flasks. After 2 h, no more diazirine **26** was present by NMR nor by gas chromatographic (GC) analysis. The results of solution photolyses of diazirine **26** are shown in Table 3. Carbene **27** can also be generated from the 2-methylcyclohexanone *p*-tosylhydrazone sodium salt (**33**) via the Bamford–Stevens reaction.[116] The gas phase results are also included in Table 3 as are the results of Wilt and Wagner.[111]

Evidence for diazo compound intermediacy. The solutions turned peach-colored for a few hours during the photolysis reactions. This can be ascribed to the transient formation of the linear diazo compound 1-diazo-2-methylcyclohexane (**32**), the valence isomer of cyclic **26**. Evidence for **32** was obtained using IR and UV/vis spectroscopy.[115a]
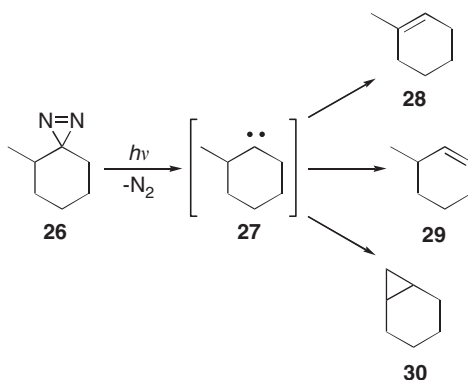
Scheme 4 Possible intramolecular reactions of 2-methylcyclohexanylidene (**27**).

RH = (a) CyD, (b) MeOH, (c) H_2O, (d) n-C_5H_{12}; Ts = p-$SO_2C_6H_4CH_3$

Scheme 5 Generation of 2-methylcyclohexanylidene (**27**) and its subsequent reactions.

Table 2 Absolute yields of **26**@CyDs

Host	(CyD/**26**)$_{NMR}$	Absolute yield (%)
α-CyD	1.85	50
β-CyD	1.14	57
γ-CyD	0.94	69

No increased C–H insertion into methyl group. In contrast to all other reaction conditions, trace amounts of insertion product **30** are produced only by the thermal Bamford–Stevens method in high-boiling NMP.[111] Formation of bis (2-methylcyclohexanylidene)hydrazine (**31**) is inhibited in MeOH, due to the short

Table 3 Effect of reaction medium on selectivity of nitrogenous 2-methylcyclohexanylidene (**27**) precursors[a]

Relative % of: methods:	28	29	28:29	30	31	36
180 °C (NMP)[b,c]	63	27	2.3	Trace		
250 °C (5 mmHg)[b]	78	22	3.6			
0.1 M n-C$_5$H$_{12}$[d]	45	21	2.1		34	
0.5 M n-C$_5$H$_{12}$[d]	25	11	2.2		64	
0.1 M MeOH[d]	43	24	1.8			33[e]
0.5 M MeOH[d]	42	23	1.8			35[e]
α-CyD[d]	72	28	2.6			
β-CyD[d]	66	34	1.9			
γ-CyD[d]	62	30	2.1		8	

[a]Error = ±3%.
[b]Precursor **33**.
[c]N-Methyl-2-pyrrolidinone, cf. Ref. 111.
[d]Precursor **26**.
[e]**36b**.

lifetime of diazo compound **32** in protic media. This same inhibition is seen with α- and β-CyD and can be attributed either to their hydroxy moieties and/or their supramolecular capabilities. Note that small amounts of **31** were formed in γ-CyD. This may be due to diffusion of long-lived **26** through γ-CyD channels or to a positive cage effect imposed upon two molecules of **26** that happen to both be included within one cavity of the larger γ-CyD clathrates.

Alkene isomer ratio unchanged. Statistically, the amount of alkene **29** that is formed via 1,2-H shift of carbene **27** should be twice that of alkene **28**, because of the 2:1 ratio of H atoms on the respective migration origins. This, however, is not the case, due to the unequal inherent migratory aptitudes of each H atom,[117] i.e., different reactivities of the migrating hydrides. Indeed, the corresponding, electron-deficient 2-methylcyclohexyl cation (**35**) yields a **28**:**29** ratio of about 5.4,[118,119] in accordance with Saytzeff's rule. The regioselectivity for the carbene **27**, however, appears to be less stringent because ratios of ca. 1.8–3.6 were observed (Table 3).

Considerable amounts of 2-methoxy-1-methylcyclohexane (**36b**) were formed in MeOH (Table 3). Methyl ether **36b** could stem from two alternative routes: (1) insertion of carbene **27** into the O–H bond of MeOH,[120] or (2) protonation of **27** and/or **32** to give carbocation **35**, which then incorporates MeOH. Therefore, the actual carbenic ratios of **28**:**29** might have been obscured due to the possible involvement of cation **35**. However, the absence of products stemming from tertiary carbocation *iso*-**35**, e.g., *iso*-**36** and **37**,[121] indicates that carbocation **35** was probably not generated during photolysis of diazirine **26**.

It was hypothesized that the tight fit of a CyD clathrate might lessen the preference of the methyl group in **26** to reside in an equatorial position (Scheme 6). If diazirine **26** were forced to adopt an axial conformation then the hydrogen at C2 would assume an equatorial position. This misalignment of the filled MO of the
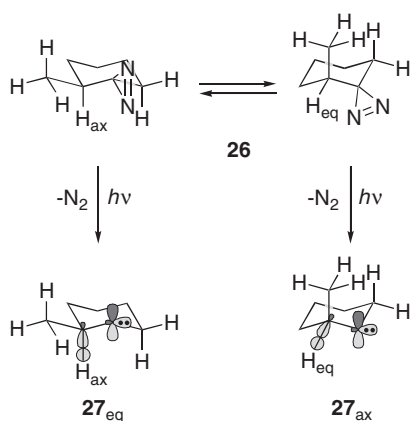
Scheme 6 Generation of two conformeric isomers of carbene **27** from an equilibrated **26**.
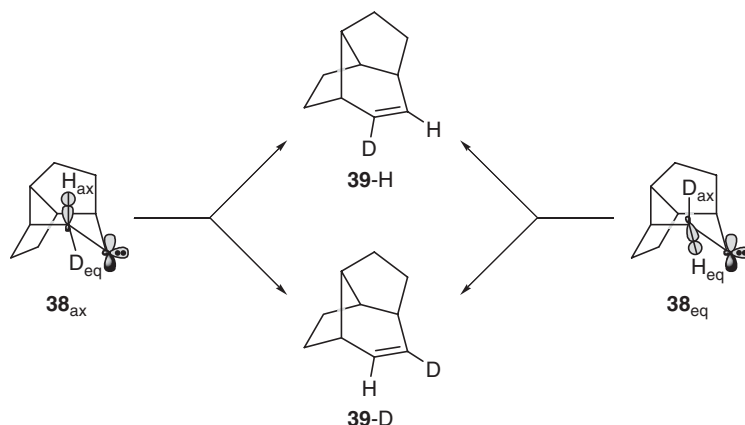
Scheme 7 Hydride migrations within tricyclo[5.3.0.0^{4,8}]decan-2-ylidene (**38**) isotopomers.

C–H bond (HOMO) with the empty orbital (LUMO) of the divalent carbon would necessarily reduce orbital overlap in **27**$_{ax}$ and concomitantly suppress the formation of alkene **28**. Of course, the conformation of **27**@CyD must resemble that of **26**@CyD, and also the classical energy barrier to a 1,2-hydride shift cannot be undermined by ultrafast quantum mechanical (QM) tunneling. The latter caveat, however, can probably be neglected at room temperature.[122] Indeed, the H/D primary kinetic isotope effect (KIE) for 1,2-H(D) shifts in scaffolded tricyclo[5.3.0.0^{4,8}]decan-2-ylidene (**38**) is quite low (Scheme 7),[112] indicating the absence of QM tunneling. Hence, the photolytic H$_{ax}$/H$_{eq}$ migration preference of 1.2 that was determined for carbene **38** is a dependable benchmark.

It should also be noted, from Scheme 6 and Fig. 9, that an axially positioned methyl group would be more susceptible to a 1,3-CH insertion. The carbon framework of axial conformer **27**$_{ax}$ mimics that of the scaffolded carbene **21**, which cannot
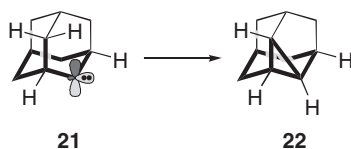
Fig. 9 Analogy of 1,3-CH insertion for 2-adamantanylidene (21).
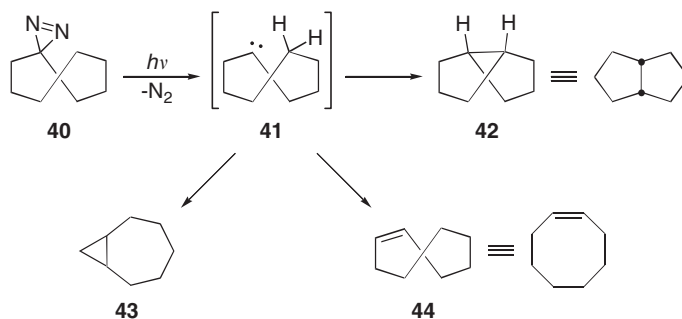
Scheme 8 Competing 1,n-CH insertions of cyclooctanylidene (41).

undergo the competing 1,2-hydride migration to afford adamantene (17). Instead, carbene 21 has been shown to have an up to 225 times enhanced 1,3-CH insertion capability to afford 2,4-didehydroadamantane (22) within supramolecular complexes, cf. NaY versus n-C_7H_{16} in Table 1. Thus, should conformational control over diazirine 26 inside CyD cavities be achieved, not only would production of the less-substituted alkene 29 be enhanced, but also the product of 1,3-CH insertion, i.e., norcarane (30), should proliferate.

Despite the hypothesis, Table 3 shows that the ratio of 28:29 was only slightly affected by solid-state supramolecular photolysis of 26@CyDs, compared to conventional methods. This is either because (1) the conformation of 26 inside CyDs is the same as in conventional media or (2) that the ring-flipped axial methyl conformer 27_{ax} is predominant, but the reaction coordinate for the QM tunneling process is independent of the torsion angle of the involved MOs in the rearrangement. However, the absence of cyclopropane 30 rules out the second conclusion in favor of the first one, according to the aforementioned analogy (Fig. 9). Finally, the lack of enhanced production of 30 is another affirmation of the crucial need for optimal orbital alignment in carbene-insertion reactions.

Cyclooctanylidene

The effect of molecular confinement on reactant conformation can be astounding. If an activated complex is deprived of its normal decay route then new reaction alternatives may arise. This is the case with the reaction intermediate cyclooctanylidene (41) (Scheme 8).[123]

Table 4 Relative allotment of long- versus short-range carbene rearrangements of cyclooctanylidene (**41**) from azicyclooctane (**40**)

Medium	**42**	**43**	**44**
n-C$_6$H$_{14}$	54	8	35
MeOH	28	9	63
α-CyD	29	14	57
β-CyD	37	9	36
γ-CyD	42	11	47
NaX	11	7	46
NaY	9	3	39
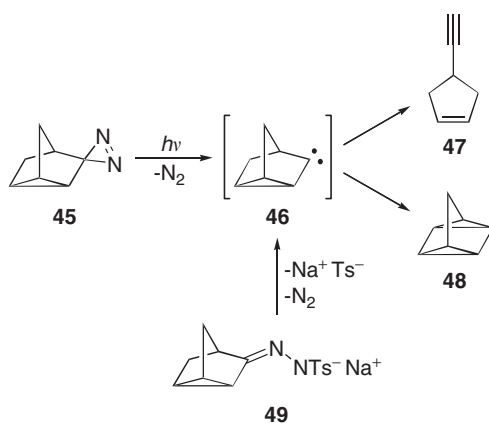
Scheme 9 Possible intramolecular reactions of 3-nortricyclanylidene (**46**).

Upon photolysis of azicyclooctane (**40**), *cis*-cyclooctene (**44**) is readily formed, but so too are products derived from intramolecular C–H insertions of carbene **41**. Of special interest is bicyclo[3.3.0]octane (**42**). Created from a 1,5-CH insertion within carbene **41** (Scheme 8),[124] *cis*-fused **42** needs space to form. Since the free volume (ΔV) of a CyD depends on the number of monomer units of which it is comprised, it is not surprising that these factors conspire to limit bicyclo[3.3.0]octane (**42**) formation when azicyclooctane (**40**) is photolyzed within α-CyD (Table 4).[42,125] The occurrence of transannular C–H insertion becomes less probable as the cavity within the molecular reaction vessel gets smaller.

3-Nortricyclanylidene

3-Nortricyclanylidene (tricyclo[2.2.1.0^{2,6}]heptan-3-ylidene, **46**) was originally generated via the Bamford–Stevens reaction of the corresponding 3-nortricyclanone *p*-tosylhydrazone sodium salt (**49**) (Scheme 9).[126] The formation of quadricyclane (tetracyclo[2.2.1.0^{2,6}.0^{3,5}]heptane, **48**) was anticipated, from an intramolecular
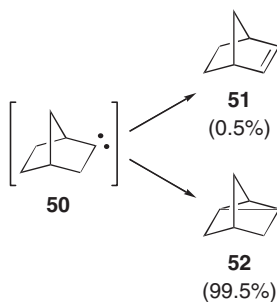
Scheme 10 Intramolecular reactions of 2-norbornanylidene (**50**).

1,3-CH insertion of carbene **46**, but was not observed. The lack of 1,3-CH insertion from carbene **46** is intriguing because 2-norbornanylidene (bicyclo[2.2.1]heptan-2-ylidene, **50**), which merely lacks the C2–C6 zero-atom bridge in **46**, undergoes 1,3-CH insertion to form nortricyclane (tricyclo[2.2.1.0²,⁶]heptane, **52**) in over 95% yield (Scheme 10).[124d,127] Instead, 4-ethynylcyclopentene (**47**) was formed via cyclopropylcarbene fragmentation (Scheme 9),[128] a process similar to the well-known Eschenmoser fragmentation.[129] The carbene rearrangement is believed to proceed through a coarctate transition state (TS) that requires strict orbital alignment of the divalent carbon with the cyclopropane ring.[130] A bilateral symmetry and an endocyclic configuration are required—both of which are perfectly exemplified by the uncomplexed carbene **46**.[131]

It is therefore reasonable to postulate that the confinement of carbene **46**, perhaps within the nanoscopic pores of CyDs and FAUs, would inhibit the fragmentation reaction and foster the 1,3-CH insertion. This reasoning is twofold: (1) there may not be enough space within the hosts' cavities for the unraveling process, **46**→**47**, and (2) distortion of the carbene's topology might concomitantly disfavor the coarctate TS and allow the 1,3-CH insertion, **46**→**48**, to finally occur.

The main challenge was to imbue CyDs and FAUs with a carbene precursor that is compatible with the hosts and the standard IC preparation. The sodium salt **49** must be kept moisture-free and, therefore, is incompatible with CyDs and FAUs, since both contain adventitious water molecules. Besides, CyD ICs are prepared from aqueous solutions! Likewise, FAU ICs are prepared by loading the zeolite with a pentane solution of the guest; salt **49** is insoluble in pentane. Therefore, a 3*H*-diazirine,[132] the previously unknown 3-azinortricyclane (3-azitricyclo[2.2.1.0²,⁶]heptane, **45**),[133] was again needed as a precursor[134] in lieu of the unsuitable Bamford–Stevens reagent **49**. Products formed during the photolysis of diazirine **45** were initially assumed to stem from carbene **46** (Scheme 11).

The α-CyD and β-CyD ICs were analyzed using ¹H NMR,[14] including 2D ROESY;[15] ICD;[17] and microanalysis.[133] The structures of the CyD ICs were concluded to be **45**@(α-CyD)₂ and (**45**@β-CyD)₂. This denotes that diazirine **45** is sandwiched between two α-CyD units but that it forms a twofold 1:1 complex with β-CyD.[18] It has been demonstrated that a guest must have an electronegative group, like −F or −OH,[15,18] to effect an opposite inclusion orientation within CyD in the
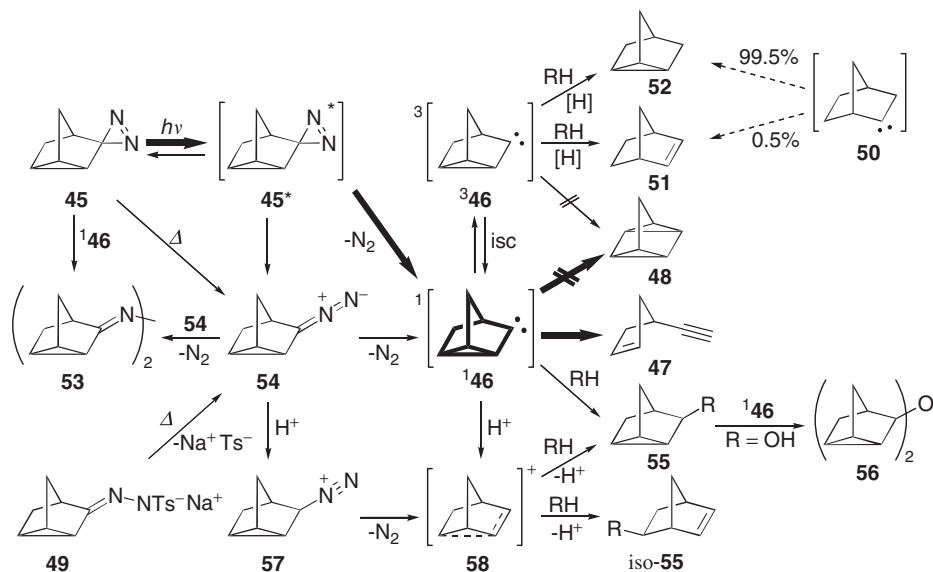
RH = (a) α-CyD, (b) β-CyD, (c) MeOH, (d) i-PrOH, (e) AcOH, (f) H_2O, (g) c-C_6H_{12}; Ts = p-$SO_2C_6H_4CH_3$.

Scheme 11   Generation of 3-nortricyclanylidene (**46**) and its subsequent reactions.

aqueous versus solid phase. Hence, it is likely that hydrophobic **45** adopts the same orientation within CyD in both phases. The FAU IC was prepared from **45** and thermally activated NaY so as to give a loading factor (⟨s⟩) of ca. 0.25, which corresponds to one filled supercage surrounded by four empty ones.[40]

Of the two possible intramolecular products, **47** and **48** (Scheme 11), only enyne **47** was observed after supramolecular photolyses of the diazirine **45** ICs. Control experiments were performed on CyDs and FAUs, both bearing **48**, to determine whether **48** is stable toward the reaction conditions. Indeed, it is. Thus, no **48** was formed from the solid-state photolyses of the **45** ICs.

The results are in accord with the proposed supramolecular structures of diazirine **45** and its hosts (vide supra). No azine, di(3-nortricyclanylidene)hydrazine (**53**), was formed upon photolysis of the dimeric **45**@(α-CyD)$_2$ complex because of a complete encapsulation of the reactive guest. Bimolecular reaction of the guests within the (**45**@β-CyD)$_2$ dimer should, of course, produce azine **53** by virtue of their geminated assemblage. Yet, the affinity of carbene **46** for the O–H bonds present in both CyDs predominated, giving O-substituted CyDs (**55a**, **55b**, iso-**55a**, and iso-**55b**), via in-nermolecular reactions,[21] that were detected using FAB MS analysis (Table 5).[133]

Clearly, the presence of azine **53** and di-3-nortricyclyl ether (3-(tricyclo[2.2.1.0^{2,6}]hep-tan-3-yloxy)tricyclo[2.2.1.0^{2,6}]heptane, **56**) after photolysis of the **45**@NaY FAU IC demonstrates that some bimolecular reactions occurred. The diffusion of ephemeral carbene **46** within the multicameral lattice was thus indicated. The principal formation of 3-nortricyclanol (tricyclo[2.2.1.0^{2,6}]heptan-3-ol, **55f**) validates that a significant amount of water still remains inside NaY even after thermal activation.

Table 5 Relative yields (%) of products formed upon photolysis of 3-azinortricyclane **(45)** in different reaction media

Medium (RH)	κ^a	52	51	53	47	55	iso-55	56	55f	ketone[b]	55:iso-55
c-C_6H_{12}	2.0	0.8	Trace	48.7	18.7	20.0		3.6	1.3	7.0	
MeOH	32.7	1.0	Trace		15.6	80.6	2.8				29
w/0.2 M DEF[c,d]		0.9	Trace		16.9	69.3	2.0				35
i-PrOH	18.3	2.1	2.3	9.9	14.2	70.4			0.6	0.5	
AcOH	6.1	Trace	Trace		14.2	84.2	1.6		Trace		53
α-CyD		14.0	Trace		6.0	80.0[e]		Trace	Trace	N/A	
β-CyD		3.8	Trace	10.0	11.5	52.0[e]		3.4	19.3	N/A	
NaY				6.0	16.3	f	1.1[g]	1.1	75.5	Trace	69

[a]Dielectric constant.
[b]3-Nortricyclanone (tricyclo[2.2.1.0^{2,6}]heptan-3-one).
[c]Diethyl fumarate.
[d]**54** + DEF → scavenger products (10.8% by GC-MS).
[e]Sum of **55** and *iso*-**55**.
[f]**55f**.
[g]*iso*-**55f**.

Although enyne **47** was previously reported to be the only product formed from carbene **46**,[126a] others were produced within the host vessels (Table 5), and also from pyrolysis of the Bamford–Stevens reagent **49**.[133] Therefore, control experiments on diazirine **45** in relevant solvents were warranted.

These trials showed a reluctance of carbene **46** to undergo intramolecular fragmentation to **47** also in the condensed phase. The hydrolysis reaction of **46** with trace amounts of H_2O, giving **55f**, was evident in each medium. Yet, the formation of 5-norbornen-2-yl-substituted products *iso*-**55** in protic media is noteworthy. Unsaturated *iso*-**55** cannot directly stem from carbene **46** (i.e., no **46**→*iso*-**55**); it derives from carbocation **58**. So, carbene protonation is indicated (**46**→**58**).[69,120,135] However, the typical product ratio that is characteristic of nonclassical carbocation **58** (i.e., **55**:*iso*-**55** = ca. 3.5) was not observed, even in the presence of diethyl fumarate (DEF).[136,137] Thus, the paucity of *iso*-**55** implies a deviation due to ion pairing of **58** with its counterion.[138]

DEF is a potent 1,3-dipolarophile that precludes the diazonium cation route (**54**→**57**→**58**) by intercepting diazo compound **54**. Indeed, the addition of DEF produced ca. 10% scavenger product which suggests that some diazo compound **54** was formed upon irradiation of diazirine **45**.[133] Barring this route should have reduced the **55**:*iso*-**55** ratio because **58** generated via pathway **49**→**54**→**57** gives an uncharacteristically[139] high ratio (**55f**:*iso*-**55f** = 24).[126g,140] That is, protonation pathway **46**→**58** should give the characteristic **55**:*iso*-**55** ratio in the presence of DEF *and* in the absence of ion pairing. It appears that carbene **46** is as Brønsted basic as its constitutional isomer 5-norbornen-2-ylidene (*iso*-**46**), which has been shown to be protonated to **58** completely under similar conditions.[141,142] The absence of unsaturated isomers of ether **56** stemming from 5-norbornen-2-ol (*iso*-**55f**) may be due to limits of detection. Alcohol **55f** has previously been shown to be stable within NaY (i.e., no **55f**→**58**).[143]

Notwithstanding, the presence of typical H-abstraction products **51** and **52** may indicate intersystem crossing (isc) of carbene **46** from the singlet to the triplet state.[144] In CyDs and cyclohexane, the concomitant oxidation of the surrounding nonpolar media rendered minor amounts of didehydro-CyDs[145] (likely via end-on abstraction of inward-pointing H3 of the nonpolar CyD cavity) and bicyclohexyl,[146] respectively. The comparatively large molar mass of the CyD could provide a collisional mechanism for the isc of **46**.[60] Nevertheless, it is surprising that the triplet state of **46** could be relatively low-lying since angle restraints[147] within the polycyclic structure and homoconjugation between the Walsh orbitals of the cyclopropane ring with the vacant p-orbital of the carbene (or carbocation)[148] center greatly favor the singlet state. Indeed, it is this interaction of the vacant p-orbital with proximate π-type bonds, i.e., bent "banana" bonds, that enhances the nucleophilicity of the carbene.

Theoretical chemistry was engaged to provide information about the propensities of carbenes to undergo exothermic 1,3-CH insertions. The transformation of **46** into **48** might be geometrically inhibited. The carbene center C1, C3, and H3 atoms describe a scalene triangle, whereby cyclopropane ring formation results from incipient C1–C3 bonding during the closely related TS (Fig. 10).

The results of AM1[149] calculations on carbene intermediates **50**, **46**, and **21** are summarized in Table 6. This semiempirical self-consistent field (SCF) method indicates the feasibility of 1,3-CH insertion of carbene **46**. Clearly, both the C1–H3 distance (r) and C1–C3–H3 angle (θ) values for **46** are intermediary, lying between those of **50** and **21**. It has previously been shown that **50** undergoes 1,3-CH insertion almost exclusively.[124d,127,150] Yet, carbene **21** mostly undergoes other types of reactions within solution.[101,103] It can, however, be compelled to undergo 1,3-CH insertion giving 2,4-didehydroadamantane (**22**) either exclusively in the gas phase[151]
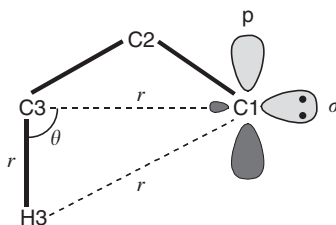
Fig. 10   The geometry of carbene 1,3-CH insertion.

Table 6   Pertinent interatomic distances within 2-norbornanylidene (**50**), 3-nortricyclanylidene (**46**), and 2-adamantanylidene (**21**) measured after geometry optimization with the AM1 Hamiltonian

Carbene	r(C1–C3) (Å)	r(C3–H3) (Å)	r(C1–H3) (Å)	θ(C1–C3–H3) (deg)
50	2.411	1.115	2.571	85.3
46	2.378	1.113	2.687	93.5
21	2.457	1.120	2.730	102.9

Table 7 Relevant enthalpies (kcal mol^{-1}) measured after geometry optimization with the AM1 Hamiltonian[a]

Carbene	$\Delta_f H^\circ$	Product	$\Delta_f H^\circ$	ΔH°
46	+133.2	**48**	+104.3	−28.9
21	+54.3	**22**	+9.3	−45.0
50	+82.3	**52**	+33.8	−48.5

[a]Ref. 133.

or appreciably in the supramolecular phase.[101,102] This mixed behavior is noteworthy. So further calculations were warranted.

According to the Bell–Evans–Polanyi principle, or the Brønsted–Evans–Polanyi rule,[152] there is a proportionality between the energy of activation (E_a) and the heat of reaction (ΔH°). That is, as a given reaction type becomes more exothermic, the E_a decreases.[153] Hence, from the Eyring equation, the rate (constant) must increase. Table 7 lists the AM1 heats of formation ($\Delta_f H^\circ$) of carbenes **46**, **21**, and **50** with those of their respective 1,3-CH insertion products, i.e., **48**,[154] **22**, and **52**. The values of ΔH° clearly show that **46→48** is the least exothermic transformation and must therefore have the highest E_a. Indeed, it must be so high that other processes, like cyclopropylcarbene fragmentation and innermolecular O–H insertion, happen more readily. Moreover, this dormant reaction of **46** should also be viewed as a 1,4-CH insertion, which is altogether uncommon—presumably due to improper orbital alignment.[124d,155] In particular, this 1,4-CH insertion would also form a cyclobutane, embedded within **48**, that is flat!

Even so, it appears that carbene **46** should also be coerced to undergo 1,3-(or 1,4-)CH insertion if an appropriate constraint is imposed. The experiments show, however, that this is not the case in the relatively spacious α-CyD dimer, in β-CyD, or in NaY supercages—all of which also have many available O–H moieties that intercept the carbene. Besides O–H insertion, the problem may be that the fragmentation,[156] whose rate likely exceeds that of 1,3-CH insertion (barring QM tunneling), needs less free volume (ΔV) for the unraveling process than originally thought. That is, when the entropy component ($\Delta S^{\ddagger}$) of the standard equation for the free energy of activation, i.e., $\Delta G^{\ddagger} = \Delta H^{\ddagger} - T\Delta S^{\ddagger}$, is rewritten in terms of volume ratios (Equation (5)), it becomes obvious that the host vessel must decrease the volume ($V^{\ddagger}$) available to the activated complex at the TS in order to increase $\Delta G^{\ddagger}$ and concomitantly inhibit the rate of **46→47**:

$$\Delta G^{\ddagger} = \Delta H^{\ddagger} - RT \ln\left(\frac{V^{\ddagger}}{V}\right) \tag{5}$$

The lifetime (τ) of 3-nortricyclanylidene (**46**) has never been measured. It is clear, however, that carbene **46** should be more stable than typical dialkylcarbenes. That is because the vacant p-orbital on the divalent carbon of **46** likely receives electron density from the bent "banana" bonds of its embedded cyclopropane ring, especially from C2.[148] The resulting electron delocalization should lower the energy of carbene
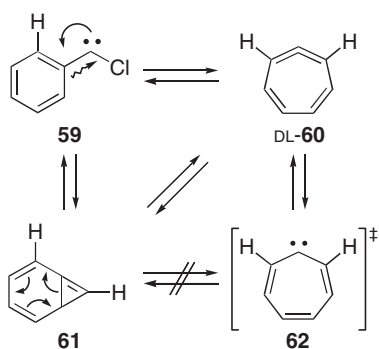
Scheme 12   Phenylcarbene (**59**) ring expansion.

46, placing it within a deeper potential energy well than that of dialkylcarbenes, which are mainly stabilized via σ-bond hyperconjugation. Presumably, carbene **46** is the species that undergoes intramolecular rearrangement in MeOH to yield modest amounts of **47** (Table 5).[157] Moreover, carbene **46** may survive long enough to form some azine **53** in lightly loaded FAU zeolites (Table 5). Therefore, it may still be possible to subdue the cyclopropylcarbene fragmentation of **46** and enhance 1,3-CH insertion under *more confining* conditions.

Phenylcarbene

The rearrangement of phenylcarbene (**59**) to 1,2,4,6-cycloheptatetraene (**60**) has been extensively studied (Scheme 12).[158] Recently, Warmuth has also reported the generation of carbene **59** within a HC.[159] Encapsulated allene **60** was protected from dimerization, so even the ^{1}H 2-D ROESY NMR spectrum of **60**@HC could be measured.

Chloro(phenyl)carbene

Photolysis of 3-chloro-3-phenyl-3H-diazirine (**63**) in Ar at 10 K generates matrix-isolated chloro(phenyl)carbene (**64**) (Scheme 13),[160] which completely undergoes ring expansion to 1-chloro-1,2,4,6-cycloheptatetraene (**65**) when exposed to short wavelength irradiation ($\lambda > 254$ nm).[161] This rearrangement proceeds by either a direct or an indirect 1,2-C shift. Indeed, neither 7-chlorobicyclo[4.1.0]hepta-2,4,6-triene (**66**) nor 2-chloro-2,4,6-cycloheptatrien-1-ylidene (**67**) was observed during prolonged irradiation ($\lambda > 338$ nm) of carbene **64**.[158c,162] Hence, cyclic allene **65** apparently derives from a direct "vinyl" migration (**64**→**65**) within the frozen argon matrix.[163,164,165] However, if 7-chlorobicyclo[4.1.0]hepta-2,4,6-triene (**66**) were to lie in a shallow potential energy well then it would be very fleeting and perhaps unobservable.[158d,e]

   Moreover, (2-chlorophenyl)carbene (*iso*-**64**) also rearranges to cyclic allene **65** (Scheme 13).[158c,160] Sander reported that the two carbenes do not interconvert,[160] which could be due to the fact that halo(phenyl)carbene **64** has a singlet GS whereas
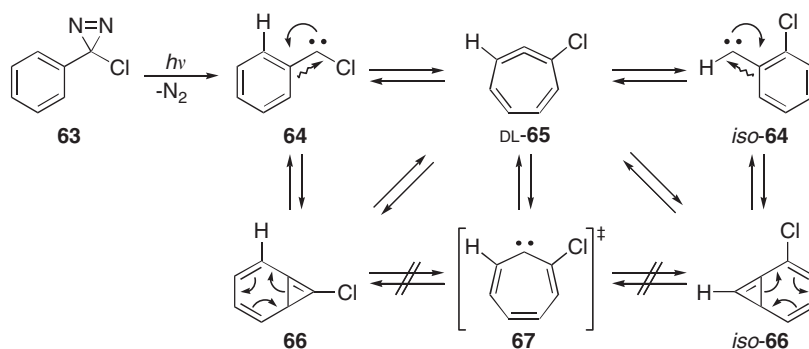
Scheme 13   Ring expansion of chloro(phenyl)carbene (**64**).

(halophenyl)carbene *iso*-**64** likely has a triplet GS. In contrast, Chapman and co-workers reported that irradiation ($\lambda > 212$ nm) of cyclic allene **65** (produced from *iso*-**64**) affords some carbene **64**.[158c] Finally, the 1,3-CH insertion of carbene **64** to 1-chloro-1*H*-cyclopropabenzene (**68**) was not observed by either research group (Equation (6)):

(6)

To determine whether room-temperature supramolecular constraint of carbene **64** could alter its reactivity by yielding ring-expanded allene **65**, triplet carbene *iso*-**64**, or benzocyclopropene **68**, diazirine **63** was prepared,[166] and then included within CyDs and FAUs prior to irradiation.[167] The photolysis of diazirine **63** is expected to form relatively "long-lived" carbene **64**, which usually decomposes via intermolecular reactions (Scheme 14).

Diazirine **63** was photolyzed in various solvents and within CyDs. The solution results are summarized in Table 8. The conventional solvents were used to gauge whatever effects the CyD hosts had on carbene **64**. Hydrocarbon solvents, like pentane (n-C_5H_{12}) and cyclohexane (c-C_6H_{12}), were used to mimic the inner cavities of CyDs, which are also nonpolar, hydrophobic environments. Tetrahydrofuran (THF) was employed because the cyclic ether resembles the D-Glc*p* monomer units of the CyDs. Moreover, since CyDs also possess many hydroxyl (O–H) groups, it seemed appropriate to perform control experiments in alcoholic solutions of diazirine **63**. Finally, chloroform (CHCl$_3$) was used to assess the spin-state of carbene **64**.

Photolysis in alcohol solution. The photolysis of diazirine **63** in anhydrous MeOH yielded (dimethoxymethyl)benzene (**73d**) (Table 8) and HCl (Scheme 15). Since the product mixture was very sensitive to moisture, it was necessary to quench the

RH = (a) α-CyD, (b) β-CyD, (c) γ-CyD, (d) MeOH, (e) i-PrOH, (f) t-BuOH, (g) H$_2$O, (h) HCl,
(i) n-C$_5$H$_{12}$ (j) c-C$_6$H$_{12}$, (k) PhH, (l) THF, (m) CHCl$_3$, (n) PhCH(OH)CH(OH)Ph (**76**).

Scheme 14   Generation of chloro(phenyl)carbene (**64**) and its subsequent reactions.

photolyzed MeOH solution with anhydrous NH$_{3(g)}$ to inhibit subsequent HCl acid-catalyzed hydrolysis of the benzaldehyde dimethyl acetal **73d** to benzaldehyde (PhCHO). To gauge the effect of ammonia on carbene **64**, anhydrous NH$_{3(g)}$ was introduced prior to photolysis of the methanolic solution of diazirine **63**. Again, only acetal **73d** was produced. Similarly, addition of anhydrous potassium carbonate (K$_2$CO$_{3(s)}$) before photolysis also made no difference.

    Condensed-phase carbenes will often react with the surrounding solvent medium, but they can also combine with other solute molecules. Indeed, these intermolecular reactions commonly occur at rates that are limited only by diffusion. Consequently, such carbenes are just short-lived intermediates. Nevertheless, arylhalocarbenes tend to have much longer lifetimes than typical alkylhalocarbenes, e.g., three orders of magnitude longer, because the latter also undergo rapid 1,2-H shift to form alkenes.[168,169] Indeed, the lifetime (τ) of singlet carbene **64** ($\lambda_{max} = 310$ nm)[170] in 2,2,4-trimethylpentane (isooctane) is reported to be ca. 3.6 μs, as determined via laser flash photolysis (LFP) of diazirine **63**.[171]

Photolysis in the supramolecular phase. The addition of benzaldehyde (PhCHO) and acetic acid (AcOH) to an *aqueous* solution of β-CyD allegedly gives 6^A,6^B-O-(benzylidene)β-CyD (**73b**) in 45% yield (Fig. 11).[172] However, that result could not be reproduced.[167] Moreover, the microanalysis, mass spectrometry, and NMR

Table 8 Relative yields (%) of products formed upon photolysis of 3-chloro-3-phenyl-3*H*-diazirine (**63**) in different reaction media

Medium (RH)	κ^a	PhCHO	69	70	72	72 h	73	Other
Neat				100				
n-C$_5$H$_{12}$ (0.01 M)	1.8	Trace	Trace	32	68^b	Trace		
n-C$_5$H$_{12}$ (0.5 M)	1.8		Trace	23	77^b			
c-C$_6$H$_{12}$ (0.1 M)	2.0	Trace	Trace	20	80^c			Trace^d
c-C$_6$H$_{12}$ (0.5 M)	2.0			61	39^c			
Benzene	2.3	2	5	83	Trace	8		2^e
CHCl$_3$ (wet)	4.7	21		Trace	33^f	46		
CDCl$_3$		3	4	57	22^g	11		3^h
THF	7.3				100^i			
i-PrOH (0.1 M)	18.3						100^j	
i-PrOH (0.5 M)	18.3	4				15	81^j	
MeOH	32.7						100^k	

^{a}Dielectric constant.
^{b}*x*-(1-Chloro-1-phenylmethyl)pentanes (**72i**).
^{c}[Chloro(cyclohexyl)methyl]benzene (**72j**).
^{d}2,5-Diphenyl-1,3,4-oxadiazole (PPD).
^{e}Biphenyl.
^{f}(1,2,2,2-Tetrachloroethyl)benzene (**72 m**).
^{g}(1,2,2,2-Tetrachloroethyl-1-*d*)benzene (**72m–d**).
^{h}Benzonitrile (PhCN).
^{i}2-(1-Chloro-1-phenylmethyl)oxolane (**72 l**).
^{j}[Di(1-methylethoxy)methyl]benzene (**73e**).
^{k}(Dimethoxymethyl)benzene (**73d**).
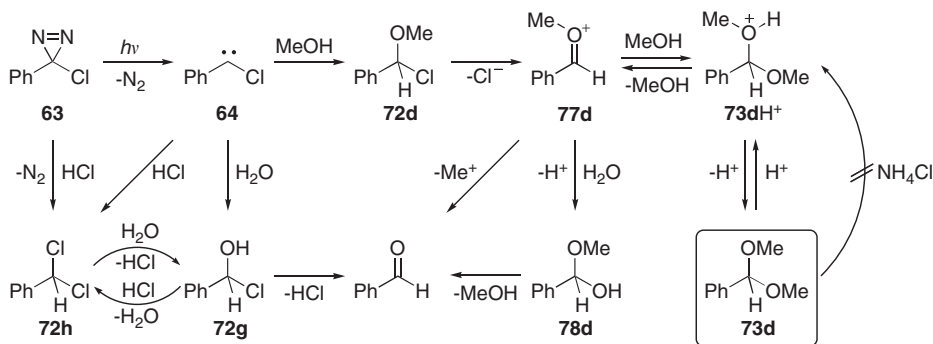
Scheme 15 Photolysis of 3-chloro-3-phenyl-3*H*-diazirine (**63**) in MeOH.

spectroscopy data that were used to characterize acetal **73b** were not made available in the patent.[172] Therefore, its formation should be regarded with skepticism. Surely, the O–H groups of the hydroxylic solvent, i.e., water, would compete with those of *β*-CyD for PhCHO. Indeed, acidified water is typically used to catabolize
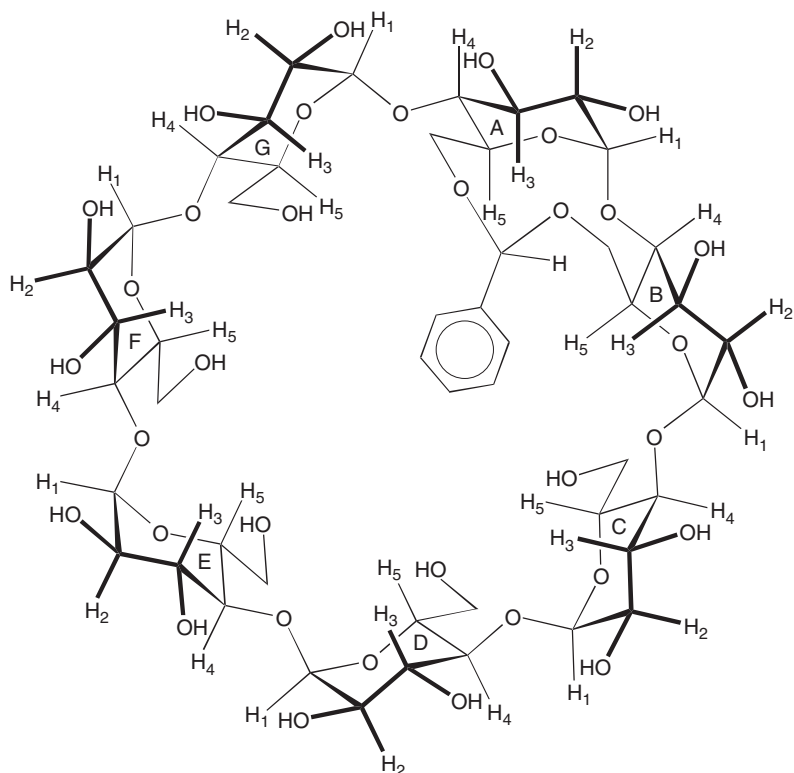
Fig. 11   Structure of $6^A,6^B$-O-(benzylidene)β-CyD (**73b**).

acetals.[173] Moreover, the preparation of benzylidene acetals from nonreducing glucopyranosides typically gives the 4,6-O-benzylidene isomers.[174] Only 2,3-O-benzylidenation of *intact* CyD should occur since they are 1,4-linked.

CyD ICs of diazirine **63** were prepared to determine the effect of supramolecular inclusion upon carbene **64**. The α-CyD and β-CyD ICs were analyzed using ^{1}H NMR,[14] including 2-D ROESY;[15] ICD;[17] and microanalysis. The integral structures of the CyD ICs were concluded to be **63@(α-CyD)$_2$** and **(63@β-CyD)$_2$**, based on their physical and chemical characteristics (vide infra). These stoichiometries denote that diazirine **63** is sandwiched between two α-CyD units, but that it forms a twofold 1:1 complex with β-CyD.[18] It has been demonstrated that a guest must have a substituent capable of hydrogen bonding, like $-F$ or $-OH$,[15,18] to effect an opposite inclusion orientation within CyD in the aqueous versus solid phase. Hence, it is likely that hydrophobic diazirine **63** adopted the same orientation within its CyD host during photolyses in both phases that were employed.

The 2-D ROESY spectrum of **63@(α-CyD)$_2$** showed cross-peaks between the phenyl ring protons of diazirine **63** with only the H3 protons of each α-CyD (Fig. 12). The absence of cross-peaks with the H5 protons of α-CyD suggests that
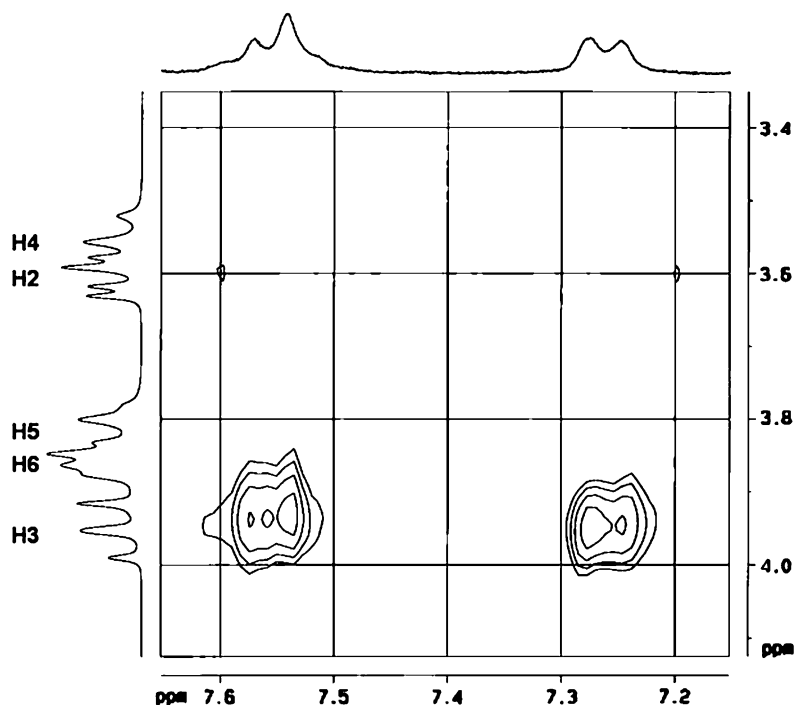
Fig. 12 250 MHz 2-D ROESY spectrum of the diazirine CyD IC **63**@(α-CyD)$_2$.

diazirine **63** does not fit entirely within one α-CyD and, therefore, requires two hosts to ensnare it. Moreover, a tight fit between the diazirine **63** guest and either α-CyD host is not indicated since neither H3 nor H5 are shifted upfield to any considerable degree, with deference to the spectrum of empty α-CyD.[14f] In contrast to the 2-D ROESY spectrum for the **63**@(α-CyD)$_2$ IC, no cross-peaks were observed for the (**63**@β-CyD)$_2$ IC.

The ICD spectrum of aqueous **63**@(α-CyD)$_2$ was also obtained.[167] Asymmetric induction by chiral α-CyD upon the chromophore of achiral diazirine **63** was made evident by the weak negative circular dichroism exhibited at $\lambda_{max} = 372$ nm. In contrast, an ICD spectrum for the (**63**@β-CyD)$_2$ complex could not be observed. However, this absence is not unexpected after considering the lack of cross-peaks in its 2-D ROESY spectrum.

Photolysis of diazirine **63** included within the cavities of CyDs presumably formed carbene **64** CyD ICs, i.e., **64**@CyD (Equation (7)). The lifetime (τ) of carbene **64** was expected to be prolonged due to the preclusion of intermolecular reactions (Scheme 14), such as azine **70** formation and solvent insertion, i.e., **64**→**72**. However, interfering *innermolecular* reactions[21] between the host and guest were indicated (vide infra). Therefore, the latent intramolecular rearrangement of carbene **64** to cyclic allene **65**, a rare transformation seen under the forbidding, low-temperature

conditions of argon matrixes,[158c,160] was not observed:

$$63@\alpha\text{-CyD: } n = 0$$
$$63@\beta\text{-CyD: } n = 1$$
$$63@\gamma\text{-CyD: } n = 2$$

$$64@\alpha\text{-CyD: } n = 0$$
$$64@\beta\text{-CyD: } n = 1$$
$$64@\gamma\text{-CyD: } n = 2$$

(7)
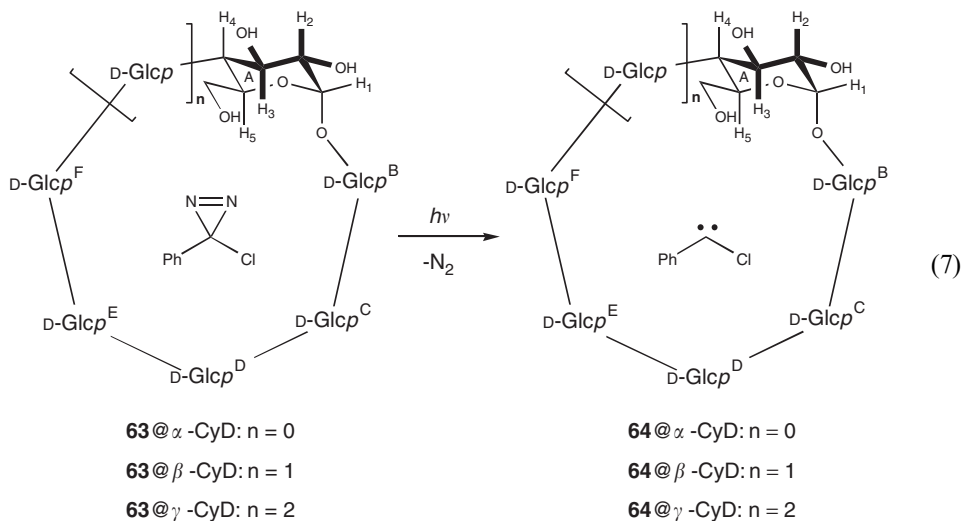
The **63**@CyD ICs were photolyzed initially in the solid state under inert atmosphere. Principally, carbene **64** appears to have reacted with adventitious H_2O, which likely resides near the perimeters of the CyDs, to give PhCHO and HCl (Equation (8); cf. Scheme 14). Of course, these hydrolysis products may also stem from **64**·CyDs, which are daughter isomers of **64**@CyDs, that derive from innermolecular reactions (Equation (9)). Therefore, such descendants were sought. Indeed, FAB MS of the products revealed the presence of new signals with masses greater than those of the unfilled CyD hosts.[167] However, the main $[M - H]^-$ signals are not attributable to **64**·CyDs, but rather to CyD hydrochlorides that could be either noncovalently bound HCl@CyD ICs or their covalently bound, constitutional isomers CyD·HCl:

$$64 + H_2O \rightarrow PhCHO + HCl \tag{8}$$

$$64 \cdot CyD + H_2O \rightarrow PhCHO + HCl + CyD \tag{9}$$

Since H_2O molecules appear to remain chemisorbed onto the "dried" CyD ICs, it was decided that photolyzing an aqueous suspension of **63**@CyD could do no further harm and might even present an advantage. In deference to the instructive MeOH results (Scheme 15), the **63**@CyD ICs were suspended in an *alkaline buffer* (to neutralize the HCl byproduct) during subsequent photolysis experiments. Hence, the HCl acid-catalyzed hydrolysis of any CyD benzylidene acetals, e.g., **73b** (Fig. 11),[172] that may have formed would be thwarted. Indeed, such detrimental effects were remedied by conducting the photolyses in aqueous alkaline buffer (vide infra).
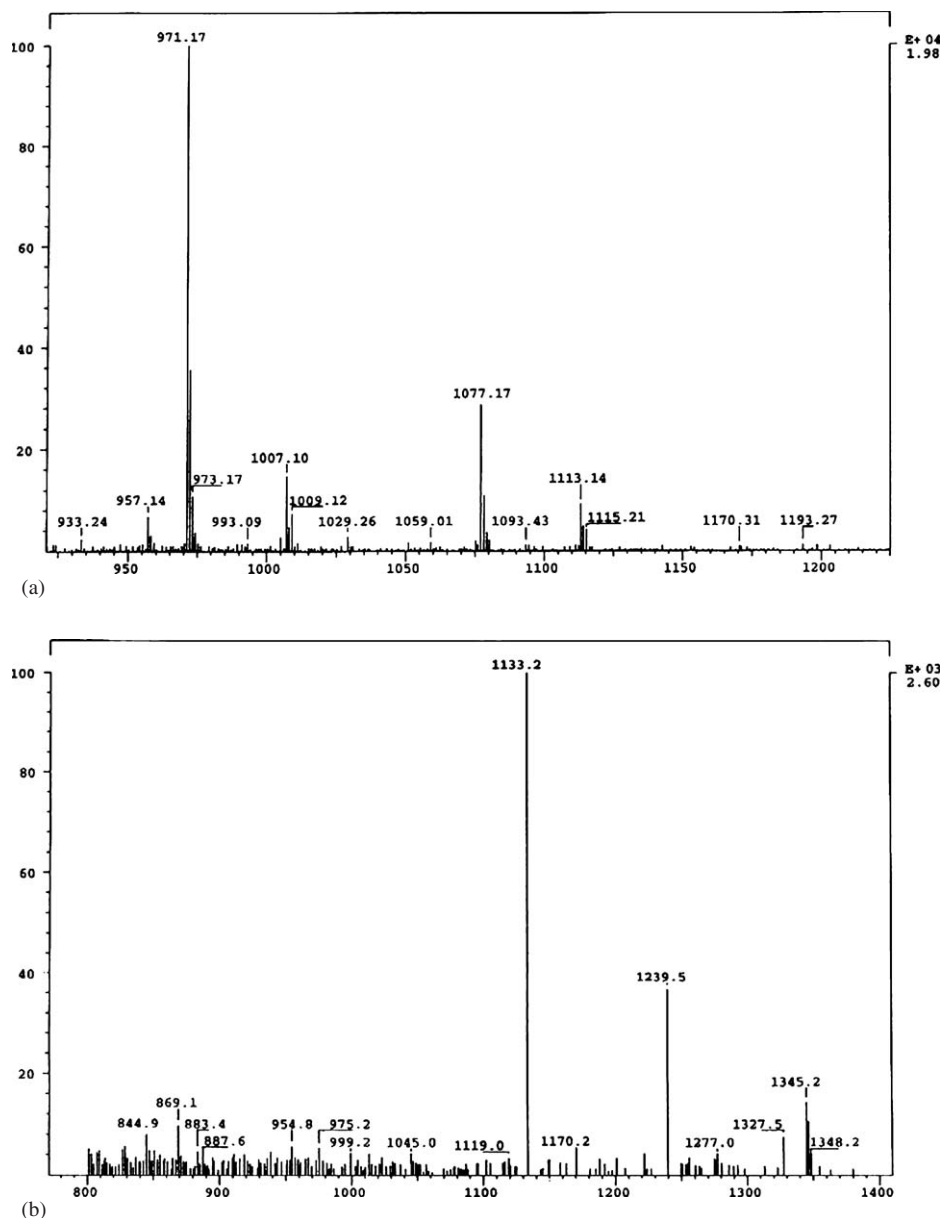
Fig. 13 FAB MS spectra of the innermolecular products formed by photolysis of diazirine **63** within (a) α-CyD and (b) β-CyD in the presence of *alkaline buffer*.

The ability of the CyDs to insulate carbene **64** from the bulk aqueous medium while still allowing HCl neutralization appears to have been realized to some extent, according to the FAB MS spectra of the **63**@CyD alkaline buffer photolysis products (Fig. 13). Still, the main [M – H]⁻ signals are not attributable to **64**·CyDs.

Instead, the spectra clearly show appreciable amounts of PhCHO·CyD (*not* PhCHO@CyD) and only traces of HCl@CyD (or CyD·HCl) byproducts. The covalently bound character of each modified PhCHO·CyD was confirmed by control experiments and RP HPLC.

Control FAB MS spectra of the independently prepared PhCHO@(α-CyD)$_2$ and (PhCHO@β-CyD)$_2$ ICs were obtained to verify that these noncovalently bound PhCHO@CyD ICs do not register a supramolecular signal.[175] Indeed, only signals from the empty CyD hosts were observed.[167] Evidently, loosely bound PhCHO is expelled from the PhCHO@CyD ICs during FAB MS analyses, leaving behind the empty CyDs.[176] This result lends support to the notion that covalently bound CyD·HCl species, rather than loosely bound HCl@CyD ICs, are responsible for the signals that were observed after unbuffered, solid-state photolyses.[167]

The FAB MS spectra of the alkaline buffer photolysis products indicated that innermolecular reactions took place between the carbene **64** guest and the CyD hosts (Fig. 13). Such supramolecular processes might entail carbene **64** insertions into the C–H bonds of the CyDs, but more likely they involve insertions into the hosts' O–H bonds (Scheme 16). However, no **64**·CyD primary insertion products, e.g., **79**, were
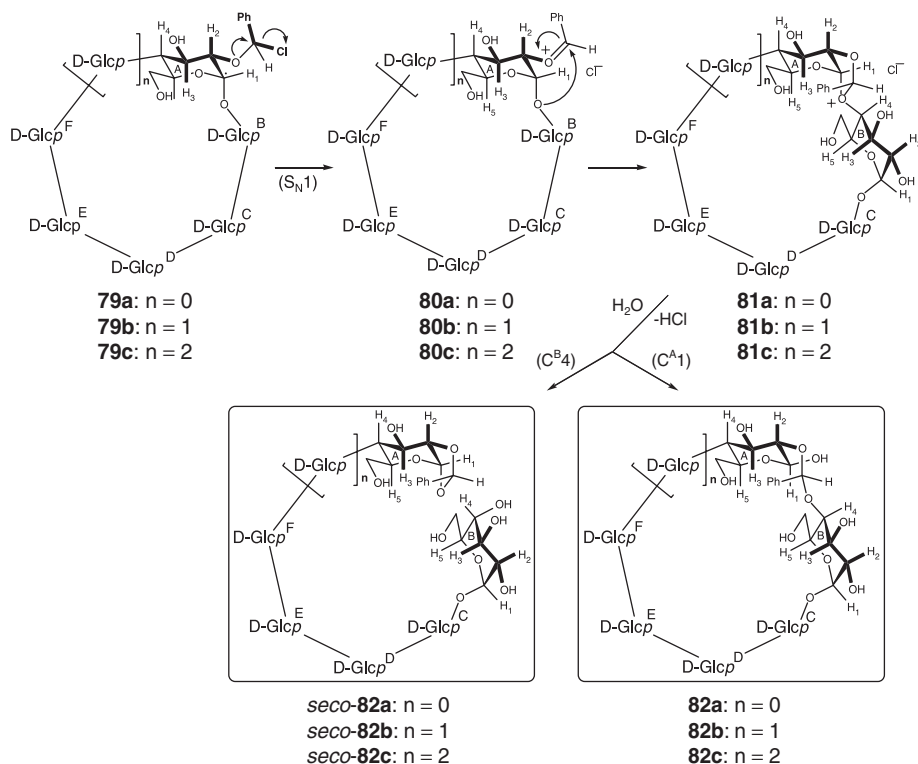
Scheme 16   Hydrolysis of O2–H inserted-CyD **79** should give FAB MS candidates **82** and/or *seco*-**82**.

Table 9 Calculated exact masses for CyD innermolecular products[a]

n	6 (α-CyD)	7 (β-CyD)[b]	8 (γ-CyD)
$[C_6(H_2O)_5]_n$	$C_{36}H_{60}O_{30}$ 972.3169	$C_{42}H_{70}O_{35}$ 1134.3698	$C_{48}H_{80}O_{40}$ 1296.4226
64@$[C_6(H_2O)_5]_n$, **64**·$[C_6(H_2O)_5]_n$, **79**	$C_{43}H_{65}ClO_{30}$ 1096.3249	$C_{49}H_{75}ClO_{35}$ 1258.3777	$C_{55}H_{85}ClO_{40}$ 1420.4306
PhCHO@$[C_6(H_2O)_5]_n$, **82**, *seco*-**82**	$C_{43}H_{66}O_{31}$ 1078.3588	$C_{49}H_{76}O_{36}$ 1240.4116	$C_{55}H_{86}O_{41}$ 1402.4645
HCl@$[C_6(H_2O)_5]_n$, $[C_6(H_2O)_5]_n$·HCl	$C_{36}H_{61}ClO_{30}$ 1008.2936	$C_{42}H_{71}ClO_{35}$ 1170.3464	$C_{48}H_{81}ClO_{40}$ 1332.3993

[a](a) $^{12}C = 12$ amu; (b) $^1H = 1.007825035$ amu; (c) $^{35}Cl = 34.96885272$ amu; (d) $^{16}O = 15.99491463$ amu. [b]For comparison, the exact mass of **73b** is 1222.4011 Da.

detected. Instead, such daughter isomers appear to have reacted further by conceptual replacement of an HCl formula unit by H_2O. To clarify the FAB MS results, a summary of exact mass calculations is given in Table 9.

To our knowledge, no carbene C–H insertion products within CyDs have ever been reported.[101,102,109,115a,125,177] Instead, formal O–H insertion appears to be preferred, and can even be chemospecific.[108,109] Therefore, one could envision an insertion into the O2–H bond by carbene **64** (Scheme 16), because the −OH groups on the C2 atoms of the smaller CyDs also point toward the apolar cavities. The resulting O–H insertion product **79** is an α-chloroether that could undergo CyD ring expansion to **82** or scission to *seco*-**82**. Cyclic **82** and acyclic *seco*-**82** might account for the observed FAB MS signal (Fig. 13, Table 9).

4 Conclusions

In summary, attempts were made to control the outcome of carbene reactions by including the corresponding 3*H*-diazirine precursors within the cavities of CyDs and FAU zeolites. Carbenes generated within the nanoscopic confines of CyDs and FAU zeolites behave differently than those arising within conventional media.

The photolyses of 2-aziadamantane (**16**) within CyD hosts give product distributions that largely depend on the type of CyD and thus the supramolecular structure. The formation of 2,4-didehydroadamantane (**22**) is essentially precluded when other inter- and innermolecular reaction channels are available. However, the formation of **22** is greatly enhanced within supramolecular confines. The amount of reduction to hydrocarbon **2**, the share of azine **19** and 2-adamantanone, the formation of CyD ethers **25a** and **25b**, and the insertion into solvent molecules yielding **25c–e** can widely be controlled by geometry and composition of the ICs. This very interesting influence of the host as mediator can be observed especially well for the photolyses of **16**, which primarily yield carbene **21**—a species that has no intramolecular pathways to stabilization.

Photolyses of 1-azi-2-methylcyclohexane (**26**) were performed within α-, β- and γ-CyDs to alter the selectivity of the carbene intermediate, 2-methylcyclohexanylidene (**27**). It was hypothesized that constriction of asymmetric carbene **27** within the CyD hosts would suppress the formation of 1-methylcyclohexene (**28**) and concomitantly enhance that of 3-methylcyclohexene (**29**) and bicyclo[4.1.0]heptane (**30**). However, no **30** was observed.

Photolyses of 3-azinortricyclane (**45**) were conducted within CyDs and FAU zeolites to alter the selectivity of the carbene intermediate, 3-nortricyclanylidene (**46**). It was hypothesized that constriction of carbene **46** within each host would suppress the formation of 4-ethynylcyclopentene (**47**) and concomitantly enhance that of quadricyclane (**48**). But only **47** was observed. Since CyD innermolecular products were also formed, control experiments in relevant solvents were performed. Both triplet-state participation and the Brønsted basicity of carbene **46** were hinted at.

Photolyses of 3-chloro-3-phenyl-3*H*-diazirine (**63**) were carried out within CyDs and FAU zeolites to foster the ring expansion of the carbene intermediate, chloro(phenyl)carbene (**64**). However, benzaldehyde (PhCHO) was formed instead of products derived from 1-chloro-1,2,4,6-cycloheptatetraene (**65**). Since CyD innermolecular products were also formed, control experiments in relevant solvents were performed. The true structure of the innermolecular product that was formed in alkaline buffer, and then observed via FAB MS and RP HPLC, has not yet been determined. The ability of the basic medium to preserve the innermolecular product and reduce the amount of PhCHO formed seems to indicate that the latter stems from the former, e.g., O–H insertion product **82**. However, the exact mechanism of PhCHO formation within the CyD ICs could not be pinpointed.

Acknowledgments

References

1. Reese, K.M. (2001). *Chem. Eng. News* **79** (21), 96
2. Wöhler, F. (1849). *Ann. Chem. Pharm.* **69**, 294–300
3. (a) Pedersen, C.J. (1967). *J. Am. Chem. Soc.* **89**, 2495–2496; (b) Pedersen, C.J. (1967). *J. Am. Chem. Soc.* **89**, 7017–7036
4. In ethylene glycol, a usual solvent, F⁻ is solvated via hydrogen bonding. Also, halide–halide exchange reaches an equilibrium. Thus, Le Châtelier's principle is employed to increase the yield, e.g., product removal
5. (a) March, J. (ed.) (1992). *Advanced Organic Chemistry* (4th edn), pp. 430–431. Wiley, New York; (b) Hassner, A. and Stumer, C. (1994). *Organic Syntheses Based on Name Reactions and Unnamed Reactions*. Pergamon, Tarrytown, NY p. 121

6. Carey, F.A. (1996). *Organic Chemistry* (3rd edn), pp. 312–313, 649–650 McGraw-Hill, New York

7. (a) Cram, D.J. and Cram, J.M. (1994). *Container Molecules and Their Guests*. Royal Society of Chemistry, Cambridge; (b) Cram, D.J. (1988). *Science* **240**, 760–767; (c) Cram, D.J. (1988). *J. Inclusion Phenom.* **6**, 397–413

8. Rebek Jr., J. (2000). *Chem. Commun. (Cambridge)*, 637–643

9. (a) Byrum, A.L. (2001). *Chem. Eng. News* **79** (30), 38–40; (b) Byrum, A. (2001). *Chem. Eng. News* **79** (26), 10

10. Schroeder, H.E. and Pedersen, C.J. (1988). *Pure Appl. Chem.* **60**, 445–451

11. 1987 Nobel lectures: (a) Cram, D.J. (1988). *Angew. Chem., Int. Ed. Engl.* **27**, 1009–1020; (b) Pedersen, C.J. (1988). *Angew. Chem., Int. Ed. Engl.* **27**, 1021–1027; (c) Lehn, J.-M. (1988). *Angew. Chem., Int. Ed. Engl.* **27**, 89–112

12. Cram, D.J., Karbach, S., Kim, Y.H., Baczynskyj, L., Marti, K., Sampson, R.M. and Kalleymeyn, G.W. (1988). *J. Am. Chem. Soc.* **110**, 2554–2560

13. The root word *carcer* means "prison" in Latin: Neufeldt, V. (1988). *Webster's New World*^{TM} *Dictionary* (3rd college edn), p. 681. Simon & Schuster, New York

14. (a) Casu, B., Reggiani, M., Gallo, G.G. and Vigevani, A. (1966). *Tetrahedron* **22**, 3061–3083; (b) Demarco, P.V. and Thakkar, A.L. (1970). *J. Chem. Soc. D*, 2–4; (c) MacNicol, D.D. (1975). *Tetrahedron Lett.*, 3325–3326; (d) Chung, W.-S., Turro, N.J., Silver, J. and le Noble, W.J. (1990). *J. Am. Chem. Soc.* **112**, 1202–1205; (e) Qi, Z.H., Mak, V., Diaz, L., Grant, D.M. and Chang, C.-J. (1991). *J. Org. Chem.* **56**, 1537–1542; (f) Salvatierra, D., Jaime, C., Virgili, A. and Sánchez-Ferrando, F. (1996). *J. Org. Chem.* **61**, 9578–9581

15. (a) Alderfer, J.L. and Eliseev, A.V. (1997). *J. Org. Chem.* **62**, 8225–8226; (b) Ivanov, P.M., Salvatierra, D. and Jaime, C. (1996). *J. Org. Chem.* **61**, 7012–7017

16. Kupfer, R., Poliks, M.D. and Brinker, U.H. (1994). *J. Am. Chem. Soc.* **116**, 7393–7398

17. (a) Krois, D. and Brinker, U.H. (1998). *J. Am. Chem. Soc.* **120**, 11627–11632; (b) Bobek, M.M., Krois, D. and Brinker, U.H. (2000). *Org. Lett.* **2**, 1999–2002

18. For an example employing X-ray diffraction upon a crystalline diazirine@CyD IC, see: Bobek, M.M., Giester, G., Kählig, H. and Brinker, U.H. (2000). *Tetrahedron Lett.* **41**, 5663–5667

19. Arnold, B.R. and Michl, J. (1993). *J. Phys. Chem.* **97**, 13348–13354

20. Cram, D.J., Tanner, M.E. and Thomas, R. (1991). *Angew. Chem., Int. Ed. Engl.* **30**, 1024–1027

21. (a) Warmuth, R. (1997). *Angew. Chem., Int. Ed. Engl.* **36**, 1347–1350; (b) Warmuth, R. (1998). *Chem. Commun. (Cambridge)*, 59–60; (c) Bradley, D. (1998). *Chem. Br.* **34** (3), 16; (d) Warmuth, R. (2000). *J. Inclusion Phenom. Macrocycl. Chem.* **37**, 1–38; (e) Warmuth, R. (2001). *Eur. J. Org. Chem.*, 423–437

22. For MCSCF and CI ab initio calculations of *o*-, *m*-, and *p*-benzyne, see: Wierschke, S.G., Nash, J.J. and Squires, R.R. (1993). *J. Am. Chem. Soc.* **115**, 11958–11967

23. Villiers, A. (1891). *C. R. Hebd. Seances Acad. Sci.* **112**, 536–538

24. Typically, starch is composed of 80% amylopectin, i.e., insoluble poly($\alpha(1\rightarrow4)$-/$\alpha(1\rightarrow6)$-D-Glc*p*) and 20% amylose, i.e., soluble poly($\alpha(1\rightarrow4)$-D-Glc*p*)

25. Feiters, M.C. (1995). In *Comprehensive Supramolecular Chemistry*, Lehn, J.-M. (ed.), Chapter 11, vol. 10. Pergamon, New York

26. Schardinger, F. (1904). *Wien. Klin. Wochenschr.* **17**, 207–209

27. (a) Cyclodextrins: D'Souza, V.T. and Lipkowitz, K.B. (eds) (1998). *Chemical Reviews*, vol. **98** (5), pp. 1741–2076. American Chemical Society, Washington, DC; (b) Wenz, G. (1994). *Angew. Chem., Int. Ed. Engl.* **33**, 803–822; (c) Saenger, W. (1980). *Angew. Chem., Int. Ed. Engl.* **19**, 344–362; (d) Bender, M.L. and Komiyama, M. (1978). *Cyclodextrin Chemistry*. Springer, Berlin

28. (a) Compare to a basketball net; (b) δ-CyD *[85220-53-7]*. is not toroidal

29. Cramer, F. and Henglein, F.M. (1957). *Chem. Ber.* **90**, 2561–2571

30. Tee, O.S., Gadosy, T.A. and Giorgi, J.B. (1996). *Can. J. Chem.* **74**, 736–744

31. Kano, K., Tamiya, Y. and Hashimoto, S. (1992). *J. Inclusion Phenom. Mol. Recognit. Chem.* **13**, 287–293

32. Bobek, M.M. (2000). *Ph.D. Dissertation*. Universität Wien, Austria

33. Cronstedt, A.F. (1756). *K. Sven. Vetenskapsakad. Handl., Stockholm* **17**, 120–123

34. Manly, R. and Holmes, J. (1989). *New Sci.* **121** (1657), 39–43

35. Pough, F.H. (1988). In *A Field Guide to Rocks and Minerals*, Peterson, R.T. (ed.) (4th edn), pp. 232–238. Houghton Mifflin, Boston

36. (a) Kresge, C.T., Leonowicz, M.E., Roth, W.J., Vartuli, J.C. and Beck, J.S. (1992). *Nature* **359**, 710–712; (b) Beck, J.S., Vartuli, J.C., Roth, W.J., Leonowicz, M.E., Kresge, C.T., Schmitt, K.D., Chu, C.T.-W., Olson, D.H., Sheppard, E.W., McCullen, S.B., Higgins, J.B. and Schlenker, J.L. (1992). *J. Am. Chem. Soc.* **114**, 10834–10843

37. Ramamurthy, V. (1991). In *Photochemistry in Organized and Constrained Media*, Ramamurthy, V. (ed.), Chapter 10. VCH, New York

38. Ramamurthy, V., Corbin, D.R., Turro, N.J., Zhang, Z. and Garcia-Garibay, M.A. (1991). *J. Org. Chem.* **56**, 255–261

39. Ramamurthy, V. and Turro, N.J. (1995). *J. Inclusion Phenom. Mol. Recognit. Chem.* **21**, 239–282

40. The limit of the sequence 1/5, 2/9, 3/13, 4/17,…,$n/(5n-(n-1)) = n/(4n+1)$ for infinite n is 0.25

41. Garcia-Garibay, M.A., Zhang, Z. and Turro, N.J. (1991). *J. Am. Chem. Soc.* **113**, 6212–6218

42. (a) Brinker, U.H. and Rosenberg, M.G. (1998). In *Advances in Carbene Chemistry*, Brinker, U.H. (ed.), vol. 2 pp. 29–44, JAI, Stamford, CT; (b) Kirmse, W. (2005). *Angew. Chem. Int. Ed.* **44**, 2476–2479

43. Szejtli, J. (1999). *Chem. Intell.* **5** (3), 38–45

44. McCoy, M. (1999). *Chem. Eng. News* **77** (9), 25–27 (see p. 26)

45. Heating NH_4X and NH_4Y zeolites expels $NH_3(g)$, yielding HX and HY zeolites, respectively

46. (a) Jacobs, P.A. and Beyer, H.K. (1979). *J. Phys. Chem.* **83**, 1174–1177; (b) Ward, J.W. (1967). *J. Catal.* **9**, 225–236

47. Hamilton, A.D. (1990). *J. Chem. Educ.* **67**, 821–828

48. 1902 Nobel Laureate in Chemistry "in recognition of the extraordinary services he has rendered by his work on sugar and purine syntheses."

49. Wedin, R. (2002). In *Chemistry*, Woods, M. (ed.), pp. 15–17, American Chemical Society, Washington, DC, Winter

50. Breslow, R. (1982). *Science* **218**, 532–537

51. Colby, D.S. (1985). *Biochemistry: A Synopsis*, pp. 56–63, Lange, Los Altos, CA

52. (a) Liu, L. and Breslow, R. (2002). *J. Am. Chem. Soc.* **124**, 4978–4979; (b) Liu, L. (2002). *Chem. Eng. News* **80** (19), 34

53. van Herwijnen, H.W.G. and Brinker, U.H. (2001). *J. Org. Chem.* **66**, 2874–2876

54. Harris, K.D.M. (1993). *Chem. Br.* **29**, 132–136

55. (a) Poon, T., Turro, N.J., Chapman, J., Lakshminarasimhan, P., Lei, X., Adam, W. and Bosio, S.G. (2003). *Org. Lett.* **5**, 2025–2028; (b) Liu, X., Chu, G., Moss, R.A., Sauers, R.R. and Warmuth, R. (2005). *Angew. Chem. Int. Ed.* **44**, 1994–1997; (c) Dagani, R. (2005). *Chem. Eng. News* **83** (9), 12

56. (a) Skell, P.S. and Woodworth, R.C. (1956). *J. Am. Chem. Soc.* **78**, 4496–4497 (Correction: (1956). *J. Am. Chem. Soc.* **78**, 6427); (b) Woodworth, R.C. and Skell, P.S. (1959). *J. Am. Chem. Soc.* **81**, 3383–3386; (c) Skell, P.S. (1985). *Tetrahedron* **41**, 1427–1428; (d), Su, M.-D. (1996). *J. Phys. Chem.* **100**, 4339–4349

57. (a) Forrester, A.R. and Sadd, J.S. (1976). *J. Chem. Soc. Chem. Commun.*, 631–632; (b) Forrester, A.R. and Sadd, J.S. (1982). *J. Chem. Soc., Perkin Trans.* 2, 1273–1278

58. Hoffmann, R., Zeiss, G.D. and Van Dine, G.W. (1968). *J. Am. Chem. Soc.* **90**, 1485–1499
59. Matsen, F.A. and Klein, D.J. (1969). *Adv. Photochem.* **7**, 1–55 (see pp. 29–32)
60. Wentrup, C. (1984). *Reactive Molecules* pp. 182–183, Wiley, New York
61. Turro, N.J. (2000). *Acc. Chem. Res.* **33**, 637–646
62. (a) Bantu, R.N., Kupfer, R. and Brinker, U.H. (1994). *Tetrahedron Lett.* **35**, 5117–5120; (b) Bantu, N.R., Kupfer, R. and Brinker, U.H. (1994). *Abstr. Pap.– Am. Chem. Soc.*, 208th, ORGN 182 (c) Takahashi, K. (1998). *Chem. Rev.* **98**, 2013–2033 (see p. 2029)
63. (a) Syamala, M.S., Nageswer Rao, B. and Ramamurthy, V. (1988). *Tetrahedron* **44**, 7234–7242; (b) Pitchumani, K., Warrier, M. and Ramamurthy, V. (1996). *J. Am. Chem. Soc.* **118**, 9428–9429; (c) Xie, R.-Q., Liu, Y.-C. and Lei, X.-G. (1992). *Res. Chem. Intermed.* **18**, 61–69; (d) Pitchumani, K., Velusamy, P., Durai Manickam, M.C. and Srinivasan, C. (1994). *Proc. Indian Acad. Sci., Chem. Sci.* **106**, 49–57
64. Bradley, D. (1992). *Chem. Br.* **28**, 870
65. Brinker, U.H. and König, L. (1984). *Chem. Lett.* 45–48
66. (a) Nickon, A. (1993). *Acc. Chem. Res.* **26**, 84–89; (b) Moss, R.A. and Ma, W. (1999). *Tetrahedron Lett.* **40**, 5101–5104; (c) Moss, R.A., Ma, W., Yan, S. and Zheng, F. (2001). *Tetrahedron Lett.* **42**, 8923–8926; (d) Merrer, D.C. and Moss, R.A. (2001). In *Advances in Carbene Chemistry*, Brinker, U.H. (ed.), vol. 3, pp. 53–113. Elsevier, Amsterdam
67. Peon, J., Polshakov, D. and Kohler, B. (2002). *J. Am. Chem. Soc.* **124**, 6428–6438
68. (a) Hine, J. (1964). *Divalent Carbon*. Ronald, New York; (b) Kirmse, W. (1969). *Carbene, Carbenoide, und Carbenanaloge*. Verlag Chemie, Weinheim; (c) Kirmse, W. (1971). *Carbene Chemistry*. (2nd edn) Academic, New York; (d) Jones Jr., M. and Moss, R.A. (eds) (1973). *Carbenes*, vol. 1. Wiley, New York; (e) Jones Jr., M. and Moss, R.A. (eds) (1975). *Carbenes*, vol. 2. Wiley, New York; (f) Jones Jr., M. (1976). *Sci. Am.* **234** (2), 101–113; (g) Jones, W.M. and Brinker, U.H. (1977). In *Pericyclic Reactions*, Marchand, A.P. and Lehr, R.E. (eds), vol. 1, Chapter 3. Academic, New York; (h) Regitz, M. (ed.) (1989). *Methoden der Organischen Chemie* (*Houben-Weyl*), vol. E19b. Thieme, Stuttgart; (i) Brinker, U.H. (ed.) (1994). *Advances in Carbene Chemistry*, vol. 1. JAI, Greenwich, CT; (j) Brinker, U.H. (ed.) (1998). *Advances in Carbene Chemistry*, vol. 2. JAI, Stamford, CT; (k) Brinker, U.H. (ed.) (2001). *Advances in Carbene Chemistry*, vol. 3. Elsevier, Amsterdam; (l) Helson, H.E. and Jorgensen, W.L. (1994). *J. Org. Chem.* **59**, 3841–3856; (m) Moss, R.A., Platz, M.S. and Jones Jr., M. (eds) (2004). *Reactive Intermediate Chemistry*. Wiley, New York
69. Kirmse, W. (2001). In *Advances in Carbene Chemistry*, Brinker, U.H. (ed.), vol. 3, pp. 1–51. Elsevier, Amsterdam
70. Closs, G.L. and Rabinow, B.E. (1976). *J. Am. Chem. Soc.* **98**, 8190–8198
71. Jackson, J.E. and Platz, M.S. (1994). In *Advances in Carbene Chemistry*, Brinker, U.H. (ed.), vol. 1, pp. 89–160. JAI, Greenwich, CT
72. Montanari, F., Quici, S. and Banfi, S. (1995). In *Comprehensive Supramolecular Chemistry*, Lehn, J.-M. (ed.), vol. 10, Chapter 13. Pergamon, New York
73. (a) Wynberg, H. (1960). *Chem. Rev.* **60**, 169–184; (b) Wynberg, H. and Meijer, E.W. (1982). *Org. React.* (*NY*) **28**, 1–36; (c) Hassner, A. and Stumer, C. (1994). *Organic Syntheses Based on Name Reactions and Unnamed Reactions*, p. 314. Pergamon, Tarrytown, NY; (d) March, J. (ed.) (1992). *Advanced Organic Chemistry* (4th edn), pp. 544–545. Wiley, New York
74. Direct S_N2 displacement of $CHCl_3$ by PhO^- has been dismissed, cf. Ref. 73a. Moreover, Coulombic repulsion between Cl_3C^- and PhO^- would hamper that interaction. Finally, C–H insertion of PhO^- by carbene-like CO, derived from the base-mediated hydrolysis of CCl_2, cannot be ruled out a priori, cf. Gattermann–Koch reaction (CO) and Kolbe–Schmitt reaction (CO_2). However, the presence of abnormal, ring-expanded aryl chlorides supports the involvement of CCl_2
75. Jiménez, M.-C., Miranda, M.-A. and Tormos, R. (1995). *Tetrahedron* **51**, 5825–5830

76. (a) Ohara, M. and Fukuda, J. (1978). *Pharmazie* **33**, 467; (b) Komiyama, M. and Hirai, H. (1981). *Bull. Chem. Soc. Jpn.* **54**, 2053–2056; (c) Komiyama, M. and Hirai, H. (1983). *J. Am. Chem. Soc.* **105**, 2018–2021

77. Joshi, G.C., Singh, N. and Pande, L.M. (1972). *Tetrahedron Lett.*, 1461–1464

78. Tabushi, I., Yoshida, Z.-I. and Takahashi, N. (1971). *J. Am. Chem. Soc.* **93**, 1820

79. In the absence of α-CyD, *p*-**5**/*o*-**5** = 0.71 (Ref. 76b), which is close to the 0.50 theoretical limit

80. (a) Aquino, A.-M., Abelt, C.-J., Berger, K.-L., Darragh, C.M., Kelley, S.-E. and Cossette, M.-V. (1990). *J. Am. Chem. Soc.* **112**, 5819–5824; (b) Acquavella, M.-F., Evans, M.-E., Farraher, S.-W., Névoret, C.-J. and Abelt, C.-J. (1994). *J. Org. Chem.* **59**, 2894–2897

81. (a) Abelt, C.J. and Pleier, J.M. (1988). *J. Org. Chem.* **53**, 2159–2162; (b) Abelt, C.J., Lokey, J.S. and Smith, S.H. (1989). *Carbohydr. Res.* **192**, 119–130; (c) Smith, S.H., Forrest, S.M., Williams Jr., D.C., Cabell, M.F., Acquavella, M.F. and Abelt, C.J. (1992). *Carbohydr. Res.* **230**, 289–297; (d) Abelt, C.J. (1992). *Insertion Reactions of Cyclodextrin-Bound Carbenes*; final report to the Petroleum Research Fund on Grant 22092–B4; College of William and Mary, Williamsburg, VA; (e) Abelt, C.J. (1992). *Minutes Int. Symp. Cyclodextrins, 6th*, 649–654; (1994). *Chem. Abstr.* **121**, 83794

82. (a) White III, W.R. and Platz, M.S. (1992). *J. Org. Chem.* **57**, 2841–2846; (b) Modarelli, D.A., Morgan, S. and Platz, M.S. (1992). *J. Am. Chem. Soc.* **114**, 7034–7041; (c) Yamamoto, N., Bernardi, F., Bottoni, A., Olivucci, M., Robb, M.A. and Wilsey, S. (1994). *J. Am. Chem. Soc.* **116**, 2064–2074

83. Wentrup, C. (1984). *Reactive Molecules* pp. 139–142, Wiley, New York

84. March, J. (ed.) (1992). *Advanced Organic Chemistry* (4th edn), p. 355. Wiley, New York

85. From the Förster cycle, $K_a^*(\mathbf{6^*} \cdot H^+) = K_a(\mathbf{6} \cdot H+) . \exp(h\Delta\nu/RT)$. For examples, see: (a) Förster, T. (1950). *Z. Elektrochem. Angew. Phys. Chem.* **54**, 42–62; (b) Klöpffer, W. (1977). *Adv. Photochem.* **10**, 311–358; (c) Frey, W., Laermer, F. and Elsaesser, T. (1991). *J. Phys. Chem.* **95**, 10391–10395

86. (a) Isaev, S.D., Zhalnina, G.G., Murzinova, Z.N., Lastovenko, S.I. and Yurchenko, A.G. (1988). *J. Org. Chem. USSR* (*Transl. of Zh. Org. Khim.*) **24**, 126–131; (b) Isaev, S.D., Kulik, N.I. and Yurchenko, A.G. (1993). *Theor. Exp. Chem.* (*Transl. Teor. Eksp. Khim.*) **29**, 213–216

87. Chang, C.-D. and Chu, C.-T.-W. (1982). *J. Catal.* **74**, 203–206

88. van Hooff, J.H.C. (1983). *J. Catal.* **79**, 242–243

89. Anderson, M.W. and Klinowski, J. (1989). *Nature* **339**, 200–203

90. Jacoby, M. (2002). *Chem. Eng. News* **80** (16), 5

91. Dagani, R. (2002). *Chem. Eng. News* **80** (24), 32–35

92. (a) Freemantle, M. (2001). *Chem. Eng. News* **79** (33), 11; (b) Freemantle, M. (1999). *Chem. Eng. News* **77** (45), 19; (c) Freemantle, M. (2000). *Chem. Eng. News* **78** (19), 57; (d) Freemantle, M. (2001). *Chem. Eng. News* **79** (24), 22; (e) Dagani, R. (1994). *Chem. Eng. News* **72** (18), 20–22; (f) Dagani, R. (1991). *Chem. Eng. News* **69** (4), 19–20; (g) Krishnamurthy, S.S. (1991). *Curr. Sci.* **60**, 619–620; (i) Bucher, G. and Winkler, M. (2002). *Nachr. Chem.* **50**, 289–293; (j) Hopkins, J.M., Bowdridge, M., Robertson, K.N., Cameron, T.S., Jenkins, H.A. and Clyburne, J.A.C. (2001). *J. Org. Chem.* **66**, 5713–5716

93. (a) Tomioka, H., Iwamoto, E., Itakura, H. and Hirai, K. (2001). *Nature* **412**, 626–628; (b) Tomioka, H., Nozaki, Y., Iwamoto, E. and Hirai, K. (2000). *Proceedings of the Conference on Reactive Intermediates and Unusual Molecules*, Bobek, M.M. (ed.), p. 3, Eigenverlag, Vienna; (c) Hirai, K. and Tomioka, H. (1999). *J. Am. Chem. Soc.* **121**, 10213–10214; (d) Tomioka, H. (1998). In *Advances in Carbene Chemistry*, Brinker, U.H. (ed.), vol. 2, pp. 175–214. JAI, Stamford, CT; (e) Tomioka, H. (1997). *Acc. Chem. Res.* **30**, 315–321; (f) Tomioka, H., Watanabe, T., Hirai, K., Furukawa, K., Takui, T. and Itoh, K. (1995). *J. Am. Chem. Soc.* **117**, 6376–6377

94. In triplet-state ESR, the zero-field splitting parameter D represents the slight energy difference between the $T_\pm$ and T_0 states, e.g., $D(11) = 3.0 \times 10^{-4}\,\text{kcal mol}^{-1}$, and is inversely related to the distance of the two unpaired electrons. See: (a) Turro, N.J. (1991). *Modern Molecular Photochemistry*, pp. 551–552. University Science Books, Mill Valley, CA; (b) Wentrup, C. (1984). *Reactive Molecules*, pp. 46–48, 176–180. Wiley, New York

95. (a) Breslow, R. (1957). *J. Am. Chem. Soc.* **79**, 1762–1763; (b) Breslow, R. (1958). *J. Am. Chem. Soc.* **80**, 3719–3726; (c) Wanzlick, H.-W. and Kleiner, H.-J. (1964). *Angew. Chem., Int. Ed. Engl.* **3**, 65; (d) Olofson, R.-A., Landesberg, J.-M., Houk, K.N. and Michelman, J.-S. (1966). *J. Am. Chem. Soc.* **88**, 4265–4266; (e) Hoffmann, R.W., Hagenbruch, B. and Smith, D.M. (1977). *Chem. Ber.* **110**, 23–36; (f) Sugimoto, H. and Hirai, K. (1985). *Tetrahedron Lett.* **26**, 883–886; (g) Kluger, R. (1987). *Chem. Rev.* **87**, 863–876

96. (a) Arduengo III, A.J., Harlow, R.L. and Kline, M. (1991). *J. Am. Chem. Soc.* **113**, 361–363; (b) Arduengo III, A.J., Dias, H.V.R., Dixon, D.A., Harlow, R.L., Klooster, W.T. and Koetzle, T.F. (1994). *J. Am. Chem. Soc.* **116**, 6812–6822; (c) Olofson, R.A., Thompson, W.R. and Michelman, J.S. (1964). *J. Am. Chem. Soc.* **86**, 1865–1866; (d) Staab, H.A., Irngartinger, H., Mannschreck, A. and Wu, M.-T. (1966). *Justus Liebigs Ann. Chem.* **695**, 55–64; (e) Regitz, M. (1996). *Angew. Chem., Int. Ed. Engl.* **35**, 725–728; (f) Herrmann, W.A. and Köcher, C. (1997). *Angew. Chem., Int. Ed. Engl.* **36**, 2162–2187; (g) Arduengo III, A.J. and Krafczyk, R. (1998). *Chem. Unserer Zeit* **32**, 6–14

97. Winberg, H.E., Carnahan, J.E., Coffman, D.D. and Brown, M. (1965). *J. Am. Chem. Soc.* **87**, 2055–2056

98. (a) Buron, C., Gornitzka, H., Romanenko, V. and Bertrand, G. (2000). *Science* **288**, 834–836; (b) Dixon, D.A., Dobbs, K.D., Arduengo III, A.J. and Bertrand, G. (1991). *J. Am. Chem. Soc.* **113**, 8782–8785; (c) Bertrand, G. (1991). *Heteroat. Chem.* **2**, 29–38; (d) Igau, A., Baceiredo, A., Trinquier, G. and Bertrand, G. (1989). *Angew. Chem., Int. Ed. Engl.* **28**, 621–622; (e) Igau, A., Grutzmacher, H., Baceiredo, A. and Bertrand, G. (1988). *J. Am. Chem. Soc.* **110**, 6463–6466

99. (a) Wanzlick, H.-W. and Kleiner, H.-J. (1961). *Angew. Chem.* **73**, 493; (b) Wanzlick, H.-W. and Schikora, E. (1961). *Chem. Ber.* **94**, 2389–2393; (c) Wanzlick, H.W. (1962). *Angew. Chem., Int. Ed. Engl.* **1**, 75–80; (d) Wanzlick, H.-W. and Ahrens, H. (1964). *Chem. Ber.* **97**, 2447–2450; (e) Lemal, D.M., Lovald, R.A. and Kawano, K.I. (1964). *J. Am. Chem. Soc.* **86**, 2518–2519; (f) Hoffmann, R.W. (1968). *Angew. Chem., Int. Ed. Engl.* **7**, 754–765; (g) Wiberg, N. (1968). *Angew. Chem., Int. Ed. Engl.* **7**, 766–779; (h) Lemal, D.M. (1998). *The Chemistry of the Amino Group*, Patai, S. (ed.), Chapter 12. Wiley, New York; (i) Arduengo III, A.J., Goerlich, J.R. and Marshall, W.J. (1995). *J. Am. Chem. Soc.*, 117, 11027–11028

100. (a) Chen, P. (1998), In: *Advances in Carbene Chemistry*, Brinker, U.H. (ed.), vol. 2, pp., 45–75, JAI, Stamford, CT; (b) Warkentin, J. (1998) In: *Advances in Carbene Chemistry*, Brinker, U.H. (Ed.), vol. 2, pp. 245–295, JAI, Stamford, CT

101. Brinker, U.H., Buchkremer, R., Kolodziejczyk, M., Kupfer, R., Rosenberg, M., Poliks, M.D., Orlando, M. and Gross, M.L. (1993). *Angew. Chem., Int. Ed. Engl.* **32**, 1344–1345

102. Kupfer, R., Poliks, M.D. and Brinker, U.H. (1994). *J. Am. Chem. Soc.* **116**, 7393–7398

103. Isaev, S.D., Yurchenko, A.G., Stepanov, F.N., Kolyada, G.G., Novikov, S.S. and Karpenko, N.F. (1973). *J. Org. Chem. USSR* (*Transl. Zh. Org. Khim.*) **9**, 745–748

104. Moss, R.A. and Chang, M.J. (1981). *Tetrahedron Lett.* **22**, 3749–3752

105. (a) Bayley, H. and Knowles, J.R. (1978). *Biochemistry* **17**, 2420–2423; (b) Bayley, H. and Knowles, J.R. (1980). *Biochemistry* **19**, 3883–3892; (c) Erni, B. and Khorana, H.G. (1980). *J. Am. Chem. Soc.* **102**, 3888–3896; (d) Brunner, J., Senn, H. and Richards, F.M. (1980). *J. Biol. Chem.* **255**, 3313–3318; (e) Nassal, M. (1983). *Liebigs Ann. Chem.*, 1510–1523

106. (a) Bally, T., Matzinger, S., Truttman, L., Platz, M.S. and Morgan, S. (1994). *Angew. Chem., Int. Ed. Engl.* **33**, 1964–1966; (b) Isaev, S.D., Kulik, N.I. and Yurchenko, A.G. (1993). *Theor. Exp. Chem.* (*Transl. Teor. Eksp. Khim.*) **29**, 80–83

107. (a) Martella, D.J., Jones Jr., M. and Schleyer, P.v.R. (1978). *J. Am. Chem. Soc.* 100, 2896–2897; (b) Jones Jr., M. (1998). In *Advances in Carbene Chemistry*, Brinker, U.H. (ed.), vol. 2, pp. 77–96, JAI, Stamford, CT

108. Krois, D., Bobek, M.M., Werner, A., Kählig, H. and Brinker, U.H. (2000). *Org. Lett.* **2**, 315–318

109. Krois, D., Brecker, L., Werner, A. and Brinker, U.H. (2004). *Adv. Synth. Catal.* **346**, 1367–1374

110. Diastereoselective 1,3-CH insertions leading to *sym*- and *as*-didehydroadamantanes have been observed for γ-substituted 2-adamantanylidenes because the carbene bridges are bent away from electron-withdrawing substituents and bent toward electron-donating substituents. For examples, see: (a) Bobek, M.M. and Brinker, U.H. (2000). *J. Am. Chem. Soc.* **122**, 7430–7431; (b) Knoll, W., Bobek, M.M., Giester, G. and Brinker, U.H. (2001). *Tetrahedron Lett*. **42**, 9161–9165; (c) Knoll, W., Bobek, M.M., Kalchhauser, H., Rosenberg, M.G. and Brinker, U.H. (2003). *Org. Lett*. **5**, 2943–2946

111. Wilt, J.W. and Wagner, W.J. (1964). *J. Org. Chem.* **29**, 2788–2789

112. Nickon, A., Stern, A.G. and Ilao, M.C. (1993). *Tetrahedron Lett.* **34**, 1391–1394

113. Liu, M.T.H. (1994). *Acc. Chem. Res.* **27**, 287–294

114. Fuchs, J.J. (1967). U.S. Patent 3 287 354. *Chem. Abstr*. **66**, 65453

115. (a) Rosenberg, M.G., Kam, S.M. and Brinker, U.H. (1996). *Tetrahedron Lett.* **37**, 3235–3238; (b) Brinker, U.H. (1996). *Carbenes in Constrained Systems*; final report to the Petroleum Research Fund on Grant 28670–AC4; State University of New York (Binghamton), Binghamton, NY

116. Bamford, W.R. and Stevens, T.S. (1952). *J. Chem. Soc.* 4735–4740

117. The inherent migratory aptitude of a group depends mainly on three factors: (i) the intrinsic migratory aptitude, (ii) the bystander substituent on the migration origin, and (iii) the spectator substituent on the migration terminus. For reviews, see: (a) Ref. 66a (b) Ref. 66d (see pp. 80–91)

118. (a) Taber, R.L. and Champion, W.C. (1967). *J. Chem. Educ.* **44**, 620; (b) Price, C.C. (1939). *J. Am. Chem. Soc.* **61**, 1847–1849; (c) Vavon, G. and Barbier, M. (1931). *Bull. Soc. Chim. Fr*. **49**, 567–582 (see pp. 569, 576); (d) Senderens, J.-B. (1922). *Ann. Chim. (Paris)* **18**, 117–145 (see p. 141); (e), Senderens, J.-B. (1912). *Ann. Chim. Phys*. **25**, 449–529 (see pp. 500–501); (f) Ipatiew, W. (1910). *Ber. Dtsch. Chem. Ges*. **43**, 3383–3387; (g) Murat, M. (1909). *Ann. Chim. Phys*. **16**, 108–126 (see p. 121); (h) Sabatier, P. and Mailhe, A. (1907). *Ann. Chim. Phys*., **10**, 527–574 (see pp. 549–550, 572); (i) Sabatier, P. and Senderens, J.-B. (1905). *Ann. Chim. Phys*. **4**, 319–488 (see p. 374)

119. The microwave-induced dehydration of the **36c**@NaY FAU IC gave **28**:**29** = 2.2. For details, see: Ipaktschi, J. and Brück, M. (1990). *Chem. Ber*. **123**, 1591–1593

120. For reactions of carbenes with alcohols, see: Kirmse, W. (1994). In *Advances in Carbene Chemistry*, Brinker, U.H. (ed.), vol. 1, pp. 1–57. JAI, Greenwich, CT

121. (a) Cawley, J.J. and Lindner, P.E. (1997). *J. Chem. Educ.* **74**, 102–104; (b) Gillis, D.B. and Creegan, F.J. (1996). *Abstr. Pap. Am. Chem. Soc., 211th*, CHED 495

122. Storer, J.W. and Houk, K.N. (1993). *J. Am. Chem. Soc.* **115**, 10426–10427

123. (a) Bradley, G.F., Evans, W.B.L. and Stevens, I.D.R. (1977). *J. Chem. Soc., Perkin Trans.* 2, 1214–1220; (b) For a review, see: Sydnes, L.K. and Brinker, U.H. (1989). In *Methoden der Organischen Chemie* (*Houben-Weyl*), Regitz, M. (ed.), vol. E19b, p. 601. Thieme, Stuttgart; (c) Baron, W.J., DeCamp, M.R., Hendrick, M.E., Jones Jr., M., Levin, R.H. and Sohn, M.B. (1973). In *Carbenes*, Jones Jr., M. and Moss, R.A. (eds), vol. 1, Chapter 1. Wiley, New York

124. (a) Wojnárovits, L., Szondy, T., Szekeres-Bursics, E. and Földiák, G. (1982). *J. Photochem.* **18**, 273–276; (b) Wojnárovits, L. (1984). *J. Chem. Soc., Perkin Trans.* 2, 1449–1451; (c) Cope, A.C., Brown, M. and Woo, G.L. (1965). *J. Am. Chem. Soc.* **87**, 3107–3110; (d) Friedman, L. and Shechter, H. (1961). *J. Am. Chem. Soc.* **83**, 3159–3160

125. Kupfer, R. and Brinker, U.H. (1995). *Liebigs Ann.*, 1721–1725

126. (a) Cristol, S.J. and Harrington, J.K. (1963). *J. Org. Chem.* **28**, 1413–1415; (b) Lemal, D.M. and Fry, A.J. (1964). *J. Org. Chem.* **29**, 1673–1676; (c) Arct, J. and Brinker, U.H. (1989). In *Methoden der Organischen Chemie* (*Houben-Weyl*), Regitz, M. (ed.), vol. E19b, pp. 337–375, Thieme, Stuttgart; (d) Sydnes, L.K. and Brinker, U.H. (1989). In *Methoden der Organischen Chemie* (*Houben-Weyl*), Regitz, M. (ed.), vol. E19b, pp. 542–576, Thieme, Stuttgart; (e) Shapiro, R.H. (1976). *Org. React.* (*NY*) **23**, 405–507; (f) Freeman, P.K., George, D.E. and Rao, V.N.M. (1963). *J. Org. Chem.* **28**, 3234–3237; (g) Kirmse, W. and Knöpfel, N. (1976). *J. Am. Chem. Soc.* **98**, 4672–4674

127. (a) Freeman, P.K., George, D.E. and Rao, V.N.M. (1964). *J. Org. Chem.* **29**, 1682–1684; (b) Kirmse, W., Meinert, T., Modarelli, D.A. and Platz, M.S. (1993). *J. Am. Chem. Soc.* **115**, 8918–8927

128. (a) Shevlin, P.B. and McKee, M.L. (1989). *J. Am. Chem. Soc.* **111**, 519–524; (b) Moss, R.A., Liu, W. and Krogh-Jespersen, K. (1993). *J. Phys. Chem.* **97**, 13413–13418; (c) Moss, R.A. (1995). *Pure Appl. Chem.* **67**, 741–747; (d) Huang, H. and Platz, M.S. (1996). *Tetrahedron Lett.* **37**, 8337–8340; (e) Huang, H. and Platz, M.S. (1998). *J. Am. Chem. Soc.* **120**, 5990–5999; (f) Ammann, J.R., Subramanian, R. and Sheridan, R.S. (1992). *J. Am. Chem. Soc.* **114**, 7592–7594; (g) Levashova, T.V., Semeikin, O.V. and Balenkova, E.S. (1980). *J. Org. Chem. USSR* (*Transl. of Zh. Org. Khim.*) **16**, 53–56; (h) Murray Jr., R.K. and Ford, T.M. (1977). *J. Org. Chem.* **42**, 1806–1808; (i) Freeman, P.K. and Pugh, J.K. (1999). *J. Am. Chem. Soc.* **121**, 2269–2273; (j) Bergman, R.G. and Rajadhyaksha, V.J. (1970). *J. Am. Chem. Soc.* **92**, 2163–2164; (k) Wills, M.S.B. and Danheiser, R.L. (1998). *J. Am. Chem. Soc.* **120**, 9378–9379

129. (a) Kirmse, W. (1998). *Eur. J. Org. Chem.*, 201–212; (b) March, J. (ed.) (1992). *Advanced Organic Chemistry*. (4th edn.) p. 1037 Wiley, New York; (c) Hassner, A. and Stumer, C. (1994). *Organic Syntheses Based on Name Reactions and Unnamed Reactions*. p. 110, Pergamon, Tarrytown, NY; (d) Mundy, B.P. and Ellerd, M.G. (1988). *Name Reactions and Reagents in Organic Synthesis*. pp. 72–73, Wiley, New York

130. Recently, diazirine rearrangement in the excited state (RIES) that mimics the result of cyclopropylcarbene fragmentation has been postulated. For examples, see: (a) Ref. 128d,e; (b) Thamattoor, D.M., Jones Jr., M., Pan, W. and Shevlin, P.B. (1996). *Tetrahedron Lett.* **37**, 8333–8336

131. (a) Herges, R. (1994). *Angew. Chem., Int. Ed. Engl.* **33**, 255–276; (b) For a related example of coarctate fragmentation of 2-furfurylcarbenes, see: Khasanova, T. and Sheridan, R.S. (1998). *J. Am. Chem. Soc.* **120**, 233–234; (c) For the relevant comparison of pseudopericyclic and coarctate reactions, see: Birney, D.M. (2000). *J. Am. Chem. Soc.* **122**, 10917–10925

132. (a) Liu, M.T.H. (ed.) (1987). *Chemistry of Diazirines*, vols. 1 and 2. CRC, Boca Raton, FL; (b) Schmitz, E. (1963). *Adv. Heterocycl. Chem.* **2**, 83–130; (c) Schmitz, E. (1979). *Adv. Heterocycl. Chem.* **24**, 63–107; (d) Schmitz, E. (1964). *Angew. Chem., Int. Ed. Engl.* **3**, 333–341; (e) Schmitz, E. (1992). In *Methoden der Organischen Chemie* (*Houben-Weyl*) Klamann, D. (ed.), vol. E16c pp. 678–728, Thieme, Stuttgart

133. Rosenberg, M.G. and Brinker, U.H. (2001). *J. Org. Chem.* **66**, 1517–1522

134. (a) Schmitz, E., Habisch, D. and Stark, A. (1963). *Angew. Chem., Int. Ed. Engl.* **2**, 548; (b) Dürr, H. and Abdel-Wahab, A.-M.A. (1995). In *Organic Photochemistry and Photobiology*, Horspool, W.M. (ed.) pp. 954–983, CRC, Boca Raton, FL

135. (a) Bethell, D., Newall, A.R., Stevens, G. and Whittaker, D. (1969). *J. Chem. Soc. B*, 749–751; (b) Bethell, D., Newall, A.R. and Whittaker, D. (1971). *J. Chem. Soc. B*, 23–31

136. (a) Schleyer, P.v.R. (1958). *J. Am. Chem. Soc.* **80**, 1700–1704; (b) Schmerling, L., Luvisi, J.P. and Welch, R.W. (1956). *J. Am. Chem. Soc.* **78**, 2819–2821; (c) Roberts, R.M.G. (1976). *J. Chem. Soc., Perkin Trans.* 2, 1183–1190; (d) Cristol, S.J., Seifert, W.K., Johnson, D.W. and Jurale, J.B. (1962). *J. Am. Chem. Soc.* **84**, 3918–3925

137. The electron-deficient radical behaves similarly: (a) Davies, D.I., Done, J.N. and Hey, D.H. (1966). *Chem. Commun. (London)* 725–726; (b) Roberts, J.D., Trumbull Jr., E.R., Bennett, W. and Armstrong, R. (1950). *J. Am. Chem. Soc.* **72**, 3116–3124

138. Carbocations stemming from *carbenes* can give deviant product ratios due to ion pairing (see Ref. 135a)

139. Carbocations stemming from *diazonium cations*, such as **57**, often give spurious product ratios (see Ref. 84)

140. For the related 5-norbornen-2-yl route, see: Kirmse, W., Knöpfel, N., Loosen, K., Siegfried, R. and Wroblowsky, H.-J. (1981). *Chem. Ber.* **114**, 1187–1191

141. Photolysis of 2-azi-5-norbornene (*iso*-**45**) is reported to give **55c**:*iso*-**55c** = 1.9. This ratio is slightly lower than usual for **58** and may also indicate some ion pairing: Kirmse, W. and Meinert, T. (1994). *J. Chem. Soc., Chem. Commun.* 1065–1066

142. The **55**:*iso*-**55** ratios obtained from carbenes **46** and *iso*-**46** indicate a *product spread* in the direction of the starting compound: March, J. (ed.) (1992). *Advanced Organic Chemistry* (4th edn), p. 328. Wiley, New York

143. (a) Azbel', B.I., Gol'dshleger, N.F., Isakov, Ya.I., Épel'baum, E.T., Yampol'skii, Yu.Yu. and Minachev, Kh.M. (1986). *Bull. Acad. Sci. USSR, Div. Chem. Sci.* (*Transl. of Izv. Akad. Nauk SSSR, Ser. Khim.*) **35**, 1122–1125; (b) Azbel', B.I., Gol'dshleger, N.F., Isakov, Ya.I., Épel'baum, E.T., Yampol'skii, Yu.Yu., Khidekel', M.L. and Minachev, Kh.M. (1984). *Dokl. Chem.* (*Transl. of Dokl. Akad. Nauk SSSR, Ser. Khim.*) **276**, 197–199

144. One may postulate that H atom transfer to excited-state diazirine **45*** leads to a diazene, 3-diazenylnortricyclane, that is responsible for the reduction

145. A carbonyl $n \to \pi^*$ electronic transition (λ = ca. 280 nm) was observed with RP HPLC analysis, cf. Ref. 109

146. Wu, G., Jones Jr., M. Walton, R. and Lahti, P.M. (1998). *J. Org. Chem.* **63**, 5368–5371

147. See Ref. 58

148. (a) March, J. (ed.) (1992). *Advanced Organic Chemistry*. (4th edn) pp. 152, 169–170, 323–324 Wiley, New York; (b) Jorgensen, W.L. and Salem, L. (1973). *The Organic Chemist's Book of Orbitals*. Academic, New York; (c) Wilcox, C.F., Loew, L.M. and Hoffmann, R. (1973). *J. Am. Chem. Soc.* **95**, 8192–8193; (d) Hoffmann, R. (1970). *Tetrahedron Lett.*, 2907–2909; (e) Macomber, R.S. (1998). *J. Chem. Educ.* **75**, 1346–1350

149. Austin Model 1, see: Dewar, M.J.S., Zoebisch, E.G., Healy, E.F. and Stewart, J.J.P. (1985). *J. Am. Chem. Soc.* **107**, 3902–3909

150. The corresponding alkyne bicyclo[2.2.1]hept-2-yne might behave like a *vic*-dicarbene that first yields carbene **46** via 1,3-CH insertion, which then forms an intermolecular cyclopropanation product. However, this pathway was not suggested. See: (a) Laird, D.W. and Gilbert, J.C. (2001). *J. Am. Chem. Soc.* **123**, 6704–6705; (b) Laird, D.W. and Gilbert, J.C. (2001). *Chem. Eng. News* **79** (28), 41

151. Isaev, S.D., Yurchenko, A.G., Stepanov, F.N., Kolyada, G.G. and Novikov, S.S. (1973). *J. Org. Chem. USSR* (*Transl. of Zh. Org. Khim.*) **9**, 436

152. Jacoby, M. (2001). *Chem. Eng. News* **79** (9), 11

153. Wentrup, C. (1984). *Reactive Molecules*, pp. 10–12 Wiley, New York

154. Experimental $\Delta_f H^\circ$(**48**) = +81.0 kcal mol^{-1}, see: (a) Steele, W.V. (1978). *J. Chem. Thermodyn.* **10**, 919–927; (b) Hall Jr., H.K., Smith, C.D. and Baldt, J.H. (1973). *J. Am. Chem. Soc.* **95**, 3197–3201

155. Bradley, G.F., Evans, W.B.L. and Stevens, I.D.R. (1977). *J. Chem. Soc., Perkin Trans. 2*, 1214–1220

156. $\Delta_f H^\circ$(**47**) = +66.3 kcal mol^{-1} as calculated by Benson group additivity method: Benson, S.W., Cruickshank, F.R., Golden, D.M., Haugen, G.R., O'Neal, H.E., Rodgers, A.S., Shaw, R. and Walsh, R. (1969). *Chem. Rev.* **69**, 279–324

157. Rearrangement in the excited state (RIES) of diazirine **45** might be the actual route to enyne **47** because MeOH, which is relatively reactive and in excess, is expected to trap carbene **46** completely

158. (a) See Ref. 68g, pp. 137–159; (b) Jones, W.M., Joines, R.C., Myers, J.A., Mitsuhashi, T., Krajca, K.E., Waali, E.E., Davis, T.L. and Turner, A.B. (1973). *J. Am. Chem. Soc.* **95**, 826–835; (c) McMahon, R.J., Abelt, C.J., Chapman, O.L., Johnson, J.W., Kreil, C.L., LeRoux, J.-P., Mooring, A.M. and West, P.R. (1987). *J. Am. Chem. Soc.* **109**, 2456–2469; (d) Wong, M.W. and Wentrup, C. (1996). *J. Org. Chem.* **61**, 7022–7029; (e) Schreiner, P.R., Karney, W.L., Schleyer, P.v.R., Borden, W.T., Hamilton, T.P. and Schaefer III, H.F. (1996). *J. Org. Chem.* 61, 7030–7039; (f) Matzinger, S. and Bally, T. (2000). *J. Phys. Chem. A* **104**, 3544–3552; (g) Geise, C.M. and Hadad, C.M. (2002). *J. Org. Chem.* **67**, 2532–2540; (h) See Ref. 105a

159. (a) Warmuth, R. and Marvel, M.A. (2000). *Angew. Chem., Int. Ed.* **39**, 1117–1119; (b) Warmuth, R. (2000). Bobek, M.M. (ed.) *Proceedings of the Conference on Reactive Intermediates and Unusual Molecules*, p. 28, Eigenverlag, Vienna; (c) See Ref. 21e

160. Sander, W.W. (1987). *Spectrochim. Acta, Part A* **43A**, 637–646

161. No range is given in Ref. 160

162. Singlet 2-chloro-2,4,6-cycloheptatrien-1-ylidene (**67**) is expected to lie at the transition state (TS) between (*R*)-1-chloro-1,2,4,6-cycloheptatetraene ((*R*)-**65**) and (*S*)-1-chloro-1,2,4,6-cycloheptatetraene ((*S*)-**65**). For an account of the related enantiomerization of DL-**60**, see Ref. 21e, p. 432

163. See Ref. 65

164. (a) Jones, W.M. (1980). In *Rearrangements in Ground and Excited States*, de Mayo, P. (ed.), vol. 1, Chapter 3. Academic, New York; (b) Kirmse, W. and Kopannia, S. (1998). *J. Org. Chem.* **63**, 1178–1184

165. Compare with the rearrangement of phenylnitrene to 1-aza-1,2,4,6-cycloheptatetraene: (a) Platz, M.S. and Gritsan, N.P. (2001). *Abstr. Pap. Am. Chem. Soc.*, 222nd, ORGN 242; (b) Platz, M.S. (1995). *Acc. Chem. Res.* **28**, 487–492; (c) Marcinek, A., Leyva, E., Whitt, D. and Platz, M.S. (1993). *J. Am. Chem. Soc.* **115**, 8609–8612

166. (a) Graham, W.H. (1965). *J. Am. Chem. Soc.* **87**, 4396–4397; (b) Padwa, A., Pulwer, M.J. and Blacklock, T.J. (1990). *Org. Synth. Coll.* **7**, 203–206

167. Rosenberg, M.G. and Brinker, U.H. (2003). *J. Org. Chem.* **68**, 4819–4832

168. Liu, M.T.H. (1994). *Acc. Chem. Res.* **27**, 287–294

169. (a) Bonneau, R. and Liu, M.T.H. In *Advances in Carbene Chemistry*, Brinker, U.H. (ed.), vol. 2, pp. 1–28, JAI, Stamford, CT; (b) Liu, M.T.H. and Bonneau, R. (1996). *J. Am. Chem. Soc.* **118**, 8098–8101

170. For the $\pi \to \pi^*$ transition. For the $\sigma \to p$ transition ($\lambda_{max} = 750$ nm), see: (a) Zuev, P.S. and Sheridan, R.S. (1994). *J. Org. Chem.* **59**, 2267–2269; (b) Sheridan, R.S. (2000). *Inter-Amer. Photochem. Soc. News.* **23** (1), 39–48

171. (a) Turro, N.J., Butcher Jr., J.A., Moss, R.A., Guo, W., Munjal, R.C. and Fedorynski, M. (1980). *J. Am. Chem. Soc.* 102, 7576–7578; (b) Naito, I., Oku, A., Otani, N., Fujiwara, Y. and Tanimoto, Y. (1996). *J. Chem. Soc., Perkin Trans. 2*, 725–729

172. Yoshinaga, M. (1993). Jpn. Patent 05 32 704, 1993; *Chem. Abstr.* **119**, 10738

173. Meskens, F.A.J. (1981). *Synthesis*, 501–522

174. (a) Evans, M.E. (1972). *Carbohydr. Res.* **21**, 473–475; (b) Horton, D. and Weckerle, W. (1975). *Carbohydr. Res.* **44**, 227–240

175. PhCHO@CyDs have been studied in the solid state using ^{13}C CP/MAS NMR: (a) Ripmeester, J.A. (1988). *J. Inclusion Phenom.* **6**, 31–40; (b) Garces, F.O., Rao, V.P., Garcia-Garibay, M.A. and Turro, N.J. (1992). *Supramol. Chem.* **1**, 65–72

176. The association constants (*K*) for PhCHO@CyD ICs in H_2O at 25 °C have been determined: K(PhCHO@α-CyD) = 1.02(4) $\times$ 10^2 M^{-1} and K(PhCHO@β-CyD) = 1.50(7) $\times$ 10^2 M^{-1}. See: Guo, Q.-X., Luo, S.-H. and Liu, Y.-C. (1998). *J. Inclusion Phenom. Mol. Recognit. Chem.* **30**, 173–182; *Chem. Abstr.* **128**, 270367

177. See Ref. 81

Computer modeling of enzyme catalysis and its relationship to concepts in physical organic chemistry

Sonja Braun-Sand, Mats H.M. Olsson and Arieh Warshel*

Department of Chemistry, University of Southern California, Los Angeles, CA 90089-1062, USA

1   Introduction

Understanding enzymatic reactions and knowing what makes them so efficient in catalyzing reactions is one of the challenges of modern biophysics. This is both of fundamental and practical interest, and is directly related to chemical catalysis. Biological systems have, however, been refined by millions of years of evolution and therefore reached an optimal performance. This makes enzyme catalysis an excellent starting point for understanding the possibilities and limitations of rational design.

This work will summarize what has been learned from theoretical studies of enzyme catalysis and relate these findings to general principles of physical organic chemistry. Our analysis will explore the factors used by enzymes to catalyze their reactions and illustrate the crucial role of reducing the "solvent", i.e., outer-sphere,

---

*Corresponding author.

reorganization energy. As will be clarified in the text, this reduction is associated with a very polar environment unlike the nonpolar environments frequently envisioned by physical organic chemists.

Before going on to a detailed discussion on contributions, it is essential to clearly define relevant concepts and systems. It should also be kept in mind that trivial suggestions such as ''enzymes work by binding the transition state (TS)'' have not given us any further insight into catalysis, the issue is rather how this is accomplished. As a starting point we consider a generic enzymatic reaction of the form:

$$E + S \overset{K}{\leftrightarrow} ES \overset{k_{cat}}{\longrightarrow} ES^{\ddagger} \to EP \to E + P \tag{1}$$

where the letters E, S and P stand for the enzyme, substrate and product, respectively. The labels ES, EP and $ES^{\ddagger}$ denote the enzyme–substrate complex, the enzyme–product complex and the TS of the enzymatic reaction, respectively. k_{cat} is the rate constant for the catalyzed reaction step and K is the ratio between the substrate association and dissociation constant, k_1/k_{-1}.

It is generally accepted (e.g., Ref. 1) that many enzymes have evolved by optimizing k_{cat}/K_M, where $K_M = (k_{-1} + k_{cat})/k_1$ and can be approximated as $K_M \approx k_{-1}/k_1 = K^{-1}$. However, this observation, and related findings, has not identified the factors responsible for the actual catalytic effect. As will be shown below, the key question is to determine how the activation barrier in the chemical step is reduced. In order to proceed further in a meaningful way, we need a reliable tool to quantify the activation barrier and to relate that with the structure and function of the enzyme. We also need to determine the individual contributions to the overall catalytic effect. Gradually it is becoming clear that this is best accomplished by computer simulation approaches.

In order to understand and analyze enzyme catalysis it is essential to define a reference reaction that is not catalyzed. The most straightforward and useful reference is water. That is, we have retained the physical environment of the bulk water, but taken away any catalyzing effect of the enzyme (see Fig. 1). Thus, understanding the origin of enzyme catalysis boils down to determining the free-energy difference between the activation barrier in water ($\Delta g_w^{\ddagger}$) and in the enzyme ($\Delta g_p^{\ddagger}$). The enzyme can, however, reduce ($\Delta g_p^{\ddagger}$) either by binding the substrate with an equal strength in the reactant state (RS) and the TS (in which case $\Delta g_p^{\ddagger} - \Delta g_w^{\ddagger} = \Delta G_{bind}$) or by reducing the activation barrier for the chemical step, $\Delta g_{cat}^{\ddagger}$, or a combination of the two. Since the factors that determine the binding energy are well understood, the real question is to determine the factors that reduce the activation barrier of the chemical step ($\Delta g_{cat}^{\ddagger}$), which is of course a question of energetics.

Experimentally, it is often difficult to directly quantify the reaction energetics and address relevant questions. Even to determine whether the enzyme works by stabilizing the RS or TS is not easily resolved, although mutational analysis of the type introduced in reference 2 (see also Ref. 3) can help in this respect. Instead, we have to focus on computer simulation studies. In doing so we will primarily address two questions: (i) what are the contributions responsible for the difference between $\Delta g_{cat}^{\ddagger}$ and $\Delta g_w^{\ddagger}$, and (ii) how do these contributions operate (i.e., do they destabilize the RS
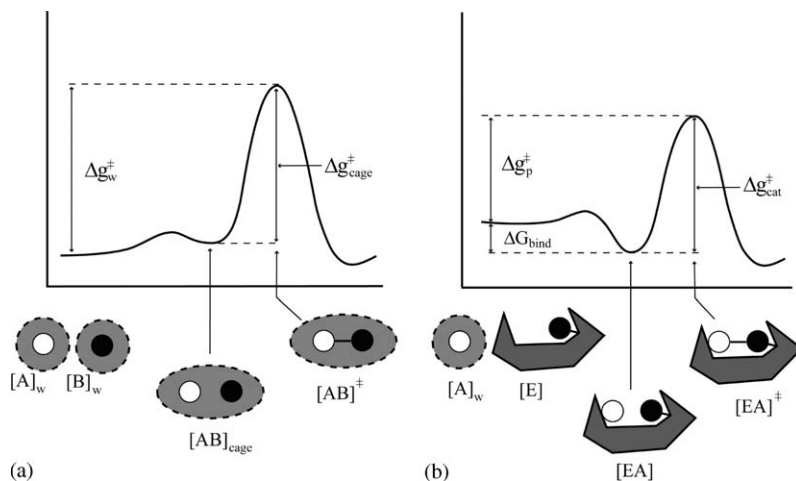
Fig. 1 Comparing the activation-free-energy profile for a reference reaction in water and the corresponding reaction in an enzyme active site. The figure illustrates the relationship between $\Delta g_{\text{cat}}^{\ddagger}$, $\Delta g_{\text{cage}}^{\ddagger}$, and $\Delta g_w^{\ddagger}$.

or stabilize the TS)? There have been many attempts to address these questions either in a direct or indirect way (e.g., see Ref. 4 for a partial list). Unfortunately, many of the current proposals have not been defined in a clear and logical way or have not been properly analyzed by their proponents. This is partially due to the difficulties analyzing energetics before the computer simulations were reliable. This has also led to numerous suggestions of enzyme catalysis that have not been clearly defined and cannot be examined conceptually or computationally. It will be shown below that it is possible to explore and quantify the origin of the catalytic power of enzymes with a clear definition of the problem and with a combination of experimental and computational studies. This can be done within the regular framework of physical organic chemistry but with a modern view of the molecular origin of these concepts.

2 Formulating chemical reactivity in solutions and in enzymes in a computationally convenient way; the empirical valence bond and other QM/MM methods

In order to gain a quantitative understanding of the catalytic power of enzymes, it is essential to be able to calculate the free-energy profiles for enzymatic reactions and the corresponding reference solution reactions. The common prescription of obtaining potential surfaces for chemical reactions involves the use of quantum mechanical (QM) computational approaches, and such approaches have become quite effective in treating small molecules in the gas phase (e.g., Ref. 5). However, here we are interested in chemical reactions in very large systems, which cannot be explored

at present by ab initio methods. Similarly, molecular mechanics (MM) simulations (e.g., Ref. 6) that have been proven to be very effective in exploring protein configurational space cannot be used to describe bond breaking and bond making reactions in proteins or solutions. The generic solution to the above problem has been provided by the development of the hybrid QM/MM approach.[7] This approach divides the simulation system (e.g., the enzyme/substrate complex) into two regions. The inner region, region I, contains the reacting fragments which are represented quantum mechanically. The surrounding protein/solvent region, region II, is represented by a MM force field. The Hamiltonian of the complete system can then be written as:

$$H = H_{QM} + H_{QM/MM} + H_{MM} \tag{2}$$

where H_{QM} is the QM Hamiltonian, $H_{QM/MM}$ the Hamiltonian that couples regions I and II, and H_{MM} the Hamiltonian of region II. H_{QM} is evaluated by any standard QM approach, which can be either ab initio or semiempirical. The total potential can then be expressed as:

$$V_{total} = \langle \Psi | H_{QM} + H_{QM/MM} + H_{MM} | \Psi \rangle = E_{QM} + \langle \Psi | H_{QM/MM} | \Psi \rangle + E_{MM} \tag{3}$$

More details about the implementation of this method are given elsewhere.[6]

QM/MM methods are now widely used in studies of complex systems in general, and enzymatic reactions in particular, and we can only mention several works (e.g., Refs. 8–19). Despite these advances, we are not yet at the stage where one can use QM/MM approaches in fully quantitative studies of enzyme catalysis. The major problem is associated with the fact that a quantitative evaluation of the potential surfaces for the reacting fragment should involve ab initio electronic structure calculations, and such calculations are too expensive to allow for the configurational averaging needed for proper free-energy calculations. Specialized approaches can help one move toward ab initio QM/MM free-energy calculations (see Ref. 20), but even these approaches are still in a development stage. Fortunately, one can use approaches that are calibrated on the energetics of the reference solution reaction to obtain reliable results with semi-empirical QM/MM studies, and the most effective way of doing so is the empirical valence bond (EVB) method described below.

As stated above, reliable studies of enzyme catalysis require accurate results for the difference between the activation barriers in enzyme and in solution. The early realization of this point led to a search for a method that could be calibrated using experimental and theoretical information of reactions in solution. It also becomes apparent that in studies of chemical reactions, it is more physical to calibrate surfaces that reflect bond properties (i.e., valence bond-based (VB-based) surfaces) than to calibrate surfaces that reflect atomic properties (e.g., molecular orbital-based surfaces). Furthermore, it appears to be very advantageous to force the potential surfaces to reproduce the experimental results of the broken fragments at infinite separation in solution. This can be easily accomplished with the VB picture. The resulting EVB method has been discussed extensively elsewhere,[21,22] but its main features will be outlined below, because it provides the most direct microscopic connection to concepts of physical organic chemistry.

The EVB is a QM/MM method that describes reactions by mixing resonance states (or more precisely diabatic states) that correspond to classical VB structures, which describe the reactant, intermediate (or intermediates) and product states. The potential energies of these diabatic states are represented by classical MM force fields of the form:

$$\varepsilon_i = \alpha_{\mathrm{gas}}^i + U_{\mathrm{intra}}^i(\mathbf{R}, \mathbf{Q}) + U_{Ss}^i(\mathbf{R}, \mathbf{Q}, \mathbf{r}, \mathbf{q}) + U_{ss}(\mathbf{r}, \mathbf{q}) \tag{4}$$

Here, $\mathbf{R}$ and $\mathbf{Q}$ represent the atomic coordinates and charges of the diabatic states, and $\mathbf{r}$ and $\mathbf{q}$ are those of the surrounding protein and solvent. α_{gas}^i is the gas-phase energy of the ith diabatic state (where all the fragments are taken to be at infinite separation), $U_{\mathrm{intra}}(\mathbf{R},\mathbf{Q})$ the intramolecular potential of the solute system (relative to its minimum); $U_{Ss}(\mathbf{R}, \mathbf{Q}, \mathbf{r}, \mathbf{q})$ represents the interaction between the solute (S) atoms and the surrounding (s) solvent and protein atoms. $U_{ss}(\mathbf{r}, \mathbf{q})$ represents the potential energy of the protein/solvent system ("ss" designates surrounding–surrounding). The ε_i of Equation (4) forms the diagonal elements of the EVB Hamiltonian (H_{ii}). The off-diagonal elements of the Hamiltonian, H_{ij}, are represented by simple exponential functions of the distances between the reacting atoms. The H_{ij} elements are assumed to be the same in the gas phase, in solutions and in proteins. The ground state (GS) energy, E_g, is obtained by solving:

$$\mathbf{H}_{\mathrm{EVB}}\mathbf{C}_{\mathrm{g}} = E_{\mathrm{g}}\mathbf{C}_{\mathrm{g}} \tag{5}$$

Here, $\mathbf{C}_{\mathrm{g}}$ is the GS eigenvector and E_g provides the EVB potential surface.

The EVB treatment provides a natural picture of intersecting electronic states, which is useful for exploring environmental effects on chemical reactions in condensed phases.[21,22] The ground-state charge distribution of the reacting species ("solute") polarizes the surroundings ("solvent"), and the charges of each resonance structure of the solute then interact with the polarized solvent.[22] This coupling enables the EVB model to represent correctly the effect of the solvent on the QM mixing of the different states of the solute. For example, in cases where ionic and covalent states are describing the solute, when the solvent stabilizes the ionic state to a greater extent the resulting GS has more ionic character and more solvation energy.

Running such molecular dynamic (MD) trajectories on the EVB surface of the RS can (in principle) provide the free-energy function, Δg, that is needed to calculate the activation energy, $\Delta g^{\ddagger}$. However, since trajectories on the reactant surface will reach the TS only rarely, it is usually necessary to run a series of trajectories on potential surfaces that gradually drive the system from the reactant to the product state.[22] The EVB approach accomplishes this by changing the system adiabatically from one diabatic state to another. In the simple case of two diabatic states, this "mapping" potential, ε_m, can be written as a linear combination of the reactant and product potentials, ε_1 and ε_2:

$$\varepsilon_m = (1 - \lambda_m)\varepsilon_1 + \lambda_m\varepsilon_2 \quad (0 \leqslant \lambda_m \leqslant 1) \tag{6}$$

When λ_m is changed from 0 to 1 in $n+1$ fixed increments ($\lambda_m = 0/n$, $1/n$, $2/n$,..., n/n), potentials with one or more of the intermediate values of λ_m will force the system to fluctuate near the TS.

The free energy, ΔG_m, associated with changing λ_m from 0 to m/n is evaluated by the well-known free-energy perturbation (FEP) procedure described elsewhere (e.g., see Ref. 22). However, after obtaining G_m we still need to obtain the free energy that corresponds to the adiabatic GS surface (the E_g of Equation (5)) along the reaction coordinate, x. This free energy (referred to as a "free-energy functional") is obtained by the FEP-umbrella sampling (FEP/US) method,[23,24] which can be written as:

$$\Delta\overline{g}(x') = \Delta G_m - \beta^{-1} \ln\langle\delta(x - x')\exp[-\beta(E_g(x) - \varepsilon_m(x))]\rangle_{\varepsilon_m} \tag{7}$$

where ε_m is the mapping potential that keeps x in the region of x'. If the changes in ε_m are sufficiently gradual, the free-energy functional, $\Delta g(x')$, obtained when several values of m overlap over a range of x', and patching together the full set of $\Delta g(x')$ gives the complete free-energy curve for the reaction. The generated reaction coordinate, x, is usually taken as the energy gap ($x = \varepsilon_1 - \varepsilon_2$). This selection[22,25] is particularly powerful when one tries to represent all of the many dimensional solvent space by a single coordinate (see Ref. 23). The FEP/US approach may be also used to obtain the free-energy functional of the isolated diabatic states. For example, the diabatic free energy, Δg_1, of the RS can be calculated as:

$$\Delta g_1(x') = \Delta G_m - \beta^{-1} \ln\langle\delta(x - x')\exp[-\beta(\varepsilon_1(x) - \varepsilon_m(x))]\rangle_{\varepsilon_m} \tag{8}$$

The diabatic free-energy profiles of the reactant and product states provide the microscopic equivalent of the Marcus' parabolas.[26,27] For example, in the case of the $(Cl^- + CH_3-Cl \rightarrow ClCH_3 + Cl^-)$ S_N2 reaction, one obtains[23] the results shown in Fig. 2.

The EVB method satisfies some of the main requirements for reliable studies of enzymatic reactions. Among the obvious advantages of the EVB approach is the facilitation of proper configurational sampling and converging free-energy calculations. This includes the inherent ability to evaluate non-equilibrium solvation effects.[28] Another important feature of the EVB method is the ability to capture correctly the linear relationship between activation free energies and reaction energies, linear free-energy relationship (LFER), observed in many important reactions (e.g., Ref. 22). Furthermore, the EVB benefits from the aforementioned ability to treat consistently and conveniently the solute–solvent coupling. This feature is essential not only in allowing one to properly model charge-separation reactions, but also in allowing for a reliable and convenient calibration. Calibrating EVB surfaces using ab initio calculations was found to provide quite reliable potential surfaces.

The seemingly simple appearance of the EVB method may have led to the initial impression that this is an oversimplified qualitative model, rather than a powerful quantitative approach. However, the model has been eventually widely adopted as a general model for studies of reactions in large molecules and in condensed phase (e.g., Refs. 29–32). Several very closely related versions have been put forward with basically the same ingredients as in the EVB method (see Ref. 33).

The reliability of the EVB approach has been challenged by some who may have assumed that it is inferior to other QM/MM approaches. This may reflect a
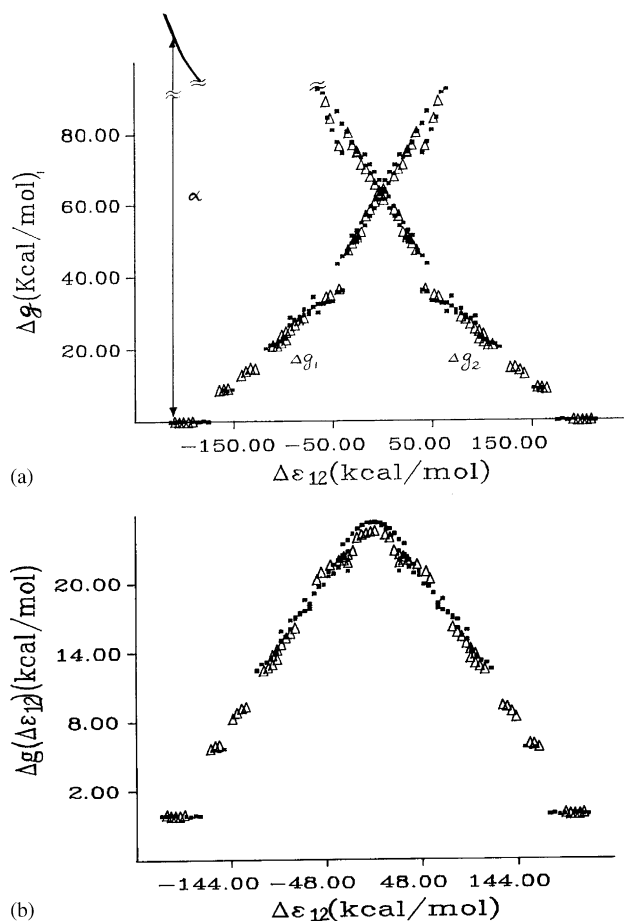
Fig. 2 (a) Free-energy functional, Δg_1 and Δg_2, for an S_N2 reaction as a function of the energy gap $\Delta\varepsilon$ (taken from Ref. 23). (b) The actual adiabatic free-energy function for the above system.

confusion between accuracy and rigorousness. Obviously, high-level ab initio calculations are much more rigorous than the EVB, but such approaches cannot be used at present to obtain the proper sampling needed for reliable calculations of activation free energies. Thus, QM/MM calculations of activation free energies are performed by semiempirical approaches which are adjusted to obtain the proper results in the solution reaction. This approach, which has been adopted from early EVB studies, is less effective than the EVB calibration procedure (the EVB calibration is especially suitable for forcing the calculated energies of the reacting fragments to reproduce the corresponding observed values).

Since we will be dealing with proton transport (PT) processes, it might be useful to clarify that the EVB and the so-called MS-EVB[34,35] (that was so effective in studies of PT in water) are more or less identical. More specifically, the so-called MS-EVB

includes typically six EVB states in the solute QM region and the location of this QM region changes if the proton moves. The QM region is surrounded by classical water molecules (the MM), whose effect is sometimes included inconsistently by solvating the charges of the gas phase QM region (this leads to inconsistent QM/MM coupling with the solute charges as explained previously (e.g., Refs. 6,28). More recently, in MS-EVB works the coupling was introduced consistently by adding the interaction with the MM water in the diagonal solute Hamiltonian. Now our EVB studies were performed repeatedly with multi-state treatment (e.g., five states in Ref. 36) and this has always been done with a consistent coupling to the MM region. Thus, the only difference that we can find between the two versions is that our EVB studies did not change the identity of the atoms in the QM region during simulations of individual chemical steps (this was done only while considering different steps). Such treatment provides the optimal strategy when one deals with processes in proteins that involve relatively high barriers, rather than with low-barrier transport processes (so that the identity of the reacting region has not changed during the simulations). Also note that the MS-EVB simulations in proteins, where we have a limited number of quantum sites, do not have to change the QM region (e.g., Ref. 37) during the simulations. Finally, in cases of high barriers, the ability to change the QM region on the fly is not useful, since the main issue is the ability to obtain a proper evaluation of the free-energy associated with climbing the barrier. Thus we conclude that the EVB and MS-EVB are identical methods, although we appreciate the elegant treatment of changing the position of the QM region during simulations, which is a very useful advance in EVB treatments of processes with a very low-activation barrier.

3   The EVB as a basis for LFER in solutions and enzymes

The approach used to obtain the EVB free-energy functionals (the Δg of Equation (7)) has been originally developed in Ref. 25 in order to provide the microscopic equivalent of the Marcus theory for electron transfer (ET) reactions.[38] This approach allows one to explore the validity of the Marcus formula and the underlying linear response approximation (LRA) on a microscopic molecular level.[39] While this point is now widely accepted by the ET community,[40] the validity of the EVB as perhaps the most general tool in microscopic LFER studies is less appreciated. This issue will be addressed below.

In order to explore the molecular basis of LFER, we have to consider a one-step chemical reaction and to describe this reaction in terms of two diabatic studies that correspond to the reactant and product states. In this case the GS adiabatic surface is given by:

$$E_{\mathrm{g}} = \frac{1}{2}\left[(\varepsilon_1 + \varepsilon_2) - \sqrt{(\varepsilon_1 - \varepsilon_2)^2 + 4H_{12}^2}\right] \tag{9}$$

With this well-defined adiabatic surface, we can explore the correlation between $\Delta g^{\ddagger}$ and ΔG^0. Now the EVB/US procedure (e.g., Ref. 22) allows one to obtain the
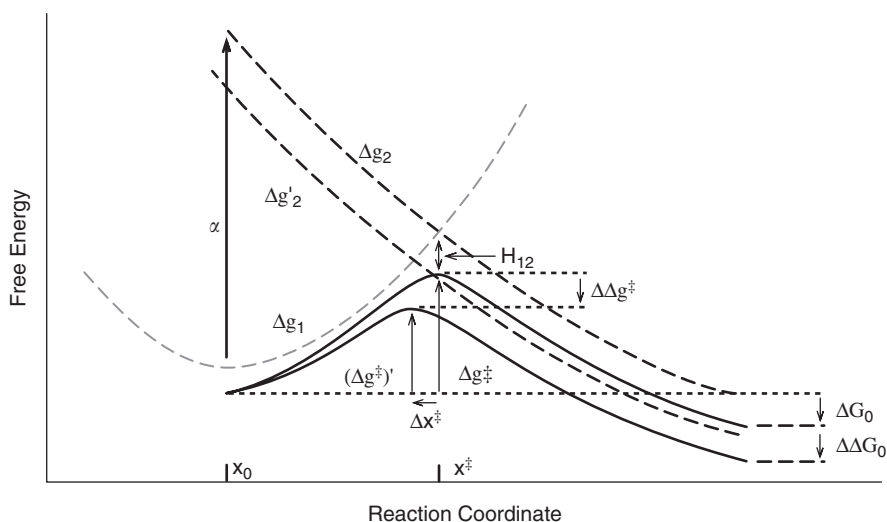
Fig. 3 A schematic description of the relationship between the free-energy difference ΔG_0 and the activation free energy $\Delta g^{\ddagger}$. The figure illustrates how a shift of Δg_2 by $\Delta \Delta G_0$ (that changes Δg_2 to $\Delta g_2'$, and ΔG_0 to $\Delta G_0 + \Delta \Delta G_0$) changes $\Delta g^{\ddagger}$ by a similar amount.

rigorous profile of the free-energy function, $\Delta \bar{g}$, that corresponds to E_g and the free-energy functions, Δg_1 and Δg_2, that correspond to ε_1 and ε_2, respectively (see Fig. 3). It is important to point out here that such profiles have been evaluated quantitatively in many EVB simulations of chemical reactions in solutions and proteins (for reviews see Refs. 21,41). The corresponding profiles provide the activation free energy, $\Delta g^{\ddagger}$, for the given chemical step. The calculated activation barrier can then be converted (e.g., see Ref. 22) to the corresponding rate constant using transition state theory (TST):

$$k_{i \rightarrow j} \cong (RT/h) \exp\{-\Delta g^{\neq}_{i \rightarrow j}/RT\} \tag{10}$$

A more rigorous expression for $k_{i \rightarrow j}$ can be obtained by multiplying the TST expression by a transmission factor that can be calculated easily by running downhill trajectories.[22] However, the corresponding correction is usually small.[4]

At this point, it is useful to consider the approximated expression for $\Delta \bar{g}$ and $\Delta g^{\ddagger}$. Here we note that with the simple two-state model of Equation (9) we can obtain a very useful approximation to the $\Delta \bar{g}$ curve. That is, using the aforementioned free-energy EVB/US formulation, we obtain the $\Delta \bar{g}$ that corresponds to the E_g and the free-energy functions, Δg_i, that correspond to the ε_i surfaces. This leads to the approximated expression:

$$\Delta \bar{g}(x) = \frac{1}{2}\left[(\Delta g_1(x) + \Delta g_2(x)) - \sqrt{(\Delta g_1(x) - (\Delta g_2(x))^2 + 4H_{12}^2(x)}\right] \tag{11}$$

This relationship can be verified in the case of small H_{12} by considering our ET studies,[39] while for larger H_{12} one should use a perturbation treatment. Now we can

exploit the fact that the Δg_i curves can be approximated by parabolas of equal curvatures (this approximated relationship was found to be valid by many microscopic simulations (e.g., Ref. 21)). This approximation can be expressed as:

$$\Delta g_i(x) = \lambda \left(\frac{x - x_o^{(i)}}{x_o^{(j)} - x_o^{(i)}} \right)^2 \tag{12}$$

where λ is the so-called "solvent reorganization energy" (which is illustrated in Fig. 3).

Using Equations (11) and (12), one obtains the Hwang Aqvist Warshel (HAW) equation, which is given in the general case by:

$$\Delta g_{i \to j}^{\neq} = (\Delta G_{i \to j}^0 + \lambda_{i \to j})^2/4\lambda - H_{ij}(x^{\neq}) + H_{ij}^2(x_0^{(i)})/(\Delta G_{i \to j}^0 + \lambda_{i \to j}) + \Gamma_{ij} \tag{13}$$

where $\Delta G_{i \to j}^0$ is the free energy of the reaction, and H_{ij} the off-diagonal term that mixes the two relevant states with the average value at the TS, $x^{\neq}$, and at the RS, $x_0^{(i)}$. Γ_{ij} is a correction that reflects the effect of tunneling and zero-point energy corrections in cases of light atom transfer reactions.

Repeated quantitative EVB studies of reactions in solutions and proteins (e.g., Refs. 21,42) established the validity of Equation (13). With this fact in mind we can take these equations as a quantitative correlation between $\Delta g_{i \to j}^{\ddagger}$ and ΔG^0. Basically, when the changes in ΔG^0 are small, we obtain a linear relationship between $\Delta g_{i \to j}^{\ddagger}$ and ΔG^0. This linear relationship, which can be obtained by simply differentiating the $\Delta g_{i \to j}^{\ddagger}$ of Equation (13) with respect to $\Delta G_{i \to j}^0$, can be expressed in the form:

$$\Delta\Delta g_{i \to j}^{\neq} = \theta \Delta\Delta G_{i \to j}^0 \tag{14}$$

where $\theta = (\Delta G_{i \to j}^0 + \lambda)/2\lambda$, and where the contribution from the last term of Equation (13) is neglected. The linear correlation coefficient depends on the magnitude of ΔG^0 and λ. At any rate, more details about this LFER or free-energy relationship (FER), and its performance in studies of chemical and biochemical problems are given elsewhere.[21–23,43–45]

The main point of Equation (14) and Fig. 3 is that the $\Delta G_{i \to j}^0$, which determines the corresponding $\Delta g_{i \to j}^{\ddagger}$, is correlated with the difference between the two minima of the $\Delta \bar{g}$ profile that correspond to state i and j, respectively.

While our ability to reproduce the observed LFER might not look like a conceptual advance, the fact the EVB provides a rigorous basis for FER in condensed phases leads to a different picture than what has been assumed in traditional LFER studies. That is, as is clear from the HAW relationship, it is essential to take into account the effect of H_{ij} on LFER studies that involve actual chemical reactions (rather than ET reactions). In such cases, H_{ij} is frequently very significant, and its neglect leads to an incorrect estimate of the relevant reorganization energy. This point has not been widely appreciated because of the fact that the correlation between $\Delta g^{\ddagger}$ and ΔG^0 does not depend so critically on H_{ij}. Thus, as long as one fits the experimentally observed relationship by phenomenological parameters, it is hard to realize that the relevant reorganization energies are underestimated in a drastic way.

A case in point is the systematic analysis of hydride transfer reactions by Kong and Warshel,[43] and S_N2 reactions,[23] which is summarized in Fig. 4.

The use of the EVB and Equation (13) in studies of reactions in solutions has been extended to studies of LFERs in enzymes. The successes of this approach have been demonstrated in studies of carbonic anhydrase,[46] p21 Ras,[44,47] and tyrosyl-tRNA synthetase.[45] At present, we view these studies as the most quantitative LFER studies of enzymes. It is also useful to point out the successes of our approach in LFER studies of electron transport in proteins (e.g., Ref. 48).

A recent study of Kiefer and Hynes[49] used an EVB formulation, with a continuum treatment of the solvent, in an attempt to derive an LFER for PT reactions. Unfortunately, they assumed that a "Marcus relation was never actually derived for PT reactions," apparently overlooking all the above works. Furthermore, their derivation ignored the crucial effect of H_{ij}. Nevertheless, it is encouraging to see again a
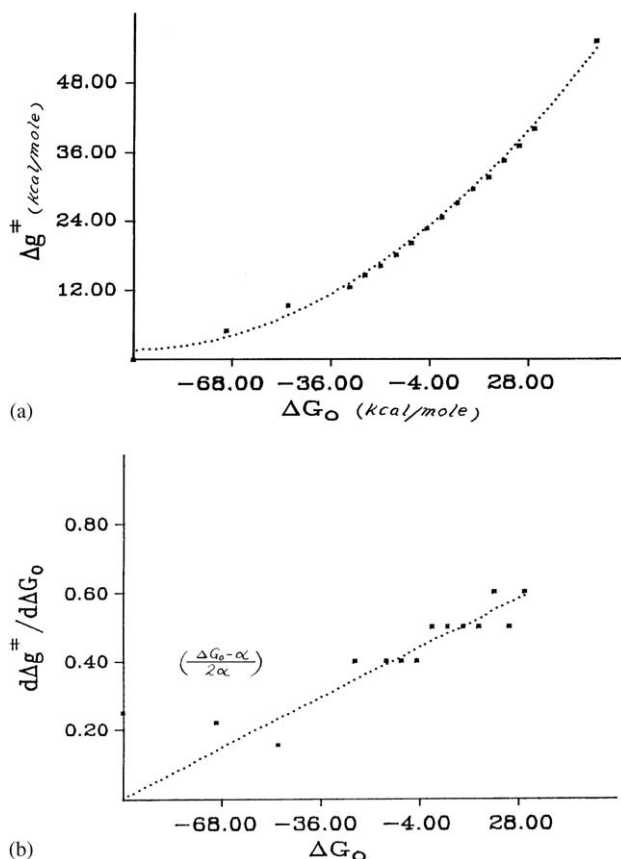
Fig. 4 (a) Calculated relationship between $\Delta g^{\neq}$ and ΔG_0 for a series of S_N2 reactions. (b) Dependence of the correlation coefficient $\delta\Delta g^{\neq}/\delta\Delta G_0$ on ΔG_0 (taken from Ref. 23).

further realization of the effectiveness of the EVB in providing a molecular basis to LFER treatments.

4 Proton transport in carbonic anhydrase as an example of the difference between microscopic and phenomenological LFERs

In order to illustrate our point about the difficulties associated with phenomenological LFER treatments of reactions in solutions and in enzymes, it is instructive to consider the studies of human carbonic anhydrase III (which will be referred to here as CA III).[50] Studies of this system[50,51] demonstrated that the rate of PT in mutants of CA III is correlated with the pK_a difference between the donor and acceptor. It was found that the observed LFER follows a Marcus' type relationship. Although this study provided an excellent benchmark for studies of PT in proteins, it also raised the question about uniqueness of the parameters deduced from phenomenological LFER studies. This issue will be explored below.

The catalytic reaction of CA III can be described in terms of two steps. The first is attack of a zinc-bound hydroxide on CO_2:[52]

$$CO_2 + EZn^{+2}(OH^-) + H_2O \rightleftharpoons HCO_3^- + EZn^{+2}(H_2O) \tag{15}$$

The reversal of this reaction is called the ''dehydration step''. The second step involves the regeneration of the OH^- by a series of PT steps:[53,54]

$$EZn^{+2}(H_2O) + B \underset{k_B}{\overset{k_{-B}}{\rightleftharpoons}} EZn^{+2}(HO^-) + BH^+ \tag{16}$$

where $K_{-B} = k_{-B}/k_B$ (in the notation of Ref. 50), BH^+ can be water, buffer in solution or the protonated form of Lys64 (other CAs have His in position 64). Previous experimental studies[50] have established an LFER that was fitted to the Marcus' equation using:

$$\Delta g^{\ddagger} = w^r + \{1 + \Delta G^0/4\Delta G_0^{\ddagger}\}^2 \Delta G_0^{\ddagger} \tag{17}$$

where the observed reaction free energy is given by:

$$-\Delta G_{obs}^0 = w^r + \Delta G^0 - w^p$$

where w^r is the work of bringing the reactants to their reacting configuration and w^p the corresponding work for the reverse reaction. ΔG^0 is the free energy of the reaction when the donor and acceptor are at their optimal distance. $\Delta G_0^{\ddagger}$ is the so-called intrinsic activation barrier, which is actually one-fourth of the corresponding reorganization energy, λ. Here we use $\Delta g^{\ddagger}$ rather than $\Delta G^{\ddagger}$ for the activation barrier, following the consideration of Ref. 22. Equation (17) can also be written in the well-known form:

$$\Delta g^{\ddagger} = w^r + (\Delta G^0 + \lambda)^2/4\lambda \tag{18}$$

The phenomenological fitting processes yielded $\lambda = 5.6\,\text{kcal}\,\text{mol}^{-1}$ and $w^r \cong 10.0\,\text{kcal}\,\text{mol}^{-1}$. The estimated value of λ appears to be in conflict with the

value deduced from computer simulation studies ($\lambda \cong 80 \, \text{kcal mol}^{-1}$ in Ref. 46. Furthermore, the large value of w^r is hard to rationalize, since the reaction involves a proton transfer between a relatively fixed donor and acceptor (residue 64 and the Zinc bound hydroxide). The very small value of λ obtained by fitting Equation (18) to experiment is not exclusive to CA III. Similarly, small values were obtained in analysis of other enzymes and are drastically different than the values obtained by actual microscopic computer simulations (note in this respect that λ cannot be measured directly).

As pointed out before,[55–57] (see also section 7) the above discrepancies reflect the following problems. First, the reaction under study may involve more than two intersecting parabolas and thus cannot be described by Equation (18). Second, although Equation (18) gives a proper description for ET reactions where the mixing between the reactant and product state (H_{12}) is small, it cannot be used for describing proton transfer or other bond-breaking reactions, where H_{12} is large. In such cases one should use the HAW expression of Eq (13).[23,46]

In order to obtain a proper molecular description of LFERs, it is essential to represent each reactant, product or intermediate by a parabolic free-energy function.[22] In the case of CA III, we describe the proton transfer from residue 64 (Lys or His) to the zinc bound hydroxyl via a bridging water molecule (and alternatively two water molecules), by considering the three states:

$$\Psi_1 = BH^+(H_2O)_b(OH^-)_a Zn^{+2}$$
$$\Psi_2 = B(H_3O^+)_b(OH^-)_a Zn^{+2}$$
$$\Psi_3 = B(H_2O)_b(H_2O)_a Zn^{+2} \tag{19}$$

where we denote by B the base at residue 64, and where Ψ_1 and Ψ_3 correspond, respectively, to the right and left sides of Equation (16). The relative free energy of these states can be estimated from the corresponding pK_as, where the pK_as of $(H_2O)_a$ and B are known from different mutations,[50] while the pK_a of $(H_2O)_b$ can be calculated by the PDLD/S-LRA approach. Note that our three-state system can be easily extended to include one more water molecule and one more state.

Just to set the problem in a clear way for further considerations, we give in Fig. 5 the potential surface for the wild-type enzyme using pK_as of 5.0 and 9.0 for $(H_2O)_a$ and Lys64 (taken from Ref. 50) and $pK_a = 0$ for $(H_2O)_b$, evaluated by the PDLD/S-LRA method as described in the previous section.

With the model of Equation (19) and with a reasonable estimate of the free energies ΔG_{12}^0 and ΔG_{23}^0 we can start to evaluate the apparent activation barrier. Before doing so, we must clarify several points: (i) A Marcus' type relationship and the corresponding LFERs are *only* valid for a two-state system ($1 \rightarrow 2$), i.e., for a reaction with a single step. However, we have a three-state process that involves a two-step mechanism ($1 \rightarrow 2 \rightarrow 3$). Fitting such a system to a Marcus type formula can lead to nonphysical parameters (e.g., too small of a value for λ). (ii) In order to use the HAW approach in a three-state system (or in a four-state system) we must consider the elementary rate constants and then consider the preequilibrium concentrations.

That is, for the reaction:

$$1 \underset{\rightleftarrows}{\overset{k_{12}}{}} 2 \underset{\rightleftarrows}{\overset{k_{23}}{}} 3 \tag{20}$$

where $K_{12} = k_{12}/k_{21}$ involves the forward and backward rate constants k_{12} and k_{21}, while $K_{23} = k_{23}/k_{32}$ involves the rate constants k_{23} and k_{32}. Note that k_{13} corresponds to k_{-B} in Equation (16). We can fit the HAW equation to $\log k_{13}$ (or $\log k_B$), but if we want to obtain the LFER for the $1 \rightarrow 3$ step we must take into account the free energy of state two. After some manipulations[58] we obtain:

$$\begin{aligned}
\Delta g_{13}^{\ddagger} &\cong \Delta G_{12}^0 + [(\Delta G_{23}^0 + \lambda_{23})^2/4\lambda_{23} - H_{23}] + w \\
&= \Delta G_{12}^0 + (\Delta g_{23}^{\ddagger})_{di} - H_{23} + w
\end{aligned} \tag{21}$$

If the rate limiting step is $1 \rightarrow 2$, then k_{12} determines k_{13} and we can write:

$$\begin{aligned}
\Delta g_{13}^{\ddagger} = \Delta g_{12}^{\ddagger} &= (\Delta G_{12}^0 + \lambda_{12})^2/4\lambda_{12} - H_{12} + w \\
&= (\Delta g_{12}^{\ddagger})_{di} - H_{12} + w
\end{aligned} \tag{22}$$

Here we neglected for convenience the $(H_{12})^2$ term in Equation (13), since the corresponding correction is small in our case.

In view of the complexity of Equations (21) and (22), we find it more convenient to try to reproduce the observed LFER by direct evaluation of these equations using the relevant calculated and observed parameters, with only a minimal adjustment procedure. Our starting point is the estimate of ΔG_{12}^0 and ΔG_{23}^0 for the different mutants studied in Ref. 50. The relevant free-energy values were obtained using the observed pK_as of $(H_2O)_a$ and B_{64}, and the calculated pK_a of $(H_2O)_b$. We used the value $\lambda_{23} \cong 80\,\text{kcal mol}^{-1}$ obtained from EVB simulations[46] as a generic value for both λ_{12} and λ_{23}. The value of $H_{ij}(x^{\ddagger})$ was taken as $18\,\text{kcal mol}^{-1}$ (which reflects a minor adjustment from the value found in Ref. 46) and $\bar{H}_{ij}(x_0)$ was taken as $10\,\text{kcal mol}^{-1}$ from an EVB study of a proton transfer from $(H_2O)_a$ to $(H_2O)_b$. With the estimated ΔG_0, λ and $\bar{H}_{ij}$, we evaluated the diabatic free-energy functions and used them to obtain the corresponding $(\Delta\Delta g^{\ddagger})_{di}$ and $\Delta\Delta g^{\ddagger}$ for several mutants, as is illustrated graphically in Figs. 5–7. The resulting dependence of $\Delta\Delta g^{\ddagger}$ on ΔG_{13} is presented in Fig. 7. As seen from the figures our model reproduced the observed trend. However, the origin of the trend is very different than that deduced from the two-state Marcus' equation. That is, the flattening of the LFER at $\Delta pK_a > 0$, which would be considered in a phenomenological analysis of a two-state model as the beginning of the Marcus' inverted region (where $\Delta G_0 = -\lambda$), is due to the behavior of the three-state system (see Ref. 58).

The extraction of λ from fitting Equation (18) to the observed LFER requires that $\lambda = -\Delta G^0$ so that $\Delta G^0 < 0$ at the point where the LFER becomes flat. This means that we must have data from regions where $\Delta G^0 < 0$. However, at least for the cases when $\Delta g_{12}^{\ddagger}$ is rate limiting, ΔG_{12}^0 cannot be negative, and the observation of the beginning of a flat LFER is actually due to other factors. It is also important to realize that λ_{out} cannot become too small and never approach 0, which is the continuum limit for a completely nonpolar environment (see discussion in Ref. 59). The
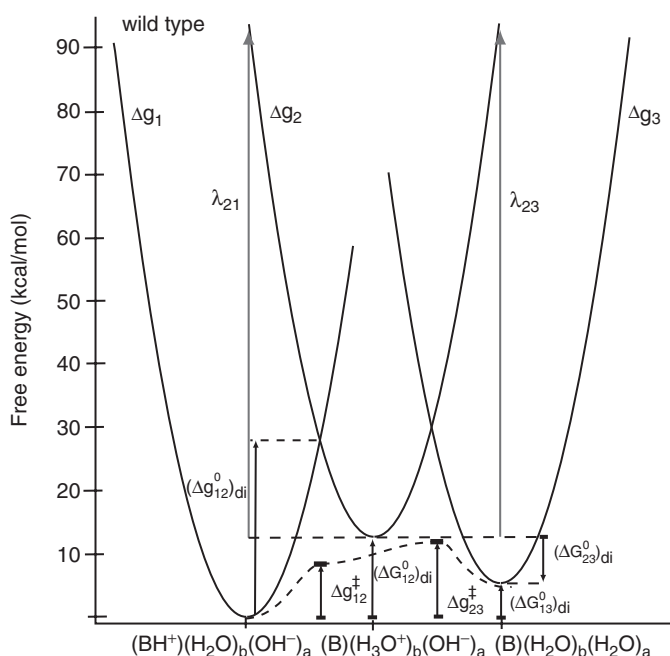
Fig. 5 Three-state description of the PT in CA III for a case where the transfer involves two water molecules (taken from Ref. 58).

reason is quite simple; the protein cannot use a nonpolar environment, since this will decrease drastically the pK_a of $(H_2O_b^+)$. Instead, proteins use polar environments with partially fixed dipoles. However, no protein can keep its dipoles completely fixed (the protein is flexible) and thus gives a nonnegligible λ_{out}. Of course, this reorganization energy is still smaller than the corresponding value for proton transfer in solutions, but it never approaches the low value obtained from fitting in a two-state Marcus' formula.[60]

As long as we obtain the value of H_{ij} from fitting to observed LFERs, it is possible to argue that both Equations (18) and (13) reflect a phenomenological fitting with a free parameter (w and λ in the case of Equation (18), and H_{ij} in the case of Equation (13)). The difference, however, is that Equation (13) and the use of three free-energy functionals reflects much more realistic physics. This is evident, e.g., from the fact that with Equation (13) we do not obtain an unrealistically large w^r. Note in this respect that ΔG_{12}^0 in Equation (21) might look like w in the phenomenological fitting to the Marcus' equation. It is also important to emphasize at this point that the present treatment is not a phenomenological treatment with many free parameters, as might be concluded by those who are unfamiliar with molecular simulations. That is, our approach is based on realistic molecular parameters obtained while starting from the X-ray structure of the protein and reproducing the relevant pK_as and reorganization energy. Reproducing the observed LFER by such an approach without adjusting the key parameters is fundamentally different than an approach
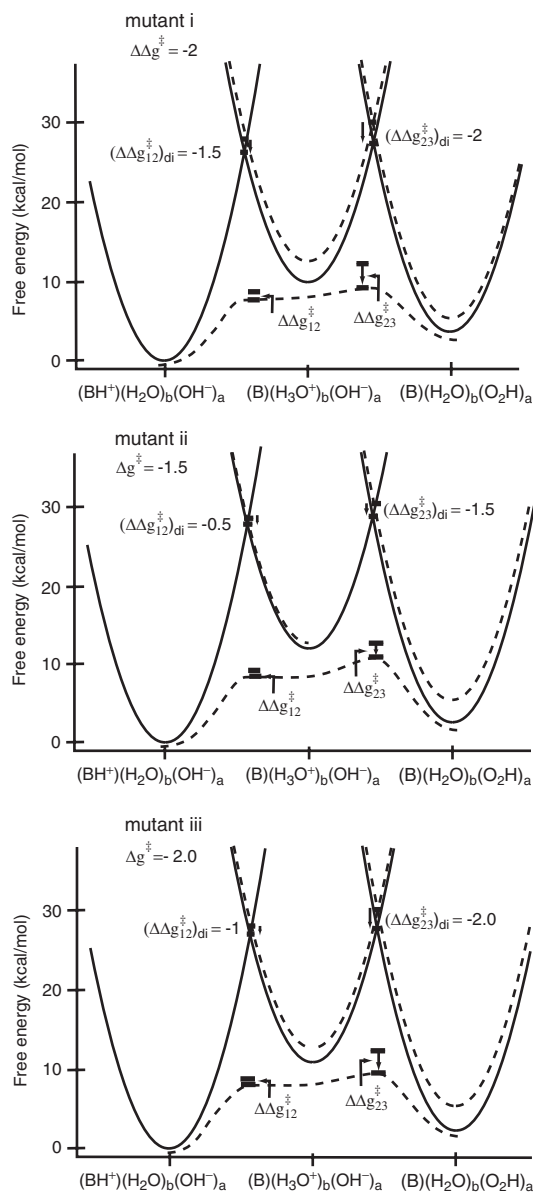
Fig. 6 Analysis of the energetics of PT in the i, ii, and iii mutants of CA III. The figure describes the three states of Equation (19) and considers their change in each of the indicated mutants (relative to the native enzyme). The figure displays the changes in the diabatic potential surfaces and the corresponding changes in the adiabatic activation barriers. The figure also gives the changes in the diabatic activation energies. The final activation barrier is taken in each case as the highest adiabatic barriers (taken from Ref. 58).
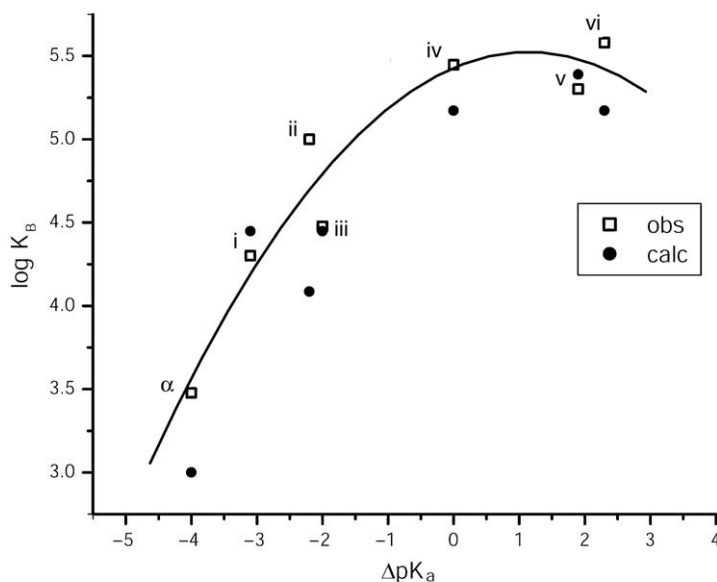
Fig. 7 Calculated and observed FER for CA III. The different systems are marked according to the notation of Ref. 58. The term ΔpK_a corresponds to the pK_a difference between the zinc-bound water and the pK_a of the given donor group ($\Delta pK_a = -\Delta G_{13}/2.3RT$).

that takes the observed LFER and adjusts free parameters in a given model to reproduce it. In such a case, one can reproduce any experiment by almost any model.

Finally, we would like to address the validity of the general use of Equation (13) and the multi-state procedure used for studies of the PTR in CA. The use of Equation (13) for subsequent PT steps might look to some as an ad hoc approach, considering the assumption that PTR processes involve the Grotthuss mechanism, which is not sensitive to the ΔG_{ij}^0 values for the sequential transfer process. However, the assumption that the Grotthuss mechanism is a key factor recently underwent a major paradigm shift, where those who supported this idea started to attribute major importance to the electrostatic barrier,[61] in agreement with our view.[62,63] Further support to this point is given below.

In order to further explore the validity of the stepwise modified Marcus' model, we developed recently[64] a simplified EVB model which represents the given conduction chain by an explicit EVB, while representing the rest of the environment (protein and solvent) implicitly. The implicit treatment forces the minima of the free-energy parabolas of the simplified model to coincide with those of the full model. The dynamics of the system are then studied by Langevin dynamics (LD) simulation. The simulation established that the rate of the PTR process is determined by the energetics of the proton along the conduction chain, once the energy of the proton in two successive sites is significantly higher than the energy of the proton in the bulk water. The model was also applied to PTR in the K64H-F198D mutant of
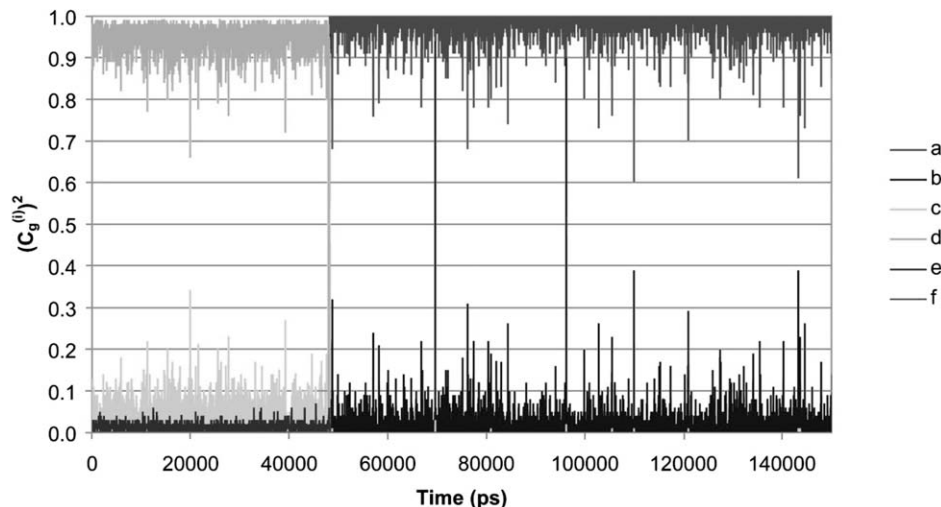
Fig. 8 The time dependence of the probability amplitude of the transferred proton for a LD trajectory for a PTR that starts at His64 and ends at OH⁻ in the overdamped version of model S/A of the K64H-F198D mutant of CA III. The calculations were accelerated by considering a case where the minimum at site d is raised by $1.2\,\mathrm{kcal\,mol^{-1}}$ (taken from Ref. 64).

CA III and reproduced the observed rate constant. Typical simulations for the case where the energy of the proton on His64 is raised by $1.2\,\mathrm{kcal\,mol^{-1}}$, in order to accelerate the calculations, are described in Fig. 8. The calculated average time for PTR from His64 to the Zn-bound hydroxide is about $5 \times 10^{-6}\,\mathrm{s}$. Correcting this result for the energy shift and the effect of using overdamped rather than underdamped Brownian dynamics (BD) simulation gives a result that is close to the observed k_B of Eq (16) ($k_\mathrm{B} = 3 \times 10^{-6}\,\mathrm{s}$). The simulation provides an additional major support for the use of the HAW model.

5   Protein reorganization energy and the preorganization concept

The previous sections established the validity of the EVB as a general tool for analyzing activation barriers in enzymes and for correlating them with different factors. Since the HAW equation reproduces the EVB trend, we may now ask which parameters contribute to the catalytic effect, and what is the molecular origin of the changes in these parameters. As shown in Fig. 9, the enzyme can reduce $\Delta g^{\ddagger}$ by reducing ΔG^0 or λ in the Marcus' formula or in the HAW equation (where it can also increase H_{12}). In fact, the question whether the catalysis is due to the reduction of ΔG^0 or λ has attracted significant interest.[60,65] Unfortunately, the real question is: what is the molecular origin of the reduction of ΔG and λ? Superficial considerations seem to suggest an almost trivial way for the reduction of λ and the corresponding
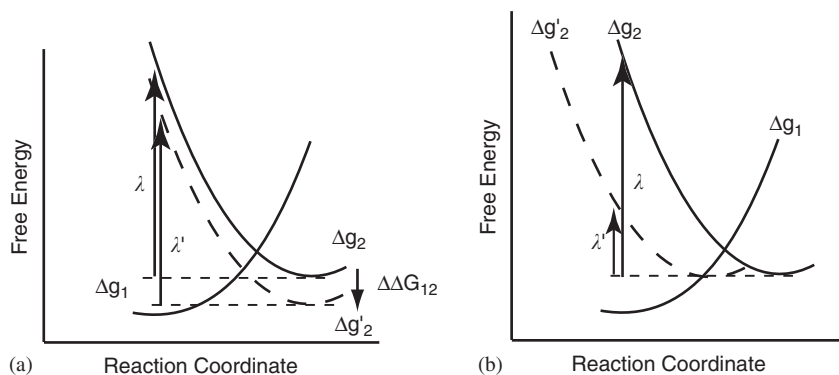
Fig. 9 Different models for reducing $\Delta g^{\ddagger}$. (a) ΔG_{12} is reduced while keeping the shape of the free-energy functionals and the reorganization energy unchanged. (b) The minimum of Δg_2 is shifted, thus changing the reorganization energy. The figure presents the given trend while considering the diabatic states. The adiabatic GS follows basically the same trend.

catalytic effect. All that is needed according to the dielectric continuum theory is reduction in the dielectric constant, and thus it is tempting to suggest that the protein reduces λ by providing a nonpolar active site and thus a low dielectric constant.[65,66]

Unfortunately, nonpolar active sites increase rather than decrease the energy of polar TSs (relative to the corresponding energy in water). Similarly, nonpolar active sites do not help in reducing the energy of charge transfer reactions where the RS is more polar than the TS, despite the reduction in reorganization energy (see Fig. 10). Apparently, enzyme active sites are polar rather than nonpolar, and the origin of the reduction of $\Delta G^{\ddagger}$ must be more complex.

Our starting point in exploring the origin for the reduction of $\Delta g^{\ddagger}$ is what was learned from computer simulation of enzymatic reactions. Such studies repeatedly showed that the difference between $\Delta g^{\ddagger}_{cat}$ and $\Delta G^{\ddagger}_{cage}$ is mainly due to electrostatic effects. The calculations indicated that enzymes "solvate" their TSs more than the corresponding TSs in the reference solution reactions.[67] The nature of this "solvation" effect appeared to be far from obvious. That is, the calculated interaction energy between the TS charges of the reacting atoms and the enzyme was found to be similar to the corresponding interaction energies in solution. This finding indicated that the "strength" of the interactions could not explain the catalytic effect. However, since the calculated electrostatic energy does account for the catalytic effect, it is clear that we must examine the entire electrostatic energy associated with the formation of the TS,[22] rather than only on the interaction energy at the TS. This includes the penalty for the reorganization of the environment upon "charging" the TS.

In order to analyze and quantify the overall electrostatic contribution associated with the binding of the TS, it is useful to evaluate the free energy of forming the TS charges in the enzyme and in solution. Performing such calculations by a FEP approach is very demanding, but fortunately they can be approximated conveniently
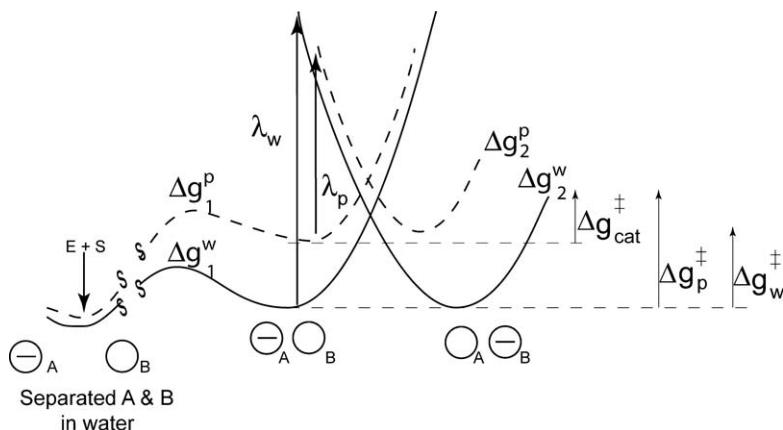
Fig. 10 Showing the effect of a hypothetical nonpolar protein on the activation energy of a charge transfer reaction. As seen from the figure, the reduction in polarity leads to small λ, but does not reduce $\Delta g^{\ddagger}$. That is, while $\Delta g^{\ddagger}_{cat}$ is indeed smaller than $\Delta g^{\ddagger}_{w}$ in such a hypothetical active site, the GS is largely destabilized relative to its energy in solution (shown on the left-hand side of the figure). Thus, we have actually a RSD mechanism and $\Delta g^{\ddagger}_{p}$, which corresponds to k_{cat}/K_{M}, is not smaller than $\Delta g^{\ddagger}_{w}$. Furthermore, no such active site has been ever found in careful studies that actually examined the corresponding polarity.

by using the LRA:[68]

$$\Delta G(Q^{\ddagger}) = 0.5(\langle U(Q = Q^{\ddagger}) - U(Q = 0)\rangle_{Q=Q^{\ddagger}}$$
$$+ \langle U(Q = Q^{\ddagger}) - U(Q = 0)\rangle_{Q=0})$$
$$= 0.5(\langle \Delta U\rangle_{Q=Q^{\ddagger}} + \langle \Delta U\rangle_{Q=0}) \tag{23}$$

where U is the solute–solvent interaction potential, Q designates the residual charges of the solute atoms with $Q^{\ddagger}$ indicating the TS charges, and $\langle \Delta U\rangle_{Q}$ designates an average over configurations obtained from an MD run with the given solute charge distribution. The first term in Equation (23) is the aforementioned interaction energy at the TS, where $Q = Q^{\ddagger}$, which is similar in the enzyme and in solution. The second term expresses the effect of the environment preorganization. If the environment is randomly oriented toward the TS in the absence of charge (as is the case in water), then the second term is 0 and we obtain:

$$\Delta G(Q^{\ddagger})_{w} = \frac{1}{2}\langle \Delta U\rangle_{Q^{\ddagger}} \tag{24}$$

where the electrostatic free energy is half of the average electrostatic potential.[56] However, in the preorganized environment of an enzyme, we obtain a significant contribution from the second term and the overall $\Delta G(Q^{\ddagger})$ is more negative than in water. This extra stabilization is responsible for the catalytic effect of the enzyme.

Another way to look at the above transition state stabilization (TSS) is to realize that in water (where the solvent dipoles are randomly oriented around the uncharged form of the TS) activation free energy includes the free energy needed to

reorganize the solvent dipoles toward the charged TS. On the other hand, the reaction in the protein costs less reorganization energy since the active site dipoles (associated with polar groups, charged groups and water molecules) are already partially preorganized toward the TS charges,[22,67] although this is associated with polar rather than nonpolar environments.

It is important to note that the reorganization energy associated with the binding of the TS charges is given by:

$$\lambda^{\neq} = 0.5(\langle \Delta U \rangle_{Q=Q^{\neq}} - \langle \Delta U \rangle_{Q=0}) \tag{25}$$

This reorganization energy is related to the well-known Marcus' reorganization energy, but it is not equal to it. More specifically, the Marcus' reorganization energy[69] is related to the transfer from the reactant to the product state, while here we deal with charging the TS (see discussion in Ref. 4). Nevertheless, calculations of the Marcus' reorganization energy in enzymes and in solution are also consistent with the above idea, and it has been repeatedly found that λ_p is smaller than λ_w (see Refs. 2,4,70,71), although this is associated with polar rather than nonpolar environments.

It is also useful to point out that the nature of the reorganization energies and the way to evaluate this quantity is still not widely recognized in the computational chemistry community. This is due in large extent to unfamiliarity with EVB-based evaluation of reorganization energy, and the difficulty to obtain this quantity by standard molecular orbital (MO) approaches. Some workers still assume, based on experimental analysis and ab initio calculations, that the reorganization energy is very small in contrast to the EVB results of Ref. 54. The reason for this is associated with the assumption that the reorganization energy can be obtained from the $\Delta G^{\ddagger}$ of Equation (17) using the relationship $\Delta G^{\ddagger} = \lambda/4$. Unfortunately, $\Delta G^{\ddagger}$ (the so-called intrinsic barrier) corresponds to the adiabatic barrier, which reflects the effect of H_{12}. A proper calculation of λ by using the diabatic functional of Equation (7) gives unique and stable results with large λ_p.[54]

Now, although all currently available consistent calculations have identified electrostatic free energies as the key element in structure–catalysis correlation, these findings may seem to be inconsistent with the many available alternative proposals. Thus, it is important to establish that those proposals which do not reflect electrostatic effects are either problematic or involve only small catalytic contributions. This point will be illustrated below, focusing on key alternative proposals.

6 Applying our concepts to different catalytic proposals

As stated above, consistent simulation studies have established electrostatic effects as the key factor in enzyme catalysis. Nevertheless, it is crucial to examine the validity of alternative proposals and the magnitude of the corresponding contributions. Such an examination will be performed below, focusing on the use of the physical organic chemistry concepts considered in the previous sections.

THE DESOLVATION PROPOSAL AND THE ASSUMPTION THAT ENZYME ACTIVE SITES ARE NONPOLAR

Many catalytic proposals involve the idea of reactant state destabilization (RSD). These proposals involve the strain proposal,[72] the entropy proposals,[73–75] and the popular concept that enzymes provide a nonpolar (sometimes described as gas phase-like) environment that destabilizes a highly charged GS (e.g., Refs. [76–79]). All of these proposals were considered elsewhere,[4,40] but in the general context of the present review, it is very useful to consider the desolvation and related proposals. The validity of the desolvation idea has been examined carefully (e.g., Ref. [22]) and was found to reflect improper thermodynamic cycles that do not use a correct reference state. This amounts to ignoring the desolvation energy associated with taking the RS from water to a hypothetical nonpolar enzyme site. With a proper reference state, one finds[22] that a polar TS is less stable in nonpolar sites than in water, and that the RSD does not help in increasing k_{cat}/K_m. Thus, there is no evolutionary pressure for this mechanism. In fact, many desolvation models (e.g., Refs. [77,80]) involve ionized residues in nonpolar environments. Such residues would be unionized in nonpolar sites. Moreover, in any specific case, when the structure of the active site is known, one finds by current electrostatic models a very polar (rather than nonpolar) active site environment near the chemically active part of the substrate. A case in point is pyruvate decarboxylase, which was put forward as a classical case of RSD by desolvation.[76] However, the structure of this enzyme[81] appeared to be very polar. Unfortunately, despite the obvious fact that groups near charges were in polar rather than nonpolar environments, it is still assumed by some (e.g., Ref. [82]) that ion pairs are stabilized in nonpolar environments, and that this is the way pyruvate decarboxylase catalyzes its reaction. However, as clarified in many of our papers, ion pairs are destabilized (relative to water) rather than stabilized.[83] Failing to realize this seemingly counterintuitive point is one of the obstacles to the application of the principles of physical organic chemistry to biological problems.

A detailed illustration of the problem with the desolvation and related RSD proposals has been given in the case of Orotidine 5′-monophosphate decarboxylase (ODCase)[79] and in the case of serine proteases.[84] Although these cases are very instructive, we chose to focus here on an example that is directly related to our discussion of S_N2 reactions. Thus, we will discuss here a recent paper by Devi-Kesavan and Gao.[85] These workers examined the origin of the catalytic power of haloalkane dehalogenase (DhlA) by a QM/MM approach. The calculations reproduce the correct trend of the catalytic effect, indicating that it is due to electrostatic effects. It was also found that the activation barrier is higher in water than in the enzyme, and that the reaction in water involves loss of solvation energy (the corresponding solvation analysis is not done in the enzyme). However, these findings were probably confused with the desolvation proposal. That is, the desolvation proposal states very clearly and unambiguously that the enzyme solvates the GS less than water does, regardless of the relative solvation of the GS and TS in water (e.g., Refs. [22,73,76]). Thus, examination of the origin of the catalytic effect should
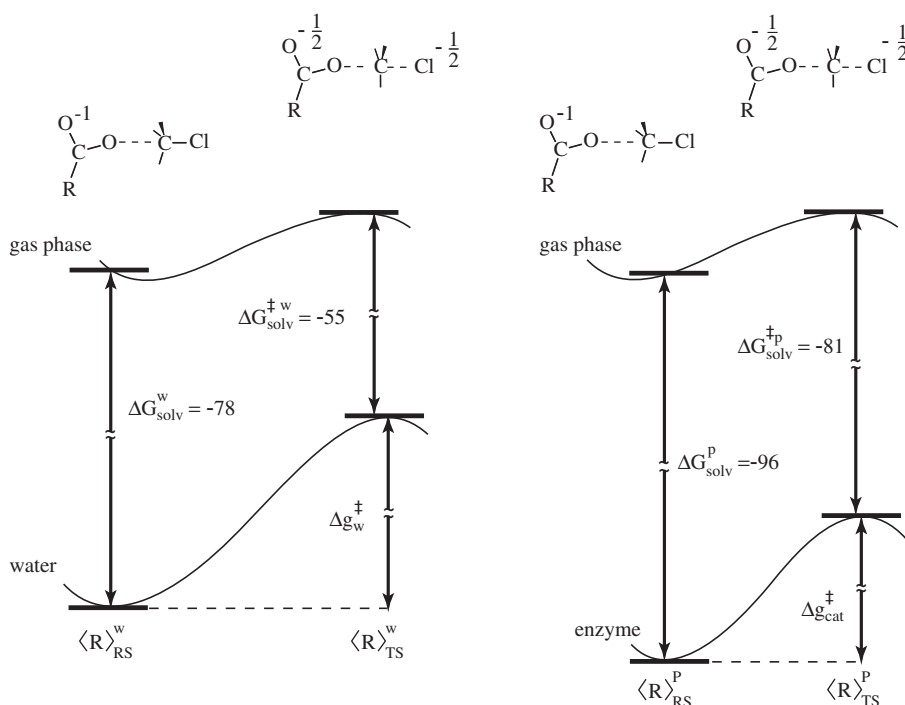
Fig. 11 Showing a schematic description of the energetics of the S_N2 reaction in DhlA and the reference water system. The figure focuses on the effects of the solvation free energies. As seen from the figure, the solvation of both the RS and TS is larger in the enzyme than in solution. Moreover, the solvation of the TS is considerably larger in the enzyme than in water. This is the origin of the catalytic effect; note however, that the catalytic effect is not directly given by this solvation difference or by the difference between the RS and TS, but by the relevant difference between the enzyme and solution reaction (see also the text). Note also that the bars on the gas-phase profile does not correspond to the gas-phase minimum (see Ref. 88).

involve comparison of the solvation of the GS in the enzyme and in water, and the solvation of the TS in the enzyme and in water (rather than comparison of the activation barriers in enzyme and in water).

In order to clarify the above point, we provide in Fig. 11 an LRA analysis of the energetics of the RS and TS. The figure considers the solvation free energies of the RS and TS, and basically reproduces most of the catalytic effect (see also Ref. 86). Now, as can be seen from the figure, the enzyme solvates the RS more (rather than less) than the solvent cage. Thus, the calculations reported in Fig. 11 are inconsistent with the desolvation proposal. Instead, as is the case with other systems that were proposed to work by the desolvation proposal (see Refs. 22,79 for discussion), the enzyme solvates the delocalized TS much more than water does (-81 versus approximately -55). Thus, TSS is the source of the catalytic power of the enzyme (see also below for the relationship of this effect to the protein preorganization).

Interestingly, the desolvation proposal requires that the charge on Asp124 (the nucleophile in the reaction) will be much less stable in the enzyme than in water. This will lead to an increase in its pK_a value and will force the Asp to accept a proton at pH 7 (see a related discussion in Ref. 79).

In conclusion, examination of the origin of the catalytic effect should involve comparison of the solvation of the GS in the enzyme and in water, and the TS in the enzyme and in water (rather than comparison of the activation barriers in enzyme and in water). However, our study (Fig. 11) has shown clearly that DhlA stabilizes (solvates) its GS as much as water does and solvates its TS much more than water does.

The problem can best be illustrated by realizing that the catalytic effect is determined by $\Delta\Delta g_p^{\ddagger} - \Delta\Delta g_w^{\ddagger}$. This quantity can be evaluated by considering the following cycle:

$$\Delta g_{cat}^{\ddagger} = (\Delta g_{gas}^{\ddagger}) + (\Delta G_{solv}^{p})_{TS} - (\Delta G_{solv}^{p})_{RS} - \Delta\Delta G_{RS^g \to RS^p}^{p}$$
$$\Delta g_{w}^{\ddagger} = (\Delta g_{gas}^{\ddagger}) + (\Delta G_{solv}^{w})_{TS} - (\Delta G_{solv}^{w})_{RS} - \Delta\Delta G_{RS^g \to RS^w}^{w} \tag{26}$$

where $\Delta\Delta G$ designates the change in solvation energies moving from the gas phase GS geometry to the RS geometry in the protein or solution system. Now, using this cycle to evaluate the catalytic effect we have:

$$\Delta\Delta g_{w \to p}^{\ddagger} = \Delta g_{cat}^{\ddagger} - \Delta g_{w}^{\ddagger} \simeq (\Delta G_{solv}^{p})_{TS} - (\Delta G_{solv}^{w})_{TS} - (\Delta G_{solv}^{p})_{RS}$$
$$+ (\Delta G_{solv}^{w})_{RS} = (\Delta\Delta G_{solv}^{\ddagger})^p - (\Delta\Delta G_{solv}^{\ddagger})^w \tag{27}$$

where for simplicity, we neglected the last terms in Equation (26), since these terms were found to be small in Ref. 86. Obviously, this expression is independent of the gas-phase barrier. Furthermore, we cannot determine this expression by only considering $(\Delta\Delta G_{solv}^{\ddagger})^w$. Thus, in order to determine the catalytic effect, we must consider the solvation in the TS and RS, both in the protein and in solution.

One might still assume that the above analysis is inconclusive, considering the arguments of Ref. 87 that the EVB approach is not reliable, in view of what they considered as the gas phase results of Ref. 86. However, first the EVB is probably still the most reliable method in evaluating the catalytic effect (see discussion in Section 2) and is clearly more reliable than the QM/MM approach of Ref. 87, whose results changed drastically from their previous value.[85] Second, what was considered as the gas phase results of Ref. 86 does not reflect the actual gas phase activation energy (since it is *not* evaluated at the gas phase minimum). This issue is further clarified in Ref. 88. Third, the analysis of Equation (20) does not depend on the EVB surface, but only on the use of reasonable solute charges, and mainly on the ability to perform reliable electrostatic calculations.

Finally, it may be instructive to consider a recent work of Dinner et al.,[89] which examined the catalytic mechanism of uracil-DNA glycosylase, suggesting that the system works by substrate autocatalysis, where presumably the burial of the polar phosphate groups stabilize the positively charged TS. While the finding of electrostatic TS stabilization is probably correct, the overall analysis is problematic. First, the use of the concept "substrate autocatalysis" is in some respects an oxymoron.

That is, obviously the correct reference state is the substrate in solution, and thus the substrate does not provide catalysis (also it is useful to note that very different theoretical models were used for the enzyme and solution reaction). The only way that parts of the substrate would stabilize the TS is that the energy of these parts plus the rest of the TS will be reduced (relative to the GS) due to the real source of catalysis, which is the protein reorganization energy. In fact, saying that the substrate's negative charge stabilizes the positively charged oxycarbenium is in some respects like saying that ion pairs in proteins are stabilized due to their gas phase Coulombic interaction. In fact, as was shown in our countless studies of related cases, (e.g., Refs. 56,90) the issue is the ability of the protein to provide larger stabilization of the ion pair (or the specific charge distribution of the given TS plus the substrate charges) than the solvent in the reference system. Finally, it is important to note that in contrast to the possible impression, the catalysis is not due to a desolvation effect where a presumably low dielectric environment increases the effect of the phosphate charges, but to a preoriented, very polar environment that stabilizes the phosphate and oxycarbenium *more* than water does.

THE NEAR ATTACK CONFORMATION PROPOSAL

An interesting proposal put forward by Bruice (e.g., Ref. 91) implies that enzyme catalysis is associated with the ability of the enzyme to bring the reacting fragments to the so-called near attack conformation (NAC). Unfortunately, the definition of this proposal was based on selecting the critical distance and angle, where the NAC is supposed to occur, rather than on free-energy surfaces that could be related directly to the difference between $\Delta g_w^{\ddagger}$ and $\Delta g_{cat}^{\ddagger}$. That is, the activation free energy can only be defined by the difference between the free energy at the TS and the lowest point at the RS minima, or by the difference between the free energy in the TS and the overall free energy of the RS (see Ref. 40). Thus, selecting an arbitrary point along the reaction coordinate as a reference for the evaluation of the activation energy cannot give unique results. In fact, in some respects the NAC proposal resembles the idea that the height scaled by a mountain climber will be smaller if the climber stops at an intermediate camp to rest. Furthermore, the NAC proposal suffers from being ill defined in several other crucial points (see Ref. 86). However, despite these problems a reasonable definition of what is meant by the NAC proposal has emerged, and it can be summarized in Fig. 12, which basically represents the current picture offered by the NAC proponents,[92,93] in a consistent way that allows one to examine this proposal. The description given in Fig. 12 relates the NAC effect to the free energies at $\langle R \rangle_{RS}^{p}$ and $\langle R \rangle_{RS}^{w}$, where R is the solute contribution to the reaction coordinate. That is, if we evaluate $\langle R \rangle_{RS}^{p}$, we may ask how much it would cost to reach $\langle R \rangle_{RS}^{p}$ in water. We may approximate the NAC free energy by:

$$\Delta G_{NAC} \approx \Delta G(R = \langle R \rangle_{RS}^{p})_w - \Delta G(R = \langle R \rangle_{RS}^{w})_w \tag{28}$$

where $\Delta G(R)_w$ is the value of the free-energy profile in water at the indicated R. In the above approximation, $\langle R \rangle_{RS}^{p}$ provides a proper definition for the NAC distance.
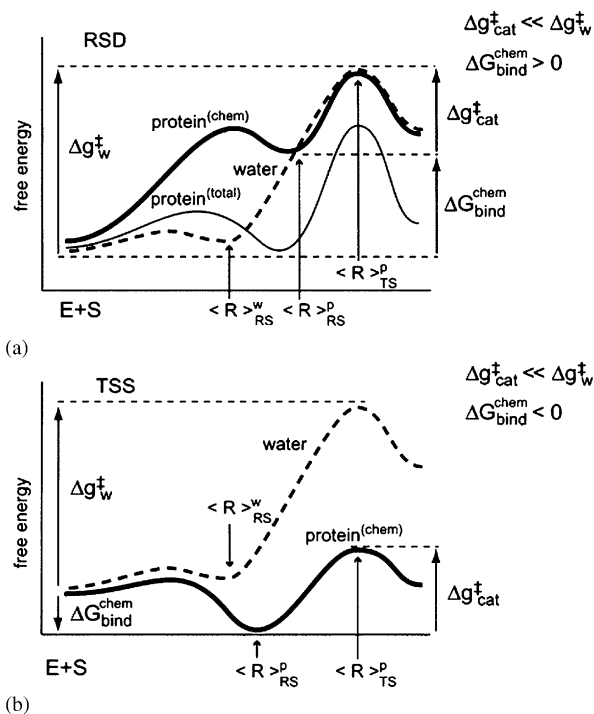
Fig. 12 Schematic description of the free-energy profiles in protein (bold and plain lines) and in water (dashed line) for the limiting cases of RSD and TSS, which are shown in the upper and lower panels, respectively. The figure focuses for simplicity on the profiles for the "chemical part" of the substrate (bold line) and describes in panel (a) the profile for the chemical plus nonreactive part of the substrate (see text). For simplicity, we consider a case where the binding of the nonreactive part is along a coordinate orthogonal to the reaction coordinate (for discussion see Ref. 92).

With the above definition, there are clear cases where it is easy to show that the NAC effect does not contribute significantly to catalysis.[86] However, in order to clarify our perspective, we will intentionally take the chorismate mutase (CM) case where the NAC effect might seem to be very significant. The catalytic reaction of this enzyme (i.e., the Claisen rearrangement of chorismate to prephenate[94]) has been the subject of a large number of theoretical studies (e.g., Refs. 95–97). A superficial examination of the results of different studies may suggest that we have here a clear case of RSD. For example, recent MD studies of Hur and Bruice[93,98] indicated that the enzyme helps in bringing the reacting atoms of the substrate to typical short distances that are rarely attained in water. Thus, they considered this NAC effect as the major reason for the catalytic power of CM. In view of this finding it is useful to examine the origin and consequences of cases where $\langle R \rangle_{RT}^{p}$ is smaller than $\langle R \rangle_{RT}^{w}$. In particular, we would like to know if this is simply a reflection of the fact that the TSS flattens the potential

surface in the enzyme and thus, $\langle R \rangle_p$ decreases, or whether it is some type of ground state destabilization (GSD). Thus, we should find out whether the NAC represents a genuine reason for catalysis, or if it merely reflects the result of electrostatic TSS.

In order to explore the above issue, we performed LRA calculations of the binding free energy of the RS and TS. The results combined with the EVB free-energy profiles are summarized in Fig. 13. Using the binding free energies established that the correct version of Fig. 13 corresponds to TSS. Thus, the apparent NAC is not the reason for the catalysis, but the result of TSS. With this in mind, we tried to find the exact reason for the apparent NAC effect. This was done by performing two sets of calculations, one set with the full EVB, and the other where we omitted the electrostatic interaction between the two carboxylates, and between the carboxylates and their surrounding environment. The results of our analysis are shown in Fig. 14. As seen from the figure, the omission of the electrostatic contribution from the carboxylates leads to disappearance of most of the catalytic effect, and the rest disappears when all residual charges of the substrate are set to zero. Thus, the main difference between the reaction in CM and in water is due to TSS electrostatic effects.

Now, the reacting system (see Fig. 13 for a schematic description) involves two negative charges, which are covalently linked to the atoms involved in the
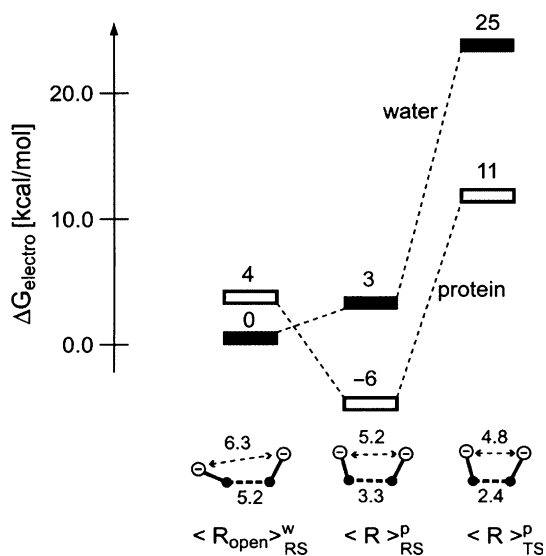
Fig. 13 LRA estimate of the electrostatic free energy for several points along the reaction coordinate of CM. Energies in kcal mol^{-1} are indicated over the corresponding bars. Distances in angstroms are given for the separation between the carboxylate charge centers (designated by (—)) and for the distances between C_1 and C_9. The relative position of the protein and water profiles are set in a way that the binding energy at $\langle R \rangle_{RS}^P$ will correspond approximately to the observed ΔG_{bind} (-5.6 kcal mol^{-1}). The TS free energy in water includes a constant term that reproduces the corresponding observed value (since the LRA electrostatic contribution does not include the intermolecular activation energy). The same constant is used for the protein TS (taken from Ref. 92).
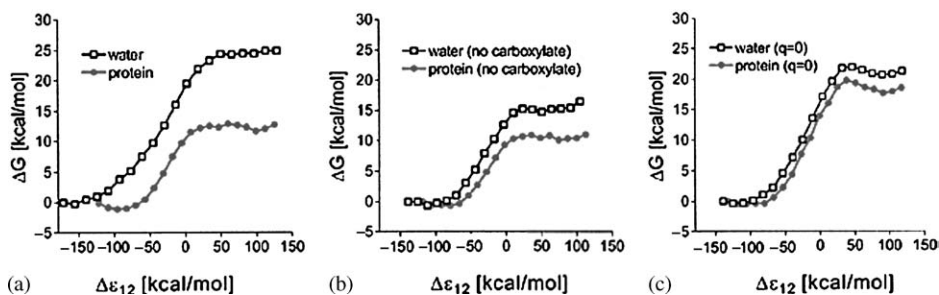
Fig. 14 Free-energy surfaces for the reaction in water and in CM for cases where (a) the complete system is included, (b) the charges of the carboxylate groups are set to zero, and (c) all the charges and residual charges of the whole substrate are set to zero.

bond-making process. Thus, a major part of the electrostatic TSS involves stabilizing the two carboxylates at a close proximity to each other. This electrostatic stabilization leads to a reduction in the average C_9–C_1 distance relative to the corresponding distance in water. Although this change in equilibrium distance can be called an NAC effect, it is simply the *result* rather than the *reason* of the catalytic effect. That is, in analyzing enzyme catalysis it is very important to determine what factors actually lead to the overall catalytic effect, and to distinguish these factors from other effects that are byproducts of the catalytic factors. For example, if an enzyme operates by electrostatic stabilization and the electrostatic effect also leads to a change of the color of the substrate, we will have to recognize the change in color is a result and not a reason.

Finally, it is instructive to consider a recent work of Hur et al.,[99] who studied different mutants of CM and found that the calculated GS energies at the NAC distance provide an excellent correlation with the corresponding observed changes in the activation free energies. These workers argued that the enzyme does not catalyze its reaction by TSS, but by a GS effect. While the calculated correlation is impressive, it does not establish the point it sets out to prove. That is, proper energy diagrams that describe the calculated results (both in papers of Bruice and co-workers and in papers that analyzed this issue (e.g. Ref. [92])) have shown that the overall effect is a TSS effect. Furthermore, the calculated NAC energies involve significant overestimates. For example, the calculated energy in water is about $8 \, \text{kcal mol}^{-1}$, which is significant larger than the estimate of about $3–5 \, \text{kcal mol}^{-1}$ obtained by others.[92,100,101] Similarly, the values obtained for some mutants are likely to involve major overestimates (they reflect an upper limit with an arbitrary definition of the NAC structure, and also reflect the assumption that the reaction coordinate is identical for the native and mutant enzyme). The most important point, however, is the fact that a much more meaningful correlation is expected between the reduction of the TSS energies and the activation energies. In fact, one does not need much calculations to realize this point, since obviously the catalysis is related to the changes in $\Delta g_{\text{cat}}^{\ddagger}$ and once we agree that we have TSS, we also per definition have a one to one correlation between $\Delta \log(k_{\text{cat}})$ and $\Delta\Delta g_{\text{cat}}^{\ddagger}$.

THE LOW-BARRIER HYDROGEN BOND PROPOSAL CAN BE BEST EXAMINED BY USING VB CONCEPTS

The catalytic role of hydrogen bonds (HBs) has been an issue of significant controversy since the identification of the oxyanion hole in subtilisin.[102] This structural observation was clearly consistent with the idea that HBs can stabilize the tetrahedral intermediate, but could not provide any estimate of the relevant catalytic energy. Subsequent theoretical studies[67,103,104] have established the idea that the overall electrostatic effect of preorganized HBs contributes in a major way to enzyme catalysis. These theoretical predictions were confirmed by mutation experiments, showing clearly that a single HB can contribute around $5\,\mathrm{kcal\,mol^{-1}}$ to an ionic TS.[105,106] The results of some specific mutation experiments were subsequently reproduced by FEP/US calculations.[103]

After the experimental demonstration of TSS by HBs, it has been proposed by several workers that HBs stabilize TSs in a special nonelectrostatic way, which was termed low-barrier hydrogen bond (LBHB).[107–109] The LBHB proposal has suggested that catalytic HBs involve a flat minimum rather than a double minimum. Unfortunately, this suggestion (which is sometimes true) does not allow one to distinguish the LBHB proposal from the previous proposal of ionic HBs (and thus, does not provide a testable definition).

In order to distinguish between ionic HBs and LBHBs, it is essential to first define the LBHB proposal in a way that reflects the energetics of the system and can be used to determine the actual catalytic contribution associated with this proposal. At present, the best way to define the LBHB proposal is to use the VB representation. This representation can be treated in a simplified two-state version of the three-state model of Coulson and Danielsson,[110,111] augmented by the EVB solvent effect.[22] Here we consider as an example the $[X^-\ H - Y \rightleftharpoons X - H\ Y^-]$ system, but the same considerations will be applicable to the $[X^-\ -\ H - B^+ \rightleftharpoons X - H\ B]$ system. At any rate, in the two-state VB representation we can describe the total wave function by:

$$\Psi = C_1\Phi_1 + C_2\Phi_2 \tag{29}$$

where $\Phi_1 = [X^-\ H - Y]$ and $\Phi_2 = [X - H\ Y^-]$ are the diabatic wave functions whose energies are E_1 and E_2, respectively. The coefficients, C_1 and C_2, and the GS free energy, E_g, are obtained by solving the two-state VB secular equation in its EVB representation, where Φ_1 and Φ_2 are assumed to be orthogonal wave functions whose off-diagonal resonance integral is the mixing term H_{12} (see Refs. 22 and 112 for this description). Now we can approximate the adiabatic GS free energy by Equation (11), which is written for the present case as follows:

$$\overline{g}(r_1, R) \cong [(g_1 + g_2) - ((g_1 - g_2)^2 + 4H_{12}^2)^{\frac{1}{2}}]/2 \tag{30}$$

where r_1 is the $H - Y$ bond length and R is the $X \cdots Y$ distance, while g_1 and g_2 are the diabatic free-energy functionals that correspond to the diabatic potential surfaces, E_1 and E_2, respectively. This expression is obtained by converting the EVB GS

potential energy, E_g, to the corresponding GS-free-energy functional, $\bar{g}$, by the EVB/US approach. We can also approximate the adiabatic free-energy barrier by:

$$\Delta \bar{g}' = \Delta g'_{\text{dia}} - H_{12} + H_{12}^2/(\lambda + \Delta G_{\text{PT}}) \tag{31}$$

where $\Delta g'_{\text{dia}}$ is the diabatic free-energy barrier obtained from the intersection of g_1 and g_2 and where the second and third terms reflect the differences between the diabatic and adiabatic energy at r' and r_1^0. Equation (31) allows us to immediately define the limits of an LBHB and an ionic HB. That is, since $\Delta g'_{\text{dia}}$ can be approximated by the Marcus' formula and can be expressed as $\Delta g'_{\text{dia}} \simeq (\lambda + \Delta G_{\text{PT}})^2/4\lambda$, we obtain $\Delta g'_{\text{dia}} \simeq \lambda/4$ when $\Delta G_{\text{PT}} \simeq 0$. Thus, we will have a single minimum or a very small barrier at $r_1 \simeq r'$ for $\Delta g'_{\text{dia}} = |H_{12}|$ and $\Delta G_{\text{PT}} \simeq 0$ (see Fig. 15). On the other hand, when $\lambda/4 \gg |H_{12}|$, we will have a double minima system, which cannot be classified as an LBHB. We also note that the LBHB proponents distinguished between a single minimum and a small barrier at $r_1 \simeq r'$, but this does not change any of our conclusions with regards to the interplay between λ and H_{12}. The situation becomes much clearer when $|\Delta G_{\text{PT}}| > 0$. In this case we have a localized ionic HB (Φ_1 or Φ_2, depending on the sign of ΔG_{PT}) and we cannot describe the system as an LBHB.

The transition between the LBHB and HB limits can be further quantified by considering the behavior of $\Delta \bar{g}'$ and asking when this barrier becomes small. This can be formulated by defining a parameter θ by:[112]

$$\theta = H_{12}/[\Delta g'_{\text{dia}} + H_{12}^2/(\lambda + \Delta G_{\text{PT}})] \tag{32}$$

This equation satisfies the relationship $\Delta \bar{g}' = H_{12}(1 - \theta)/\theta$, where $\Delta \bar{g}'$ is the adiabatic free-energy barrier of Equation (31). Now, when $\theta \geqslant 1$ we have $\Delta \bar{g}' \leqslant 0$, and the system can be classified as an LBHB.

The above analysis allows one to see how the interplay between the covalent mixing H_{12} and the electrostatic (solvation) effects are reflected by λ and ΔG_{PT},
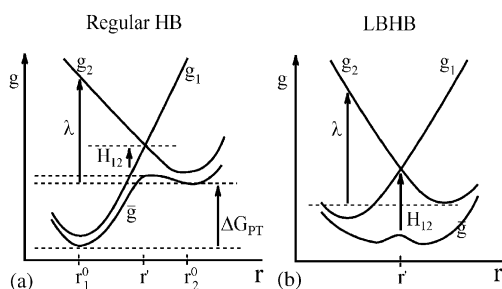
Fig. 15 (a) A two-state VB model for an ionic hydrogen bonded system (see Ref. 114). The free energies g_1 and g_2 correspond to the states $[X^- H - Y]$ and $[X - H Y^-]$. The GS surface, E_g, (with a corresponding free-energy surface and gmacr) is obtained from the mixing of the two states. The donor and the acceptor are held at a distance R. The equilibrium distances for isolated $X-H$ and $H-Y$ fragments are designated by r_1^0 and r_2^0. λ and ΔG_{PT} designate the reorganization energy and proton transfer energies, respectively. (b) A two-state VB model in the LBHB limit. In this case, $\Delta G_{\text{PT}} \approx 0$ and $H_{12} \geqslant \lambda/4$.

which determines the nature of ionic HBs. It is also important to note that ΔG_{PT} is linearly correlated with the pK_a difference between the donor and acceptor, and thus we have a clear relationship between the LBHB character and ΔG_{PT}. Now, when $\theta \leqslant 1$ and when the minimum of the adiabatic GS is near r_1^0, we can use perturbation theory and write:

$$C_2^2(r \simeq r_1^0) = (H_{12}/(g_2 - g_1))_{r \simeq r_1^0}^2 = (H_{12}/[\lambda + \Delta G_{PT} + H_{12}^2/(\lambda + \Delta G_{PT})])^2 \qquad (33)$$

Note that $g_2 - g_1$ is rigorously equal to $E_2 - E_1$.[39] The magnitude of C_2^2 can tell us how much delocalization we still have in the given HB. At any rate, we established here that the existence of a LBHB is defined in terms of the competition between H_{12} and $(\lambda + \Delta G_{PT})$. In other words, we are dealing here with a competition between the localized $[X - H \ Y^-]$, $[X^- \ H - Y]$ pictures, and the delocalized $[X^{-\frac{1}{2}} \cdots H \cdots Y^{-\frac{1}{2}}]$ picture. In the gas phase, the delocalized picture tends to dominate, while in solution the localized picture is more important.

With the above limiting cases in mind we can ask what is new in the LBHB proposal. Obviously the idea that HBs, which are preorganized to stabilize ionic TSs, contribute to catalysis is not new (see above). Thus, the only new element in the LBHB proposal is the idea that the covalent delocalized character, which leads to the single energy minimum, is the origin of the catalytic effect. In this respect, it should be clear that HBs in solution have a significant covalent character (for an early demonstration see Ref. 113). Furthermore, for the LBHB proposal to be valid the covalent character must be larger in the enzyme than in solution, and the corresponding difference must be the source of the HB catalytic effect. Obviously, these issues cannot be examined without evaluating the relevant energies.

At this point it is important to clarify that the entire issue of the validity of the LBHB proposal is related to the interaction between the environment and the VB states of the given ionic HB (in the gas phase we will frequently have LBHBs). Now, the LBHB proponents, who originally assigned to LBHBs in enzymes the enormous energy of $\sim 20 \, kcal \, mol^{-1}$, of gas phase LBHB (e.g., Ref. 107), argued that the enzyme environment is nonpolar and thus should lead presumably to gas phase-like LBHB. However, such desolvation arguments are not useful without actual calculations of the relevant polarity and the corresponding solvation effect. Here it is important to point out that all consistent studies demonstrate that enzyme sites are very polar (e.g., Ref. 22). Performing such calculations in a reliable way is the best way to examine the LBHB proposal.

This review will not examine specific LBHB proposals since this was done in many of our works, including a very recent one.[114] Instead we would only like to emphasize the importance of a well-defined, testable definition. We would also like to take exception with more traditional definitions that unfortunately led the LBHB proponents to a circular logic. The landmark work of Hibbert and Emsley[115] classified HBs according to what they called weak, intermediate and strong HBs. Now, while the review of Ref. 115 is very instructive, it does not address the effect of the environment on the nature of HBs and thus, in contrast to the EVB approach, cannot be used to analyze this crucial effect or to examine the LBHB proposal.

Furthermore, and more importantly, the notion of strength of HBs, which is reasonable when one deals with HBs in a single phase (e.g., gas or solution), becomes extremely problematic when one deals with HBs in proteins. Here what counts is the energy relative to the corresponding energy in water (stability rather than force). The best way to see this fact is to realize that an ionic HB is very strong in the gas phase, but much less stable than the "weak" HBs in water (see Ref. 112 for a clear demonstration of this issue). Once we avoid the ill-defined concept of "strength" we are back to the above VB definition of the relative energy of the two VB states.

One of the most crucial ingredients for following the LBHB "controversy" is the ability to judge different arguments at their face value. Thus, it is useful to examine the arguments that the LBHB proposal also applies to asymmetric HBs (e.g., Ref. 116). One can perhaps trace this proposal to the statement in Ref. 108, that when the fractional charge (δ) on the donor can be between 50% to almost 100%, we can have an LBHB. Unfortunately, if we allow the fractional charge to be close to 100%, we clearly cannot have an LBHB proposal, since this contradicts the assumption of equal pK_a ($\Delta G_{PT} \simeq 0$), which is shared by all the LBHB proponents including Frey et al.[108] Having $\delta \sim 1$ corresponds exactly to the localized ionic HB concept, which means that assigning such a system as an LBHB cannot be a new proposal (see above). Apparently the suggestion that an asymmetric HB is compatible with the LBHB proposal is simply inconsistent with the requirement of having a new proposal or having $\Delta pK_a \sim 0$. In other words, the common case of asymmetric single minimum ionic HBs is not an LBHB, but a clear case where the ΔpK_a is large. Note in this respect that the idea that an LBHB may involve asymmetric charge distribution is in clear contrast with the molecular figures presented by the LBHB proponents (e.g., Scheme 1 in Ref. 117).

It is also important to point out that the LBHB cannot be defined by such terms as short strong HB (SSHB), since an ionic HB can also be short. Furthermore, in contrast to statements (e.g., Ref. 116) that the LBHB proposal does *not* imply that the proton is found at equal distance from the donor and acceptor, this is exactly the requirement from a consistently defined LBHB model. That is, if we have a large ΔG_{PT}, we can have an asymmetric HB with $[X^- H - Y]$ as a dominant form so that the proton will be attached to Y. Since this will be clearly an ionic HB, we conclude that the identification of an LBHB with a single minimum system is *only* valid when the minimum is at the center of the $X \cdots Y$ vector.

As much as the definition of the LBHB proposal is concerned, it is important to address the repeated attempts to use experimental observations as operational definitions of this proposal (e.g., Refs. 109,117). Apparently, such a definition confuses the *interpretation* of experiments with experimental facts. As has been shown in the Ref. 114, most experimental-based definitions of the LBHB proposal are equally consistent with the existence of an ionic HB. Several experiments (e.g., studies of the N–H distance) are much more consistent with the ionic HB than the LBHB picture. However, the most crucial issue is the relative energy of the VB states or the ΔpK_a (or ΔG_{PT}) in the protein active site at the TS. Now, since the corresponding ΔpK_as cannot be determined experimentally (even in cases of TS analogues we do not have

experimental assignment of all the relevant protonation states[114]), it is essential to use theoretical calculations to address the validity of the LBHB proposal. At present, all consistent theoretical studies indicate that LBHBs do not contribute to enzyme catalysis (see also discussion in Ref. 114).

DYNAMICAL PROPOSALS AND MISUNDERSTANDINGS OF THE STATIC NATURE OF THE REORGANIZATION ENERGY

The proposal that special ''dynamical'' effects play a major role in enzyme catalysis (e.g., Refs. 118,119) has become quite popular in recent years (e.g., Refs. 120–128). However, a significant part of this popularity reflects confusion about the nature of dynamical effects and the requirement from catalytic contributions, which must be related to the reference reaction in solution. Apparently, some workers overlooked the difference between the well-known fact that all chemical and biological processes involve atomic motions and the existence of true dynamical contributions to catalysis. Since this issue has been analyzed in great length in several recent reviews[4,40] we consider here only some key points.

The dynamical proposal can be expressed in terms of several alternative definitions. Yet, in order to exhibit dynamical contribution to catalysis, any definition must find a different magnitude of dynamical contributions to the rate constant in the enzyme and in water. All the reasonable definitions result with very small dynamical contributions.[40] Rigorously speaking, it is agreed in the chemical physics community (see references in Ref. 4) that all the dynamical effects are contained in the transmission factor, that corrects the absolute rate theory for re-crossing of the reactive trajectories (see Ref. 40 for a clear definition). All reported simulation studies (e.g., Refs. 4,103) found that the transmission factors are similar in enzymes and in solution, and do not differ much from unity in the enzyme (e.g., Refs. 4,125).

Dynamical effects can also be defined in terms of the availability of special coherent motions. In this way, the dynamical proposal implies that enzymes ''activate'' special types of coherent motions, which are not available in the solution reaction. Now, the difference between the reaction in enzyme and in solution cannot be accounted for by evaluating the corresponding $\Delta g^{\ddagger}$ using nondynamical Monte Carlo (MC) methods. In other words, if the results from MC and MD are identical, then we do not have dynamical contributions to catalysis. Careful and systematic studies (e.g., Refs. 4,129) have shown that the reactions in both enzymes and solutions involved large electrostatic fluctuations. However, these fluctuations follow the Boltzmann distribution, and thus, do not provide dynamical contributions to catalysis.

Attempts to imply that dynamical effects are associated with the so-called non-equilibrium solvation effects[125] have been shown to be very problematic (see Ref. 4). Furthermore, it has been clearly demonstrated that the difference between the non-equilibrium solvation effects in enzyme and solution is an integral part of the difference between the corresponding activation barriers.[4]

The suggestion that the relaxation of the solvent is very different in enzymes and solution, and that this should have catalytic implications, was also promoted in a

recent work of Nam et al.[87] These workers concluded that the dynamics in DhlA and the reference solution reaction are very different and that "in aqueous solution there is a significant electrostatic effect, which is reflected by the slow relaxation of the solvent. On the other hand, there is no strong electrostatic coupling in the enzyme and the major effect on the reaction coordinate motion is intermolecular energy relaxation." This proposal might have created the impression that enzyme catalysis originates from the slow dynamics of the reference reaction. However, as was emphasized recently[88] the dynamical effects (that reflect the time of arrival of a reactive trajectory to the TS) are similar in enzymes and solution, and the catalysis is due to the difference in the time of producing a reactive trajectory, which is due to the difference in activation free energy and the corresponding difference in the solvent reorganization free energy.

As discussed elsewhere (e.g., Ref. 129), the time-dependent energy gap tells us about the reactive fluctuations, and as seen from the figure, these fluctuations look quite similar in the enzyme and the water reactions. However, in order to quantify the similarity between the two sets of fluctuations, it is essential to examine the autocorrelation of the energy gap, C(t). This autocorrelation has been introduced in our early works as a tool for getting a qualitative estimate of the transmission factor (see Ref. 23), and as a quantitative tool for determining the projections of the enzyme modes on the reaction coordinate.[130,131] At any rate, the C(t) values for the reaction of DhlA and the corresponding solution reaction are presented in Fig. 16, where they are decomposed to the total contribution, and to the contribution of the solvent coordinate. As seen from the figure, the C(t)s of both the enzyme and the solution reactions have a similar fast relaxation (which determines the main physics of the transmission factor) and then a slower component which is larger in the
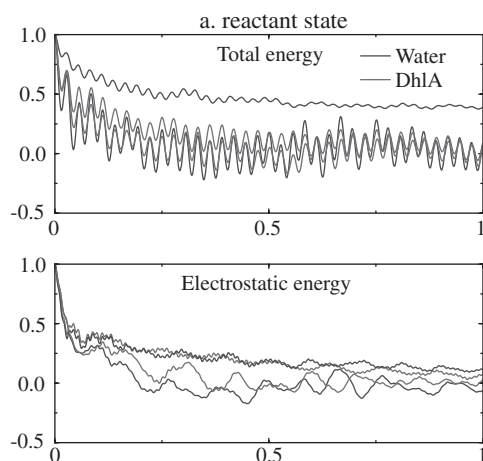
Fig. 16 The autocorrelation of the energy gap for the reaction of DhlA and the reference reaction. The figure provides the analysis for the total energy gap, $\varepsilon_1 - \varepsilon_2$ (top) and for the electrostatic contribution (the solvent coordinate) to the gap (bottom) at the RS (see Ref. 88).

solution reaction. However, the difference between the two systems becomes much smaller when one considers their solvent coordinate (Fig. 16).

Before we continue in the discussion of the significance of our analysis, it is useful to consider related results of Nam et al.[87] These workers used a QM/MM MO approach, which does not provide a diabatic energy gap or the corresponding $C(t)$. Instead, they evaluated the force autocorrelation, $C(t)_F$, which is a valid but somewhat less direct measure of the solvation dynamics than $C(t)$. It was found that $C(t)_F$ relaxes more slowly in water than in DhlA. Furthermore, the $C(t)_F$ of the enzyme also showed some oscillations. The finding that $C(t)$ can be somewhat different in the enzyme and in water is not new and has been reported by Villa and Warshel.[4] Unfortunately, the study of Nam et al.[87] did not provide a separate analysis for the solute and solvent coordinate. Such an analysis is quite challenging when one uses standard QM/MM studies.

With the above results in mind, we can identify the following problems with the analysis of Nam et al.:

(i) Attributing special significance to the slower relaxation of the solution reaction overlooks the fact that most workers in the dynamics community (e.g., Ref. 132) expect that the $C(t)$ of the enzyme will have slower components than $C(t)$ in solution, since water is well known as a very fast solvent.[133]

(ii) A consistent analysis of the type presented in Fig. 16, that actually examines $C(t)$ for the solvent coordinate, finds it to be similar for the enzyme and solution reaction.

(iii) Detailed analysis of "downhill" dynamics (Fig. 17)[88] has demonstrated that the overall dynamics in the solute–solvent coordinate space is similar in DhlA and in solution, regardless of the slow component in $C(t)$ of the solute in DhlA.

(iv) Finally, and most importantly, our recent study[88] has demonstrated that the dynamical effects do not contribute to the differences between the rate constants in the enzyme and solution reaction, and thus do not contribute to catalysis. It was also clarified that the difference in the "reorganization relaxation," if any, is basically irrelevant to catalysis, while the nondynamical reorganization energy is the key factor in enzyme catalysis.

At this point one may wonder about experimental support for the dynamical hypothesis. Here we would like to point out that at present, there is no experimental finding that can be used to consistently support this proposal. In fact, most experiments that were used to support the dynamical proposal have not compared the catalyzed and uncatalyzed reaction, and have not addressed the issue of catalysis (see discussion in Ref. 4). Instructive nuclear magnetic resonance (NMR) experiments (e.g., Ref. 126) demonstrated the involvement of different motions in enzymatic reactions. The obvious existence of motions that have components along the reaction coordinate does not constitute a dynamical effect unless these motions are shown to be coherent. Probably, all the motional effects identified so far are related to entropic factors (i.e., to a change in the available configurational space) rather than to real dynamical effects.
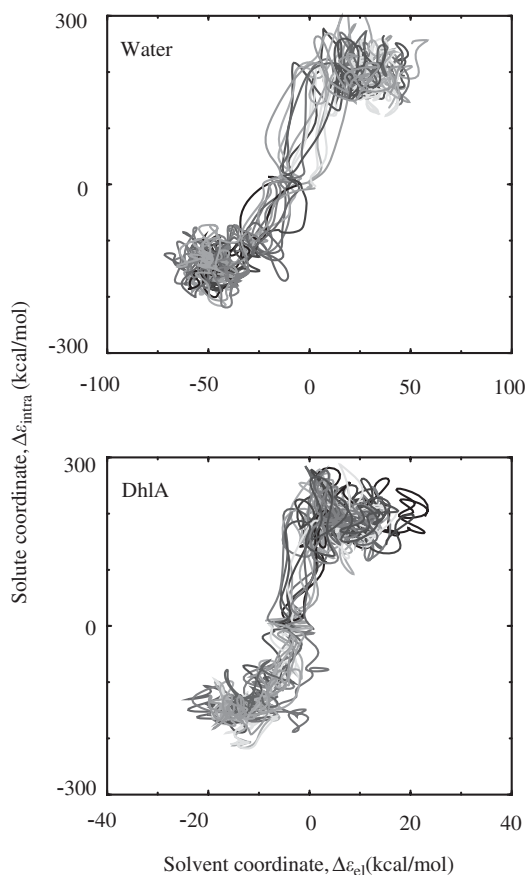
Fig. 17 Showing the behavior of downhill trajectories running for 200 fs on the GS EVB surface for the DhlA system (bottom) and the water reference system (top). The figure shows the trajectories separated into solvent and intra-molecular solute components. The time reversal of these trajectories corresponds to the actual reactive trajectories.

In summary, it is useful to recognize that consistent simulation studies found no evidence for dynamical contributions to catalysis.[4] Studies that were used to invoke such effects (e.g., Ref. 122) did not evaluate any actual activation free energy or transmission factors, and a recent study[87] that did calculate the relevant activation free energy could not produce any correlation between its calculated dynamical effects and the actual rate constant.

TUNNELING AND RELATED EFFECTS

Recent studies (see Refs. 4,127) have suggested that vibrationally enhanced tunneling (VET) plays a major role in enzyme catalysis. Some workers (e.g., Ref. 128)

assumed that there exists here an entirely new phenomenon that makes TST inapplicable to enzymatic reactions. However, the VET effect is not new and is common to many chemical reactions in solution.[25,134,135] Moreover, the VET is strongly related to TST. That is, when the solvent fluctuates and changes the energy gap (see Refs. [25,129]) the light atom sees a fluctuating barrier that allows, in some cases, for a larger rate of tunneling. As shown in Ref. [129], these fluctuations are taken into account in the statistical factor of the classical TST and the same is true when quantum effects are taken into account. Thus, the recent finding that the solvent coordinates should be considered in tunneling studies is not new and does not mean that this effect is important in catalysis.

Hwang et al.[131] were the first to calculate the contribution of tunneling and other nuclear quantum effects to enzyme catalysis. Since then, and in particular in the past few years, there has been a significant increase in simulations of QM-nuclear effects in enzyme reactions. The approaches used range from the quantized classical path (QCP) (e.g., Refs. [4,57,136]), the centroid path integral approach,[137,138] and vibrational TS theory,[139] to the molecular dynamics with quantum transition (MDQT) surface hopping method.[140] Most studies did not yet examine the reference water reaction, and thus could only evaluate the QM contribution to the enzyme rate constant, rather than the corresponding catalytic effect. However, studies that explored the actual catalytic contributions (e.g., Refs. [4,57,136]) concluded that the QM contributions are similar for the reaction in the enzyme and in solution, and thus, do not contribute to catalysis.

Interestingly, the MDQT approach of Hammes-Schiffer and coworkers[140] allowed them to explore the QM transmission factor. It was found that even with QM considerations, the transmission factor is not so different than unity, and thus, we do not have a large dynamical correction to the TST rate constant.

Finally, it is important to clarify some recent misunderstandings about the assertion that the reorganization energy and gate opening fluctuations are dynamical effects,[141] as well as the assumption that the description of PT processes by curve crossing formulations (e.g., Ref. [142]) provide a new "dynamical" insight. Now, the view of PT in solutions and proteins as a curve crossing process has been formulated in early realistic simulation studies[25,129,143] with and without quantum corrections. The phenomenologic formulation of such models has already been introduced quite early by Kuznetsov and Ulstrup.[144] Furthermore, the fact that the fluctuations of the environment in enzymes and solution determined the rate constants of PT reactions has been demonstrated in realistic microscopic simulations of Warshel.[25,129] However, as clarified in these works, the time dependence of these fluctuations does not provide a useful way to determine the rate constant. That is, the electrostatic fluctuations of the environment are determined by the corresponding Boltzmann probability and do not represent a dynamical effect. In other words, the rate constant is determined by the time it takes the system to produce a reactive trajectory, multiplied by the time it takes such trajectories to move to the TS. The time needed to generate a reactive trajectory is determined by the corresponding Boltzmann probability and the actual time it takes the reactive trajectory to reach the TS, which is on the order of picoseconds and is more or less constant in different

systems. As to the suggestion that the reorganization energy or the "gate opening" fluctuations are dynamical effects, first, the solvent reorganization energy, which determines the amplitude of the solvent fluctuations, is not a "static dynamic effect" (as proposed in Ref. 141) but a unique measure of the free-energy associated with the reorganization of the solvent from its reactant to its product configuration (see Ref. 39 for a more rigorous definition). Second, describing the chance of reaching a given solvent configuration as a dynamical gate opening is not useful or predictive. This probability is entirely determined by the corresponding Boltzmann probability,[39] which is determined by ΔG and λ (see discussion in Refs. 28,129).

7   Concluding remarks

This work addressed the issue of enzyme catalysis focusing on the principle of physical organic chemistry and the power of computer simulation approaches. It was shown that when such concepts as reorganization energy and Marcus' parabolas are formulated in a consistent microscopic way, they could be used to explore the origin of enzyme catalysis. It was also clarified that phenomenological applications of the Marcus' formula or related expressions can lead to problematic conclusions.

The use of the EVB approach is shown to provide a powerful quantitative bridge between the classical concepts of physical organic chemistry and the actual energetics of enzymatic reactions. This approach provides quantitative LFERs in enzymes and solution, and allows us to quantify catalytic effects and to define them in terms of the relevant reorganization energies, reaction free energies, and the pre-organization of enzyme active sites.

The concepts outlined in this work provide a powerful way for examining, and sometimes eliminating, different catalytic proposals. Here it is important to realize that we are now at a stage where one can use well-defined energy-based concepts and reliable simulation approaches to actually determine the contribution of different catalytic effects. It is becoming apparent that in contrast to some suggestions (e.g., Ref. 145) it is unlikely that enzymes can in a "synergistic" way make catalytic contributions (e.g., strain, dynamics, entropy, etc.) to catalyze their reactions. In fact, it appears that it is quite hard for the protein environment to change the activation barrier by most proposed effects, and that only the electrostatic effect of pre-organized active sites is capable of leading to *large* catalytic effects. Of course, examining the above statement requires one to use clear definitions of the type presented in this work.

Acknowledgments

References

1. Radzicka, A. and Wolfenden, R. (1995). *Science* **267**, 90–92
2. Warshel, A. (1998). Electrostatic origin of the catalytic power of enzymes and the role of preorganized active sites. *J. Biol. Chem.* **273**, 27035–27038
3. Kienhofer, A., Kast, P. and Hilvert, D. (2003). Selective stabilization of the chorismate mutase transition state by a positively charged hydrogen bond donor. *J. Am. Chem. Soc.* **125** (11), 3206–3207
4. Villa, J. and Warshel, A. (2001). Energetics and dynamics of enzymatic reactions. *J. Phys. Chem. B* **105**, 7887–7907
5. Pople, J.A. (1999). Quantum chemical models (Nobel lecture). *Angew. Chem. Int. Ed. Engl.* **38**, 1894–1902
6. Shurki, A. and Warshel, A. (2003). Structure/function correlations of proteins using MM, QM/MM and related approaches; methods, concepts, pitfalls and current progress. *Advan. Protein Chem.* **66**, 249–312
7. Warshel, A. and Levitt, M. (1976). Theoretical studies of enzymic reactions: dielectric, electrostatic and steric stabilization of the carbonium ion in the reaction of lysozyme. *J. Mol. Biol.* **103**, 227–249
8. Théry, V., et al. (1994). Quantum mechanical computations on very large molecular systems: the local self-consistent field method. *J. Comp. Chem.* **15**, 269–282
9. Zhang, Y., Liu, H. and Yang, W. (2000). Free energy calculation on enzyme reactions with an efficient iterative procedure to determine minimum energy paths on a combined ab initio QM/MM potential energy surface. *J. Chem. Phys.* **112** (8), 3483–3492
10. Gao, J. (1996). Hybrid quantum and molecular mechanical simulations: an alternative avenue to solvent effects in organic chemistry. *Acc. Chem. Res.* **29**, 298–305
11. Bakowies, D. and Thiel, W. (1996). Hybrid models for combined quantum mechanical and molecular approaches. *J. Phys. Chem.* **100**, 10580–10594
12. Field, M.J., Bash, P.A. and Karplus, M. (1990). A combined quantum mechanical and molecular mechanical potential for molecular dynamics simulations. *J. Comp. Chem.* **11**, 700–733
13. Friesner, R. and Beachy, M.D. (1998). Quantum mechanical calculations on biological systems. *Curr. Op. Struct. Biol.* **8**, 257–262
14. Monard, G. and Merz, K.M. (1999). Combined quantum mechanical/molecular mechanical methodologies applied to biomolecular systems. *Acc. Chem. Res.* **32**, 904–911
15. Garcia-Viloca, M., Gonzalez-Lafont, A. and Lluch, J.M. (2001). A QM/MM study of the racemization of vinylglycolate catalysis by mandelate racemase enzyme. *J. Am. Chem. Soc.* **123**, 709–721
16. Marti, S., et al. (2001). Transition structure selectivity in enzyme catalysis: a QM/MM study of chorismate mutase. *Theor. Chem. Acc.* **105**, 207–212
17. Field, M. (2002). Stimulating enzyme reactions: challenges and perspectives. *J. Comp. Chem.* **23**, 48–58
18. Mulholland, A.J., Lyne, P.D. and Karplus, M. (2000). Ab *initio* QM/MM study of the citrate synthase mechanism: a low-barrier hydrogen bond is not involved. *J. Am. Chem. Soc.* **122**, 534–535
19. Cui, Q., et al. (2001). A QM/MM implementation of the self-consistent charge density functional tight binding (SCC-DFTB) method. *J. Phys. Chem. B* **105**, 569–585
20. Strajbl, M., Hong, G. and Warshel, A. (2002). Ab-initio QM/MM simulation with proper sampling: "first principle" calculations of the free energy of the auto-dissociation of water in aqueous solution. *J. Phys. Chem.* **106**, 13333–13343
21. Aqvist, J. and Warshel, A. (1993). Simulation of enzyme reactions using valence bond force fields and other hybrid quantum/classical approaches. *Chem. Rev.* **93**, 2523–2544
22. Warshel, A. (1991). *Computer Modeling of Chemical Reactions in Enzymes and Solutions.* Wiley, New York

23. Hwang, J.-K., et al. (1988). Simulation of free energy relationships and dynamics of S_N2 reactions in aqueous solution. *J. Am. Chem. Soc.* **110**, 5297–5311

24. Warshel, A. (1991). *Computer Modeling of Chemical Reactions in Enzymes and Solutions*. Wiley, New York

25. Warshel, A. (1982). Dynamics of reactions in polar solvents. Semiclassical trajectory studies of electron-transfer and proton-transfer reactions. *J. Phys. Chem.* **86**, 2218–2224

26. Marcus, R.A. (1964). Chemical and electrochemical electron transfer theory. *Ann. Rev. Phys. Chem.* **15**, 155–196

27. Marcus, R.A. (1993). Electron-transfer reactions in chemistry – theory and experiment (Nobel lecture). *Angew. Chem. Int. Ed. Engl.* **32**, 1111–1121

28. Villa, J. and Warshel, A. (2001). Energetics and dynamics of enzymatic reactions. *J. Phys. Chem. B.* **105**, 7887–7907

29. Billeter, S.R., et al. (2001). Hydride transfer in liver alcohol dehydrogenase: quantum dynamics, kinetic isotope effects, and role of enzyme motion. *J. Am. Chem. Soc.* **123**, 11262–11272

30. Vuilleumier, R. and Borgis, D. (1998). Quantum dynamics of an excess proton in water using an extended empirical valence-bond hamiltonian. *J. Phys. Chem. B* **102**, 4261–4264

31. Smondyrev, A.M. and Voth, G.A. (2002). Molecular dynamics simulation of proton transport near the surface of a phospholipid membrane. *Biophys. J.* **82**, 1460–1468

32. Billeter, S.R., et al. (2001). Hybrid approach for including electronic and nuclear quantum effects in molecular dynamics simulations of hydrogen transfer reactions in enzymes. *J. Chem. Phys.* **114**, 6925–6936

33. Florian, J. (2002). Comment on molecular mechanics for chemical reactions. *J. Phys. Chem. A* **106** (19), 5046–5047

34. Vuilleumier, R. and Borgis, D. (1998). An extended empirical valence bond model for describing proton transfer in $H^+(H_2O)_n$ clusters and liquid water. *Chem. Phys. Lett.* **284**, 71–77

35. Schmitt, U.W. and Voth, G.A. (1998). Multistate empirical valence bond model for proton transport in water. *J. Phys. Chem. B* **102**, 5547–5551

36. Warshel, A. and Russell, S. (1986). Theoretical correlation of structure and energetics in the catalytic reaction of trypsin. *J. Am. Chem. Soc.* **108**, 6569–6579

37. Cuma, M., Schmitt, U.W. and Voth, G.A. (2001). A multi-state empirical valence bond model for weak acid dissociation in aqueous solution. *J. Phys. Chem. A* **105** (12), 2814–2823

38. Marcus, R.A. (1964). Chemical and electrochemical electron transfer theory. *Ann. Rev. Phys. Chem.* **15**, 155

39. King, G. and Warshel, A. (1990). Investigation of the free energy functions for electron transfer reactions. *J. Chem. Phys.* **93**, 8682–8692

40. Warshel, A. and Parson, W.W. (2001). Dynamics of biochemical and biophysical reactions: insight from computer simluations. *Q. Rev. Biophys.* **34**, 563–670

41. Warshel, A. (2003). Computer simulations of enzyme catalysis: methods, progress, and insights. *Annu. Rev. Biophy. Biomol. Struct.* **32**, 425–443

42. Warshel, A. (1985). *Simulating the Energetics and Dynamics of Enzymatic Reactions. Specificity in Biological Interactions*. Vol. 55. 1984: Pontificiae Academiae Scientiarum Scripta Varia. 60

43. Kong, Y. and Warshel, A. (1995). Linear free energy relationships with quantum mechanical corrections: classical and quantum mechanical rate constants for hydride transfer between NAD^+ analogues in solutions. *J. Am. Chem. Soc.* **117**, 6234–6242

44. Schweins, T. and Warshel, A. (1996). Mechanistic analysis of the observed linear free energy relationships in p21 ras and related systems. *Biochemistry* **35**, 14232–14243

45. Warshel, A., Schweins, T. and Fothergill, M. (1994). Linear free energy relationships in enzymes. *Theoretical analysis of the reaction of tyrosyl-tRNA synthetase. J. Am. Chem. Soc.* **116**, 8437–8442

46. Warshel, A., Hwang, J.K. and Åqvist, J. (1992). Computer simulations of enzymatic reactions: examination of linear free-energy relationships and quantum-mechanical corrections in the initial proton-transfer step of carbonic anhydrase. *Faraday Discuss* **93**, 225

47. Schweins, T., et al. (1996). Linear free energy relationships in the intrinsic and GTPase activating protein-stimulated guanosine 5′-triphosphate hydrolysis of p21 ras. *Biochemistry* **35**, 14225–14231

48. Warshel, A., Chu, Z.T. and Parson, W.W. (1989). Dispersed polaron simulations of electron transfer in photosynthetic reaction centers. *Science* **246**, 112–116

49. Kiefer, P.M. and Hynes, J.T. (2002). Nonlinear free energy relations for adiabatic proton transfer reactions in a polar environment I. Fixed proton donor–acceptor separation. *J. Phys. Chem. A.* **106** (9), 1834–1849

50. Silverman, D.N., et al. (1993). Rate-equilibria relationships in intramolecular proton transfer in human carbonic anhydrase III. *Biochemistry* **34**, 10757–10762

51. Silverman, D.N. (2000). Marcus rate theory applied to enzymatic proton transfer. *Biochem. Biophys. Acta.* **1458** (1), 88–103

52. Åqvist, J., Fothergill, M. and Warshel, A. (1993). Computer simulation of the CO_2/HCO_3^- interconversion step in human carbonic anhydrase I. *J. Am. Chem. Soc.* **115**, 631–635

53. Silverman, D.N. and Lindskog, S. (1988). Catalytic mechanism of carbonic anhydrase. *Acc. Chem. Res.* **21**, 30–36

54. Åqvist, J. and Warshel, A. (1992). Computer simulation of the initial proton transfer step in human carbonic anhydrase I. *J. Mol. Biol.* **224**, 7–14

55. Schweins, T., et al. (1995). Substrate-assisted catalysis as a mechanism for GTP hydrolysis of p21 ras and other GTP-binding proteins. *Nature Struct. Biol.* **2** (1) 36–44

56. Warshel, A. and Russell, S.T. (1984). Calculations of electrostatic interactions in biological systems and in solutions. *Q. Rev. Biophys.* **17**, 283–421

57. Hwang, J.-K. and Warshel, A. (1996). How important are quantum mechanical nuclear motions in enzyme catalysis?. *J. Am. Chem. Soc.* **118**, 11745–11751

58. Schutz, C.N. and Warshel, A. (2004). Analyzing free energy relationships for proton translocations in enzymes; carbonic anhydrase revisited. *J. Phys. Chem. B* **108** (6), 2066–2075

59. Muegge, I., et al. (1997). The reorganization energy of cytochrome c revisited. *J. Phys. Chem. B* **101**, 825–836

60. Gerlt, J.A. and Gassman, P.G. (1993). An explanation for rapid enzyme-catalyzed proton abstraction from carbon acids: importance of late transition states in concerted mechanisms. *J. Am. Chem. Soc.* **115**, 11552–11568

61. Yarnell, A. (2004). Blockade in the cell's waterway. *C&EN* **82** (4), 42–44

62. Warshel, A. (1979). Conversion of light energy to electrostatic energy in the proton pump of halobacterium halobium. *Photochem. Photobiol.* **30**, 285–290

63. Burykin, A. and Warshel, A. (2003). What really prevents proton transport through aquaporin? Charge self-energy versus proton wire proposals. *Biophys. J.* **85**, 3696–3706

64. Braun-Sand, S., Strajbl, M. and Warshel, A. (2004). Studies of proton translocations in biological systems: simulating proton transport in carbonic anhydrase by EVB based models. *Biophys. J.* **87**, 2221–2239

65. Albery, W.J. and Knowles, J.R. (1976). Free energy profile for the reaction catalyzed by triosephosphate isomerase. *Biochemistry* **15**, 5627–5631

66. Krishtalik, L.I. (1980). Catalytic acceleration of reactions by enzymes. Effect of screening of a polar medium by a protein globule. *J. Theor. Biol.* **86**, 757–771

67. Warshel, A. (1978). Energetics of enzyme catalysis. *Proc. Natl. Acad. Sci. USA* **75**, 5250–5254

68. Lee, F.S., et al. (1992). Calculations of antibody-antigen interactions: microscopic and semi-microscopic evaluation of the free energies of binding of phosphorylcholine analogs to McPC603. *Prot. Eng.* **5**, 215–228

69. Marcus, R.A. (1956). On the theory of oxidation-reduction reactions involving electron transfer I. *J. Chem. Phys.* **24**, 966–978

70. Yadav, A., et al. (1991). Role of solvent reorganization energies in the catalytic activity of enzymes. *J. Am. Chem. Soc.* **113**, 4800–4805

71. Åqvist, J. and Fothergill, M. (1996). Computer simulation of the triosephosphate isomerase catalyzed reaction. *J. Biol. Chem.* **271**, 10010–10016

72. Phillips, D.C. (1966). *Sci. Amer.* **215**, 78–90

73. Jencks, W.P. (1987). *Catalysis in Chemistry and Enzymology*. Dover, New York

74. Kollman, P.A., et al. (2001). Elucidating the nature of enzyme catalysis utilizing a new twist on an old methodology: quantum mechanical-free energy calculations on chemical reactions in enzymes and in aqueous solution. *Acc. Chem. Res.* **34**, 72–79

75. Blow, D. (2000). So do we understand how enzymes work?. *Structure* **8**, R77–R81

76. Crosby, J., Stone, R. and Lienhard, G.E. (1970). Mechanisms of thiamine-catalyzed reactions. Decarboxylation of 2-(1-carboxy-1-hydroxyethyl)-3,4-dimethylthiazolium chloride. *J. Am. Chem. Soc.* **92**, 2891–2900

77. Lee, J.K. and Houk, K.N. (1997). A proficient enzyme revisited: the predicted mechanism for orotidine monophosphate decarboxylase. *Science* **276**, 942–945

78. Dewar, M.J.S. and Storch, D.M. (1985). Alternative view of enzyme reactions. *Proc. Natl. Acad. Sci. USA* **82**, 2225–2229

79. Warshel, A., et al. (2000). Remarkable rate enhancement of orotidine 5′-monophosphate decarboxylase is due to transition state stabilization rather than ground state destabilization. *Biochemistry* **39**, 14728–14738

80. Lightstone, F.C., et al. (1997). Non-enzymatic and enzymatic hydrolysis of alkyl halides: a haloalkane dehalogenation enzyme evolved to stabilize the gas-phase transition state of an S_N2 displacement reaction. *Proc. Natl. Acad. Sci. USA* **94**, 8417–8420

81. Arjunan, P., et al. (1996). Crystal structure of the thiamin diphosphate-dependent enzyme pyruvate decarboxylase from the yeast saccharomyces cerevisiae at 2.3 Å Resolution. *J. Mol. Biol.* **256**, 590–600

82. Jordan, F., Li, H. and Brown, A. (1999). Remarkable stabilization of zwitterionic intermediates may account for a billion-fold rate acceleration by thiamin diphosphate-dependent decarboxylases. *Biochemistry* **38** (20), 6369–6373

83. Warshel, A., Russell, S.T. and Churg, A.K. (1984). Macroscopic models for studies of electrostatic interactions in proteins: limitations and applicability. *Proc. Natl. Acad. Sci. USA* **81**, 4785–4789

84. Warshel, A., Åqvist, J. and Creighton, S. (1989). Enzymes work by solvation substitution rather than by desolvation. *Proc. Natl. Acad. Sci. USA* **86**, 5820–5824

85. Devi-Kesavan, L.S. and Gao, J. (2003). Combined QM/MM study of the mechanism and kinetic isotope effect of the nucleophilic substitution reaction in haloalkane dehalogenase. *J. Am. Chem. Soc.* **125** (6), 1532–1540

86. Shurki, A., et al. (2002). How much do enzymes really gain by restraining their reacting fragments?. *J. Am. Chem. Soc.* **124** (15), 4097–4107

87. Nam, K., et al. (2004). Dynamics of an enzymatic substitution reaction in haloalkane dehalogenase. *J. Am. Chem. Soc.* **126** (5), 1369–1376

88. Olsson, M.H.M. and Warshel, A. (2004). Solute–solvent dynamics and energetics in enzyme catalysis: the S_N2 reaction of dehalogenase as a general benchmark. *J. Am. Chem. Soc.* **126**, 15167–15179

89. Dinner, A.R., Blackburn, G.M. and Karplus, M. (2001). Uracil-DNA glycosylase acts by substrate autocatalysis. *Nature* **413** (6857), 752–755

90. Sham, Y.Y., Muegge, I. and Warshel, A. (1998). The effect of protein relaxation on charge–charge interactions and dielectric constants of proteins. *Biophys. J.* **74**, 1744–1753

91. Bruice, T.C. (2002). A view at the millennium: the efficiency of enzymatic catalysis. *Acc. Chem. Res.* **35** (3), 139–148

92. Strajbl, M., et al. (2003). Apparent NAC effect in chorismate mutase reflects electrostatic transition state stabilization. *J. Am. Chem. Soc.* **125** (34), 10228–10237

93. Hur, S. and Bruice, T.C. (2002). The mechanism of catalysis of the chorismate to pre-phenate reaction by the *Escherichia coli* mutase enzyme. *Proc. Natl. Acad. Sci.* **99**, 1176–1181

94. Haslam, E. (1993). *Shikimic Acid: Metabolism and Metabolites*. Wiley, New York

95. Martí, S., et al. (2000). A QM/MM study of the conformational equilibria in the chorismate mutase active site. The role of the enzymatic deformation energy contribution. *J. Phys. Chem. B* **104**, 11308–11315

96. Khanjin, N.A., Snyder, J.P. and Menger, F.M. (1999). Mechanism of chorismate mutase: contribution of conformational restriction to catalysis in the claisen rearrangement. *J. Am. Chem. Soc.* **121**, 11831–11846

97. Guo, H., et al. (2001). Substrate conformational transitions in the active site of chorismate mutase: their role in the catalytic mechanism. *Proc. Natl. Acad. Sci. USA* **98**, 9032–9037

98. Hur, S. and Bruice, T.C. (2003). Enzymes do what is expected (chalcone isomerase versus chorismate mutase). *J. Am Chem. Soc.* **125**, 1472–1473

99. Hur, S., Newby, Z.E.R. and Bruice, T.C. (2004). Transition state stabilization by general acid catalysis, water expulsion, and enzyme reorganization in *Medicago sativa* chalcone isomerase. *Proc. Natl. Acad. Sci. USA* **101** (9), 2730–2735

100. Ranaghan, K.E., et al. (2004). Transition state stabilization and substrate strain in enzyme catalysis: ab initio QM/MM modelling of the chorismate mutase reaction. *Organ. Biomol. Chem.* **2** (7), 968–980

101. Guimaraes, C.R.W., et al. (2003). Contributions of conformational compression and preferential transition state stabilization to the rate enhancement by chorismate mutase. *J. Am. Chem. Soc.* **125** (23), 6892–6899

102. Alden, R.A., et al. (1971). Subtilisin: a stereochemical mechanism involving transition-state stabilization. *Biochem. Biophys. Res. Commun.* **45**, 337

103. Warshel, A., Sussman, F. and Hwang, J.-K. (1988). Evaluation of catalytic free energies in genetically modified proteins. *J. Mol. Biol.* **201**, 139–159

104. Rao, S.N., et al. (1987). Free energy perturbation calculations on binding and catalysis after mutating asn 155 in subtilisin. *Nature* **328**, 551–554

105. Leatherbarrow, R.J., Fersht, A.R. and Winter, G. (1985). Transition-state stabilization in the mechanism of tyrosyl-tRNA synthetase revealed by protein engineering. *Proc. Natl. Acad. Sci. USA* **82**, 7840–7844

106. Carter, P. and Wells, J.A. (1990). Functional interaction among catalytic residues in subtilisin BPN'. *Proteins: Struct. Func. Gen.* **6**, 240–248

107. Cleland, W.W. and Kreevoy, M.M. (1994). Low-barrier hydrogen bonds and enzymic catalysis. *Science* **264**, 1887–1890

108. Frey, P.A., Whitt, S.A. and Tobin, J.B. (1994). A low-barrier hydrogen bond in the catalytic triad of serine proteases. *Science* **264**, 1927–1930

109. Cleland, W.W., Frey, P.A. and Gerlt, J.A. (1998). The low-barrier hydrogen bond in enzymatic catalysis. *J. Biol. Chem.* **273**, 22529–22532

110. Coulson, C.A. and Danielsson, U. Ionic and covalent contributions to the hydrogen bond. Part I. *Ark. Fys.* **8**, 239–244

111. Coulson, C.A. and Danielsson, U. (1954). Ionic and covalent contributions to the hydrogen bond. Part II. *Ark. Fys.* **8**, 245–255

112. Warshel, A. and Papazyan, A. (1996). Energy considerations show that low-barrier hydrogen bonds do not offer a catalytic advantage over ordinary hydrogen bonds. *Proc. Natl. Acad. Sci. USA* **93**, 13665–13670
113. Warshel, A. and Weiss, R.M. (1980). An empirical valence bond approach for comparing reactions in solutions and in enzymes. *J. Am. Chem. Soc.* **102** (20), 6218–6226
114. Schutz, C.N. and Warshel, A. (2004). The low-barrier hydrogen bond (LBHB) proposal revisited: the case of the Asp…His pair in serine proteases. *Proteins* **55** (3), 711–723
115. Hibbert, F. and Emsley, J. (1990). Hydrogen bonding and chemical reactivity. *Adv. Phys. Org. Chem.* **26**, 255–279
116. Halkides, C.J., Wu, Y.Q. and Murray, C.J. (1996). A low-barrier hydrogen bond in subtilisin: 1H and 15N NMR studies with peptidyl trifluoromethyl ketones. *Biochemistry* **35** (49), 15941–15948
117. Lin, J., et al. (1998). Fractionation factors and activation energies for exchange of the low-barrier hydrogen bonding proton in peptidyl trifluoromethyl ketone complexes of chymotrypsin. *Proc. Natl. Acad. Sci.* **95** (25), 14664–14668
118. Careri, G., Fasella, P. and Gratton, E. (1979). Enzyme dynamics: the statistical physics approach. *Ann. Rev. Biophys. Bioeng.* **8**, 69–97
119. Karplus, M. and McCammon, J.A. (1983). Dynamics of proteins: elements and function. *Ann. Rev. Biochem.* **53**, 263–300
120. Kohen, A., et al. (1999). Enzyme dynamics and hydrogen tunnelling in a thermophilic alcohol dehydrogenase. *Nature* **399**, 496–499
121. Basran, J., Sutcliffe, M.J. and Scrutton, N.S. (1999). Enzymatic H-transfer requires vibration-driven extreme tunneling. *Biochemistry* **38**, 3218–3222
122. Radkiewicz, J.L. and Brooks, C.L.III (2000). Protein dynamics in enzymatic catalysis: exploration of dihydrofolate reductase. *J. Am. Chem. Soc.* **122**, 225–231
123. Cameron, C.E. and Benkovic, S.J. (1997). Evidence for a functional role of the dynamics of glycine-121 of Escherichia coli dihydrofolate reductase obtained from kinetic analysis of a site-directed mutant. *Biochemistry* **36**, 15792–15800
124. Berendsen, H.J.C. and Hayward, S. (2000). Collective protein dynamics in relation to function. *Curr. Opin. Struct. Biol.* **10**, 165–169
125. Neria, E. and Karplus, M. (1997). Molecular dynamics of an enzyme reaction: proton transfer in TIM. *Chem. Phys. Lett.* **267**, 23–30
126. Eisenmesser, E.Z., et al. (2002). Enzyme dynamics during catalysis. *Science* **295**, 1520–1523
127. Kohen, A. and Klinman, J.P. (1999). Hydrogen tunneling in biology. *Chem. Biol.* **6**, R191–R198
128. Sutcliffe, M.J. and Scrutton, N.S. (2000). Enzyme catalysis: over-the-barrier or through-the-barrier?. *Trends Biochem. Sci.* **25**, 405–408
129. Warshel, A. (1984). Dynamics of enzymatic reactions. *Proc. Natl. Acad. Sci. USA* **81**, 444–448
130. Warshel, A. and Hwang, J.-K. (1986). Simulation of the dynamics of electron transfer reactions in polar solvents: semiclassical trajectories and dispersed polaron approaches. *J. Chem. Phys.* **84**, 4938–4957
131. Hwang, J.-K., et al. (1991). Simulations of quantum mechanical corrections for rate constants of hydride-transfer reactions in enzymes and solutions. *J. Phys. Chem.* **95**, 8445–8448
132. Nandi, N., Bhattacharyya, K. and Bagchi, B. (2000). Dielectric relaxation and solvation dynamics of water in complex chemical and biological systems. *Chem. Rev.* **100** (6), 2013–2045
133. Maroncelli, M. and Fleming, G.R. (1988). Computer simulation of the dynamics of aqueous solvation. *J. Chem. Phys.* **89** (8), 5044–5069
134. Borgis, D. and Hynes, J.T. (1991). Molecular-dynamics simulation for a model non-adiabatic proton transfer reaction in solution. *J. Chem. Phys.* **94**, 3619–3628

135. German, E.K. (1981). *J. Chem. Soc. Faraday Trans. 1* **77**, 397–412
136. Feierberg, I., Luzhkov, V. and Åqvist, J. (2000). Computer simulation of primary kinetic isotope effects in the proposed rate limiting step of the glyoxalase I catalyzed reaction. *J. Biol. Chem.* **275**, 22657–22662
137. Gillan, M.J. (1987). Quantum-classical crossover of the transition rate in the damped double well. *J. Phys. C. Solid State Phys.* **20**, 3621–3641
138. Voth, G.A. (1996). Path-integral centroid methods in quantum statistical mechanics and dynamics. *Adv. Chem. Phys.* **93**, 135–218
139. Alhambra, C., et al. (2000). Quantum dynamics of hydride transfer in enzyme catalysis. *J. Am. Chem. Soc.* **122** (34), 8197–8203
140. Billeter, S.R., Webb, S.P., Agarwal, P.K., Iordanov, T. and Hammes-Schiffer, S. (2001). Hydride transfer in liver alcohol dehydrogenase: quantum dynamics, kinetic isotope effects, and role of enzyme motion. *J. Am. Chem. Soc.* **123**, 11262–11272
141. Knapp, M.J. and Klinman, J.P. (2002). Environmentally coupled hydrogen tunneling – linking catalysis to dynamics. *Eur. J. Biochem.* **269** (13), 3113–3121
142. Borgis, D. and Hynes, J.T. (1996). Curve crossing formulation for proton transfer reactions in solution. *J. Phys. Chem.* **100**, 1118–1128
143. Warshel, A. and Chu, Z.T. (1990). Quantum corrections for rate constants of diabatic and adiabatic reactions in solutions. *J. Chem. Phys.* **93**, 4003
144. Kuznetsov, A.M. and Ulstrup, J. (1999). Proton and hydrogen atom tunnelling in hydrolytic and redox enzyme catalysis. *Canad. J. Chem. Rev. Canad. Chim.* **77** (5–6), 1085–1096
145. Li, G.H. and Cui, Q. (2003). What is so special about Arg 55 in the catalysis of cyclophilin A? Insights from hybrid QM/MM simulations. *J. Am. Chem. Soc.* **125** (49), 15028–15038

Cumulative Index of Authors

Cumulative Index of Titles

Author Index